CRANFIELD INSTITUTE OF TECHNOLOGY

COLLEGE OF AERONAUTICS

Ph.D. Thesis

R. GHADIMI

NONLINEAR DYNAMIC ANALYSIS OF OFFSHORE STRUCTURES

Supervisor: Professor C.L.Kirk

March 1986

To my Parents - with my sincere thanks

for your constant love and support

ABSTRACT

In this thesis consideration is given to a selection of nonlinear dynamic problems in the field of offshore engineering. Hydrodynamic loading on fixed horizontal and vertical tubular members and the dynamic response of articulated towers together with the distribution of shear force and bending moment along the tower are investigated using various wave theories. Effects of nonlinear convective acceleration terms in the calculation of fluid inertia forces and moments are examined and attention is given to integration of wave forces up to the free surface for vertical members. Calculation of fluid loading at the displaced position of the articulated tower and any Mathieu type instabilities that may occur have been considered. The dynamic analysis of a damaged Single Anchor Leg Storage (SALS) system subject to loss of buoyancy in the yoke chamber is studied. The equations of motion of the yoke/riser system are derived assuming large displacements and solved in the time domain. Time histories of the response, variations of the riser tension, velocities of riser top end and the time histories of pivot reactions are given. Natural periods and mode shapes for small displacements of the system are calculated. Two methods of simulating random seas, both represented by a sum of harmonic wave components, are used to simulate second order low frequency (slow drift) force on a tanker in head seas by Pinkster's time domain method. In one method the wave amplitudes are generated randomly from a Rayleigh distribution and in the other they are obtained deterministically via the wave spectrum. Time histories of slow drift force and response together with simulation results with various duration lengths are presented and compared. Estimates of the extreme vessel response and its relation to rms value are compared with the result of a commonly used method of determining peak/rms ratios. The results of these investigations highlight the importance of accurately simulating nonlinear effects in both fixed, floating and compliant offshore structures from the point of view of safe design and operation of such systems.

CONTENTS

	Page
ABSTRACT	i
CONTENTS	ii
LIST OF FIGURES	v
LIST OF TABLES	viii
ACKNOWLEDGEMENTS	ix
CHAPTER ONE - INTRODUCTION	1
1.1 Linear and Nonlinear Waves	2
1.1.1 Morison's Equation for Fixed Structural Members	2
1.1.2 Nonlinear Wave Theories	3
1.1.3 Nonlinear Inertia Force	4
1.1.4 Free Surface Effects	5
1.1.5 Hydrodynamic Loading and Response of Articulated Towers	5
1.2 Large Displacements and The Single Anchor Leg Storage (SALS) System	8
1.3 Simulation of Nonlinear and Random Wave Loading and Dynamic Response	10
1.4 Outline of the Main Text and the Scope of the Present Work	13
CHAPTER TWO - WAVE FORCES AND RESPONSE OF FIXED AND COMPLIANT OFFSHORE STRUCTURES UNDER LINEAR AND NONLINEAR WAVE EXCITATION	19
2.0 Introduction	19
2.1 Fixed Cylindrical Members	19
2.2 Articulated Tower	22
2.2.1 Equation of Motion	23
2.2.2 Fluid Loading	26
2.2.3 Distribution of Shear Force and Bending Moment	33
2.2.4 Dynamic Stability	35
2.3 Numerical Data	45
2.4 Results	49
2.5 Discussion	100
CHAPTER THREE - DYNAMIC ANALYSIS OF DAMAGED SINGLE ANCHOR LEG STORAGE (SALS) SYSTEM	115
3.0 Introduction	115
3.1 Mathematical Model	115

3.2 Articulated Riser 119
3.2.1 Kinetic Energy of Links (Structural) 119
3.2.2 Potential Energy of Links 125
3.2.3 Generalised Fluid Forces 126
3.3 Yoke Structure 134
3.3.1 Yoke Kinetic Energy (Structural) 134
3.3.2 Potential Energy of Yoke 148
3.3.3 Generalised Wave Forces on Buoy 151
3.3.4 Change of Buoyancy Force due to Yoke Submersion 159
3.4 Tanker Bow Pivot Motions 161
3.5 Geometric Constraints 161
3.6 Lagrange's Constrained Equations of Motion 162
3.7 Natural Frequencies and Mode Shapes for Small Oscillations 179
3.8 Velocity of Riser Top Articulated Joint 184
3.9 Riser Top Tension and Support Reactions 185
3.10 Static Offset of Tanker 193
3.11 Numerical Data 196
3.12 Results 198
3.13 Discussion 218

CHAPTER FOUR - SIMULATION OF RANDOM SEAS AND ASSOCIATED SECOND ORDER RANDOM PHENOMENA 227
4.0 Introduction 227
4.1 First Order Random Seas 227
4.2 Second Order Random Seas 230
4.3 A Statistically Realistic Model of Random Seas 234
4.4 Slow Drift Force on Tanker (Pinkster's Time Domain Method) 235
4.5 Second Order Surge Response of Tanker 238
4.6 Numerical Data 241
4.7 Results 241
4.8 Discussion 261

CHAPTER FIVE - CONCLUSIONS 265

REFERENCES 269

APPENDIX A - NONLINEAR WAVE THEORIES AND SECOND ORDER NONLINEAR RANDOM WAVES

APPENDIX B - SALS SYSTEM RESPONSE TRANSFER FUNCTIONS

APPENDIX C - FORCE COEFFICIENTS

LIST OF FIGURES

		Page
1.1	Jacket Production Platform	15
1.2	Comparison of Local and Total Horizontal Accelerations	15
1.3	Articulated Towers	16
1.4	Typical Arrangement of a Ball Joint	17
1.5	Maureen Field Articulated Loading Folumn	17
1.6	General Arrangement of SALS	18
1.7	Riser Links	18
2.1	Fixed Horizontal Cylinder	20
2.2	Fixed Vertical Cylinder	22
2.3-2.18	Hydrodynamic Loading on a Horizontal Cylinder	57
2.19-2.28	Hydrodynamic Loading on a Vertical Cylinder	73
2.29-2.30	Motion Response of an Articulated Tower to Regular Waves	83
2.31-2.32	Distribution of Shear Force along an Articulated Tower	85
2.33-2.34	Distribution of Bending Moment along an Articulated Tower	87
2.35-2.36	Motion Response of an Articulated Tower to Regular Waves	89
2.37-2.38	Distribution of Shear Force along an Articulated Tower	91
2.39-2.40	Distribution of Bending Moment along an Articulated Tower	93
2.41-2.43	Motion Response of an Articulated Tower to Regular Waves	97
3.1	Initial Configuration	115
3.2	Static Offset Position	115
3.3	Schematic of Damaged SALS	116
3.4	Instantaneous Position of Riser Links	127
3.5	Yoke Configuration	133
3.6	Vertical Displacement of Yoke Centre of Gravity	148
3.7	Instantaneous Position of Yoke Structure	152
3.8	Virtual Displacements of Buoy due to kth Link Virtual Displacements	157
3.9	Virtual Displacement of Yoke	158

3.10	Forces Acting on the System	185
3.11	Variation of Buoyancy Force with Yoke Submersion	198
3.12	Response of a Damaged SALS System	199
3.13-3.16	Damaged SALS System.Natural Periods and Mode Shapes	201
3.17	Damaged SALS System.Riser Top Tension and Support Reactions	206
3.18-3.20	Response of a Damaged SALS System	207
3.21	Damaged SALS System.Pivot Motions and Velocity of Riser Top	210
3.22-3.23	Damaged SALS System.Riser Top Tension and Support Reactions	211
3.24	Damaged SALS System.Pivot Motions and Velocity of Riser Top	213
3.25-3.26	Response of a Damaged SALS System	214
3.27	Damaged SALS System.Riser Top Tension and Support Reactions	216
4.1	Power Spectral Density	229
4.2	Random Sea Surface Realizations	242
4.3	Power Spectral Density of Simulated Random Sea Surface	242
4.4	Diagonal Cosine Transfer Function of Longitudinal Slow Drift Force on a Tanker in Head Seas	243
4.5	Time Histories of Slow Drift Force on a Tanker	244
4.6	Power Spectral Densities of Slow Drift Force on a Tanker	245
4.7	Time Histories of Slowly Varying Surge Response of a Tanker	246
4.8	Time Histories of Slow Drift Force on a Tanker	247
4.9	Power Spectral Densities of Slow Drift Force on a Tanker	248
4.10	Time Histories of Slowly Varying Surge Response of a Tanker	249
4.11-4.18	Simulation Results for Low Frequency Surge Response of a Tanker in Head Seas	253

A1	Coordinate System, Definition Sketch	A1
A2-A35	Stokes Fifth Order Wave Coefficients	A27
A36	Cnoidal Waves - Coordinate System	A74
B1	Schematic of SALS	B1
B2-B3	Vessel Transfer Functions for Surge, Heave and Pitch	B6
C1	Drag Coefficient versus Reynold's Number	C1
C2	Inertia Coefficient versus Reynold's Number	C1
C3	Slow Drift Force Coefficient on VLCC	C2
C4	Nondimensional Damping Matrix for an Oscillating Column	C2
C5	Nondimensional Added Inertia Matrix for an Oscillating Column	C3

LIST OF TABLES

		Page
2.1-2.4	R_e and K_c values for a Horizontal Cylinder	52
2.5-2.8	R_e and K_c values for a Vertical Cylinder	54
2.9	Dimensionless Properties of Wave Cases Considered	95
3.1	a and b Parameters for Yoke Upper Plane	136
3.2	Parameters x_s and y_s for Yoke Lower Plane	140
3.3	Parameters α and β for Sides of Yoke	143
3.4	Particulars of Tanker	196
3.5	Approximate Mean Loads and Static Offset of Tanker	197
3.6	SALS System - Summary of Results for Wave Cases Considered	217
4.1	Quadratic Transfer Function of Longitudinal Slow Drift Force on a Tanker in Head Seas	241
A1-A3	Values of kd.Stokes 5th Order Waves	A25

ACKNOWLEDGEMENTS

I would like to express my deepest gratitude to Professor C.L.Kirk for his continued help, advice and encouragement during the course of my studies at Cranfield.

Special thanks are given to Dr.R.S.Langley for the valuable suggestions and stimulating discussions during the preparation of this work.

Appreciation is extended to all Ph.D students and staff at the College of Aeronautics, in particular Mr.M.Nabavian, Mr.R.K.Joshi, Mr.A.D.Trim and Mr.P.S.Jhita for their friendship and moral support.

Many thanks to Mrs.Tricia Forrest-Holden for her accurate typing of this manuscript.

The financial assistance given by the Science and Engineering Research Council and the College of Aeronautics, C.I.T. is also gratefully acknowledged.

CHAPTER ONE

INTRODUCTION

In the design and analysis of fixed, floating and compliant offshore structures many nonlinear physical quantities and mechanisms exist that are difficult to quantify and interpret in relation to hydrodynamic loading and dynamic response in random sea states. For example with small diameter structures probably the most controversial and significant nonlinearity is the viscous drag force component. There is also the choice of finite amplitude wave theory to be made and the decision of whether or not to evaluate fluid forces at the instantaneous dynamic position of an oscillating structure. In addition low frequency second order wave forces in random seas derive from a nonlinear mechanism and lead to resonant low frequency motions of floating systems that are damped primarily by nonlinear fluid forces.

Structural nonlinearities of practical significance are present in catenary moorings for semi-submersible vessels and other types of floating structures. Again in a damaged state a floating system or one of its components may contain nonlinear stiffness or buoyancy forces.

Thus a strict categorization of nonlinearities is not possible for all systems as each design will possess non-linearities of varying degree and magnitude.

It should also be remembered that nonlinear means "not linear" thus a linear spring with a time varying stiffness coefficient is not a nonlinearity as in the case of Mathieu's equation.

The aim of this thesis is to present a theoretical and computational study of a selection of nonlinear mechanisms and to demonstrate their importance or otherwise in the design context.

Considerable research has been carried out in this field over the past 20 years or so and it is hoped that this thesis will enhance the understanding of nonlinear phenomena in relation to the safe design of all classes of offshore structures.

1.1 Linear and Nonlinear Waves

1.1.1 Morison's equation for fixed structural members

One of the common types of fixed offshore structure is the jacket platform (Fig.1.1) the substructure of which consists of a steel tubular space frame which is subjected to Morison type loading. The fluid induced forces and moments in the jacket and at the base of the legs can play a major role in the design of both the frame and the piled foundations of the structure and for an economic and reliable design good estimation of fluid loading is essential.

For small diameter members used in jackets diffraction effects are negligible and the formulation proposed by Morison et al (62), known as the Morison equation, is most commonly used in research and engineering to estimate the fluid loading. For example, the force per unit length acting on a fixed vertical member of diameter D is

$$F = \frac{1}{2}\rho C_D D (u+V_c)|u+V_c| + \rho\frac{\pi D^2}{4} C_m \frac{du}{dt} \quad (1.1)$$

where ρ = fluid density, u = horizontal particle velocity, C_D, C_m = drag and inertia coefficients respectively, V_c = coplanar current velocity.

The assumption of current and wave induced velocity acting in the same direction is a gross idealization as waves tend to propagate parallel to the wind whereas currents tend to propagate at about 45^o to the wind due to the Coriolis effects of the earth's rotation. Furthermore the current vector rotates with depth in an anti-clockwise direction in the northern hemisphere and hence the resultant fluid velocity vector $\underset{\sim}{u}+\underset{\sim}{V_c}$ is never in reality coplanar. For design purposes however the worst case is taken to be when both velocity components act in the same direction.

It is evident that for calculation of the loads realistic estimates of fluid particle kinematics are necessary. Unfortunately the mathematical modelling of finite amplitude wave motion is complex and in spite of many elegant analyses simple solutions rarely exist. The derivation of linear and

nonlinear wave theories exist in many textbooks on hydrodynamics, e.g. Lamb (52), Ippen (39) and Le Mehaute (55). The major difficulty in finding a solution to the nonlinear boundary value problem describing the wave motion is that one of the boundaries, namely the free surface, is unknown. This leads to the inevitable approximate solutions to the problem and the development of various kinds of wave theories.

1.1.2 Nonlinear wave theories

Assuming infinitesimal waves and neglecting the nonlinear terms in the equations of fluid motion gives a first approximation to the wave motion known as the small amplitude, Airy or linear wave theory. In 1847 Stokes introduced a perturbation procedure by which successive approximations to the solution could be performed and Skjelbreia and Hendrickson (77) extended Stokes finite amplitude wave theory to the 5th order. Their approach is conceptually simple although algebraically complex and involves the numerical solution of a pair of nonlinear equations which can easily be performed making the theory attractive for engineering use. Dean's (15) stream function theory presented a numerical solution to the two dimensional problem by minimising the error in the fit with the nonlinear dynamic free surface boundary condition and representing the flow field by a stream function. Dean (16) also computed and tabulated various parameters suitable for engineering applications, such as the fluid velocities and accelerations, for a wide range of environmental conditions.

Since higher order solutions to Stokes finite amplitude wave theories are obtained using perturbation, they are only suitable for weakly nonlinear waves and their application to steep waves or for shallow water can lead to large errors in wave kinematics. In 1895 Kortweg and DeVries developed the fundamental theory for periodic waves in the shallow water range in which they expressed the 1st order approximation to the wave elevation in terms of the Jacobian elliptic function Cn and hence it was termed "Cnoidal wave

theory". Laitone (50) obtained the 2nd order approximation to the cnoidal theory and Fenton (23) extended it to any desirable order, however, he found no practical justification in going beyond the 5th order.

It must be pointed out that a tremendous amount of literature related to the various aspects of the water wave theories exists and for brevity most will not be mentioned. For an extensive review of the published work related to nonlinear wave theories the reader is referred to Chapter 4 of the book by Sarpkaya and Isaacson (75) where more than 220 publications are referenced.

Comparisons between the predictions of different wave theories are usually based on estimations of the fluid particle kinematics alone, however, it is intended here to compare the predicted fluid forces and the response of ocean structures corresponding to typical design wave conditions. This is carried out in Chapter 2 where predictions of linear and nonlinear wave theories suitable for engineering purposes are discussed. Derivation of the wave theories employed are given in Appendix A.

1.1.3 Nonlinear inertia forces

In equation (1.1) it is usually assumed that the only nonlinearity arises from the quadratic drag term and the acceleration term $\left(\frac{du}{dt}\right)$ in the inertial part is frequently replaced by the local acceleration term $\left(\frac{\partial u}{\partial t}\right)$ which is the change in the velocity with respect to time only. Therefore in calculating the fluid inertia forces by Morison's equation the derivatives of u with respect to space, known as the convective acceleration terms, are normally ignored. Isaacson (40) studied the nonlinear inertia forces acting on a sphere, a horizontal cylinder and a vertical cylinder using Morison's equation and Stokes 2nd and 5th order theories. He found that the inertia forces calculated in the conventional manner, i.e. by letting $\frac{du}{dt} \simeq \frac{\partial u}{\partial t}$, generally overestimates the actual force. Fig.1.2 shows a comparison of local and total acceleration terms indicating that for nonlinear wave flows

the effect of convective acceleration terms can become significant and therefore it is important to illustrate their influence on the fluid loading under typical sea conditions. This is investigated in Chapter 2.

1.1.4 Free surface effects

Since the small amplitude (linear) wave theory is not applicable to regions of the waves above the still water level (SWL), for calculation of the total force on vertical members, integration of equation (1.1) is usually carried only up to SWL and therefore the effect of free surface elevation, at which particle velocity is high, is normally not taken into account.

Wheeler (88) proposed an empirical modification ('stretching') of the depth decay function to linear wave theory to allow for such effects. Although his modification has no theoretical justification and its use in the expressions for the horizontal and vertical fluid motions violate Laplace's equation, Wheeler suggests that this error is not necessarily important from a practical point of view of performing wave force calculations. For nonlinear waves especially in shallow waters the free surface elevation can take up a significant portion of the fluid region and therefore neglecting the effect of variable structural wetted length could lead to large errors in calculated wave forces. The effect of variable submergence on both fixed and compliant vertical members is examined in Chapter 2 using various wave theories.

1.1.5 Hydrodynamic loading and response of articulated towers

Equation (1.1) is also commonly used to estimate the fluid loads acting on compliant structures. This is done by replacing the velocity term in the equation by an expression representing the relative velocity and by including the added mass effects in the inertia part of the force. Fig. 1.3 shows a compliant offshore structure, the articulated tower, which basically consists of a rigid shaft connected

to a gravity base via a ball joint and is maintained in a vertical position by the buoyancy force. Apart from providing an articulation, the joint design (Fig.1.4)must allow for the passage of pipes and transfer of oil to the upper parts of the tower. The sliding faces of the spherical shells are normally made of corrosion-proof material and are separated by a sliding layer of PTFE elements. In order to prevent damage to the internal pipelines any rotation of the bearing about the vertical axis is taken up by a cardan joint which transmits all torsional moments to the base. The joint connecting the column to the gravity base can therefore prove to be expensive to manufacture and for its design a reliable estimate of the maximum loads or maximum tower inclination must be specified. Articulated buoyant towers have been employed as flare structures or tanker loading terminals and their application to deep water drilling and production units can offer many economic advantages. Since the fluid loads due to passage of waves are reacted by the inertia relief of the articulated structure, the induced stresses are therefore lower than those encountered by a fixed tower. Kokkinowrachos and Butt (46) discussed the design principles, motion optimisation and technical feasibility of the articulated tower concept and carried out a parameter study for the use of concrete articulated towers as loading terminals in moderate and deep waters. They concluded that satisfactory behaviour of the structure together with high standard of safety and efficient maintenance can be achieved and gave an account of the fabrication and installation processes related to articulated towers. Their parameter studies were extended by Kokkinowrachos and Mitzlaff (47) to 3, 4 and 5 legged structures (Fig.1.3) for water depths of 250 and 300 metres with balljoints at both ends of each leg allowing the upper deck to move horizontally, however, they did not discuss any practical problems associated with safety, construction or installation. An example of problems experienced is the case of Mobil's SPMI system (Fig.1.3) in

the North Sea Beryl field (see Offshore Engineer (24)). A few months after its installation, in December 1975, the locking device which secured the Beryl column to the base failed during a storm resulting in a freely drifting tower which was later caught by a Dutch tug. It was reconnected with an extra lock in 1976 but two years later there were further problems with the rotating head which had to be replaced. In 1980/81 cracks appeared in the welds of the lattice structure imposing a need for grinding and rewelding. Finally during a storm in January 1985 the top of the tower broke from the supporting column, possibly along a weld due to fatigue, and the tower was taken out of service. To replace the system Mobil considered other alternatives, their cost, maintenance, reliability and endurance and again chose to use an articulated tower which is reflective of the company's belief in the advantages that the system can offer. Granville and Fisher (27) described the concept, design, construction and installation of the Maureen field Articulated Loading Column (ALC), shown in Fig.1.5, and suggested that the successful completion of the project points the way to the development of ALC. It is therefore thought that an examination of the hydrodynamic loading and the response of articulated towers carried out in Chapter 2 can also yield useful results.

The dynamics of articulated towers have been studied by many authors. Kirk and Jain (43) gave an analysis of the articulated tower subject to non-collinear waves and current using linear wave theory and showed that the tower can undergo a complex whirling motion even in regular waves. Chakrabarti and Cotter (10) studying the motion of articulated tower based their analysis on the assumption that the current and wave loads are collinear and linearised the quadratic drag terms using linear wave theory and some of their theoretical results did not correlate well with the experiments. In a later paper (11) they included the effect of lift force produced by eddy formation and shedding causing transverse oscillations of the tower in a uni-directional wave field. They found that such transverse

oscillations can be as high as 30% of the inline motions, however, it was stressed that their data for the lift coefficients were unreliable. A random dynamic analysis in the frequency domain, using spectral techniques and linear wave theory, of articulated platforms was carried out by Kirk and Bose (44) for the combined action of collinear waves and current forces and including the slowly varying drift forces and moments. Their results for 3 designs of articulated platforms showed that the slowly varying resonant motions of the structure can induce considerable increases in column bending moments due to the deck weight. Olsen et al (68) analysed the articulated Single Point Mooring (SPM) system and developed a computer program (NV429) capable of evaluating the system behaviour with and without a tanker in regular waves. The computed results for horizontal and vertical force at wave frequency acting at the base joint together with the bending moment at top of the lattice tower, with no tanker present, did not agree well with the model test results, and they suggested that further experiments should be carried out. The problem of dynamic instabilities associated with the parametric excitations of marine structures was brought into focus by McIver (59) who illustrated that calculation of wave forces at the displaced position of a compliant system leads to time dependent stiffness coefficients and the Mathieu-Hill type equations describing the motion. This is discussed in Chapter 2 and the influence of the nonlinear drag damping in the dynamic stability of articulated towers is also investigated.

1.2 Large Displacements and the Single Anchor Leg Storage (SALS) System

For marginal oilfields, such as the Beryl field, transportation of crude via an offshore loading terminal can prove to be more economical than laying a pipeline. Since 1960 SPM systems have been extensively used as loading or offloading oil terminals for tankers and today there are about 300 SPMs in operation worldwide. In an SPM system the

tanker is moored at one point only, usually the bow, so that the vessel can swing freely about the mooring point and can take up the position of least resistance to the combination of wind, waves and current, i.e. it can 'weathervane'. One such system in which the vessel is moored to the sea bed via a yoke/riser assembly is the Single Anchor Leg Storage (SALS) system shown in Fig.1.6. The concept of the SALS was originally proposed by Single Buoy Mooring Inc., and was further developed by Shell International Petroleum. In this system the tanker is permanently moored by a buoyant rigid yoke and a tensioned riser. Weathervaning is made possible by means of a roller bearing situated at the riser top and the crude can be offloaded to a shuttle tanker moored alongside or behind the storage vessel. The yoke structure is attached to the tanker by hinges allowing it to rotate in the vertical plane about the pivot connection and consists of welded tubular steel frame. The cylindrical buoyancy tank provides the mooring restoring force (or the riser tension) in the system. The riser, articulated at top and bottom, is made up of a number of heavy forged steel links (Fig.1.7) connected by steel pins and shackle plates. To allow for installation flexibility the ends of the links are set at right angles to each other and the flexible production riser or hose is attached to the chain by flexible supports. More information about various types of SPMs and further details of the SALS system can be found in Ref.(2). Eykhout and Foolen (21) give the description, design concept and construction of a SALS system installed in Castellon field offshore Spain. A linearised random dynamic analysis of the SALS system taking account of the 1st and 2nd order wave forces acting on the structure in head seas was presented by Langley and Kirk (53). They gave the system transfer functions for motions and yoke pivot reactions together with the variation of RMS values for various parameters, such as riser tension and pivot reactions, as a function of significant wave height H_s. Kirk (45) gave an approximate analytical approach assuming

a deterministic wave environment and stressed that for the particular system considered, wave heights greater than about 20m can cause a loss of tension in the articulated riser during part of the load cycle which can lead to 'snatch' loads in the riser links. The loss of tension in the riser can also be initiated by a damaged buoyancy cylinder in which flooding of the chamber due to fatigue cracks at the welded joints has taken place. This would subsequently lead to a slack chain susceptible to high stresses caused by snatch loads and detrimental to the integrity of the structure. An investigation into the behaviour of the damaged SALS system subject to environmental loads is therefore of practical use. This problem is considered in Chapter 3 and since large motions of the slack yoke/riser system can take place a nonlinear dynamic analysis is carried out to predict the system response to regular waves.

1.3 Simulation of Nonlinear and Random Wave Loading and Dynamic Response

Apart from very few cases it is not possible to arrive at exact analytical solutions to the differential equations describing nonlinear motion. An account of the basic ideas relating to the dynamic behaviour of nonlinear systems, analytical solution methods in nonlinear vibrations and stability theory can be found in the textbook given by Hagedorn (32). Perturbation, equivalent linearisation, harmonic balance or other analytical methods commonly used in applied mechanics, electronics, biology and other branches of science or engineering can only provide approximate solutions but can also give a physical insight into the nature of a given problem, however, owing to the present day excellent computational facilities accurate and reliable solutions can be found using numerical techniques. In connection with statistical analysis and simulation of nonlinear random processes the rapid growth in computer technology and the advent of the new generation of computers, commonly referred to as the supercomputers, means that

larger and more complex mathematical models and algorithms can be efficiently handled at very high speed. The main features of the supercomputer architecture are their use of multiple processing units instead of the conventional single Central Processing Unit (single CPU), e.g. the CRAY X-MP/48 has 4 processor units, together with vector processing capabilities, high transfer rate of disk drives and a large memory space. Multiple and vector processing means that the execution of many operations can be performed simultaneously and in parallel rather than one by one. For example if in one line of a computer program there are a number of multiplications which are then added together, all variables involved can be read from the central memory at once and all the multiplications can be carried out in parallel instead of sequentially. The use of supercomputers in both research and industry especially in the fields of computational fluid dynamics, weather forecasting and oilfield reservoir simulation has increased. Many oil producing companies such as EXXON, Chevron, ARAMCO, Sun Exploration and Production Co., already use supercomputers for exploration data processing, reservoir simulation and seismic analysis. Next generation machines, such as HEP-2 manufactured by Denelcor Inc., which are said to be 500 times faster and more powerful than any currently available supercomputer have already been introduced. It is therefore anticipated that time domain simulation techniques with higher speed and efficiency will be used to solve the problems involving nonlinear and random phenomena.

Random simulation techniques suitable for offshore engineering and design purposes were described by Borgman (6) who suggested the use of the fast or finite Fourier transform (FFT) algorithm introduced by Cooley and Tukey (14) which had proved to be an efficient method of computing the discrete Fourier transform of a time series. Longuet-Higgins (57) applied the statistical theory of stationary random noise developed by Rice (73) to the random process of the sea surface elevation by expressing the 1st order wave elevation as the sum of a large number

of infinitesimal wavelets each having independent phases, better known as the wave superposition or the Monte Carlo method, i.e.

$$\eta(t) = \sum_{m=1}^{N} a_m \cos(\omega_m t + \psi_m) \qquad (1.2)$$

in which a_m , ω_m , ψ_m are the mth amplitude, frequency and random phase angle respectively. As shown by Hasselmann (34) the second order solution to random seas can be derived using the perturbation method for Stokesian waves. The second order contributions occur at frequencies which are determined by the sum and differences of their 1st order counterparts (see Appendix A). Hudspeth and Chen (37) extended the digital simulation of unidirectional linear random seas to the second order utilizing a FFT algorithm. In simulating a Gaussian sea by equation (1.2) it is commonly assumed that a_m can be calculated deterministically from the wave spectrum, i.e. the randomness is only due to ψ_m , however as pointed out by Rice and Tucker et al (83) this is only valid when $N \longrightarrow \infty$ and this deterministic method, in which a_m are calculated directly from the wave spectrum, cannot model a random Gaussian sea when a limited number of frequency components is used. Tucker et al illustrated that for an accurate model a_m must be generated randomly from a Rayleigh distribution such that the random nature of the record arises from both a_m and ψ_m and suggested that the errors in simulation using the deterministic approach can significantly influence the wave group statistics. Spansberg and Jacobson (78) investigated experimentally the effect of wave grouping on the 2nd order low frequency or 'slow drift' motions of a semi-submersible and found that in beam seas the succession of the waves, or the wave 'groupiness', has a profound effect on the 2nd order part of the force and sway response of the vessel. The two above mentioned methods of simulating random seas, one in which the wave amplitudes are found deterministically from the

wave spectrum the other with randomly generated amplitudes, are considered in Chapter 4 in more detail and are used to simulate the slow drift force and low frequency response of a tanker in head seas.

While the second order forces are generally small compared to the 1st order wave forces, the low natural frequency of a floating system invariably falls within the range of the low frequency second order spectrum leading to large amplitude resonant motions due to low levels of damping present. The accurate estimation of extreme vessel response then becomes important when the design of the vessel mooring system is considered. The second order response of the tanker in random seas is considered in Chapter 4 where the results of simulated response are presented.

1.4 Outline of the Main Text and the Scope of the Present Work

A brief introduction to the various problems examined in this thesis has been given. Much of the published work not mentioned here are referenced in the main text where their importance and relevance become more apparent.

Chapter 2 investigates the evaluation of hydrodynamic forces acting on fixed and moving tubular members using linear and nonlinear wave theories. The theories employed are: Linear or Airy, 'stretched' Airy, Stokes 5th, stream function and 5th order cnoidal. Morison's equation is used and the effect of nonlinear inertia forces arising from the convective acceleration terms is considered. Integration of fluid forces is extended to the free surface for vertical members and results are discussed. The equation of motion of the articulated tower is presented taking into account the effect of variable submergence. The distribution of shear force and bending moments along the tower is investigated. Dynamic stability of the tower is examined by calculating the fluid loads, predicted by Stokes 5th and stream function theories, at the displaced position of the tower and the effect of nonlinear drag damping on stability

is examined. Results of hydrodynamic loading relating to a selection of wave data chosen from typical 50 year storm conditions in the North Sea are presented and predictions of the various wave theories are compared. Simulation results for the response of articulated tower are given and discussed.

Chapter 3. This chapter presents the nonlinear dynamic analysis of damaged SALS system. It is assumed that the system can undergo large displacements. The marine environment is represented by coplanar regular waves and current. The constrained nonlinear equations of motion are derived using the Lagrangian method. The changes in buoyancy force due to yoke submersion are taken into account. Neglecting damping and using an incremental method, the natural frequencies and mode shapes for small oscillations of the system are formulated. Expressions for the riser tension and support reactions are given and results for the system response are presented. Time histories of the riser top tension and forces at the supports are included and snatch loads are discussed.

Chapter 4. Here an introduction is given to the efficient method of simulating linear and nonlinear random seas and the evaluation of the slow drift force on a tanker using Pinkster's time domain method (7I). Two methods of simulating random seas, one with deterministic the other with random wave amplitudes, using wave superposition are considered and compared. Simulation results for the low frequency second order response of a tanker in head seas are given and an estimation of the peak values at practical levels of damping is considered.

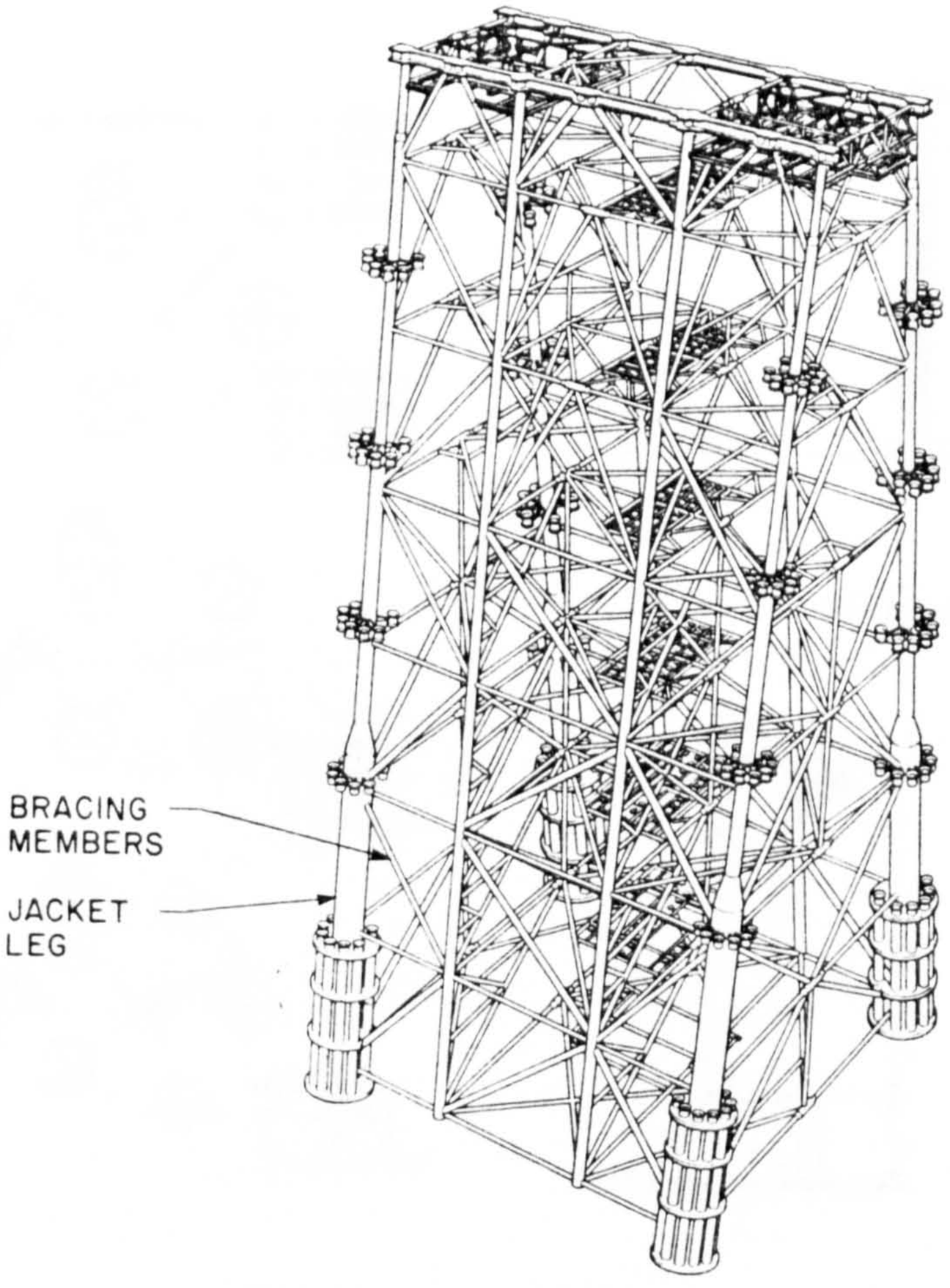

FIGURE 1.1. JACKET PRODUCTION PLATFORM

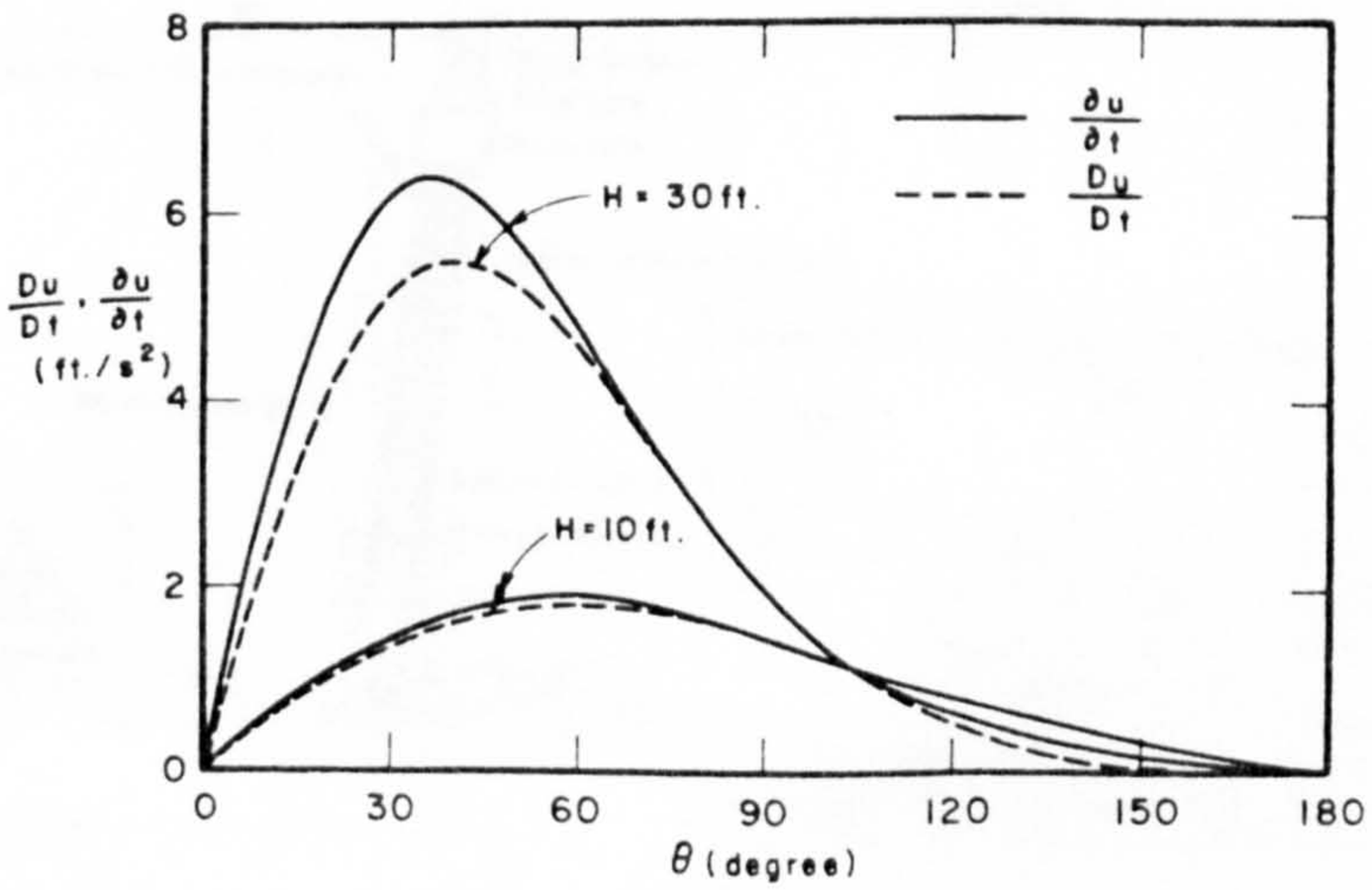

FIGURE 1.2. COMPARISON OF LOCAL AND TOTAL HORIZONTAL ACCELERATIONS (75). (25ft below MWL, wave period = 14 sec, water depth = 50ft).

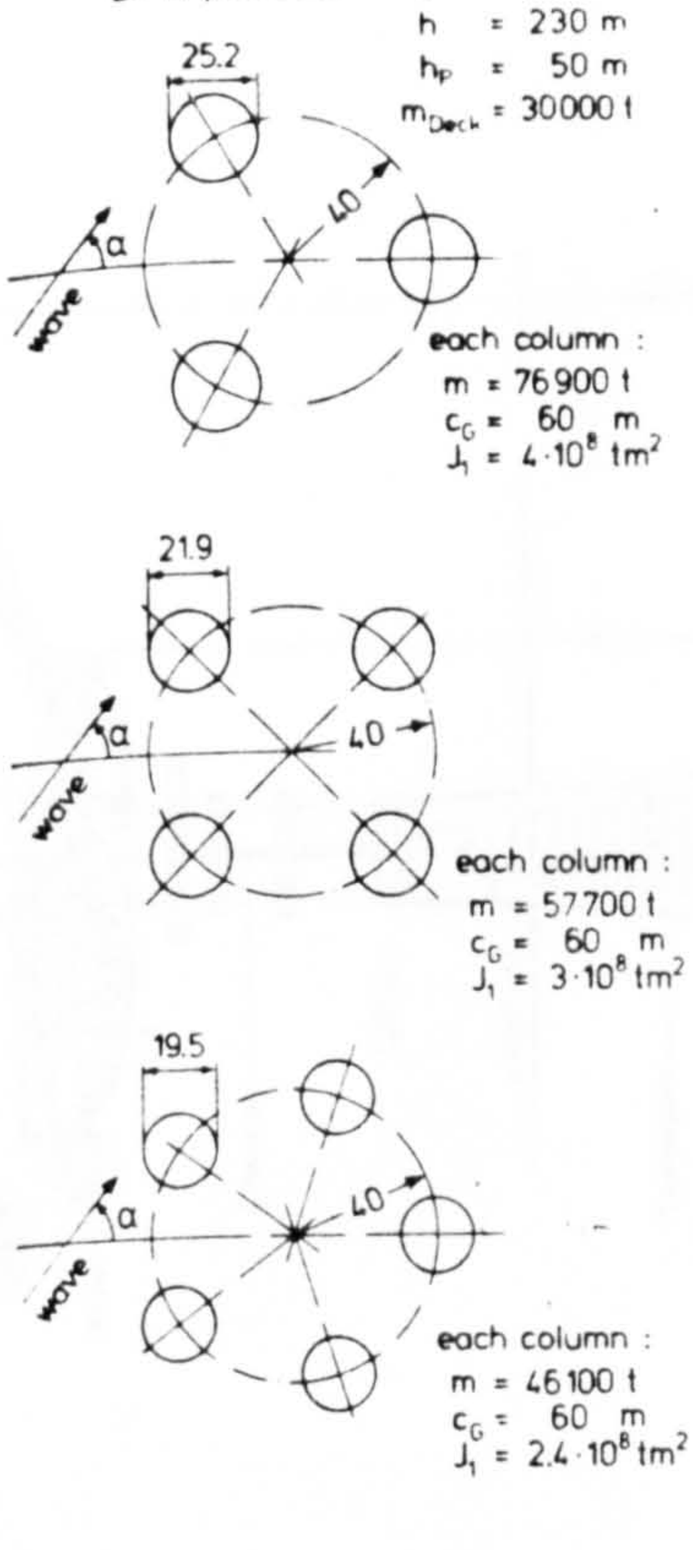

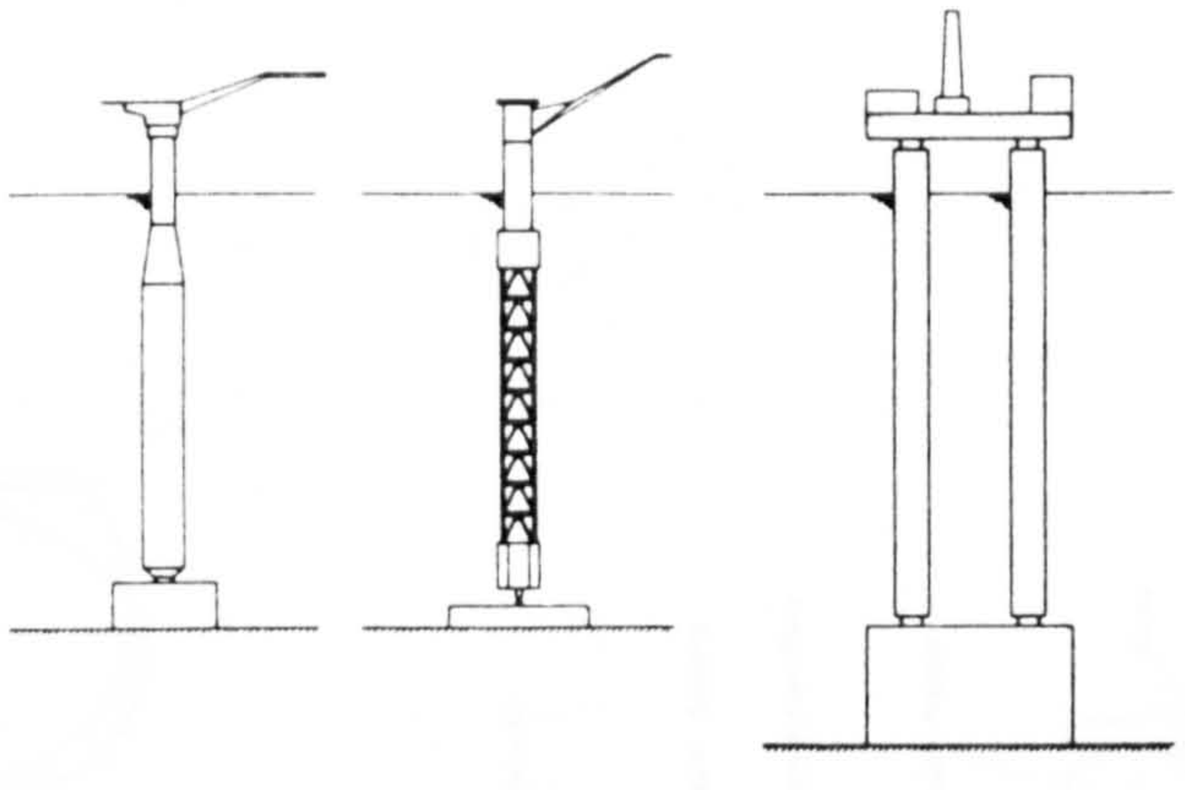

Articulated structures

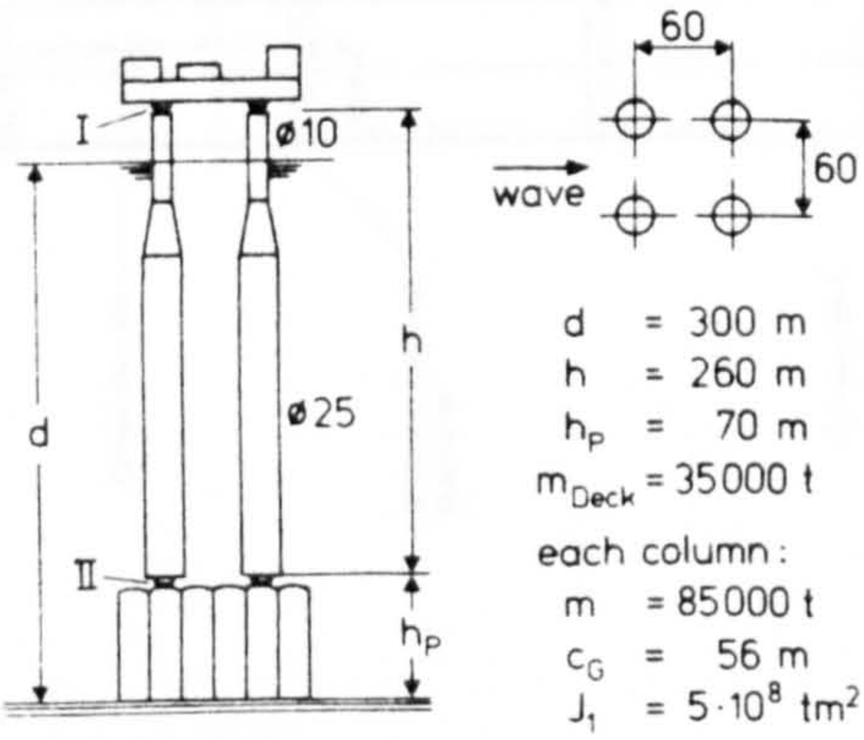

Multi-column platforms

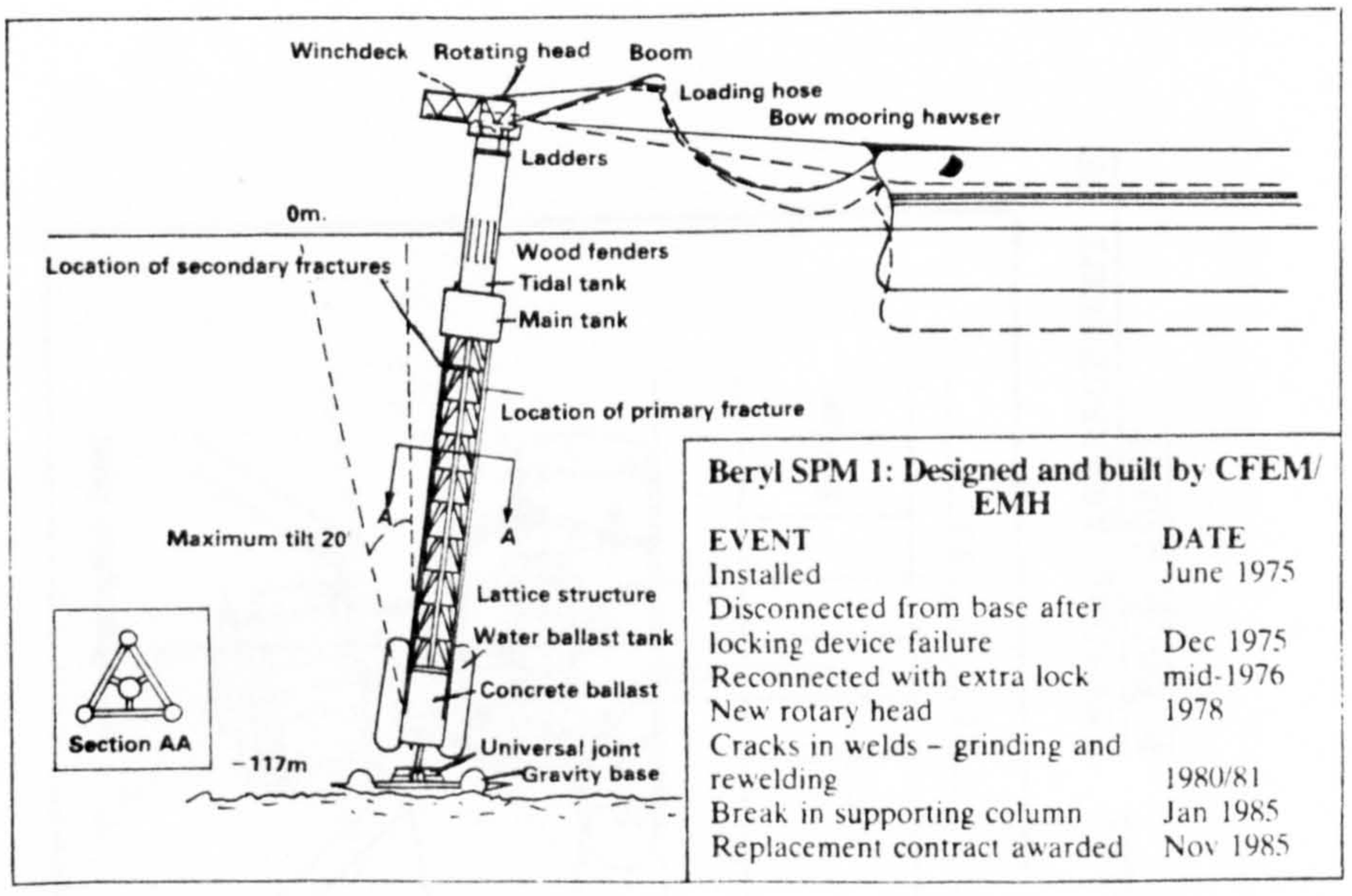

FIGURE 1.3. ARTICULATED TOWERS

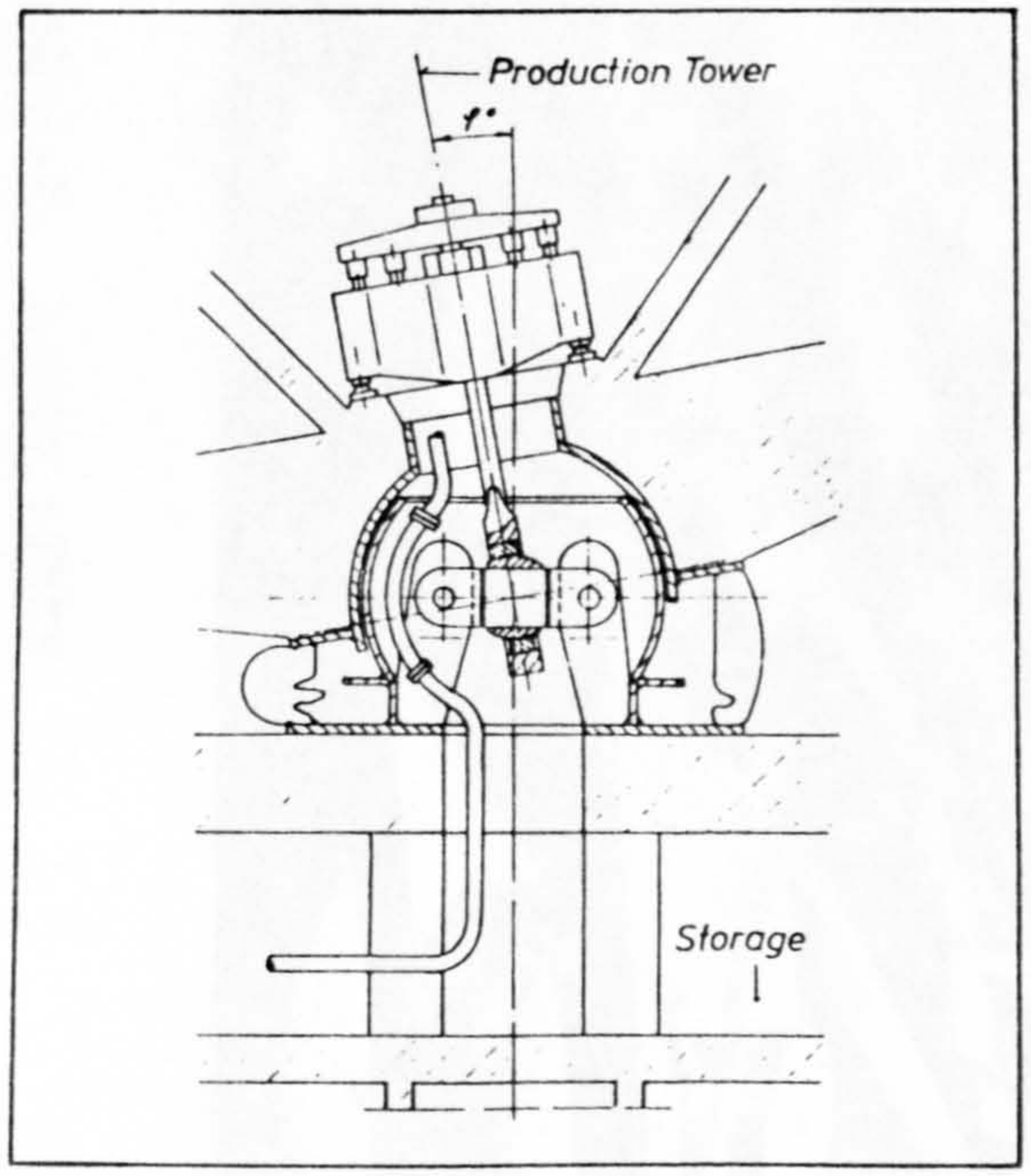

FIGURE 1.4. TYPICAL ARRANGEMENT OF A BALL JOINT

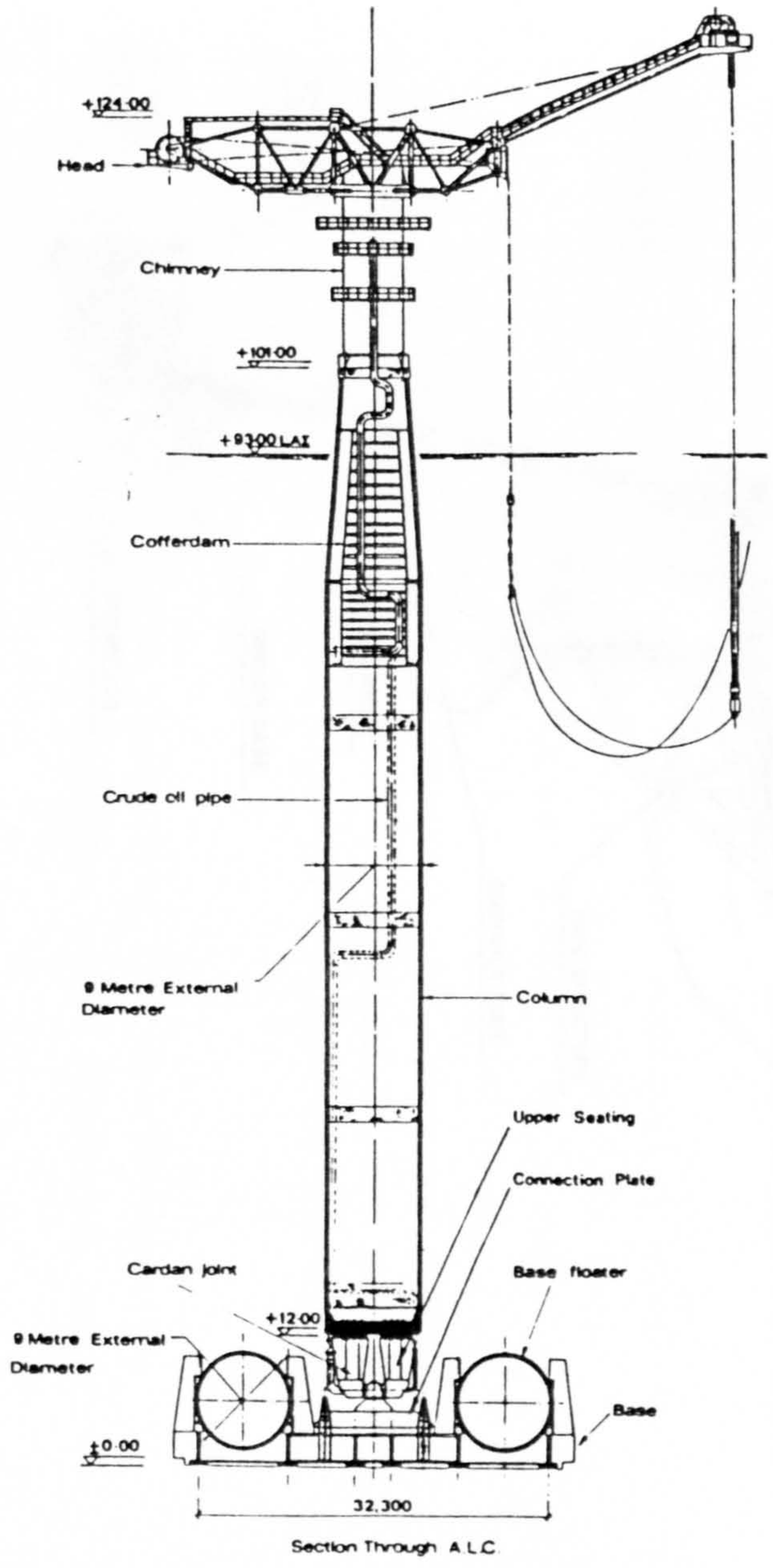

FIGURE 1.5. MAUREEN FIELD ARTICULATED LOADING COLUMN

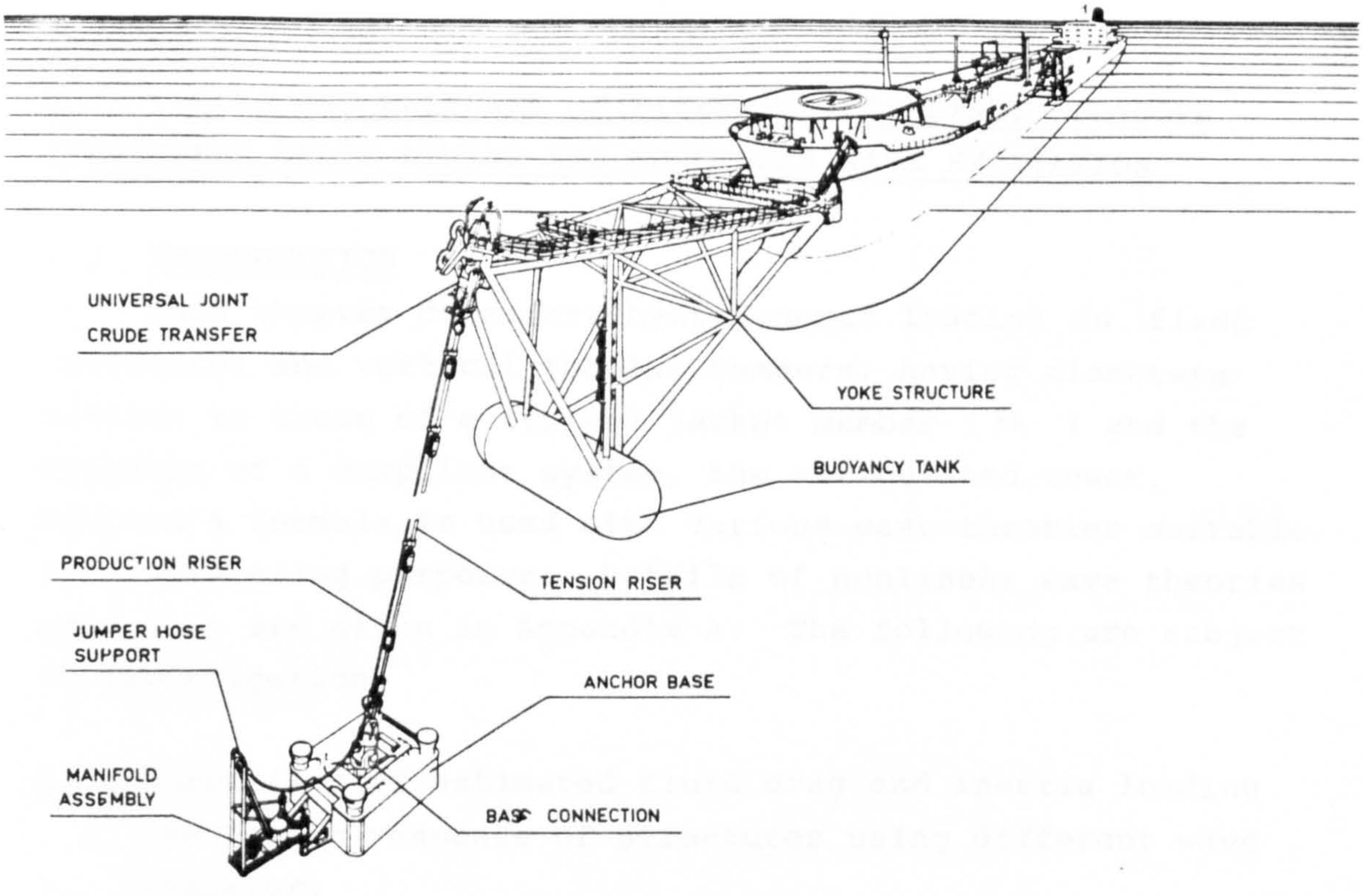

FIGURE 1.6. GENERAL ARRANGEMENT OF SALS

FIGURE 1.7. RISER LINKS

CHAPTER TWO

WAVE FORCES AND RESPONSE OF FIXED AND COMPLIANT OFFSHORE STRUCTURES UNDER LINEAR AND NONLINEAR WAVE EXCITATION

2.0 INTRODUCTION

This chapter considers hydrodynamic loading on fixed horizontal and vertical tubular members, having diameters similar to those of a typical jacket member (36) and the dynamics of a compliant system, the articulated tower. Morison's formula is used with various wave theories suitable for engineering purposes. Details of nonlinear wave theories used here are given in Appendix A. The following are subject to investigation:

1. Comparison of estimated fluid drag and inertia loading and motion response of structures using different wave theories.
2. Effect of integration of forces up to the free surface elevation for vertical members
3. Calculation of fluid loading at instantaneous position of articulated tower and prediction of possible dynamic instabilities.
4. Effect of convective acceleration terms in calculation of fluid inertia forces and moments in Morison's equation.

2.1 FIXED CYLINDRICAL MEMBERS

Figure 2.1 shows a horizontal cylinder of diameter D fixed at depth γ_c below the mean water level. The x,y coordinate system is fixed directly above the cylinder with origin O lying on the undisturbed free surface. The wave travels in direction x perpendicular to the longitudinal axis of the cylinder. Using Morison's formula (62) we can write

Drag force per unit length,

$$\delta F_d = \tfrac{1}{2} \rho C_D D (u^2 + v^2) \qquad (2.1.1)$$

where u and v are horizontal and vertical fluid particle velocities respectively.

ρ = fluid density,
C_D = drag coefficient,
C_m = inertia coefficient

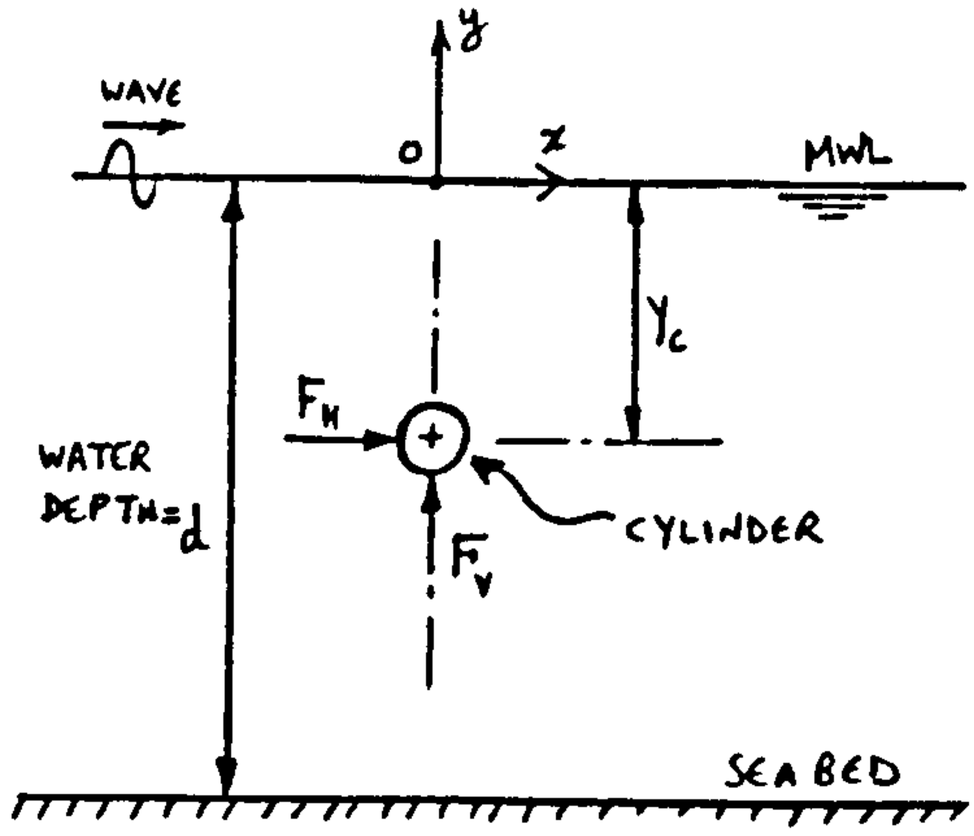

Fig.2.1. Fixed Horizontal Cylinder

From (2.1.1) we get

Horizontal drag force per unit length,

$$\delta F_{dx} = \frac{1}{2} \rho C_D D u \sqrt{u^2 + v^2} \qquad (2.1.2)$$

Vertical drag force per unit length,

$$\delta F_{dy} = \frac{1}{2} \rho C_D D v \sqrt{u^2 + v^2} \qquad (2.1.3)$$

Horizontal fluid inertia force per unit length,

$$\delta F_{ix} = \rho C_m \left(\frac{\pi D^2}{4} \right) \frac{du}{dt} \qquad (2.1.4)$$

Vertical fluid inertia force per unit length,

$$\delta F_{iy} = \rho C_m \left(\frac{\pi D^2}{4} \right) \frac{dv}{dt} \qquad (2.1.5)$$

where the total acceleration terms are given by the sum of linear and nonlinear terms as follows:

$$\frac{du}{dt} = \overbrace{\frac{\partial u}{\partial t}}^{\text{LOCAL}} + \overbrace{u\frac{\partial u}{\partial x} + v\frac{\partial u}{\partial y}}^{\text{CONVECTIVE}} \qquad (2.1.6)$$

$$\frac{dv}{dt} = \frac{\partial v}{\partial t} + u\frac{\partial v}{\partial x} + v\frac{\partial v}{\partial y} \qquad (2.1.7)$$

Adding (2.1.2) and (2.1.4) we have

Total horizontal wave force
per unit length,

$$F_H = \frac{1}{2}\rho C_D D u\sqrt{u^2+v^2} + \rho C_m \cdot \frac{\pi D^2}{4} \cdot \frac{du}{dt} \qquad (2.1.8)$$

Total vertical wave force,
per unit length,

$$F_V = \frac{1}{2}\rho C_D D v\sqrt{u^2+v^2} + \rho C_m \frac{\pi D^2}{4} \frac{dv}{dt} \qquad (2.1.9)$$

and resultant wave force
per unit length,

$$F_R = \sqrt{F_H^2 + F_V^2} \qquad (2.1.10)$$

for a vertical cylinder as shown in Figure 2.2 the horizontal force at depth y on an element dy is given by

$$\delta F = \left[\frac{1}{2}\rho C_D D u|u| + \rho C_m \frac{\pi D^2}{4} \frac{du}{dt} \right] dy \qquad (2.1.11)$$

Total force at base,

$$F_b = \int_{-d}^{\eta} \delta F \qquad (2.1.12)$$

where η = wave elevation at cylinder.

Similarly base moment is

$$M_b = \int_{-d}^{\eta} \delta F\,(d+y) \qquad (2.1.13)$$

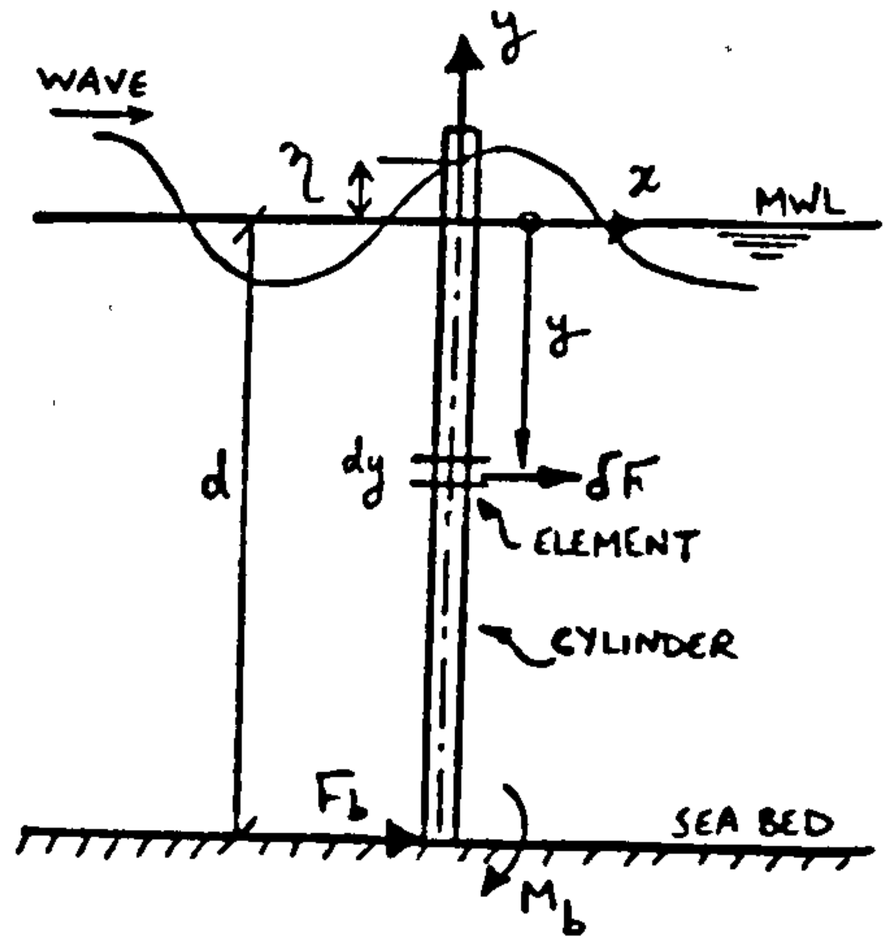

Fig.2.2. Fixed Vertical Cylinder

In evaluating fluid particle velocities and accelerations the following wave theories are used:

1. Airy or Linear wave theory
2. 'Stretched' or modified Airy due to Wheeler (88)
3. 5th order Stokes (77)
4. Stream Function (16)
5. 5th order Cnoidal (23)

2.2 ARTICULATED TOWER

A mathematical model for articulated tower is shown below. The following terminology will be used:

M_p = deck mass,

m_s = structural mass of tower per unit length,

m_a = added mass of tower per unit length,

m_b = ballast mass per unit length,

D = external diameter of tower

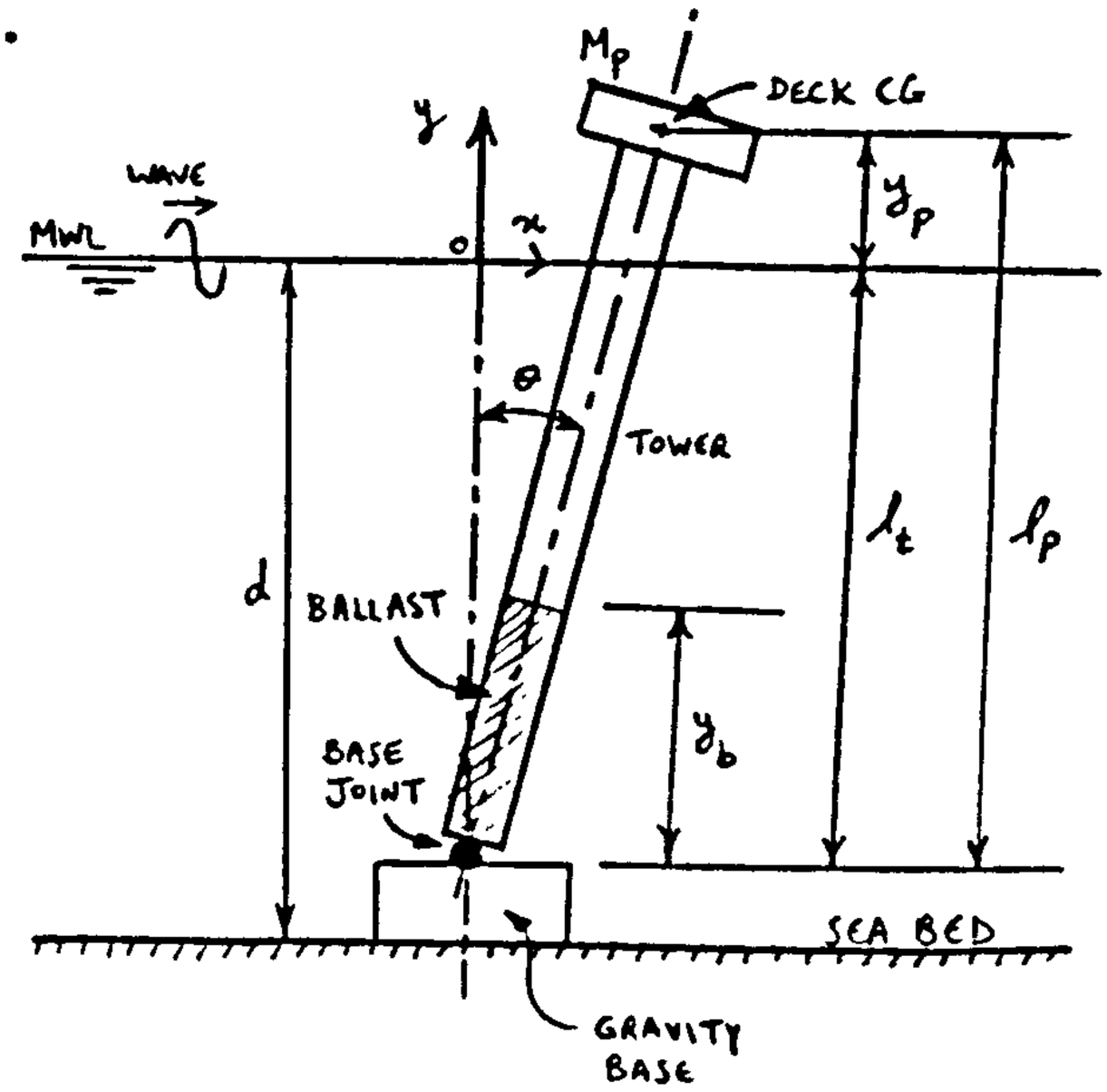

η = wave elevation at instantaneous position of tower,
θ = angular displacement of tower from vertical,
d = water depth,
x, y = coordinate system directly above base joint with origin fixed at the mean water level,
g = gravitational acceleration,
H = wave height.

It is assumed that:

1. Angular displacements are small.
2. Bending stiffness of tower is large and rigid body motions are dominant
3. Wave and current act in the same direction
4. The base joint has zero rotational stiffness and damping.

2.2.1 Equation of Motion

The equation of motion of the system can be derived using Lagrange's method, details of which can be found in texts dealing with the subject of dynamics (e.g. see (81)).

Motion of tower is represented by Lagrange's equation as

$$\frac{d}{dt}\left(\frac{\partial T}{\partial \dot{\theta}}\right) - \frac{\partial T}{\partial \theta} + \frac{\partial V}{\partial \theta} = M_I + M_D - C\dot{\theta} \qquad (2.2.1)$$

where

T = kinetic energy
V = potential energy
M_I, M_D = exciting moment of inertia and drag forces respectively
C = wave damping coefficient

Taking an element of length dy along the tower as shown, we have

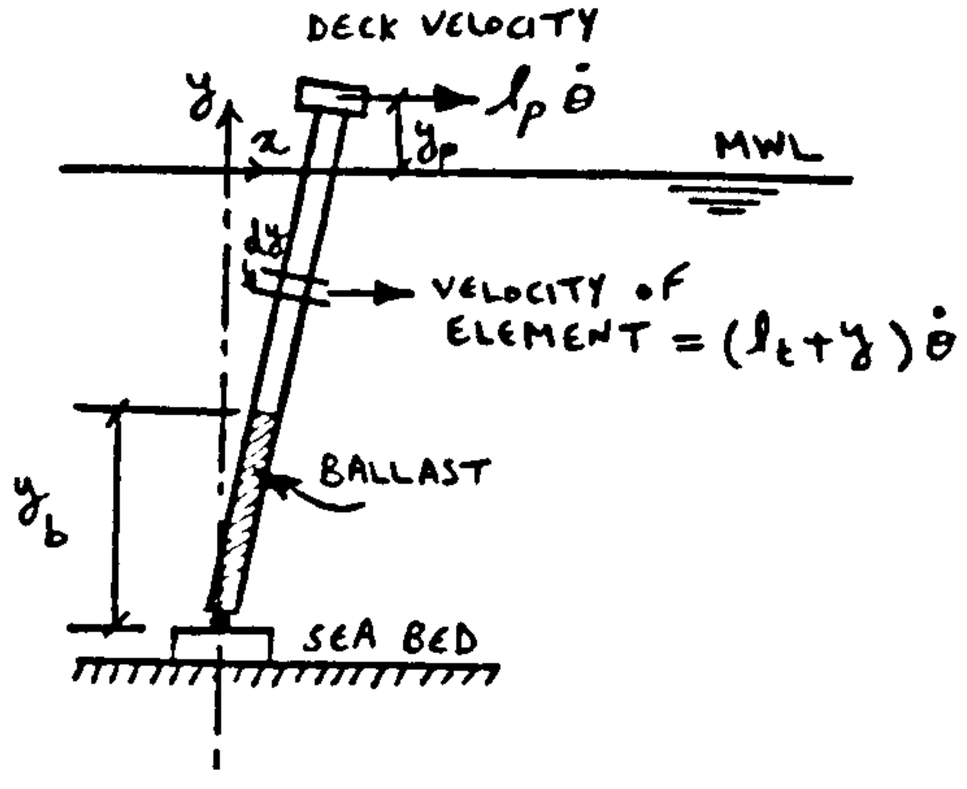

kinetic energy

$$T = \frac{1}{2}\int_{-l_t}^{y_p} m_s \left[(l_t + y)\,\dot{\theta} \right]^2 dy \qquad \text{(COLUMN STRUCTURE)}$$

$$+ \frac{1}{2}\int_{-l_t}^{l} m_a \left[(l_t + y)\,\dot{\theta} \right]^2 dy \qquad \text{(COLUMN ADDED MASS)}$$

$$+ \frac{1}{2} M_p (l_p \dot{\theta})^2 \qquad \text{(DECK)}$$

$$+ \frac{1}{2}\int_{-l_t}^{-(l_t + y_b)} m_b \left[(l_t + y)\dot{\theta} \right]^2 dy \qquad \text{(BALLAST)} \qquad (2.2.2)$$

From equation (2.2.2) we get

$$\frac{d}{dt}\left(\frac{\partial T}{\partial \dot{\theta}}\right) = \frac{1}{3}\left[m_s l_p^3 + m_a (\eta + l_t)^3 + m_b y_b^3 + 3 M_p l_p^2 \right] \ddot{\theta} \qquad (2.2.3)$$

and

$$\frac{\partial T}{\partial \theta} = 0 \qquad (2.2.4)$$

Assuming small angles, i.e. $\sin\theta \simeq \theta$ and $\cos\theta \simeq 1 - \frac{\theta^2}{2}$
Vertical displacement of deck = $l_p \frac{\theta^2}{2}$

Similarly,

Vertical displacement of Centre of Gravity of Ballast = $y_b \frac{\theta^2}{2}$

and

Vertical displacement of Centre of Gravity of Tower = $\frac{l_p \theta^2}{4}$

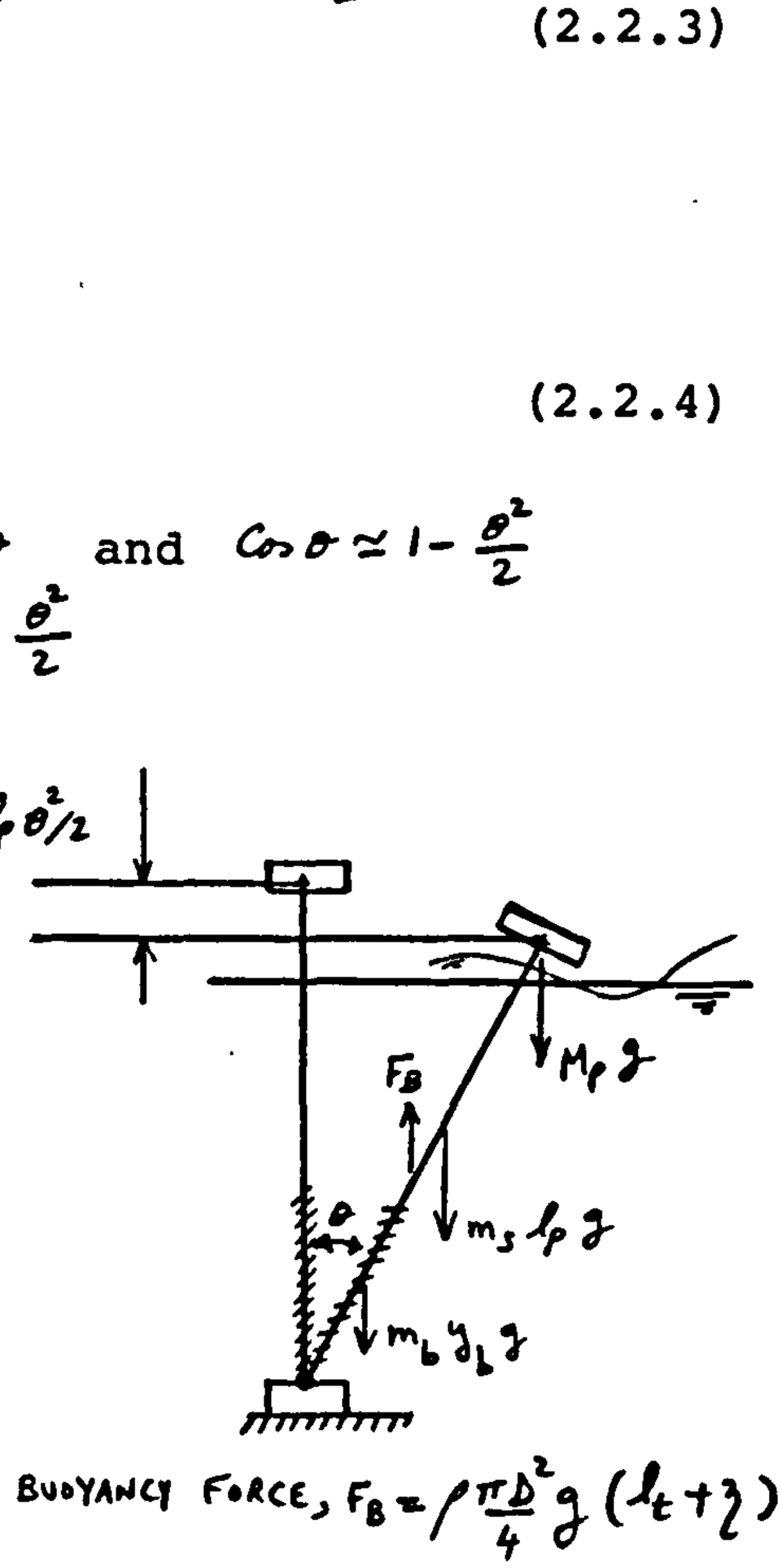

BUOYANCY FORCE, $F_B = \rho \frac{\pi D^2}{4} g (l_t + \zeta)$

Therefore, increase in potential energy

$$V = -g\left[M_p l_p + m_b \frac{y_b^2}{2} + m_s \frac{l_p^2}{2} - \rho \frac{\pi D^2}{8}(l_t+\eta)^2\right]\frac{\theta^2}{2} \qquad (2.2.5)$$

Hence

$$\frac{\partial V}{\partial \theta} = -g\left[M_p l_p + m_b \frac{y_b^2}{2} + m_s \frac{l_p^2}{2} - \rho \frac{\pi D^2}{8}(l_t+\eta)^2\right]\theta \qquad (2.2.6)$$

Substituting (2.2.3), (2.2.4) and (2.2.6) into (2.2.1) and rearranging we have

$$I\ddot{\theta} + C\dot{\theta} + K_o\theta = M_I + M_D \qquad (2.2.7)$$

where

$$I = \frac{1}{3}\left[m_s l_p^3 + m_a(l_t+\eta)^3 + m_b y_b^3 + 3M_p l_p^2\right] \qquad (2.2.8)$$

$$K_o = -g\left[M_p l_p + m_b \frac{y_b^2}{2} + m_s \frac{l_p^2}{2} - \rho \frac{\pi D^2}{8}(l_t+\eta)^2\right] \qquad (2.2.9)$$

Fluid added mass and potential damping corresponding to dissipation of energy in radiated waves can be found numerically using finite element and boundary integral methods (see (60), (26) and (92)). Eatock-Taylor and Duncan (19) give added inertia and damping coefficients of a doubly articulated column in regular waves in non-dimensional form (see Appendix C). Damping and added-mass coefficients for the first mode of the doubly articulated column can be used for a singly articulated tower. From Appendix C

$$\bar{M}^* = \rho \frac{\pi D^2}{4}\int_{-l_t}^{0} y^2\, dy = \rho \frac{\pi D^2}{12} l_t^3 \qquad (2.2.10)$$

and

$$m_a = \alpha_{11} \rho \frac{\pi D^2}{4} \qquad (2.2.11)$$

$$c = \beta_{11} \bar{M}^* \omega = \beta_{11} \rho \frac{\pi D^2}{12} \ell_t^3 \omega \qquad (2.2.12)$$

where

α_{11} = non-dimensional added inertia coefficient for first mode

β_{11} = non-dimensional damping coefficient for first mode

ω = wave frequency

2.2.2 Fluid Loading

Fluid inertia and drag forces acting on an element at distance y from the mean water level are given by Morison's equation as

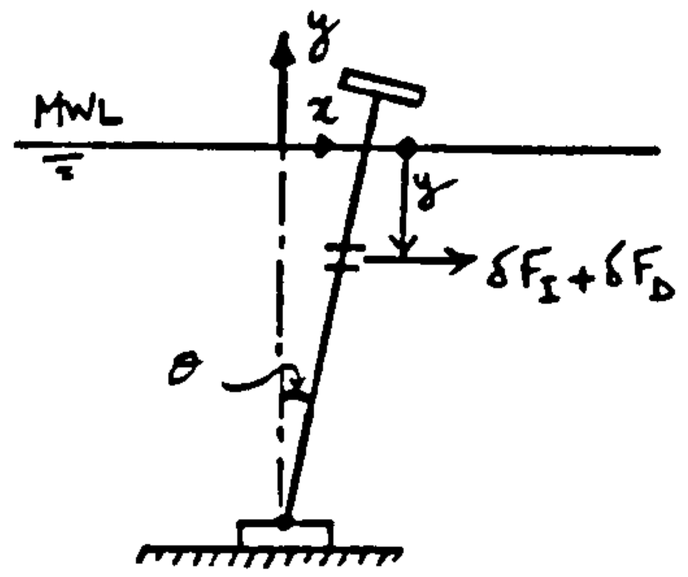

Inertia, $$\delta F_I = C_m \rho \frac{\pi D^2}{4} \dot{u} \, dy \qquad (2.2.13)$$

Drag $$\delta F_D = \frac{1}{2} \rho C_D D \left[u + V_c(y) - (d+y)\dot{\theta}\right] \times \left|u + V_c(y) - (d+y)\dot{\theta}\right| dy \qquad (2.2.14)$$

where $V_c(y)$ = current velocity at element.

In predicting fluid particle kinematics the following wave theories will be used:

1. Airy
2. 'Modified' or 'Stretched' Airy
3. Stokes fifth order
4. Stream Function.

In 2 an empirical modification is applied to the Airy wave theory. The depth decay function $\cosh[k(d+y)]$ in expressions for u and $\dot{u}$ is replaced by $\cosh\left[kd\left(\frac{d+y}{d+\eta}\right)\right]$

to include surface elevation effects.

For the above mentioned water wave theories we can write;

$$u = A_u \sum_{n=1}^{N} G_n \cosh\left[\frac{nk}{a}(d+y)\right] \cos\left[n(kx-\omega t)\right] \qquad (2.2.15)$$

$$\dot{u} = B_u \sum_{n=1}^{N} P_n \cosh\left[\frac{nk}{a}(d+y)\right] \sin\left[n(kx-\omega t)\right] \qquad (2.2.16)$$

For Airy Wave Theory

$$\left.\begin{aligned} a &= 1 \\ N &= 1 \\ A_u &= \frac{\omega H}{2\sinh(kd)} \\ G_n &= 1 \\ B_u &= \frac{\omega^2 H}{2\sinh(kd)} \\ P_n &= 1 \end{aligned}\right\} \qquad (2.2.17)$$

For 'Stretched' Airy Theory as above except for

$$a = \frac{d+\zeta}{d} \qquad (2.2.18)$$

For Stokes Fifth Order Wave Theory

$$\left.\begin{aligned} a &= 1 \\ N &= 5 \\ A_u &= \sqrt{gd} \\ G_n &= b_n \\ B_u &= g \\ P_n &= d_n \end{aligned}\right\} \qquad (2.2.19)$$

For Stream Function Wave Theory

$$
\begin{aligned}
&a = 1 \\
&N = \text{ORDER OF STREAM FUNCTION} \\
&A_u = -k \\
&G_n = n \cdot X(n) \\
&B_u = -k\omega \\
&P_n = n^2 \cdot X(n)
\end{aligned}
\qquad \Bigg\} \qquad (2.2.20)
$$

To find the fluid induced inertia moment at any section, say $y = y_e$, we can write

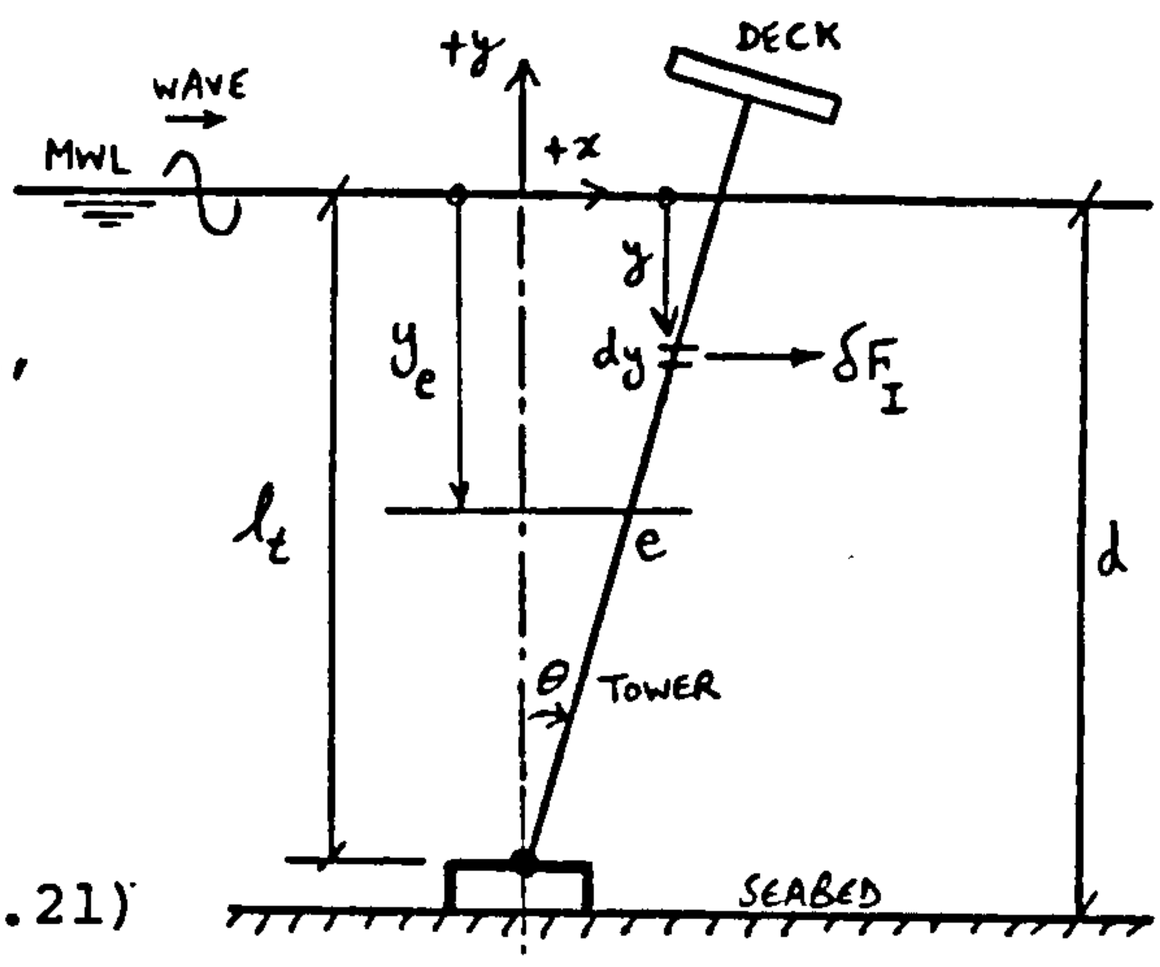

$$M_e^I = \int_{y_e}^{l} \delta F_I (y - y_e) \qquad (2.2.21)$$

Substituting for $\dot{u}$ from (2.2.16) into (2.2.13) and for δF_I into (2.2.21) we have

$$
M_e^I = C_m \rho \frac{\pi D^2}{4} B_u \sum_{n=1}^{N} \left\{ P_n \int_{y_e}^{l} \left[\cosh\left[\frac{nk}{a}(d+y) \right] \cdot \sin[n(kx - \omega t)] \cdot (y - y_e) \cdot dy \right] \right\} \qquad (2.2.22)
$$

Equation (2.2.22) can be evaluated at the instantaneous tower position by letting

$$x = (l_t + y)\theta$$

Substituting for x into (2.2.22) and letting

$$Z_n = \int_{y_e}^{l} \cosh\left[\frac{nk}{a}(d+y)\right] \cdot \sin n\left[k(l_t+y)\theta - \omega t\right] \cdot (y-y_e)\,dy \qquad (2.2.23)$$

$$; n = 1, 2, \ldots, N$$

Equation (2.2.22) can then be written

$$M_e^I = C_m \rho \frac{\pi D^2}{4} B_u \sum_{n=1}^{N} P_n \cdot Z_n \qquad (2.2.24)$$

Integrating (2.2.23) triply by parts gives

$$Z_n = Z_n^{(1)} - \frac{a}{nk} Z_n^{(2)} - a\theta Z_n^{(3)} \qquad (2.2.25)$$

where

$$Z_n^{(1)} = \frac{a(\eta - y_e)}{nk} \sinh(\alpha_n) \cdot \sin(\gamma_n) \qquad (2.2.26)$$

$$\alpha_n = \frac{nk}{a}(d+\eta) \qquad (2.2.27)$$

$$\gamma_n = n\left[k(l_t+\eta)\theta - \omega t\right] \qquad (2.2.28)$$

$$Z_n^{(2)} = Z_n^{(4)} - a\theta Z_n^{(5)} \qquad (2.2.29)$$

$$Z_n^{(4)} = \frac{a}{nk}\left\{\cosh(\alpha_n) \cdot \sin(\gamma_n) - \cosh(\varepsilon_n) \cdot \sin(\mu_n)\right\} \qquad (2.2.30)$$

$$\varepsilon_n = \frac{nk}{a}(d + y_e) \tag{2.2.31}$$

$$\mu_n = n\left[k(l_t + y_e)\theta - \omega t\right] \tag{2.2.32}$$

$$Z_n^{(5)} = Z_n^{(6)} + a\theta Z_n^{(2)} \tag{2.2.33}$$

$$Z_n^{(6)} = \frac{a}{nk}\left\{\sinh(\alpha_n).\cos(\gamma_n) - \sinh(\varepsilon_n).\cos(\mu_n)\right\} \tag{2.2.34}$$

$$Z_n^{(3)} = Z_n^{(7)} + a\theta Z_n - \frac{a}{nk} Z_n^{(5)} \tag{2.2.35}$$

$$Z_n^{(7)} = \frac{a}{nk}(\eta - y_e)\cosh(\alpha_n)\cos(\gamma_n) \tag{2.2.36}$$

Substituting equations (2.2.26 - 2.2.36) into (2.2.25) and neglecting θ^2 terms for small angles we have

$$Z_n = Z_n^{(1)} - \frac{a}{nk} Z_n^{(4)} + a\theta\left\{\frac{2a}{nk} Z_n^{(6)} - Z_n^{(7)}\right\} \tag{2.2.37}$$

Note. In the above equations η is calculated at instantaneous position of tower hence $\eta = \eta(l_t\theta)$
Now total fluid induced moment at e can be written as

$$M_e = M_e^I + M_e^D \tag{2.2.38}$$

where

$$M_e^D = \int_{y_e}^{\ell} \delta F_D (y - y_e) \tag{2.2.39}$$

Similarly fluid induced shear force at e can be expressed as

$$F_e = F_e^I + F_e^D \qquad (2.2.40)$$

where from (2.2.16)

$$F_e^I = C_m \rho \frac{\pi D^2}{4} \left[B_u \sum_{n=1}^{N} P_n \int_{y_e}^{l} \cosh \frac{nk}{a}(d+y) \cdot \sin\left[n\{k(l_t+y)\theta - \omega t\}\right] dy \right. \qquad (2.2.41)$$

and

$$F_e^D = \int_{y_e}^{l} \delta F_D \qquad (2.2.42)$$

Integrating (2.2.41) by parts gives

$$F_e^I = C_m \rho \frac{\pi D^2}{4} B_u \sum_{n=1}^{N} P_n \cdot L_n \qquad (2.2.43)$$

where neglecting θ^2 terms we have

$$L_n = L_n^{(1)} - a\theta L_n^{(2)} \qquad (2.2.44)$$

$$L_n^{(1)} = \frac{a}{nk}\left\{\sinh(\alpha_n)\cdot\sin(\gamma_n) - \sinh(\varepsilon_n)\cdot\sin(\mu_n)\right\} \qquad (2.2.45)$$

$$L_n^{(2)} = \frac{a}{nk}\left\{\cosh(\alpha_n)\cdot\cos(\gamma_n) - \cosh(\varepsilon_n)\cdot\cos(\mu_n)\right\} \qquad (2.2.46)$$

Equations (2.2.24) and (2.2.43) give moments and forces at depth $y = y_e$ below MWL. To evaluate the moment about the

pivot, i.e. M_I and M_D in (2.2.7) we can write

$$M_I = M_e^I \Big|_{y_e = -l_t} \tag{2.2.47}$$

and

$$M_D = M_e^D \Big|_{y_e = -l_t} \tag{2.2.48}$$

Evaluating (2.2.47) we get

$$M_I = C_m \rho \frac{\pi D^2}{4} B_u \sum_{n=1}^{N} P_n \cdot F_n \tag{2.2.49}$$

where

$$F_n = F_n^{(1)} - \frac{a}{nk} F_n^{(2)} + a\theta \left\{ \frac{2a}{nk} F_n^{(3)} - F_n^{(4)} \right\} \tag{2.2.50}$$

$$F_n^{(1)} = \frac{a}{nk} (\eta + l_t) \cdot \sinh(\alpha_n) \cdot \sin(\gamma_n) \tag{2.2.51}$$

$$F_n^{(2)} = \frac{a}{nk} \left\{ \cosh(\alpha_n) \cdot \sin(\gamma_n) + \cosh(\xi_n) \cdot \sin(n\omega t) \right\} \tag{2.2.52}$$

$$\xi_n = \frac{nk}{a} (d - l_t) \tag{2.2.53}$$

$$F_n^{(3)} = \frac{a}{nk} \left\{ \sinh(\alpha_n) \cdot \cos(\gamma_n) - \sinh(\xi_n) \cdot \cos(n\omega t) \right\} \tag{2.2.54}$$

$$F_n^{(4)} = \frac{a}{nk} (\eta + l_t) \cdot \cosh(\alpha_n) \cdot \cos(\gamma_n) \tag{2.2.55}$$

2.2.3 Distribution of Shear Force and Bending Moment

The total forces on the structure are shown below. Neglecting potential damping total shear force at e is

$$\mathcal{T}_e = F_e - M_p \cdot l_p \cdot \ddot{\theta} - \int_{y_e}^{(l_p - l_t)} m_s (d+y) \ddot{\theta}\, dy - \int_{y_e}^{2} m_a (d+y) \ddot{\theta}\, dy -$$

$$\int_{y_e}^{(y_b - l_t)} m_b (d+y) \ddot{\theta}\, dy + \int_{y_e}^{(l_p - l_t)} m_s g \theta\, dy -$$

$$\int_{y_e}^{2} \delta F_B \theta\, dy + \int_{y_e}^{(y_b - l_t)} m_b g \theta\, dy +$$

$$M_p g \theta \qquad (2.2.56)$$

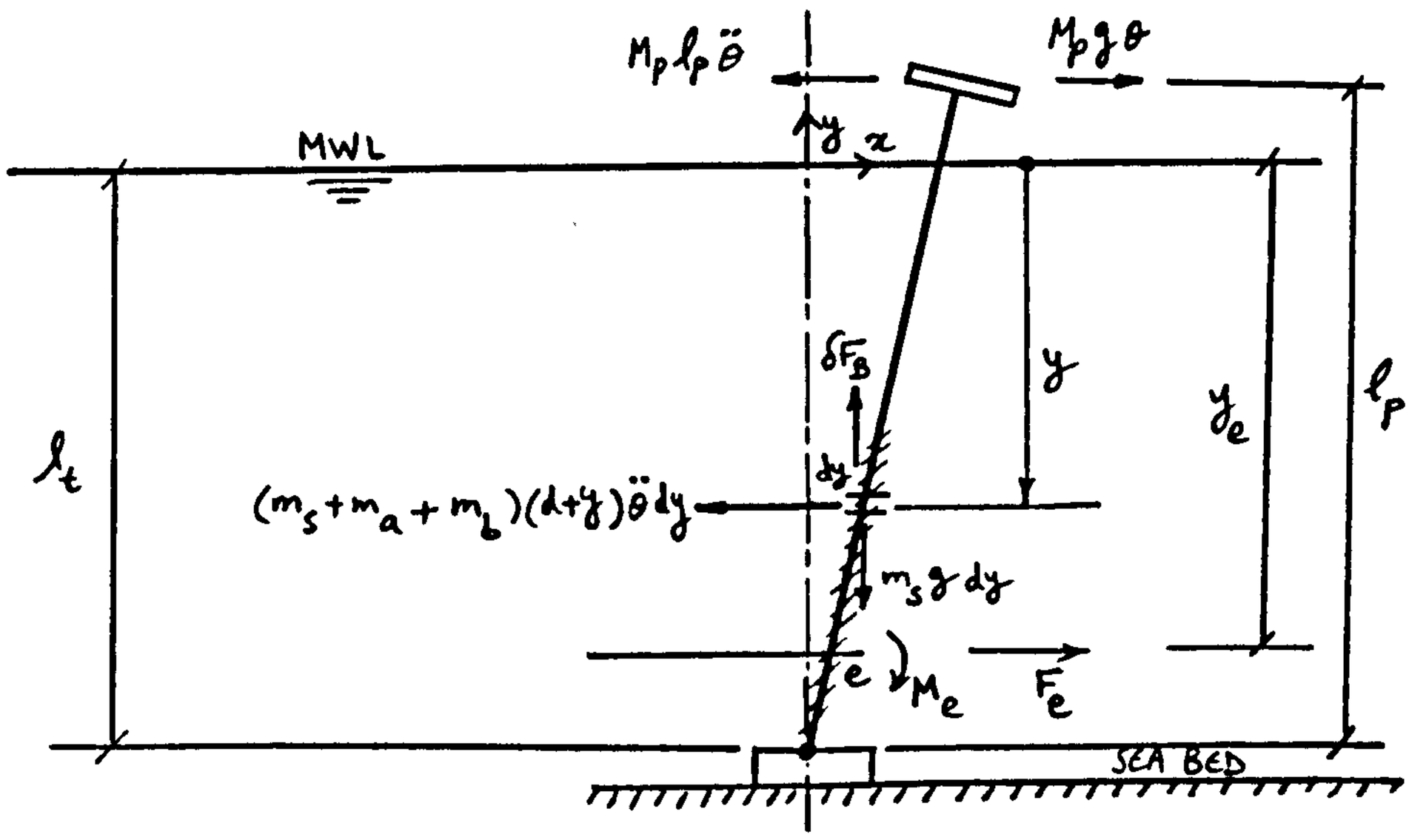

where δF_B = buoyancy force on element given by

$$\delta F_B = \rho \frac{\pi D^2}{4} g \, dy \qquad (2.2.57)$$

Substituting for δF_B in (2.2.56) and integrating we get

$$\begin{aligned} \mathcal{T}_e = F_e - \ddot{\theta} \Big\{ & M_p l_p + m_s \left[(l_p - l_t - y_e) l_t + \tfrac{1}{2}(l_p - l_t)^2 + \tfrac{1}{2} y_e^2 \right] + \\ & m_a \left[(\eta - y_e) l_t + \tfrac{1}{2}\eta^2 - \tfrac{1}{2} y_e^2 \right] + \\ & m_b \left[(y_b - l_t - y_e) l_t + \tfrac{1}{2}(y_b - l_t)^2 - \tfrac{1}{2} y_e^2 \right] \Big\} + \\ & g\theta \left\{ M_p + m_s (l_p - l_t - y_e) - \rho \frac{\pi D^2}{4} (\eta - y_e) + m_b (y_b - l_t - y_e) \right\} \end{aligned} \qquad (2.2.58)$$

Note

If $y_b - l_t \leq y_e$ then expressions involving m_b in (2.2.58) are set to zero, and if $\eta \leq y_e$ then expressions related to fluid loading are neglected. These also apply to expression for bending moment given by the following.

Total bending moment at e,

$$\begin{aligned} \sim_e = M_e - M_p l_p \ddot{\theta} (l_p - l_t - y_e) - & \int_{y_e}^{(l_p - l_t)} m_s (l_t + y) \ddot{\theta} (y - y_e) dy - \\ & \int_{y_e}^{\eta} m_a (l_t + y) \ddot{\theta} (y - y_e) dy - \int_{y_e}^{(y_b - l_t)} m_b (l_t + y) \ddot{\theta} (y - y_e) dy + \end{aligned}$$

$$\int_{y_e}^{(l_p-l_t)} m_s g\,\theta\,(y-y_e)\,dy \;-\; \int_{y_e}^{l} \delta F_B\,\theta\,(y-y_e)\,dy \;+$$

$$\int^{(y_b-l_t)} m_b g\,\theta\,(y-y_e)\,dy + M_p g\,\theta\,(l_p-l_t-y_e)$$

$$y_e$$

(2.2.59)

Integrating (2.2.59) we have

$$\alpha_e = M_e - \ddot{\theta}\Big\{ M_p l_p (l_p-l_t-y_e) + m_s\big[(l_p-l_t)^3/3 + y_e^3/6 + l_t(l_p-l_t-y_e)^2/2 - y_e(l_p-l_t)^2/2\big] + m_a\big[\eta^3/3 + y_e^3/6 + l_t(\eta-y_e)^2/2 - \eta^2 y_e/2\big] + m_b\big[(y_b-l_t)^3/3 + y_e^3/6 + l_t(y_b-l_t-y_e)^2/2 - y_e(y_b-l_t)^2/2\big]\Big\} +$$

$$g\theta\Big\{ m_s(l_p-l_t-y_e)^2/2 + m_b(y_b-l_t-y_e)^2/2 - \rho\frac{\pi D^2}{8}(\eta-y_e)^2 + M_p(l_p-l_t-y_e)\Big\}$$

(2.2.60)

2.2.4 Dynamic Stability

In this section we consider the possibility of Mathieu type instabilities of an articulated column under periodic wave forces. For large diameter columns which are inertia dominated equation (2.2.7) can be written as

$$I\ddot{\theta} + c\dot{\theta} + K_o\theta = M_I \qquad (2.2.61)$$

Neglecting surface elevation (2.2.8) gives

$$I = \frac{1}{3}\left[m_s \ell_p^3 + m_a \ell_t^3 + m_b y_b^3 + 3 M_p \ell_p^2 \right] \qquad (2.2.62)$$

and (2.2.9) becomes

$$K_o = -g\left[M_p \ell_p + m_b \frac{y_b^2}{2} + m_s \frac{\ell_p^2}{2} - \rho \frac{\pi D^2}{8} \ell_t^2 \right] \qquad (2.2.63)$$

M_I is calculated from (2.2.49) in which for Stokes Fifth Order or Stream Function wave theories equations (2.2.50 - 2.2.55) give

$$F_n = \frac{1}{nk}\left\{ \ell_t \sinh(nkd)\sin[n(k\ell_t\theta - \omega t)] - \right.$$
$$\frac{1}{nk}\left[\cosh(nkd)\sin[n(k\ell_t\theta-\omega t)] + \cosh[nk(d-\ell_t)]\sin(n\omega t)\right] +$$
$$\frac{2\theta}{nk}\left[\sinh(nkd)\cos[n(k\ell_t\theta-\omega t)] - \sinh[nk(d-\ell_t)]\cos(n\omega t)\right] -$$
$$\left.\theta\ell_t\cosh(nkd)\cos[n(k\ell_t\theta-\omega t)]\right\} \quad , \; n=1,2,\ldots,N \qquad (2.2.64)$$

For small angles

$$\sin[n(k\ell_t\theta - \omega t)] \simeq nk\ell_t\theta\cos(n\omega t) - \sin(n\omega t) \qquad (2.2.65)$$

$$\cos[n(k\ell_t\theta - \omega t)] \simeq \cos(n\omega t) + nk\ell_t\theta\sin(n\omega t) \qquad (2.2.66)$$

Thus equation (2.2.64) becomes

$$F_n = \cos(n\omega t)\left\{ l_t^2 \sinh(nkd) + \frac{2}{nk}\left[-l_t \cosh(nkd) + \frac{1}{nk}\sinh(nkd) - \frac{1}{nk}\sinh[nk(d-l_t)]\right]\right\}\theta +$$

$$\frac{1}{nk}\sin(n\omega t)\left\{-l_t \sinh(nkd) + \frac{1}{nk}\cosh(nkd) - \frac{1}{nk}\cosh[nk(d-l_t)]\right\}$$

(2.2.67)

Substituting (2.2.67) in (2.2.49) we have

$$M_I = \sum_{n=1}^{N} \left\{ f_n \sin(n\omega t) - k_n \cos(n\omega t)\cdot\theta \right\} \qquad (2.2.68)$$

which contains a time varying stiffness term which can give rise to Mathieu instabilities. In Stokes Fifth Order and Stream Function wave theories

$$f_n = C_m \rho \frac{\pi D^2}{4} \cdot \frac{Bu \cdot P_n}{(nk)^2}\left[-nk\, l_t \sinh(nkd) + \cosh(nkd) - \cosh[nk(d-l_t)]\right]$$

(2.2.69)

$$k_n = C_m \rho \frac{\pi D^2}{4} \cdot \frac{Bu \cdot P_n}{(nk)^2}\left[-(nk\, l_t)^2 \sinh(nkd) + 2nk\, l_t \cosh(nkd) - 2\sinh(nkd) + 2\sinh[nk(d-l_t)]\right]$$

(2.2.70)

Substituting (2.2.68) into (2.2.61) and rearranging we have a linear equation with the time varying stiffness

$$I\ddot{\theta} + c\dot{\theta} + \left[k_0 + \sum_{n=1}^{N} k_n \cos(n\omega t)\right]\theta = \sum_{n=1}^{N} f_n \sin(n\omega t) \quad (2.2.71)$$

Assuming that the solution to (2.2.71) consists of transient and steady state components we consider the stability of

$$I\ddot{\theta} + c\dot{\theta} + \left[k_0 + \sum_{n=1}^{N} k_n \cos(n\omega t)\right]\theta = 0 \quad (2.2.72)$$

A solution is then assumed to consist of product of a characteristic component and a periodic function (Floquet's theory, Ref.(5)). The periodic function is expanded into a Fourier series form and the solution is written as

$$\theta = e^{\lambda t}\left\{\frac{1}{2}\gamma_0 + \sum_{m=1}^{\infty}\left[\alpha_m \sin(m\omega t) + \gamma_m \cos(m\omega t)\right]\right\} \quad (2.2.73)$$

where λ , γ_0 , α_m and γ_m are constants.

Thus the stability of system depends upon the parameter λ which can be determined using a method given by Takahashi (80) in which an eigenvalue problem is formulated and use is made of Bolotin's harmonic balance method (5) in which coefficients of $\cos(m\omega t)$ and $\sin(m\omega t)$ are equated to form the equations in the unknowns α_m and γ_m . From (2.2.73) we get

$$\dot{\theta} = e^{\lambda t}\left\{\lambda\left[\frac{1}{2}\gamma_0 + \sum_{m=1}^{\infty}\alpha_m \sin(m\omega t) + \gamma_m \cos(m\omega t)\right] + \sum_{m=1}^{\infty} m\omega\left[\alpha_m \cos(m\omega t) - \gamma_m \sin(m\omega t)\right]\right\} \quad (2.2.74)$$

and

$$\ddot{\theta} = e^{\lambda t}\left\{ \lambda^2 \left[\tfrac{1}{2}\gamma_0 + \sum_{m=1}^{\infty} x_m \sin(m\omega t) + \gamma_m \cos(m\omega t)\right] + \right.$$

$$2\lambda\left[\sum_{m=1}^{\infty} m\omega \left(x_m \cos(m\omega t) - \gamma_m \sin(m\omega t)\right)\right] -$$

$$\left. \sum_{m=1}^{\infty} (m\omega)^2 \left(x_m \sin(m\omega t) + \gamma_m \cos(m\omega t)\right) \right\}$$

(2.2.75)

Substituting (2.2.73 - 2.2.75) into (2.2.72) and truncating the Fourier series to M terms, we have

$$I\left\{ \lambda^2 \left[\tfrac{1}{2}\gamma_0 + \sum_{m=1}^{M} x_m \sin(m\omega t) + \gamma_m \cos(m\omega t)\right] + 2\lambda\left[\sum_{m=1}^{M} m\omega \left(x_m \cos(m\omega t) - \gamma_m \sin(m\omega t)\right)\right] - \right.$$

$$\left. \sum_{m=1}^{M} (m\omega)^2 \left(x_m \sin(m\omega t) + \gamma_m \cos(m\omega t)\right)\right\} +$$

$$c\lambda\left\{ \tfrac{1}{2}\gamma_0 + \sum_{m=1}^{M} x_m \sin(m\omega t) + \gamma_m \cos(m\omega t)\right\} + c\left\{ \sum_{m=1}^{M} m\omega \left(x_m \cos(m\omega t) - \gamma_m \sin(m\omega t)\right)\right\} +$$

$$\tfrac{1}{2} K_0 \gamma_0 + K_0 \left\{ \sum_{m=1}^{M} x_m \sin(m\omega t) + \gamma_m \cos(m\omega t)\right\} + \tfrac{1}{2}\gamma_0 \sum_{n=1}^{N} K_n \cos(n\omega t) +$$

$$\tfrac{1}{2} \sum_{n=1}^{N} \sum_{m=1}^{M} K_n \left\{ x_m \left[\sin(m+n)\omega t + \sin(m-n)\omega t\right] + \right.$$

$$\left. \gamma_m \left[\cos(m+n)\omega t + \cos(m-n)\omega t\right]\right\} + \tfrac{1}{2} \sum_{n=1}^{N} K_n b_n = 0$$

(2.2.76)

In order to be able to use the harmonic balance method we write the double series

$$\sum_{n=1}^{N}\sum_{m=1}^{M} K_n \left\{ a_m \left[\sin(m+n)\omega t + \sin(m-n)\omega t \right] \right\} =$$

$$\sum_{m=1}^{M} \sin(m\omega t) \left\{ \sum_{\substack{n=1 \\ n\neq m}}^{N} \mathrm{sgn}(m-n)\, K_n\, x_{|m-n|} + \sum_{\substack{n=1 \\ n\neq M-m}}^{N} K_n\, x_{m+n} \right\}$$

, FOR $M \geq N$

(2.2.77)

where $\mathrm{Sgn}(m-n)$ is the sign of $(m-n)$

Also

$$\sum_{n=1}^{N}\sum_{m=1}^{M} K_n\, y_m \left[\cos(m+n)\omega t + \cos(m-n)\omega t \right] =$$

$$\sum_{m=1}^{M} \cos(m\omega t) \left\{ \sum_{\substack{n=1 \\ n\neq m}}^{N} K_n\, y_{|m-n|} + \sum_{\substack{n=1 \\ n\neq M-m}}^{N} K_n\, y_{m+n} \right\}$$

, FOR $M \geq N$

(2.2.78)

Note that it is assumed that the Fourier series consist of at least N frequency components, i.e. $M \geq N$

Now applying the harmonic balance method yields the following homogeneous equations:

Coefficients of constant term:

$$(I\lambda^2 + c\lambda + k_0)\, y_0 + \sum_{n=1}^{N} K_n\, y_n = 0 \qquad (2.2.79)$$

Coefficients of $\cos(m\omega t)$:

$$I\lambda^2 y_m + 2\lambda x_m m\omega - I y_m (m\omega)^2 + c\lambda y_m + c x_m m\omega +$$

$$K_0 y_m + \frac{1}{2} y_0 K_m + \frac{1}{2}\left\{ \sum_{\substack{n=1 \\ n\neq m}}^{N} K_n y_{|m-n|} + \sum_{\substack{n=1 \\ n\neq M-m}}^{N} K_n y_{m+n} \right\} = 0$$

$$; m = 1, 2, \ldots, M \qquad (2.2.80)$$

Coefficients of $\sin(m\omega t)$:

$$I\lambda^2 x_m - 2I\lambda y_m m\omega - I x_m (m\omega)^2 + c\lambda x_m - c y_m m\omega + K_0 x_m +$$

$$\frac{1}{2}\left\{ \sum_{\substack{n=1 \\ n\neq m}}^{N} \operatorname{sgn}(m-n) K_n x_{|m-n|} + \sum_{\substack{n=1 \\ n\neq M-m}}^{N} K_n x_{m+n} \right\} = 0$$

$$; m = 1, 2, \ldots, M \qquad (2.2.81)$$

Equations (2.2.79 - 2.2.81) form (2M+1) homogeneous equations which can be written in matrix form as

$$\left[\lambda^2 \cdot \left[I_2\right] + \lambda \cdot \left[I_1\right] + \left[I_0\right] \right] \left\{ z \right\} = \left\{ 0 \right\} \qquad (2.2.82)$$

where $\left[I_2\right]$ is a diagonal matrix of size (2M+1)x(2M+1) with diagonal elements equal to I.

and

$$\{Z\} = \begin{Bmatrix} y_0 \\ y_1 \\ y_2 \\ \vdots \\ y_M \\ x_1 \\ x_2 \\ \vdots \\ x_M \end{Bmatrix} \qquad (2.2.83)$$

and $\{0\}$ is a null vector.

Equation (2.2.82) can be written as

$$[I_0]\{Z\} = -\lambda^2 [I_2]\{Z\} - \lambda[I_1]\{Z\} \qquad (2.2.84)$$

Taking

$$\lambda\{Z\} = \{W\} \qquad (2.2.85)$$

and multiplying (2.2.84) by $[I_2]^{-1}$ we have

$$[I_2]^{-1}[I_0]\{Z\} = -\lambda\{W\} - [I_2]^{-1}[I_1]\{W\} \qquad (2.2.86)$$

Equation (2.2.86) can be written in the form

$$\begin{bmatrix} [0] & [I^*] \\ \hline -[\hat{I}_2]^{-1}[I_0] & -[\hat{I}_2]^{-1}[I_1] \end{bmatrix} \begin{Bmatrix} \{z\} \\ \hline \{w\} \end{Bmatrix} = \lambda \begin{Bmatrix} \{z\} \\ \hline \{w\} \end{Bmatrix} \qquad (2.2.87)$$

Note: $[\hat{I}_2]^{-1}$ is a diagonal matrix with elements $\frac{1}{I}$ and $[0]$ is a null matrix. $[I^*]$ is the unit matrix.

Equation (2.2.87) suggests that λ is the eigenvalue of the real and unsymmetric $2(2M+1)x2(2M+1)$ matrix on the left hand side and consists of pairs of complex numbers. If the real part of λ is positive then solution in (2.2.73) is unbounded as $t \to \infty$ and system is unstable. If real part of λ is negative or zero then solution is bounded and system is stable.

Using Stokes fifth order wave theory and truncating the Fourier series in (2.2.73) at the fifth component, i.e. M = N = 5, elements of the 22 x 22 matrix on left hand side of (2.2.87), matrix $[D]$, can be written as

$$D_{ij} = 1 \quad \text{FOR} \quad \begin{cases} i = 1, 2, \ldots, 11 \\ j = i+11 \end{cases}$$

$$D_{12\,j} = -(K_{j-1})/I \quad , j = 1, 2, \ldots, 6$$

$$D_{jj} = -C/I \quad , j = 12, 13, \ldots, 22$$

$$D_{13\,1} = D_{15\,5} = D_{16\,4} = D_{16\,6} = D_{17\,5} = D_{20\,10} = D_{21\,9} = D_{21\,11} = D_{22\,10} = -k_1/2I$$

$$D_{13\,2} = (\omega^2 - k_0/I - k_2/2I)$$

$$D_{13\,3} = D_{14\,2} = -(k_1 + k_3)/2I$$

$D_{13\ 4} = D_{15\ 2} = -(K_2 + K_4)/2I$

$D_{13\ 5} = D_{16\ 2} = -(K_3 + K_5)/2I$

$D_{13\ 6} = D_{16\ 1} = D_{17\ 2} = D_{18\ 11} = D_{22\ 7} = -K_4/2I$

$D_{13\ 7} = -C\omega/I$, $D_{13\ 8} = -2\omega$, $D_{14\ 1} = D_{14\ 5} = D_{15\ 6} = D_{16\ 3} = D_{17\ 4} = D_{19\ 10} = -K_2/2I$

$D_{20\ 11} = D_{21\ 8} = D_{22\ 9} = -K_2/2I$, $D_{14\ 3} = (4\omega^2 - K_0/I - K_4/2I)$

$D_{14\ 4} = D_{15\ 3} = -(K_1 + K_5)/2I$, $D_{14\ 6} = D_{15\ 1} = D_{17\ 3} = D_{19\ 11} = D_{22\ 8} = -K_3/2I$

$D_{14\ 8} = -2C\omega/I$, $D_{14\ 19} = -4\omega$, $D_{15\ 4} = (9\omega^2 - K_0/I)$, $D_{15\ 9} = -3C\omega/I$

$D_{15\ 20} = -6\omega$, $D_{16\ 5} = 16\omega^2 - K_0/I$, $D_{16\ 10} = -4C\omega/I$, $D_{16\ 21} = -8\omega$

$D_{17\ 1} = -K_5/2I$, $D_{17\ 6} = 25\omega^2 - K_0/I$, $D_{17\ 11} = -5C\omega/I$, $D_{17\ 22} = -10\omega$

$D_{18\ 2} = C\omega/I$, $D_{18\ 7} = (\omega^2 - K_0/I + K_2/2I)$, $D_{18\ 8} = D_{19\ 7} = (K_3 - K_1)/2I$

$D_{18\ 9} = D_{20\ 7} = (K_4 - K_2)/2I$, $D_{18\ 10} = D_{21\ 7} = (K_5 - K_3)/2I$, $D_{18\ 3} = 2\omega$

$D_{19\ 3} = 2C\omega/I$, $D_{19\ 8} = (4\omega^2 - K_0/I + K_4/2I)$, $D_{19\ 9} = D_{20\ 8} = (K_5 - K_1)/2I$

$D_{19\ 14} = 4\omega$, $D_{20\ 4} = 3C\omega/I$, $D_{20\ 9} = (9\omega^2 - K_0/I)$, $D_{20\ 15} = 6\omega$

$D_{21\ 5} = 4C\omega/I$, $D_{21\ 10} = 16\omega^2 - K_0/I$, $D_{21\ 16} = 8\omega$

$D_{22\ 6} = 5C\omega/I$

$D_{22\ 11} = (25\omega^2 - K_0/I)$

$D_{22\ 17} = 10\omega$

AND THE REST OF D_{ij} ARE EQUAL TO ZERO.

2.3 NUMERICAL DATA

The following wave data are used:

(1)

H = 25.2m, d = 100m, T = 11.3 sec

giving

(H/d) = 0.25, $(\omega^2 d/g)$ = 3.15

Stream Function coefficients (16) are

$X(1)/H.T.g = -0.931214 \times 10^{-2}$, $X(2)/H.T.g. = -0.168029 \times 10^{-4}$
$X(3)/H.T.g = -0.938674 \times 10^{-7}$, $X(4)/H.T.g. = -0.939917 \times 10^{-9}$
$X(5)/H.T.g = -0.900754 \times 10^{-11}$, $X(6)/H.T.g. = -0.823671 \times 10^{-13}$
$X(7)/H.T.g = -0.194169 \times 10^{-14}$

Phase Angle (deg)	0	10	20	30	50	75	100	130	180
(ℓ/H)	0.611	0.586	0.521	0.434	0.243	0.025	-0.15	-0.329	-0.38

(H/Breaking height) = H/H_B = 0.75

Wave length/$(\frac{gT^2}{2\pi})$ = $(\frac{L}{L_o})$ = 1.12519

Note that phase angle refers to $(kx-\omega t)$ term in Appendix A.

(2)

H = 22m, d = 70.5m, T = 15 sec.

(H/d) = 0.31, $(\omega^2 d/g)$ = 1.26

$X(1)/H.T.g = -0.374631 \times 10^{-1}$, $X(2)/H.T.g = -0.577025 \times 10^{-3}$
$X(3)/H.T.g = -0.126846 \times 10^{-5}$, $X(4)/H.T.g = -0.661278 \times 10^{-7}$
$X(5)/H.T.g = -0.290160 \times 10^{-8}$

Phase Angle (deg)	0	10	20	30	50	75	100	130	180
(η/H)	0.593	0.576	0.527	0.453	0.270	0.038	-0.152	-0.345	-0.407

$(H/H_B) = 0.5, \quad (L/L_o) = 0.931055$

(3)

H = 18.76m, d = 40m, T = 11.31 sec

$(H/d) = 0.47, (\omega^2 d/g) = 1.26$

$X(1)/H.T.g = -0.369772 \times 10^{-1}$, $X(2)/H.T.g = -0.111087 \times 10^{-2}$
$X(3)/H.T.g = -0.22037 \times 10^{-4}$, $X(4)/H.T.g = -0.59101 \times 10^{-6}$
$X(5)/H.T.g = -0.517059 \times 10^{-7}$, $X(6)/H.T.g = -0.357964 \times 10^{-8}$
$X(7)/H.T.g = -0.424772 \times 10^{-9}$

Phase Angle (deg)	0	10	20	30	50	75	100	130	180
(η/H)	0.653	0.616	0.528	0.420	0.207	-0.010	0.165	-0.305	-0.347

$(H/H_B) = 0.75, \quad (L/L_o) = 0.981055$

(4)

H = 12.8m, d = 100m, T = 8 sec

$(H/d) = 0.128, (\omega^2 d/g) = 6.28$

$X(1)/H.T.g = -0.596822 \times 10^{-3}$, $X(2)/H.T.g = -0.581606 \times 10^{-7}$
$X(3)/H.T.g = -0.289623 \times 10^{-10}$

Phase Angle (deg)	0	10	20	30	50	75	100	130	180
(η/H)	0.609	0.585	0.522	0.436	0.245	0.026	-0.149	-0.330	-0.391

$(H/H_B) = 0.75$, $(L/L_o) = 1.132813$

(5)

H = 21.3m, d = 250m, T = 12.65 sec

$(H/d) = 0.085$, $(\omega^2 d/g) = 6.29$

$X(1)/H.T.g = -0.433331 \times 10^{-3}$, $X(2)/H.T.g = -0.100012 \times 10^{-7}$

$X(3)/H.T.g = -0.160018 \times 10^{-11}$, $X(4)/H.T.g = -0.331298 \times 10^{-15}$

Phase Angle (deg)	0	10	20	30	50	75	100	130	180
(η/H)	0.569	0.554	0.513	0.450	0.286	0.062	-0.137	-0.356	-0.431

$(H/H_B) = 0.5$, $(L/L_o) = 1.065234$

Articulated Towers

Two cases are considered, particulars of which are given below.

H (m)	d (m)	T (s)	M_p (Kg)	m_s (Kg/m)	m_b (Kg/m)	m_a (Kg/m)	D (m)	l_p (m)	l_t (m)	y_b (m)	α_{11}	β_{11}
25.2	100	11.3	10^6	2.546×10^4	6.963×10^4	8.050×10^4	10	119	94	20	1.00	0.037
21.3	250	12.65	3.4×10^7	8×10^4	6.3×10^5	7.61×10^5	30	280	240	100	1.05	0.200

Drag and inertia coefficients are given in Section 2.4 with the results. Bending moments and shear forces are calculated at 35 stations along the tower as shown below. The current profile can be taken as

$$V_c(y) = V_t\,(1 + y/d)^{\frac{1}{7}} + V_w\,(1 + y/50)$$

where V_t = tidal contribution, V_w = wind induced (zero below 50m from MWL)

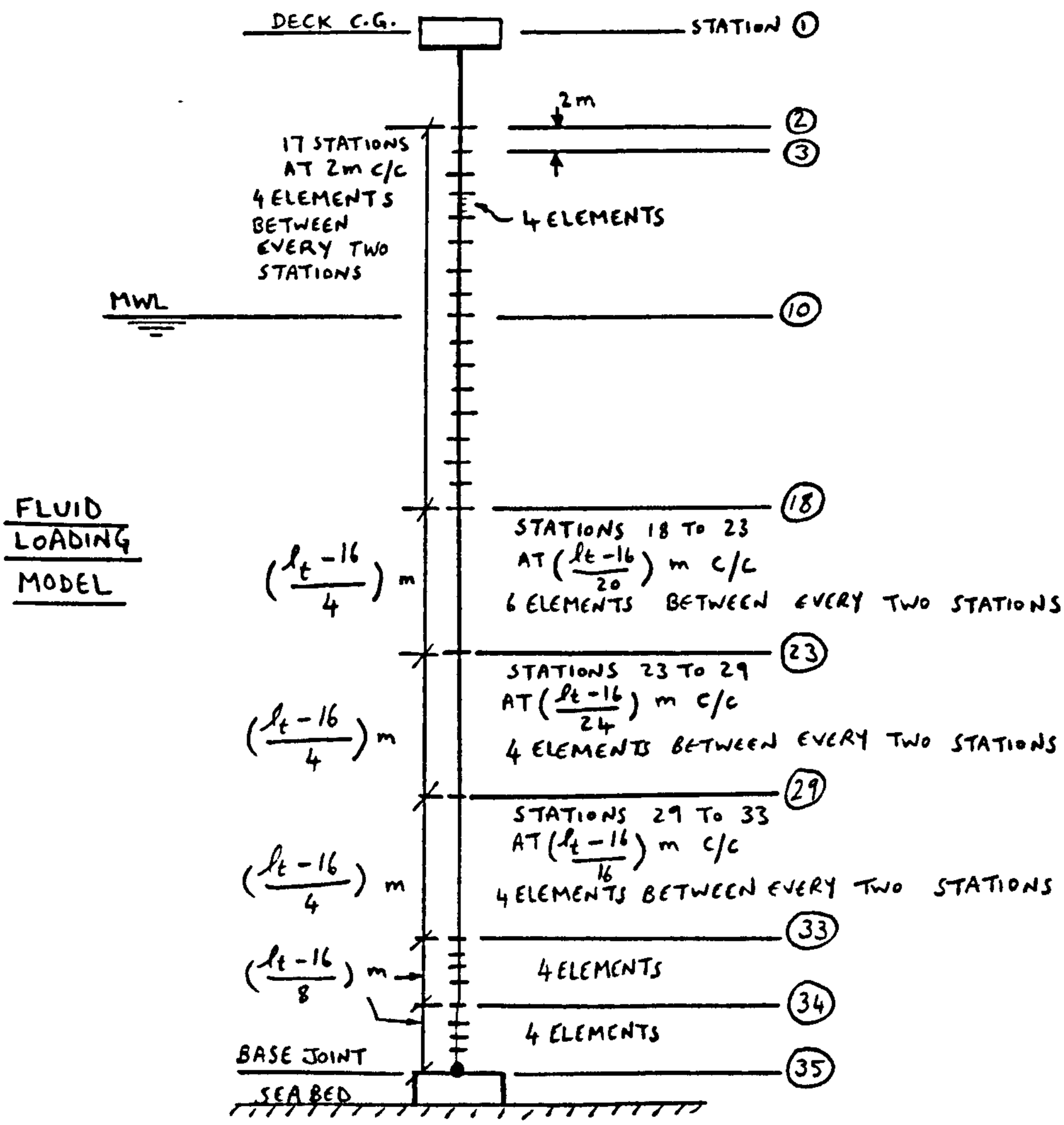

2.4 Results

STOKES FIFTH ORDER WAVE COEFFICIENTS

****

WAVE HEIGHT=18.76 (m)

WAVE PERIOD=11.31 (sec)

WATER DEPTH= 40.00 (m)

==========

a1=0.213249E+00 a2=0.583586E-01 a3=0.192941E-01 a4=0.512862E-02 a5=0.191983E-02
b1=0.128221E+00 b2=0.734259E-02 b3=0.119249E-03 b4=-.962612E-05 b5=0.157190E-06
d1=0.143837E+00 d2=0.164737E-01 d3=0.401319E-03 d4=-.387069E-04 d5=0.881676E-06

WAVE NUMBER=0.321725E-01

****

WAVE HEIGHT=22.00 (m)

WAVE PERIOD=15.00 (sec)

WATER DEPTH= 70.50 (m)

==========

a1=0.149767E+00 a2=0.269211E-01 a3=0.593265E-02 a4=0.124073E-02 a5=0.328990E-03
b1=0.885094E-01 b2=0.266529E-02 b3=0.263643E-05 b4=-.125201E-05 b5=0.270549E-07
d1=0.993889E-01 d2=0.598581E-02 d3=0.988151E-05 d4=-.562361E-05 d5=0.151902E-06

WAVE NUMBER=0.192017E-01

****

WAVE HEIGHT=12.80 (m)

WAVE PERIOD= 8.00 (sec)

WATER DEPTH= 100.00 (m)

==========

a1=0.602831E-01 a2=0.117418E-01 a3=0.346715E-02 a4=0.761366E-03 a5=0.249724E-03
b1=0.105832E-02 b2=0.166062E-06 b3=0.529823E-10 b4=0.386753E-16 b5=-.138938E-19
d1=0.265383E-02 d2=0.832830E-06 d3=0.398577E-09 d4=0.387926E-15 d5=-.174199E-18

WAVE NUMBER=0.557113E-01

STOKES FIFTH ORDER WAVE COEFFICIENTS
****

WAVE HEIGHT=25.20 (m)

WAVE PERIOD=11.30 (sec)

WATER DEPTH= 100.00 (m)
==========

a1=0.118493E+00	a2=0.235409E-01	a3=0.699460E-02	a4=0.154957E-02	a5=0.512183E-03
b1=0.233043E-01	b2=0.691883E-04	b3=0.233652E-06	b4=0.736229E-09	b5=-.327690E-11
d1=0.413716E-01	c2=0.245657E-03	d3=0.124439E-05	d4=0.522805E-08	d5=-.290870E-10

WAVE NUMBER=0.281177E-01

STOKES FIFTH ORDER WAVE COEFFICIENTS
****

WAVE HEIGHT=21.30 (m)

WAVE PERIOD=12.65 (sec)

WATER DEPTH= 250.00 (m)
==========

a1=0.414424E-01	a2=0.550322E-02	a3=0.110920E-02	a4=0.202651E-03	a5=0.484455E-04
b1=0.542772E-03	b2=0.225947E-07	b3=0.375468E-11	b4=0.137471E-17	b5=-.257434E-21
c1=0.130095E-02	c2=0.113283E-06	d3=0.282435E-10	d4=0.137878E-16	d5=-.322746E-20

WAVE NUMBER=0.230269E-01

5th ORDER CNOIDAL WAVE COEFFICIENTS

WAVE HEIGHT= 18.76 (m)
WAVE PERIOD= 11.31 (sec)
WATER DEPTH= 40.00 (m)

m= 0.601748
h= 33.394238(m)
Epsilon/m= 0.933420
Alpha= 0.702394
K(m)= 1.951461(rad)
K"(m)= 1.770309(rad)
WAVE CELERITY= 15.916565(m/s)
WAVE LENGTH/WATER DEPTH Ratio= 4.50

WAVE HEIGHT= 22.00 (m)
WAVE PERIOD= 15.00 (sec)
WATER DEPTH= 70.50 (m)

m= 0.451656
h= 61.542272(m)
Epsilon/m= 0.791483
Alpha= 0.693896
K(m)= 1.815150(rad)
K"(m)= 1.697354(rad)
WAVE CELERITY= 20.648907(m/s)
WAVE LENGTH/WATER DEPTH Ratio= 4.39

Yc (m)	Reynolds No.				Keulegan-Carpenter No.			
	A	S5	SF	CN	A	S5	SF	CN
-15.0	.24E+07	.24E+07	.25E+07	.23E+07	66.8	68.0	68.2	63.9
-30.0	.19E+07	.19E+07	.20E+07	.19E+07	53.4	54.0	54.2	51.5

A=Airy wave theory
S5=Stokes 5th Order
SF=Stream Function
CN=5th Order Cnoidal

TABLE 2.1 Re AND Kc VALUES FOR A HORIZONTAL CYLINDER
(H= 22.00 m,T= 15.00 sec,d= 70.5 m,D= 0.9 m)

Yc (m)	Reynolds No.				Keulegan-Carpenter No.			
	A	S5	SF	CN	A	S5	SF	CN
-10.0	.26E+07	.26E+07	.26E+07	.23E+07	54.7	54.6	53.6	48.4
-20.0	.20E+07	.20E+07	.20E+07	.19E+07	42.6	42.4	41.4	40.3

A=Airy wave theory
S5=Stokes 5th Order
SF=Stream Function
CN=5th Order Cnoidal

TABLE 2.2 Re AND Kc VALUES FOR A HORIZONTAL CYLINDER
(H= 18.76 m,T= 11.31 sec,d= 40.0 m,D= 0.9 m)

Yc (m)	Reynolds No.				Keulegan-Carpenter No.			
	A	S5	SF	CN	A	S5	SF	CN
-10.0	.16E+07	.15E+07	.15E+07		23.8	22.7	22.6	
-20.0	.30E+06	.87E+06	.86E+06		12.7	12.9	12.8	

A=Airy wave theory
S5=Stokes 5th Order
SF=Stream Function
CN=5th Order Cnoidal

TABLE 2.3 Re AND Kc VALUES FOR A HORIZONTAL CYLINDER
(H= 12.80 m,T= 8.00 sec,d= 100.0 m,D= 0.9 m)

Yc (m)	Reynolds No.				Keulegan-Carpenter No.			
	A	S5	SF	CN	A	S5	SF	CN
-15.0	.26E+07	.25E+07	.25E+07		55.1	52.1	52.0	
-20.0	.23E+07	.22E+07	.22E+07		47.1	45.2	45.1	

A=Airy wave theory
S5=Stokes 5th Order
SF=Stream Function
CN=5th Order Cnoidal

TABLE 2.4 Re AND Kc VALUES FOR A HORIZONTAL CYLINDER
(H= 25.20 m, T= 11.30 sec, d= 100.0 m, D= 0.9 m)

Yc (m)	Reynolds No.				Keulegan-Carpenter No.			
	A	S5	SF	CN	A	S5	SF	CN
0.0	.10E+08	.11E+08	.11E+08	.11E+08	25.9	26.7	26.8	26.7
-5.0	.95E+07	.97E+07	.98E+07	.95E+07	23.7	24.3	24.4	23.8
-10.0	.87E+07	.89E+07	.89E+07	.85E+07	21.8	22.2	22.3	21.3
-15.0	.80E+07	.82E+07	.82E+07	.77E+07	20.0	20.4	20.5	19.2
-20.0	.74E+07	.75E+07	.75E+07	.70E+07	18.5	18.8	18.9	17.5
-30.0	.64E+07	.65E+07	.65E+07	.62E+07	16.0	16.2	16.3	15.5
-50.0	.52E+07	.52E+07	.52E+07	.55E+07	12.9	13.0	13.0	14.6
-70.0	.47E+07	.48E+07	.48E+07	.60E+07	11.9	12.0	12.0	14.9

A=Airy wave theory
S5=Stokes 5th Order
SF=Stream Function
CN=5th Order Cnoidal

TABLE 2.5 Re AND Kc VALUES FOR A VERTICAL CYLINDER
(H= 22.00 m, T= 15.00 sec, d= 70.5 m, D= 3.0 m)

Yc (m)	Reynolds No.				Keulegan-Carpenter No.			
	A	S5	SF	CN	A	S5	SF	CN
0.0	.12E+08	.12E+08	.12E+08	.16E+08	22.1	22.4	22.2	30.4
-5.0	.10E+08	.10E+08	.99E+07	.10E+08	19.0	19.1	18.8	19.2
-10.0	.87E+07	.87E+07	.85E+07	.82E+07	16.4	16.4	16.1	11.7
-15.0	.76E+07	.76E+07	.74E+07	.53E+07	14.4	14.3	14.0	10.0
-20.0	.68E+07	.67E+07	.66E+07	.56E+07	12.8	12.7	12.4	10.6
-30.0	.57E+07	.57E+07	.56E+07	.65E+07	10.8	10.8	10.5	12.3

A=Airy wave theory
S5=Stokes 5th Order
SF=Stream Function
CN=5th Order Cnoidal

TABLE 2.6 Re AND Kc VALUES FOR A VERTICAL CYLINDER
(H= 18.76 m, T= 11.31 sec, d= 40.0 m, D= 3.0 m)

Yc (m)	Reynolds No.				Keulegan-Carpenter No.			
	A	S5	SF	CN	A	S5	SF	CN
0.0	.10E+08	.91E+07	.91E+07		13.4	12.1	12.1	
-5.0	.73E+07	.68E+07	.68E+07		9.8	9.1	9.0	
-10.0	.54E+07	.51E+07	.51E+07		7.1	6.8	6.8	
-15.0	.39E+07	.38E+07	.38E+07		5.2	5.1	5.1	
-20.0	.29E+07	.29E+07	.29E+07		3.8	3.9	3.8	
-30.0	.15E+07	.17E+07	.16E+07		2.0	2.2	2.2	
-50.0	.43E+06	.54E+06	.54E+06		0.6	0.7	0.7	
-70.0	.13E+06	.18E+06	.18E+06		0.2	0.2	0.2	
-100.0	.37E+05	.66E+05	.67E+05		0.0	0.1	0.1	

A=Airy wave theory
S5=Stokes 5th Order
SF=Stream Function
CN=5th Order Cnoidal

TABLE 2.7 Re AND Kc VALUES FOR A VERTICAL CYLINDER
(H= 12.80 m, T= 8.00 sec, d= 100.0 m, D= 3.0 m)

Yc (m)	Reynolds No.				Keulegan-Carpenter No.			
	A	S5	SF	CN	A	S5	SF	CN
0.0	.14E+08	.13E+08	.13E+08		26.5	24.2	24.2	
-5.0	.12E+08	.11E+08	.11E+08		22.6	20.9	20.9	
-10.0	.10E+08	.96E+07	.96E+07		19.3	18.0	18.0	
-15.0	.88E+07	.83E+07	.83E+07		16.5	15.6	15.6	
-20.0	.75E+07	.72E+07	.72E+07		14.1	13.6	13.5	
-30.0	.55E+07	.54E+07	.54E+07		10.4	10.2	10.2	
-50.0	.30E+07	.32E+07	.32E+07		5.7	6.0	6.0	
-70.0	.18E+07	.20E+07	.20E+07		3.3	3.8	3.8	
-100.0	.12E+07	.15E+07	.15E+07		2.2	2.8	2.8	

A=Airy wave theory
S5=Stokes 5th Order
SF=Stream Function
CN=5th Order Cnoidal

TABLE 2.8 Re AND Kc VALUES FOR A VERTICAL CYLINDER
(H= 25.20 m,T= 11.30 sec,d= 100.0 m,D= 3.0 m)

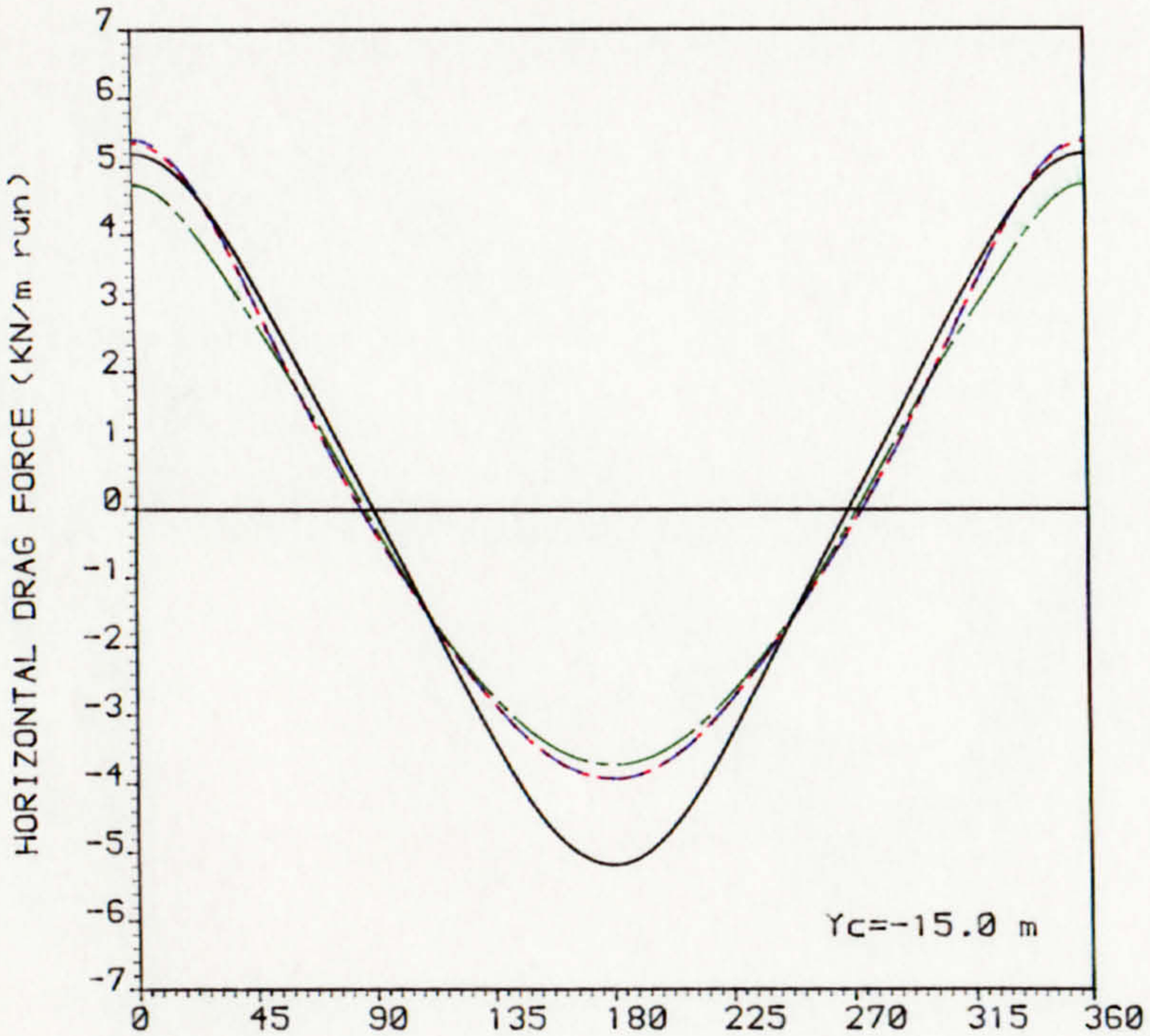

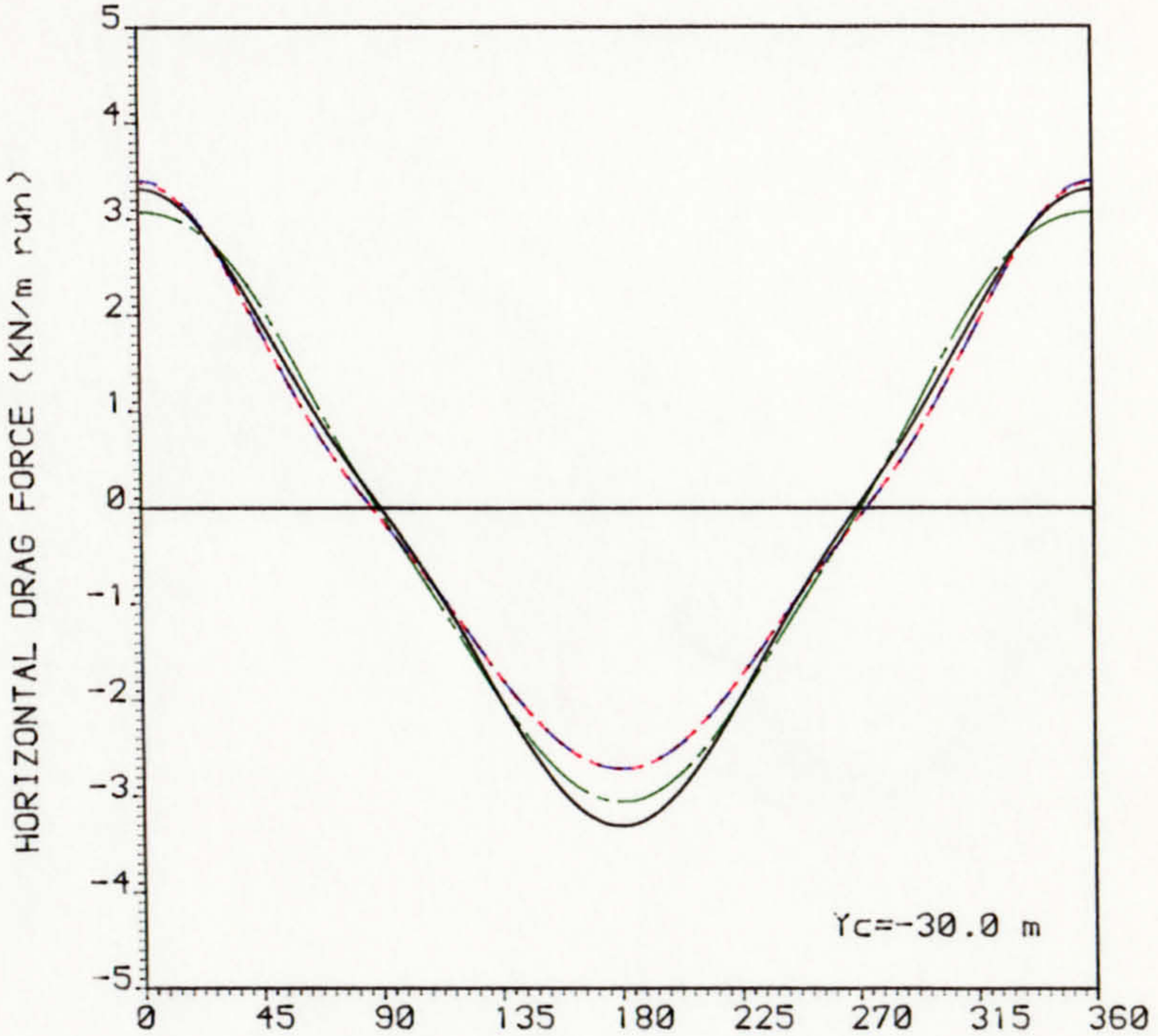

_____ AIRY	H= 22.00 (m)	Cd= .70	H/d= .31
..... 5th Order STOKES	T= 15.00 (sec)	Cm= 2.00	$w^2 d/g$= 1.26
_ __ . 5th Order STREAM FUNCTION	d= 70.50 (m)		
__ _ __ 5th Order CNOIDAL	Cylinder Dia.= .90 (m)		

FIG 2.3 HYDRODYNAMIC LOADING ON A HORIZONTAL CYLINDER

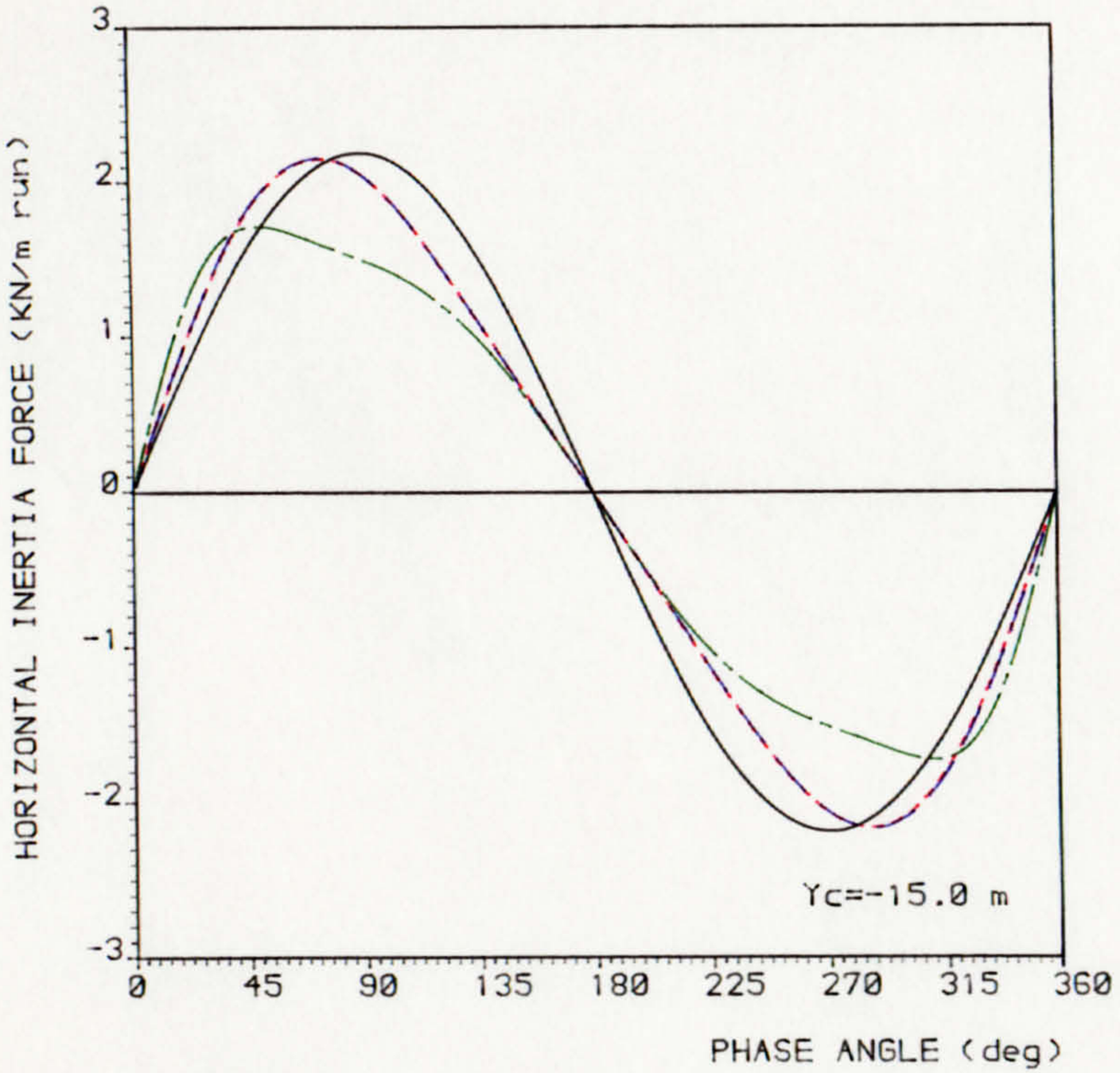

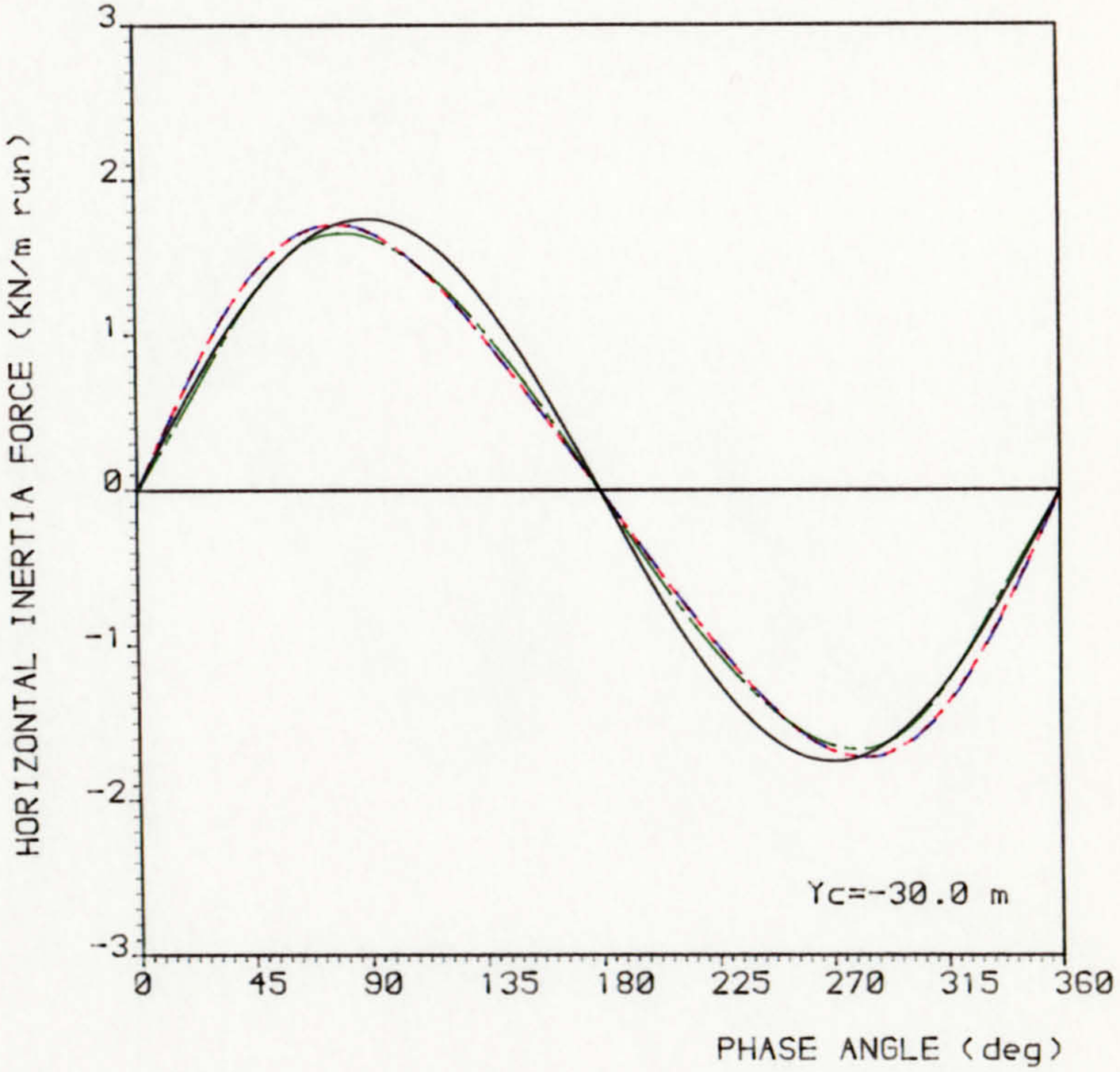

——— AIRY	H= 22.00 (m)	Cd= .70	H/d= .31
..... 5th Order STOKES	T= 15.00 (sec)	Cm= 2.00	$w^2 d/g$= 1.26
_ _ _ 5th Order STREAM FUNCTION	d= 70.50 (m)		
___ 5th Order CNOIDAL	Cylinder Dia.= .90 (m)		

FIG 2.4 HYDRODYNAMIC LOADING ON A HORIZONTAL CYLINDER

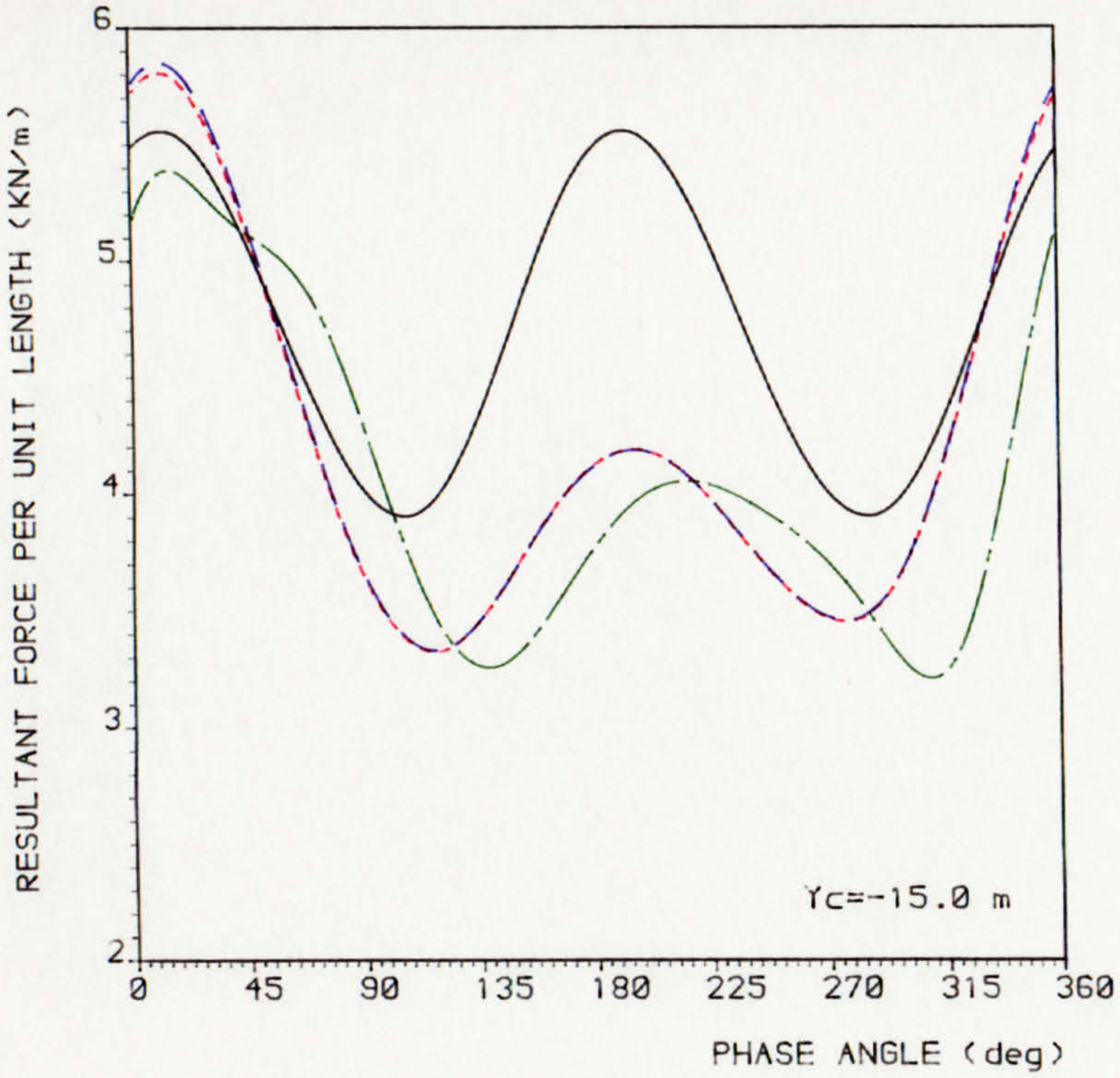

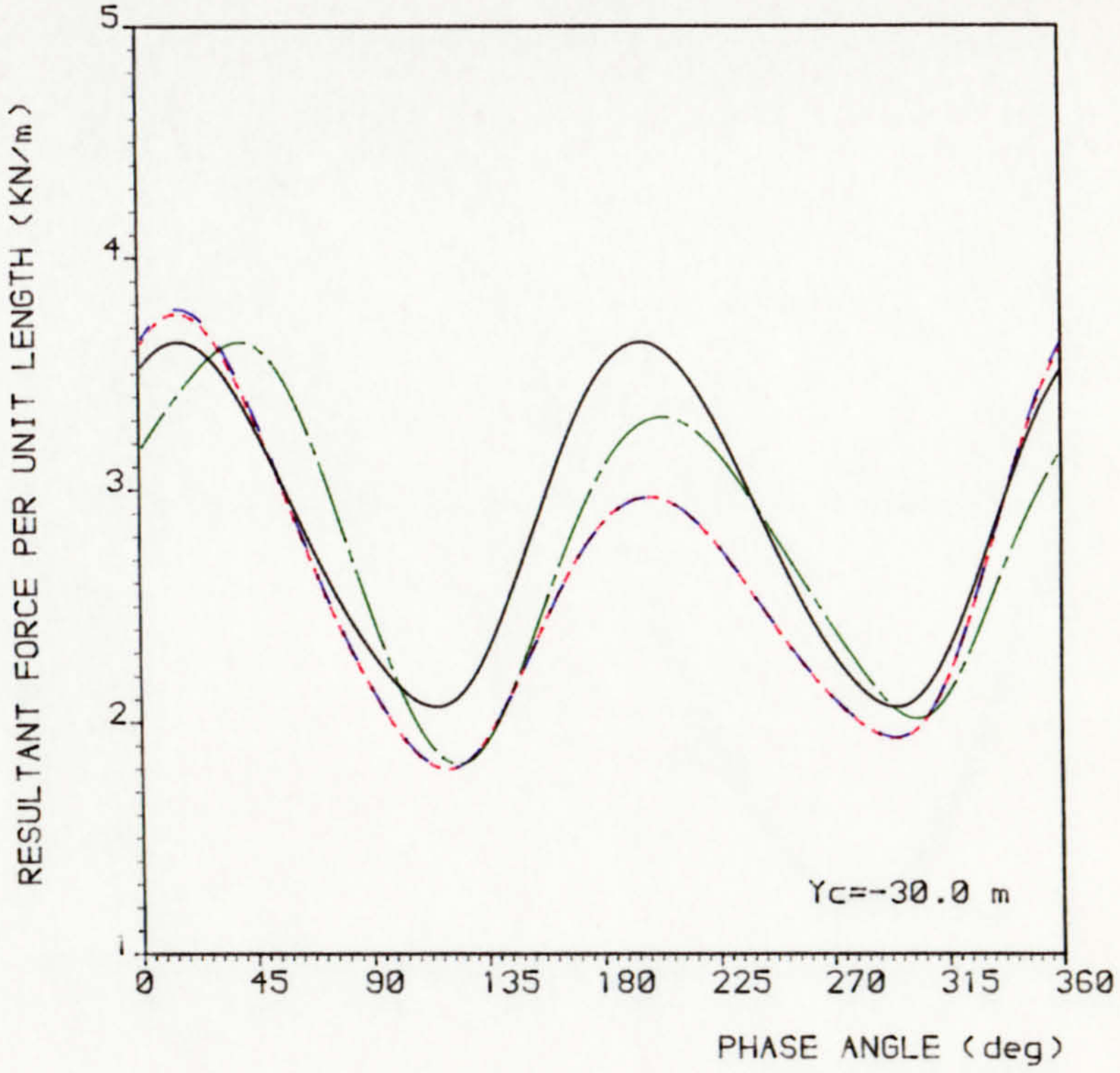

——— AIRY	H= 22.00 (m)	Cd= .70	H/d= .31
- - - - - 5th Order STOKES	T= 15.00 (sec)	Cm= 2.00	$w^2 d/g$= 1.26
— — — 5th Order STREAM FUNCTION	d= 70.50 (m)		
— — — 5th Order CNOIDAL	Cylinder Dia.= .90(m)		

FIG 2.5 HYDRODYNAMIC LOADING ON A HORIZONTAL CYLINDER

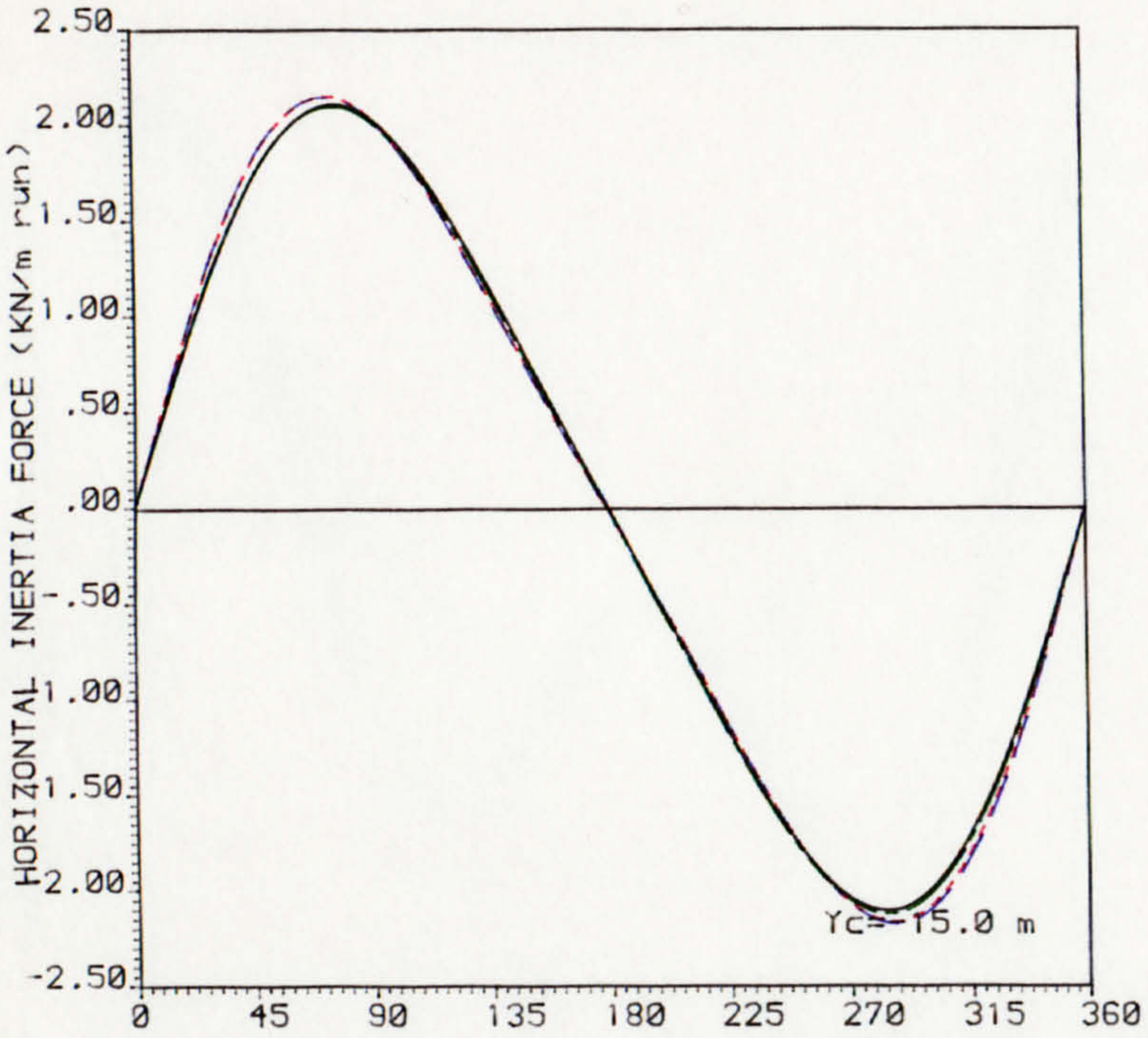

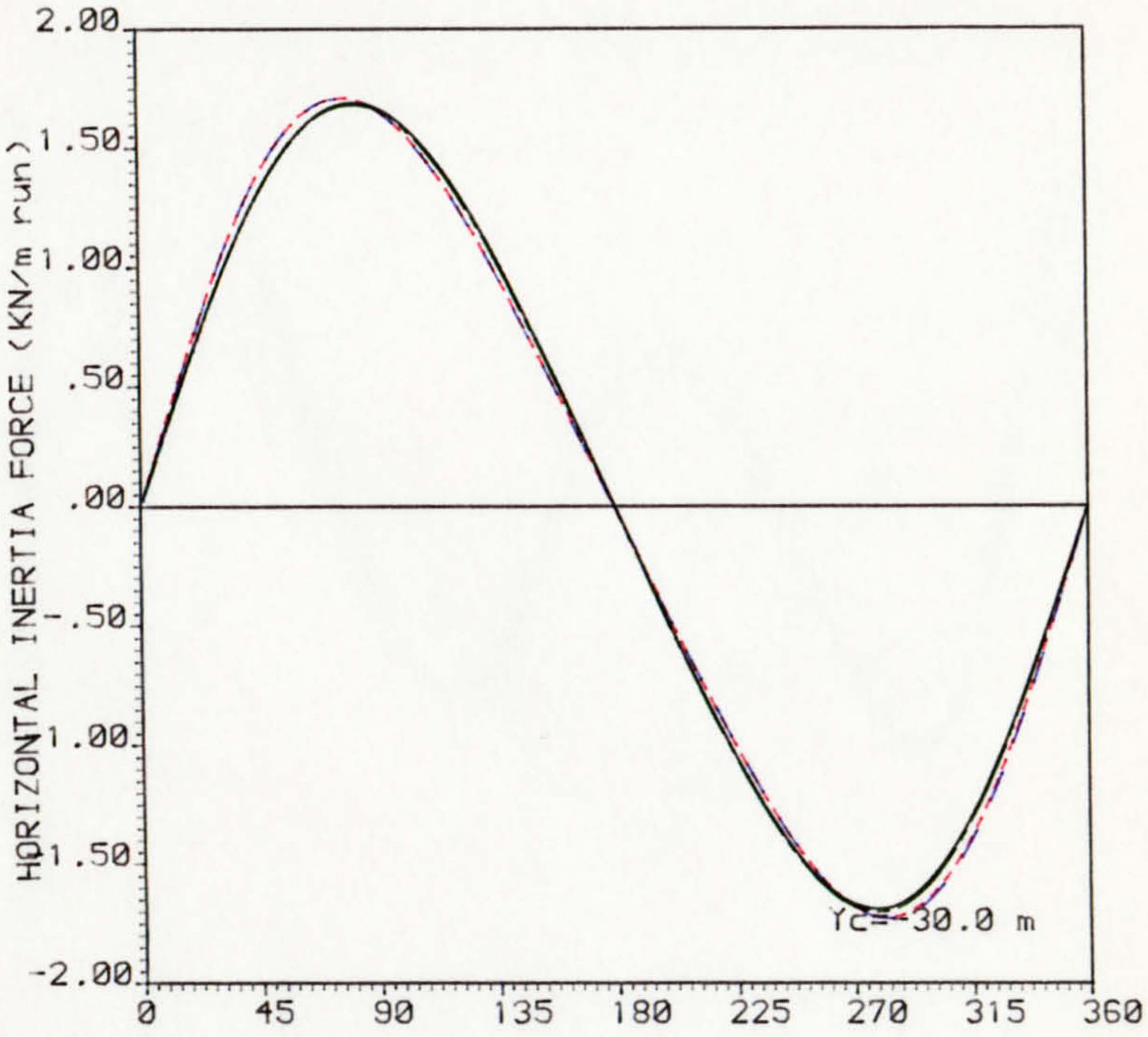

_____ 5th Order STOKES++	H= 22.00 (m)	Cd= .70	H/d= .31
..... 5th Order STOKES	T= 15.00 (sec)	Cm= 2.00	$w^2 d/g$= 1.26
_ _ _ 5th Order STREAM FUNCTION	d= 70.50 (m)		
_ _ _ 5th Order STREAM FUNCTION++	Cylinder Dia.= .90 (m)	++ CONVECTIVE ACCELERATION terms included	

FIG 2.6 HYDRODYNAMIC LOADING ON A HORIZONTAL CYLINDER

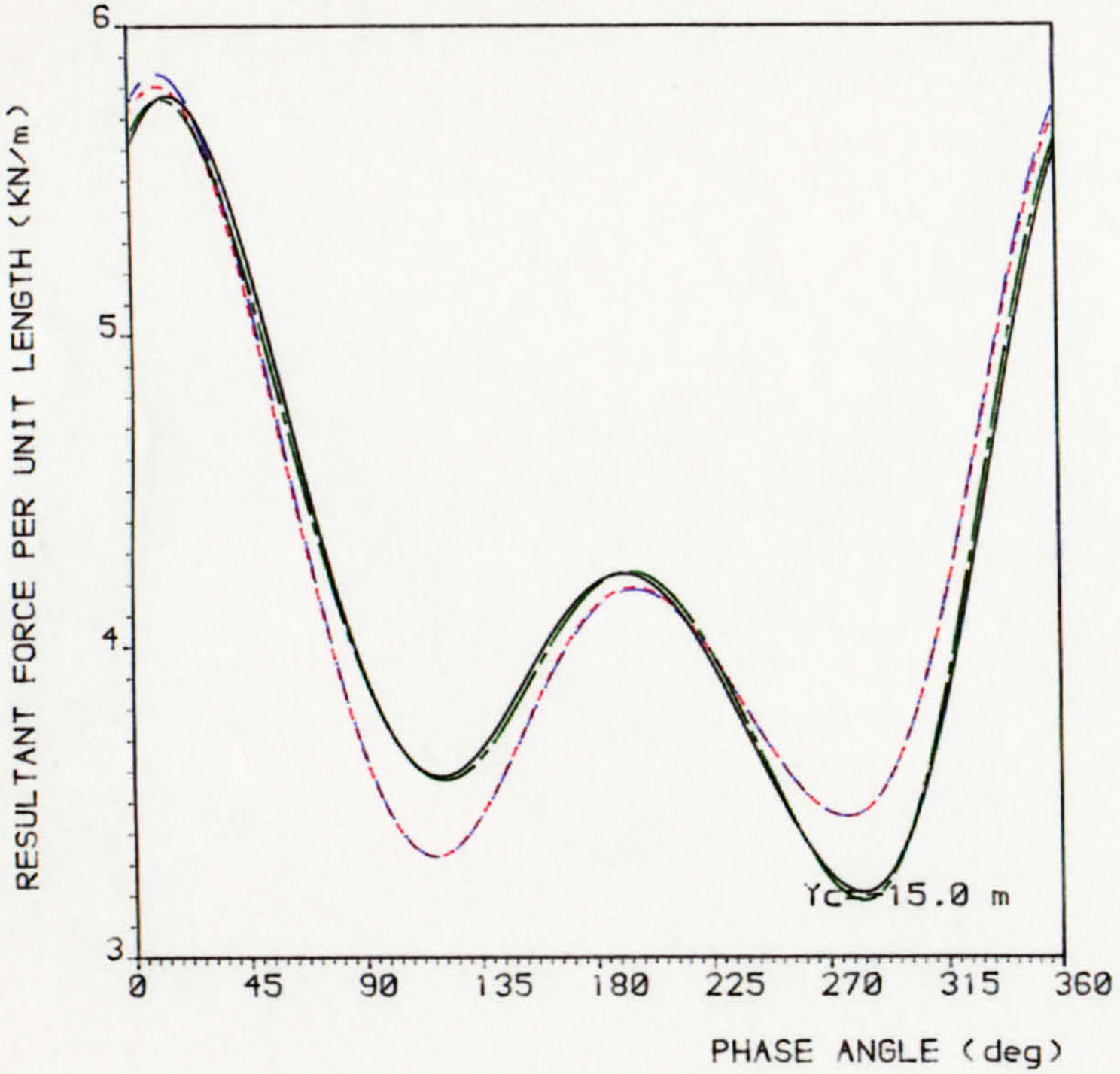

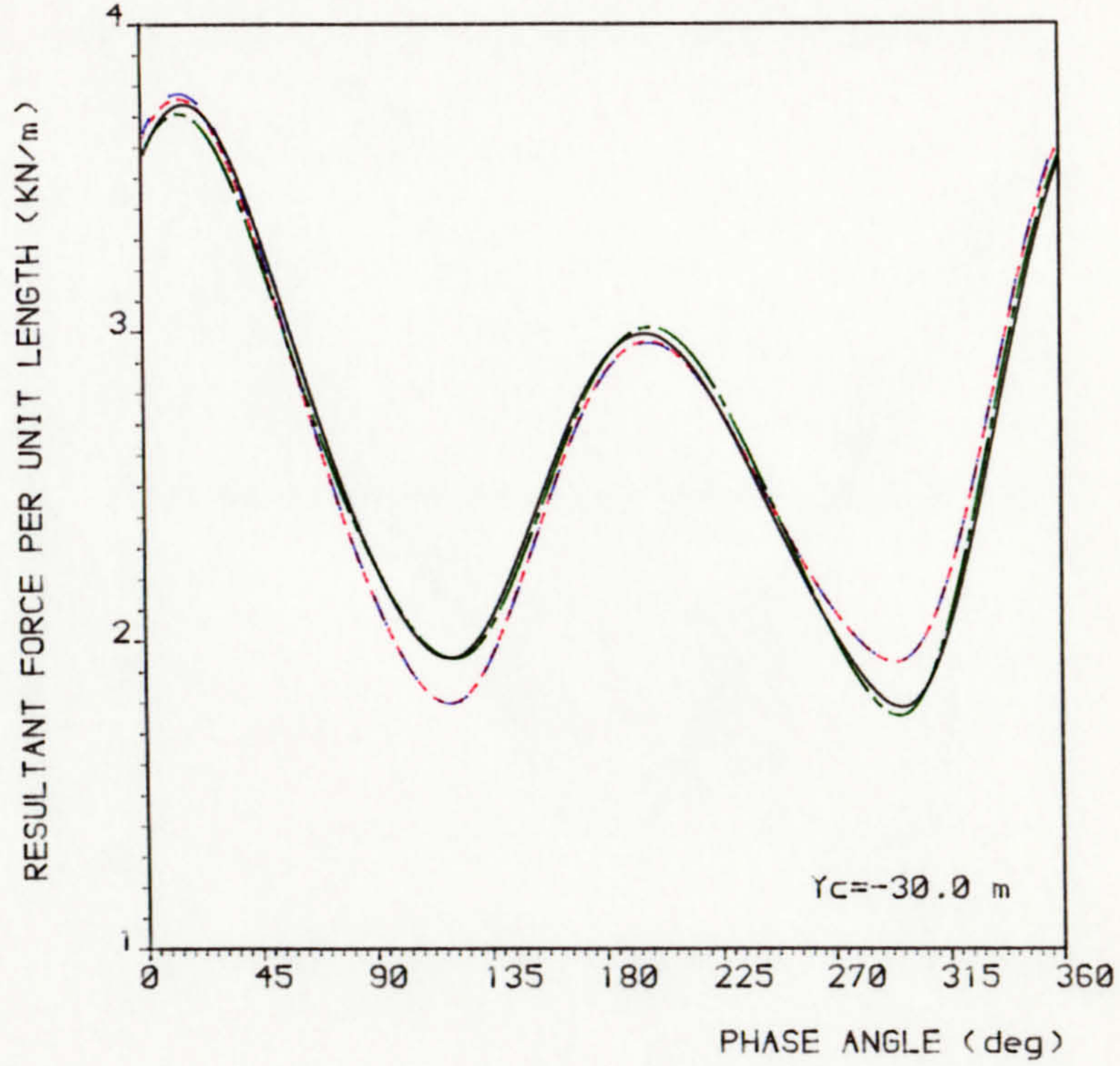

_____ 5th Order STOKES++	H= 22.00 (m)	Cd= .70	H/d= .31
- - - - - 5th Order STOKES	T= 15.00 (sec)	Cm= 2.00	$w^2 d/g$= 1.26
_ _ _ _ 5th Order STREAM FUNCTION	d= 70.50 (m)		
_ _ _ _ 5th Order STREAM FUNCTION++	Cylinder Dia.= .90 (m)	++ CONVECTIVE ACCELERATION terms included	

FIG 2.7 HYDRODYNAMIC LOADING ON A HORIZONTAL CYLINDER

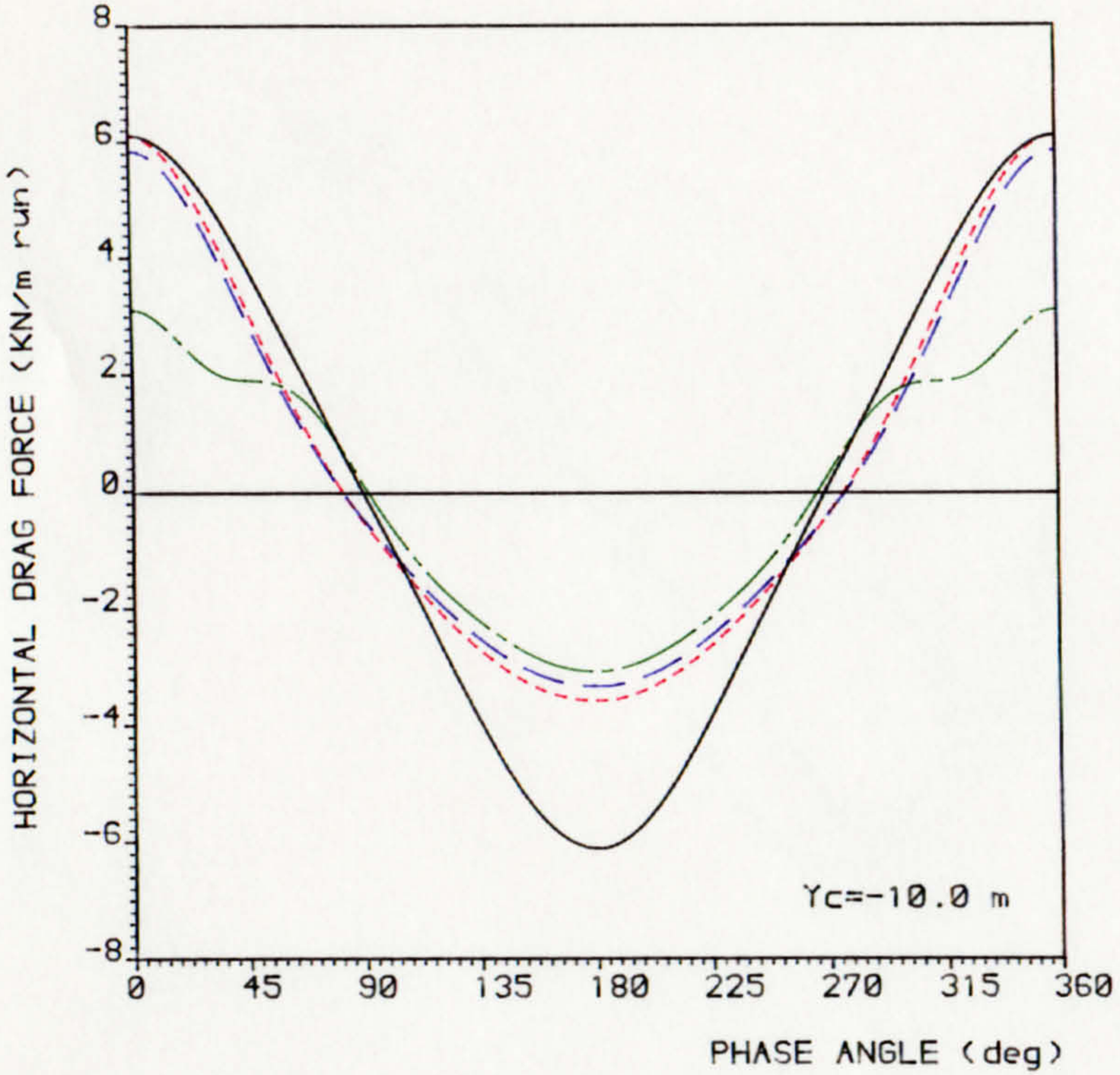

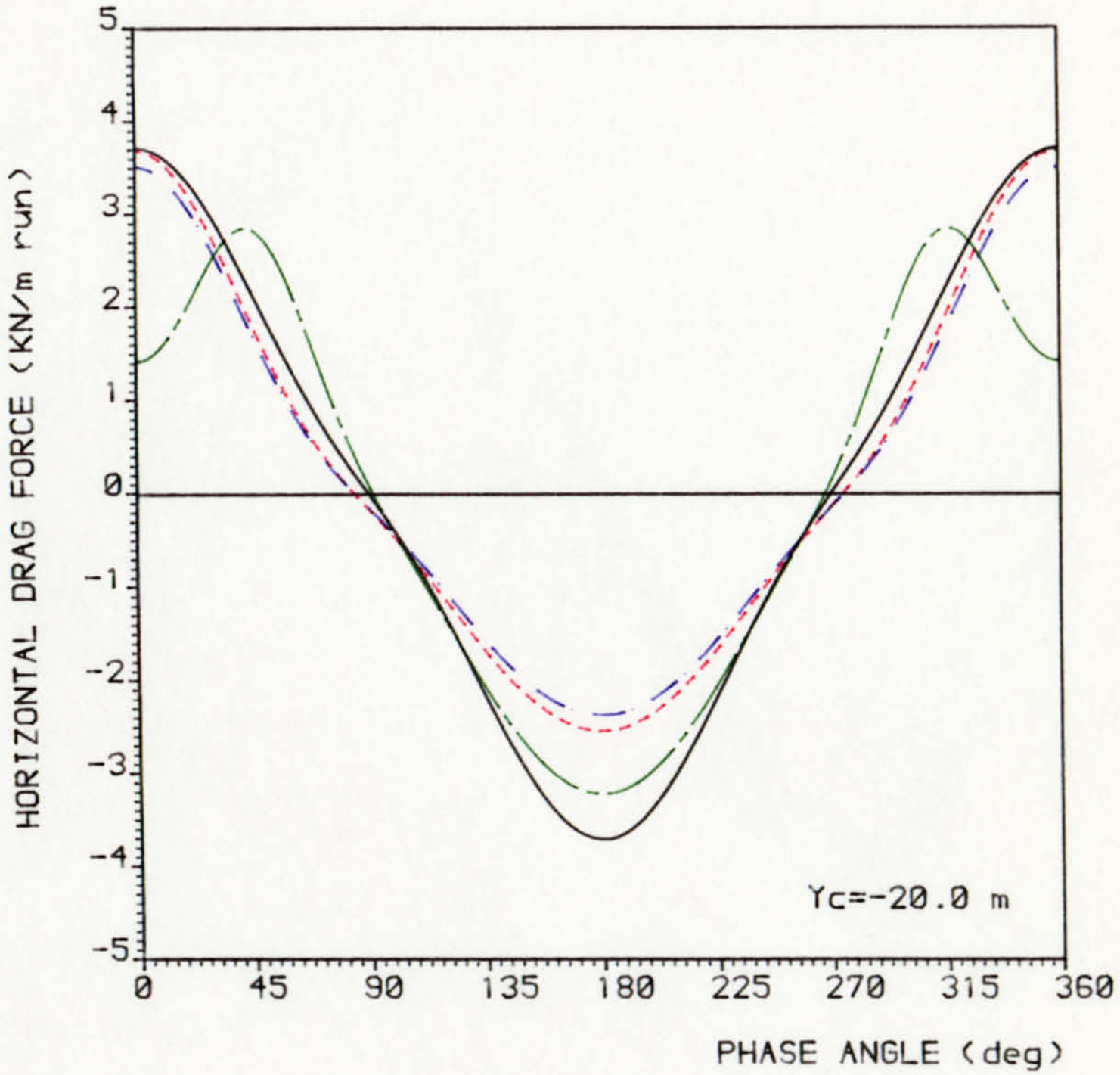

——— AIRY	H= 18.76 (m)	Cd= .70	H/d= .47
- - - - - 5th Order STOKES	T= 11.32 (sec)	Cm= 2.00	$w^2 d/g$= 1.26
— — — . 7th Order STREAM FUNCTION	d= 40.00 (m)		
——— 5th Order CNOIDAL	Cylinder Dia.= .90 (m)		

FIG 2.8 HYDRODYNAMIC LOADING ON A HORIZONTAL CYLINDER

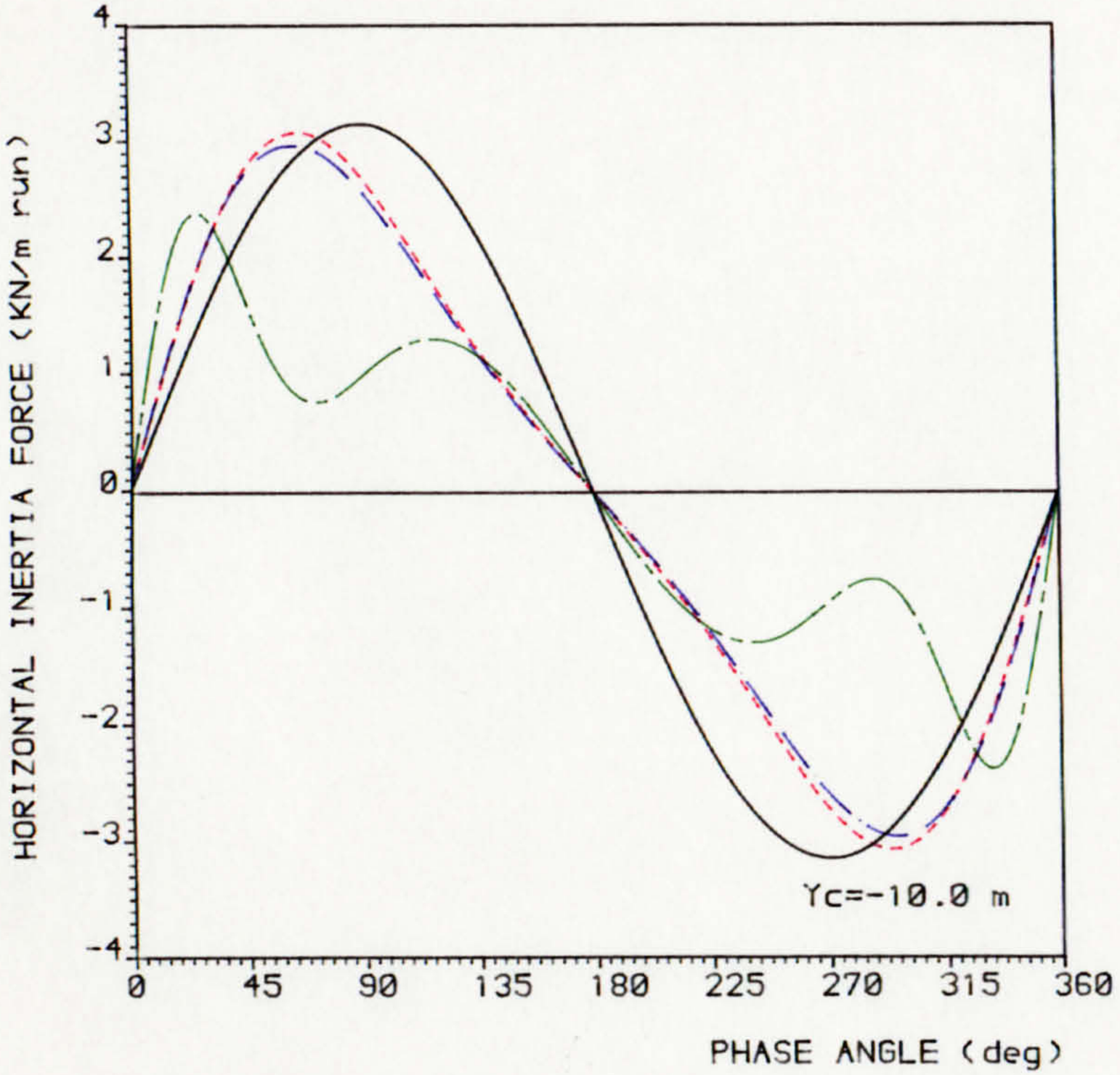

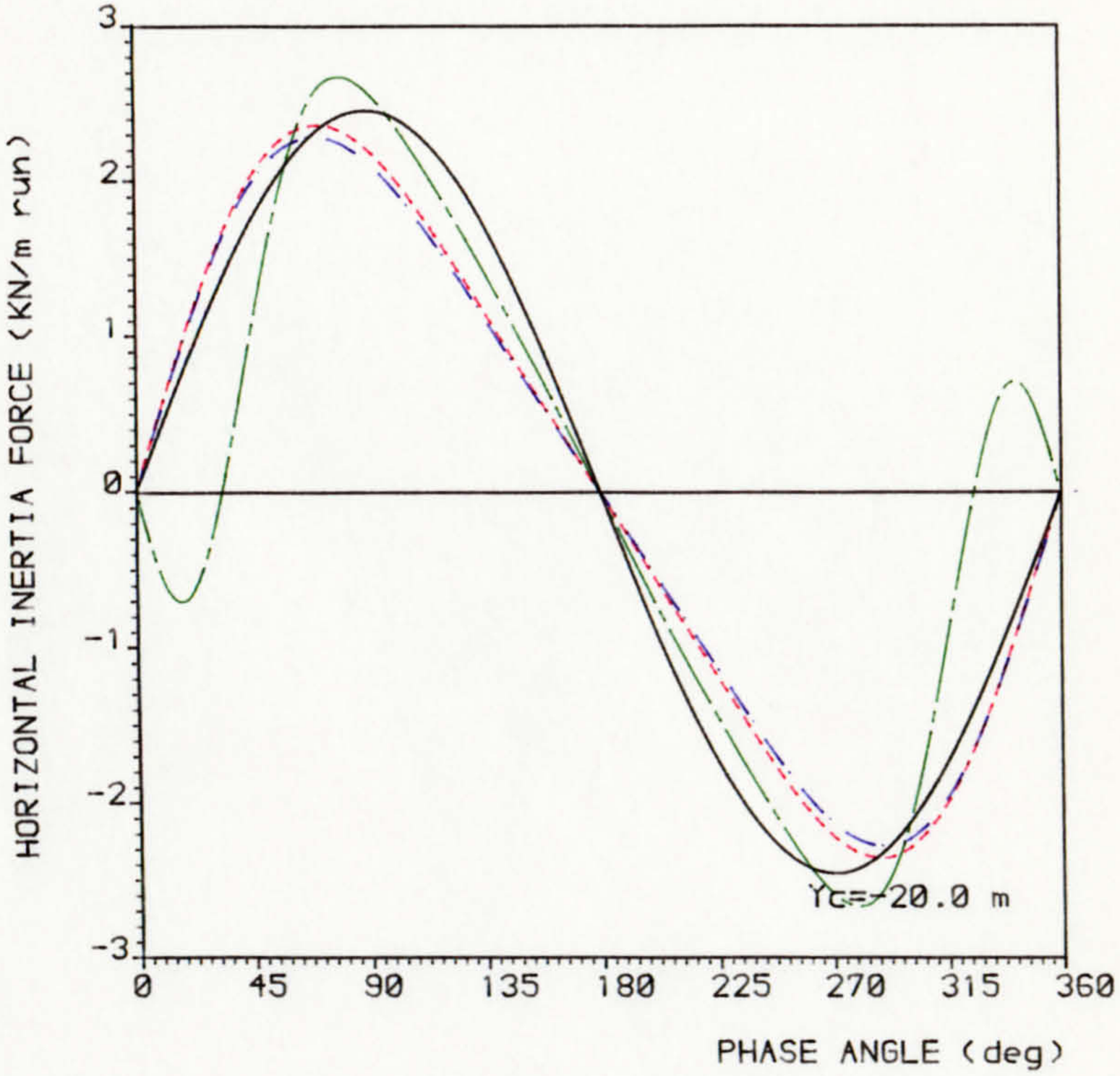

——— AIRY	H= 18.76 (m)	Cd= .70	H/d= .47
- - - - - 5th Order STOKES	T= 11.32 (sec)	Cm= 2.00	$W^2 d/g$= 1.26
— — 7th Order STREAM FUNCTION	d= 40.00 (m)		
— — — 5th Order CNOIDAL	Cylinder Dia.= .90 (m)		

FIG 2.9 HYDRODYNAMIC LOADING ON A HORIZONTAL CYLINDER

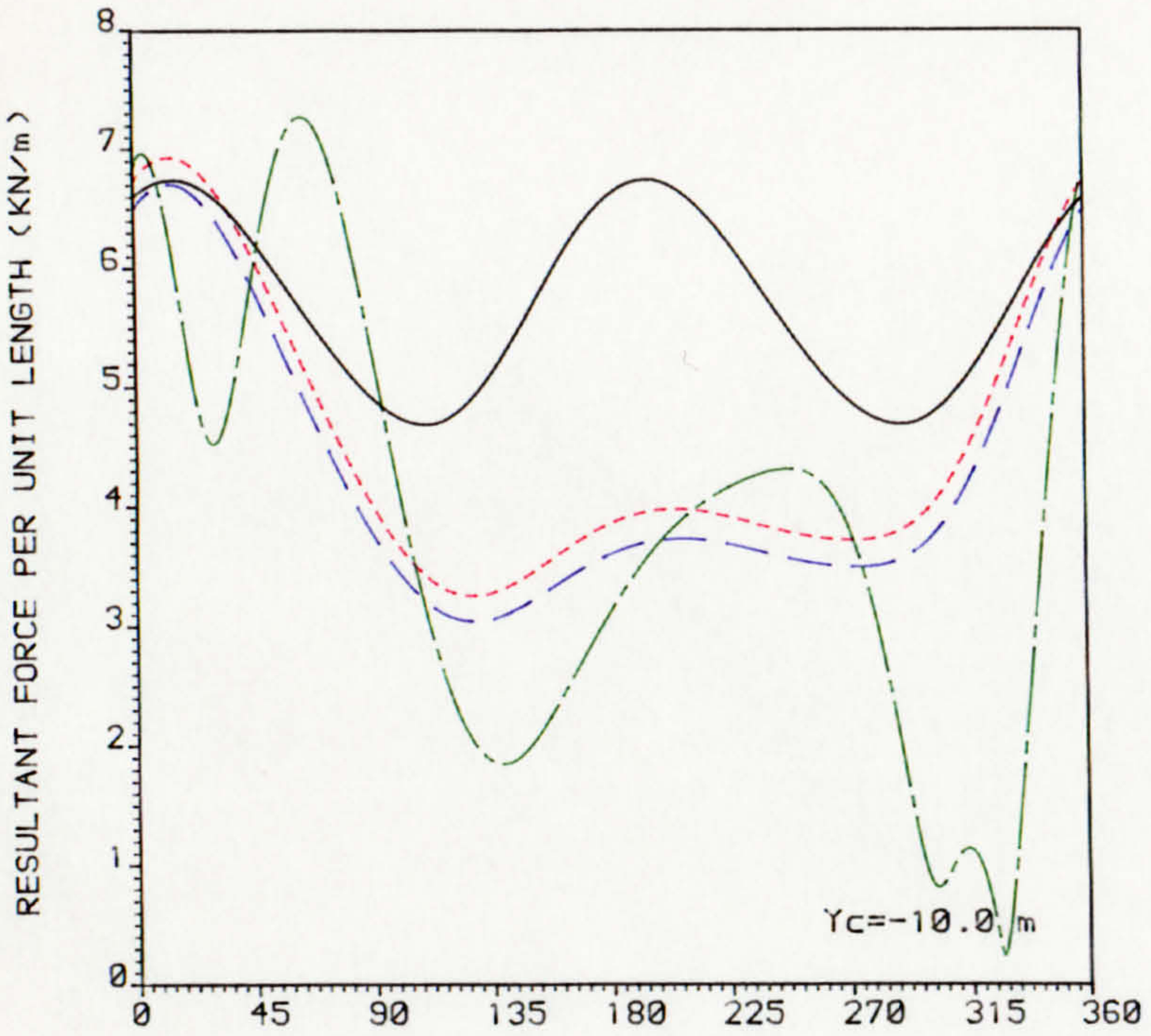

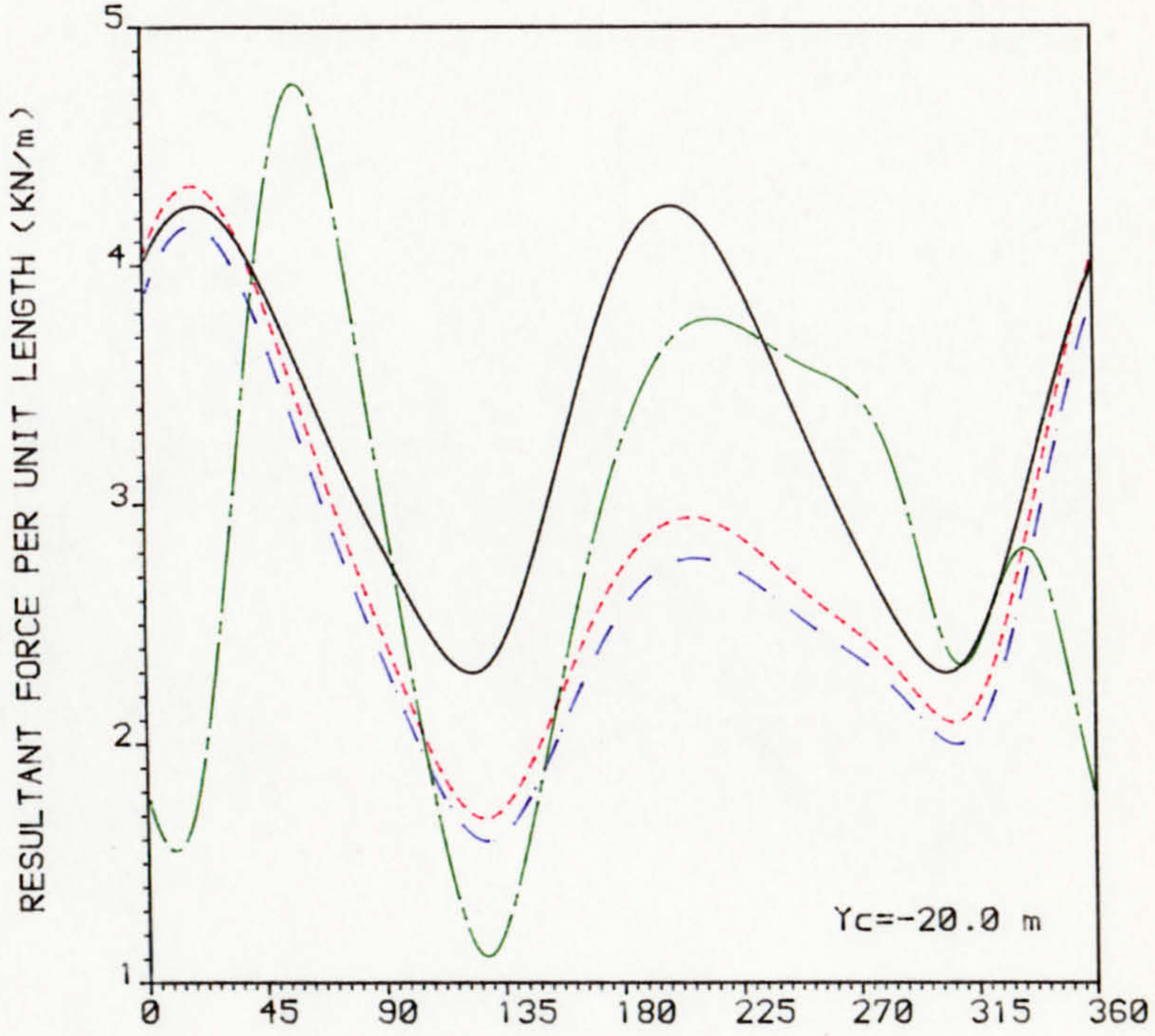

——— AIRY	H= 18.76 (m)	Cd= .70	H/d= .47
- - - - - 5th Order STOKES	T= 11.32 (sec)	Cm= 2.00	$w^2 d/g$= 1.26
— — . 7th Order STREAM FUNCTION	d= 40.00 (m)		
— — — 5th Order CNOIDAL	Cylinder Dia.= .90(m)		

FIG 2.10 HYDRODYNAMIC LOADING ON A HORIZONTAL CYLINDER

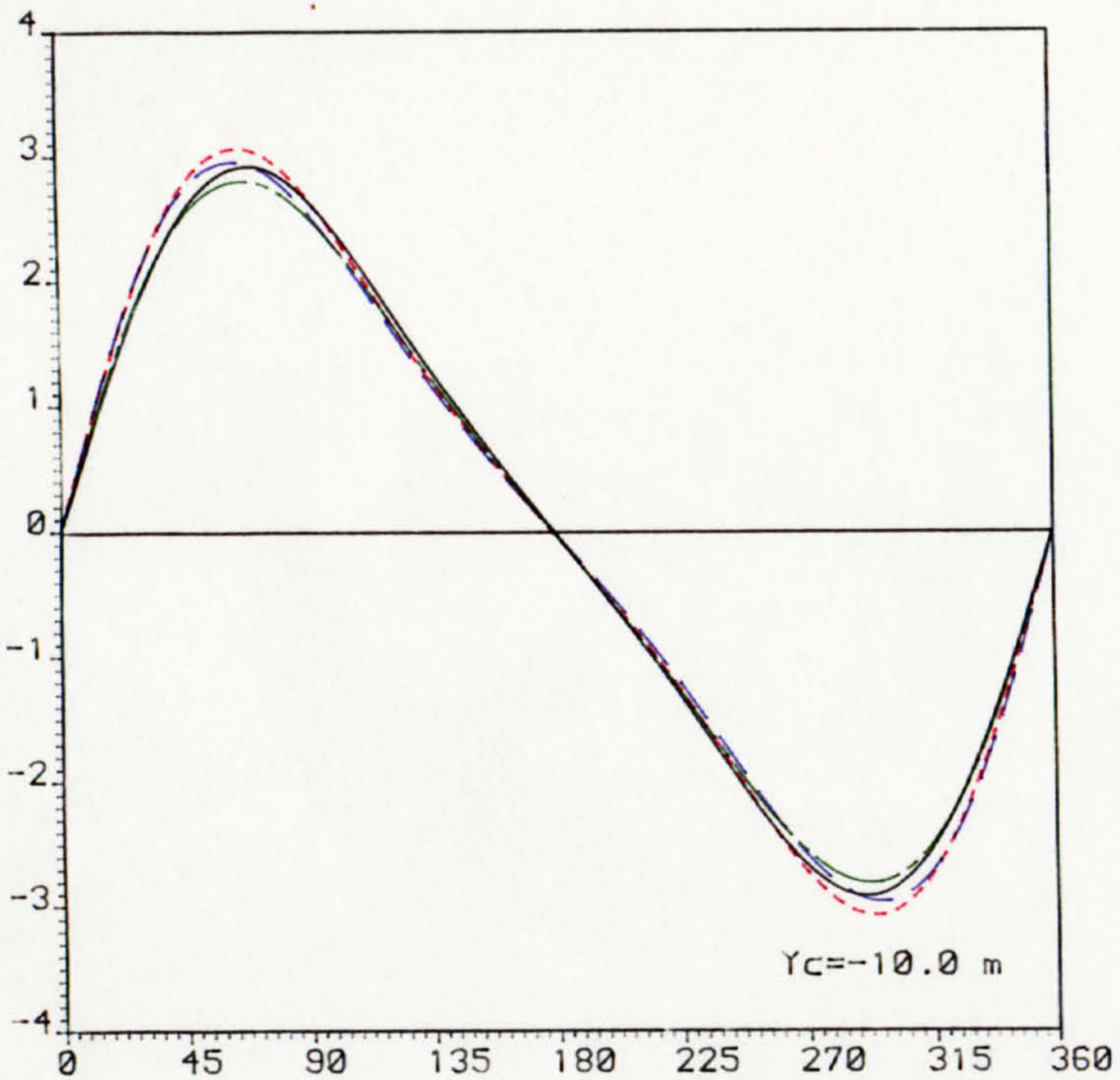

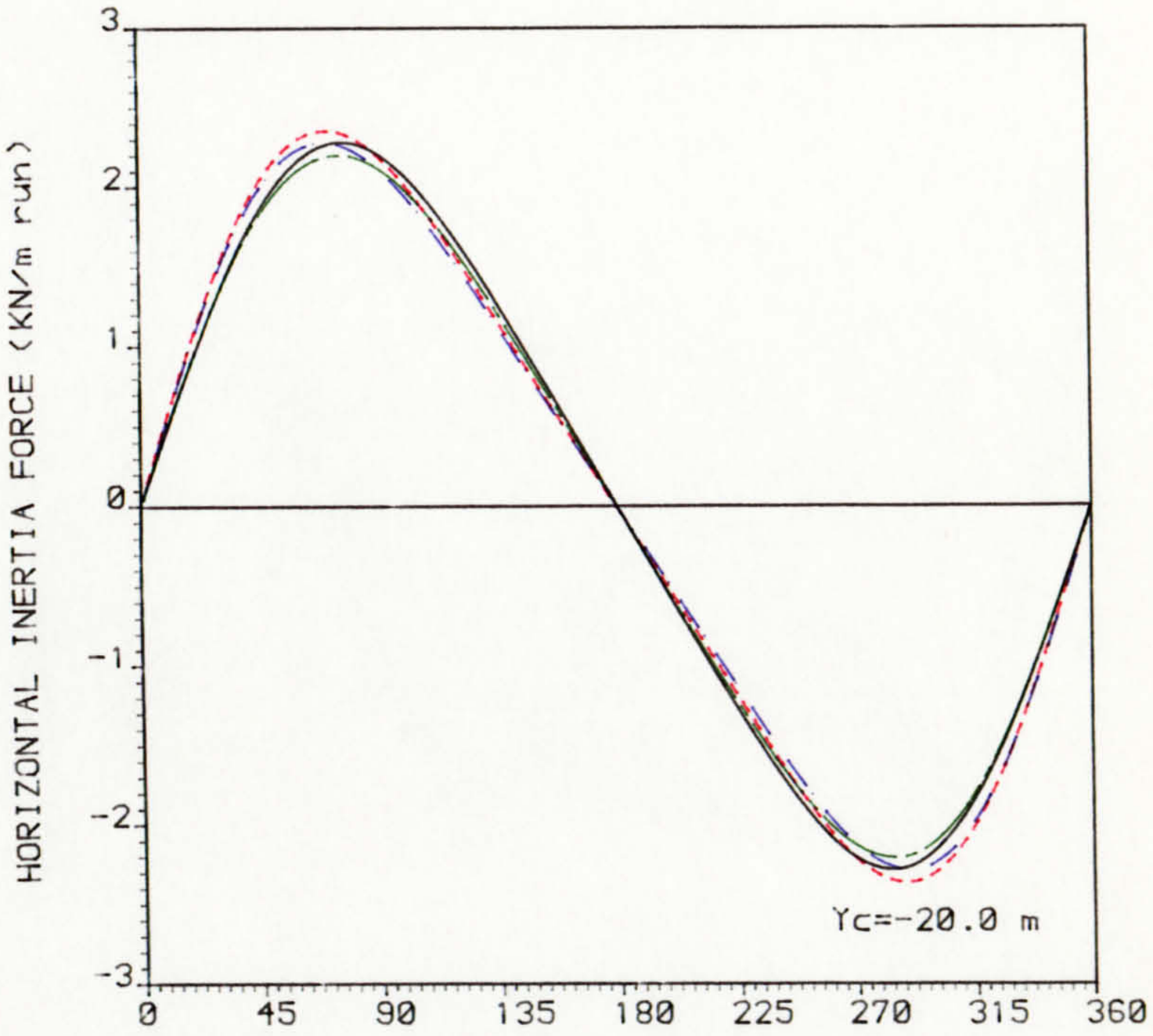

_____ 5th Order STOKES++	H= 18.76 (m)	Cd= .70	H/d= .47
----- 5th Order STOKES	T= 11.32 (sec)	Cm= 2.00	$w^2 d/g$= 1.26
__ __ 7th Order STREAM FUNCTION	d= 40.00 (m)		
__ __ 7th Order STREAM FUNCTION++	Cylinder Dia.= .90 (m)	++ CONVECTIVE ACCELERATION terms included	

FIG 2.11 HYDRODYNAMIC LOADING ON A HORIZONTAL CYLINDER

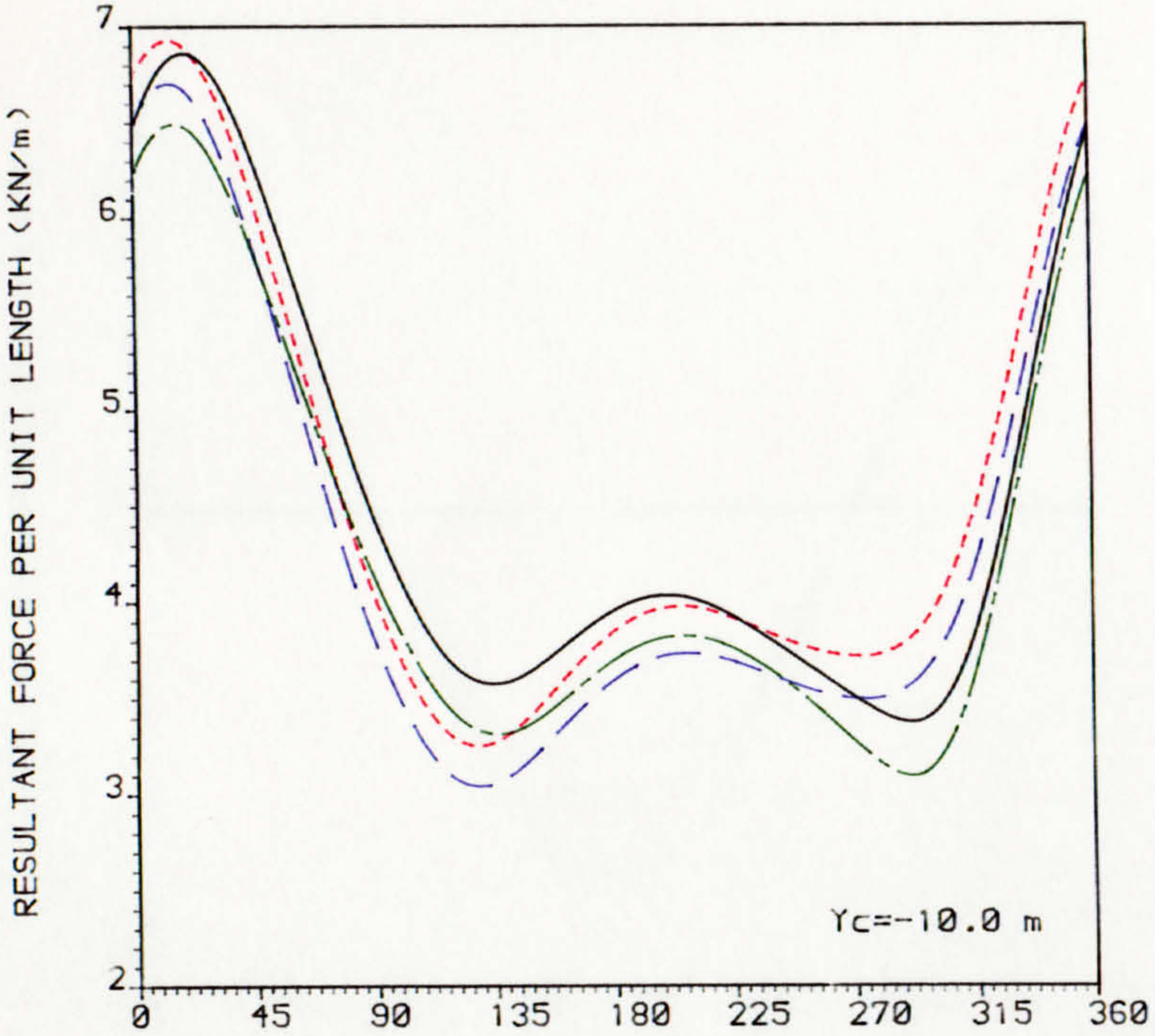

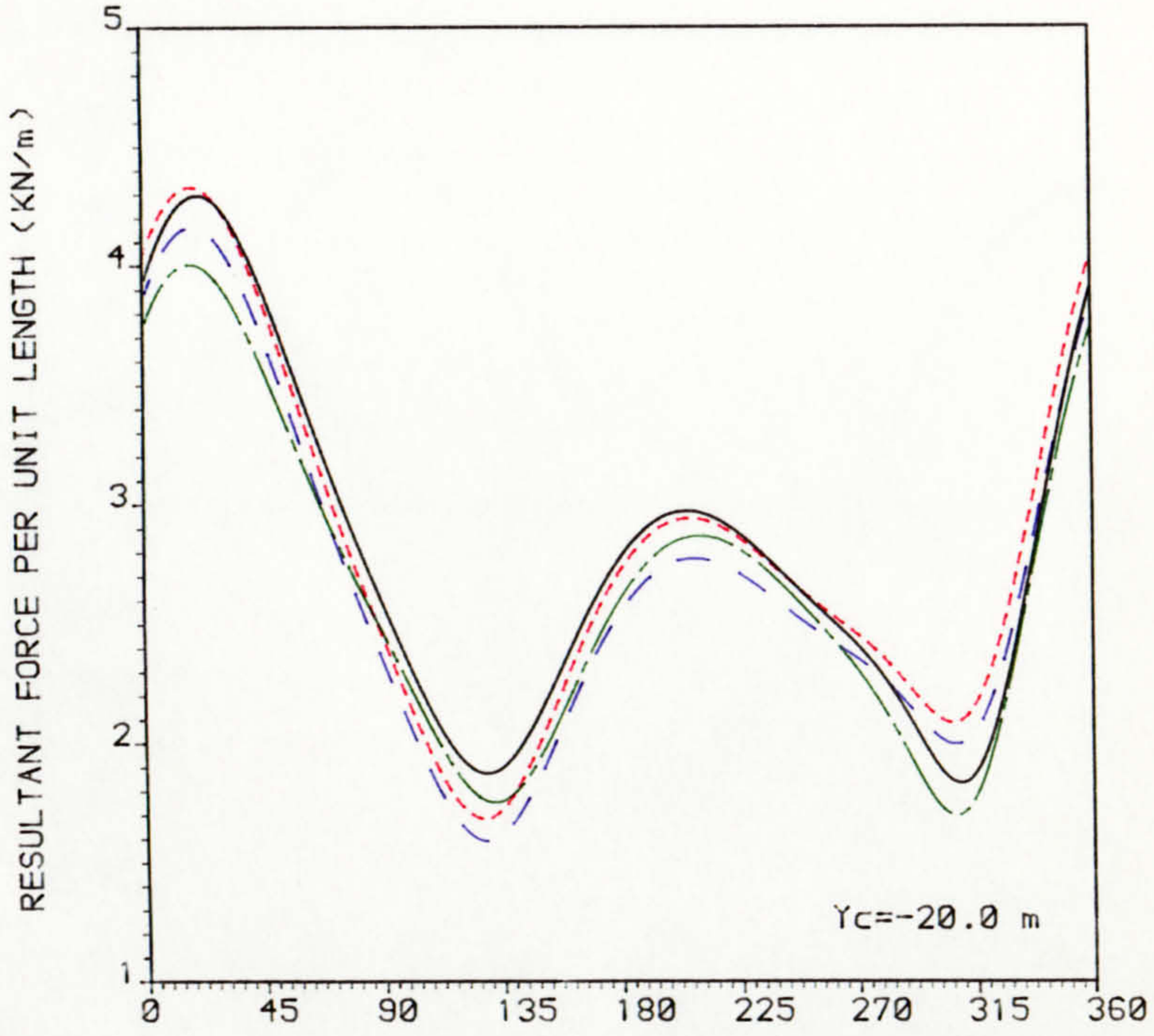

_____ 5th Order STOKES++	H= 18.76 (m)	Cd= .70	H/d= .47
_ _ _ _ _ 5th Order STOKES	T= 11.32 (sec)	Cm= 2.00	$w^2 d/g$= 1.26
_ __ _ 7th Order STREAM FUNCTION	d= 40.00 (m)		
___ _ _ 7th Order STREAM FUNCTION++	Cylinder Dia.= .90 (m)	++ CONVECTIVE ACCELERATION terms included	

FIG 2.12 HYDRODYNAMIC LOADING ON A HORIZONTAL CYLINDER

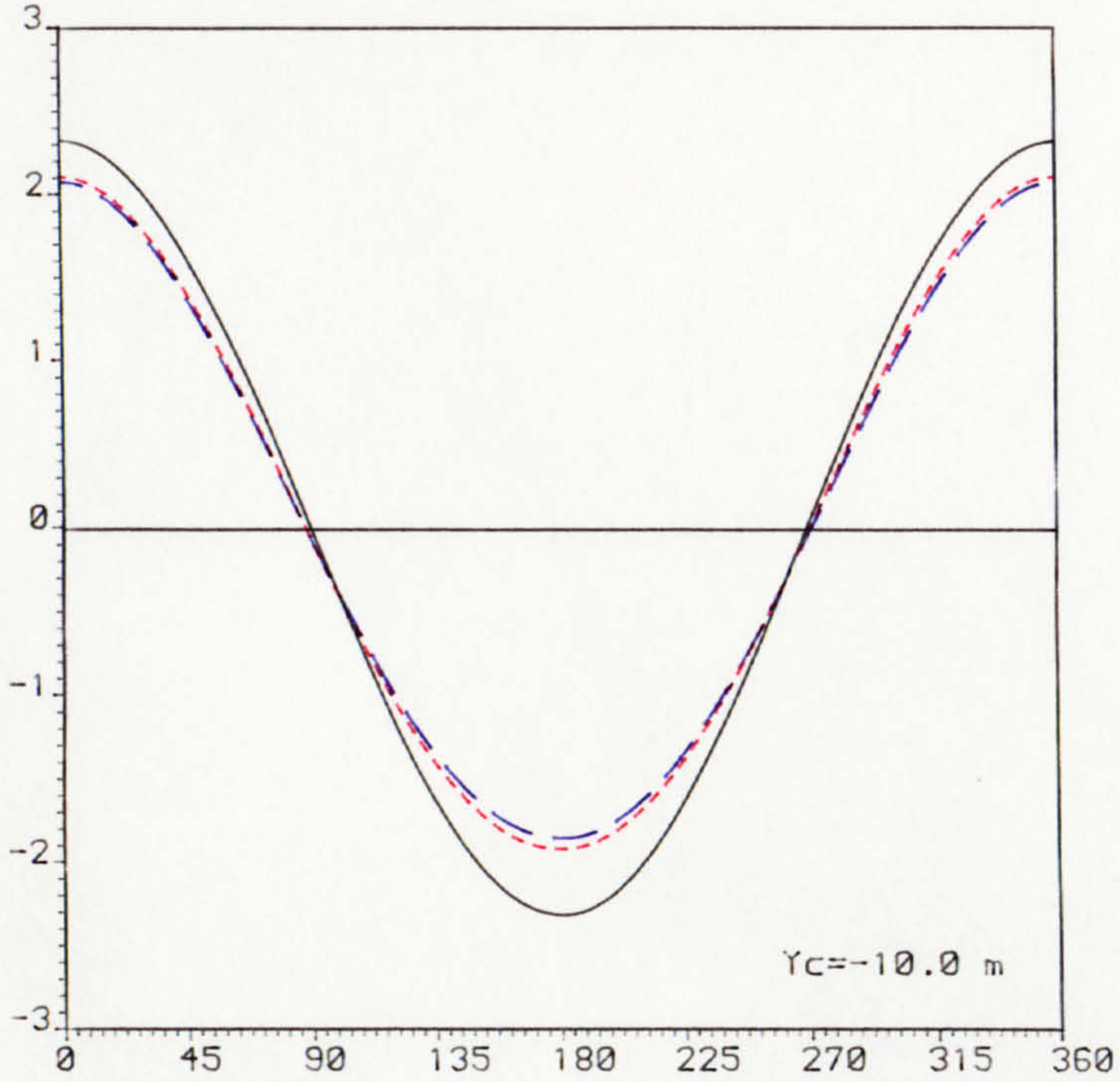

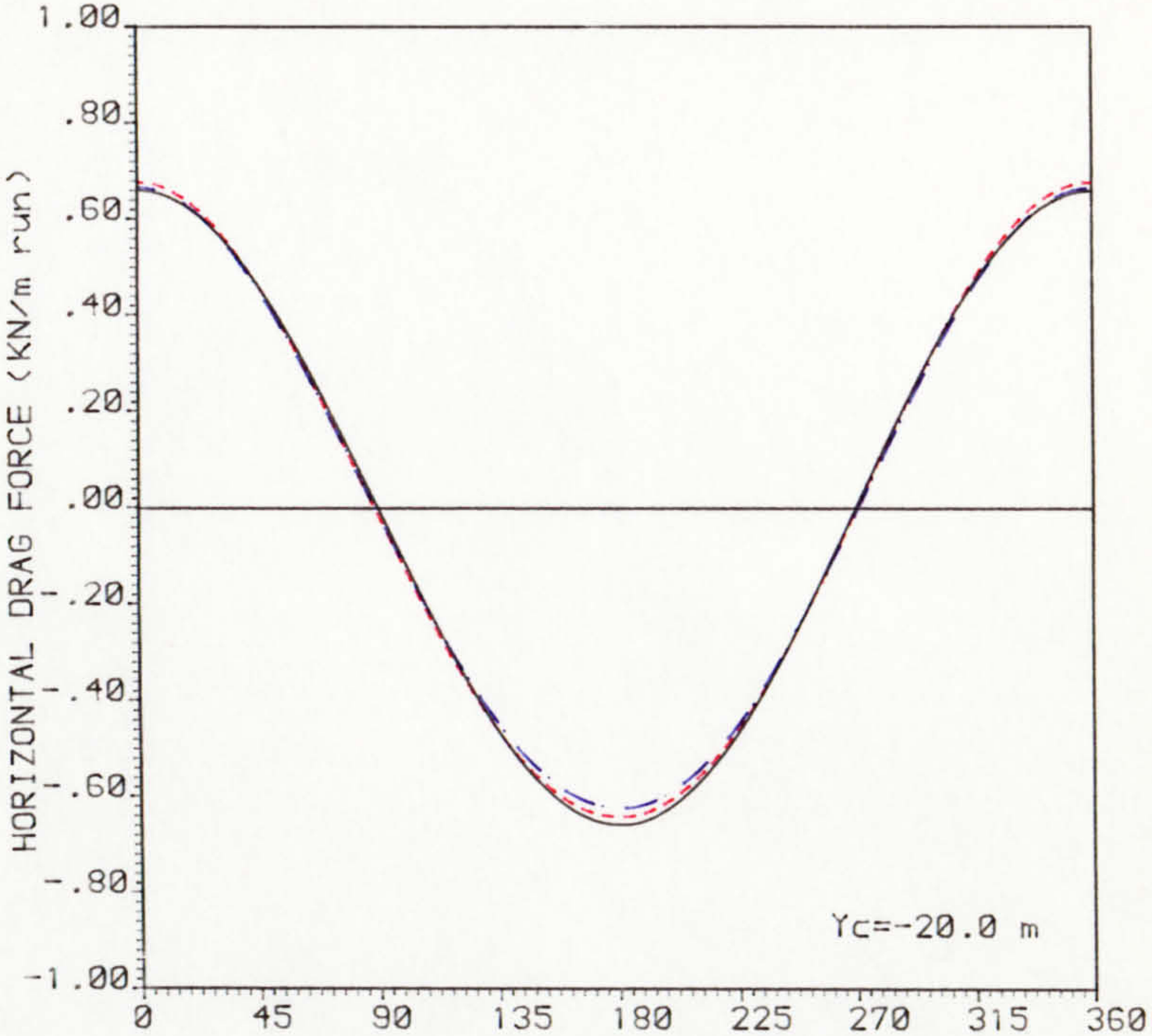

——— AIRY
..... 5th Order STOKES
— — 3rd Order STREAM FUNCTION

H= 12.80 (m)
T= 8.00 (sec)
d= 100.00 (m)
Cylinder Dia.= .90 (m)

Cd= .70
Cm= 2.00

H/d= .13
w^2 d/g= 6.29

FIG 2.13 HYDRODYNAMIC LOADING ON A HORIZONTAL CYLINDER

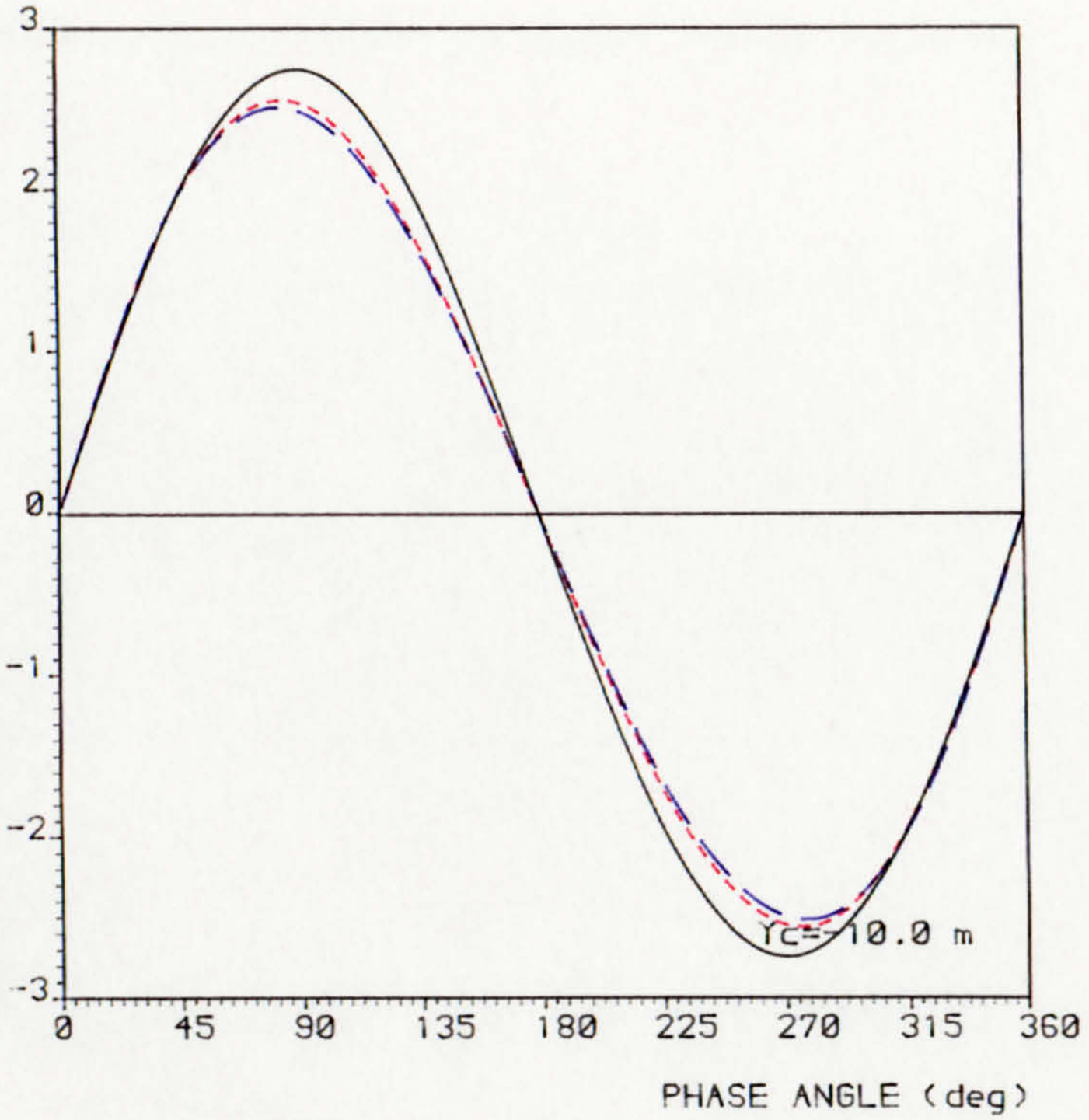

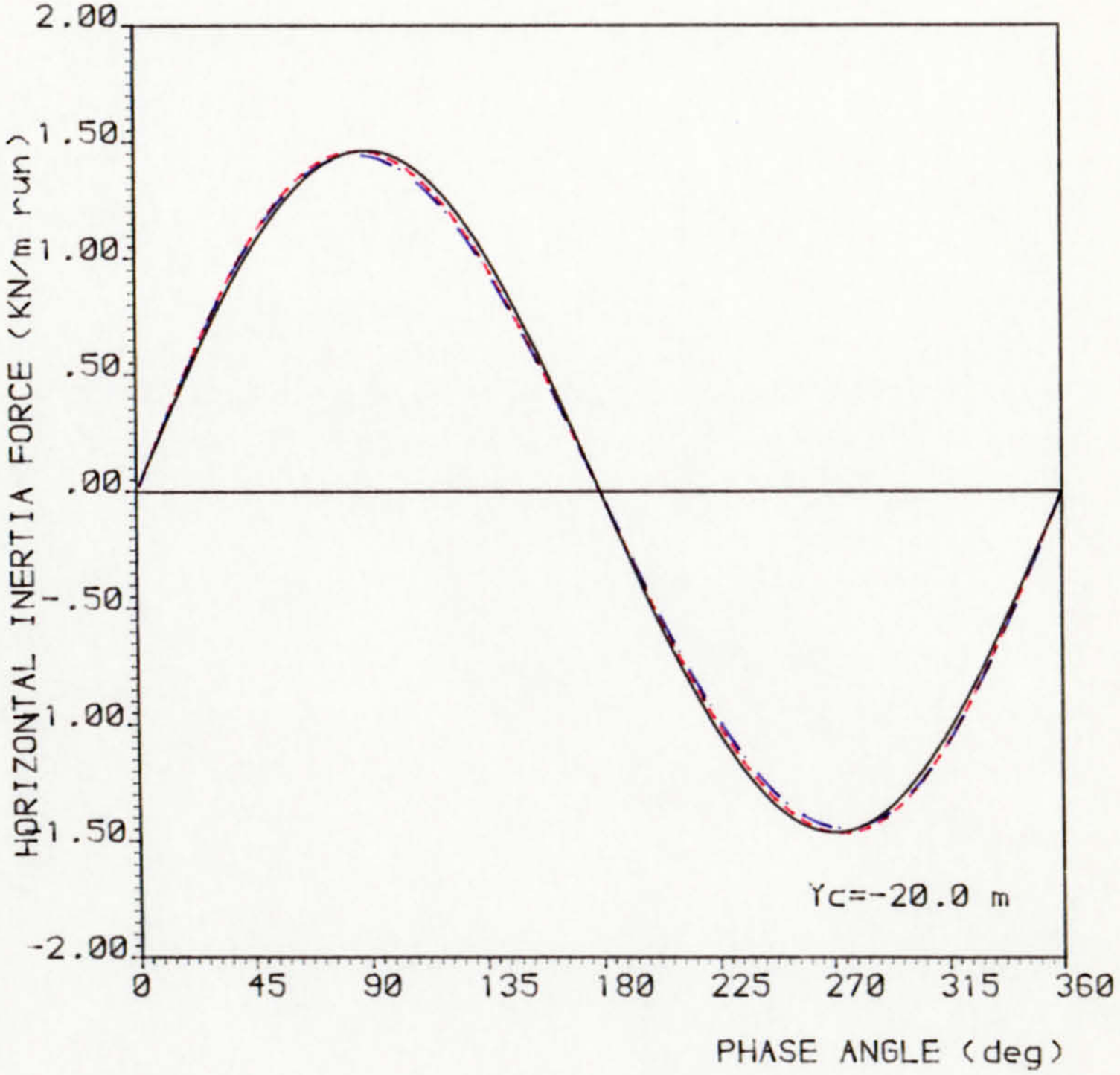

_____ AIRY	H= 12.80 (m)	Cd= .70	H/d= .13
- - - - - 5th Order STOKES	T= 8.00 (sec)	Cm= 2.00	$w^2 d/g$= 6.29
_ __ _ 3rd Order STREAM FUNCTION	d= 100.00 (m)		
	Cylinder Dia.= .90 (m)		

FIG 2.14 HYDRODYNAMIC LOADING ON A HORIZONTAL CYLINDER

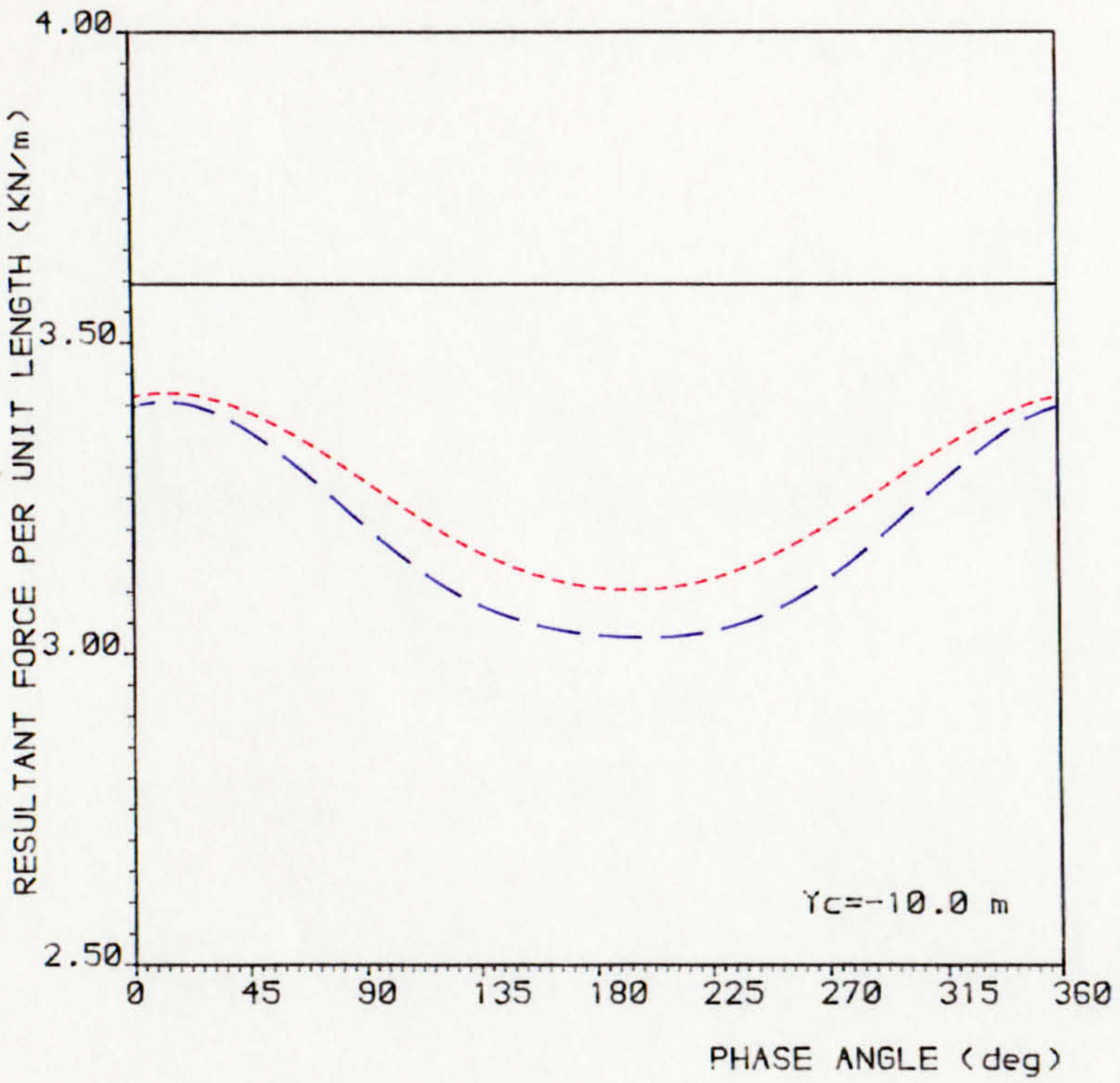

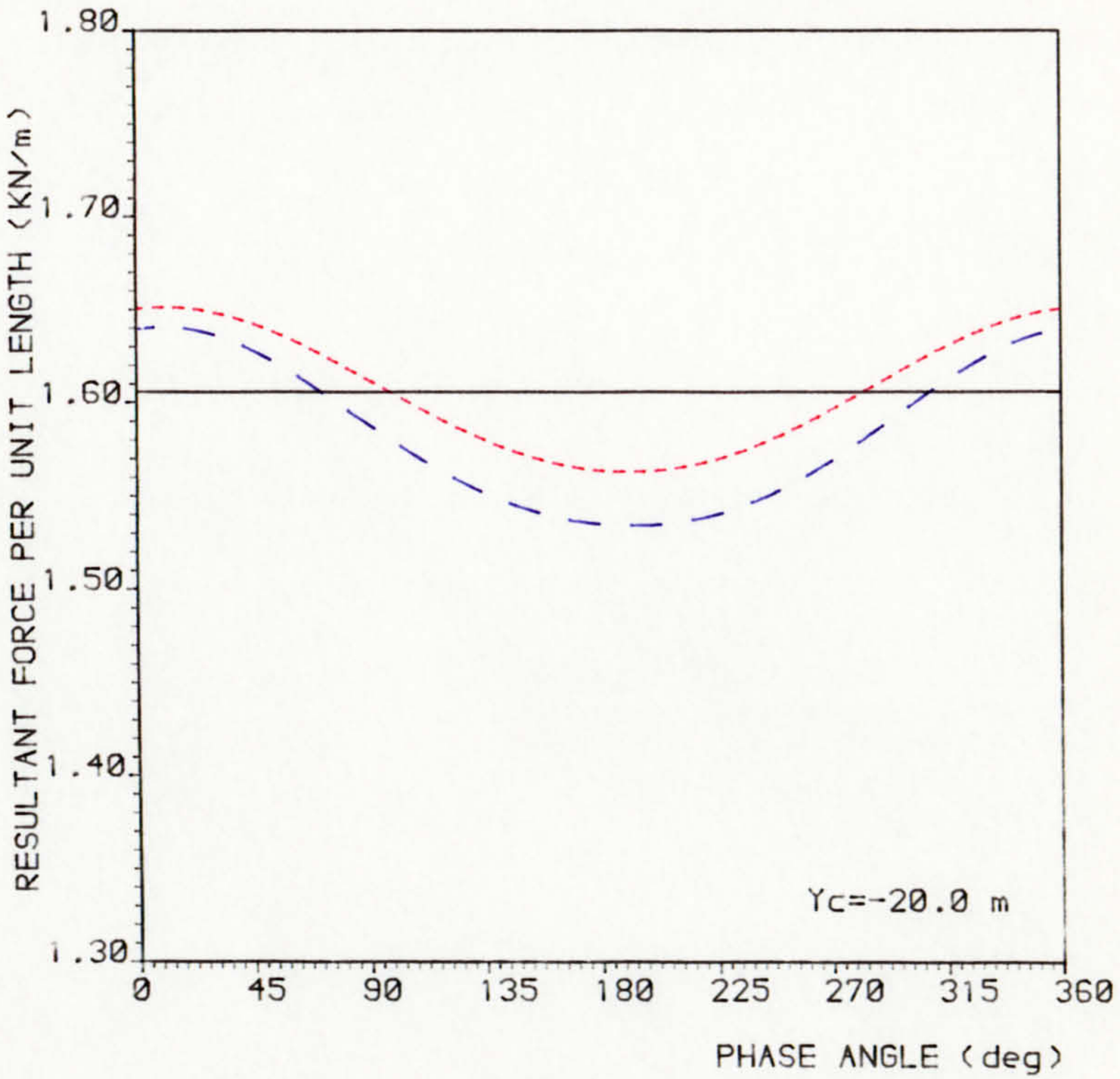

_____ AIRY	H= 12.80 (m)	Cd= .70	H/d= .13
----- 5th Order STOKES	T= 8.00 (sec)	Cm= 2.00	$w^2 d/g$= 6.29
_ __ . 3rd Order STREAM FUNCTION	d= 100.00 (m)		
	Cylinder Dia.= .90(m)		

FIG 2.15 HYDRODYNAMIC LOADING ON A HORIZONTAL CYLINDER

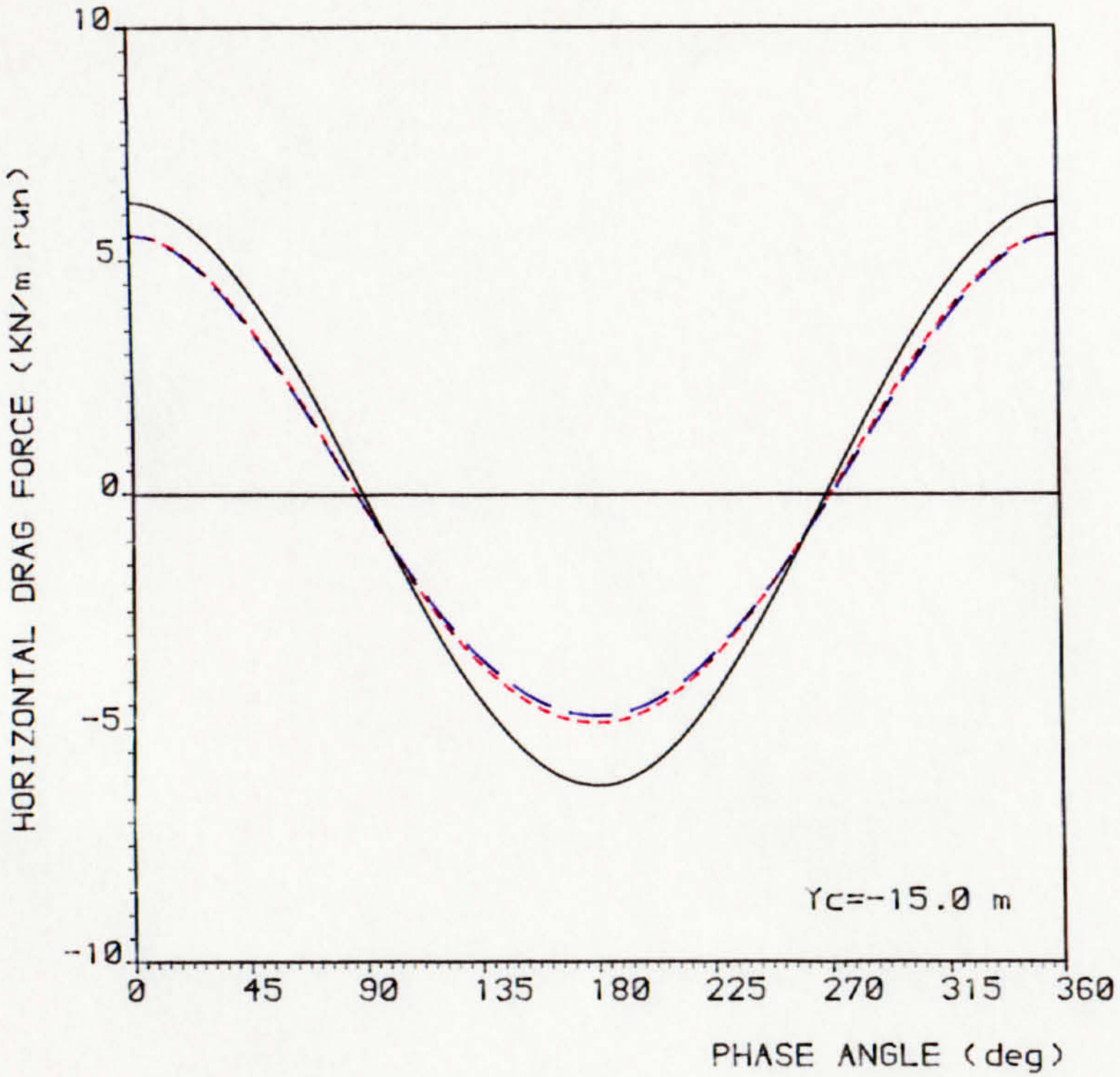

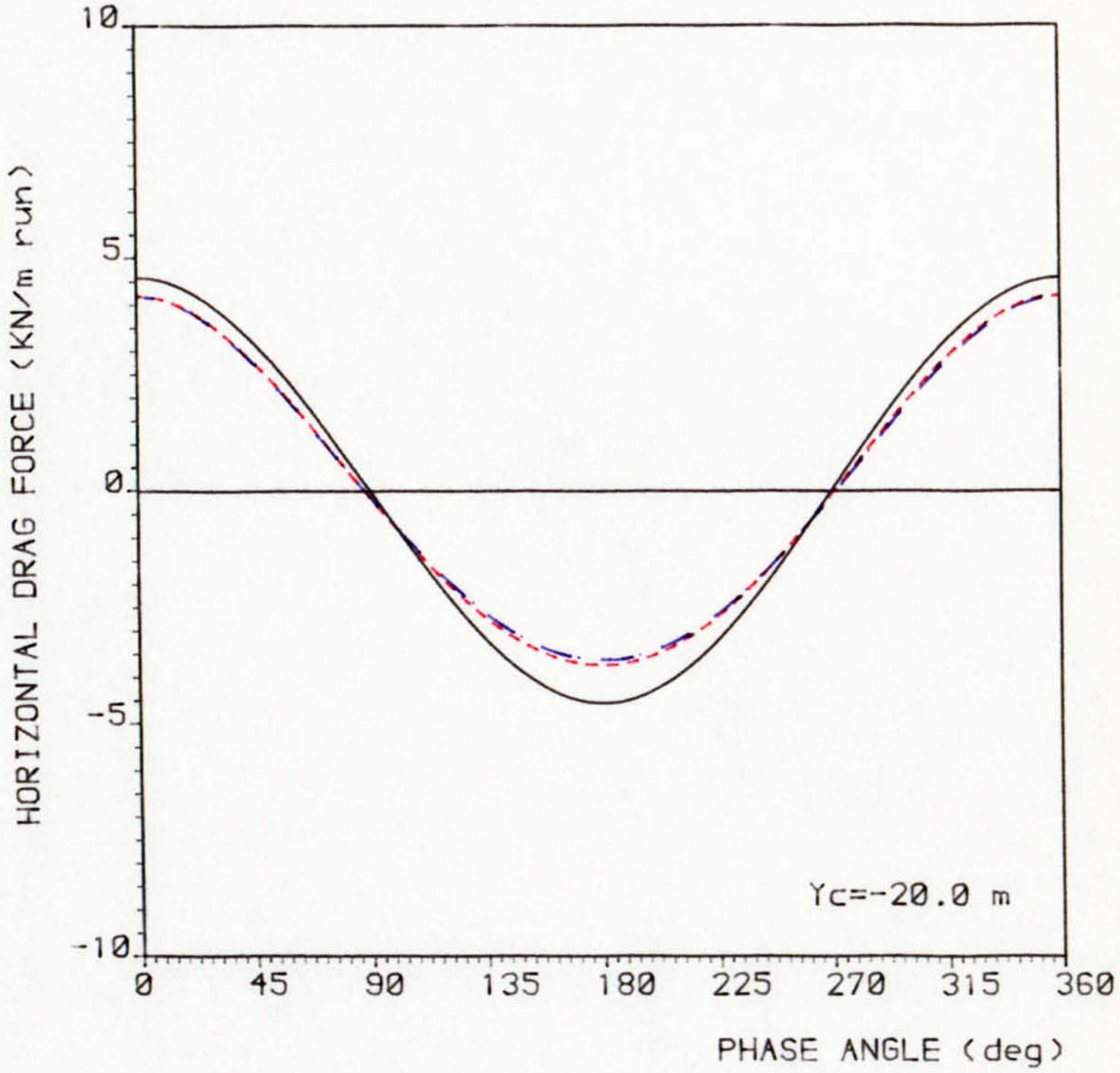

——— AIRY
------ 5th Order STOKES
_ __ . 7th Order STREAM FUNCTION

H= 25.20 (m)
T= 11.30 (sec)
d= 100.00 (m)
Cylinder Dia.= .90 (m)

Cd= .70
Cm= 2.00

H/d= .25
w^2 d/g= 3.15

FIG 2.16 HYDRODYNAMIC LOADING ON A HORIZONTAL CYLINDER

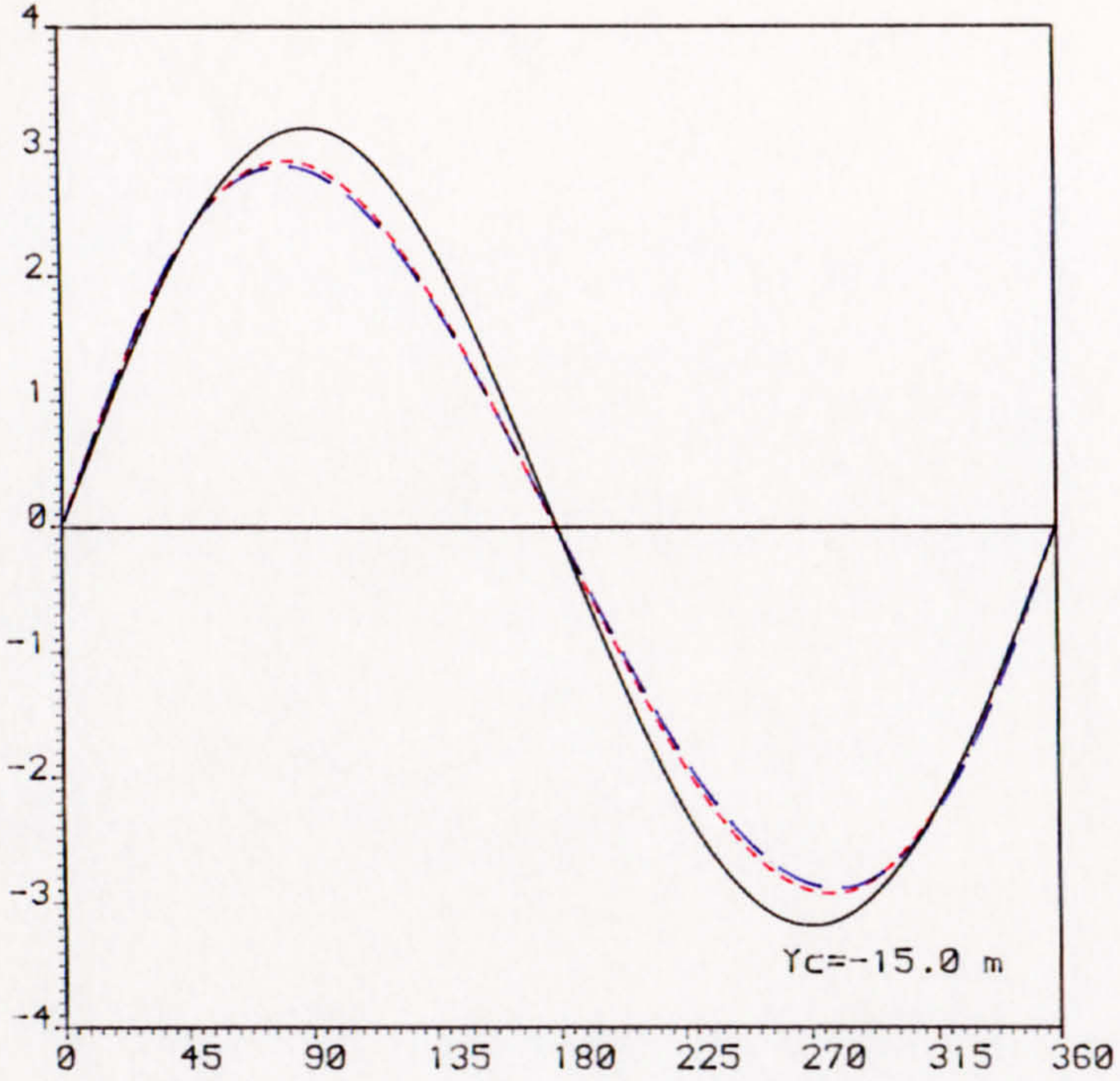

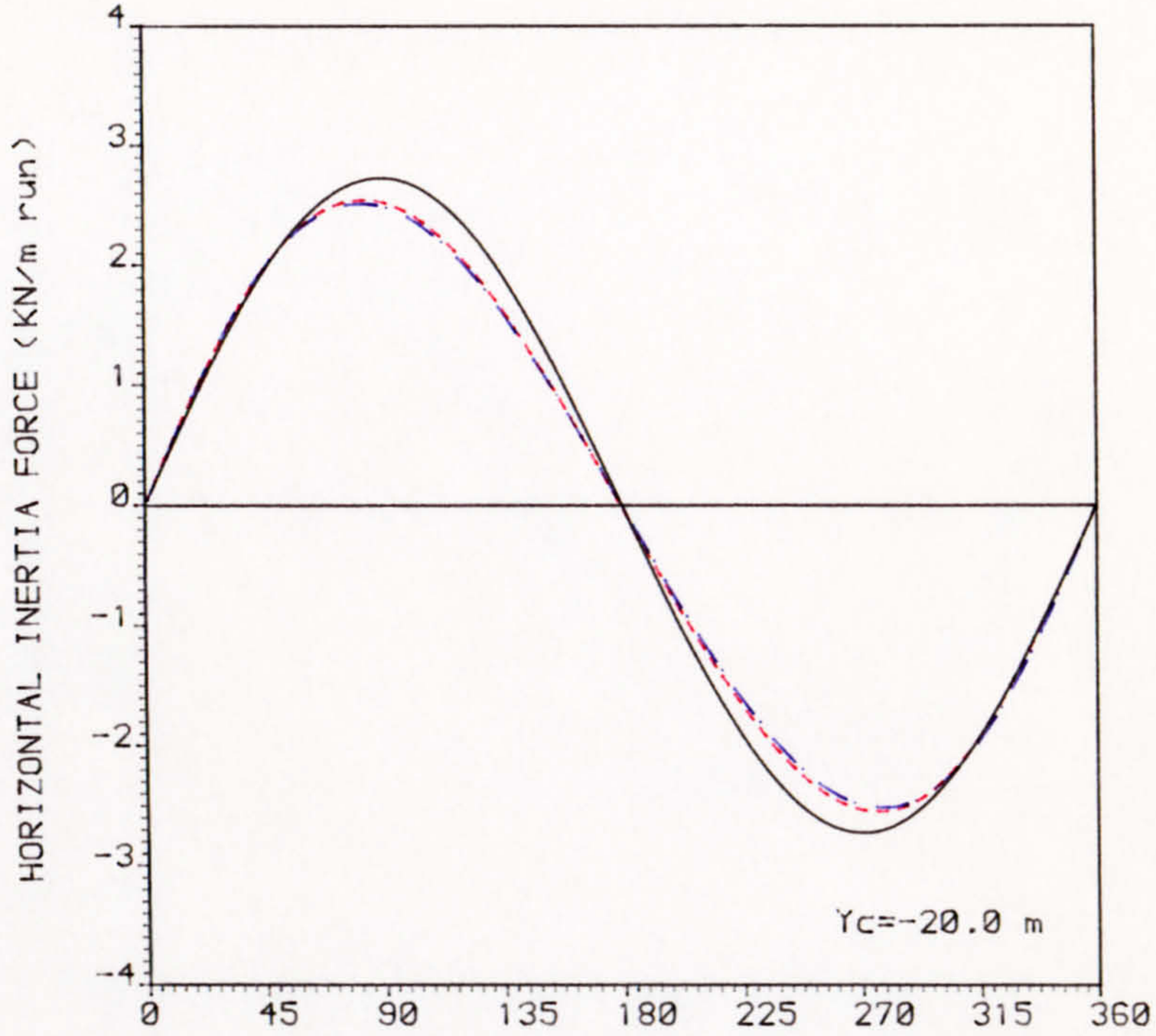

_____ AIRY
..... 5th Order STOKES
_ _ _ 7th Order STREAM FUNCTION

H= 25.20 (m)
T= 11.30 (sec)
d= 100.00 (m)
Cylinder Dia.= .90 (m)

Cd= .70
Cm= 2.00

H/d= .25
$w^2 d/g$= 3.15

FIG 2.17 HYDRODYNAMIC LOADING ON A HORIZONTAL CYLINDER

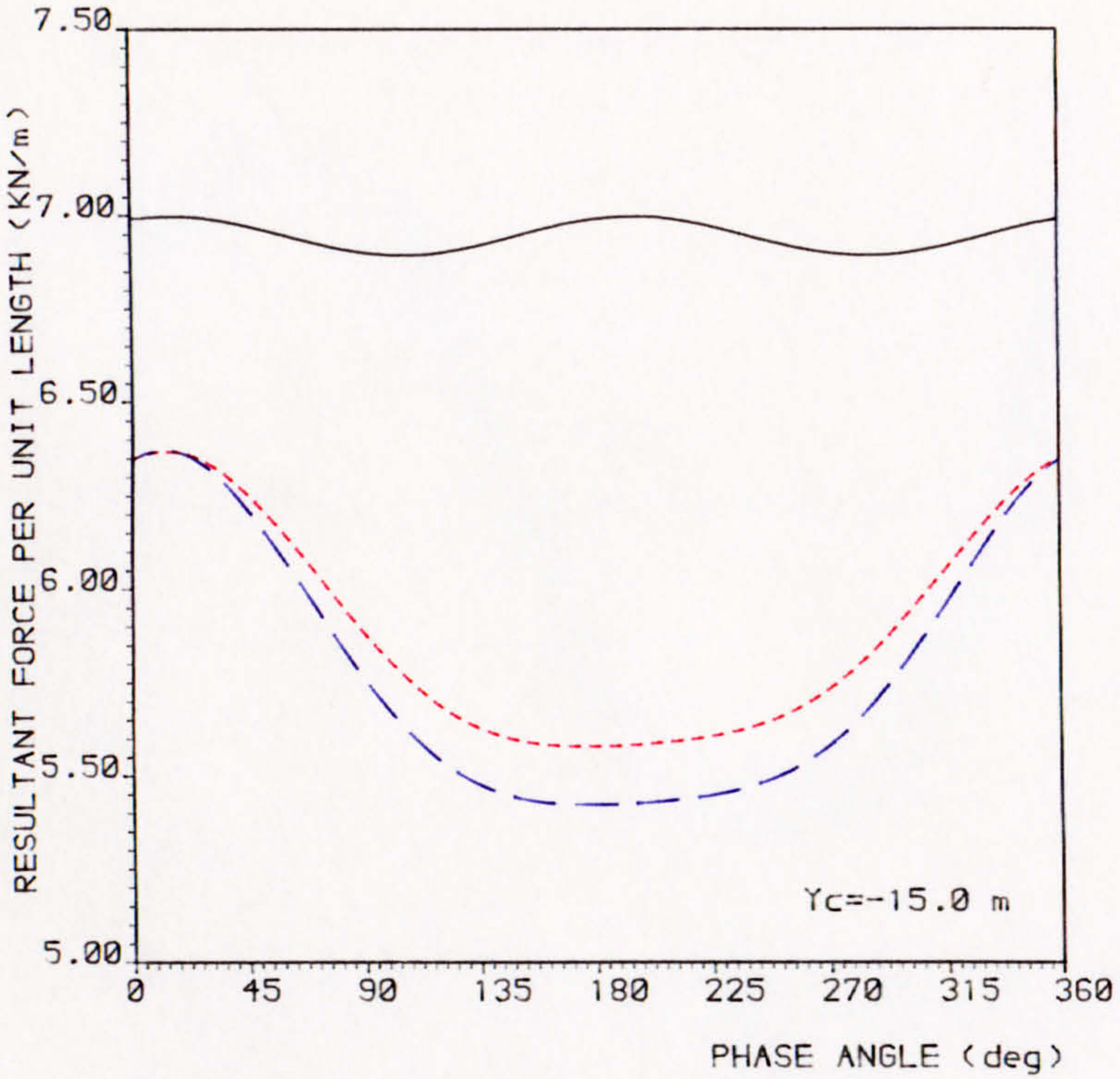

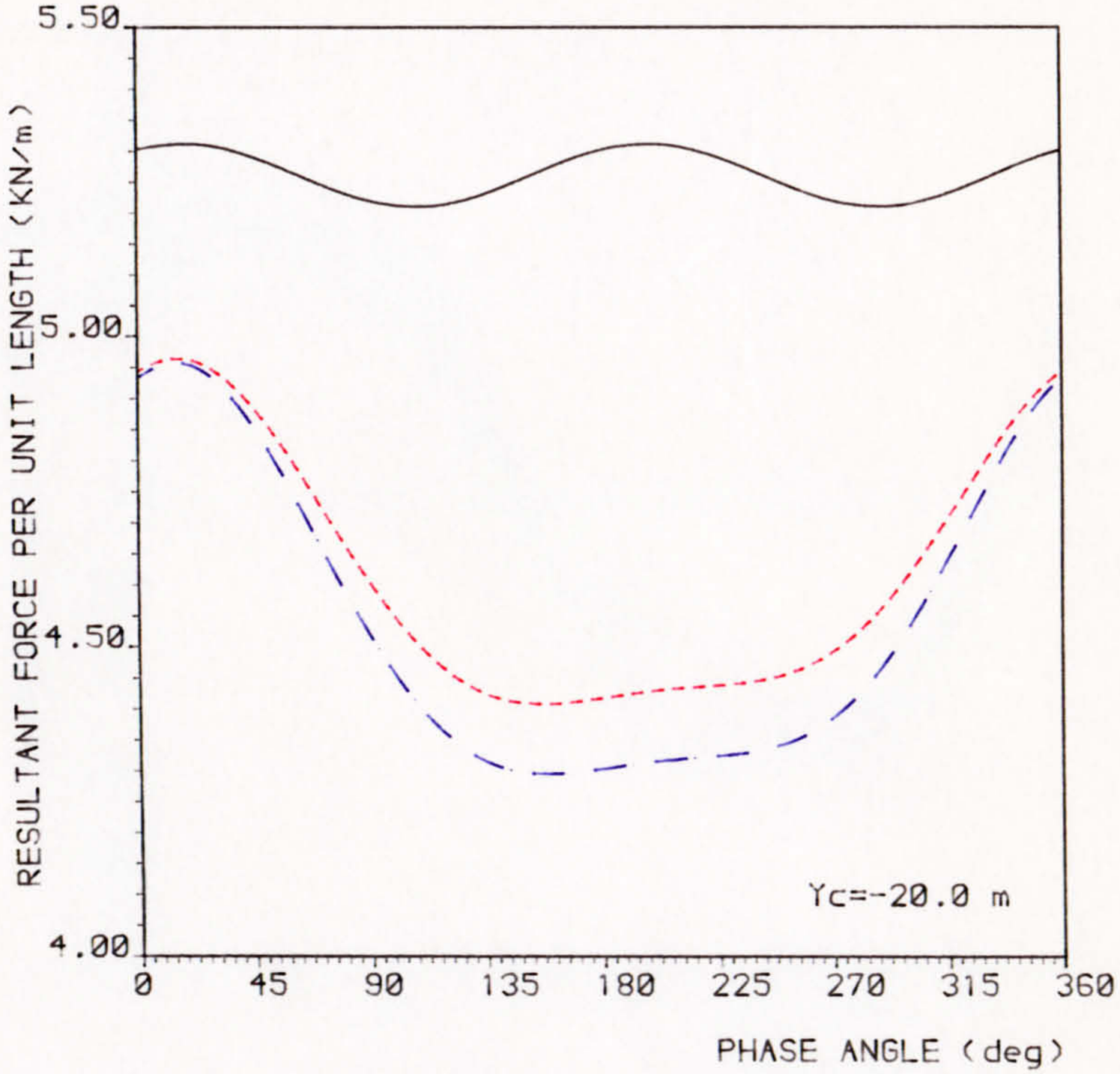

——— AIRY
----- 5th Order STOKES
_ _ . 7th Other STREAM FUNCTION

H= 25.20 (m)
T= 11.30 (sec)
d= 100.00 (m)
Cylinder Dia.= .90(m)

Cd= .70
Cm= 2.00

H/d= .25
$w^2 d/g$= 3.15

FIG 2.18 HYDRODYNAMIC LOADING ON A HORIZONTAL CYLINDER

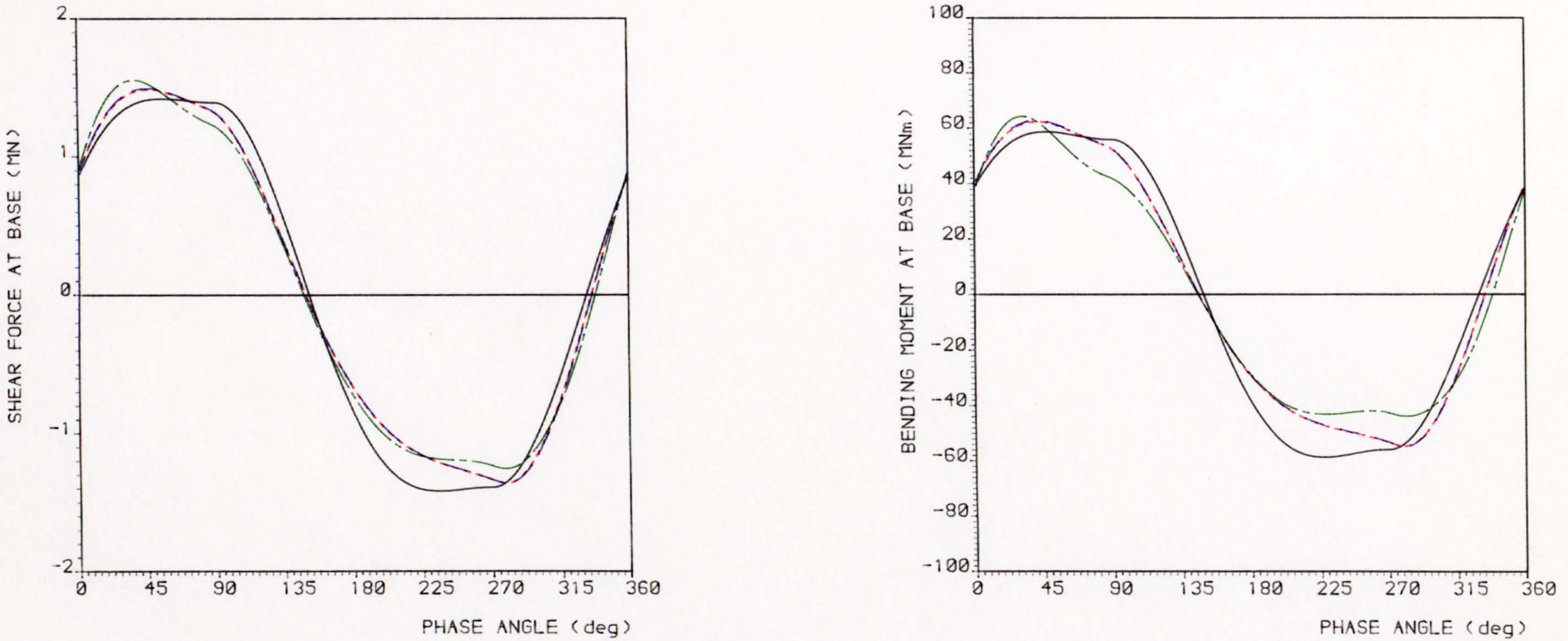

——— AIRY

------ 5th Order STOKES

_ _ . 5th Order STREAM FUNCTION

—_—_ 5th Order CNOIDAL

H= 22.00 (m)
T= 15.00 (sec)
d= 70.50 (m)
Cylinder Dia.= 3.00(m)

Cd= .70
Cm= 2.00
NOTE: Loads integrated up to M.W.L

H/d= .31
w^2 d/g= 1.26

FIG 2.19 HYDRODYNAMIC LOADING ON A VERTICAL CYLINDER

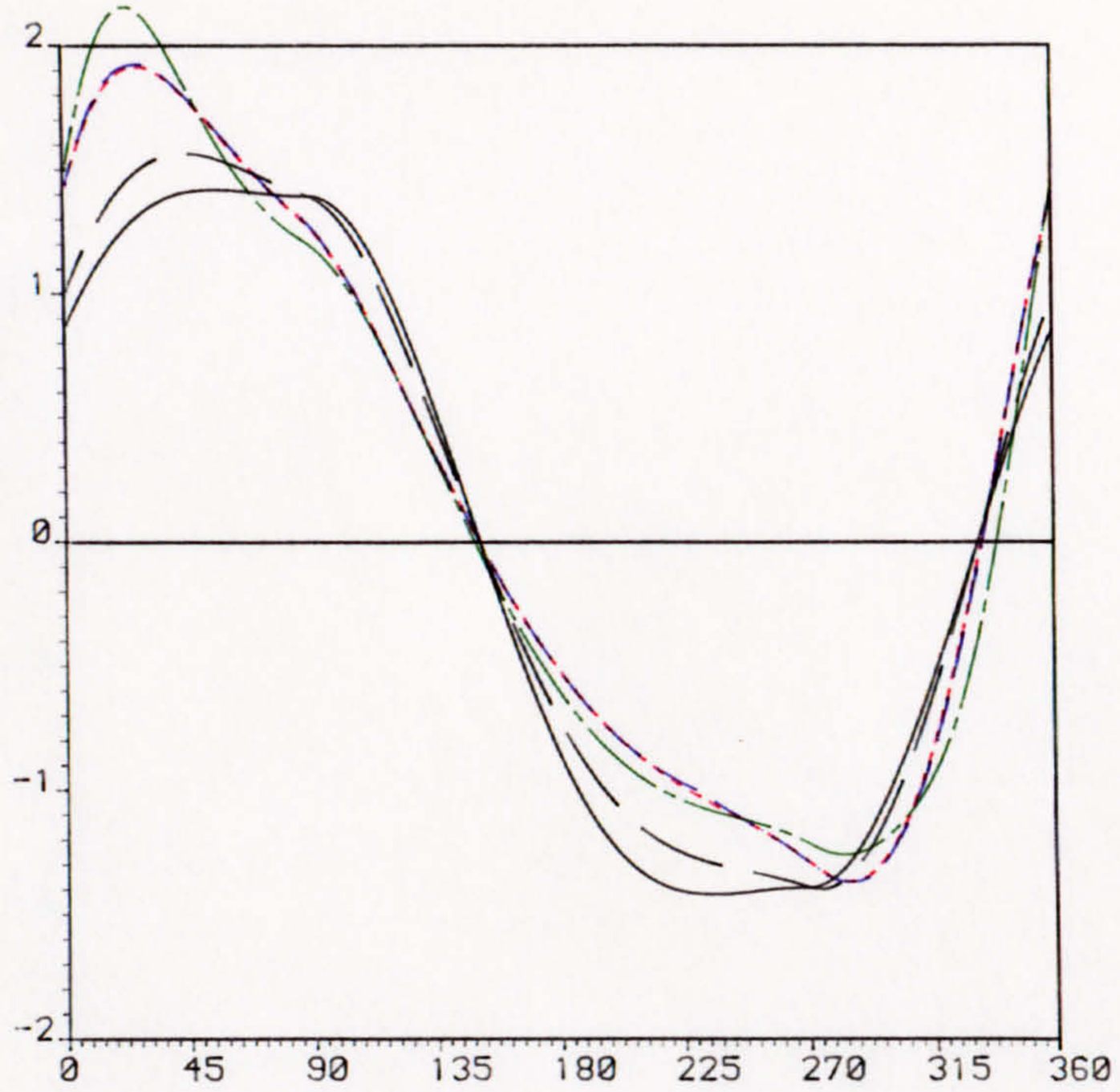

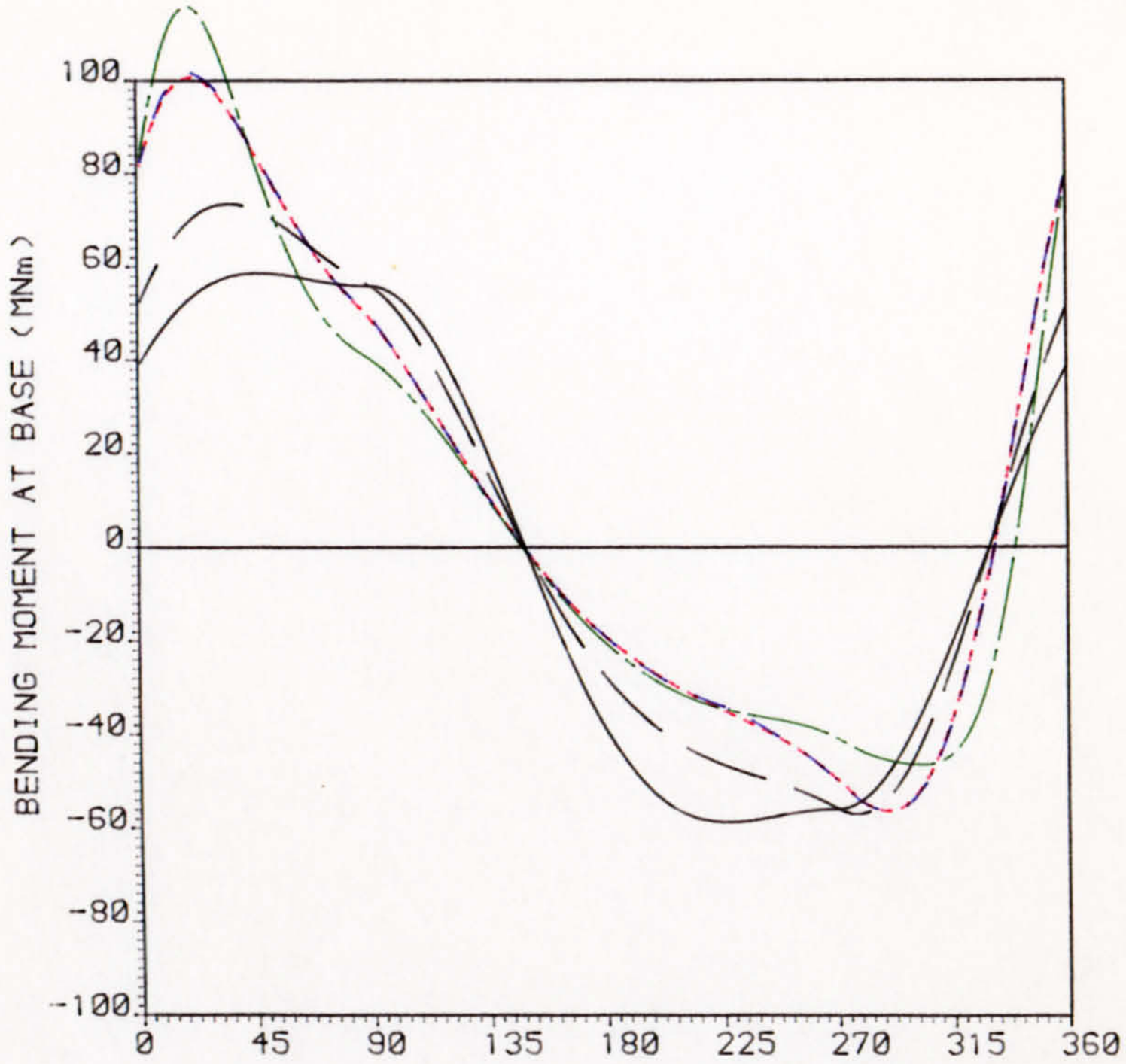

_____ AIRY, _____ "Stretched" AIRY
..... 5th Order STOKES
_ __ . 5th Order STREAM FUNCTION
__ __ 5th Order CNOIDAL

H= 22.00 (m)
T= 15.00 (sec)
d= 70.50 (m)
Cylinder Dia.= 3.00(m)

Cd= .70
Cm= 2.00

H/d= .31
$w^2 d/g$= 1.26

NOTE: Loads integrated up to instantaneous level of surface elevation

FIG 2.20 HYDRODYNAMIC LOADING ON A VERTICAL CYLINDER

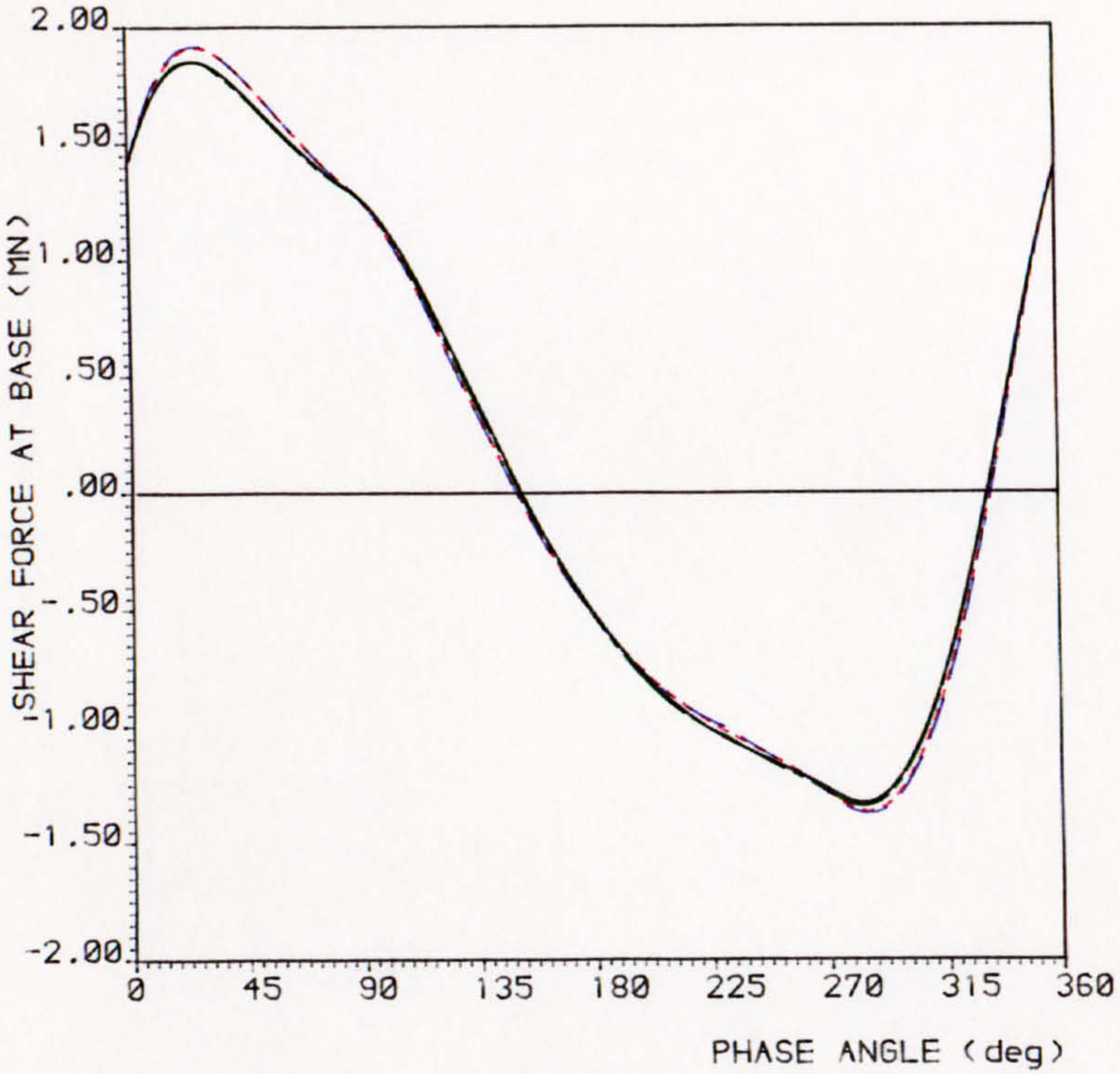

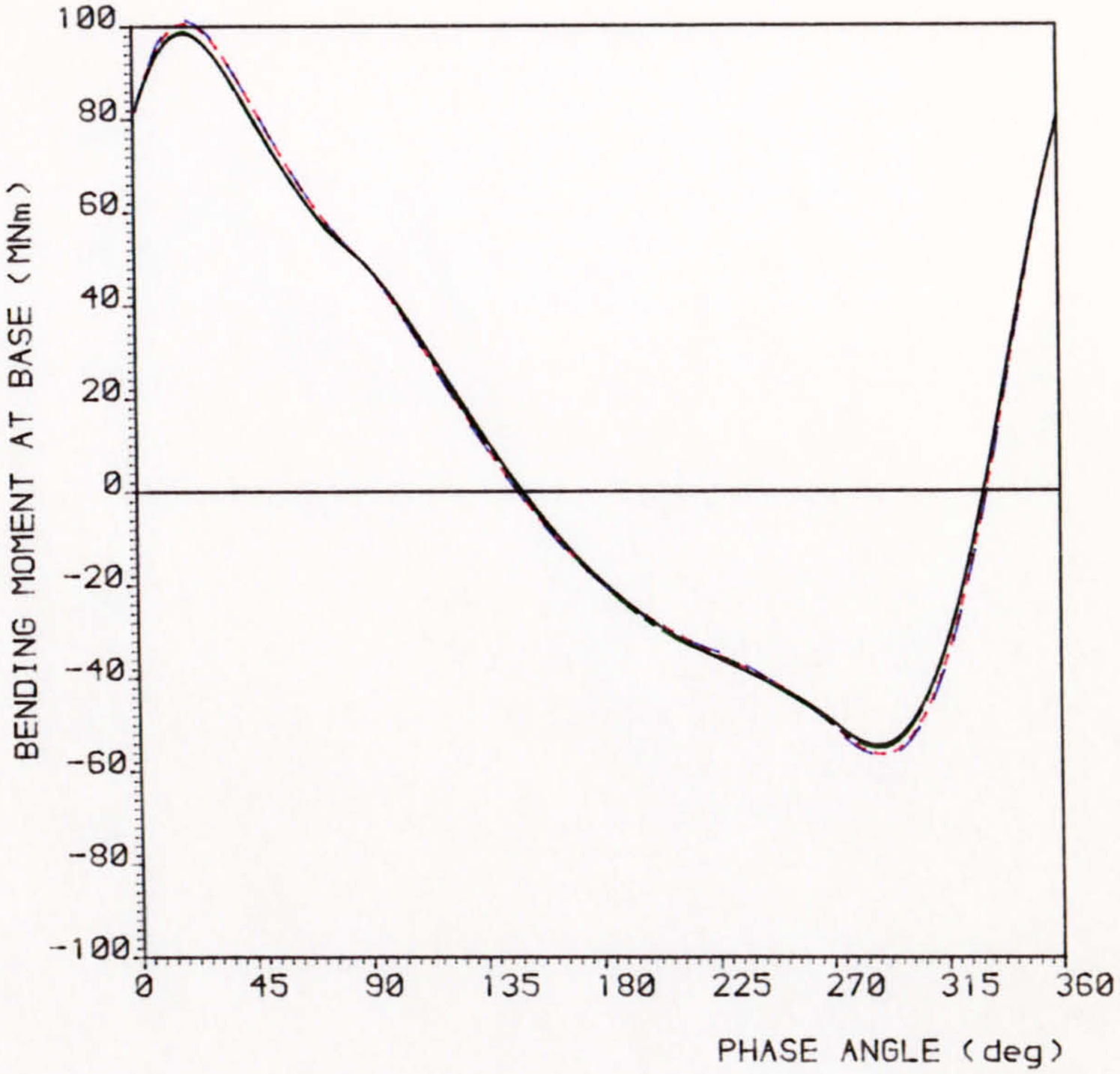

_____ 5th Order STOKES++
------ 5th Order STOKES
_ __ . 5th Order STREAM FUNCTION
__ __ 5th Order STREAM FUNCTION++

H= 22.00 (m)
T= 15.00 (sec)
d= 70.50 (m)
Cylinder Dia.= 3.00(m)

Cd= .70
Cm= 2.00
NOTE: Loads integrated up to instantaneous level of surface elevation.
++ CONVECTIVE ACCELERATION terms included

H/d= .31
$w^2 d/g$= 1.26

FIG 2.21 HYDRODYNAMIC LOADING ON A VERTICAL CYLINDER

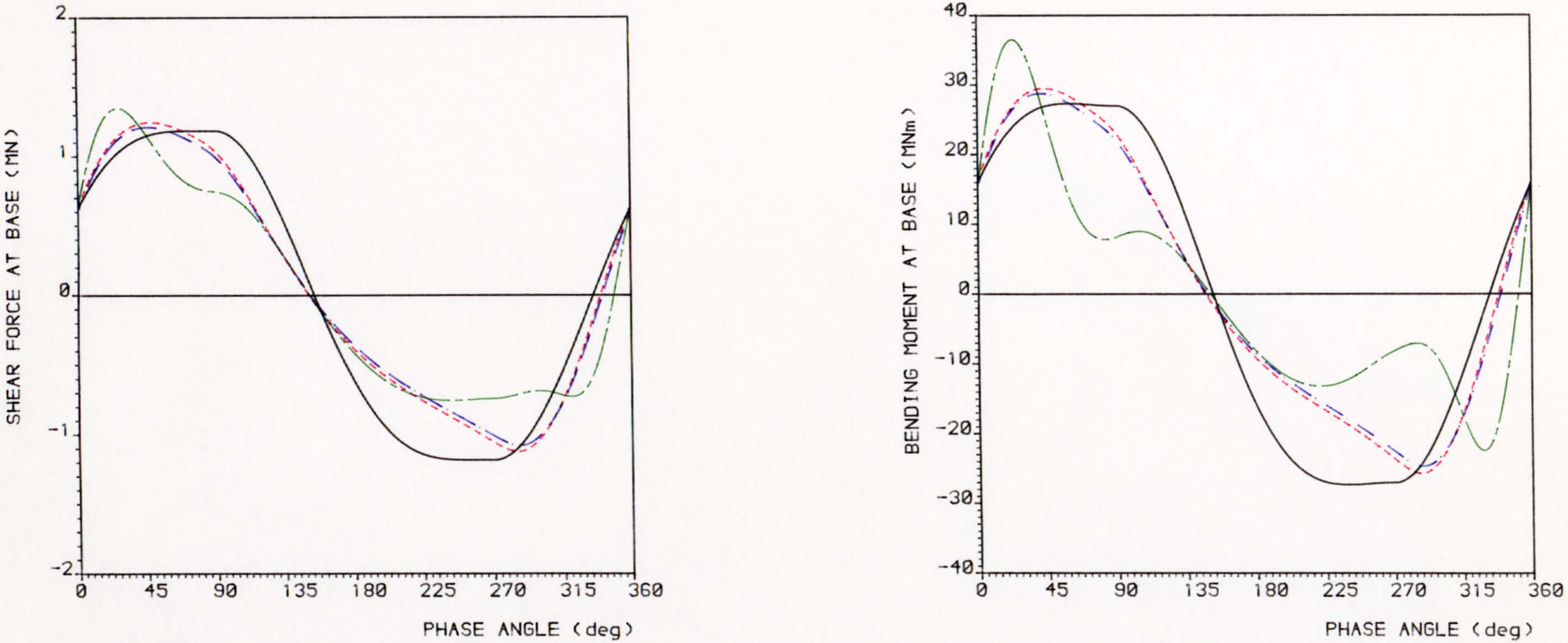

AIRY
5th Order STOKES
7th Order STREAM FUNCTION
5th Order CNOIDAL

H= 18.76 (m)
T= 11.32 (sec)
d= 40.00 (m)
Cylinder Dia.= 3.00(m)

Cd= .70
Cm= 2.00
NOTE: Loads integrated up to M.W.L

H/d= .47
$w^2 d/g$= 1.26

FIG 2.22 HYDRODYNAMIC LOADING ON A VERTICAL CYLINDER

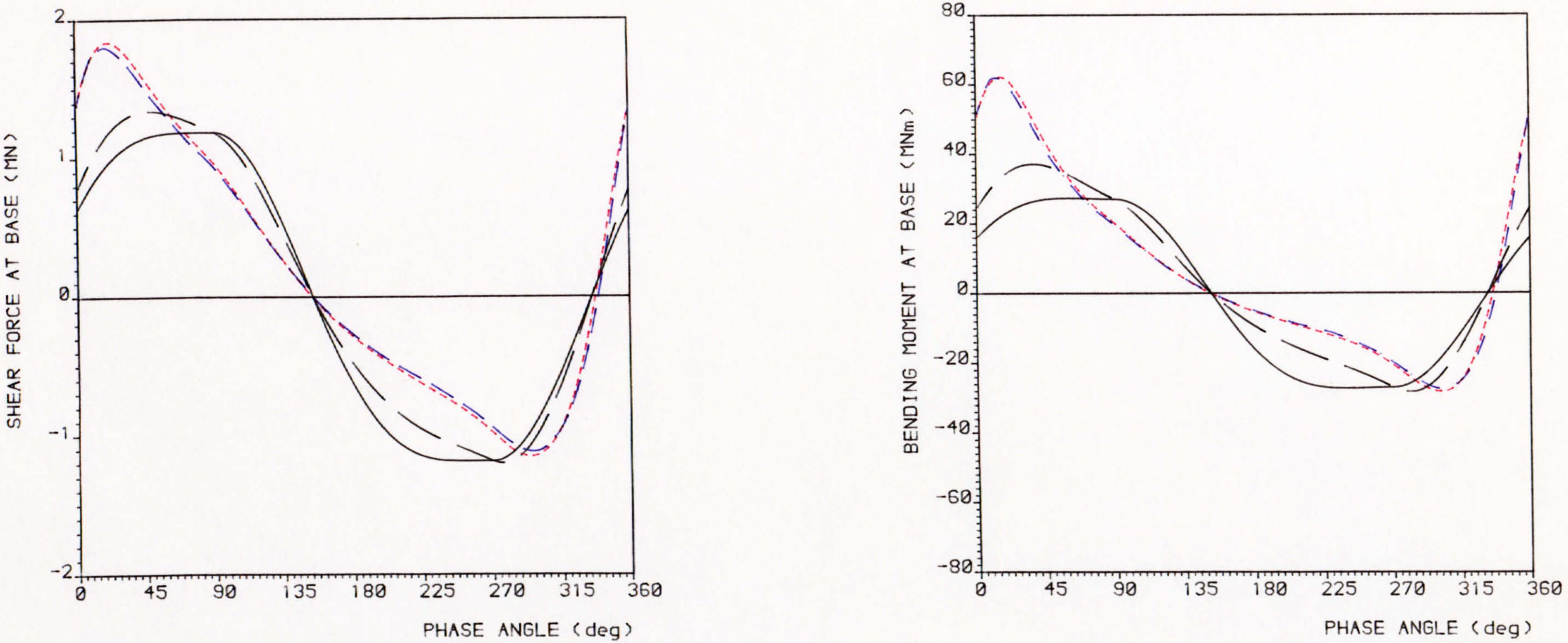

——— AIRY, — — "Stretched" AIRY
----- 5th Order STOKES
_ __ . 7th Order STREAM FUNCTION

H= 18.76 (m)
T= 11.32 (sec)
d= 40.00 (m)
Cylinder Dia.= 3.00(m)

Cd= .70
Cm= 2.00

H/d= .47
$w^2 d/g$= 1.26

NOTE: Loads integrated up to instantaneous level of surface elevation

FIG 2.23 HYDRODYNAMIC LOADING ON A VERTICAL CYLINDER

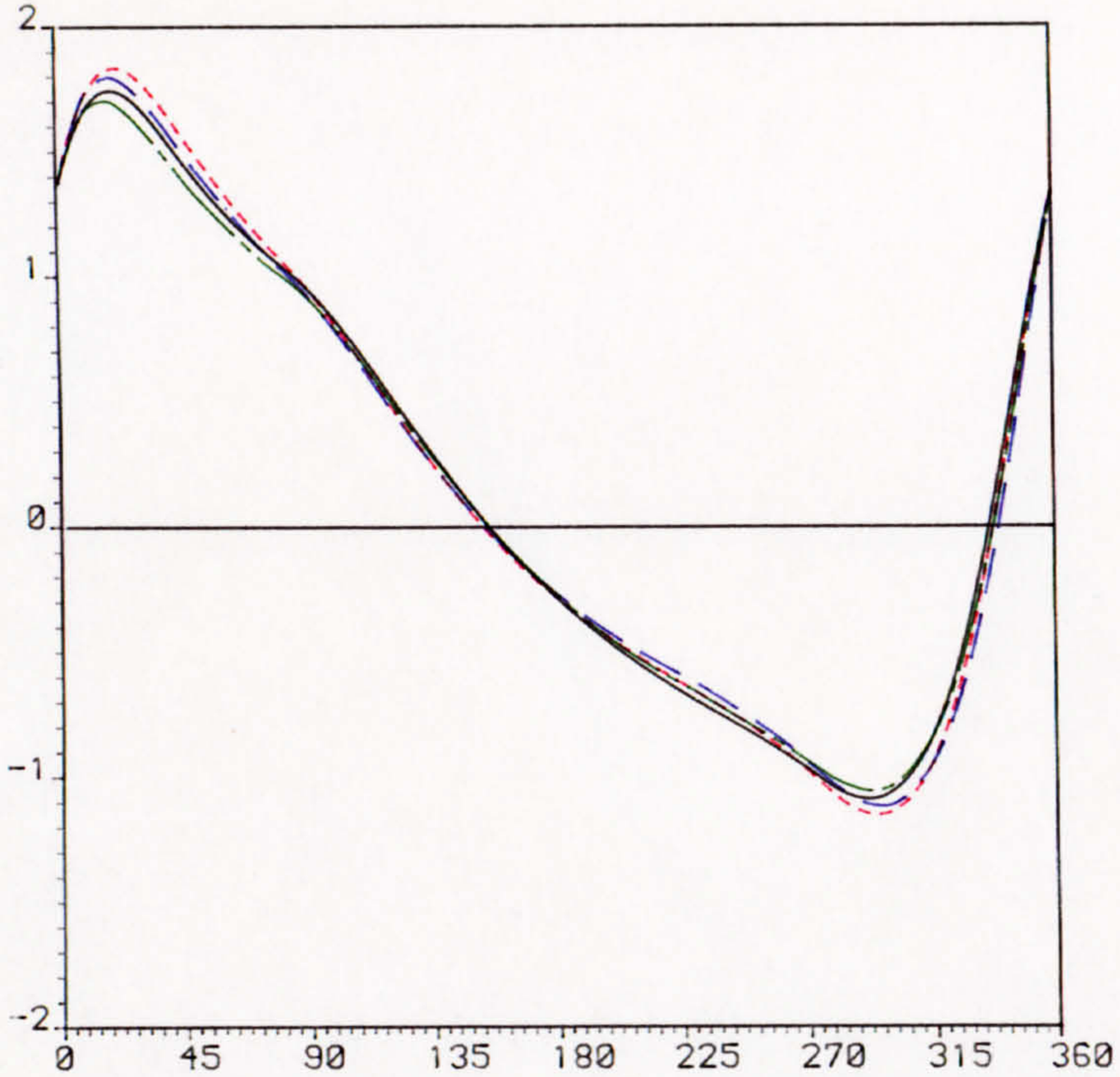

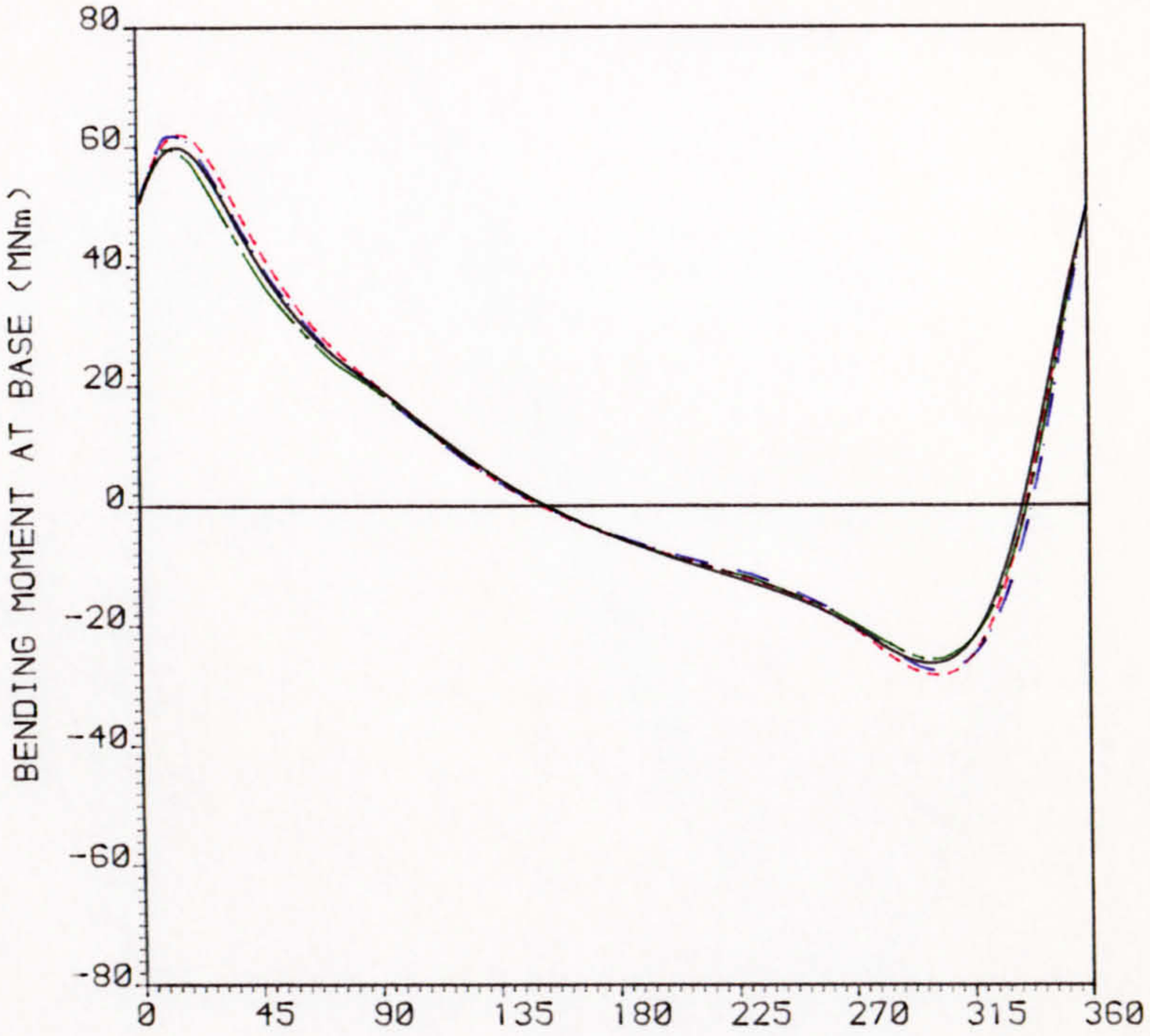

_____ 5th Order STOKES++
_ _ _ _ _ 5th Order STOKES
_ _ _ . 7th Order STREAM FUNCTION
_ _ _ _ 7th Order STREAM FUNCTION++

H= 18.76 (m)
T= 11.32 (sec)
d= 40.00 (m)
Cylinder Dia.= 3.00(m)

Cd= .70
Cm= 2.00

H/d= .47
$w^2 d/g$= 1.26

NOTE: Loads integrated up to instantaneous level of surface elevation.
++ CONVECTIVE ACCELERATION terms included

FIG2.24 HYDRODYNAMIC LOADING ON A VERTICAL CYLINDER

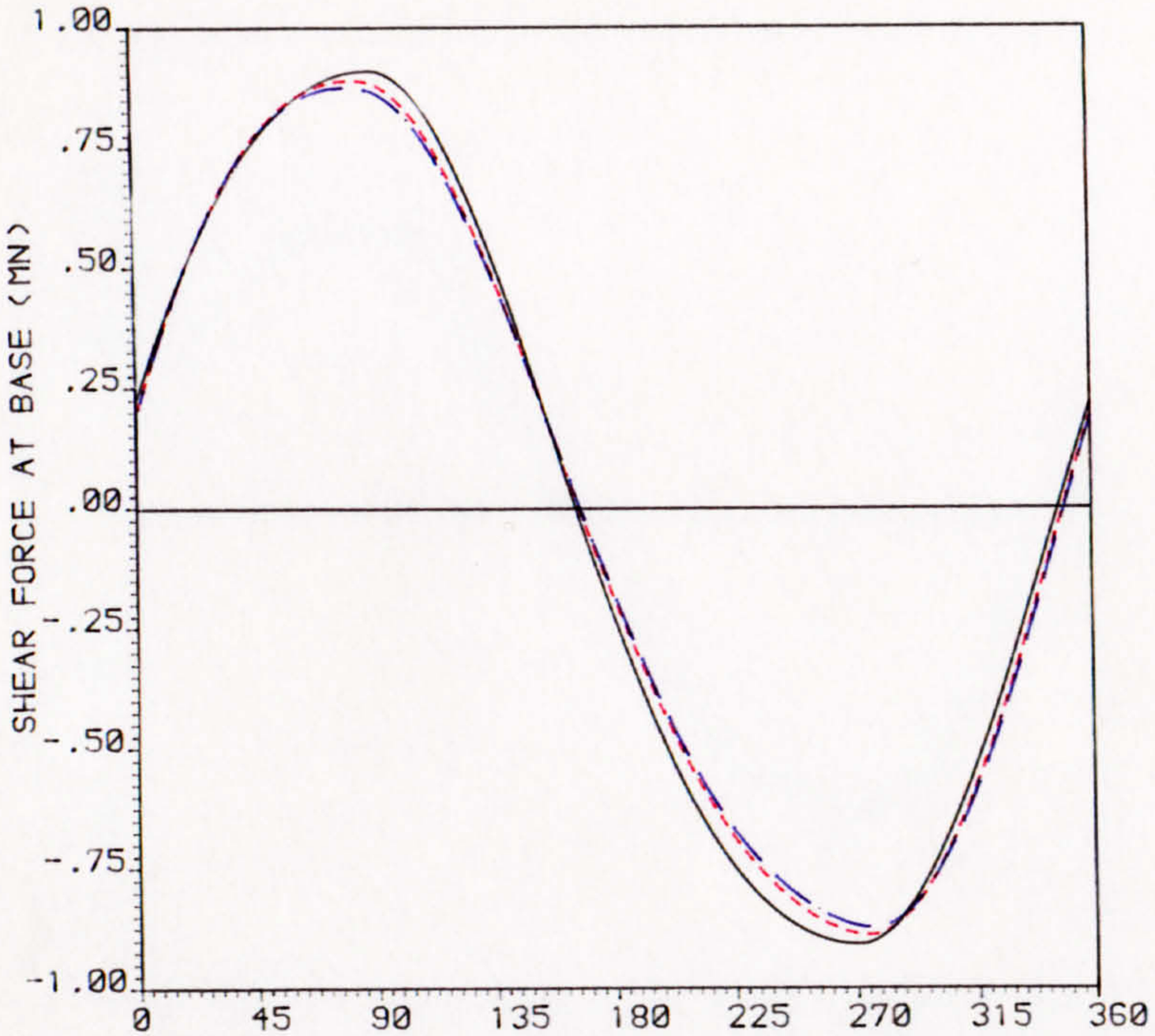

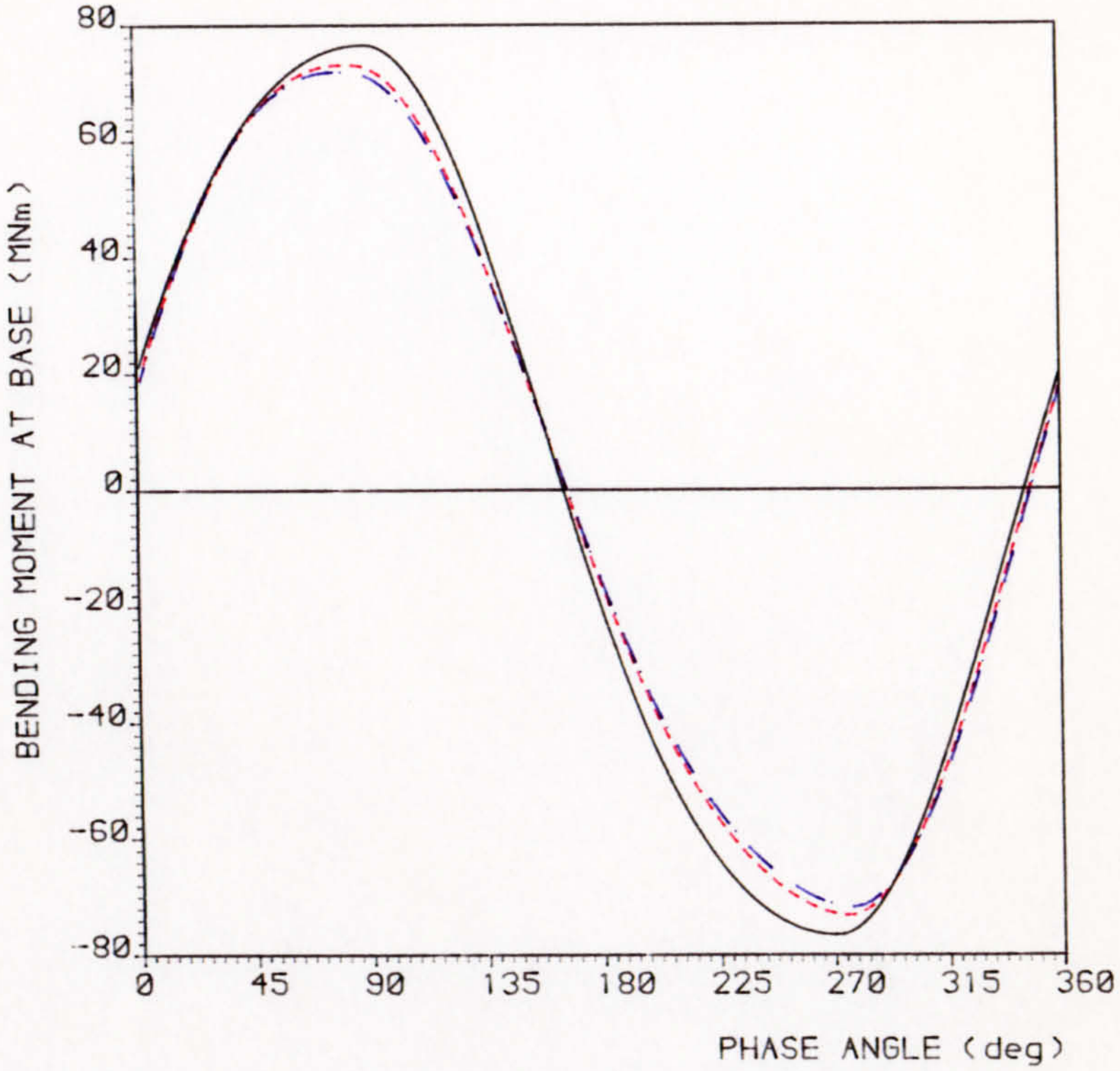

——— AIRY
------ 5th Order STOKES
— — 3rd Order STREAM FUNCTION

H= 12.80 (m)
T= 8.00 (sec)
d= 100.00 (m)
Cylinder Dia.= 3.00(m)

Cd= .70
Cm= 2.00
NOTE: Loads integrated up to M.W.L

H/d= .13
$w^2 d/g$= 6.29

FIG 2.25 HYDRODYNAMIC LOADING ON A VERTICAL CYLINDER

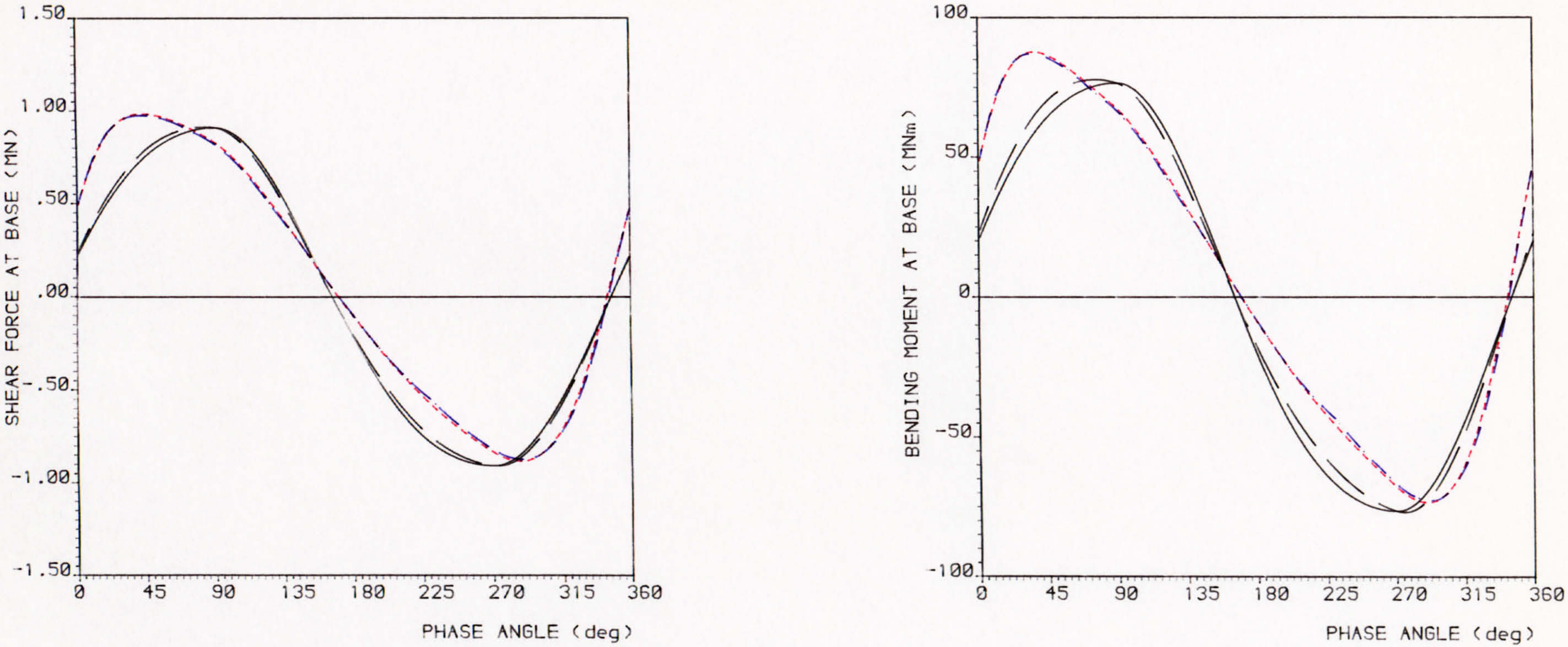

——— AIRY, ——— "Stretched" AIRY
----- 5th Order STOKES
_ _ _ . 3rd Order STREAM FUNCTION

H= 12.80 (m)
T= 8.00 (sec)
d= 100.00 (m)
Cylinder Dia.= 3.00(m)

Cd= .70
Cm= 2.00
NOTE: Loads integrated up to instantaneous level of surface elevation

H/d= .13
w^2 d/g= 6.29

FIG 2.26 HYDRODYNAMIC LOADING ON A VERTICAL CYLINDER

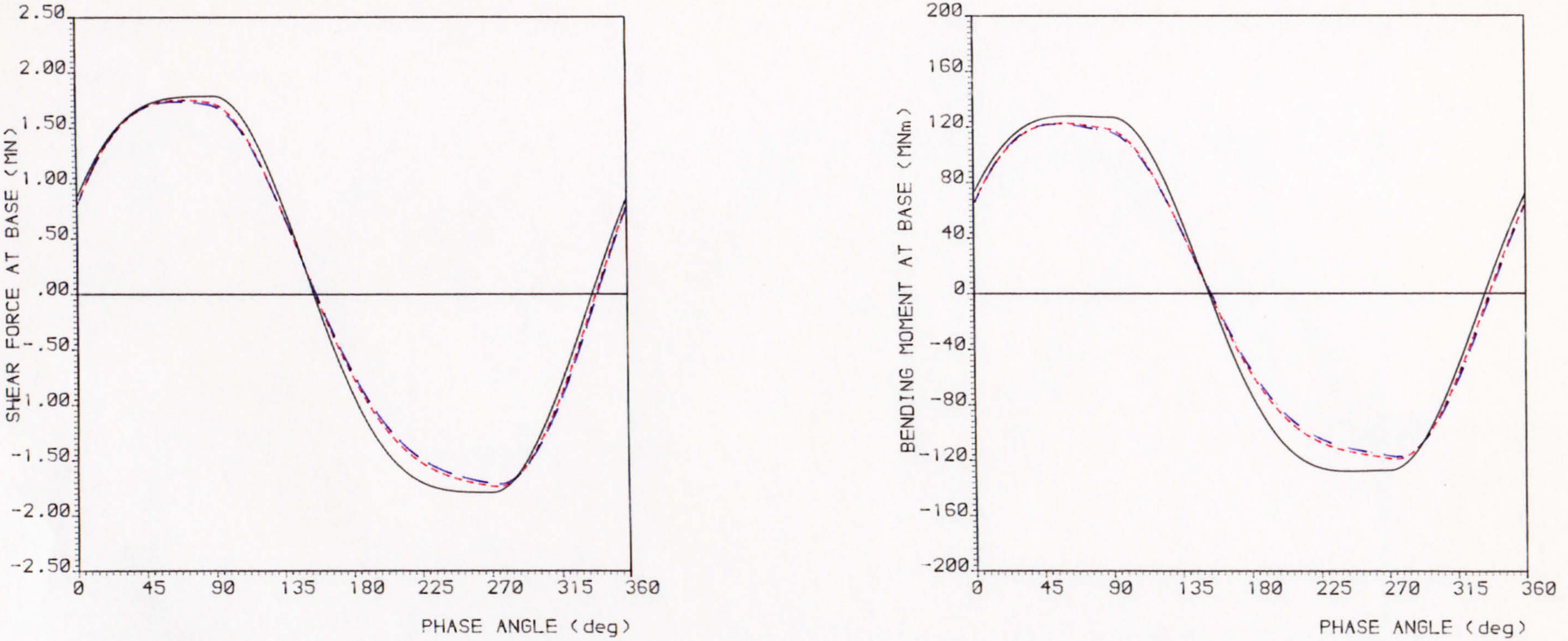

——— AIRY
..... 5th Order STOKES
_ __ . 7th Order STREAM FUNCTION

H= 25.20 (m)
T= 11.30 (sec)
d= 100.00 (m)
Cylinder Dia.= 3.00(m)

Cd= .70
Cm= 2.00
NOTE: Loads integrated up to M.W.L

H/d= .25
$w^2 d/g$= 3.15

FIG 2.27 HYDRODYNAMIC LOADING ON A VERTICAL CYLINDER

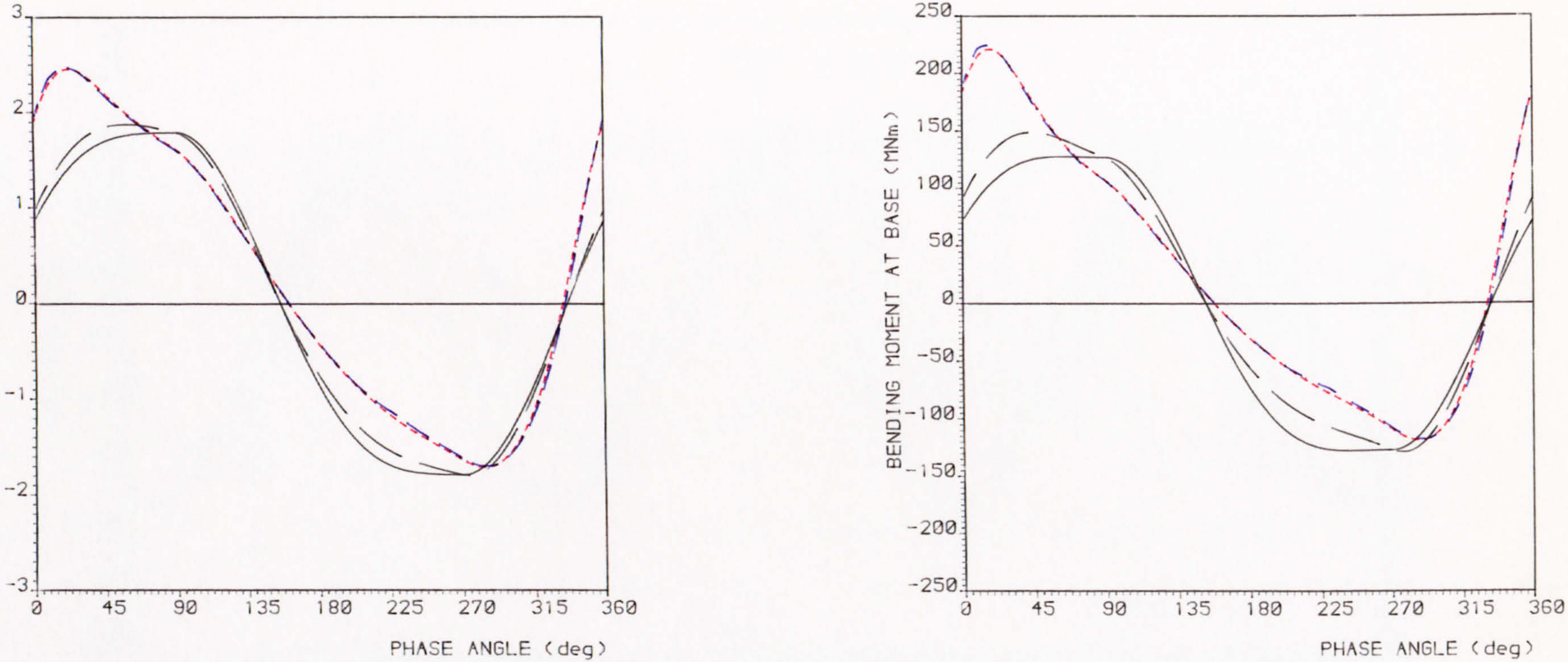

——— AIRY, __ ___ "Stretched" AIRY
----- 5th Order STOKES
_ __ . 7th Order STREAM FUNCTION

H= 25.20 (m)
T= 11.30 (sec)
d= 100.00 (m)
Cylinder Dia.= 3.00(m)

Cd= .70
Cm= 2.00

H/d= .25
$w^2 d/g$= 3.15

NOTE: Loads integrated up to instantaneous level of surface elevation

FIG 2.28 HYDRODYNAMIC LOADING ON A VERTICAL CYLINDER

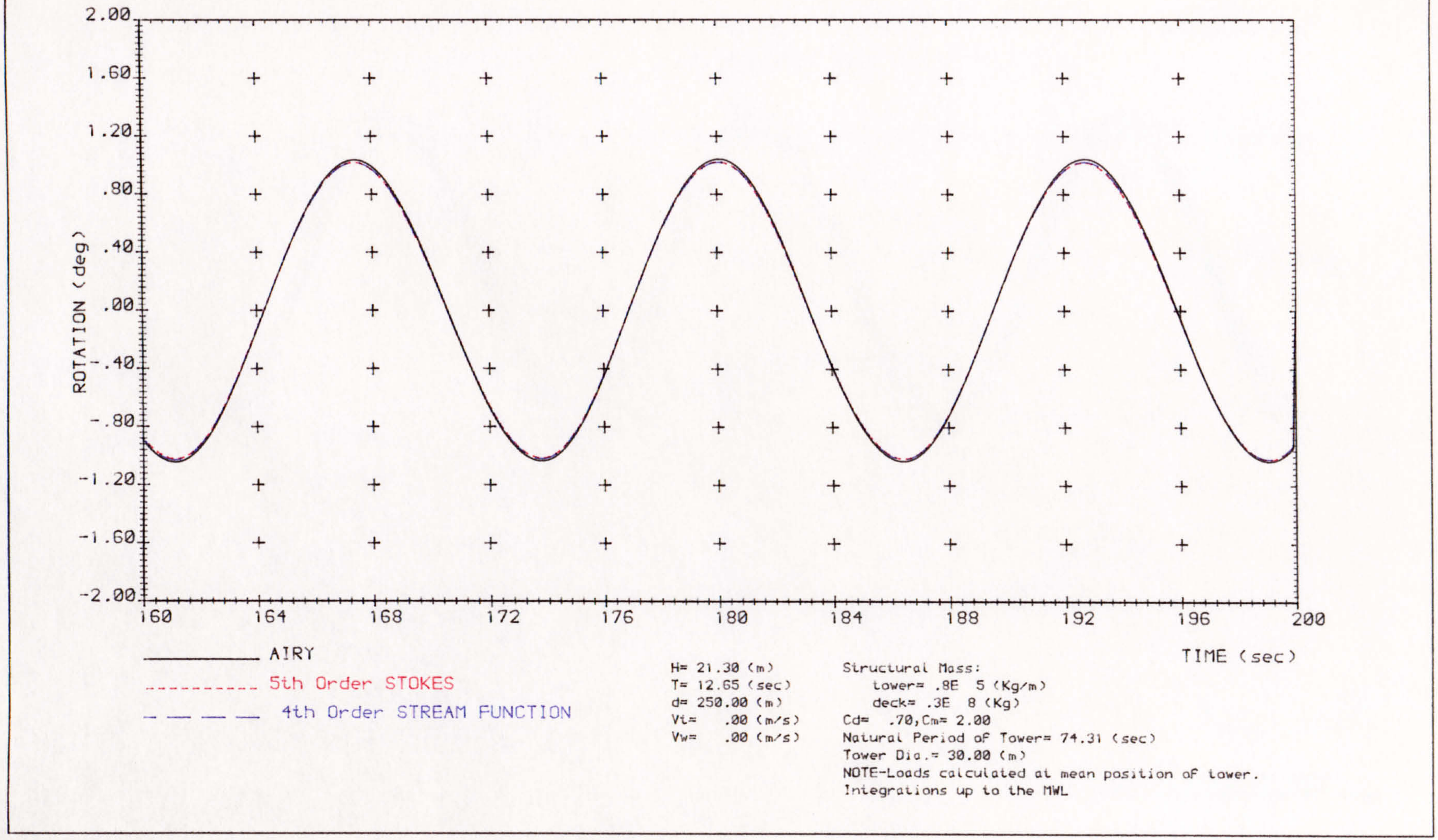

FIG **2.29** *MOTION RESPONSE OF AN ARTICULATED TOWER TO REGULAR WAVES*

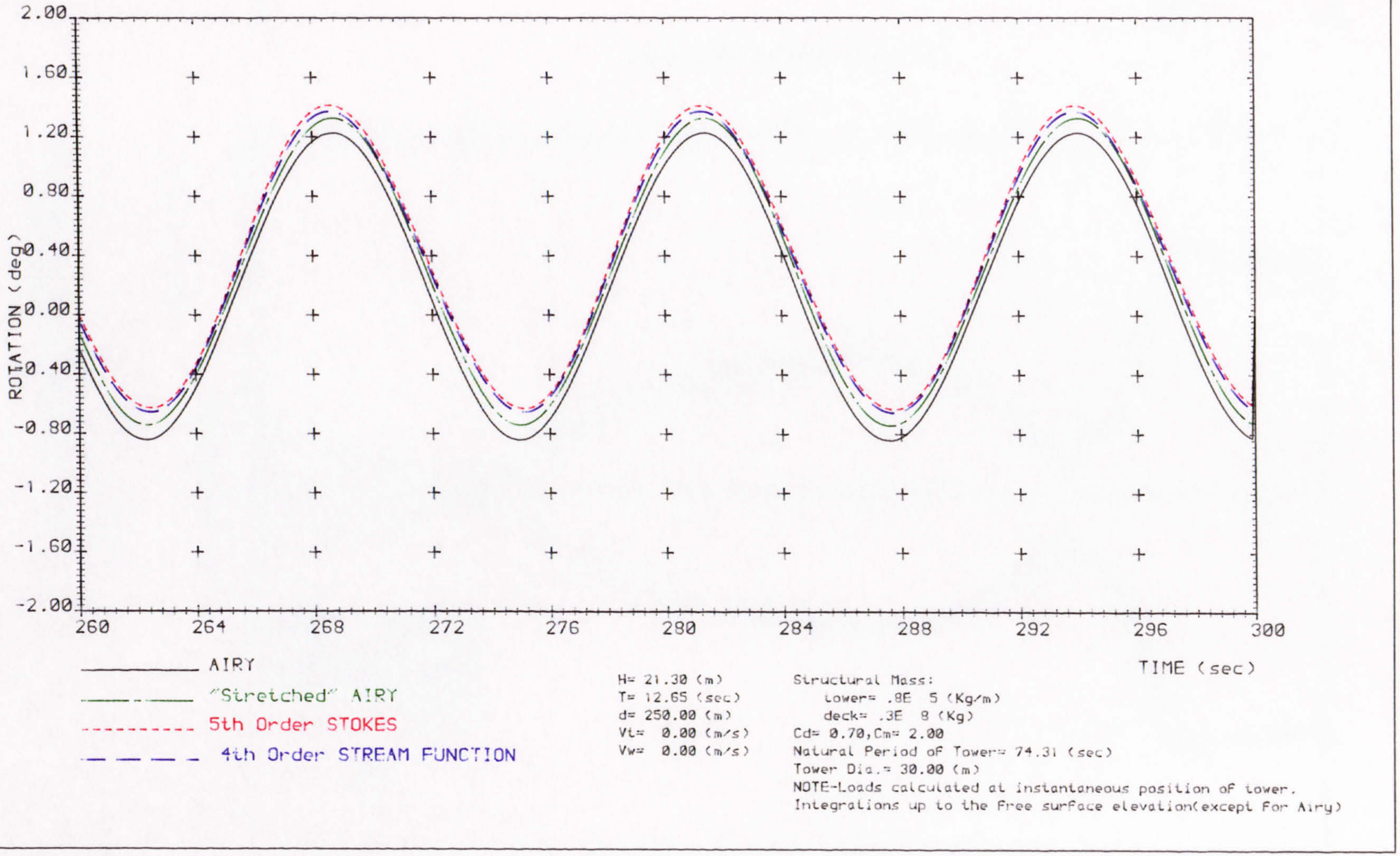

FIG 2.30 MOTION RESPONSE OF AN ARTICULATED TOWER TO REGULAR WAVES

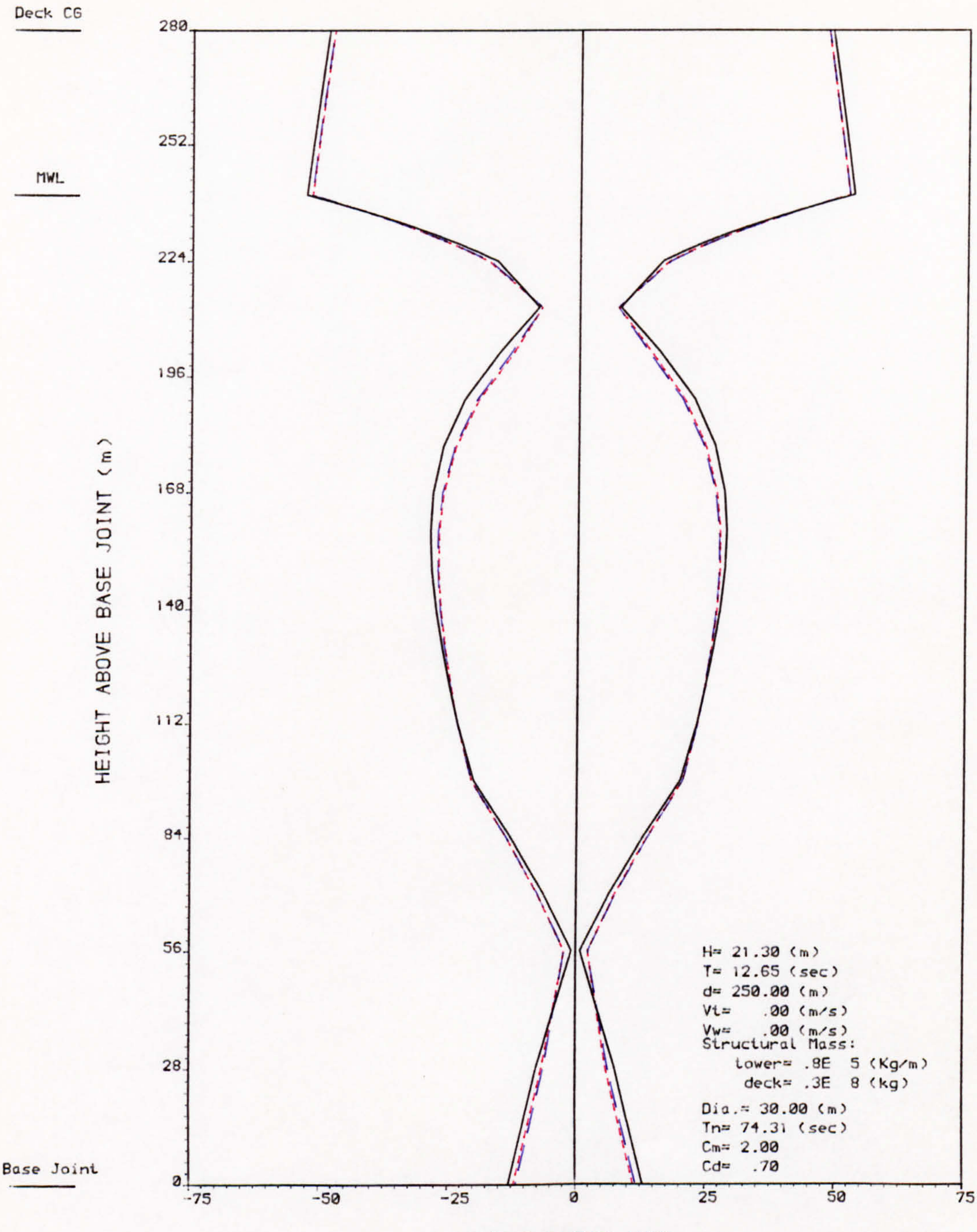

NOTE-Loads calculated at mean position of tower.
Integrations up to the MWL

FIG 2.31 DISTRIBUTION OF SHEAR FORCE ALONG AN ARTICULATED TOWER

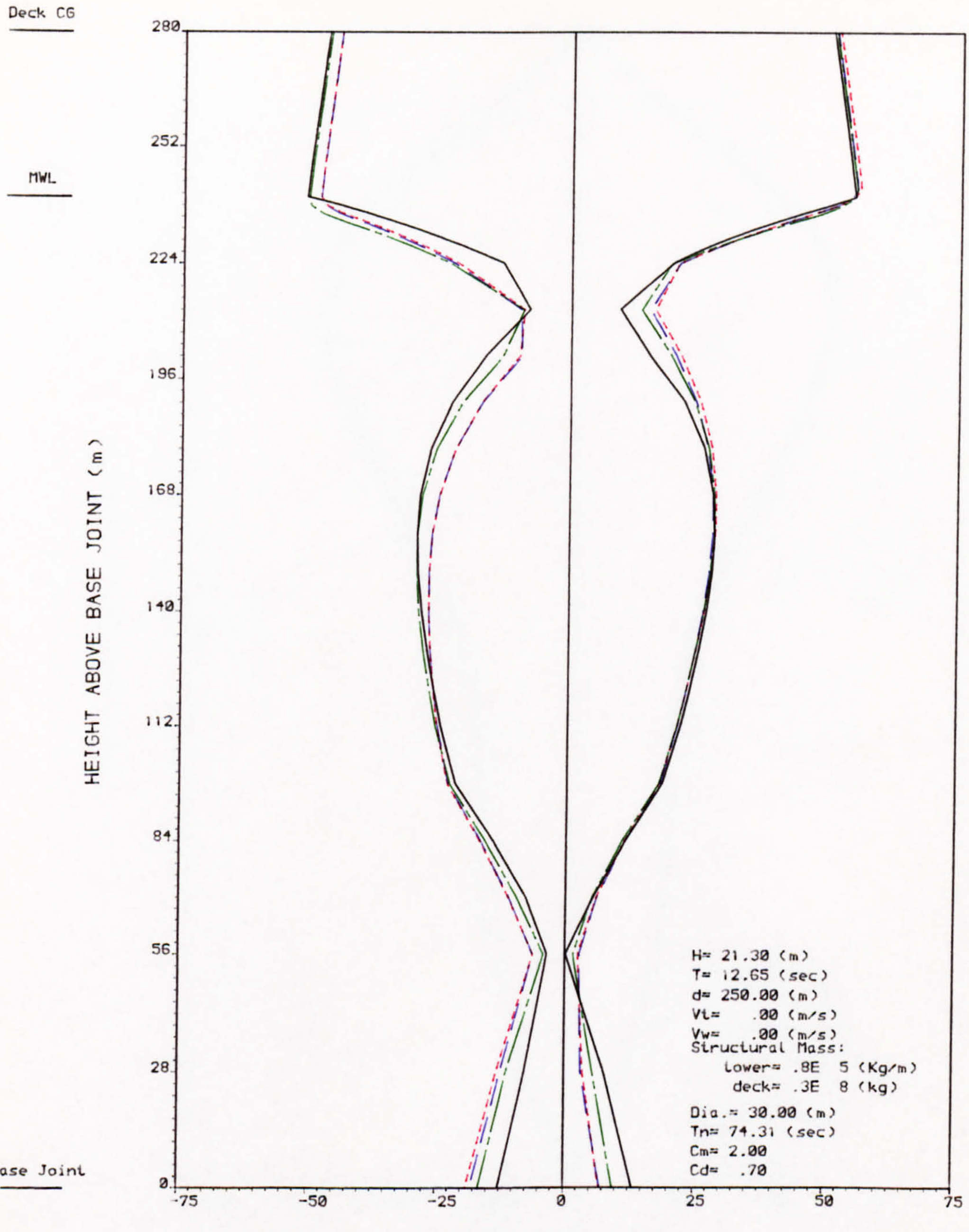

FIG 2.32 DISTRIBUTION OF SHEAR FORCE ALONG AN ARTICULATED TOWER

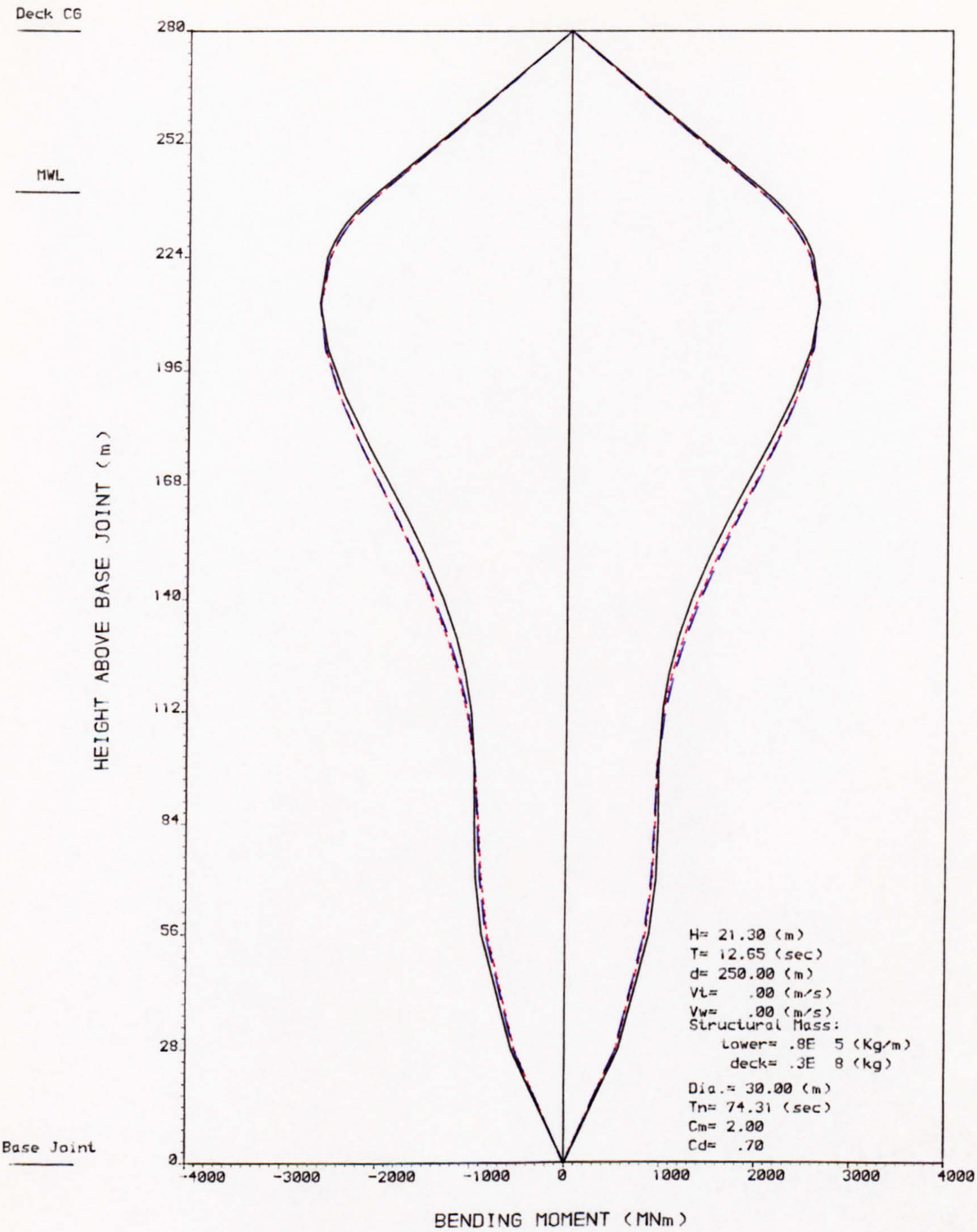

NOTE-Loads calculated at mean position of tower.
Integrations up to the MWL

FIG 2.33 DISTRIBUTION OF BENDING MOMENT ALONG AN ARTICULATED TOWER

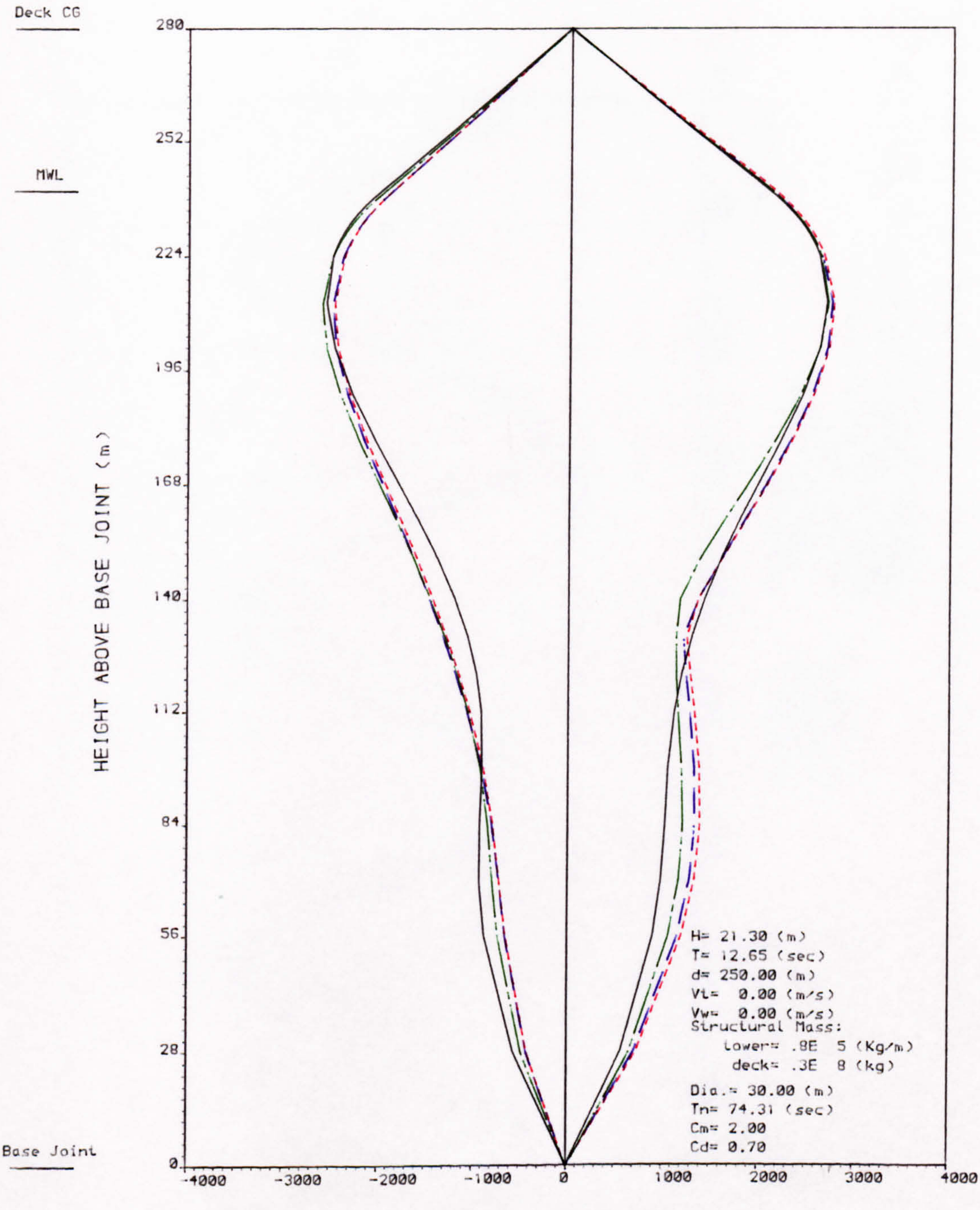

NOTE-Loads calculated at instantaneous position of tower.
Integrations up to the free surface elevation(except for Airy)

FIG 2.34 DISTRIBUTION OF BENDING MOMENT ALONG AN ARTICULATED TOWER

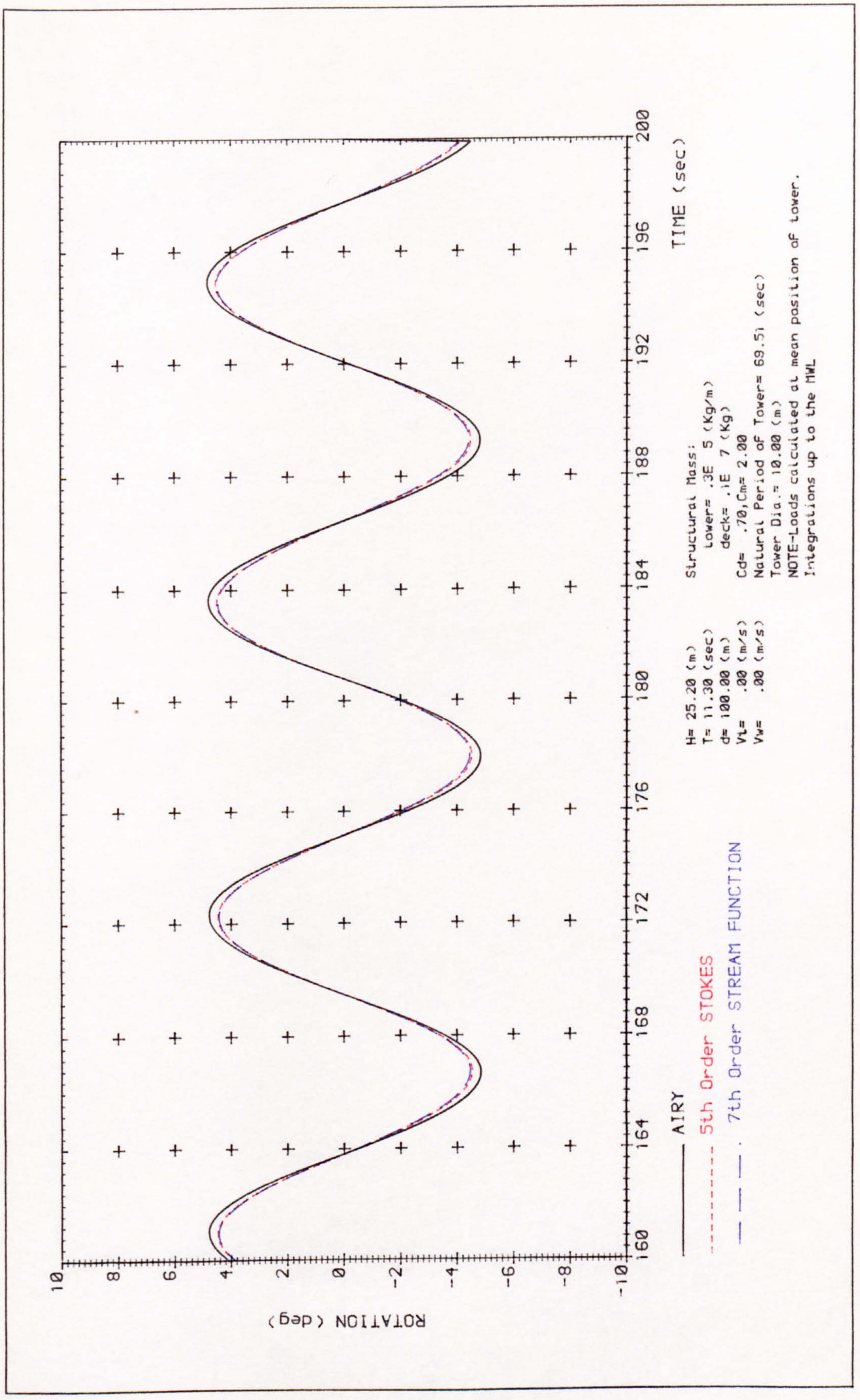

FIG 2.35 MOTION RESPONSE OF AN ARTICULATED TOWER TO REGULAR WAVES

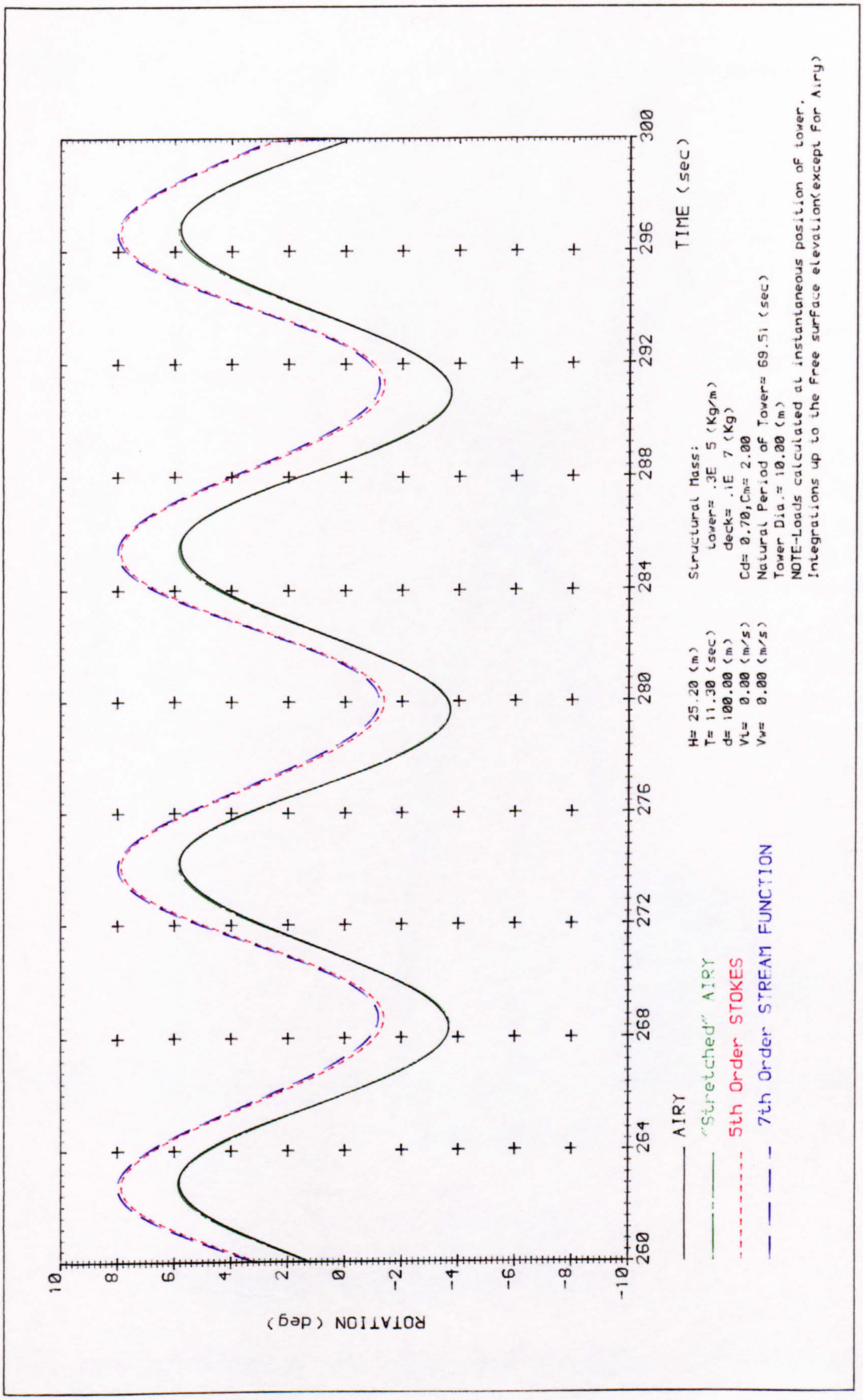

FIG 2.36 MOTION RESPONSE OF AN ARTICULATED TOWER TO REGULAR WAVES

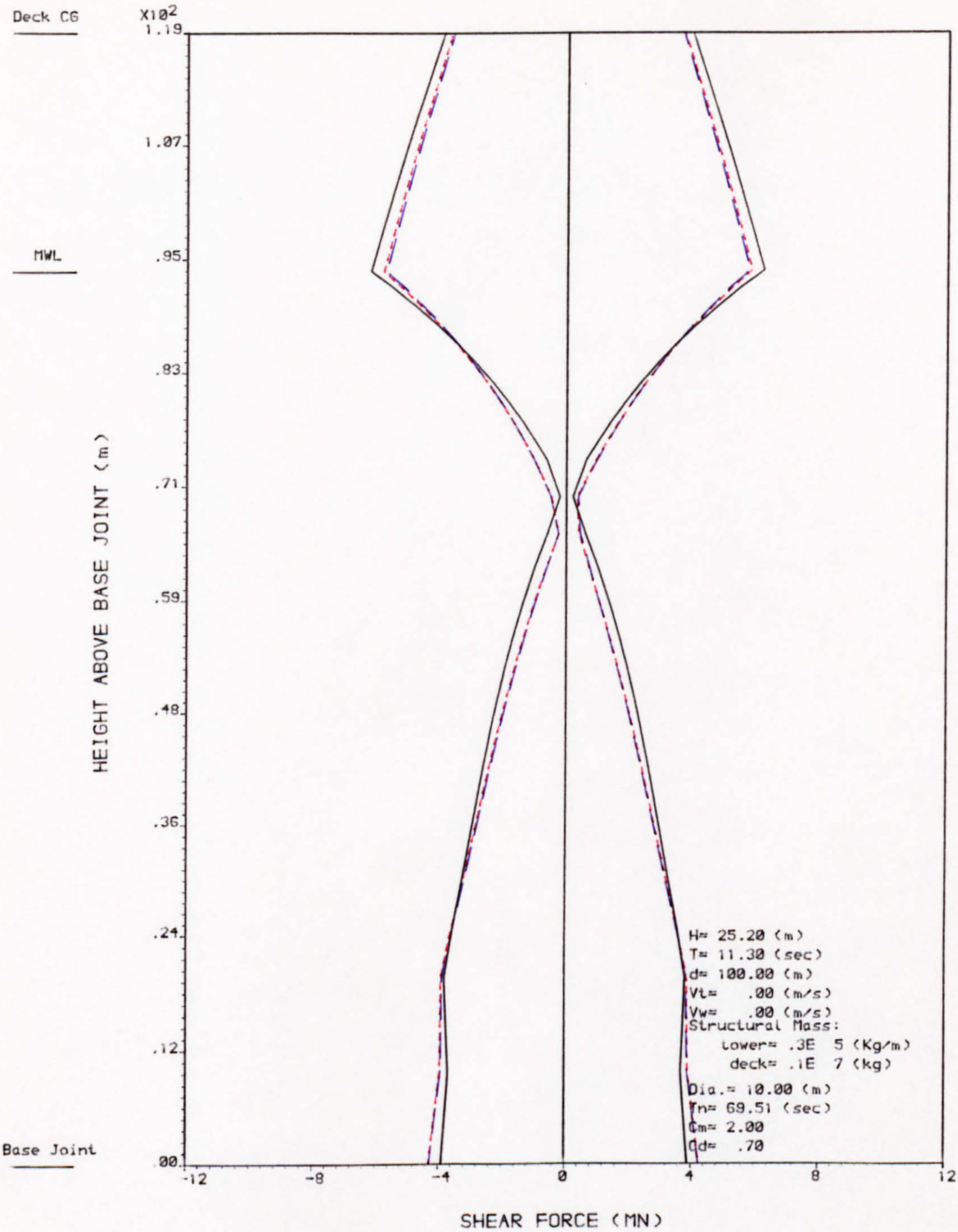

NOTE-Loads calculated at mean position of tower.
Integrations up to the MWL

FIG 2.37 DISTRIBUTION OF SHEAR FORCE ALONG AN ARTICULATED TOWER

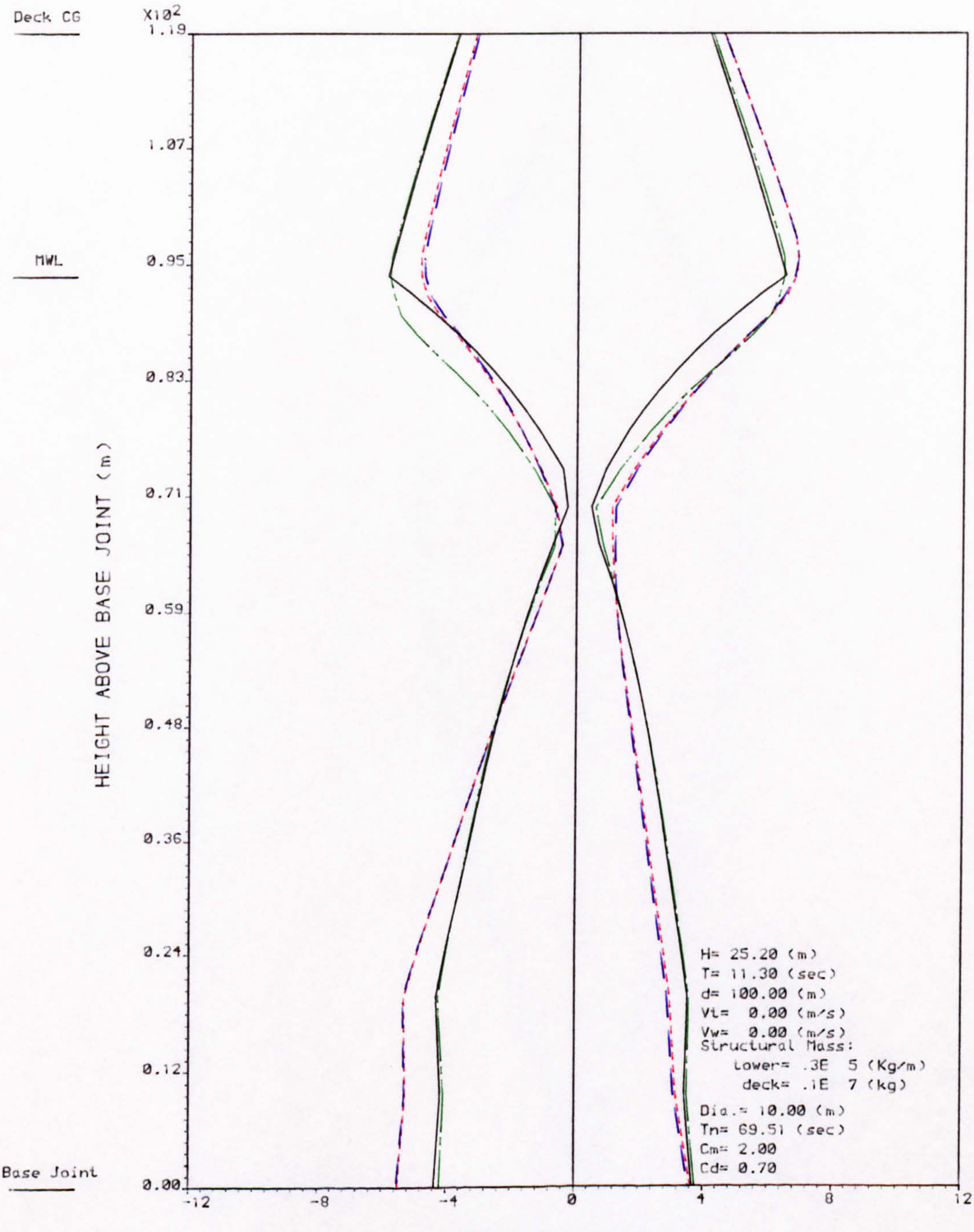

FIG 2.38 DISTRIBUTION OF SHEAR FORCE ALONG AN ARTICULATED TOWER

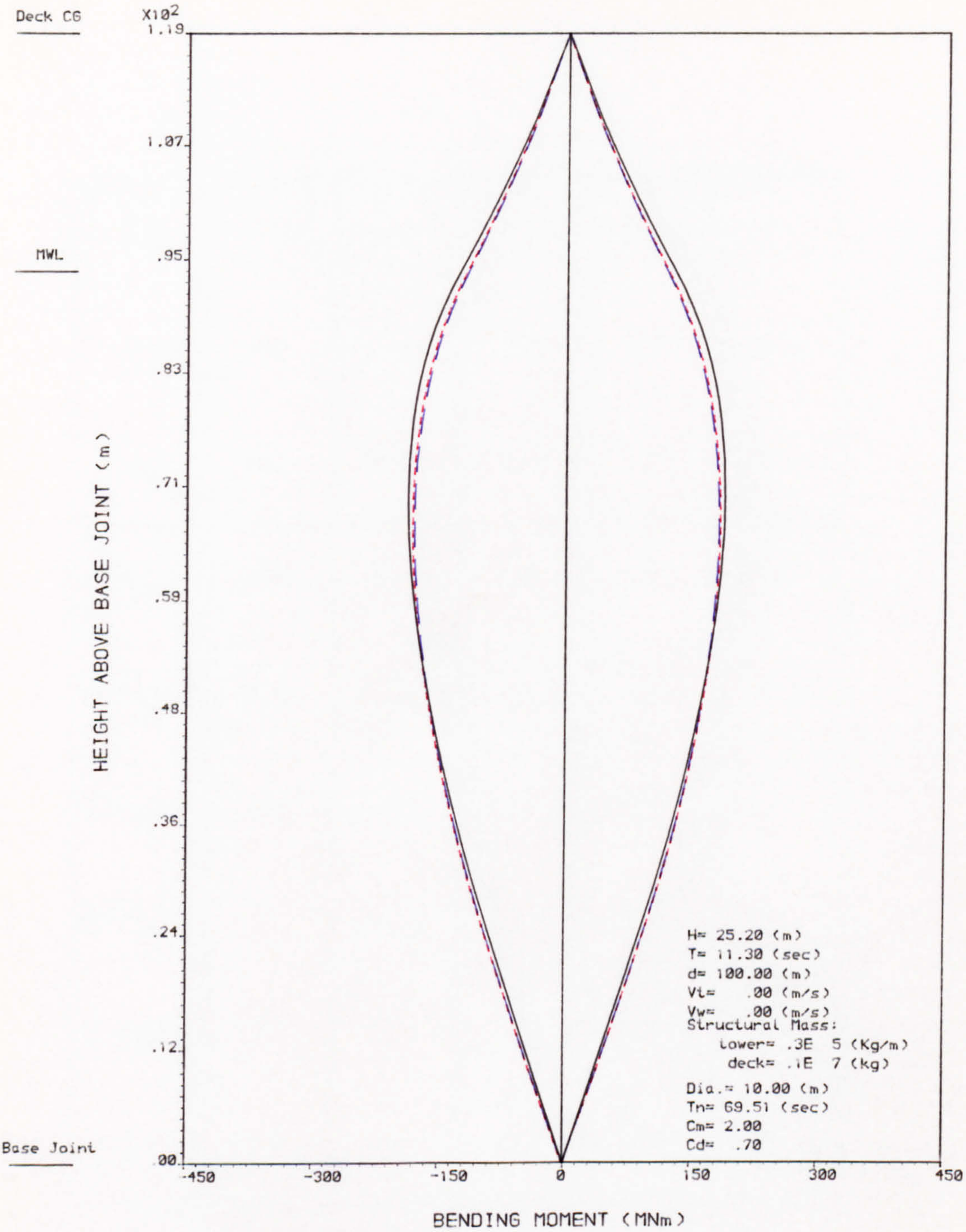

NOTE-Loads calculated at mean position of tower.
Integrations up to the MWL

FIG 2.39 DISTRIBUTION OF BENDING MOMENT ALONG AN ARTICULATED TOWER

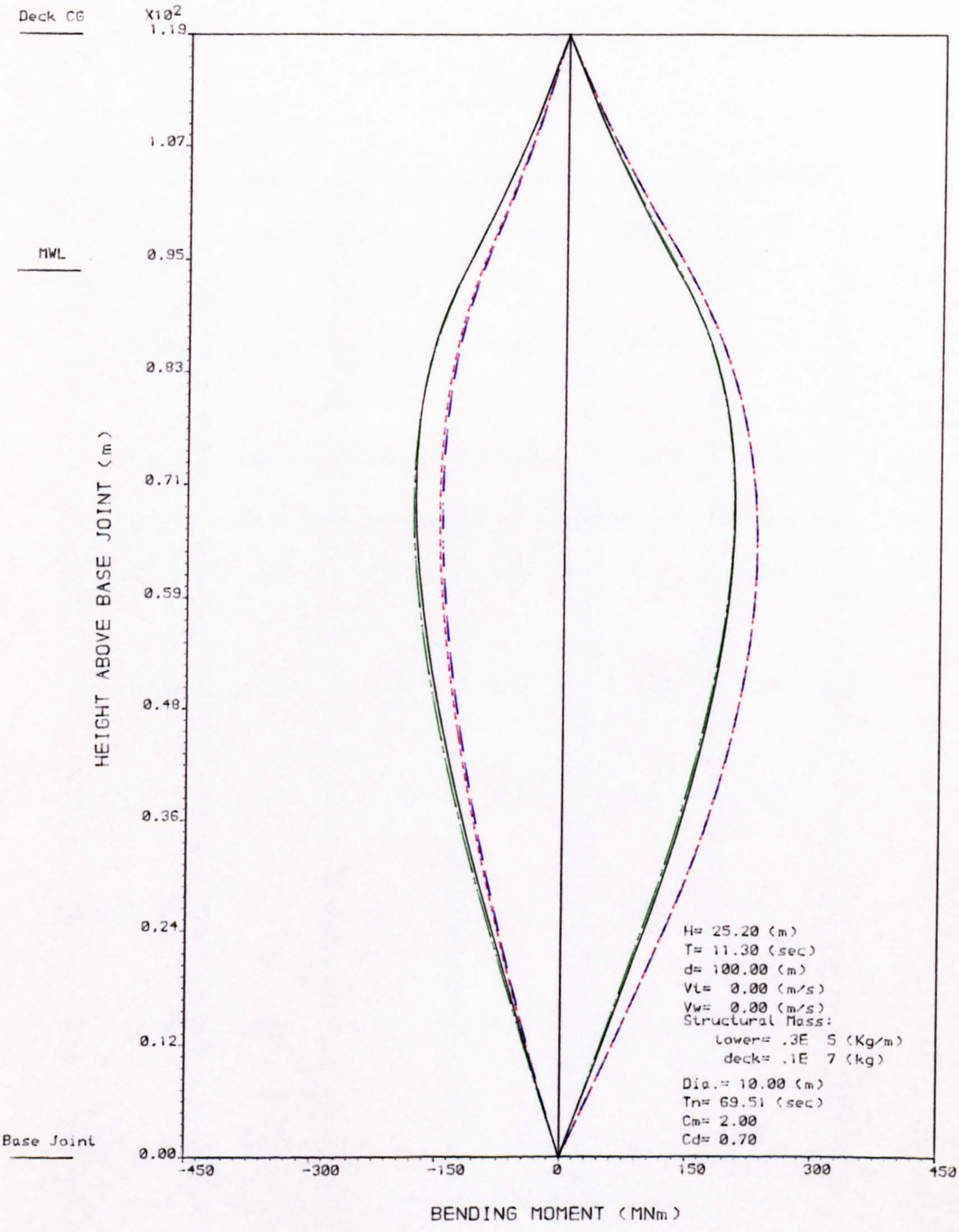

FIG **2.40** *DISTRIBUTION OF BENDING MOMENT ALONG AN ARTICULATED TOWER*

H (m)	12.8	22.0	25.2	18.76	21.3
T (s)	8.0	15.0	11.3	11.32	12.65
d (m)	100.0	70.5	100.0	40.0	250.0
(H/d)	0.128	0.31	0.25	0.47	0.085
$(\omega^2 d/g)$	6.28	1.26	3.15	1.26	6.29
(H/L) *	0.113	0.067	0.113	0.096	0.080
(L/d) *	1.1	4.6	2.2	4.9	1.1
$(H/L)(L/d)^3$	0.15	6.50	1.25	11.30	0.10
(H/H_B)	0.75	0.50	0.75	0.75	0.50

* Wave length predicted by Stream Function theory

TABLE 2.9. Dimensionless Properties of Wave Cases Considered

```
  ARTICULATED TOWER.DYNAMIC STABILITY
  ***********************************
  *Stokes 5th order wave*
 Wave ht.=25.2m,Wave period=11.30sec,Water depth=100.0m
 Structural mass= 0.255E+05Kg/m,Deck mass= 0.100E+07Kg
 Damping ratio= 0.050,Natural period= 69.5sec
 LARGEST REAL PART OF EIGENVALUES=  -0.450E-02 (SYSTEM STABLE)
*****************************************************************
*****************************************************************
FORTRAN STOP
```

```
  ARTICULATED TOWER.DYNAMIC STABILITY
  ***********************************
  *Stokes 5th order wave*
 Wave ht.=20.0m,Wave period=17.10sec,Water depth=100.0m
 Structural mass= 0.250E+05Kg/m,Deck mass= 0.300E+06Kg
 Damping ratio= 0.020,Natural period= 34.2sec
*****************************************************************
 LARGEST REAL PART OF EIGENVALUES=   0.205E-01 (SYSTEM UNSTABLE)
*****************************************************************
FORTRAN STOP
```

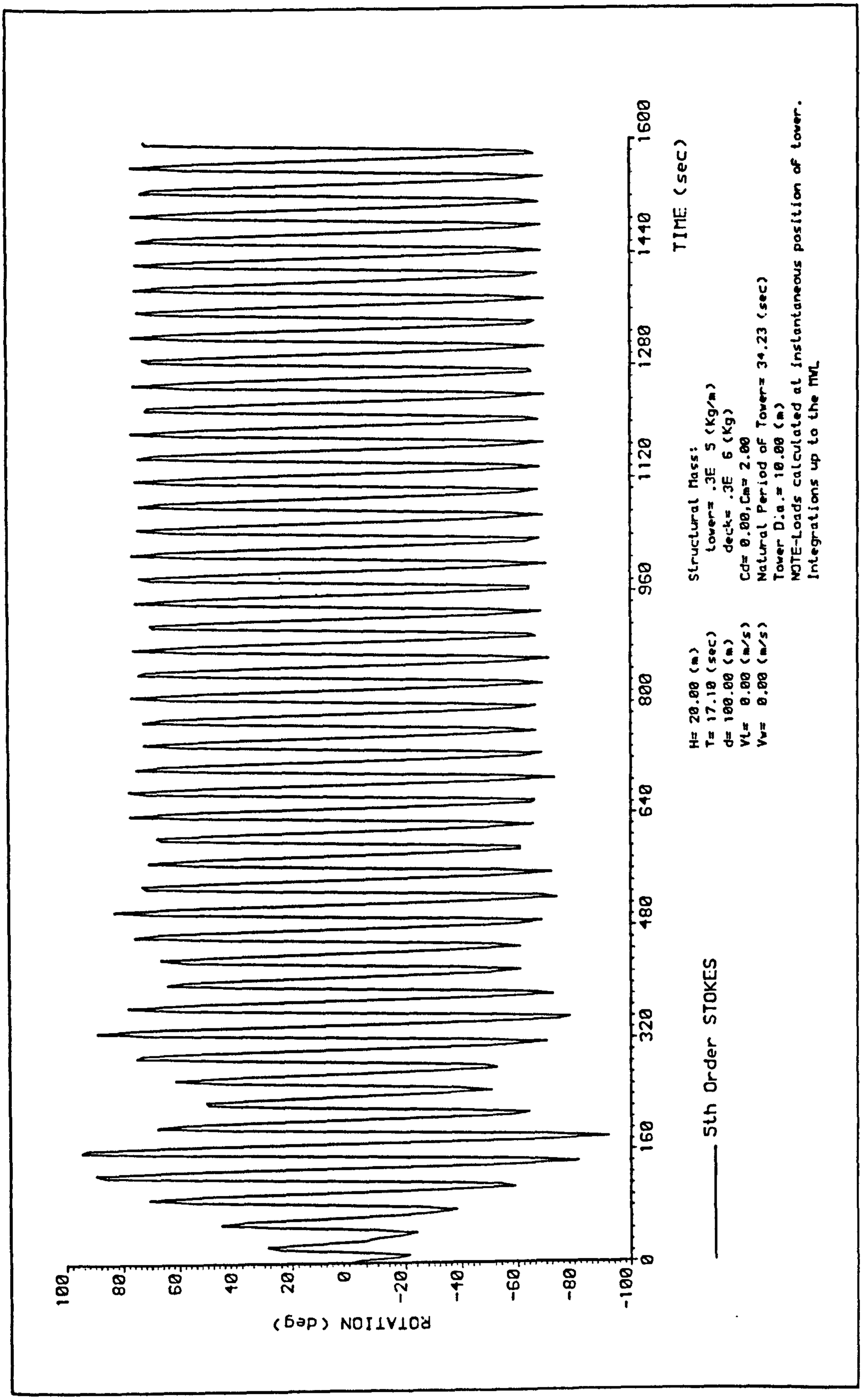

FIG 2.4 MOTION RESPONSE OF AN ARTICULATED TOWER TO REGULAR WAVES

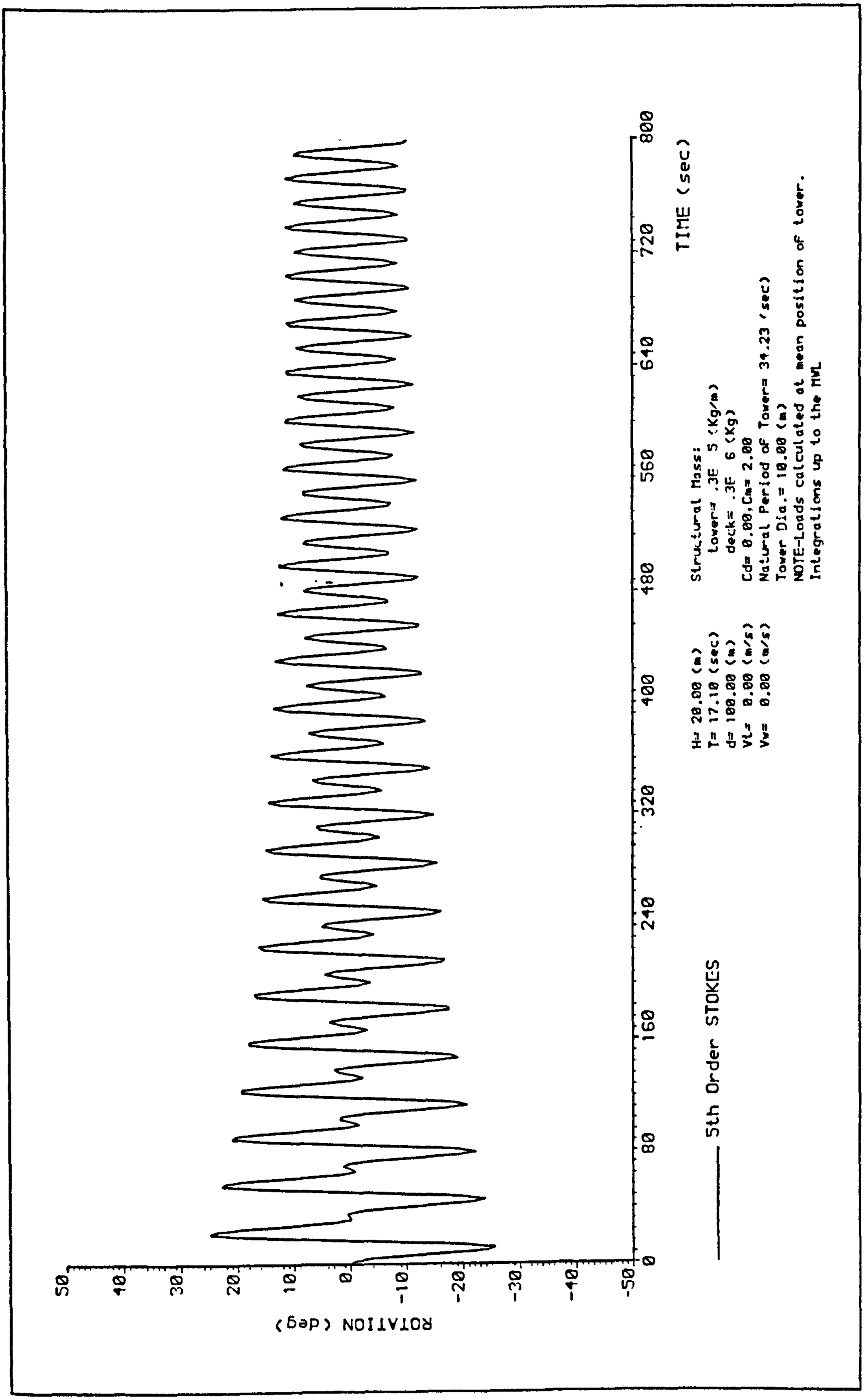

FIG 2.42 MOTION RESPONSE OF AN ARTICULATED TOWER TO REGULAR WAVES

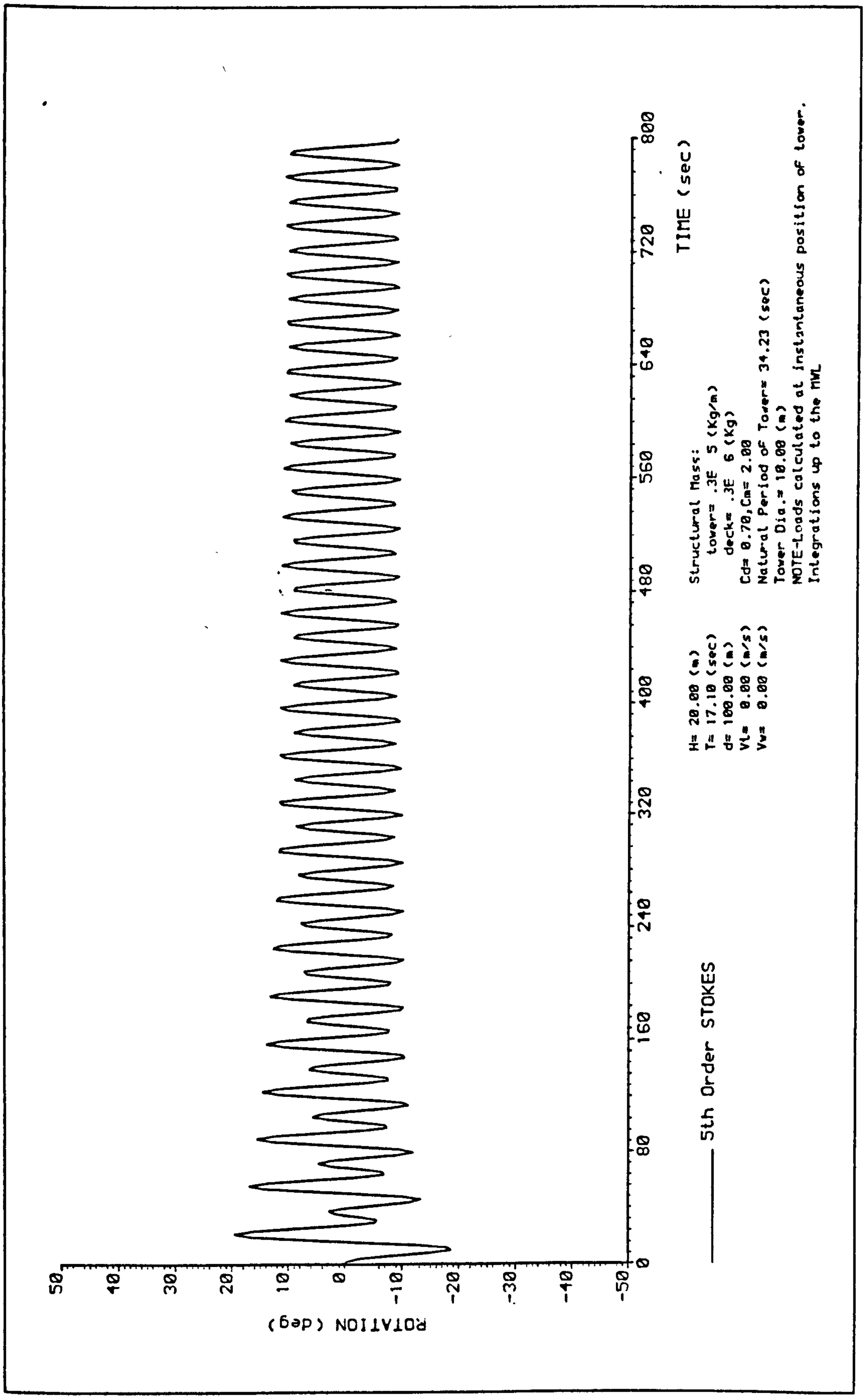

FIG 2.43 *MOTION RESPONSE OF AN ARTICULATED TOWER TO REGULAR WAVES*

2.5 DISCUSSION

(a) Comparison of Wave Forces and Wave Theories

The wave data selected in Section 2.3 were chosen from some typical fifty year storm conditions in the North Sea given by BS 6235 (7). Two computer programs, S5 and CN5, were developed to give fifth order Stokes and fifth order Cnoidal wave coefficients respectively. In program S5, due to the large values of sinh and cosh terms, use was made of a quadruple precision facility on a VAX 11/782 computer. The two parameters λ and (kd) given by equations (A.2.29) and (A.2.30) in Appendix A were calculated correct to twelve decimal places in each case. Convergence was rapid and in most cases five or six iterations were sufficient to give the required accuracy. A modified version of program S5 was used to give the wave coefficients for a variety of conditions and results are presented graphically in Appendix A, together with tables of non-dimensional wave number (kd). In program CN5 parameter m (see equation A.4.47 of Appendix A) is found using the method of bisection and is calculated accurate up to fifteen decimal places. Elliptic functions given by equations (A.4.57 - A.4.65) are calculated such that summation terms involved converge to an accuracy of fifteen decimal places. Accuracy in both programs were extended to twenty decimal places to check the values of wave coefficients but this made no contribution to the results. Stream Function wave coefficients were taken from Ref.(16). One of the disadvantages of the Stream Function method is that an explicit expression for surface elevation is not readily available (wave elevation is found numerically at points along the wave length, see Appendix A) and non-dimensional values for the surface elevation, at sixteen points along the wave length, given by Dean had to be used. When integration of loads were carried out up to the instantaneous level of surface elevation the intermediate values for wave elevation were calculated by interpolation using the subroutine E O1 AAF (65) which interpolates from

a table of function values using Aitken's technique of successive linear interpolations (see Ref.(25)).

Selection of drag and inertia coefficients was based on the results of experiments of Sarpkaya (76) who gives C_D and C_m values for cylinders in steady and harmonically oscillating flows as function of Reynold's and Keulegan-Carpenter numbers (see Fig.c1,c2 Appendix C). These experiments have been carried out in a U-shaped vertical water tunnel and the drag and inertia coefficients evaluated through the use of Fourier-averaging technique (see Ref.(75), pp.89-92). In the analysis it has been assumed that for cases considered the use of a particular wave theory does not affect the choice of values of C_D and C_m . Tables 2.1 - 2.8 show values of Reynold's number, $R_e = U_m \cdot D/\nu$, and Keulegan-Carpenter number, $K_c = \frac{U_m \cdot T}{D}$ (where U_m is taken as the maximum fluid particle velocity normal to the cylinder and ν is the kinematic viscosity of fluid taken as 1.5×10^{-6} m^2/s for sea water), calculated for the fixed cylindrical members studied here. It can be seen that due to the high values of Re ($>7 \times 10^5$) , C_D and C_m remain the same values for all cases considered here. Bishop's results (4) from the second Christchurch Bay tower agree well with Sarpkaya's results for C_D and C_m in oscillating flow and show that force coefficients do not vary with Re over the range of conditions tested (Re = 2×10^5 to 2×10^6). It is expected that as Re is increased still further the position of flow transition (from linear to turbulent) behind the cylinder becomes insensitive to changes in Re and therefore at higher Re, in the order of 10^7 as encountered here, the wake width and force coefficients are likely to remain constant, however additional experiments, although difficult to perform, are needed to evaluate the coefficients at such high Reynold's numbers.

In table 2.7 Re becomes small at very large depths which can result in a different set of values for C_D and C_m but due to the exponential decay of fluid particle

velocities and accelerations with depth the drag and inertia forces at these depths are very small. In this case at a depth of 70m velocities and accelerations are about 2% of those at the mean water level resulting in almost zero contribution to drag force and negligible effect on overall fluid inertia loading.

A great deal of uncertainty still exists when estimating values of drag and inertia coefficients. The flow conditions in the real ocean environment can significantly differ from the idealized steady, harmonically oscillating or wavy flows simulated under laboratory conditions. Measurements in the ocean environment can be very costly and accurate results are not easy to obtain or interpret. The interaction of waves and ocean currents gives rise to an even more complex flow around the structure. There is very little information available on the effect of wave-current interaction on the hydrodynamic loading of offshore structures and much investigation remains to be carried out to assess the accuracy of conventional methods of vectorially superposing wave and current velocity profiles in Morison's equation. Also orbital motion of fluid particles can result in a different set of C_D and C_m values for horizontal members in comparison to vertical cylinders. Experimental results of Maull and Norman (58) with horizontal cylinders in a wave tank, Koterayama (49) and Ramberg and Niedzwecki (72) have all been carried out at low Re and Kc values not applicable here and experiments at much higher Reynold's and Keulegan-Carpenter numbers need to be carried out.

Figures 2.3 - 2.18 show predictions of hydrodynamic loading on a fixed horizontal cylinder using various wave theories. The suitability of one wave theory over another for use in a particular engineering situation is not easy to assess. It can depend upon the environmental characteristics under consideration as well as the ease with which the wave kinematics can be estimated to the required accuracy. In addition, comparison of wave theories based on theoretical grounds may not necessarily reflect the conclusions which

might be drawn from experimental investigations carried out in the laboratory or in the ocean. Unfortunately accurate experimental results for particle velocities and accelerations under extreme design conditions and comparisons with wave theories are not available and some of the published results may be subject to instrumentation errors. For example experiments of Le Mehaute et al (56) have been criticized by other authors (see Ref.(82) and (16)) for bad use of apparatus and Chakrabarti (9) has attributed the reason for poor correlation between his wave tank results for fluid particle velocities and analytical results of Stream Function theory partly to the measuring instrument that he employed. Clearly then more accurate and extensive measurement programs are necessary in order to assess the suitability of wave theories for prediction of wave kinematics and fluid loading on offshore structures. In the absence of adequate experimental data the theoretical comparisons of wave theories by Dean (17), based on the degree to which various wave theories satisfy the free surface boundary conditions, and the range of suitability for various wave theories as suggested by Le Mehaute (55) together with site measurements of Hudspeth et al (38) and Ohmart and Gratz (66) indicate that the Stream Function wave theory can give accurate results for the intermediate and deep water conditions.

Loadings for fixed cylinders were calculated at one degree intervals in the phase plane. For the cases considered predictions of Stream Function and Stokes fifth order wave theories, despite the use of two different techniques in their development, one perturbation and the other error minimization in the free surface boundary conditions, are in good agreement. Results of field measurements by Ohmart and Gratz taken during two storms, Edith and Delia, in the Gulf of Mexico also indicate that Stokes fifth order and Stream Function wave theories would yield identical results. Since in the development of Stokes fifth order theory the higher order terms in the expressions for wave kinematics are found using a perturbation method,

for accurate results the successive terms in the derived expressions must be of an order smaller than their lower harmonic counterparts. Referring to equation (A.2.4) in Appendix A the ratio of first two successive terms can be written as $r = \lambda^2 \cdot B_{22} / \lambda = \lambda / \sinh^3(kd)$ where λ is a parameter found numerically, and therefore results are valid when this ratio becomes small. Noting that for shallow water (kd) or $\sinh(kd) \to 0$ and using the first order approximation $\lambda \simeq \frac{\pi H}{L}$ in equation (A.2.4), where L is the wave length, we have $r = \frac{1}{8\pi^2}\left[\left(\frac{H}{L}\right)\left(\frac{L}{d}\right)^3\right]$ where the term in square brackets is better known as the Ursell parameter. This shows that theoretically, results of Stokes fifth order wave theory can become inaccurate for long waves in shallow waters except for very small wave heights. The highest value of $\left(\frac{L}{d}\right)$ for the cases considered in this thesis was found to be 4.9 by the predictions of Stream Function or Stokes fifth order theories and 4.5 using predictions of fifth order cnoidal theory (indicating a 9% difference in the estimated value of wave lengths) corresponding to a wave height H = 18.76m, period T = 11.3 sec and water depth d = 40 metres. For this value of $\left(\frac{L}{d}\right)$ or lower wave length/water depth ratios, i.e. all cases considered here, the wave tank results of Iwagaki and Sakai (41) and Le Mehaute et al, as concluded by Fenton (23), suggest that stokes fifth order theory is more suitable when $\frac{L}{d} < 8$ and fifth order Cnoidal theory can be used otherwise. These agree well with recommendations of Laitone (51) on the limiting conditions for Cnoidal and Stokes waves. Therefore it seems that for the wave cases considered in this chapter the results of Cnoidal wave theory are not accurate.

Figures 2.3 and 2.4 show the horizontal components of fluid induced drag and inertia forces acting on a horizontal cylinder fixed at two various levels in the sea. The ratio $\left(\frac{L}{d}\right)$ in this case is approximately 4.6 and prediction of fifth order Cnoidal theory for the maximum drag force at a depth 15m below the mean water level gives an under-

estimation of about 14% as compared to the results given by Stream Function and Stokes fifth. For maximum inertia force the underprediction is even higher and exceeds a value of 26%. Compared to Stream Function and Stokes fifth in this case the linear (Airy) theory underestimates the maximum horizontal drag force by less than 4%, the maximum resultant force by more than 5% and overpredicts the maximum value of horizontal inertia force by about 3%. As the waves become steeper and in shallower waters predictions of the Airy theory can become less accurate. As shown in Figures 2.16-2.18 for a wave steepness of 0.11, corresponding to H = 25.2m, T = 11.3 sec and d = 100m, at a depth 15m below MWL the Airy theory gives much higher values for fluid loading on the cylinder as compared to the results of Stream Function and Stokes fifth order wave theories. The differences were found to be approximately 13.5% for maximum horizontal drag and 10% for maximum horizontal inertia forces. Note that these values correspond to a relative depth $(-\gamma_c/d)=0.15$ and that at a larger depth $\gamma_c=-20m$ differences become smaller. This is mainly due to the fact that the contributions of higher harmonics become rapidly small at large depths below MWL (see equations 2.2.15 and 2.2.16). Referring to Figure 2.13 it can be seen that the difference between predictions of Airy and higher order theories for maximum drag force acting at a relative depth of 0.1 is about 10% while at $(-\gamma_c/d)=0.2$ differences are almost zero.

Figure 2.15 shows the resultant drag + inertia force on a horizontal cylinder in deep water ($kd\simeq 5.6$ by Stream Function and Stokes fifth order theories). In this case $\cosh(ky)\simeq\sinh(ky)\simeq\frac{1}{2}e^{ky}$ and when using linear wave theory the terms for (horizontal and vertical forces)^2 as in equation (2.1.10) yield sine and cosine terms which cancel out giving an almost constant resultant force at each depth. It can be seen that in this case the Airy theory in comparison to higher order theories overestimates the resultant force by more than 5% at a depth 10m below MWL.

Figures 2.8 - 2.12 show the results when the Ursell parameter $U_R = 11.3$. As mentioned earlier at high values of U_R predictions by Stokes fifth can become inaccurate and it can be seen that deviations from the results of Stream Function theory are significant. In Figure 2.8 at relative depths of 0.25 and 0.5 predictions by Stokes fifth for maximum horizontal drag force is about 5% higher than the results obtained by Stream Function. However differences are less for maximum horizontal inertia and resultant forces as shown in Figures 2.9 and 2.10.

The inclusion of convective acceleration terms in the expression for inertia force in Morison's formula was investigated for the cases mentioned above using Stream Function and Stokes fifth order theories. It was found that for two cases with $U_R = 0.15$ and 1.25 (see table 2.9) the convective acceleration terms made virtually no contribution to the values of horizontal inertia and resultant forces acting on the horizontal cylinder. Also for the case with $U_R = 6.5$ inclusion of these nonlinear terms reduced the maximum horizontal inertia force for both $Y_c = -15\,m$ and $-30\,m$ by only 2% as shown in Figure 2.6, and the maximum resultant force was reduced by an even smaller amount. For a more extreme case with $U_R = 11.3$, as shown in figures 2.11 and 2.12, neglecting convective acceleration terms resulted in higher, although not more than 5%, values for the maximum forces. Therefore for the cases considered it is shown that convective acceleration terms in the Morison's equation have little effect on the values of maximum fluid induced inertia and resultant forces acting on a fixed horizontal cylinder, however for highly nonlinear waves with large Ursell parameters ($U_R > 11$) such effects can become significant.

Apart from the estimation of maximum wave loads on structural members, determination of the stress ranges that structural elements may undergo becomes important in design. In the deterministic approach to fatigue damage calculations it is usually assumed that the equation

characterizing the fatigue behaviour under constant amplitude loading includes the stress range raised to a power, say q, taken from S-N curves (see for example ref.(33) pp.269-273). For the types of welded steel joints typically used offshore BS 6235 gives average values of 3 and 3.5 for the parameter q, and therefore errors in estimating stress ranges can significantly affect the calculations involved in assessment of fatigue damage. For example if q = 3 and the stress range is underpredicted by 5% then using Miner's rule the contribution of that particular wave component to fatigue damage would be under-estimated by nearly 16%. For the fixed horizontal cylinders studied the Airy theory invariably overpredicted the force range compared to the results by Stokes fifth and Stream Function. In the worst case (see figure 2.8) the differences for estimation of the range in horizontal drag force exceeded 26%. Assuming a linear relationship between force and stress, this alone can result in more than 100% error in the estimated contribution to fatigue damage by this wave component. For the same case the differences between predictions by Stream Function and Stokes fifth are about 22% in this respect. Figures 2.6, 2.7, 2.11 and 2.12 show the effect of including the convective acceleration terms in Morison's equation on the calculated force range. In figure 2.12 at $\gamma_c = -10$ m the range is about 8% less when the total acceleration of the fluid is considered indicating that although in some cases convective terms have little influence on values of maximum loads their effect on values of stress range can become significant. However it must be pointed out that the overall effect of such errors in the calculation of fatigue damage is not easy to assess and depends on the particular long term wave histogram, i.e. the number of waves. Also it is emphasised that although Airy theory may often overpredict the stress range, when the fundamental frequency of the structure lies close to a multiple of the exciting frequency then the higher wave harmonics may cause resonant vibrations which in turn may lead to even higher stress levels not predicted by the Airy theory.

Figures 2.19 - 2.28 show the hydrodynamic loading on a 3m diameter fixed vertical cylinder. These results, showing the shear forces and bending moments at the base, can give an indication of the differences in predicting fluid loading on vertical legs and piled foundations of a fixed offshore platform using various wave theories. Again results of Stream Function and Stokes fifth show good agreement and for the cases studied the differences in estimating maximum loads were less than 4%. Integration of drag force terms along the cylinder was carried out numerically using Simpson's rule. For all cases and when integration of loads were carried out up to the MWL only, the results of Airy theory for maximum fluid induced base shear force were in good agreement with predictions of Stream Function and Stokes fifth with differences less than 6%. For values of maximum bending moment differences were slightly higher and for the worst case (see figure 2.22) there was an underprediction of about 7.5% by the Airy theory. Differences between the results of 'stretched' Airy theory and other methods were found to be high when integration of loads were extended to the surface elevation. In all cases results of 'stretched' Airy method were lower than those predicted by Stream Function and Stokes fifth. For the maximum shear force these underpredictions varied from 7% (figure 2.26) to more than 34% (figure 2.23). For maximum bending moments the corresponding differences are even larger and range from 12% up to about 67%. Extension of load integrations to the level of the wave elevation had a marked effect on all results. For example referring to figures 2.27 and 2.28 we can see that when loads are calculated up to the free surface level predictions by Stream Function theory for maximum shear force increase by more than 43% and the value of maximum bending moment is almost 80% higher. Similarly for the worst case, as shown in figures 2.22 and 2.23, results of Stream Function theory differ by almost 50% for maximum shear force and 100% for value of maximum bending moment. Note that in this case

the wave height is almost half the water depth ($\frac{H}{d}=0.47$) resulting in such high differences when integrations are extended to the surface elevation. If results of Airy theory (calculations up to MWL) and Stream Function theory (integrations up to wave elevation) are compared for this case the difference in prediction of maximum shear force is about 52% and for maximum bending moment reaches a value of 132%. It is pointed out that the accuracy of nonlinear wave theories for particle velocities and accelerations under wave crests and troughs is not exactly known. On a theoretical basis Chaplin and Anastasiou (12) compared the predictions of Stream Function and Stokes fifth order theories for horizontal velocity and vertical acceleration at the crest level of the steepest wave in deep water to values of wave celerity and $(-\frac{1}{2}g)$ respectively since, as suggested by Stokes (79), a suitable criterion for the highest wave is that the crest particle velocity reaches wave celerity and any further increase in height i.e. increase in particle velocity will cause the crest to spill or topple. Their comparisons show that both wave theories underestimate the crest horizontal velocity and vertical acceleration. However the errors diminish rapidly away from the surface. In contrast Gudmestad and Connor (31) with reference to experimental results of Nath and Kobune (63) and Delft Hydraulics Laboratory (18) suggest that Airy, Stream Function and Stokes higher order wave theories overpredict the values of horizontal crest velocities and underestimate the corresponding values under wave troughs in deep water. Clearly more experimental data using accurate measurement techniques are required to establish the validity of predictions of nonlinear wave theories for particle velocities and accelerations near the free surface zone. Large differences found in estimated values of maximum shear force and bending moments here show that the important effect of variable submergence cannot be ignored and it can be a major factor in offshore design. The importance of load range in connection with fatigue analysis

was mentioned earlier. Integration of loads up to the instantaneous level of wave elevation showed large increases in the values of load range. Comparing predictions of Stream Function theory in figures 2.22 and 2.23 the difference between values of shear force range is about 28% and that of base moment exceeds 52%. Integration of loads up to the surface elevation, as pointed out by Basu and Jain (3) can also lead to occurence of superharmonic resonant excitations at frequencies equal to multiples of the wave frequency which in turn induce higher stress levels and more fatigue damage.

Figures 2.21 and 2.24 show the effect of convective accelerations terms on fluid loading on a vertical cylinder when loads are integrated up to the free surface level. For the worst case (figure 2.24) studied inclusion of total acceleration terms in the fluid inertia force of Morison's equation reduced the maximum values of shear force and base moment by less than 6%.

b. <u>Articulated Column</u>

Figures 2.29 - 2.40 show the results of computer programs ALT1 and ALT2 for the articulated column. The equation of motion was solved in the time domain by calling the subroutine $D_{O2}BBF$ (65) which uses a variable step - variable order Runge-Kutta-Merson algorithm for time integrations. In order to reduce the initial transient oscillations the wave height was gradually increased from zero at t = 0 to its value H at t = 40 seconds. The simulation was then carried further until transients died out. Damping ratios $\left(\frac{C}{2\sqrt{I \cdot K_0}}\right)$ of 10m and 30m diameter towers for cases considered were found to be 0.05 and 0.28 respectively. The largest diffration parameter (tower diameter/wave length ratio, D/L) for the cases considered was found to be 0.11. Since a value $\frac{D}{L} = 0.2$ can be taken as a limit above which diffraction effects become important (see for example Ref.(75)) it was assumed that scattering of incident waves due to presence of structure is negligible.

Figure 2.29 shows the response of an articulated tower to a regular wave (with no current) using predictions of Airy, Stream Function and Stokes fifth order wave theories with loads integrated up to MWL only. This case represents a relatively low wave height in deep water conditions with $(\frac{H}{d})=0.085$, $(\frac{L}{d})=1.1$ and Ursell parameter $U_R \simeq 0.1$ and as can be seen there is good agreement between results of Airy and nonlinear theories considered here. Note that where it is suggested that loads are integrated up to MWL, the effect of variable submergence on the restoring buoyancy moment and added inertia terms (see equations 2.2.8 and 2.2.9) have also been excluded. Figure 2.30 shows the steady state response when variable submergence effects are taken into account and loads are calculated at the instantaneous position of tower. Agreement between results of 'stretched' Airy, Stream Function and Stokes fifth order theories are within 2-4% however differences with predictions of linear wave theory are large. In this case 'stretching' of Airy theory increases the maximum response by about 28% and comparing results of Stream Function theory in figures 2.29 and 2.30 there is an increase of about 34% in the value of maximum steady state response. The increase appears in the form of a mean offset about the initial undisturbed position of the tower. Note that there is no current acting and that this offset is partly caused by calculation of loads at instantaneous location of tower since results of Airy theory (with integrations up to MWL only) show a similar trend. The reason for such offset can be attributed to additional terms with non-zero averages, which are introduced into the equation of motion when nonlinear effects are included. A perturbed solution to a single degree of freedom dynamical system with a time varying stiffness (see Hooft (35)) also shows that such effects can give rise to oscillations at a zeroth multiple of exciting frequency. Comparing results of Airy theory in figures 2.29 and 2.30 we can see that for this case the mean offset increases the maximum response by more than 17% therefore although the maximum tower displacement

(about 5m at MWL) is less than 2% of the wave length (266m by prediction of Stokes fifth), calculation of loads at the instantaneous position of the tower can have a significant influence on the maximum response. For D = 10m, as shown in figures 2.35 and 2.36, using Airy theory this offset implied an increase of about 20% in response while the maximum tower displacement at MWL is less than 4% of wave length. Comparing figures 2.35 and 2.36 it can be seen that maximum response, as predicted by Stream Function theory, becomes more than 75% higher when nonlinear effects of variable submergence and tower position are taken into account.

Figures 2.31 - 2.34 show the distribution of extreme shear force and bending moments for D = 30m. Both maximum and minimum values at steady state have been plotted so that the range of force and moment are also given. In the analysis (section 2.2.3) it was assumed that loads due to potential damping are negligible. As shown by Eatock-Taylor et al (20) the radiated wave potential can be expressed in a series form having both trigonometric and hyperbolic depth decay functions and it may be possible to derive the exact distribution of potential damping forces along the tower by some algebraic manipulation however since structures considered here are inertia dominated with frequency ratios (exciting frequency/natural frequency) exceeding a value of 6, potential damping can be ignored and the results for distribution of shear force and bending moment along the tower would not be affected.

Referring to the results of Airy theory in figures 2.31 - 2.34 it can be seen that for this case calculation of loads at the instantaneous location of the tower has little effect on the shear forces and bending moments. However effects of surface elevation are significant and 'stretched' Airy theory predicted more than 25% increase in the base shear force. Comparing results of Stream Function theory for maximum force at the base joint (figures 2.31 and 2.32) the difference is about 52% but maximum bending moments in the column (figures 2.33 and 2.34) differ by not more than

6.5%. Note that since inclusion of surface effects and calculation of loads at the instanteous position of the tower can influence response characteristics of the structure, loads acting at locations above the fluid region, say at deck C.G., can also be affected.For D = 10m differences between predictions of Airy and nonlinear theories for loadings along the tower are large in most cases. Even when integration of loads is carried up to MWL only maximum base shear force as predicted by Airy theory was underestimated by more than 10% in comparison to the results of Stream Function and Stokes fifth order theories (figure 2.37). The effect of calculating the loads at instantaneous position of tower on the results of Airy theory, as shown in figures 2.37 - 2.40, was to increase the values of base shear force and maximum bending moment by 13% and 8% respectively. Therefore in this case such effect alone has a noticeable influence on the loading of the tower. The effect of variable submergence and tower position on predictions of Stream Function theory for this case was found to be the increase in values of maximum shear force at base joint and maximum bending moment along the tower by amounts of 28% and 24% respectively.

c. Dynamic Instability

Results of computer program STA for dynamic stability analysis of towers are given on page 96 . For calculation of the eigenvalues given by equation (2.2.87) subroutine F_{02} AAF (65) was called which reduces a real unsymmetric matric to Hessenberg form and uses the QR algorithm (see Wilkinson and Reinsch (90)) in the main program. Although a 22 x 22 sparse matrix was under consideration the necessary reduction to simpler form and calculation of eigenvalues for cases studied took only a few seconds on a VAX 11/782 computer. The method presented in section 2.2.4 includes the effects of higher frequency components up to the fifth harmonic and can also be extended to be used for doubly articulated columns or for stability analysis of

multidegree of freedom systems with similar time varying stiffness terms and linear damping. To assess the effect of nonlinear drag moment on the dynamic stability D = 10m was considered. The exciting frequency is twice the natural frequency of tower and as predicted by the eigenvalue analysis, with a damping ratio of 0.02 and no drag loading, the system is unstable which is verified by the time simulation shown in figure 2.41. Note that although the response shown in figure 2.41 does not grow with time this does not imply stability since the simulation model represented by the equation of motion for small displacements cannot accurately predict the response characteristics at such unstable conditions. Therefore the large angular displacements exhibited by the system are sufficient indication of instability and an unacceptable design configuration and in figure 2.42 it is shown that when loads are calculated at the mean position of the tower such large motions are not predicted.

Figure 2.43 shows the dynamic response when the effect of quadratic drag damping is included and loads are calculated at the instantaneous position of the tower. It can be seen that transient motions decay with time and the system becomes stable with maximum angular displacements of about ± 10 degrees at steady state. Therefore quadratic drag damping can play a significant role in stabilising an articulated tower and time domain analysis remains the most reliable method of determining the behaviour of the system.

CHAPTER THREE
DYNAMIC ANALYSIS OF DAMAGED SINGLE ANCHOR LEG STORAGE (SALS) SYSTEM

3.0 INTRODUCTION

A physical description of this problem was given in Chapter One, in this Chapter a mathematical model is developed and equations of motion of the system are derived. It is assumed that large displacements may occur and the problem is solved in time domain

3.1 MATHEMATICAL MODEL

For development of the theoretical model, the initial configuration of the SALS in its undisturbed static equilibrium position is shown in Figure 3.1. The system is assumed to weather vane in the direction of wave propagation and under the action of coplanar wind, ocean currents and second order slow drift wave forces so that it takes up a new position in Figure 3.2, where X_s = tanker static offset from its initial configuration.

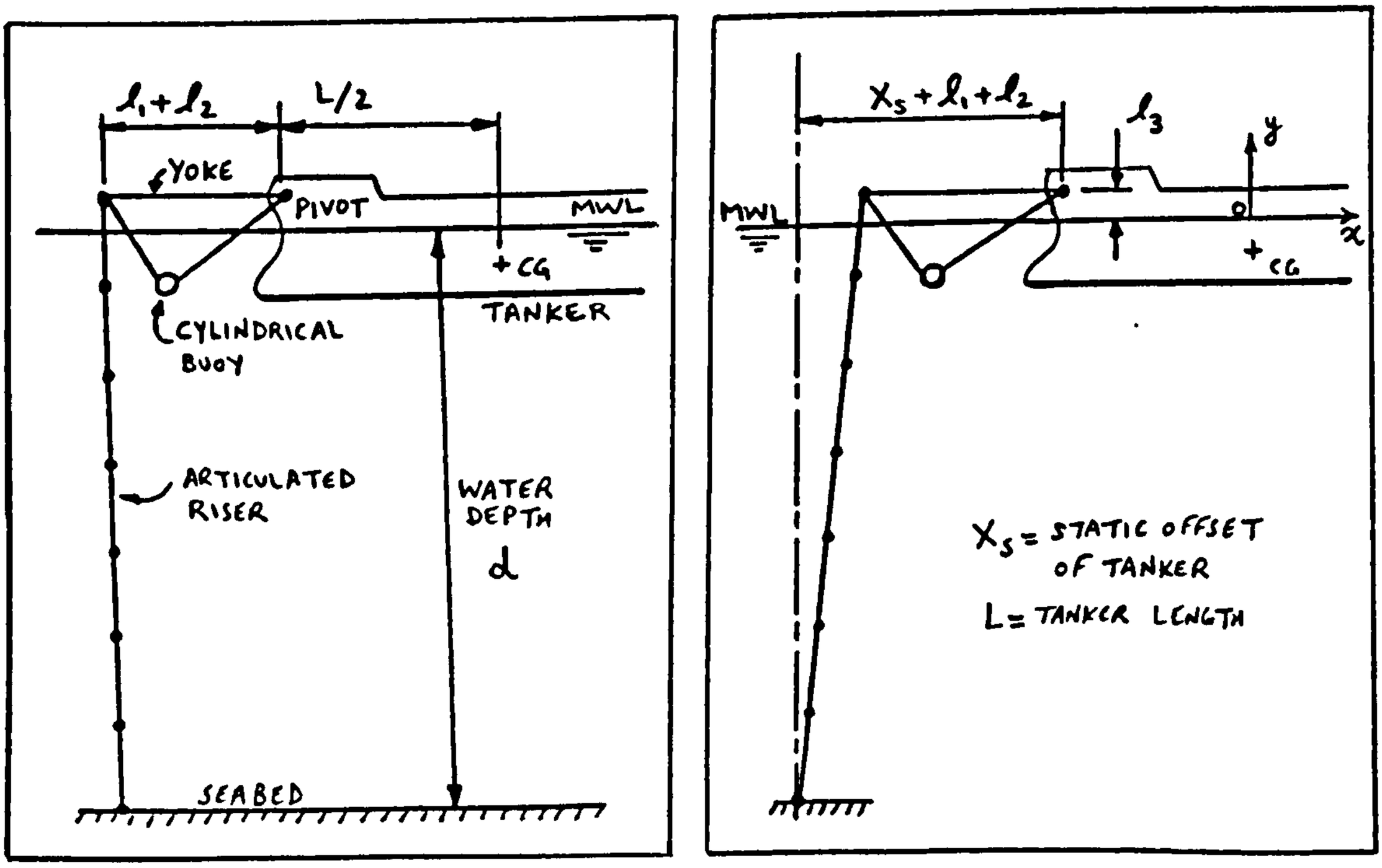

FIG.3.1. INITIAL CONFIGURATION-FIG.3.2. STATIC OFFSET POSITION

The x, y coordinate system in Figures 3.2 and 3.3 is the reference for wave loading calculations and is fixed amidships of the vessel with the origin O at M.W.L. Figure 3.3 shows the system under the action of waves when there is a reduction in riser tension caused by loss of buoyancy. $x_p(t)$ and $y_p(t)$ denote horizontal and vertical high frequency motions of the pivot respectively. In the analysis the vessel motion is assumed to be independent of the riser/buoy system and uncoupled from it. Thus the prescribed pivot motion x_p, y_p due to vessel surge, heave and pitch act as constraints on the riser system. The articulated riser is assumed to consist of N links and the generalised coordinates are chosen as the angles θ_1, $\theta_2, \theta_3, \ldots, \theta_N$ etc., with clockwise rotations taken as positive. ϕ = angle between upper part of yoke structure and the vertical.

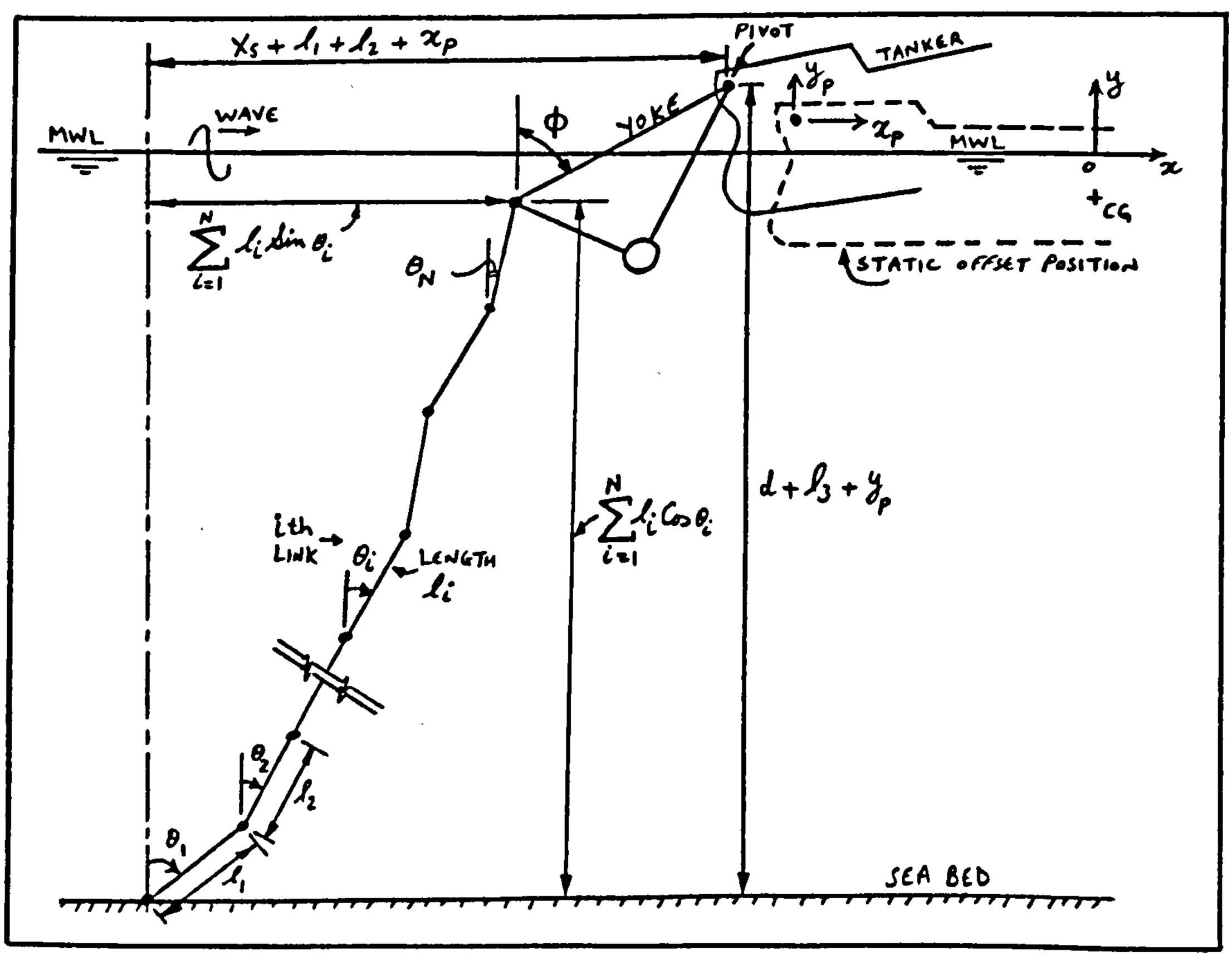

FIG.3.3 SCHEMATIC OF DAMAGED SALS SYSTEM.

The dynamic analysis considers only tanker surge, heave and pitch motions and for the riser/yoke system large angular displacements may occur and thus hydrodynamic forces are calculated at the instantaneous position of the structure.

The system has $(N-1)$ degrees of freedom and horizontal and vertical distances between the pivot and riser bottom end impose two geometric constraints. The dynamic analysis is based on the following assumptions:

1) Slow drift oscillations occur at much lower frequencies than high frequency motions due to first order wave forces. Thus the dynamic response can be evaluated with reference to a prescribed static offset position and the slowly varying pivot motions can be ignored.

2) Friction in the riser connections and the elastic deformations are negligible

3) The centre of gravity of the tanker is amidships, thus uncoupling heave and pitch motions.

4) The ocean environment is represented by a single regular wave coplanar with a steady current profile.

5) Fluid forces on the structure can be obtained from Morison's equation using linear wave theory. It is assumed that Froude-Krylov hypothesis holds and that diffraction and interference effects due to the presence of tanker are negligible.

6) Wave inertia exciting forces on the small cross section of the riser links are negligible in comparison with the drag force.

7) Wave forces on yoke bracing members are small in comparison to those on the buoy.

8) Potential damping forces on the riser and cylindrical buoy are small compared to those caused by nonlinear viscous effects

9) Yoke and riser motions have negligible effect on tanker motions.

10) Added mass and potential damping coefficients of the vessel are obtained using Grim's data (29) and (45) based on strip theory.

The equations of motion of the constrained riser/yoke system can be written by Lagrange's equation

$$\frac{d}{dt}\left(\frac{\partial T}{\partial \dot{\theta}_k}\right) - \frac{\partial T}{\partial \theta_k} + \frac{\partial V}{\partial \theta_k} = Q_k + \sum_{q=1}^{N_c} \lambda_q \frac{\partial f_q}{\partial \theta_k} \qquad (3.1.1)$$

$$; k = 1, 2, \ldots, N$$

where

T = total kinetic energy of system = $T_L + T_y$

T_L = kinetic energy of riser links

T_y = kinetic energy of yoke structure

V = increase in total potential energy of system = $V_L + V_y$

V_L = increase in potential energy of links

V_y = increase in potential energy of yoke

θ_k = generalised angluar coordinate of k^{th} link

Q_k = generalised force corresponding to θ_k

N_c = number of constraint equations

λ_q = Lagrange multipliers

Equation (3.1.1) will be developed fully in the following sections.

3.2 ARTICULATED RISER

3.2.1 Kinetic Energy of Links (Structural)

Taking an element ds distance s from the lower joint, along the i^{th} link as shown, we have

Horizontal displacement of element from p

$$x_i = \left\{ \sum_{j=1}^{i-1} l_j \sin(\theta_j) \right\} + s \sin(\theta_i) \quad (3.2.1)$$

Vertical displacement of element

$$y_i = \left\{ \sum_{j=1}^{i-1} l_j [1 - \cos(\theta_j)] \right\} + s [1 - \cos(\theta_i)] \quad (3.2.2)$$

Differentiating (3.2.1) and (3.2.2) with respect to time gives the velocity components of the element

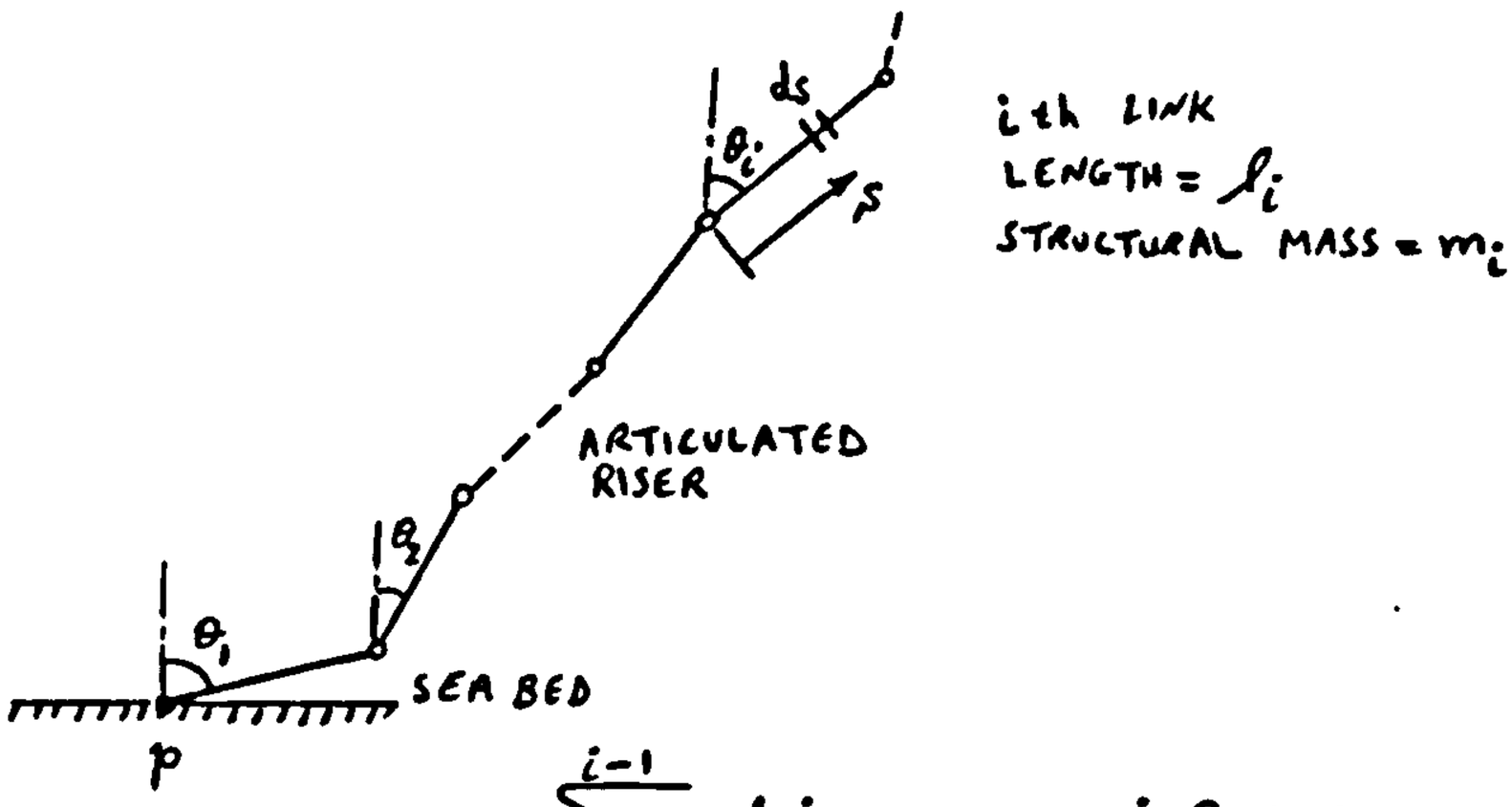

$$\dot{x}_i = \sum_{j=1}^{i-1} l_j \dot{\theta}_j \cos(\theta_j) + s \dot{\theta}_i \cos(\theta_i) \quad (3.2.3)$$

$$\dot{y}_i = \sum_{j=1}^{i-1} l_j \dot{\theta}_j \sin(\theta_j) + s \dot{\theta}_i \sin(\theta_i) \quad (3.2.4)$$

Taking δ_{m_i} as the structural mass per unit length of i^{th} link (added mass will be considered later) and δT_i the associated kinetic energy, then

$$\delta T_i = \frac{1}{2} \delta_{m_i} (\dot{x}_i^2 + \dot{y}_i^2) \, ds \quad (3.2.5)$$

Substituting for $\dot{x}_i$ and $\dot{y}_i$ from (3.2.3) and (3.2.4) into (3.2.5) gives

$$\delta T_i = \frac{1}{2}\delta m_i \Big\{ \Big[\sum_{j=1}^{i-1} l_j \dot{\theta}_j \cos(\theta_j) \Big]^2 + 2s \sum_{j=1}^{i-1} l_j \dot{\theta}_j \cos(\alpha_{ij}) + s^2 \dot{\theta}_i^2 + \Big[\sum_{j=1}^{i-1} l_j \dot{\theta}_j \sin(\theta_j) \Big]^2 \Big\} ds \qquad (3.2.6)$$

where

$$\alpha_{ij} = (\theta_i - \theta_j) \qquad (3.2.7)$$

Total kinetic energy of i^{th} link, T_i , is

$$T_i = \int_0^{l_i} \delta T_i \qquad (3.2.8)$$

Substituting for δT_i from (3.2.6) in (3.2.8) and integrating with respect to s gives

$$T_i = \frac{1}{2} m_i \Big\{ \Big[\sum_{j=1}^{i-1} l_j \dot{\theta}_j \cos(\theta_j) \Big]^2 + l_i \dot{\theta}_i \sum_{j=1}^{i-1} l_j \dot{\theta}_j \cos(\alpha_{ij}) + \frac{l_i^2}{3} \dot{\theta}_i^2 + \Big[\sum_{j=1}^{i-1} l_j \dot{\theta}_j \sin(\theta_j) \Big]^2 \Big\} \qquad (3.2.9)$$

Expanding (3.2.9) gives

$$T_i = \frac{1}{2} m_i \Big\{ \left[l_1 \dot{\theta}_1 \cos(\theta_1) + l_2 \dot{\theta}_2 \cos(\theta_2) + \cdots + l_{i-1} \dot{\theta}_{i-1} \cos(\theta_{i-1}) \right]^2 +$$

$$l_i \dot{\theta}_i \left[l_1 \dot{\theta}_1 \cos(\alpha_{i1}) + l_2 \dot{\theta}_2 \cos(\alpha_{i2}) + \cdots + l_{i-1} \dot{\theta}_{i-1} \cos(\alpha_{i\ i-1}) \right] +$$

$$\left[l_1 \dot{\theta}_1 \sin(\theta_1) + l_2 \dot{\theta}_2 \sin(\theta_2) + \cdots + l_{i-1} \dot{\theta}_{i-1} \sin(\theta_{i-1}) \right]^2 +$$

$$\frac{1}{3} l_i^2 \dot{\theta}_i^2 \Big\} \qquad (3.2.10)$$

Partial differentiation of (3.2.10) with respect to $\dot{\theta}_k$ gives

$$\frac{\partial T_i}{\partial \dot{\theta}_k} = m_i \left\{ l_k \sum_{j=1}^{i-1} \cos(\alpha_{jk}) l_j \dot{\theta}_j + \frac{1}{2} l_i l_k \dot{\theta}_i \cos(\alpha_{ik}) \right\} \quad ; \ k<i \qquad (3.2.11)$$

$$\frac{\partial T_i}{\partial \dot{\theta}_k} = \frac{1}{3} m_k l_k^2 \dot{\theta}_k + \frac{1}{2} l_k \sum_{p=1}^{k-1} m_p l_p \cos(\alpha_{pk}) \dot{\theta}_p \quad ; k=i \qquad (3.2.12)$$

$$\frac{\partial T_i}{\partial \dot{\theta}_k} = 0 \quad ; \ k>i \qquad (3.2.13)$$

Differentiating (3.2.11, 12 and 13) with respect to time we get

$$\frac{d}{dt}\left(\frac{\partial T_i}{\partial \dot{\theta}_k}\right) = m_i \Big\{ l_k \sum_{j=1}^{i-1} l_j \dot{\theta}_j \left[(\dot{\theta}_k - \dot{\theta}_j) \sin(\alpha_{jk}) \right] +$$

$$l_j \cos(\alpha_{jk}) \ddot{\theta}_j +$$

$$\frac{1}{2} l_i l_k \dot{\theta}_i \left[(\dot{\theta}_k - \dot{\theta}_i) \sin(\alpha_{ik}) \right] +$$

$$\frac{1}{2} l_i l_k \cos(\alpha_{ik}) \ddot{\theta}_i \Big\} \quad ; k<i \qquad (3.2.14)$$

$$\frac{d}{dt}\left(\frac{\partial T_i}{\partial \dot{\theta}_k}\right) = \frac{1}{3} m_k l_k^2 \ddot{\theta}_k + \frac{1}{2} l_k \sum_{p=1}^{k-1} m_p l_p \left[(\dot{\theta}_k - \dot{\theta}_p) \sin(\alpha_{pk}) + \ddot{\theta}_p \cos(\alpha_{pk}) \right] \quad ; k=i$$

(3.2.15)

$$\frac{d}{dt}\left(\frac{\partial T_i}{\partial \dot{\theta}_k}\right) = 0 \quad ; k>i$$

(3.2.16)

Total kinetic energy of all links is then

$$T_L = \sum_{i=1}^{N} T_i \qquad (3.2.17)$$

Hence

$$\frac{d}{dt}\left(\frac{\partial T_L}{\partial \dot{\theta}_k}\right) = \sum_{i=1}^{N} \frac{d}{dt}\left(\frac{\partial T_i}{\partial \dot{\theta}_k}\right) \qquad (3.2.18)$$

Substituting in the right hand side of (3.2.18) from (3.2.14, 15 and 16) and noting in the summation that $i>k$ or $i=k+1$ to N gives

$$\frac{d}{dt}\left(\frac{\partial T_L}{\partial \dot{\theta}_k}\right) = \sum_{i=k+1}^{N} \Bigg[m_i \Big\{ l_k \sum_{j=1}^{i-1} l_j \dot{\theta}_j \left[(\dot{\theta}_k - \dot{\theta}_j) \sin(\alpha_{jk}) \right] + l_j \cos(\alpha_{jk})\, \ddot{\theta}_j \; + \; \tfrac{1}{2} l_i l_k \dot{\theta}_i (\dot{\theta}_k - \dot{\theta}_i) \sin(\alpha_{ik}) + \tfrac{1}{2} l_i l_k \cos(\alpha_{ik})\, \ddot{\theta}_i \Big\} \Bigg] +$$

$$\tfrac{1}{3} m_k l_k^2 \ddot{\theta}_k + \tfrac{1}{2} l_k \sum_{p=1}^{k-1} m_p l_p \left[(\dot{\theta}_k - \dot{\theta}_p) \dot{\theta}_p \sin(\alpha_{pk}) + \cos(\alpha_{pk})\, \ddot{\theta}_p \right] \qquad (3.2.19)$$

If all links are identical with mass m and length l (3.2.19) simplifies to

$$\frac{d}{dt}\left(\frac{\partial T_L}{\partial \dot{\theta}_k}\right) = m l^2 \Bigg\{ \sum_{i=k+1}^{N} \sum_{j=1}^{i-1} \left[\dot{\theta}_j (\dot{\theta}_k - \dot{\theta}_j) \sin(\alpha_{jk}) + \ddot{\theta}_j \cos(\alpha_{jk}) \right] +$$

$$\tfrac{1}{2} \sum_{i=k+1}^{N} \left[\dot{\theta}_i (\dot{\theta}_k - \dot{\theta}_i) \sin(\alpha_{ik}) + \cos(\alpha_{ik}) \ddot{\theta}_i \right] +$$

$$\tfrac{1}{3} \ddot{\theta}_k + \tfrac{1}{2} \sum_{p=1}^{k-1} \left[(\dot{\theta}_k - \dot{\theta}_p) \dot{\theta}_p \sin(\alpha_{pk}) + \cos(\alpha_{pk}) \ddot{\theta}_p \right] \Bigg\} \qquad (3.2.20)$$

In the context of the subsequent matrix formulation of the equations of motion, $\dot{\theta}_k$, $\ddot{\theta}_k$ represent diagonal terms and $\dot{\theta}_j$, $\ddot{\theta}_j$ represent off-diagonal terms. We thus have to devise a method for separating these terms from equation (3.2.20). By expanding

the first term of the equation and substituting values of k and j a pattern emerged from which the following identity was established.

$$\sum_{i=k+1}^{N} \sum_{j=1}^{i-1} A_{kj} = (N-k) \sum_{q=1}^{K} A_{kq} + \sum_{r=k+1}^{N-1} (N-r) A_{kr} \qquad (3.2.21)$$

where A_{Kj} represents the first term of equation (3.2.20). This can then be written as

$$\frac{d}{dt}\left(\frac{\partial T_L}{\partial \dot{\theta}_k}\right) = m\ell^2 \left\{ (N-k+\tfrac{1}{3})\ddot{\theta}_k + (N-k+\tfrac{1}{2}) \sum_{j=1}^{k-1} D_{jk} + \sum_{r=k+1}^{N} (N-r+\tfrac{1}{2}) D_{rK} \right\} \qquad (3.2.22)$$

where

$$D_{jk} = \dot{\theta}_j (\dot{\theta}_k - \dot{\theta}_j) \sin(\alpha_{jk}) + \cos(\alpha_{jk})\, \ddot{\theta}_j \quad ; k = 1, 2, \ldots, N \qquad (3.2.23)$$

Note: In (3.2.22) the summation term $\sum_{r=k+1}^{N}$ is set to zero when $k=N$. Similarly from (3.2.9) we get

$$\frac{\partial T_i}{\partial \theta_k} = m_i \left\{ l_k \dot{\theta}_k \sum_{j=1}^{i-1} l_j \dot{\theta}_j \sin(\alpha_{jk}) + \tfrac{1}{2} l_i l_k \dot{\theta}_i \dot{\theta}_k \sin(\alpha_{ik}) \right\} \quad ; k<i \qquad (3.2.24)$$

$$\frac{\partial T_i}{\partial \theta_k} = \tfrac{1}{2} m_i \left\{ l_k \dot{\theta}_k \sum_{j=1}^{i-1} l_j \dot{\theta}_j \sin(\alpha_{jk}) \right\} \quad ; k=i \qquad (3.2.25)$$

$$\frac{\partial T_i}{\partial \theta_k} = 0 \quad ; k>i \qquad (3.2.26)$$

Hence for identical links

$$\frac{\partial T_i}{\partial \theta_k} = m\ell^2 \left\{ \dot{\theta}_k \sum_{j=1}^{i-1} \dot{\theta}_j \sin(\alpha_{jk}) + \tfrac{1}{2} \dot{\theta}_i \dot{\theta}_k \sin(\alpha_{ik}) \right\} \quad ; k<i \qquad (3.2.27)$$

$$\frac{\partial T_i}{\partial \theta_k} = \frac{1}{2} m \ell^2 \left\{ \dot{\theta}_k \sum_{j=1}^{k-1} \dot{\theta}_j \sin(\alpha_{jk}) \right\} \quad ; k=i \tag{3.2.28}$$

$$\frac{\partial T_i}{\partial \theta_k} = 0 \quad ; k>i \tag{3.2.29}$$

Thus using equation (3.2.21) we have

$$\frac{\partial T_L}{\partial \theta_k} = m\ell^2 \dot{\theta}_k \left\{ (N-k+\tfrac{1}{2}) \sum_{j=1}^{k-1} \dot{\theta}_j \sin(\alpha_{jk}) + \sum_{r=k+1}^{N} (N-r+\tfrac{1}{2}) \dot{\theta}_r \sin(\alpha_{rk}) \right\} \tag{3.2.30}$$

$$; k = 1, 2, \ldots, N$$

3.2.2 Potential Energy of Links

If the links are of uniform cross section, using equation (3.2.2) we have

Vertical displacement of C.G. of i^{th} link $= \sum_{j=1}^{i-1} \ell_j [1-\cos(\theta_j)] + \frac{\ell_i}{2} [1-\cos(\theta_i)]$ (3.2.31)

Increase of potential energy of i^{th} link

$$V_i = -w_i' \left\{ \sum_{j=1}^{i-1} \ell_j [1-\cos(\theta_j)] + \frac{\ell_i}{2} [1-\cos(\theta_i)] \right\} \tag{3.2.32}$$

Where w_i' = weight of i^{th} link in fluid. Increase in total potential energy in links,

$$V_L = \sum_{i=1}^{N} V_i \tag{3.2.33}$$

or

$$V_L = -\left\{ \sum_{i=1}^{N} \sum_{j=1}^{i-1} w_i' \ell_j [1-\cos(\theta_j)] + \sum_{i=1}^{N} w_i' \frac{\ell_i}{2} [1-\cos(\theta_i)] \right\} \tag{3.2.34}$$

For identical links equation (3.2.34) can be written as

$$V_L = -w'\ell \left\{ \sum_{i=1}^{N} \sum_{j=1}^{i-1} [1 - \cos(\theta_j)] + \frac{1}{2} \sum_{i=1}^{N} [1 - \cos(\theta_i)] \right\} \qquad (3.2.35)$$

where w' = weight of each link in fluid.

Noting that

$$\sum_{i=1}^{N} \sum_{j=1}^{i-1} A_j = \sum_{P=1}^{N-1} (N-P) A_P \qquad (3.2.36)$$

we get

$$V_L = -w'\ell \sum_{i=1}^{N} (N - i + \tfrac{1}{2}) [1 - \cos(\theta_i)] \qquad (3.2.37)$$

Partial differentiation of (3.2.37) with respect to θ_k gives

$$\frac{\partial V_L}{\partial \theta_k} = -w'\ell (N - k + \tfrac{1}{2}) \sin(\theta_k) \quad ; k = 1, 2, \ldots, N \qquad (3.2.38)$$

3.2.3 Generalised Fluid Forces

The instantaneous x and y coordinate of an element of the j^{th} link are shown in Figure 3.4 and referring to Figure 3.3 we have

Instantaneous x-coordinate of element on j^{th} link,

$$X_j = -\left[X_s + \ell_1 + \ell_2 + \frac{L}{2} - \sum_{i=1}^{j-1} \ell_i \sin(\theta_i) - \frac{1}{2} \sin(\theta_j) \right] \qquad (3.2.39)$$

where L is the tanker length.

Instantaneous y-coordinate of element of j^{th} link

$$y_j = -\left[d - \sum_{i=1}^{j-1} l_i \cos\theta_i - s\cos(\theta_j)\right] \qquad (3.2.40)$$

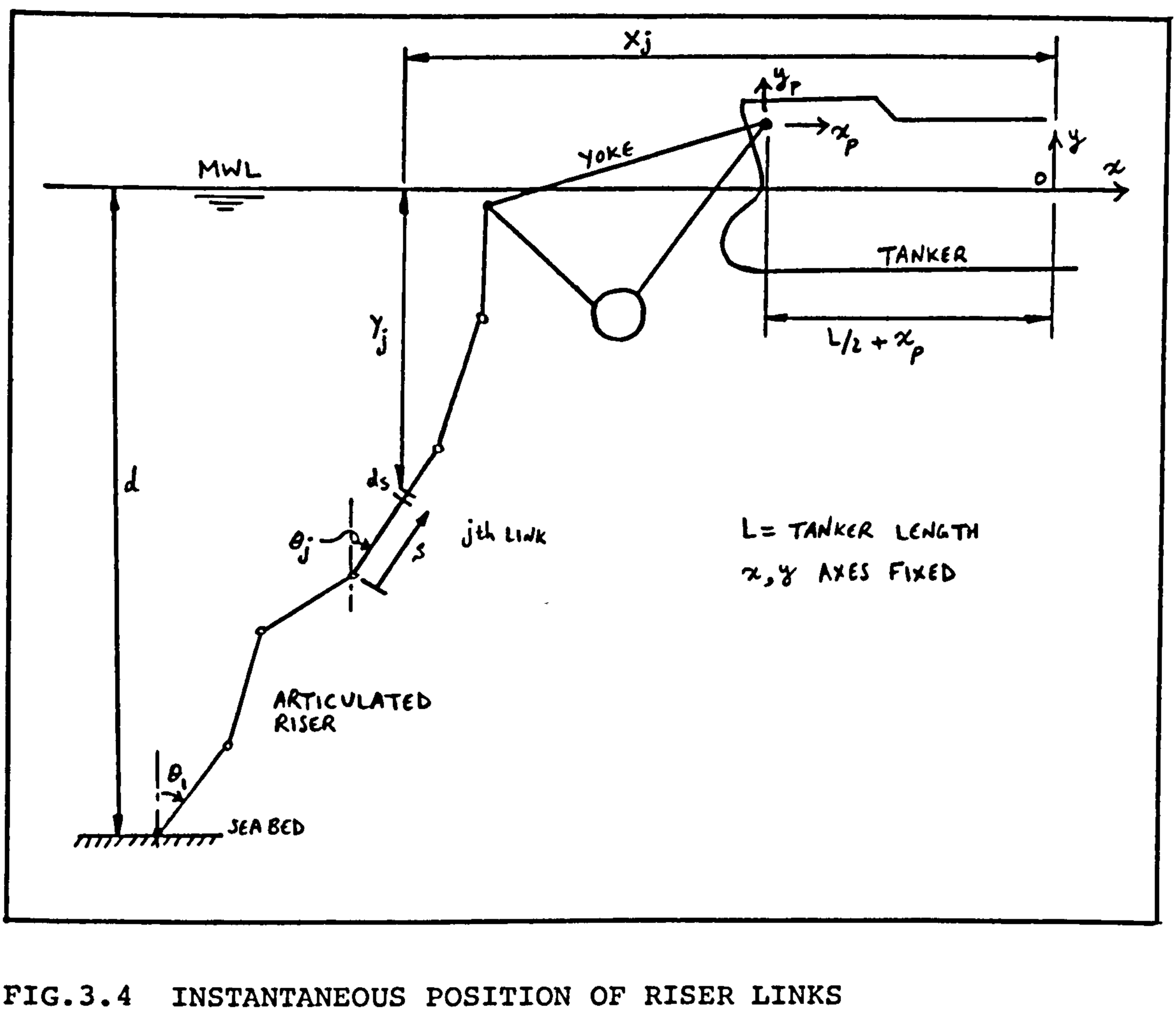

FIG.3.4 INSTANTANEOUS POSITION OF RISER LINKS

The velocity components of fluid and element are shown below:

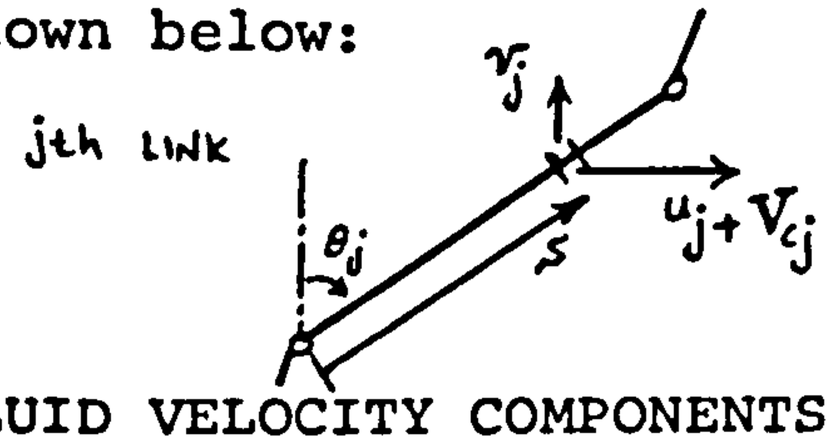

FLUID VELOCITY COMPONENTS

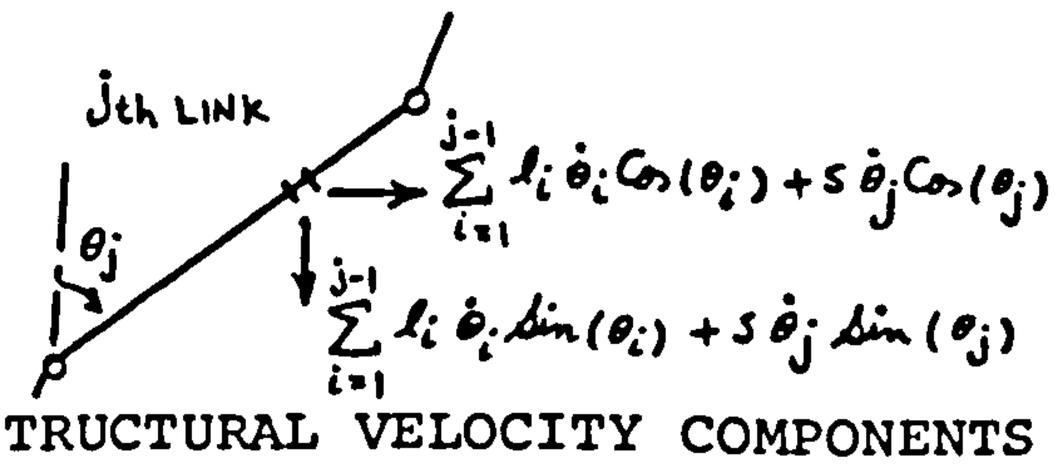

STRUCTURAL VELOCITY COMPONENTS

where u_j and v_j = horizontal and vertical fluid particle velocities respectively and V_{cj} = current velocity at element.

Fluid velocity component normal to the link is shown below:

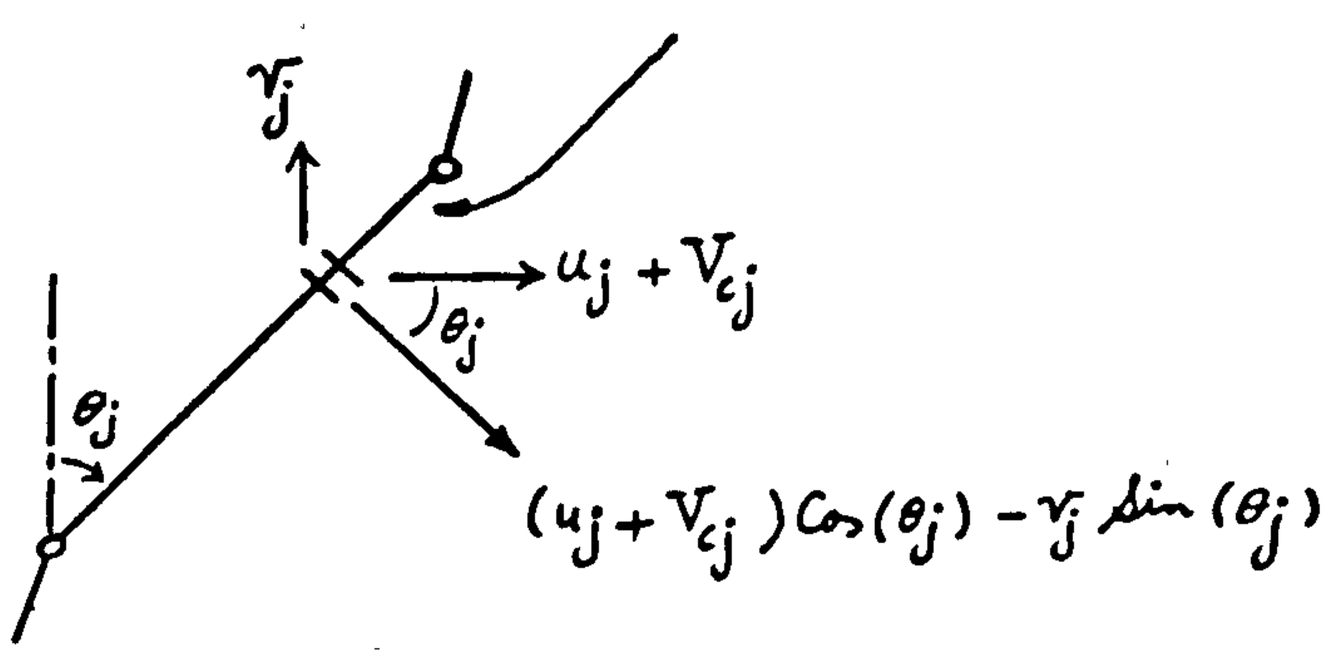

FLUID VELOCITY NORMAL TO j^{th} LINK

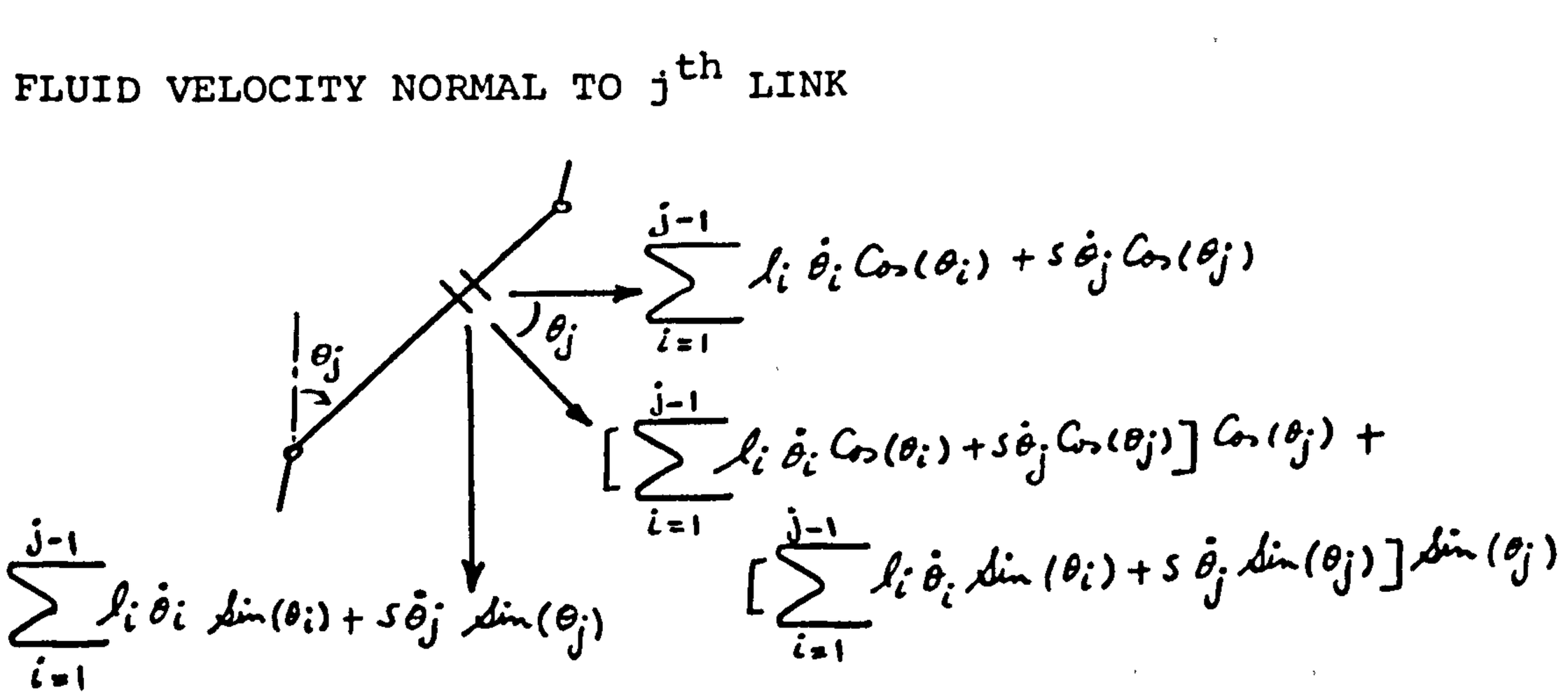

STRUCTURAL VELOCITY COMPONENT NORMAL TO j^{th} LINK

Relative fluid velocity normal to j^{th} link

$$V_j = [u_j + V_{cj} - \sum_{i=1}^{j-1} l_i \dot{\theta}_i \cos(\theta_i)]\cos(\theta_j) - [v_j + \sum_{i=1}^{j-1} l_i \dot{\theta}_i \sin(\theta_i)]\sin(\theta_j) - s\dot{\theta}_j \quad (3.2.41)$$

From linear wave theory

$$u_j = \frac{\omega H}{2} \frac{\cosh k(d+y_j)}{\sinh(kd)} \cos(k x_j - \omega t) \quad (3.2.42)$$

$$v_j = \frac{\omega H}{2} \frac{\sinh k(d+y_j)}{\sinh(kd)} \sin(kx_j - \omega t) \qquad (3.2.43)$$

and $\omega^2 = g k \tanh(kd)$

where

ω = circular wave frequency
H = wave height
k = wave number

Drag force on element is given by

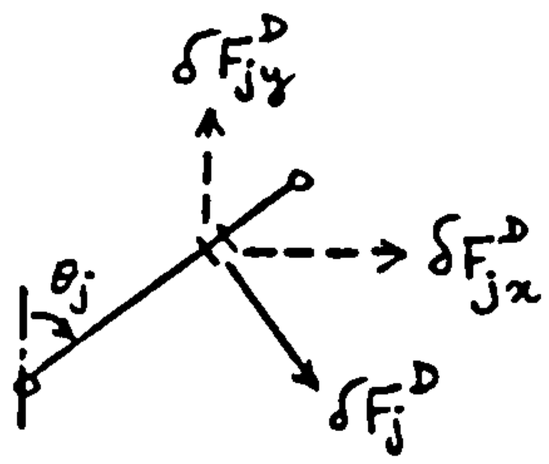

$$\delta F_j^D = \frac{1}{2} \rho C_D D_l V_j |V_j| ds \qquad (3.2.44)$$

where

C_D = Drag coefficient (assumed to be equal for all links)
D_l = Link diameter or width
ρ = Fluid density

Horizontal components of drag force on element of j^{th} link

$$\delta F_{jx}^D = \frac{1}{2} \rho C_D D_l |V_j| V_j \cos(\theta_j) ds \qquad (3.2.45)$$

Vertically,

$$\delta F_{jy}^{D} = -\frac{1}{2} \rho C_D D_e |V_j| V_j \sin(\theta_j)\, ds \qquad (3.2.46)$$

Now work done by drag force acting on element of j^{th} link when the k^{th} link undergoes a virtual displacement $\delta\theta_k$ and all other displacements remain fixed can be found as follows:

Removing the constraints from the system, i.e. assuming that top end of riser is free, horizontal displacement of element on j^{th} link after a virtual displacement $\delta\theta_k$ at k^{th} link is

$$\delta x_{jk} = l_k \delta\theta_k \cos(\theta_k) \qquad ; j \neq k \qquad (3.2.47)$$

vertically,

$$\delta y_{jk} = -l_k \delta\theta_k \sin(\theta_k) \qquad ; j \neq k \qquad (3.2.48)$$

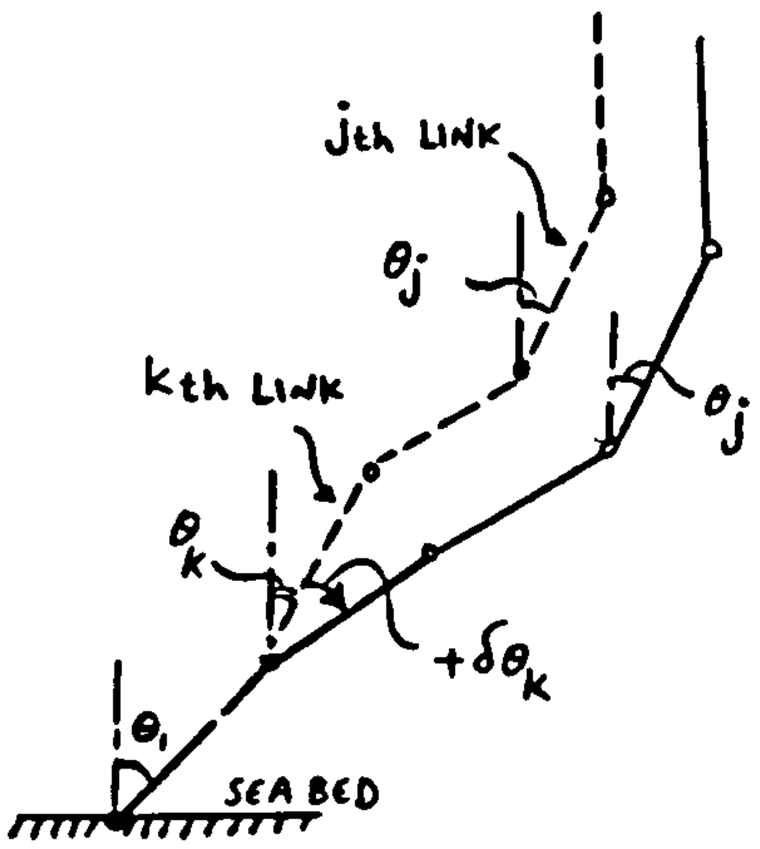

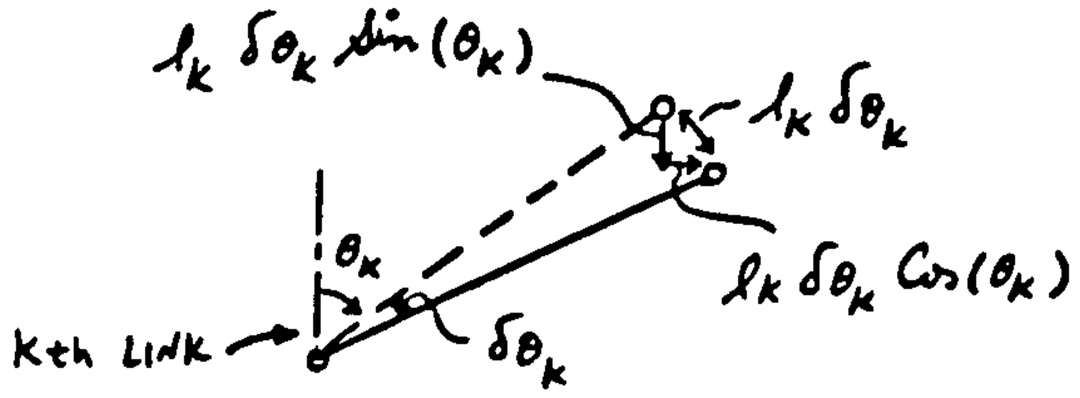

<u>Note</u>: $+\delta\theta_k$ causes displacements in the direction of δF_{jx}^{D} but in the opposite direction to δF_{jy}^{D}

Work done by drag force acting on element of j^{th} link when k^{th} link undergoes a virtual displacement $\delta\theta_k$ is

$$\delta W_{jk} = \delta F^D_{jx} \cdot \delta x_{jk} + \delta F^D_{jy} \cdot \delta y_{jk} \tag{3.2.49}$$

Substituting for δx_{jk} and δy_{jk} from (3.2.47) and (3.2.48) into (3.2.49) and integrating gives

Work done by drag force on j^{th} link,

$$W_{jk} = \int_0^{l_j} \delta W_{jk} = \int_0^{l_j} l_k \left[\delta F^D_{jx} \cdot \cos(\theta_k) - \delta F^D_{jy} \cdot \sin(\theta_k) \right] \delta\theta_k \quad ; j \neq k \tag{3.2.50}$$

Similarly, work done by drag force acting on k^{th} link itself

$$W_{kk} = \int_0^{l_k} \left[\delta F^D_{kx} \cdot \cos(\theta_k) - \delta F^D_{ky} \cdot \sin(\theta_k) \right] s \cdot \delta\theta_k \tag{3.2.51}$$

Therefore the total work done by drag force acting on links when the k^{th} link undergoes a virtual displacement is given by

$$W_{k\ell} = \sum_{j=k+1}^{N} \left\{ \int_0^{l_j} l_k \left[\delta F^D_{jx} \cdot \cos(\theta_k) - \delta F^D_{jy} \cdot \sin(\theta_k) \right] \delta\theta_k \right\} + \int_0^{l_k} \left[\delta F^D_{kx} \cdot \cos(\theta_k) - \delta F^D_{ky} \cdot \sin(\theta_k) \right] s \cdot \delta\theta_k \tag{3.2.52}$$

For identical links equation (3.2.52) simplifies to

$$W_{kl} = l \sum_{j=k+1}^{N} \left\{ \int_0^l [\, \delta F_{jx}^D \cdot \cos(\theta_k) - \delta F_{jy}^D \cdot \sin(\theta_k)\,] \, \delta\theta_k \right\} +$$

$$\int_0^l [\, \delta F_{kx}^D \cdot \cos(\theta_k) - \delta F_{ky}^D \cdot \sin(\theta_k)\,] \, s \cdot \delta\theta_k \qquad (3.2.53)$$

The generalised force Q_{kl} corresponding to the k^{th} link is then given by

$$Q_{kl} = W_{kl} \,/\, \delta\theta_k \qquad (3.2.54)$$

Using (3.2.45), (3.2.46) and (3.2.53), equation (3.2.54) can be written as

$$Q_{kl} = \tfrac{1}{2} \rho C_D D_l \int_0^l \left[l \sum_{j=k+1}^{N} \cos(\alpha_{kj}) \, |V_j| V_j + |V_k| V_k \cdot s \right] ds \quad ; k = 1, 2, \ldots, N \qquad (3.2.55)$$

where $\alpha_{kj} = (\theta_k - \theta_j)$

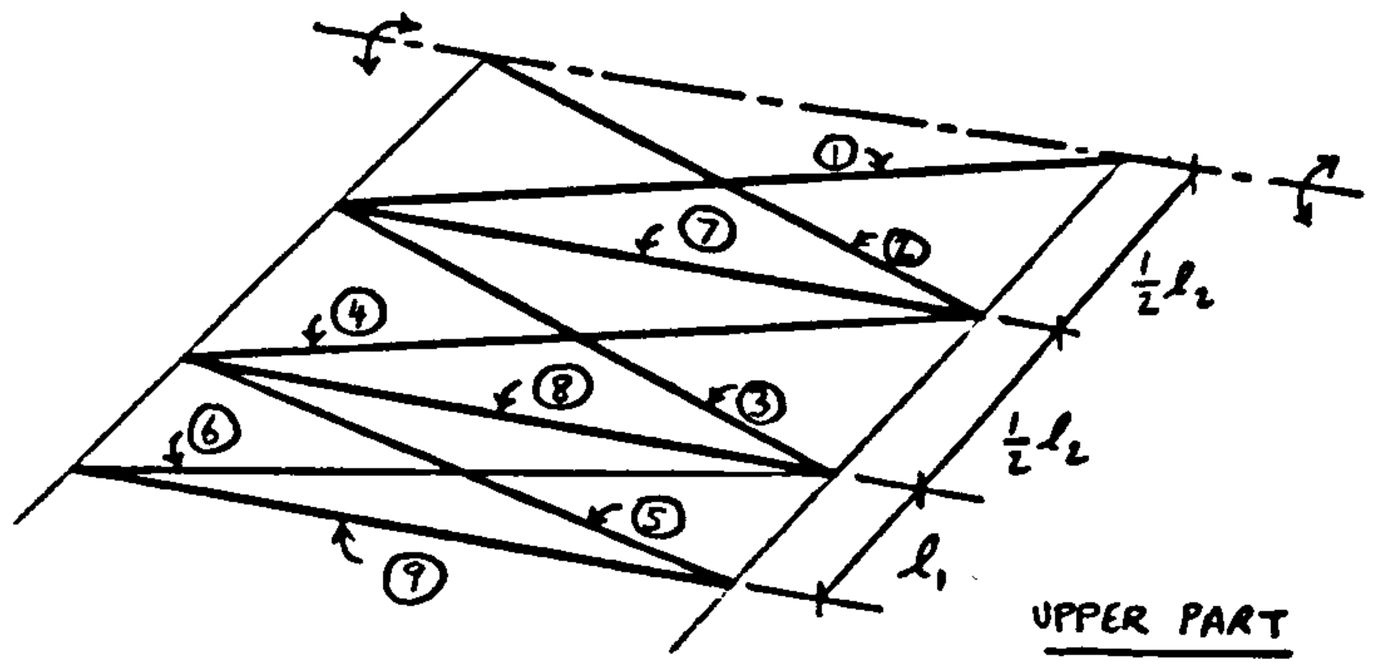

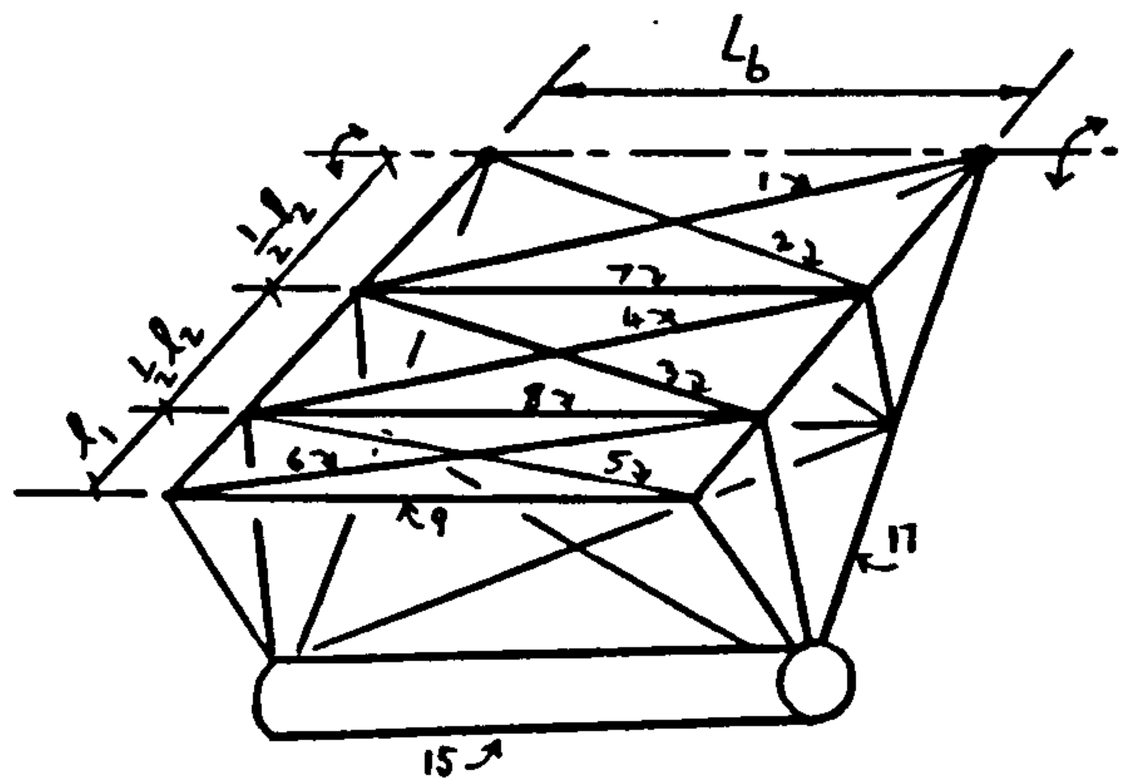

M_j = MASS OF jth MEMBER

$M_1 = M_2 = M_3 = M_4$

$M_5 = M_6$

$M_7 = M_8 = M_9$

$M_{10} = M_{11} = M_{13} = M_{14}$

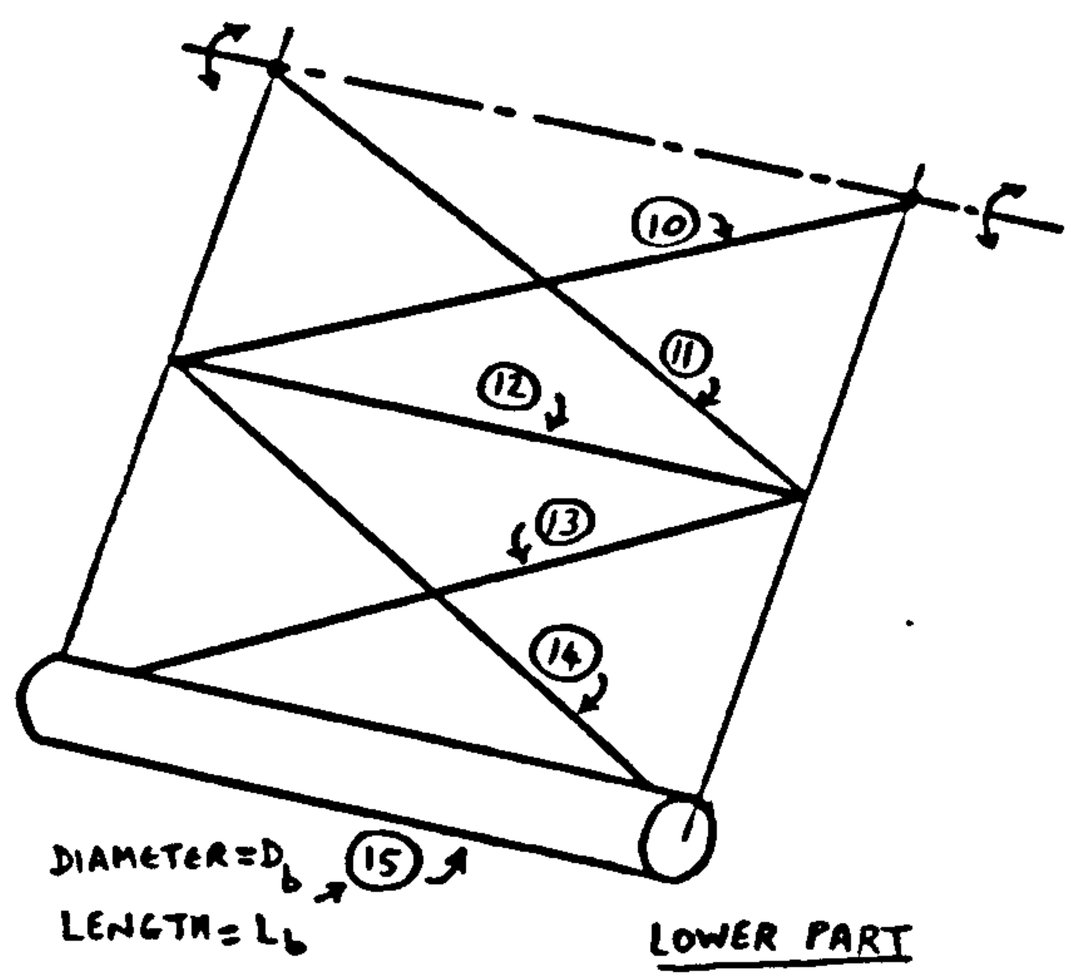

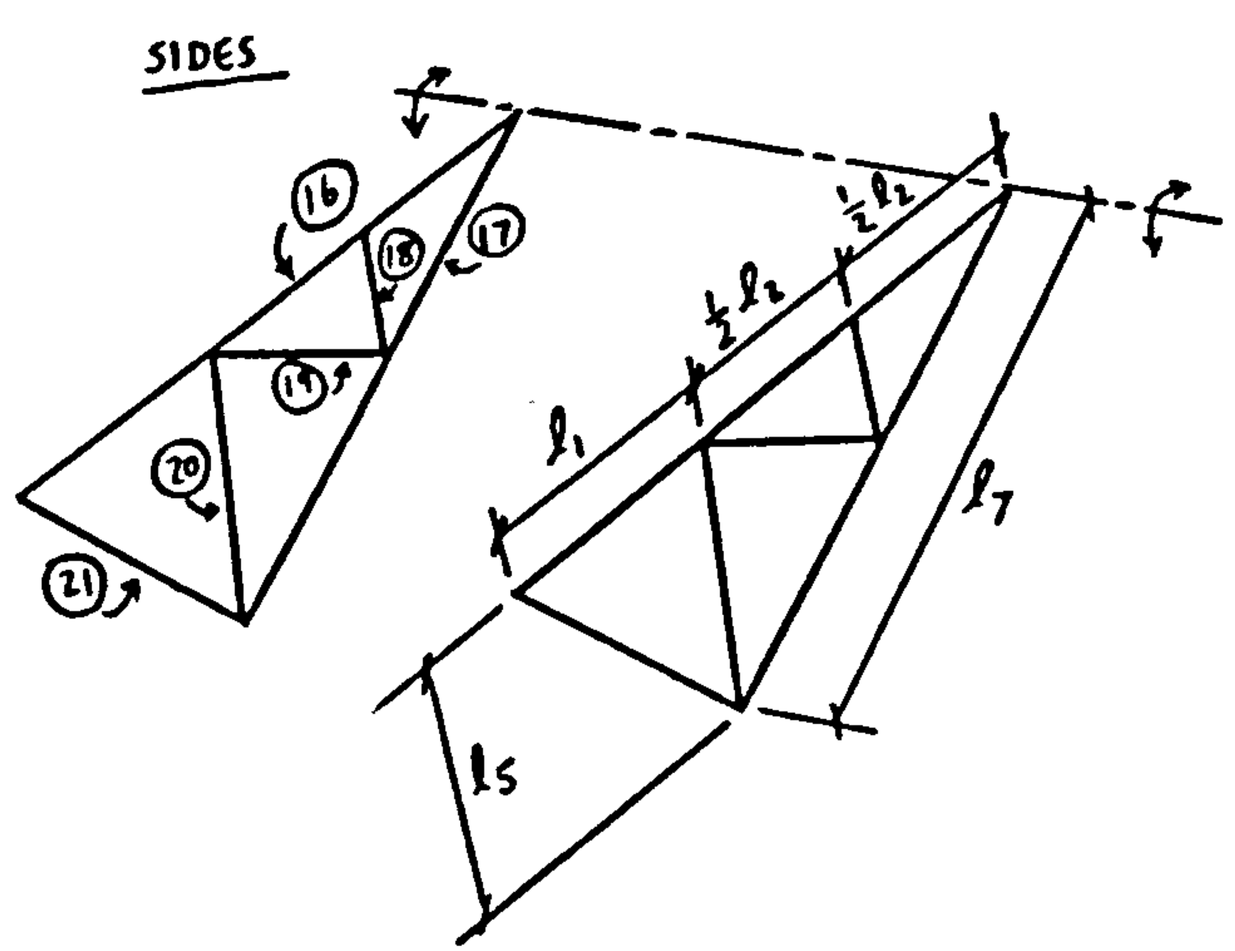

FIGURE 3.5. YOKE CONFIGURATION

3.3 YOKE STRUCTURE

For the purpose of incorporating the constraints on the system it is necessary and convenient to derive the kinetic energy of the yoke in terms of the riser coordinates and yoke rigid body rotation

The dimensions and geometrical configuration of the yoke structure are shown in Fig.3.5 in which (j) indicates the j^{th} member and M_j its structural mass.

3.3.1 Yoke Kinetic Energy (Structural)

Expressions for the structural kinetic energy and its derivatives are developed by considering individual members of the yoke framework and cylindrical buoy in Fig.3.5.

Upper plane members:

For the upper part we consider a bracing member shown below lever arm,

$$\ell_s = a + \frac{s(b-a)}{L_j} \qquad (3.3.1)$$

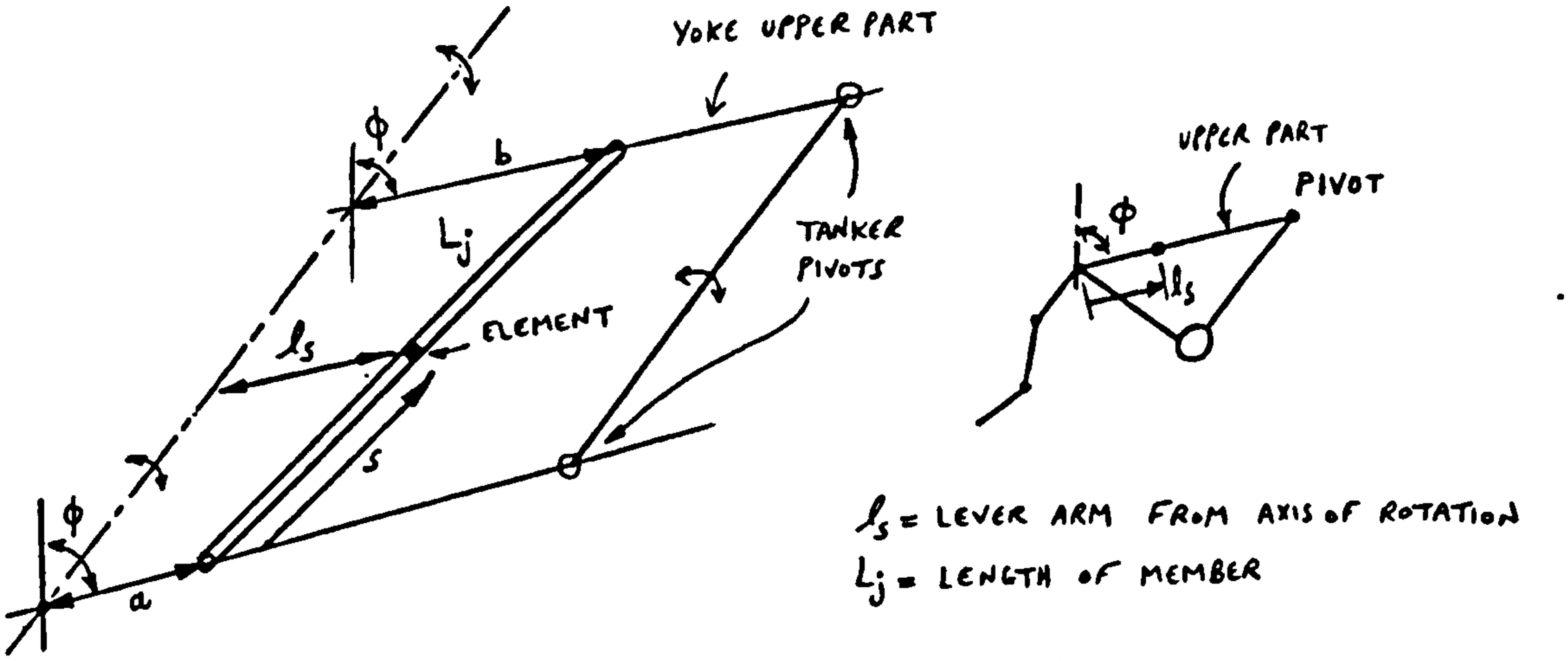

Assuming identical riser links of length ℓ we have

$$\text{Horizontal displacement of element on } L_j = \ell \sum_{i=1}^{N} \sin(\theta_i) + \ell_s \sin\phi \qquad (3.3.2)$$

$$\text{Vertical displacement of element} = \ell \sum_{i=1}^{N} [1-\cos(\theta_i)] + \ell_s [1-\cos(\phi)] \qquad (3.3.3)$$

where ϕ = angle of yoke upper plane to vertical.

Differentiating (3.3.2) and (3.3.3) with respect to time

Horizontal velocity of element $= \left[l \sum_{i=1}^{N} \dot{\theta}_i \cos(\theta_i) \right] + l_s \dot{\phi} \cos(\phi)$ (3.3.4)

Vertical velocity of element $= \left[l \sum_{i=1}^{N} \dot{\theta}_i \sin(\theta_i) \right] + l_s \dot{\phi} \sin(\phi)$ (3.3.5)

Therefore kinetic energy of j^{th} upper plane member, T_j^u is

$$T_j^u = \frac{1}{2} \delta M_j \int_0^{L_j} \left\{ \left[l \sum_{i=1}^{N} \dot{\theta}_i \cos(\theta_i) + l_s \dot{\phi} \cos(\phi) \right]^2 + \left[l \sum_{i=1}^{N} \dot{\theta}_i \sin(\theta_i) + l_s \dot{\phi} \sin(\phi) \right]^2 \right\} ds \quad (3.3.6)$$

where δM_j = structural mass per unit length of j^{th} member

The kinetic energy of the fluid added mass is considered later.

From (3.3.6) we get

$$\frac{d}{dt}\left(\frac{\partial T_j^u}{\partial \dot{\phi}}\right) = l M_j \left(\frac{a+b}{2}\right) \left\{ -\dot{\phi} \sin(\phi) \sum_{i=1}^{N} \dot{\theta}_i \cos(\theta_i) + \cos(\phi) \left[\sum_{i=1}^{N} \ddot{\theta}_i \cos(\theta_i) - \dot{\theta}_i^2 \sin(\theta_i) \right] + \dot{\phi} \cos(\phi) \sum_{i=1}^{N} \dot{\theta}_i \sin(\theta_i) + \sin(\phi) \left[\sum_{i=1}^{N} \ddot{\theta}_i \sin(\theta_i) + \dot{\theta}_i^2 \cos(\theta_i) \right] \right\} + \frac{1}{3} M_j (a^2 + ab + b^2) \ddot{\phi} \quad (3.3.7)$$

Referring to Fig.3.5, the derivatives of kinetic energy of upper plane are

$$\frac{d}{dt}\left(\frac{\partial T_t}{\partial \dot{\phi}}\right) = \sum_{j=1}^{9} \frac{d}{dt}\left(\frac{\partial T_j^u}{\partial \dot{\phi}}\right) \qquad (3.3.8)$$

Table 3.1 gives a and b parameters appearing in (3.3.7) for various members of upper part. Substituting for a and b from Table 3.1 into (3.3.7) for each member and using (3.3.8) we get equation (3.3.9)

Member	a	b
1	$l_1 + l_2$	$l_1 + (\frac{l_2}{2})$
2	$l_1 + (\frac{l_2}{2})$	$l_1 + l_2$
3	l_1	$l_1 + (\frac{l_2}{2})$
4	$l_1 + (\frac{l_2}{2})$	l_1
5	0	l_1
6	l_1	0
7	$l_1 + (\frac{l_2}{2})$	$l_1 + (\frac{l_2}{2})$
8	l_1	l_1
9	0	0

TABLE 3.1. a AND b PARAMETERS FOR YOKE UPPER PLANE

$$\frac{d}{dt}\left(\frac{\partial T_t}{\partial \dot{\phi}}\right) = l\left\{\sum_{i=1}^{N} \ddot{\theta}_i \cos(\alpha_{i\phi}) - \dot{\theta}_i(\dot{\theta}_i - \dot{\phi})\sin(\alpha_{i\phi})\right\} \times$$

$$\left[2M_1(2l_1 + l_2) + M_5 \cdot l_1 + M_7(2l_1 + l_2/2)\right] +$$

$$\frac{1}{3}\ddot{\phi}\left[4M_1(3l_1^2 + 3l_1l_2 + l_2^2) + \right.$$

$$\left. 2M_5 \cdot l_1^2 + M_7(6l_1^2 + 3l_1l_2 + \frac{3}{4}l_2^2)\right]$$

(3.3.9)

where

$$\alpha_{i\phi} = (\theta_i - \phi)$$

similarly

$$\frac{d}{dt}\left(\frac{\partial T_t}{\partial \dot{\theta}_k}\right) = 2\left(2M_1 + M_5 + \frac{3}{2}M_7\right)\left\{\ell^2 \sum_{i=1}^{N} \ddot{\theta}_i \cos(\alpha_{ik}) + \dot{\theta}_i(\dot{\theta}_k - \dot{\theta}_i)\sin(\alpha_{ik})\right\} +$$

$$\ell\left[2M_1(2\ell_1 + \ell_2) + M_5\ell_1 + M_7(2\ell_1 + \ell_2/2)\right] \times$$

$$\left\{\ddot{\phi}\cos(\alpha_{k\phi}) + \dot{\phi}(\dot{\phi} - \dot{\theta}_k)\sin(\alpha_{k\phi})\right\}$$

(3.3.10)

$$\frac{\partial T_t}{\partial \phi} = \left[\ell\dot{\phi}\sum_{i=1}^{N} \dot{\theta}_i \sin(\alpha_{i\phi})\right]\left[2M_1(2\ell_1 + \ell_2) + M_5\ell_1 + M_7\left(2\ell_1 + \frac{\ell_2}{2}\right)\right]$$

(3.3.11)

$$\frac{\partial T_t}{\partial \theta_k} = 2\left(2M_1 + M_5 + \frac{3}{2}M_7\right)\left\{-\ell^2\dot{\theta}_k \sum_{i=1}^{N} \dot{\theta}_i \sin(\alpha_{ki})\right\} -$$

$$\ell\dot{\phi}\dot{\theta}_k \sin(\alpha_{k\phi})\left[2M_1(2\ell_1 + \ell_2) + M_5\ell_1 + M_7\left(2\ell_1 + \frac{\ell_2}{2}\right)\right]$$

(3.3.12)

Lower Plane:

For the lower plane of yoke as shown in Fig.3.5 and below, taking an element on j^{th} member we can write

$$\sin(\delta) = \frac{y_s}{r_s} \quad , \quad \cos(\delta) = \frac{x_s}{r_s}$$

Horizontal displacement of element =

$$\ell \sum_{i=1}^{N} \sin(\theta_i) - r_s \left[\sin(\delta) - \sin(\delta+\phi) \right]$$

(3.3.13)

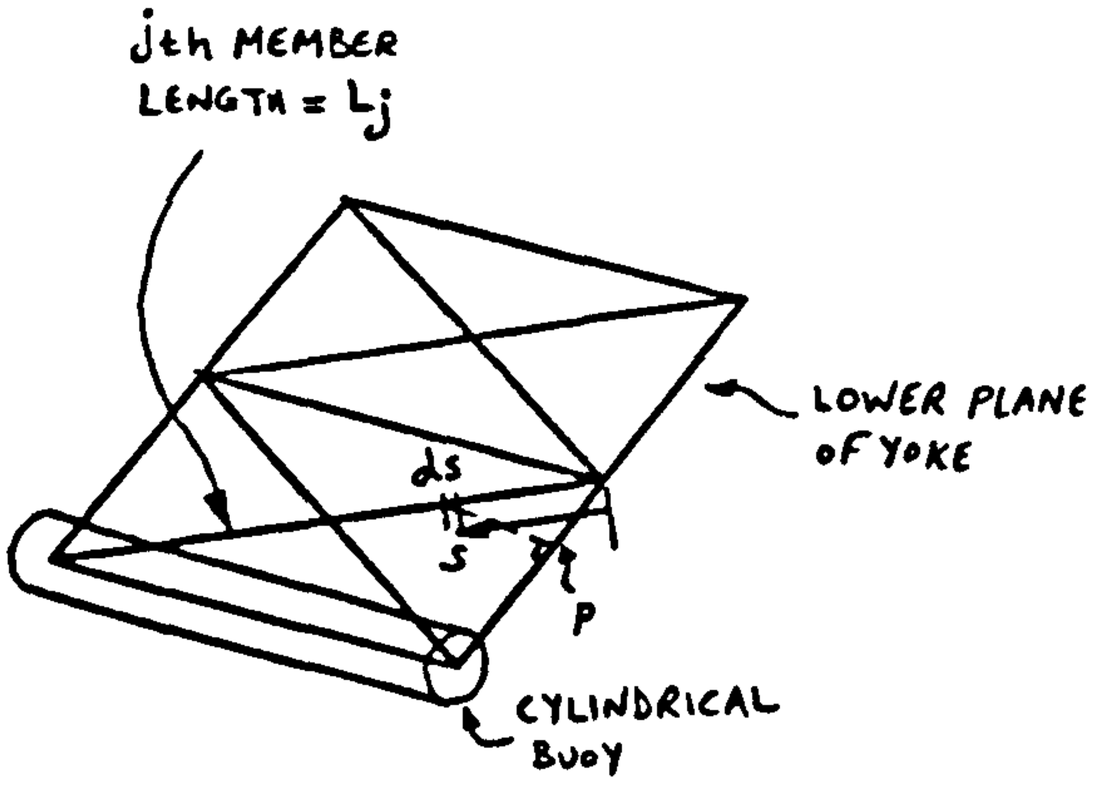

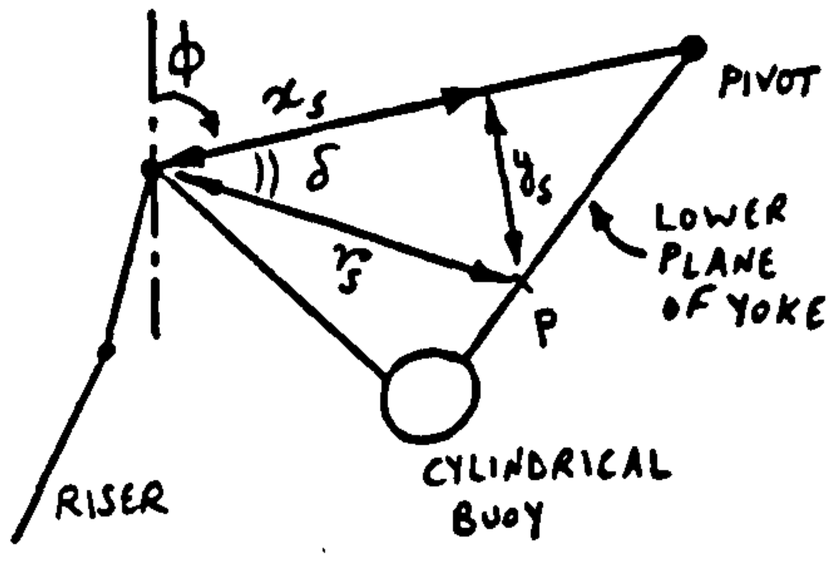

Vertical displacement of element =

$$\ell \sum_{i=1}^{N} \left[-\cos(\theta_i) + 1 \right] +$$

$$r_s \left[\cos(\delta) - \cos(\delta+\phi) \right]$$

(3.3.14)

Differentiating (3.3.13) and (3.3.14) with respect to time gives

Horizontal velocity of element , u_x =

$$\ell \sum_{i=1}^{N} \dot{\theta}_i \cos(\theta_i) +$$

$$\dot{\phi} \left[x_s \cos(\phi) - y_s \sin(\phi) \right] \qquad (3.3.15)$$

Vertical velocity of element, $u_y = \ell \sum_{i=1}^{N} \dot{\theta}_i \sin(\theta_i) + \dot{\phi}\,[x_s \sin(\phi) + y_s \cos(\phi)]$ (3.3.16)

Kinetic energy due to member j, $T_j = \frac{1}{2}\delta M_j \int_o^{L_j} (u_x^2 + u_y^2)\, ds$ (3.3.17)

Substituting for u_x and u_y from (3.3.15) and (3.3.16) into (3.3.17) and differentiating with respect to $\dot{\phi}$ gives

$$\frac{\partial T_j}{\partial \dot{\phi}} = \delta M_j \int_o^{L_j} \left\{ \ell \sum_{i=1}^{N} \dot{\theta}_i \left[x_s \cos(\alpha_{i\phi}) + y_s \sin(\alpha_{i\phi}) \right] + \dot{\phi}\,(x_s^2 + y_s^2) \right\} ds \quad (3.3.18)$$

For total kinetic energy of lower plane, T_ℓ, we have

$$\frac{d}{dt}\left(\frac{\partial T_\ell}{\partial \dot{\phi}}\right) = \frac{d}{dt} \sum_{j=10}^{15} \left(\frac{\partial T_j}{\partial \dot{\phi}}\right) \quad (3.3.19)$$

Evaluating (3.3.18) for individual members using values of x_s and y_s given in Table 3.2, and adding up and differentiating using (3.3.19) we have

$$\frac{d}{dt}\left(\frac{\partial T_l}{\partial \dot{\phi}}\right) = l \sum_{i=1}^{N} \ddot{\theta}_i \Big\{ \left[2M_{10}(2l_1+l_2) + M_{12}(l_1+l_2/2) + M_{15}\, l_1\right] Cos(\alpha_i\phi) +$$

$$l_5\left[2M_{10} + M_{12}/2 + M_{15}\right] Sin(\alpha_i\phi) \Big\} +$$

$$\dot{\theta}_i \Big\{ -\left[2M_{10}(2l_1+l_2) + M_{12}(l_1+l_2/2) + \right.$$

$$\left. M_{15}\, l_1\right](\dot{\theta}_i - \dot{\phi})\, Sin(\alpha_i\phi) +$$

$$l_5\left[2M_{10} + M_{12}/2 + M_{15}\right](\dot{\theta}_i - \dot{\phi})\, Cos(\alpha_i\phi) \Big\} +$$

$$\ddot{\phi}\left[2M_{10}\left(2l_1^2 + 3l_1l_2 + \tfrac{5}{3}l_2^2 + \tfrac{2}{3}l_5^2\right) + \right.$$

$$\left. M_{12}\left(l_1^2 + l_1l_2 + l_7^2/4\right) + M_{15}\left(l_5^2 + l_1^2\right)\right]$$

(3.3.20)

Member	x_s	y_s
10	$l_1 + l_2 - s\, l_2/2l_{10}$	$s\, l_5/2l_{10}$
11	DITTO	DITTO
12	$l_1 + l_2/2$	$l_5/2$
13	$l_1 + l_2/2 - s\, l_2/2l_{13}$	$l_5/2 + s\, l_5/2l_{13}$
14	DITTO	DITTO
15	l_1	l_5

TABLE 3.2. PARAMETERS x_s AND y_s FOR YOKE LOWER PLANE

Similarly

$$\frac{d}{dt}\left(\frac{\partial T_\ell}{\partial \dot{\theta}_k}\right) = \ell^2 (4M_{10} + M_{12} + M_{15}) \sum_{i=1}^{N} \left\{ \ddot{\theta}_i \cos(\alpha_{ik}) + \dot{\theta}_i (\dot{\theta}_k - \dot{\theta}_i) \sin(\alpha_{ik}) \right\} +$$

$$\ell \ddot{\phi} \left\{ \left[2M_{10} (2l_1 + l_2) + M_{12} (l_1 + l_2/2) + M_{15} l_1 \right] \cos(\alpha_{k\phi}) + \right.$$

$$\left. l_5 \left[2M_{10} + M_{12}/2 + M_{15} \right] \sin(\alpha_{k\phi}) \right\} +$$

$$\ell \dot{\phi} (\dot{\theta}_k - \dot{\phi}) \left\{ l_5 \left[2M_{10} + M_{12}/2 + M_{15} \right] \cos(\alpha_{k\phi}) - \right.$$

$$\left. \left[2M_{10} (2l_1 + l_2) + M_{12} (l_1 + l_2/2) + M_{15} l_1 \right] \sin(\alpha_{k\phi}) \right\}$$

(3.3.21)

$$\frac{\partial T_\ell}{\partial \phi} = \ell \dot{\phi} \sum_{i=1}^{N} \dot{\theta}_i \left\{ \left[2M_{10} (2l_1 + l_2) + M_{12} (l_1 + l_2/2) + M_{15} l_1 \right] \sin(\alpha_{i\phi}) - \right.$$

$$\left. l_5 \left[2M_{10} + \tfrac{1}{2} M_{12} + M_{15} \right] \cos(\alpha_{i\phi}) \right\}$$

(3.3.22)

$$\frac{\partial T_\ell}{\partial \theta_k} = (4M_{10} + M_{12} + M_{15}) \ell^2 \dot{\theta}_k \sum_{i=1}^{N} \dot{\theta}_i \sin(\alpha_{ik}) +$$

$$\ell \dot{\phi} \dot{\theta}_k \left\{ \left[-2M_{10} (2l_1 + l_2) - M_{12} (l_1 + \tfrac{1}{2} l_2) - M_{15} l_1 \right] \sin(\alpha_{k\phi}) + \right.$$

$$\left. l_5 \left[2M_{10} + \tfrac{1}{2} M_{12} + M_{15} \right] \cos(\alpha_{k\phi}) \right\}$$

(3.3.23)

Side Members:

For the sides of yoke structure, we consider an element on member j as shown below.

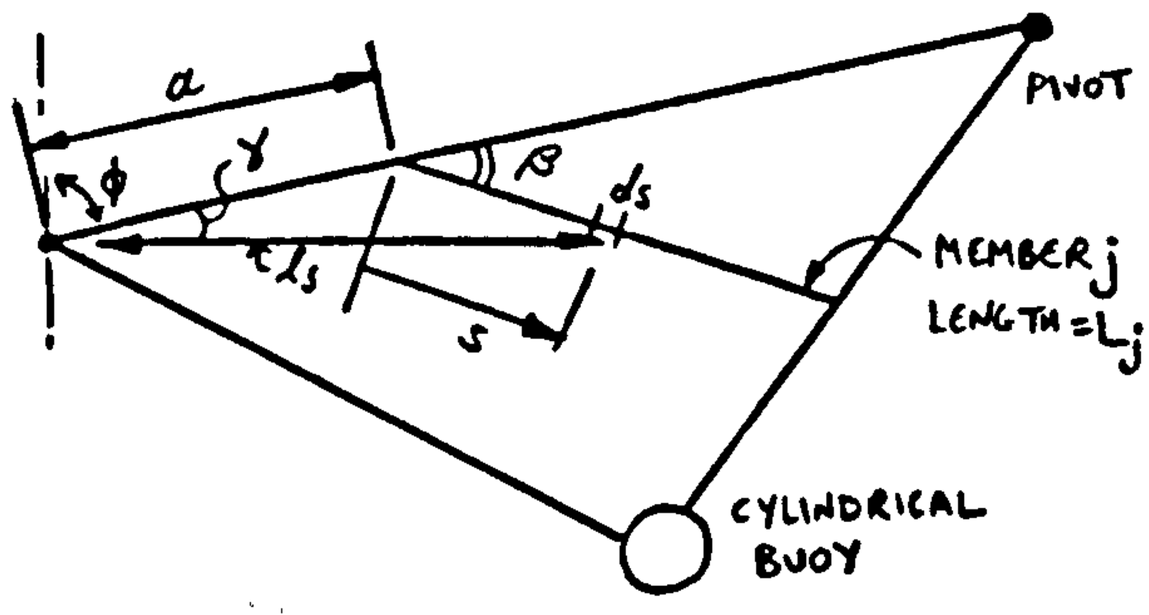

Horizontal displacement of element =

$$\ell \sum_{i=1}^{N} \sin(\theta_i) + l_s [\sin(\gamma+\phi) - \sin(\gamma)] \qquad (3.3.24)$$

Vertical displacement of element =

$$\ell \sum_{i=1}^{N} [1 - \cos(\theta_i)] + l_s [\cos(\gamma) - \cos(\gamma+\phi)] \qquad (3.3.25)$$

Noting that

$$l_s \cdot \sin(\gamma) = s \cdot \sin(\beta)$$

$$l_s \cdot \cos(\gamma) = a + s \cdot \cos(\beta)$$

Horizontal velocity of element , u_x =

$$\ell \sum_{i=1}^{N} \dot{\theta}_i \cos(\theta_i) + \dot{\phi}[\cos(\phi) \cdot (a + s\cos(\beta)) - \sin(\phi) \cdot s \cdot \sin(\beta)] \qquad (3.3.26)$$

Vertical velocity of element , u_y =

$$\ell \sum_{i=1}^{N} \dot{\theta}_i \sin(\theta_i) + \dot{\phi}[\sin(\phi) \cdot (a + s\cos(\beta)) + \cos(\phi) \cdot s \cdot \sin(\beta)] \qquad (3.3.27)$$

Using (3.3.26) and (3.3.27) in (3.3.17) and differentiating we get

$$\frac{\partial T_j}{\partial \dot{\phi}} = M_j \Big[\ell \sum_{i=1}^{N} \dot{\theta}_i \Big\{ \Big(a + \tfrac{1}{2} L_j \cos(\beta)\Big) \cdot \cos(\alpha_i \phi) + \tfrac{1}{2} L_j \sin(\beta) \cdot \sin(\alpha_i \phi) \Big\} + \dot{\phi} \Big\{ a^2 + a L_j \cos(\beta) + \tfrac{1}{3} L_j^2 \Big\} \Big] \qquad (3.3.28)$$

Noting that derivatives corresponding to kinetic energy of sides, T_s , can be written as

$$\frac{d}{dt}\left(\frac{\partial T_s}{\partial \dot{\phi}}\right) = 2 \sum_{j=16}^{21} \frac{d}{dt}\left(\frac{\partial T_j}{\partial \dot{\phi}}\right) \qquad (3.3.29)$$

and using parameters a and β as given in Table 3.3 for individual members we can write

Member	a	β
16	0	0
17	$(\ell_1+\ell_2)$	$\cos^{-1}(-\ell_2/\ell_7)$
18	$(\ell_1+\frac{1}{2}\ell_2)$	$\pi/2$
19	ℓ_1	$\cos^{-1}(\ell_2/2\ell_{19})$
20	ℓ_1	$\pi/2$
21	0	$\cos^{-1}(\ell_1/\ell_{21})$

TABLE 3.3 PARAMETERS a AND β FOR SIDES OF YOKE

$$\frac{d}{dt}\left(\frac{\partial T_s}{\partial \dot{\phi}}\right) = \ddot{\phi} \Big\{ \tfrac{2}{3} M_{16} (\ell_1+\ell_2)^2 + 2M_{17}\left(\tfrac{1}{3}\ell_7^2 + \ell_1^2 + \ell_1\ell_2\right) + M_{18}\left[2\left(\ell_1+\tfrac{1}{2}\ell_2\right)^2 + \tfrac{1}{6}\ell_5^2\right] + M_{19}\left(2\ell_1^2 + \ell_1\ell_2 + \tfrac{1}{6}\ell_7^2\right) +$$

$$2M_{20}\left(l_1^2+\tfrac{1}{3}l_5^2\right)+\tfrac{2}{3}M_{21}\left(l_5^2+l_1^2\right)\Big\}\ +$$

$$l\sum_{i=1}^{N}\Big\{\ddot{\theta}\Big\{C_{os}(\alpha_{i\phi})\left[M_{16}(l_1+l_2)+(2l_1+l_2)(M_{17}+M_{18})+M_{19}(2l_1+\tfrac{1}{2}l_2)+\right.$$

$$\left.l_1(2M_{20}+M_{21})\right]+$$

$$\sin(\alpha_{i\phi})\left[M_{17}+\tfrac{1}{2}M_{18}+\tfrac{1}{2}M_{19}+M_{20}+M_{21}\right]l_5\ \Big\}\ +$$

$$\dot{\theta}_i(\dot{\theta}_i-\dot{\phi})\Big\{C_{os}(\alpha_{i\phi})\left[M_{17}+\tfrac{1}{2}M_{18}+\tfrac{1}{2}M_{19}+M_{20}+M_{21}\right]l_5-$$

$$\sin(\alpha_{i\phi})\left[M_{16}(l_1+l_2)+(M_{17}+M_{18})(2l_1+l_2)+\right.$$

$$\left.M_{19}(2l_1+\tfrac{1}{2}l_2)+l_1(2M_{20}+M_{21})\right]\Big\}\Big\}$$

(3.3.30)

Similarly

$$\frac{d}{dt}\left(\frac{\partial T_s}{\partial\dot{\theta}_k}\right)=\left[2l^2\sum_{j=16}^{21}M_j\right]\sum_{i=1}^{N}\ddot{\theta}_i\,C_{os}(\alpha_{ik})+\dot{\theta}_i(\dot{\theta}_k-\dot{\theta}_i)\sin(\alpha_{ik})+$$

$$l\ddot{\phi}\Big\{C_{os}(\alpha_{k\phi})\left[M_{16}(l_1+l_2)+(M_{17}+M_{18})(2l_1+l_2)+\right.$$

$$\left.M_{19}(2l_1+\tfrac{1}{2}l_2)+l_1(2M_{20}+M_{21})\ \right]+$$

$$l_5\sin(\alpha_{k\phi})\left[M_{17}+\tfrac{1}{2}(M_{18}+M_{19})+M_{20}+M_{21}\right]\ \Big\}+$$

$$l\dot{\phi}(\dot{\theta}_k-\dot{\phi})\Big\{l_5\,C_{os}(\alpha_{k\phi})\left[M_{17}+\tfrac{1}{2}(M_{18}+M_{19})+M_{20}+M_{21}\right]-$$

$$\sin(\alpha_{k\phi})\left[M_{16}(l_1+l_2)+(M_{17}+M_{18})(2l_1+l_2)+\right.$$

$$\left.M_{19}(2l_1+\tfrac{1}{2}l_2)+l_1(2M_{20}+M_{21})\right]\Big\}$$

(3.3.31)

$$\frac{\partial T_s}{\partial \phi} = l\dot{\phi}\sum_{i=1}^{N}\dot{\theta}_i\Big\{\Big[M_{16}(l_1+l_2)+(M_{17}+M_{18})(2l_1+l_2)+M_{19}(2l_1+\tfrac{1}{2}l_2)+(2M_{20}+M_{21})l_1\Big]\sin(\alpha_{i\phi})-l_5\Big[M_{17}+\tfrac{1}{2}(M_{18}+M_{19})+M_{20}+M_{21}\Big]\cos(\alpha_{i\phi})\Big\}$$

(3.3.32)

and

$$\frac{\partial T_s}{\partial \theta_k} = l\dot{\theta}_k\Big\{\Big[2l\sum_{j=16}^{21}M_j\Big]\sum_{i=1}^{N}\dot{\theta}_i\sin(\alpha_{ik})+\dot{\phi}\Big[l_5\cos(\alpha_{k\phi})\Big(M_{17}+\tfrac{1}{2}(M_{18}+M_{19})+M_{20}+M_{21}\Big)-\sin(\alpha_{k\phi})\Big(M_{16}(l_1+l_2)+(M_{17}+M_{18})(2l_1+l_2)+M_{19}(2l_1+\tfrac{1}{2}l_2)+(2M_{20}+M_{21})l_1\Big)\Big]\Big\}$$

(3.3.33)

For total kinetic energy of yoke, T_y , we can write

$$\frac{d}{dt}\left(\frac{\partial T_y}{\partial \dot{\phi}}\right)=\frac{d}{dt}\left(\frac{\partial T_t}{\partial \dot{\phi}}\right)+\frac{d}{dt}\left(\frac{\partial T_l}{\partial \dot{\phi}}\right)+\frac{d}{dt}\left(\frac{\partial T_s}{\partial \dot{\phi}}\right) \qquad (3.3.34)$$

$$\frac{d}{dt}\left(\frac{\partial T_y}{\partial \dot{\theta}_k}\right)=\frac{d}{dt}\left(\frac{\partial T_t}{\partial \dot{\theta}_k}\right)+\frac{d}{dt}\left(\frac{\partial T_l}{\partial \dot{\theta}_k}\right)+\frac{d}{dt}\left(\frac{\partial T_s}{\partial \dot{\theta}_k}\right) \qquad (3.3.35)$$

$$\frac{\partial T_y}{\partial \phi} = \frac{\partial T_t}{\partial \phi} + \frac{\partial T_l}{\partial \phi} + \frac{\partial T_s}{\partial \phi} \qquad (3.3.36)$$

$$\frac{\partial T_y}{\partial \theta_k} = \frac{\partial T_t}{\partial \theta_k} + \frac{\partial T_l}{\partial \theta_k} + \frac{\partial T_s}{\partial \theta_k} \qquad (3.3.37)$$

Substituting for right hand side of (3.3.34) from (3.3.9), (3.3.20) and (3.3.30) gives

$$\frac{d}{dt}\left(\frac{\partial T_y}{\partial \dot{\phi}}\right) = l \sum_{i=1}^{N} \ddot{\theta}_i \left\{ \cos(\alpha_{i\phi}) \cdot A_m + \sin(\alpha_{i\phi}) \cdot B_m \right\} +$$

$$(\dot{\theta}_i - \dot{\phi})\dot{\theta}_i \left\{ \cos(\alpha_{i\phi}) \cdot B_m - \sin(\alpha_{i\phi}) \cdot A_m \right\} + \qquad (3.3.38)$$

$$\ddot{\phi} . D_m$$

where

$$A_m = \Big\{ (2l_1 + l_2)\left[2(M_1 + M_{10}) + M_{17} + M_{18} \right] + (2l_1 + \tfrac{1}{2} l_2)(M_7 + M_{19}) +$$

$$M_{12}\left(l_1 + \tfrac{1}{2} l_2\right) +$$

$$M_{16}(l_1 + l_2) + l_1 (M_5 + M_{15} + 2M_{20} + M_{21}) \Big\}$$

(3.3.39)

$$B_m = l_5 \left\{ 2M_{10} + M_{15} + M_{17} + M_{20} + M_{21} + \tfrac{1}{2}(M_{12} + M_{18} + M_{19}) \right\}$$

(3.3.40)

$$D_m = \Big\{ \tfrac{4}{3} M_1 (3l_1^2 + 3l_1 l_2 + l_2^2) + \tfrac{2}{3} M_5 l_1^2 + \tfrac{1}{3} M_7 (6l_1^2 + 3l_1 l_2 + \tfrac{3}{4} l_2^2) +$$

$$2M_{10}(2l_1^2 + 3l_1 l_2 + \tfrac{5}{3} l_2^2 + \tfrac{2}{3} l_5^2) + M_{12}(l_1^2 + l_1 l_2 + \tfrac{1}{4} l_7^2) +$$

$$M_{15}(l_5^2 + l_1^2) + \tfrac{2}{3} M_{16}(l_1 + l_2)^2 + 2M_{17}(\tfrac{1}{3} l_7^2 + l_1^2 + l_1 l_2) +$$

$$M_{18}\left[2(l_1 + \tfrac{1}{2} l_2)^2 + \tfrac{1}{6} l_5^2 \right] + M_{19}(2l_1^2 + l_1 l_2 + \tfrac{1}{6} l_7^2) +$$

$$2M_{20}(l_1^2 + \tfrac{1}{3} l_5^2) + \tfrac{2}{3} M_{21}(l_5^2 + l_1^2) \Big\}$$

(3.3.41)

Substituting for the right hand side of (3.3.35) from (3.3.10), (3.3.21) and (3.3.31) gives

$$\frac{d}{dt}\left(\frac{\partial T_y}{\partial \dot{\theta}_k}\right) = \ell^2 E_m \sum_{i=1}^{N} \left[\ddot{\theta}_i \cos(\alpha_{ik}) + \dot{\theta}_i (\dot{\theta}_k - \dot{\theta}_i) \sin(\alpha_{ik}) \right] +$$

$$\ell \ddot{\phi} \left\{ \cos(\alpha_{k\phi}) \cdot A_m + \sin(\alpha_{k\phi}) \cdot B_m \right\} +$$

$$\ell \dot{\phi}(\dot{\phi} - \dot{\theta}_k) \left\{ \sin(\alpha_{k\phi}) \cdot A_m - \cos(\alpha_{k\phi}) \cdot B_m \right\}$$

(3.3.42)

where

$$E_m = \left\{ 2(2M_1 + M_5 + \tfrac{3}{2}M_7) + 4M_{10} + M_{12} + M_{15} + 2\sum_{j=16}^{21} M_j \right\}$$

(3.3.43)

Substituting for the right hand side of (3.3.36) from (3.3.11), (3.3.22) and (3.3.32) we have

$$\frac{\partial T_y}{\partial \phi} = \ell \dot{\phi} \sum_{i=1}^{N} \dot{\theta}_i \left[A_m \sin(\alpha_{i\phi}) - B_m \cos(\alpha_{i\phi}) \right]$$

(3.3.44)

Substituting for the right hand side of (3.3.37) from (3.3.12), (3.3.23) and (3.3.33) gives

$$\frac{\partial T_y}{\partial \theta_k} = \ell^2 \dot{\theta}_k E_m \sum_{i=1}^{N} \dot{\theta}_i \sin(\alpha_{ik}) +$$

$$\ell \dot{\theta}_k \dot{\phi} \left[-A_m \sin(\alpha_{k\phi}) + B_m \cos(\alpha_{k\phi}) \right] \qquad (3.3.45)$$

3.3.2 Potential Energy of Yoke

Variation in buoyancy due to yoke motion is considered in section 3.3.4. Assuming that the total buoyancy force, F_B , acts at the centre of the submerged buoy as shown in Fig.3.6 we have

Vertical displacement of C.G. (upwards) =

$$-l\sum_{i=1}^{N}[1-\cos(\theta_i)] + l_G[\sin(\mu)+\cos(\mu+\phi)] \qquad (3.3.46)$$

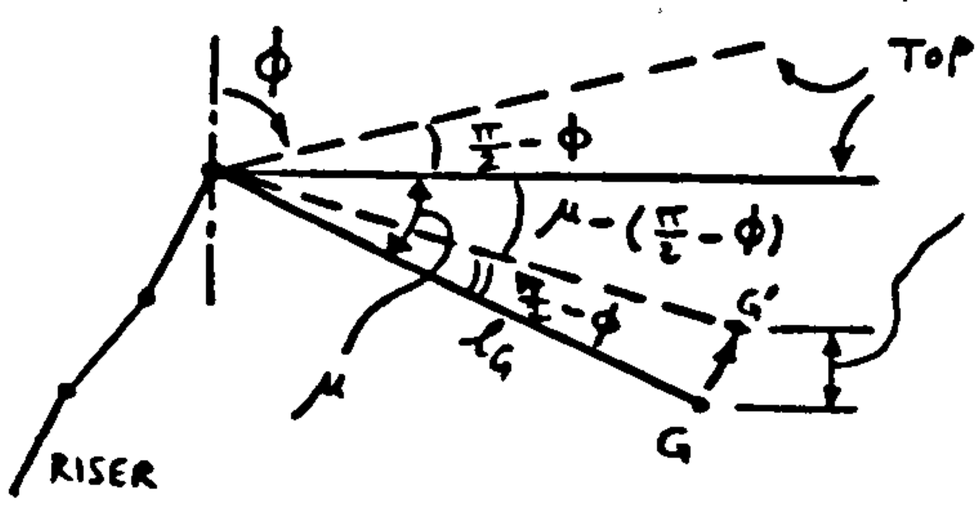

$l_G[\sin(\mu)-\sin(\mu-\frac{\pi}{2}+\phi)] =$

$l_G[\sin(\mu)+\cos(\mu+\phi)]$

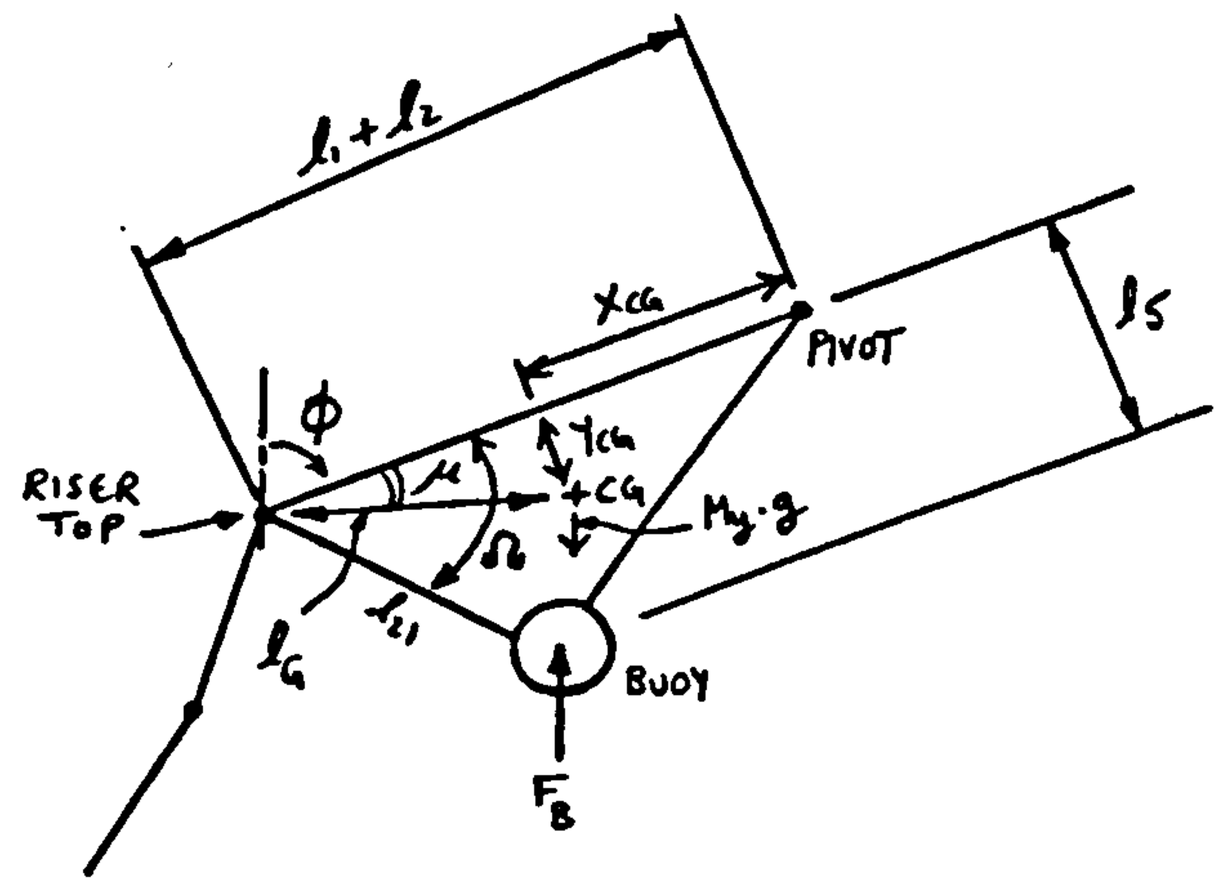

FIG.3.6 VERTICAL DISPLACEMENT OF YOKE CENTRE OF GRAVITY

M_y = total structural mass of yoke

l_G = distance of yoke centre of gravity (C.G.) from riser top

Vertical displacement
of buoy (upwards) =

$$-l\sum_{i=1}^{N}[1-\cos(\theta_i)] + l_{21}[\sin(\Omega)+\cos(\Omega+\phi)] \qquad (3.3.47)$$

Increase in potential energy
due to displacement of C.G. =

$$M_y g\left\{-l\sum_{i=1}^{N}[1-\cos(\theta_i)] + l_G[\sin(\mu)+\cos(\mu+\phi)]\right\} \qquad (3.3.48)$$

Increase in potential energy
due to buoyancy force F_B =

$$-F_B\left\{-l\sum_{i=1}^{N}[1-\cos(\theta_i)] + l_{21}[\sin(\Omega)+\cos(\Omega+\phi)]\right\} \qquad (3.3.49)$$

Adding up (3.3.48) and (3.3.49) we have

Total increase in potential energy
of yoke

$$V_y = [F_B - M_y g]\left\{l\sum_{i=1}^{N}[1-\cos(\theta_i)]\right\} +$$

$$M_y g\, l_G[\sin(\mu)+\cos(\mu+\phi)] -$$

$$F_B\, l_{21}[\sin(\Omega)+\cos(\Omega+\phi)] \qquad (3.3.50)$$

Differentiating (3.3.50) with respect to ϕ we have

$$\frac{\partial V_y}{\partial \phi} = -M_y g\, l_c \sin(\mu+\phi) + F_B\, l_{21} \sin(\Omega+\phi) \qquad (3.3.51)$$

Substituting for $\sin(\mu+\phi)$ and $\sin(\Omega+\phi)$ in (3.3.51) from the following

$$\sin(\mu+\phi) = \frac{Y_{CG}}{l_G}\cos(\phi) + \frac{(l_1+l_2-X_{CG})}{l_G}\sin(\phi) \qquad (3.3.52)$$

$$\sin(\Omega+\phi) = \frac{l_5}{l_{21}}\cos(\phi) + \frac{l_1}{l_{21}}\sin(\phi) \qquad (3.3.53)$$

we get

$$\frac{\partial V_y}{\partial \phi} = -M_y g\,[\, Y_{CG}\cdot\cos(\phi) + (l_1+l_2-X_{CG})\sin(\phi)\,] +$$

$$F_B\,[\, l_5\cdot\cos(\phi) + l_1\cdot\sin(\phi)\,] \qquad (3.3.54)$$

Differentiating (3.3.50) with respect to θ_k

$$\frac{\partial V_y}{\partial \theta_k} = l\,[\, F_B - M_y g\,]\sin(\theta_k) \qquad (3.3.55)$$

For the yoke structure under consideration, X_{CG} and Y_{CG} found by moment equilibrium can be expressed as

$$X_{CG} = \Big\{ \ell_2 \big[2 (M_1 + M_5 + M_{10} + M_{20} + M_{21}) + \tfrac{1}{2}(5M_7 + M_{12} + 3M_{19}) + M_{15} + M_{16} + M_{17} + M_{18} \big] + \ell_1 \big[M_5 + M_7 + M_{16} + M_{21} \big] \Big\} / M_y \tag{3.3.56}$$

$$Y_{CG} = \Big\{ \ell_5 \big[\tfrac{1}{2}(3M_7 + M_{12} + M_{19}) + 2(M_{10} + M_{20}) + M_{15} + M_{17} + M_{18} + M_{21} \big] \Big\} / M_y \tag{3.3.57}$$

Note: F_B is a function of time and changes with variations in yoke submergence level and is given in Section 3.3.4.

3.3.3 Generalised Wave Forces on Buoy

In this section we derive expressions for the generalised wave inertia and drag forces on the buoy due to wave motion. As shown in Fig.3.7, the coordinates of the buoy can be written as

$$x_b = -\Big\{ X_s + \ell_1 + \ell_2 + \tfrac{L}{2} - \ell \sum_{i=1}^{N} \sin(\theta_i) - \ell_{21} \sin(\Omega + \phi) \Big\} \tag{3.3.58}$$

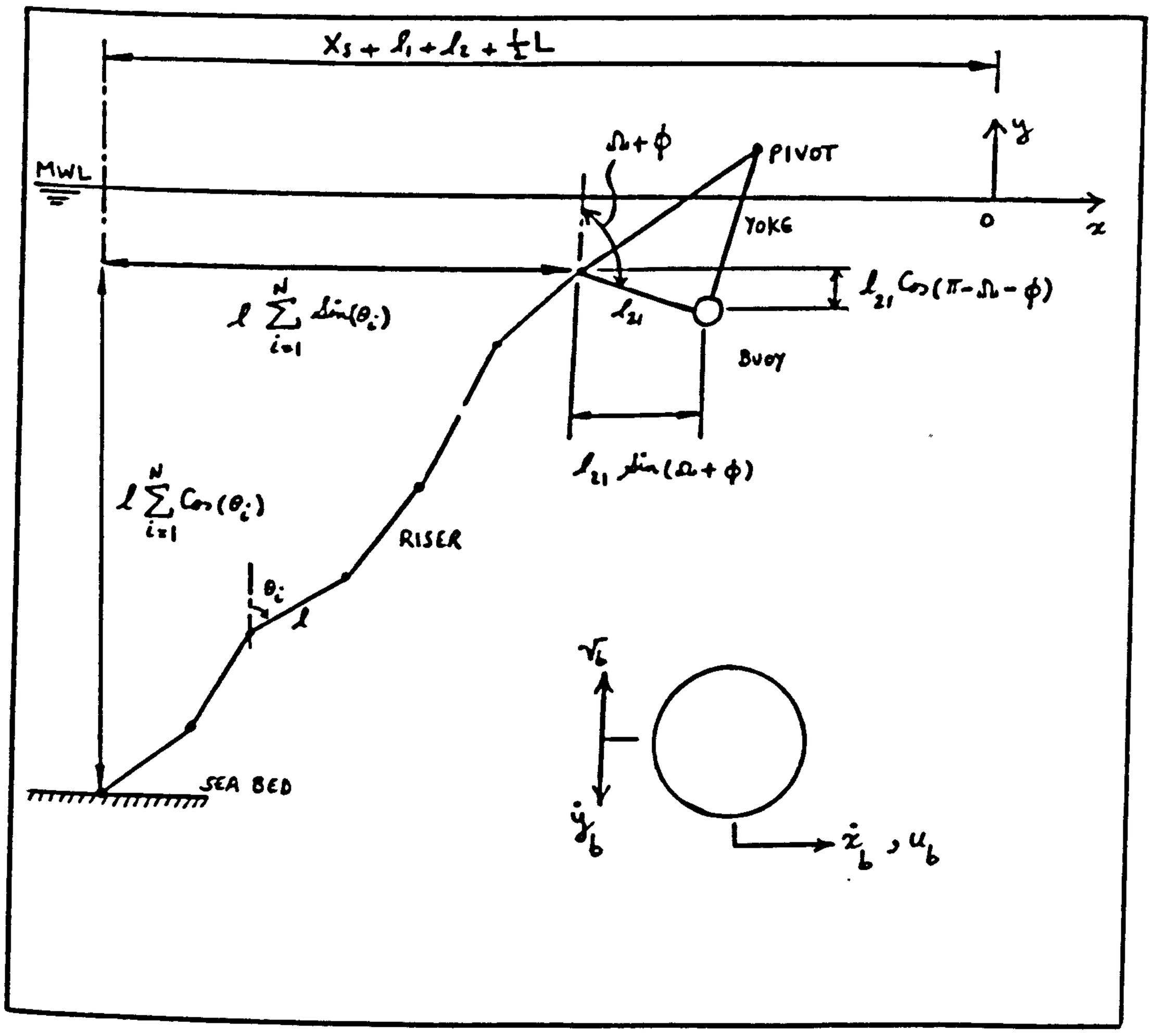

FIG.3.7. INSTANTANEOUS POSITION OF YOKE STRUCTURE

Substituting for $\sin(\Omega+\phi)$ from (3.3.53) into (3.3.58) gives

$$x_b = -X_s - (l_1+l_2) - \frac{1}{2}L + l\sum_{i=1}^{N}\sin(\theta_i) + l_5\cos(\phi) + l_1\sin(\phi) \qquad (3.3.59)$$

$$y_b = -\left\{ d - l \sum_{i=1}^{N} \cos(\theta_i) - l_{21} \cos(\Omega + \phi) \right\} \qquad (3.3.60)$$

Noting that

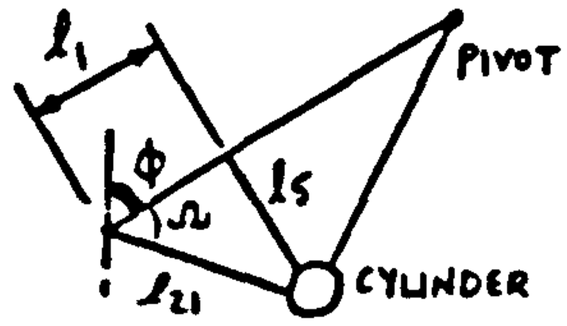

$$l_{21} \cos(\Omega + \phi) = l_1 \cos(\phi) - l_5 \sin(\phi)$$

Equation (3.3.60) can be written as

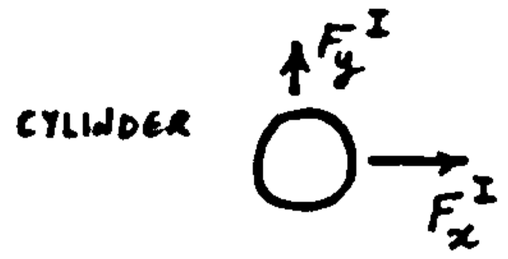

$$y_b = -d + l \sum_{i=1}^{N} \cos(\theta_i) + l_1 \cos(\phi) - l_5 \sin(\phi) \qquad (3.3.61)$$

Inertia Force

Fluid inertia force on buoy from Morison's formula is

In x-direction,

$$F_x^I = \rho \frac{\pi D_b^2}{4} C_m L_b \dot{u} \qquad (3.3.62)$$

In y-direction,

$$F_y^I = \rho \frac{\pi D_b^2}{4} C_m L_b \dot{v} \qquad (3.3.63)$$

where D_b = buoy diameter

C_m = inertia coefficient

$\dot{u}$ and $\dot{v}$ are horizontal and vertical fluid particle accelerations respectively given by linear wave

theory as

$$\dot{u} = \frac{\omega^2 H}{2} \frac{\cosh k(d+y_b)}{\sinh(kd)} \sin(kx_b - \omega t) \tag{3.3.64}$$

$$\dot{v} = \frac{-\omega^2 H}{2} \frac{\sinh k(d+y_b)}{\sinh(kd)} \cos(kx_b - \omega t) \tag{3.3.65}$$

Drag Force

Horizontal displacement of buoy $= \ell \sum_{i=1}^{N} \sin(\theta_i) + l_5 \cos(\phi) + l_1 \sin(\phi)$

Velocity of cylinder in x-direction

$$\dot{x}_b = \ell \sum_{i=1}^{N} \dot{\theta}_i \cos(\theta_i) + \dot{\phi}[l_1 \cos(\phi) - l_5 \sin(\phi)] \tag{3.3.66}$$

From (3.3.47)

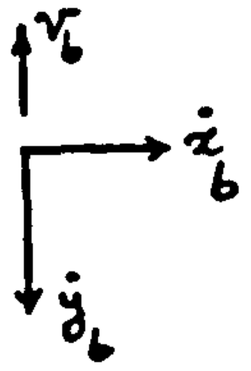

Velocity of cylinder in y-direction

$$\dot{y}_b = \ell \sum_{i=1}^{N} \dot{\theta}_i \sin(\theta_i) + \dot{\phi}[l_1 \sin(\phi) + l_5 \cos(\phi)] \tag{3.3.67}$$

Fluid particle velocities at instantaneous position of buoy are:

In x-direction

$$u_b = \frac{\omega H}{2} \frac{\cosh k(d+y_b)}{\sinh (kd)} \cos (kx_b - \omega t) \qquad (3.3.68)$$

In y-direction

$$v_b = \frac{\omega H}{2} \frac{\sinh k(d+y_b)}{\sinh (kd)} \sin (kx_b - \omega t) \qquad (3.3.69)$$

Relative velocities at instantaneous position of buoy are

In x-direction

$$U_b = u_b + V_c(y_b) - \dot{x}_b \qquad (3.3.70)$$

In y-direction

$$V_b = v_b + \dot{y}_b \qquad (3.3.71)$$

Resultant drag force on buoy

$$F_R = \frac{1}{2} \rho C_D D_b L_b (U_b^2 + V_b^2) \qquad (3.3.72)$$

Horizontal component of drag force

$$F_x^D = F_R \frac{U_b}{\sqrt{U_b^2 + V_b^2}}$$

or

$$F_x^D = \frac{1}{2} \rho \cdot C_D \cdot D_b \cdot L_b \cdot U_b \sqrt{U_b^2 + V_b^2} \qquad (3.3.73)$$

Similarly vertical component of drag force on cylinder,

$$F_y^D = \frac{1}{2} \rho C_D D_b L_b V_b \sqrt{U_b^2 + V_b^2} \qquad (3.3.74)$$

Total forces acting on cylinder are

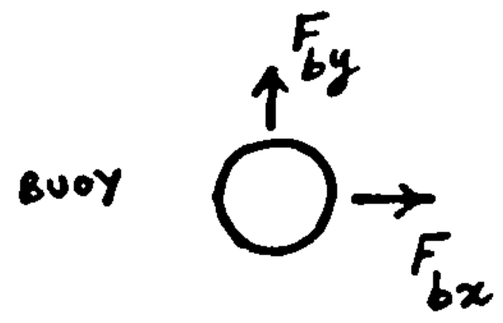

In x-direction,

$$F_{bx} = F_x^I + F_x^D \qquad (3.3.75)$$

In y-direction,

$$F_{by} = F_y^I + F_y^D \qquad (3.3.76)$$

Generalised wave forces on buoy:

Horizontal displacement of buoy due to a virtual link displacement $\delta\theta_k$ of k^{th} link,

$$\delta x_{bk} = l . \delta\theta_k . \cos(\theta_k) \qquad (3.3.77)$$

Vertically,

$$\delta y_{bk} = -l . \delta\theta_k . \sin(\theta_k) \qquad (3.3.78)$$

Let F_{bx} and F_{by} denote total x and y components of wave force on buoy. Then work done by F_b is

$$\delta W_{kb} = F_{bx} \cdot \delta x_{bk} + F_{by} \cdot \delta y_{bk} \qquad (3.3.79)$$

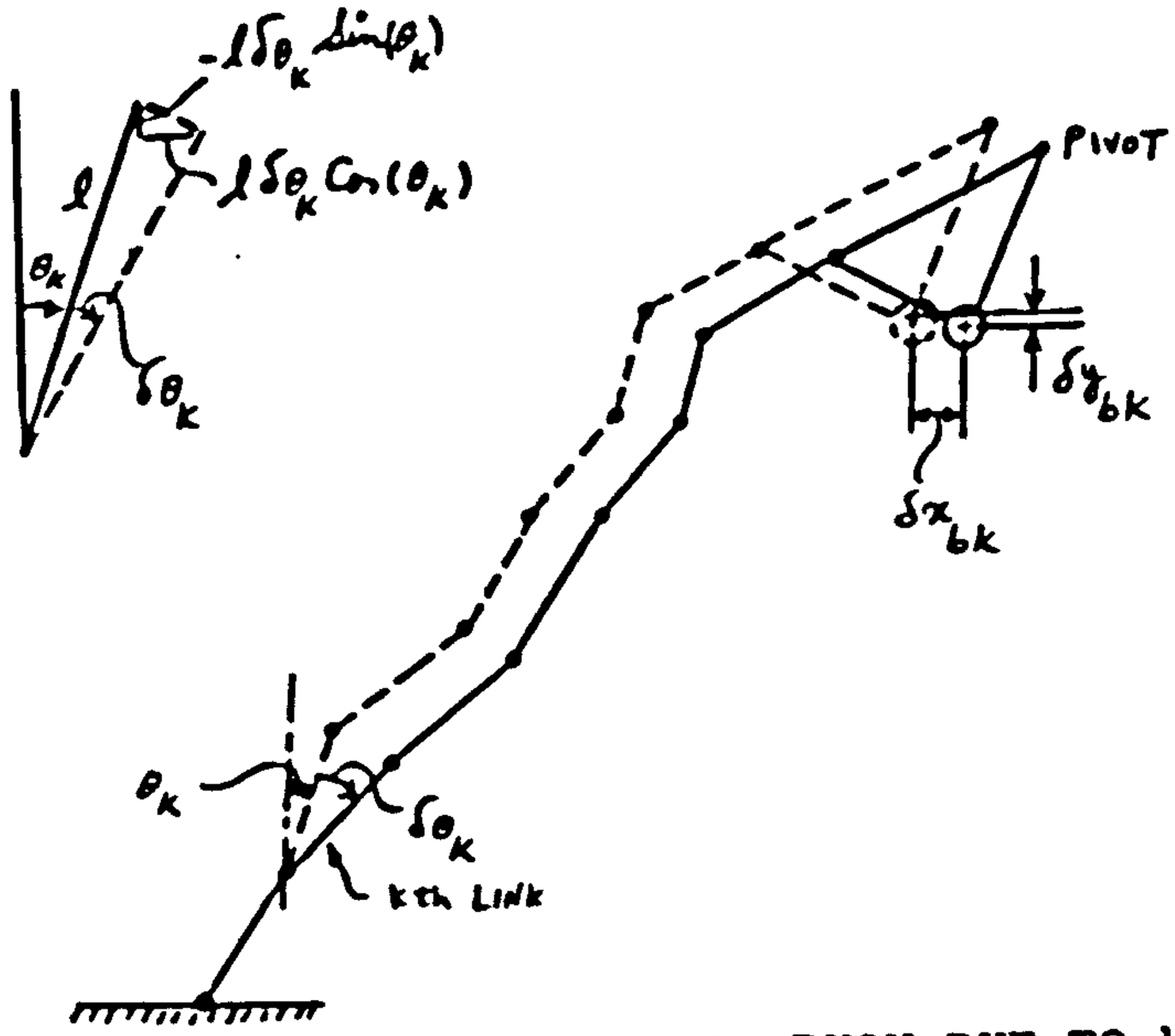

FIG.3.8. VIRTUAL DISPLACEMENTS OF BUOY DUE TO k^{th} LINK

Substituting for δx_{bk} and δy_{bk} from (3.3.77) and (3.3.78) into (3.3.79) gives

$$\delta W_{kb} = l\left[F_{bx} \cdot \cos(\theta_k) - F_{by} \cdot \sin(\theta_k)\right] \delta\theta_k \qquad (3.3.80)$$

Generalised wave force on buoy corresponding to θ_k

$$Q_{kb} = \frac{\delta W_{kb}}{\delta\theta_k} = l\left[F_{bx} \cdot \cos(\theta_k) - F_{by} \cdot \sin(\theta_k)\right] \qquad (3.3.81)$$

Work done due to a virtual displacement $\delta\phi$ of yoke can be found by reference to Figure 3.9.

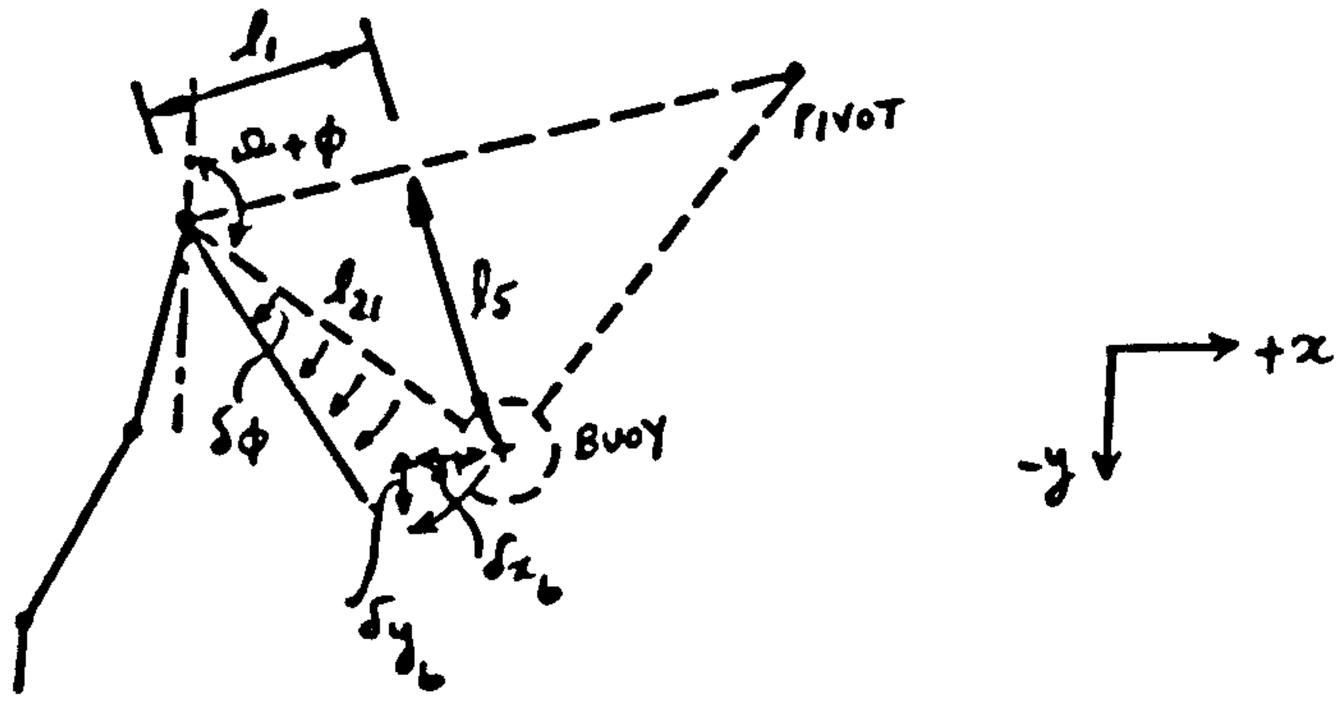

FIG.3.9. VIRTUAL DISPLACEMENT OF YOKE

Horizontal displacement of buoy,

$$\delta x_b = -\left[l_5 \sin(\phi) - l_1 \cos(\phi)\right]\delta\phi \qquad (3.3.82)$$

Vertical displacement of buoy,

$$\delta y_b = -\left[l_5 \cos(\phi) + l_1 \sin(\phi)\right]\delta\phi \qquad (3.3.83)$$

Work done by forces acting on buoy,

$$\delta W_y = F_{bx} \cdot \delta x_b + F_{by} \cdot \delta y_b \qquad (3.3.84)$$

Generalised force corresponding to ϕ is

$$Q_\phi = \delta W_y / \delta\phi \qquad (3.3.85)$$

Substituting for δx_b and δy_b from (3.3.82) and (3.3.83) into (3.3.84) and then (3.3.85) we have

$$Q_\phi = F_{bx}\left[\ell_1 \cos(\phi) - \ell_5 \sin(\phi)\right] - F_{by}\left[\ell_1 \sin(\phi) + \ell_5 \cos(\phi)\right] \qquad (3.3.86)$$

3.3.4 Change of Buoyancy Force due to Yoke Submersion

In reality the change in buoyancy due to motion of the yoke relative to the wave free surface elevation should be considered. However, since the wave forces are calculated using linear wave theory up to the mean water level only, a similar simplification is made for calculation of the variation in the submerged volume of the yoke.

To find the variation in buoyancy force due to yoke motion we derive a relationship between the wetted lengths of yoke members relative to mean water level and angle ϕ. For an arbitrary side member as shown below (also see Fig.3.5) we can write

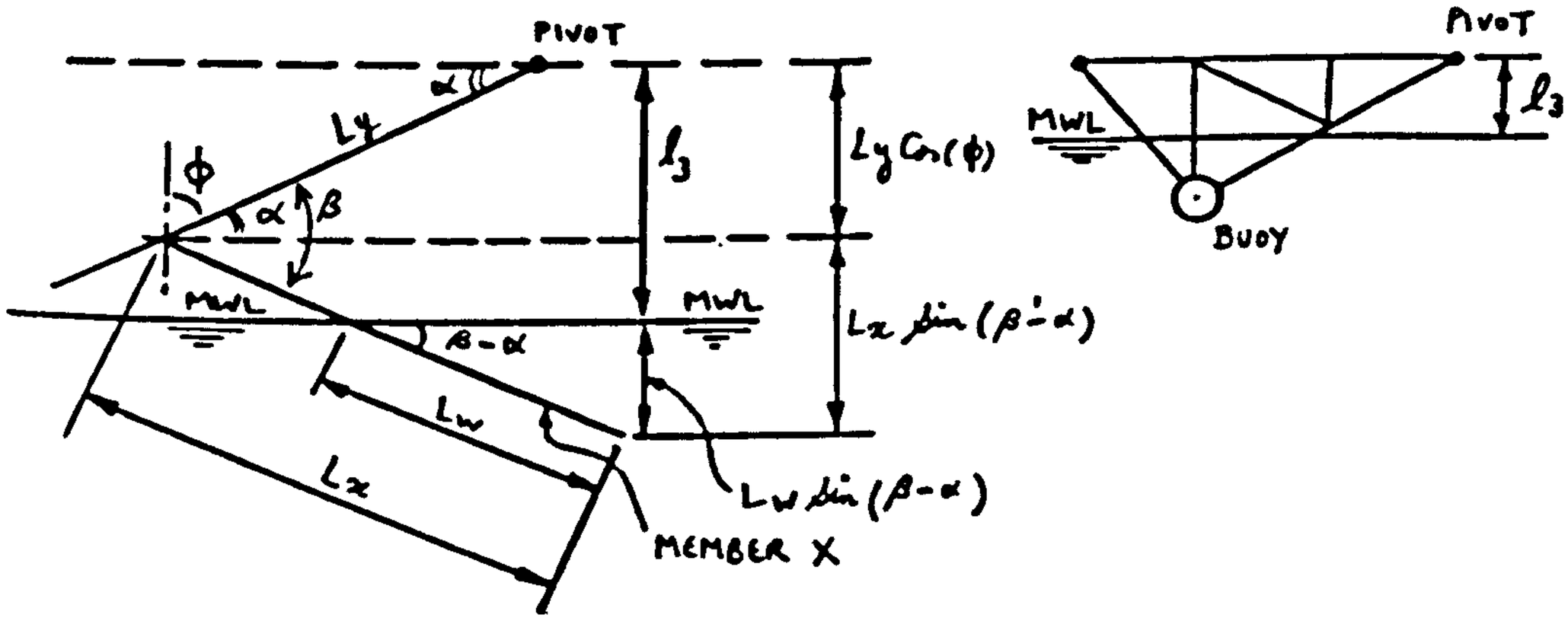

$$\ell_3 = L_y \cos(\phi) + (L_x - L_w)\sin(\beta - \alpha) \qquad (3.3.87)$$

but

$$\alpha = \frac{\pi}{2} - \phi$$

Substituting for α

$$L_W = \frac{\ell_3 + L_x \cos(\beta + \phi) - L_y \cos(\phi)}{\cos(\beta + \phi)} \qquad (3.3.88)$$

Note: For top longitudinals $\beta = \pi$ in (3.3.88) and $(L_x + L_y)$ is length of member.

If $L_W < 0$ member is not submerged.

For verticals $\beta = \frac{\pi}{2}$

For the upper and lower planes of yoke, as shown below, the wetted length of diagonal bracing members can be found from

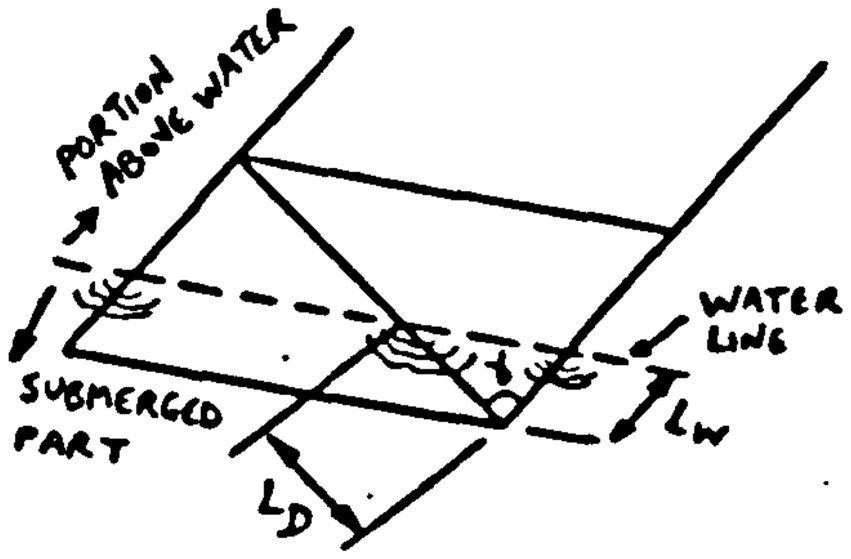

$$L_D = \frac{L_W}{\cos(\gamma)} \quad ; \gamma \neq \frac{\pi}{2} \qquad (3.3.89)$$

Once the wetted length of all members at each value of ϕ are found, buoyancy force can be calculated as a function of ϕ.

Total buoyancy force can be written as

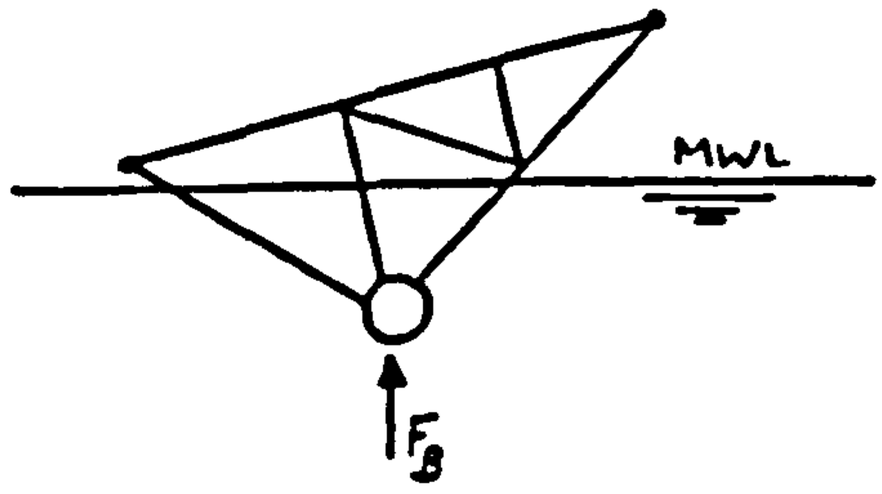

$$F_B = \rho g \frac{\pi}{4} \sum_{i=1}^{S} L_{W_i} \; D_i^2 \qquad (3.3.90)$$

where

L_{W_i} = wetted length of i^{th} member

S = total number of submerged members (including the buoy)

D_i = diameter of i^{th} member

3.4 Tanker Bow Pivot Motions

Tanker surge x_G, heave y_G and pitch θ_G caused by regular wave motions, give rise to bow pivot motions as follows;

Horizontal Displacement $$x_p = x_G - l_3' \theta_G \quad (3.4.1)$$

Horizontal Velocity, $$\dot{x}_p = \dot{x}_G - l_3' \dot{\theta}_G \quad (3.4.2)$$

Horizontal Acceleration $$\ddot{x}_p = \ddot{x}_G - l_3' \ddot{\theta}_G \quad (3.4.3)$$

Vertical Displacement $$y_p = y_G - \tfrac{1}{2} L \theta_G \quad (3.4.4)$$

Vertical Velocity $$\dot{y}_p = \dot{y}_G - \tfrac{1}{2} L \dot{\theta}_G \quad (3.4.5)$$

Vertical Acceleration $$\ddot{y}_p = \ddot{y}_G - \tfrac{1}{2} L \ddot{\theta}_G \quad (3.4.6)$$

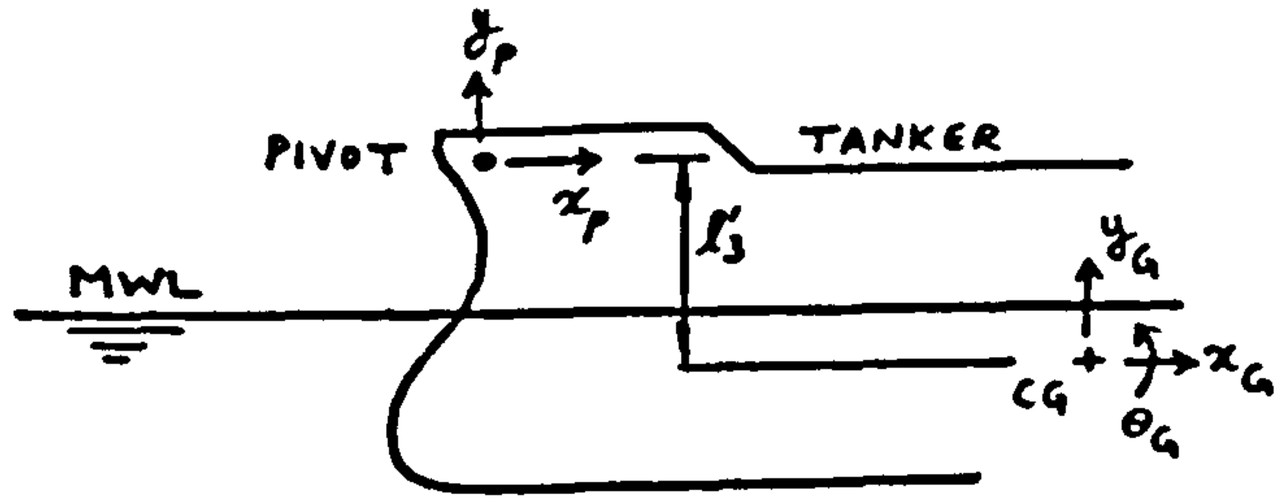

Tanker motions can be evaluated using transfer functions given by Kirk (45) (see Appendix B)

3.5 Geometric Constraints

The two geometric constraints on the system arise from the prescribed hoirzontal and vertical displacements x_p, y_p . Referring to figure 3.3 and equation (3.1.1) the two equations of constraint are

Horizontally,

$$f_1 = (l_1 + l_2)\sin(\phi) + l\sum_{i=1}^{N}\sin(\theta_i) - X_s - (l_1 + l_2) - x_p = 0 \quad (3.5.1)$$

Vertically,

$$f_2 = (l_1 + l_2)\cos(\phi) + l\sum_{i=1}^{N}\cos(\theta_i) - d - l_3 - y_p = 0 \qquad (3.5.2)$$

3.6 Lagrange's Constrained Equations of Motion

For an M-degree of freedom system the equations of motion are usually written in terms of generalised coordinates, however, in some cases the set of coordinates involved in the dynamic analysis exceeds the number of degrees of freedom of the system, say by N_c , and therefore one must impose N_c equations of constraint to the system. Equations of constraint are related to equations of motion by the use of time functions λ_i $(i = 1, 2, \ldots, N_c)$ known as Lagrange multipliers as in equation (3.1.1).

Differentiating (3.5.1) and (3.5.2) with respect to the generalised coordinates θ_k and ϕ we get

$$\frac{\partial f_1}{\partial \theta_k} = l\cos(\theta_k) \qquad ; k = 1, 2, \ldots, N \qquad (3.6.1)$$

$$\frac{\partial f_1}{\partial \phi} = (l_1 + l_2)\cos(\phi) \qquad (3.6.2)$$

$$\frac{\partial f_2}{\partial \theta_k} = -l\sin(\theta_k) \qquad ; k = 1, 2, \ldots, N \qquad (3.6.3)$$

$$\frac{\partial f_2}{\partial \phi} = -(l_1 + l_2)\sin(\phi) \qquad (3.6.4)$$

Substituting equations (3.6.1) to (3.6.4) into (3.1.1) we have

$$\frac{d}{dt}\left(\frac{\partial T}{\partial \dot{\theta}_k}\right) - \frac{\partial T}{\partial \theta_k} + \frac{\partial V}{\partial \theta_k} = Q_k + \lambda_1 \cdot l \cdot \cos(\theta_k) - \lambda_2 \cdot l \cdot \sin(\theta_k) \qquad (3.6.5)$$

where

$$\frac{d}{dt}\left(\frac{\partial T}{\partial \dot{\theta}_k}\right)=\frac{d}{dt}\left(\frac{\partial T_L}{\partial \dot{\theta}_k}\right)+\frac{d}{dt}\left(\frac{\partial T_y}{\partial \dot{\theta}_k}\right) \qquad (3.6.6)$$

(LINKS, YOKE)

$$; k=1,2,\ldots,N$$

are given by equations (3.2.22) and (3.3.38) respectively and

$$\frac{\partial T}{\partial \theta_k}=\frac{\partial T_L}{\partial \theta_k}+\frac{\partial T_y}{\partial \theta_k} \qquad (3.6.7)$$

$$; k=1,2,\ldots,N$$

are given by equations (3.2.30) and (3.3.45). Also

$$\frac{\partial V}{\partial \theta_k}=\frac{\partial V_L}{\partial \theta_k}+\frac{\partial V_y}{\partial \theta_k} \qquad (3.6.8)$$

$$; k=1,2,\ldots,N$$

are evaluated from equations (3.2.38) and (3.3.55). The generalised forces are given by

$$Q_k = Q_{k\ell} + Q_{kb} \qquad ; k=1,2,\ldots,N \qquad (3.6.9)$$

which can be evaluated using equations (3.2.55) and (3.3.81). For the yoke:

$$\frac{d}{dt}\left(\frac{\partial T_y}{\partial \dot{\phi}}\right)-\frac{\partial T_y}{\partial \phi}+\frac{\partial V_y}{\partial \phi}=Q_\phi+\lambda_1(\ell_1+\ell_2)\cos(\phi)-\lambda_2(\ell_1+\ell_2)\sin(\phi) \qquad (3.6.10)$$

where the left hand side is evaluated using equations (3.3.42, 3.3.44 and 3.3.54) and Q_ϕ is found from (3.3.86). Equations (3.6.5) and (3.6.10) provide (N+1) equations to be

solved. The (N+3) unknowns are θ_k $(k=1,2,\ldots,N)$, ϕ and the Lagrange multipliers λ_1 and λ_2. Making use of the two constraints, equations (3.5.1) and (3.5.2), all unknowns can thus be found. Lagrange multipliers can be found from the equations of motion of the yoke and the Nth link in terms of $\theta_k, \dot{\theta}_k, \ddot{\theta}_k$ $(k=1,\ldots,N)$ and $\phi, \dot{\phi}, \ddot{\phi}$. Substituting these into the remaining equations gives (N-1) equations involving $\theta_k, \dot{\theta}_k, \ddot{\theta}_k$ $(k=1,\ldots,N)$ and $\phi, \dot{\phi}, \ddot{\phi}$. Now $\theta_N, \dot{\theta}_N, \ddot{\theta}_N$ and $\phi, \dot{\phi}, \ddot{\phi}$ can be evaluated from the constraint equations as follows:

The constraint equations (3.5.1) and 3.5.2) can be written as

$$(l_1+l_2)\sin(\phi) = X_s + l_1 + l_2 + x_p - l\sum_{i=1}^{N-1}\sin(\theta_i) - l\sin(\theta_N) \qquad (3.6.11)$$

$$(l_1+l_2)\cos(\phi) = d + l_3 + y_p - l\sum_{i=1}^{N-1}\cos(\theta_i) - l\cos(\theta_N) \qquad (3.6.12)$$

Let

$$A = X_s + l_1 + l_2 + x_p - l\sum_{i=1}^{N-1}\sin(\theta_i) \qquad (3.6.13)$$

$$B = d + l_3 + y_p - l\sum_{i=1}^{N-1}\cos(\theta_i) \qquad (3.6.14)$$

Squaring (3.6.11), (3.6.12) and adding using (3.6.13) and (3.6.14) gives

$$a_1\sin(\theta_N) + b_1\cos(\theta_N) + c_1 = 0 \qquad (3.6.15)$$

where

$$a_1 = 2Al \tag{3.6.16}$$

$$b_1 = 2Bl \tag{3.6.17}$$

$$c_1 = (l_1 + l_2)^2 - A^2 - B^2 - l^2 \tag{3.6.18}$$

To solve (3.6.15) for θ_N assume

$$x_1 = \tan\left(\frac{\theta_N}{2}\right) \tag{3.6.19}$$

$$\sin(\theta_N) = \frac{2\tan\left(\frac{\theta_N}{2}\right)}{1+\tan^2\left(\frac{\theta_N}{2}\right)} = \frac{2x_1}{1+x_1^2} \tag{3.6.20}$$

$$\cos(\theta_N) = \frac{1-\tan^2\left(\frac{\theta_N}{2}\right)}{1+\tan^2\left(\frac{\theta_N}{2}\right)} = \frac{1-x_1^2}{1+x_1^2} \tag{3.6.21}$$

Substituting for $\sin(\theta_N)$ and $\cos(\theta_N)$ from (3.6.20 and 3.6.21) into (3.6.15) we have

$$(c_1 - b_1)x_1^2 + 2a_1x_1 + (b_1 + c_1) = 0 \tag{3.6.22}$$

giving

$$x_1 = \frac{-a_1 \pm \sqrt{a_1^2 - c_1^2 + b_1^2}}{(c_1 - b_1)} \qquad (3.6.23)$$

Substituting for x_1 from (3.6.23) into (3.6.20) and (3.6.21) gives θ_N in terms of θ_K $(K=1, 2, \ldots, (N-1))$. Now ϕ can be found from (3.6.11 and 3.6.12)

$$\sin(\phi) = [A - l \sin(\theta_N)] / (l_1 + l_2) \qquad (3.6.24)$$

$$\cos(\phi) = [B - l \cos(\theta_N)] / (l_1 + l_2) \qquad (3.6.25)$$

Differentiating (3.6.11 and 3.6.12) with respect to t gives

$$(l_1 + l_2)\dot{\phi}\cos(\phi) + l\dot{\theta}_N \cos(\theta_N) = \dot{x}_p - l\sum_{i=1}^{N-1} \dot{\theta}_i \cos(\theta_i) \qquad (3.6.26)$$

$$-(l_1 + l_2)\dot{\phi}\sin(\phi) - l\dot{\theta}_N \sin(\theta_N) = \dot{y}_p + l\sum_{i=1}^{N-1} \dot{\theta}_i \sin(\theta_i) \qquad (3.6.27)$$

From equations (3.6.13 and 3.6.14)

$$\dot{A} = \dot{x}_p - l\sum_{i=1}^{N-1} \dot{\theta}_i \cos(\theta_i) \qquad (3.6.28)$$

$$\dot{B} = \dot{y}_p + l\sum_{i=1}^{N-1} \dot{\theta}_i \sin(\theta_i) \qquad (3.6.29)$$

$$S_\phi = (l_1 + l_2)\sin(\phi) \qquad (3.6.30)$$

$$C_\phi = (l_1 + l_2)\cos(\phi) \qquad (3.6.31)$$

$$S_N = l\sin(\theta_N) \qquad (3.6.32)$$

$$C_N = l\cos(\theta_N) \qquad (3.6.33)$$

To solve for $\dot{\theta}_N$ and $\dot{\phi}$ in (3.6.26 and 3.6.27) we can write

$$\begin{bmatrix} C_\phi & C_N \\ -S_\phi & -S_N \end{bmatrix} \begin{Bmatrix} \dot{\phi} \\ \dot{\theta}_N \end{Bmatrix} = \begin{Bmatrix} \dot{A} \\ \dot{B} \end{Bmatrix} \qquad (3.6.34)$$

giving

$$\dot{\phi} = (\dot{A}\cdot S_N + \dot{B}\cdot C_N)/\Delta \qquad (3.6.35)$$

$$\dot{\theta}_N = (-\dot{A}\cdot S_\phi - \dot{B}\cdot C_\phi)/\Delta \qquad (3.6.36)$$

where

$$\Delta = C_\phi\cdot S_N - S_\phi\cdot C_N \qquad (3.6.37)$$

Differentiating (3.6.26 and 3.6.27) with respect to t and writing the resulting equations in matrix form we have

$$\begin{bmatrix} C_\phi & C_N \\ -S_\phi & -S_N \end{bmatrix} \begin{Bmatrix} \ddot{\phi} \\ \ddot{\theta}_N \end{Bmatrix} = \begin{Bmatrix} \ddot{C} \\ \ddot{D} \end{Bmatrix} \qquad (3.6.38)$$

where

$$\ddot{C} = \ddot{A} + S_\phi \cdot \dot{\phi}^2 + S_N \cdot \dot{\theta}_N^2 \qquad (3.6.39)$$

$$\ddot{D} = \ddot{B} + C_\phi \cdot \dot{\phi}^2 + C_N \cdot \dot{\theta}_N^2 \qquad (3.6.40)$$

$$\ddot{A} = \ddot{x}_p - l \sum_{i=1}^{N-1} [\ddot{\theta}_i \cos(\theta_i) - \dot{\theta}_i^2 \sin(\theta_i)] \qquad (3.6.41)$$

$$\ddot{B} = \ddot{y}_p + l \sum_{i=1}^{N-1} [\ddot{\theta}_i \sin(\theta_i) + \dot{\theta}_i^2 \cos(\theta_i)] \qquad (3.6.42)$$

Equations (3.6.8) to (3.6.42) give

$$\ddot{\phi} = \frac{1}{\Delta} \Big\{ S_N \ddot{x}_p + l^2 \sum_{i=1}^{N-1} [\ddot{\theta}_i \sin(\alpha_{iN}) + \dot{\theta}_i^2 \cos(\alpha_{iN})] + l(l_1+l_2)\dot{\phi}^2 \cos(\alpha_{N\phi}) + l^2 \dot{\theta}_N^2 + C_N \ddot{y}_p \Big\} \qquad (3.6.43)$$

$$\ddot{\theta}_N = -\frac{1}{\Delta} \Big\{ S_\phi \ddot{x}_p + l(l_1+l_2) \sum_{i=1}^{N-1} [\ddot{\theta}_i \sin(\alpha_{i\phi}) + \dot{\theta}_i^2 \cos(\alpha_{i\phi})] + (l_1+l_2)^2 \dot{\phi}^2 + l(l_1+l_2)\dot{\theta}_N^2 \cos(\alpha_{N\phi}) + C_\phi \ddot{y}_p \Big\} \qquad (3.6.44)$$

where

$$\alpha_{iN} = \theta_i - \theta_N \qquad (3.6.45)$$

$$\alpha_{i\phi} = \theta_i - \phi \qquad (3.6.46)$$

$$\alpha_{N\phi} = \theta_N - \phi \qquad (3.6.47)$$

Lagrange multipliers, λ_1 , λ_2 , can be found from the equations of motion of the yoke and the Nth link using (3.6.5) and (3.6.10)

$$E_N = \lambda_1 \cdot C_N - \lambda_2 \cdot S_N \qquad (3.6.48)$$

$$E_\phi = \lambda_1 \cdot C_\phi - \lambda_2 \cdot S_\phi \qquad (3.6.49)$$

where

$$E_N = \frac{d}{dt}\left(\frac{\partial T}{\partial \dot{\theta}_N}\right) - \frac{\partial T}{\partial \theta_N} + \frac{\partial V}{\partial \theta_N} - Q_N \qquad (3.6.50)$$

$$E_\phi = \frac{d}{dt}\left(\frac{\partial T}{\partial \dot{\phi}}\right) - \frac{\partial T}{\partial \phi} + \frac{\partial V}{\partial \phi} - Q_\phi \qquad (3.6.51)$$

Equations (3.6.48 and 3.6.49) give

$$\lambda_1 = \frac{1}{\Delta}\left(E_\phi \cdot S_N - E_N \cdot S_\phi\right) \qquad (3.6.52)$$

$$\lambda_2 = \frac{1}{\Delta}\left(-E_N \cdot C_\phi + E_\phi \cdot C_N\right) \qquad (3.6.53)$$

Note: When $\Delta = o$ i.e. $\phi = \theta_N$ (see equation 3.6.37), λ_1 and λ_2 cannot be evaluated from equations of motion of yoke and the Nth link but must be found from another pair of equations, say corresponding to θ_i and θ_j, given by (3.6.5). If $\Delta = o$ for all equations then we have $\theta_k = \phi$; $k = 1,2,\ldots,N$ indicating that system is fully taut, as shown below, and that Lagrange multipliers introduce infinitely large stiffness terms in the equations of motion

Evaluating equations (3.6.6) to (3.6.8) and substituting into (3.6.5) gives the left hand side of (3.6.5)

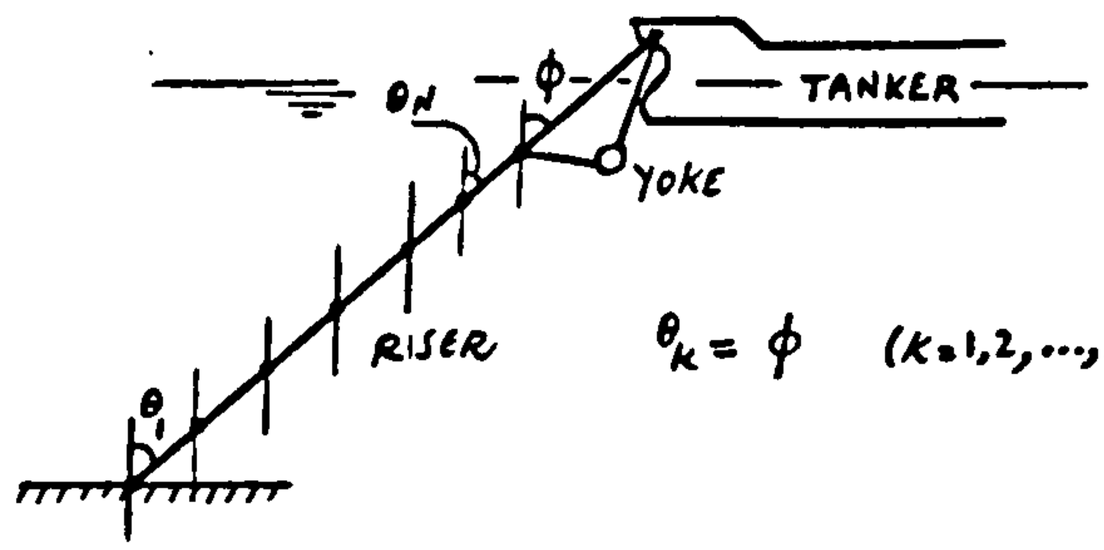

$\theta_k = \phi \quad (k = 1,2,\ldots,N)$

$$\frac{d}{dt}\left(\frac{\partial T}{\partial \dot\theta_k}\right) - \frac{\partial T}{\partial \theta_k} + \frac{\partial V}{\partial \theta_k} = m\ell^2\left(N-K+\tfrac{1}{3}\right)\ddot\theta_k +$$

$$m\ell^2\left(N-K+\tfrac{1}{2}\right)\sum_{j=1}^{K-1}\left[\cos(\alpha_{kj})\,\ddot\theta_j + \dot\theta_j^2 \sin(\alpha_{kj})\right] +$$

$$m\ell^2 \sum_{r=K+1}^{N}\left[(N-r+\tfrac{1}{2})\cos(\alpha_{kr})\,\ddot\theta_r + \dot\theta_r^2 \sin(\alpha_{kr})\right] +$$

$$\ell^2 E_m \sum_{i=1}^{N}\left[\ddot\theta_i \cos(\alpha_{ik}) - \dot\theta_i^2 \sin(\alpha_{ik})\right] +$$

$$\ell\ddot\phi\left[\cos(\alpha_{k\phi})\cdot A_m + \sin(\alpha_{k\phi})\cdot B_m\right] +$$

$$\ell\dot\phi^2\left[\sin(\alpha_{k\phi})\cdot A_m - \cos(\alpha_{k\phi})\cdot B_m\right] +$$

$$\ell\sin(\theta_k)\left[F_B - M_y g - w'(N-k+\tfrac{1}{2})\right] \qquad (3.6.54)$$

; $k = 1,2,\ldots,N$

Substituting for $\ddot{\phi}$ and $\ddot{\theta}_N$ from (3.6.43 and 3.6.44) into (3.6.54) we have

$$\frac{d}{dt}\left(\frac{\partial T}{\partial \dot{\theta}_k}\right) - \frac{\partial T}{\partial \theta_k} + \frac{\partial V}{\partial \theta_k} =$$

$$\ell^2 \ddot{\theta}_k \left\{ m\left(N-K+\tfrac{1}{3}\right) + G_k \sin(\alpha_{k\phi}) + E_m + H_k \sin(\alpha_{kN}) \right\} +$$

$$\ell^2 \sum_{j=1}^{K-1} \ddot{\theta}_j \left\{ m\left(N-K+\tfrac{1}{2}\right) \cos(\alpha_{kj}) + G_k \sin(\alpha_{j\phi}) + E_m \cos(\alpha_{jk}) + H_k \sin(\alpha_{jN}) \right\} +$$

$$\ell^2 \sum_{r=k+1}^{N-1} \ddot{\theta}_r \left\{ \left(N-r+\tfrac{1}{2}\right) \cos(\alpha_{kr}) + G_k \sin(\alpha_{r\phi}) + E_m \cos(\alpha_{rk}) + H_k \sin(\alpha_{rN}) \right\} +$$

$$\ell^2 \dot{\theta}_k^2 \left\{ G_k \cos(\alpha_{k\phi}) + H_k \cos(\alpha_{kN}) \right\} +$$

$$\ell^2 \sum_{j=1}^{K-1} \dot{\theta}_j^2 \left\{ m\left(N-K+\tfrac{1}{2}\right) \sin(\alpha_{kj}) + G_k \cos(\alpha_{j\phi}) - E_m \sin(\alpha_{jk}) + H_k \cos(\alpha_{jN}) \right\} +$$

$$\ell^2 \sum_{r=K+1}^{N-1} \dot{\theta}_r^2 \left\{ \left(N-r+\tfrac{1}{2}\right) \sin(\alpha_{kr}) + G_k \cos(\alpha_{r\phi}) - E_m \sin(\alpha_{rk}) + H_k \cos(\alpha_{rN}) \right\} +$$

$$\ell \dot{\phi}^2 \left\{ (l_1+l_2) G_k + (l_1+l_2) H_k \cos(\alpha_{N\phi}) + \sin(\alpha_{K\phi}) \cdot A_m - \cos(\alpha_{K\phi}) \cdot B_m \right\} +$$

$$\ell^2 \dot{\theta}_N^2 \left\{ G_k \cos(\alpha_{N\phi}) + \left(E_m + \tfrac{1}{2} m\right) \sin(\alpha_{kN}) + H_k \right\} +$$

$$\ell \ddot{x}_p \left\{ G_k \sin(\phi) + H_k \sin(\theta_N) \right\} +$$

$$\ell \ddot{y}_p \left\{ G_k \cos(\phi) + H_k \cos(\theta_N) \right\} +$$

$$\ell \sin(\theta_k) \left\{ F_B - M_y g - w'\left(N-k+\tfrac{1}{2}\right) \right\} \qquad ; k = 1, 2, \ldots, (N-1)$$

(3.6.55)

where

$$G_k = -(E_m + \tfrac{1}{2}m)\cos(\alpha_{kN})\; l(l_1+l_2)/\Delta \qquad (3.6.56)$$

$$H_k = \frac{l}{\Delta}\left[A_m \cos(\alpha_{k\phi}) + B_m \sin(\alpha_{k\phi})\right] \qquad (3.6.57)$$

Using (3.6.50) and (3.6.54) we can write

$$E_N = l^2 \sum_{i=1}^{N-1} (\ddot{\theta}_i \;\; A_i^*) + l \sum_{i=1}^{N-1} (\dot{\theta}_i^2 \;\; B_i^*) + C^* - Q_N \qquad (3.6.58)$$

where

$$A_i^* = \left\{\sin(\alpha_{i\phi})\left[G_N - (l_1+l_2)a^*\right] + \cos(\alpha_{iN})\left[E_m + \tfrac{1}{2}m\right] + H_N \sin(\alpha_{iN})\right\} \qquad (3.6.59)$$

$$a^* = \frac{l}{\Delta}\left[\tfrac{1}{3}m + G_N \sin(\alpha_{N\phi}) + E_m\right] \qquad (3.6.60)$$

$$G_N = -E_m\, l\,(l_1+l_2)/\Delta \qquad (3.6.61)$$

Note that the term $\frac{1}{2}m$ in (3.6.56) must be set to zero when $K=N$ as it arises from terms in $\sum_{r=K+1}^{N} A_r$ i.e. $A_r = 0$ WHEN $r \geq N$.

$$H_N = \frac{l}{\Delta}\left[A_m \cos(\alpha_{N\phi}) + B_m \sin(\alpha_{N\phi})\right] \qquad (3.6.62)$$

$$B_i^* = \left\{\cos(\alpha_{i\phi})\left[G_N - (l_1+l_2)\,a^*\right] - \sin(\alpha_{iN})\left[E_m + \tfrac{1}{2}m\right] + H_N \cos(\alpha_{iN})\right\} \qquad (3.6.63)$$

$$C^* = l^2 \dot{\theta}_N^2 \left\{ -(l_1+l_2) a^* \cos(\alpha_{N\phi}) + 2[G_N \cos(\alpha_{N\phi}) + H_N] \right\} +$$

$$l \ddot{x}_P \left\{ -a^* S_\phi + G_N \sin(\phi) + H_N \sin(\theta_N) \right\} +$$

$$l \ddot{y}_P \left\{ -a^* C_\phi + G_N \cos(\phi) + H_N \cos(\theta_N) \right\} +$$

$$l \dot{\phi}^2 \left\{ -a^* (l_1+l_2)^2 + (l_1+l_2)[G_N + H_N \cos(\alpha_{N\phi})] + A_m \sin(\alpha_{N\phi}) - B_m \cos(\alpha_{N\phi}) \right\} +$$

$$l \sin(\theta_N) \left\{ F_B - M_y g - \frac{w'}{2} \right\} \qquad (3.6.64)$$

Similarly using (3.6.51) we have

$$E_\phi = l \sum_{i=1}^{N-1} (\ddot{\theta}_i \; D_i^*) + l \sum_{i=1}^{N-1} (\dot{\theta}_i^2 \; E_i^*) + F^* - Q_\phi \qquad (3.6.65)$$

where

$$D_i^* = A_m \cos(\alpha_{i\phi}) + [B_m - (l_1+l_2) H_N] \sin(\alpha_{i\phi}) + \frac{l}{\Delta} D_m \sin(\alpha_{iN}) \qquad (3.6.66)$$

$$E_i^* = [B_m - (l_1+l_2) H_N] \cos(\alpha_{i\phi}) - A_m \sin(\alpha_{i\phi}) + \frac{l}{\Delta} D_m \cos(\alpha_{iN}) \qquad (3.6.67)$$

$$F^* = l \dot{\theta}_N^2 \left\{ [B_m - (l_1+l_2) H_N] \cos(\alpha_{N\phi}) - A_m \sin(\alpha_{N\phi}) + \frac{l}{\Delta} D_m \right\} +$$

$$\ddot{x}_P \left\{ -S_\phi \; H_N + \frac{l}{\Delta} D_m \sin(\theta_N) \right\} + \ddot{y}_P \left\{ -C_\phi \; H_N + \frac{Dm}{\Delta} \; C_N \right\} +$$

$$\dot{\phi}^2 \left\{ -(l_1+l_2)^2 \; H_N + \frac{l}{\Delta} D_m (l_1+l_2) \cos(\alpha_{N\phi}) \right\} +$$

$$\cos(\phi)[F_B \, l_5 - M_y \, g \, Y_{CG}] + \sin(\phi)[F_B \, l_1 - M_y \, g \, (l_1 + l_2 - X_{CG})] \qquad (3.6.68)$$

Substituting for E_N and E_ϕ from (3.6.58) and (3.6.65) into (3.6.48) and (3.6.49) and rearranging we get

$$\lambda_1 = \frac{1}{\Delta}\left\{ \ell \sum_{i=1}^{N-1} \ddot{\theta}_i \left(D_i^* S_N - A_i^* \ell S_\phi \right) + \dot{\theta}_i^2 \left(E_i^* S_N - B_i^* \ell S_\phi \right) + \right.$$

$$\left. S_N \left(F^* - Q_\phi \right) + S_\phi \left(Q_N - C^* \right) \right\}$$

(3.6.69)

$$\lambda_2 = \frac{1}{\Delta}\left\{ \ell \sum_{i=1}^{N-1} \ddot{\theta}_i \left(D_i^* C_N - A_i^* \ell C_\phi \right) + \dot{\theta}_i^2 \left(E_i^* C_N - B_i^* \ell C_\phi \right) + \right.$$

$$\left. C_N \left(F^* - Q_\phi \right) + C_\phi \left(Q_N - C^* \right) \right\}$$

(3.6.70)

Substituting for the left hand side of equation (3.6.5) from (3.6.55) and for λ_1 and λ_2 from (3.6.69 and 3.6.70) and rearranging gives

$$\ell^2 \ddot{\theta}_k \left\{ m\left(N-k+\tfrac{1}{3}\right) + \sin\left(\alpha_{k\phi}\right)\left[G_k - \frac{\ell}{\Delta}\left(l_1+l_2\right) A_k^* \right] + E_m + \sin\left(\alpha_{kN}\right)\left[H_k + \frac{\ell}{\Delta} D_k^* \right] \right\} +$$

$$\ell^2 \sum_{j=1}^{k-1} \ddot{\theta}_j \left\{ m\left(N-k+\tfrac{1}{2}\right)\cos\left(\alpha_{kj}\right) + G_k \sin\left(\alpha_{j\phi}\right) + E_m \cos\left(\alpha_{jk}\right) + H_k \sin\left(\alpha_{jN}\right) + \right.$$

$$\left. \frac{\ell}{\Delta} D_j^* \sin\left(\alpha_{kN}\right) - \frac{\ell}{\Delta}\left(l_1+l_2\right) A_j^* \sin\left(\alpha_{k\phi}\right) \right\} +$$

$$\ell^2 \sum_{r=k+1}^{N-1} \ddot{\theta}_r \left\{ \left(N-r+\tfrac{1}{2}\right)\cos\left(\alpha_{kr}\right) + G_k \sin\left(\alpha_{r\phi}\right) + E_m \cos\left(\alpha_{rk}\right) + H_k \sin\left(\alpha_{rN}\right) + \right.$$

$$\left. \frac{\ell}{\Delta} D_r^* \sin\left(\alpha_{kN}\right) - \frac{\ell}{\Delta} A_r^* \left(l_1+l_2\right) \sin\left(\alpha_{k\phi}\right) \right\} =$$

$$-\ell^2 \sum_{j=1}^{k-1} \dot{\theta}_j^2 \left\{ \left[m\left(N-k+\tfrac{1}{2}\right) + E_m \right] \sin\left(\alpha_{kj}\right) + G_k \cos\left(\alpha_{j\phi}\right) + H_k \cos\left(\alpha_{jN}\right) + \right.$$

$$\left. \frac{\ell}{\Delta} E_j^* \sin\left(\alpha_{kN}\right) - \frac{\ell}{\Delta} B_j^* \left(l_1+l_2\right) \sin\left(\alpha_{k\phi}\right) \right\} -$$

$$l^2\,\dot{\theta}_k^2\left\{G_k\,\mathrm{Cos}(\alpha_{k\phi})+H_k\,\mathrm{Cos}(\alpha_{kN})+\frac{l}{\Delta}E_k^*\,\mathrm{Sin}(\alpha_{kN})-\right.$$

$$\left.\frac{l}{\Delta}B_k^*\,(l_1+l_2)\,\mathrm{Sin}(\alpha_{k\phi})\right\}-$$

$$l^2\sum_{r=k+1}^{N-1}\dot{\theta}_r^2\left\{\left[(N-r+\tfrac{1}{2})+E_m\right]\mathrm{Sin}(\alpha_{kr})+G_k\,\mathrm{Cos}(\alpha_{r\phi})+\right.$$

$$H_k\,\mathrm{Cos}(\alpha_{rN})+\frac{l}{\Delta}E_r^*\,\mathrm{Sin}(\alpha_{kN})-$$

$$\left.\frac{l}{\Delta}B_r^*\,(l_1+l_2)\,\mathrm{Sin}(\alpha_{k\phi})\right\}-$$

$$l\,\dot{\phi}^2\left\{(l_1+l_2)\left[G_k+H_k\,\mathrm{Cos}(\alpha_{N\phi})\right]+\right.$$

$$A_m\,\mathrm{Sin}(\alpha_{k\phi})-B_m\,\mathrm{Cos}(\alpha_{k\phi})+$$

$$\frac{l}{\Delta}\mathrm{Sin}(\alpha_{kN})\left[-(l_1+l_2)^2\,H_N+\frac{l}{\Delta}D_m\,(l_1+l_2)\,\mathrm{Cos}(\alpha_{N\phi})\right]-$$

$$\frac{l(l_1+l_2)}{\Delta}\mathrm{Sin}(\alpha_{k\phi})\left[-a^*\,(l_1+l_2)^2+(l_1+l_2)\left(G_N+H_N\,\mathrm{Cos}(\alpha_{N\phi})\right)+\right.$$

$$\left.A_m\,\mathrm{Sin}(\alpha_{N\phi})-B_m\,\mathrm{Cos}(\alpha_{N\phi})\right]\Big\}-$$

$$l^2\,\dot{\theta}_N\left\{G_k\,\mathrm{Cos}(\alpha_{N\phi})+(E_m+\tfrac{1}{2}m)\,\mathrm{Sin}(\alpha_{kN})+H_k+\right.$$

$$\frac{l}{\Delta}\mathrm{Sin}(\alpha_{kN})\left[\left(B_m-(l_1+l_2)H_N\right)\mathrm{Cos}(\alpha_{N\phi})-A_m\,\mathrm{Sin}(\alpha_{N\phi})+\frac{l}{\Delta}D_m\right]-$$

$$\left.\frac{l(l_1+l_2)}{\Delta}\mathrm{Sin}(\alpha_{k\phi})\left[\mathrm{Cos}(\alpha_{N\phi})\left(2G_N-(l_1+l_2)a^*\right)+2H_N\right]\right\}-$$

$$l\ddot{y}_p\left\{G_k\cos(\phi)+H_k\cos(\theta_N)-\frac{l(l_1+l_2)}{\Delta}\sin(\alpha_{k\phi})\left[-a^*\ C_\phi+G_N\cos(\phi)+H_N\cos(\theta_N)\right]+\right.$$

$$\left.\frac{l}{\Delta}\sin(\alpha_{kN})\left[-C_\phi\ H_N+\frac{Dm}{\Delta}\ C_N\right]\ \right\}-$$

$$l\ddot{x}_p\left\{G_k\sin(\phi)+H_k\sin(\theta_N)+\frac{l}{\Delta}\sin(\alpha_{kN})\left[-S_\phi\ H_N+\frac{Dm}{\Delta}\ S_N\ \right]-\right.$$

$$\left.\frac{l(l_1+l_2)}{\Delta}\sin(\alpha_{k\phi})\left[-a^*\ S_\phi+G_N\sin(\phi)+H_N\sin(\theta_N)\right]\right\}-$$

$$l\sin(\theta_k)\left\{F_B-M_y g-w'(N-k+\tfrac{1}{2})\right\}+Q_k\ -$$

$$\frac{l^2}{\Delta}\sin(\alpha_{kN})\left\{\cos(\phi)\left[F_B\ l_5-M_y g\ Y_{cG}\right]+\sin(\phi)\left[F_B\ l_1-M_y g(l_1+l_2-X_{cG})-Q_\phi\right\}+\right.$$

$$\frac{l(l_1+l_2)}{\Delta}\sin(\alpha_{k\phi})\left\{S_N\left[F_B-M_y g-\frac{w'}{2}\right]-\ Q_N\right\}$$

$$;\ k=1,2,\cdots,(N-1)$$

(3.6.71)

Equation (3.6.71) can be solved using a time step integration algorithm. At each time step values of θ_N, $\dot{\theta}_N$, ϕ, $\dot{\phi}$ are evaluated in terms of θ_k $(k=1,2,\cdots,N-1)$ using equations (3.6.20, 3.6.21, 3.6.24, 3.6.25, 3.6.35 and 3.6.36). Equation (3.6.71) for k=1,2,.... ,(N-1) can be written in matrix form as

$$\{\ddot{\theta}\}=[I]^{-1}\left\{-[C]\{\dot{\theta}^2\}+\frac{1}{l^2}\{P\}+\frac{1}{l^2}[K]\{\sin(\theta)\}+\frac{1}{l^2}\{Q\}\right\}$$

(3.6.72)

where

$\{\ddot{\theta}\}$ is accelerations vector of size (N-1)

$[I]$ is inertia matrix of size (N-1)x(N-1) whose elements are

$$I_{ki} = \cos(\alpha_{ki})\left[m'(N-i+\tfrac{1}{2}) + E'_m\right] + G'_k \sin(\alpha_{i\phi}) + H'_k \sin(\alpha_{iN}) + \frac{\ell}{\Delta} D'^{*}_i \sin(\alpha_{kN}) - \frac{\ell}{\Delta} A'^{*}_i (l_1+l_2)\sin(\alpha_{k\phi}) \quad ; k \neq i$$

(3.6.73)

$$I_{kk} = m'(N-k+\tfrac{1}{3}) + \sin(\alpha_{k\phi})\left[G'_k - \frac{\ell}{\Delta}(l_1+l_2)A'^{*}_k\right] + E'_m + \sin(\alpha_{kN})\left(H'_k + \frac{\ell}{\Delta} D'^{*}_k\right)$$

(3.6.74)

where a dash indicates structural mass + added mass in the corresponding expression. $[C]$ is an (N-1)x(N-1) matrix with elements

$$C_{ki} = \sin(\alpha_{ki})\left[(N-i+\tfrac{1}{2}) + E_m\right] + G'_k \cos(\alpha_{i\phi}) + H'_k \cos(\alpha_{iN}) - \frac{\ell}{\Delta}\left[-E'^{*}_i \sin(\alpha_{kN}) + B'^{*}_i (l_1+l_2)\sin(\alpha_{k\phi})\right] \quad ; K<i$$

(3.6.75)

$$C_{kK} = G'_k \cos(\alpha_{K\phi}) + H'_k \cos(\alpha_{kN}) - \frac{\ell}{\Delta}\left[-E'^{*}_K \sin(\alpha_{kN}) + B'^{*}_k (l_1+l_2)\sin(\alpha_{k\phi})\right]$$

(3.6.76)

$$C_{ki} = \sin(\alpha_{ki})\left[m(N-k+\tfrac{1}{2}) + E_m\right] + G'_k \cos(\alpha_{i\phi}) + H'_k \cos(\alpha_{iN}) - \frac{\ell}{\Delta}\left[-E'^{*}_i \sin(\alpha_{kN}) + B'^{*}_i (l_1+l_2)\sin(\alpha_{k\phi})\right] \quad ; K>i$$

(3.6.77)

Elements of $\{P\}$, a vector of size (N-1), are

$$P_k = -l\dot{\phi}^2 \Big\{ (l_1+l_2)\left[G'_k + H'_k \cos(\alpha_{N\phi})\right] + A_m \sin(\alpha_{k\phi}) - B_m \cos(\alpha_{k\phi}) +$$

$$\frac{l}{\Delta}\sin(\alpha_{kN})\left[-(l_1+l_2)^2 H'_N + \frac{l}{\Delta} D'_m (l_1+l_2)\cos(\alpha_{N\phi})\right] -$$

$$\frac{l(l_1+l_2)}{\Delta}\sin(\alpha_{k\phi})\left[-a'^*(l_1+l_2)^2 + (l_1+l_2)\left(G'_N + H'_N\cos(\alpha_{N\phi})\right) + A_m \sin(\alpha_{N\phi}) - B_m\cos(\alpha_{N\phi})\right] \Big\} -$$

$$l^2\dot{\theta}_N^2 \Big\{ G'_k\cos(\alpha_{N\phi}) + (E_m + \tfrac{1}{2}m)\sin(\alpha_{kN}) + H'_k +$$

$$\frac{l}{\Delta}\sin(\alpha_{kN})\left[\left(B_m - (l_1+l_2)H'_N\right)\cos(\alpha_{N\phi}) - A_m\sin(\alpha_{N\phi}) + \frac{l}{\Delta}D'_m\right] -$$

$$\frac{l(l_1+l_2)}{\Delta}\sin(\alpha_{k\phi})\left[\cos(\alpha_{N\phi})\left(-(l_1+l_2)a'^* + 2G'_N\right) + 2H'_N\right] \Big\} -$$

$$l\ddot{x}_p \Big\{ G'_k\sin(\phi) + H'_k\sin(\theta_N) + \frac{l}{\Delta}\sin(\alpha_{kN})\left[-S_\phi H'_N + \frac{D'_m}{\Delta}S_N\right] -$$

$$\frac{l(l_1+l_2)}{\Delta}\sin(\alpha_{k\phi})\left[-a'^* S_\phi + G'_N\sin(\phi) + H'_N\sin(\theta_N)\right] \Big\} -$$

$$l\ddot{y}_p \Big\{ G'_k\cos(\phi) + H'_k\cos(\theta_N) - \frac{l(l_1+l_2)}{\Delta}\sin(\alpha_{k\phi})\left[-a'^* C_\phi + G'_N\cos(\phi) + H'_N\cos(\theta_N)\right] +$$

$$\frac{l}{\Delta}\sin(\alpha_{kN})\left[-C_\phi H'_N + \frac{D'_m}{\Delta}C_N\right] \Big\} -$$

$$\frac{l^2}{\Delta}\sin(\alpha_{kN})\Big\{ \cos(\phi)\left[F_B l_5 - M_y g Y_{CG}\right] +$$

$$\sin(\phi)\left[F_B l_1 - M_y g (l_1+l_2-X_{CG})\right] - Q_\phi \Big\} +$$

$$\frac{l(l_1+l_2)}{\Delta}\sin(\alpha_{k\phi})\Big\{ S_N\left[F_B - M_y g - \frac{w'}{2}\right] - Q_N \Big\}$$

(3.6.78)

$[k]$ is an (N-1)x(N-1) diagonal stiffness matrix with elements

$$K_{kk} = \ell\left[w'(N-k+\tfrac{1}{2}) - F_B + M_y g\right] \qquad (3.6.79)$$

$\{Q\}$ is the generalised force vector of size (N-1) whose elements can be evaluated using equation (3.6.9)

3.7 Natural Frequencies and Mode Shapes for Small Oscillations

Neglecting damping terms equation (3.6.71) gives the equation of motion of the kth link as

$$\sum_{i=1}^{N-1} I_{ki} \cdot \ddot{\theta}_i + q_k(\theta_1, \theta_2, \ldots, \theta_k, \ldots, \theta_{N-1}, \theta_N, \phi) = F_k \qquad (3.7.1)$$

where

$$q_k = -\frac{1}{\ell}\sin(\theta_N)\left[F_B - M_y g - \frac{w'}{2}\right]\frac{\sin(\alpha_{k\phi})}{\sin(\alpha_{N\phi})} -$$

$$\frac{1}{\ell}\left[w'(N-k+\tfrac{1}{2}) - F_B + M_y g\right]\sin(\theta_k) +$$

$$\frac{1}{\ell(\ell_1+\ell_2)}\frac{\sin(\alpha_{kN})}{\sin(\alpha_{N\phi})}\left\{\cos(\phi)\left[F_B \ell_5 - M_y g Y_{CG}\right] + \sin(\phi)\left[F_B \ell_1 - M_y g(\ell_1+\ell_2-X_{CG})\right]\right\}$$

$$; k = 1, 2, \ldots, N-1 \qquad (3.7.2)$$

and F_k is the force which in the case of free vibrations only includes static loads. Expanding (3.7.1) about a static equilibrium position (with no tanker motions) gives

$$\sum_{i=1}^{N-1} I_{ki} \cdot \Delta\ddot{\theta}_i + \Delta q_k = \Delta F_k = 0 \qquad ; k = 1, 2, \ldots, N-1 \qquad (3.7.3)$$

where Δ indicates a small increment and we have

$$\Delta q_k = \sum_{i=1}^{N-1} \left[\frac{\partial q_k}{\partial \theta_i} \bigg|_s \cdot \Delta\theta_i \right] + \frac{\partial q_k}{\partial \theta_N} \bigg|_s \cdot \Delta\theta_N + \frac{\partial q_k}{\partial \phi} \bigg|_s \cdot \Delta\phi$$

$$; k = 1, 2, \ldots, N-1 \qquad (3.7.4)$$

where $|_s$ indicates evaluation about static equilibrium position. Substituting (3.7.4) into (3.7.3) we get

$$\sum_{i=1}^{N-1} (I_{ki} \cdot \ddot{\theta}_i) + \sum_{i=1}^{N-1} \left[\frac{\partial q_k}{\partial \theta_i} \bigg|_s \cdot \Delta\theta_i \right] + \frac{\partial q_k}{\partial \theta_N} \bigg|_s \cdot \Delta\theta_N + \frac{\partial q_k}{\partial \phi} \bigg|_s \cdot \Delta\phi = 0$$

$$; k = 1, 2, \ldots, N-1 \qquad (3.7.5)$$

Constraint equations (3.6.11 and 3.6.12) with zero tanker motions can be written as

$$(l_1 + l_2) \sin(\phi) = X_s + l_1 + l_2 - l \sum_{i=1}^{N-1} \sin(\theta_i) - l \sin(\theta_N) \qquad (3.7.6)$$

and

$$(l_1 + l_2) \cos(\phi) = d + l_3 - l \sum_{i=1}^{N-1} \cos(\theta_i) - l \cos(\theta_N) \qquad (3.7.7)$$

In incremental form (3.7.6) and (3.7.7) give

$$\Delta\phi \cdot (l_1 + l_2) \cdot \cos(\phi) = -l \sum_{i=1}^{N-1} \Delta\theta_i \cdot \cos(\theta_i) - l \cdot \cos(\theta_N) \cdot \Delta\theta_N \qquad (3.7.8)$$

and

$$-\Delta\phi \cdot (l_1 + l_2) \cdot \sin(\phi) = l \sum_{i=1}^{N-1} \Delta\theta_i \cdot \sin(\theta_i) + l \cdot \sin(\theta_N) \cdot \Delta\theta_N \qquad (3.7.9)$$

Note that here ϕ and θ_i (i=1,2,.... ,N) are static equilibrium angles. From (3.7.8 and 3.7.9) we have

$$\Delta\phi = \frac{l^2}{\Delta} \sum_{i=1}^{N-1} \Delta\theta_i \cdot \sin(\alpha_{iN}) \qquad (3.7.10)$$

$$\Delta\theta_N = \frac{-l(l_1+l_2)}{\Delta} \sum_{i=1}^{N-1} \Delta\theta_i \cdot \sin(\alpha_{i\phi}) \qquad (3.7.11)$$

Substituting for $\Delta\phi$ and $\Delta\theta_N$ from (3.7.10) and (3.7.11) into (3.7.5) we get

$$\sum_{i=1}^{N-1} I_{ki} \cdot \Delta\ddot{\theta}_i + \sum_{i=1}^{N-1} \left\{ \left.\frac{\partial q_k}{\partial \theta_i}\right|_s - \frac{l(l_1+l_2)}{\Delta} \sin(\alpha_{i\phi}) \cdot \left.\frac{\partial q_k}{\partial \theta_N}\right|_s + \left. \frac{l^2}{\Delta} \sin(\alpha_{iN}) \frac{\partial q_k}{\partial \phi} \right|_s \right\} \Delta\theta_i = 0 \qquad (3.7.12)$$

Equation (3.7.12) for k=1,2,.....,N-1 can be written in matrix form as

$$\left[I \right] \left\{ \Delta\ddot{\theta} \right\} + \left[K' \right] \left\{ \Delta\theta \right\} = \left\{ 0 \right\} \qquad (3.7.13)$$

where $[K']$ is the 'tangent' stiffness matrix of size (N-1)x(N-1) whose elements are

$$K'_{ki} = \left.\frac{\partial q_k}{\partial \theta_i}\right|_s - \frac{l(l_1+l_2)}{\Delta} \sin(\alpha_{i\phi}) \left.\frac{\partial q_k}{\partial \theta_N}\right|_s + \left. \frac{l^2}{\Delta} \sin(\alpha_{iN}) \frac{\partial q_k}{\partial \phi} \right|_s$$

$$; K, i = 1, 2, \ldots, N-1 \qquad (3.7.14)$$

and from (3.7.2) we get

$$\frac{\partial q_k}{\partial \phi} = -\frac{1}{l}\sin(\theta_N)\left[F_B - M_y\cdot g - \frac{w'}{2}\right]\frac{\sin(\alpha_{kN})}{\sin^2(\alpha_{N\phi})} +$$

$$\frac{\sin(\alpha_{kN})}{l(l_1+l_2)\sin^2(\alpha_{N\phi})}\left\{\cos(\theta_N)\left[F_B\cdot l_5 - M_y\cdot g\cdot Y_{cG}\right] + \sin(\theta_N)\left[F_B\cdot l_1 - M_y\cdot g\cdot(l_1+l_2-X_{cG})\right]\right\}$$

$$; k = 1, 2, \ldots, N-1 \qquad (3.7.15)$$

and

$$\frac{\partial q_k}{\partial \theta_N} = \frac{1}{l}\frac{\sin(\alpha_{k\phi})}{\sin^2(\alpha_{N\phi})}\left\{\left[F_B - M_y\cdot g - \frac{w'}{2}\right]\sin(\phi) -\right.$$

$$\frac{1}{(l_1+l_2)}\cos(\phi)\left[F_B\cdot l_5 - M_y\cdot g\cdot Y_{cG}\right] -$$

$$\left.\frac{1}{(l_1+l_2)}\sin(\phi)\left[F_B\cdot l_1 - M_y\cdot g\cdot(l_1+l_2-X_{cG})\right]\right\}$$

$$; k = 1, 2, \ldots, N-1 \qquad (3.7.16)$$

and noting that $\frac{\partial q_k}{\partial \theta_i} = 0$ for $i \neq k$ we have

$$\frac{\partial q_k}{\partial \theta_k} = -\frac{1}{l}\sin(\theta_N)\left[F_B - M_y\cdot g - \frac{w'}{2}\right]\frac{\cos(\alpha_{k\phi})}{\sin(\alpha_{N\phi})} -$$

$$\frac{1}{l}\left[w'(N-k+\tfrac{1}{2}) - F_B + M_y\cdot g\right]\cos(\theta_k) +$$

$$\frac{1}{l(l_1+l_2)}\frac{\cos(\alpha_{kN})}{\sin(\alpha_{N\phi})}\left\{\cos(\phi)\left[F_B\cdot l_5 - M_y\cdot g\cdot Y_{cG}\right] +\right.$$

$$\left.\sin(\phi)\left[F_B\cdot l_1 - M_y\cdot g\cdot(l_1+l_2-X_{cG})\right]\right\}$$

$$; k = 1, 2, \ldots, N-1 \qquad (3.7.17)$$

In equation (3.7.13) $\{0\}$ is the null vector of size (N-1). Substituting for derivatives of q_k from (3.7.15, 3.7.16 and 3.7.17) into (3.7.14) we get

$$K'_{ki} = \frac{\ell^2(\ell_1+\ell_2)}{\Delta^3}\left\{\left[-F_B\cdot\ell_2 + (\ell_1+\ell_2)\frac{W'}{2} + M_y\cdot g\cdot X_{cg}\right]\left[\sin(\alpha_{i\phi})\cdot\sin(\alpha_{k\phi})\cdot S_\phi + \sin(\alpha_{iN})\cdot\sin(\alpha_{kN})\cdot S_N\right] + \left[F_B\cdot\ell_5 - M_y\cdot g\cdot Y_{cg}\right]\left[\sin(\alpha_{i\phi})\cdot\sin(\alpha_{k\phi})\cdot C_\phi + \sin(\alpha_{iN})\cdot\sin(\alpha_{kN})\cdot C_N\right]\right\}$$

$$; \; k \neq i \qquad (3.7.18)$$

Note that $K'_{ik} = K'_{ki}$, and

$$K'_{kk} = \frac{\ell^2(\ell_1+\ell_2)}{\Delta^3}\left\{\left[-F_B\cdot\ell_2 + (\ell_1+\ell_2)\frac{W'}{2} + M_y\cdot g\cdot X_{cg}\right]\times \left[\sin^2(\alpha_{k\phi})\cdot S_\phi + \sin^2(\alpha_{kN})\cdot S_N\right] + \left[F_B\cdot\ell_5 - M_y\cdot g\cdot Y_{cg}\right]\left[\sin^2(\alpha_{k\phi})\cdot C_\phi + \sin^2(\alpha_{kN})\cdot C_N\right]\right\} + \frac{\partial q_k}{\partial \theta_k} \qquad (3.7.19)$$

letting

$$[R] = [I]^{-1}[K'] \qquad (3.7.20)$$

and referring to equation (3.7.13), eigenvalues of $[R]$ give natural frequencies of the system and eigenvector of $[R]$ gives the mode shape coefficients.

3.8 Velocity of Riser Top Articulated Joint

Equations (3.2.3) and (3.2.4) give

Horizontal velocity of riser top,

$$\dot{x}_N = \ell \sum_{i=1}^{N} \dot{\theta}_i \cos(\theta_i) \qquad (3.8.1)$$

Vertical velocity of riser top

$$\dot{y}_N = -\ell \sum_{i=1}^{N} \dot{\theta}_i \sin(\theta_i) \qquad (3.8.2)$$

But from (3.6.23 to 3.6.33) we have

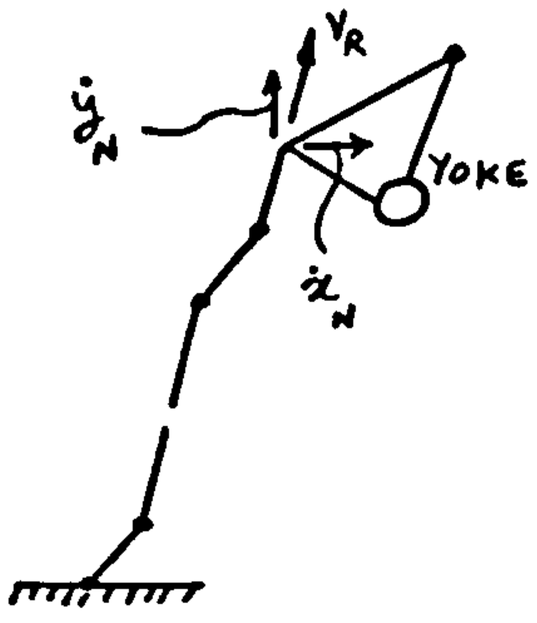

$$\ell \sum_{i=1}^{N} \dot{\theta}_i \cos(\theta_i) = \dot{x}_p - C_\phi \cdot \dot{\phi} \qquad (3.8.3)$$

$$-\ell \sum_{i=1}^{N} \dot{\theta}_i \sin(\theta_i) = \dot{y}_p + S_\phi \cdot \dot{\phi} \qquad (3.8.4)$$

Substituting (3.8.3) into (3.8.1) and (3.8.4) into (3.8.2)

$$\dot{x}_N = \dot{x}_p - C_\phi \cdot \dot{\phi} \qquad (3.8.5)$$

$$\dot{y}_N = \dot{y}_p + S_\phi \cdot \dot{\phi} \qquad (3.8.6)$$

Velocity along the Nth link,

$$V_R = \dot{x}_N \cdot \sin(\theta_N) + \dot{y}_N \cdot \cos(\theta_N) \qquad (3.8.7)$$

Substituting for $\dot{x}_N$ and $\dot{y}_N$ from (3.8.5) and (3.8.6) into (3.8.7) gives

$$V_R = \left[\dot{x}_p - C_\phi \cdot \dot{\phi}\right] \sin(\theta_N) + \left[\dot{y}_p + S_\phi \cdot \dot{\phi}\right] \cos(\theta_N)$$

(3.8.8)

3.9 Riser Top Tension and Support Reactions

Forces acting on the system and support reactions are shown in figure 3.10.

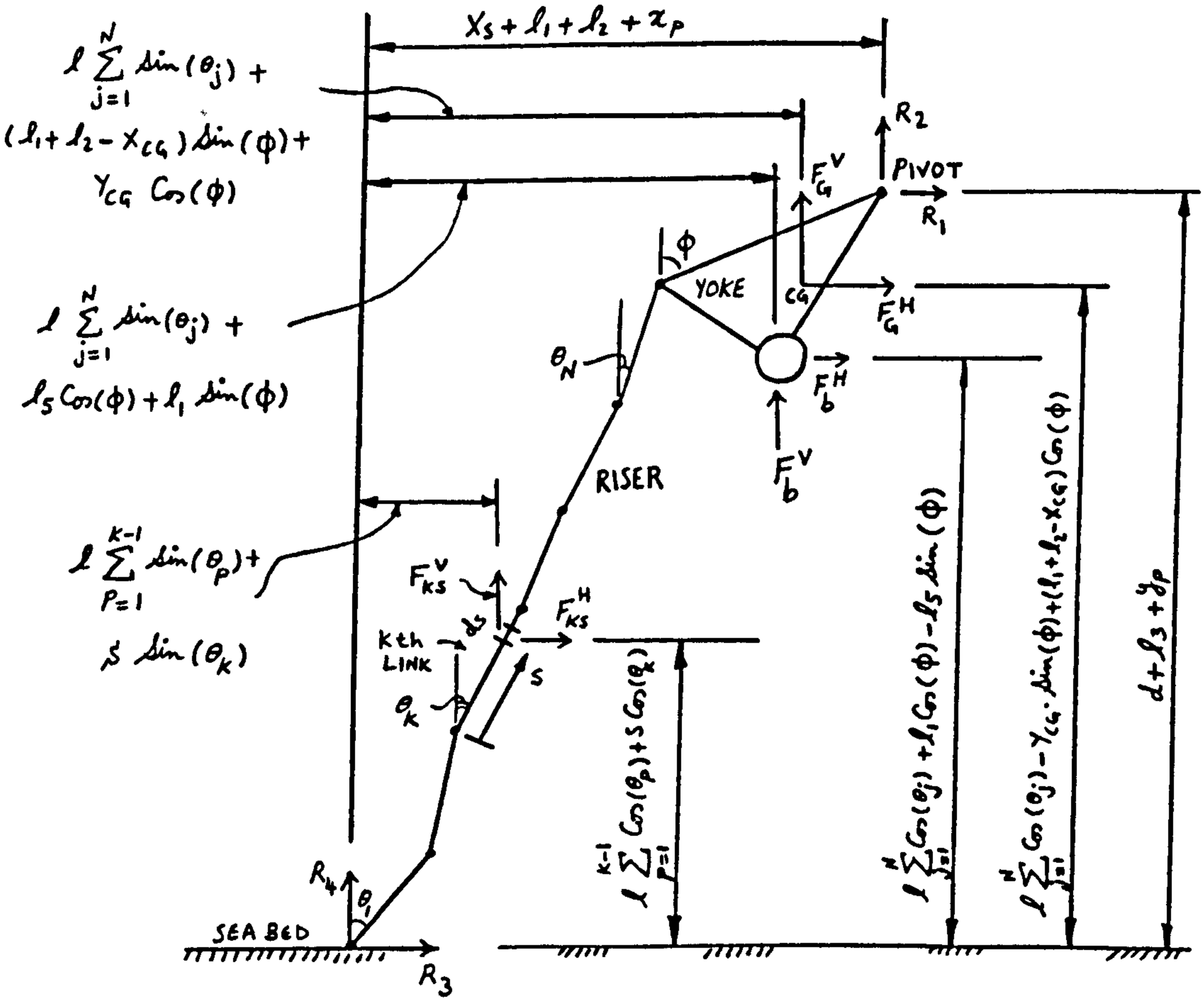

Figure 3.10. Forces Acting on the System

F_{KS}^H and F_{KS}^V are the horizontal and vertical components of force acting on element ds of kth link and at distance s from lower pin respectively. For

horizontal force equilibrium

$$R_3 + \sum_{K=1}^{N} \left\{ \int_o^{\ell} F_{KS}^H \right\} + F_b^H + F_G^H + R_1 = o \qquad (3.9.1)$$

vertically,

$$R_4 + \sum_{K=1}^{N} \left\{ \int_o^{\ell} F_{KS}^V \right\} + F_b^V + F_G^V + R_2 = o \qquad (3.9.2)$$

where

R_1 = horizontal reaction at tanker bow pivot

R_2 = vertical reaction at pivot

R_3 = horizontal reaction at sea bed

R_4 = vertical reaction at sea bed

F_G^H, F_G^V = horizontal and vertical forces acting on centre of gravity of yoke respectively

F_b^H, F_b^V = horizontal and vertical forces acting on cylindrical buoy respectively.

Taking bending moments about the riser top articulated joint we have

$$\begin{aligned} & R_1(\ell_1+\ell_2)\cos(\phi) - R_2(\ell_1+\ell_2)\sin(\phi) - \\ & F_G^H[\,Y_{CG}\sin(\phi) - (\ell_1+\ell_2-X_{CG})\cos(\phi)\,] - \\ & F_G^V[\,Y_{CG}\cos(\phi) + (\ell_1+\ell_2-X_{CG})\sin(\phi)\,] - \\ & F_b^H[\,\ell_5\sin(\phi) - \ell_1\cos(\phi)\,] - \\ & F_b^V[\,\ell_5\cos(\phi) + \ell_1\sin(\phi)\,] \qquad = o \end{aligned} \qquad (3.9.3)$$

and taking moments about the pin joint at sea bed

$$R_1(d+\ell_3+y_p)-R_2(x_s+\ell_1+\ell_2+x_p)+$$

$$F_G^H\left[\ell\sum_{j=1}^{N}\cos(\theta_j)-y_{CG}\sin(\phi)+(\ell_1+\ell_2-x_{CG})\cos(\phi)\right]-$$

$$F_G^V\left[\ell\sum_{j=1}^{N}\sin(\theta_j)+(\ell_1+\ell_2-x_{CG})\sin(\phi)+y_{CG}\cos(\phi)\right]+$$

$$F_b^H\left[\ell\sum_{j=1}^{N}\cos(\theta_j)+\ell_1\cos(\phi)-\ell_5\sin(\phi)\right]-$$

$$F_b^V\left[\ell\sum_{j=1}^{N}\sin(\theta_j)+\ell_5\cos(\phi)+\ell_1\sin(\phi)\right]+$$

$$\sum_{K=1}^{N}\left\{\int_0^{\ell}F_{KS}^H\left[\ell\sum_{P=1}^{K-1}\cos(\theta_p)+s\cos(\theta_k)\right]-F_{KS}^V\left[\ell\sum_{P=1}^{K-1}\sin(\theta_p)+s\sin(\theta_k)\right]\right\}=0 \qquad (3.9.4)$$

Equations (3.9.1) to (3.9.4) can be written in the form

$$\begin{bmatrix} C_\phi & -S_\phi & 0 & 0 \\ X_1 & X_2 & 0 & 0 \\ 1 & 0 & 1 & 0 \\ 0 & 1 & 0 & 1 \end{bmatrix} \begin{Bmatrix} R_1 \\ R_2 \\ R_3 \\ R_4 \end{Bmatrix} = \begin{Bmatrix} F_1 \\ F_2 \\ F_3 \\ F_4 \end{Bmatrix} \qquad (3.9.5)$$

where

$$X_1 = d+\ell_3+y_p \qquad (3.9.6)$$

$$X_2 = -(X_s + \ell_1 + \ell_2 + x_p) \qquad (3.9.7)$$

$$F_1 = F_G^H \left[Y_{CG} \sin(\phi) - (\ell_1 + \ell_2 - X_{CG}) \cos(\phi) \right] +$$

$$F_G^V \left[Y_{CG} \cos(\phi) + (\ell_1 + \ell_2 - X_{CG}) \sin(\phi) \right] +$$

$$F_b^H \left[\ell_5 \sin(\phi) - \ell_1 \cos(\phi) \right] + F_b^V \left[\ell_5 \cos(\phi) + \ell_1 \sin(\phi) \right] \qquad (3.9.8)$$

$$F_2 = -\ell \left[\sum_{j=1}^{N} \cos(\theta_j) \right] \left[F_G^H + F_b^H \right] + F_G^H \left[Y_{CG} \sin(\phi) - (\ell_1 + \ell_2 - X_{CG}) \cos(\phi) \right] +$$

$$\ell \left[\sum_{j=1}^{N} \sin(\theta_j) \right] \left[F_G^V + F_b^V \right] + F_G^V \left[(\ell_1 + \ell_2 - X_{CG}) \sin(\phi) + Y_{CG} \cos(\phi) \right] -$$

$$F_b^H \left[\ell_1 \cos(\phi) - \ell_5 \sin(\phi) \right] + F_b^V \left[\ell_5 \cos(\phi) + \ell_1 \sin(\phi) \right] -$$

$$\sum_{k=1}^{N} \left\{ \int_o^{\ell} F_{ks}^H \left[\ell \sum_{p=1}^{k-1} \cos(\theta_p) + s \cos(\theta_k) \right] - F_{ks}^V \left[\ell \sum_{p=1}^{k-1} \sin(\theta_p) + s \sin(\theta_k) \right] \right\} \qquad (3.9.9)$$

$$F_3 = -\sum_{K=1}^{N} \left\{ \int_o^{\ell} F_{ks}^H \right\} - F_b^H - F_G^H \qquad (3.9.10)$$

$$F_4 = -\sum_{K=1}^{N} \left\{ \int_o^{\ell} F_{ks}^V \right\} - F_b^V - F_G^V \qquad (3.9.11)$$

Equation (3.9.5) gives

$$\begin{Bmatrix} R_1 \\ R_2 \\ R_3 \\ R_4 \end{Bmatrix} = \begin{bmatrix} X_2/X_3 & S_\phi/X_3 & 0 & 0 \\ -X_1/X_3 & C_\phi/X_3 & 0 & 0 \\ -X_2/X_3 & -S_\phi/X_3 & 1 & 0 \\ X_1/X_3 & -C_\phi/X_3 & 0 & 1 \end{bmatrix} \begin{Bmatrix} F_1 \\ F_2 \\ F_3 \\ F_4 \end{Bmatrix}$$

(3.9.12)

where

$$X_3 = C_\phi \cdot X_2 + S_\phi \cdot X_1$$

(3.9.13)

Force components F_{ks}^H and F_{ks}^V in figure 3.10 can be written as

$$F_{ks}^H = \delta F_k^H + \delta F_{kx}^D \qquad (3.9.14)$$

$$F_{ks}^V = \delta F_k^V + \delta F_{ky}^D + \rho \frac{\pi D_l^2}{4} g \, ds - \delta m \, g \, ds \qquad (3.9.15)$$

where δF_{kx}^D , δF_{ky}^D = horizontal and vertical components of drag force on the element given by equations (3.2.45) and (3.2.46) respectively.

δF_k^H , δF_k^V = horizontal and vertical components of inertia (structural) force.

Differentiating equations (3.2.3) and (3.2.4) with respect to t gives the horizontal and vertical components of acceleration at the element. Therefore we can write

$$\delta F_k^H = -\delta m' \ell\, ds \sum_{j=1}^{k-1} \left(\ddot{\theta}_j \cos(\theta_j) \right) +$$

$$\delta m\ \ell\, ds \sum_{j=1}^{k-1} \left(\dot{\theta}_j^2 \sin(\theta_j) \right) -$$

$$\delta m' s\, ds\ \ddot{\theta}_k \cos(\theta_k) +$$

$$\delta m\ s\, ds\ \dot{\theta}_k^2 \sin(\theta_k)$$

(3.9.16)

$$\delta F_k^V = \delta m' \ell\, ds \sum_{j=1}^{k-1} \left(\ddot{\theta}_j \sin(\theta_j) \right) +$$

$$\delta m\ \ell\, ds \sum_{j=1}^{k-1} \left(\dot{\theta}_j^2 \cos(\theta_j) \right) +$$

$$\delta m' s\, ds\ \ddot{\theta}_k \sin(\theta_k) +$$

$$\delta m\ s\, ds\ \dot{\theta}_k^2 \cos(\theta_k) \qquad (3.9.17)$$

where $\delta m'$ = structural + added mass of each link per unit length. Similarly forces acting on yoke (see figure 3.10) can be expressed as

$$F_G^H = -M'_y \left\{ \ell \sum_{j=1}^{N} \left(\ddot{\theta}_j \cos(\theta_j) \right) - Y_{CG}\ \ddot{\phi} \sin(\phi) + (l_1 + l_2 - X_{CG})\, \ddot{\phi} \cos(\phi) \right\} +$$

$$M_y \left\{ \ell \sum_{j=1}^{N} \left(\dot{\theta}_j^2 \sin(\theta_j) \right) + Y_{CG}\ \dot{\phi}^2 \cos(\phi) + (l_1 + l_2 - X_{CG})\, \dot{\phi}^2 \sin(\phi) \right\} \qquad (3.9.18)$$

$$F_G^V = M'_y \left\{ \ell \sum_{j=1}^{N} \left(\ddot{\theta}_j \sin(\theta_j) \right) + (l_1 + l_2 - X_{CG})\, \ddot{\phi} \sin(\phi) + Y_{CG}\ \ddot{\phi} \cos(\phi) \right\} +$$

$$M_y \left\{ \ell \sum_{j=1}^{N} \left(\dot{\theta}_j^2 \cos(\theta_j) \right) + (l_1 + l_2 - X_{CG})\, \dot{\phi}^2 \cos(\phi) - Y_{CG}\ \dot{\phi}^2 \sin(\phi) \right\} -$$

$$M_y\, g \qquad (3.9.19)$$

$$F_b^H = F_{bx} - M'_b \left\{ \ell \sum_{j=1}^{N} \left[\ddot{\theta}_j \cos(\theta_j) \right] - \ell_5 \ddot{\phi} \sin(\phi) + \ell_1 \ddot{\phi} \cos(\phi) \right\} \quad (3.9.20)$$

$$F_b^V = F_B + F_{by} + M'_b \left\{ \ell \sum_{j=1}^{N} \left[\ddot{\theta}_j \sin(\theta_j) \right] + \ell_1 \ddot{\phi} \sin(\phi) + \ell_5 \ddot{\phi} \cos(\phi) \right\} \quad (3.9.21)$$

where M'_y = structural mass of yoke + added mass of bracing members

M'_b = added mass of cylindrical buoy

F_{bx} and F_{by} are given by (3.3.75) and (3.3.76) respectively.

Now reactions R_1, R_2, R_3, R_4 can be evaluated using (3.9.12). The horizontal and vertical forces, r_k^H and r_k^V as shown below, at top of kth link can be found as follows:

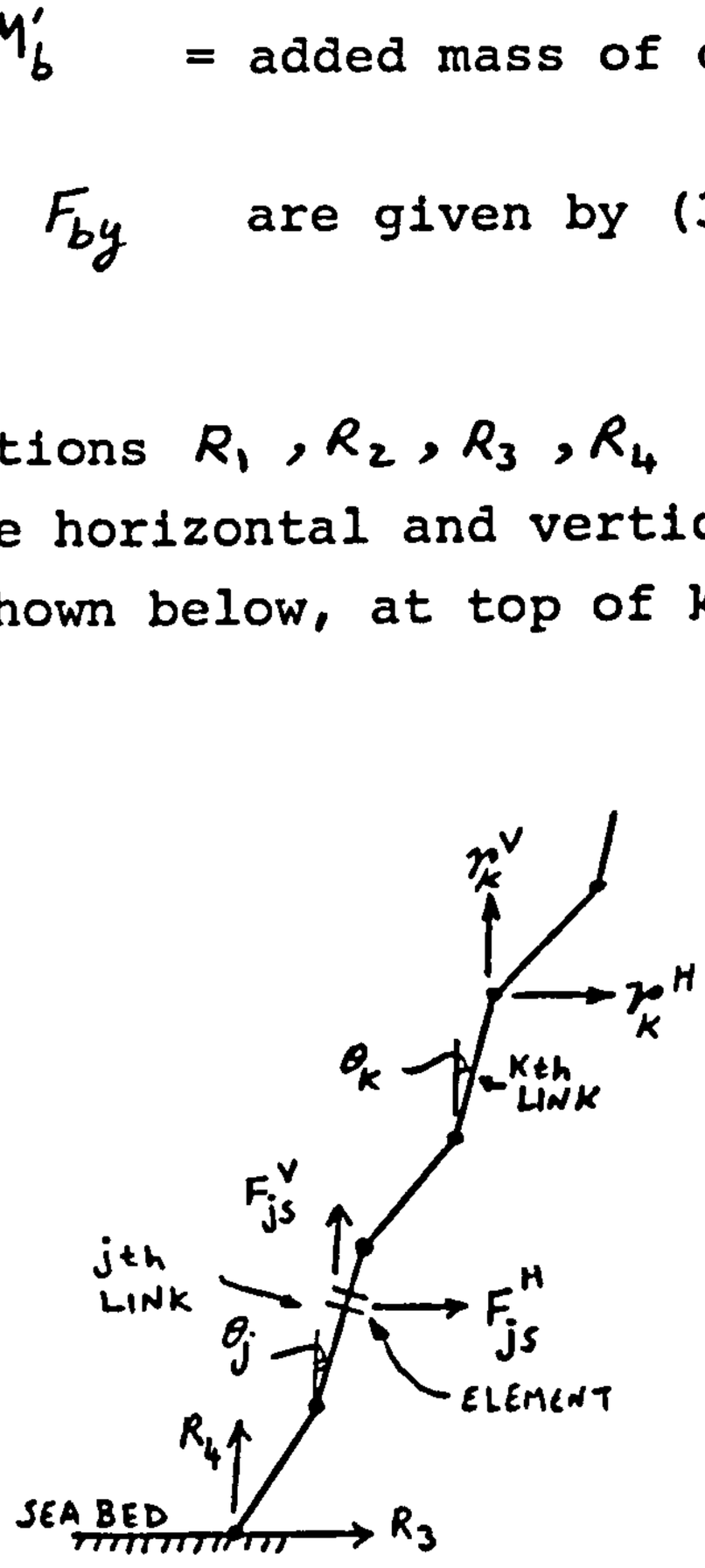

Horizontal force equilibirum gives

$$T_k^H + \sum_{j=1}^{K} \left\{ \int_o^{\ell} F_{js}^H \right\} + R_3 = 0 \qquad (3.9.22)$$

Vertical force equilibrium

$$T_k^V + \sum_{j=1}^{K} \left\{ \int_o^{\ell} F_{js}^V \right\} + R_4 = 0 \qquad (3.9.23)$$

Alternatively we can write

$$T_k^H = T_{k-1}^H - \int_o^{\ell} F_{ks}^H \qquad ; k=2,3,\ldots,N \qquad (3.9.24)$$

$$T_k^V = T_{k-1}^V - \int_o^{\ell} F_{ks}^V \qquad ; k=2,3,\ldots,N \qquad (3.9.25)$$

with

$$T_1^H = -R_3 - \int_o^{\ell} F_{1s}^H \qquad (3.9.26)$$

$$T_1^V = -R_4 - \int_o^{\ell} F_{1s}^V \qquad (3.9.27)$$

Force along the kth link, T_k (tension +ve) is

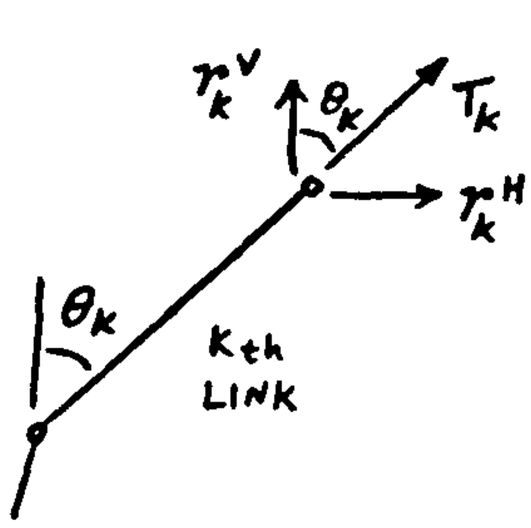

$$T_k = T_k^V \cdot \cos(\theta_k) + T_k^H \cdot \sin(\theta_k) \qquad (3.9.28)$$

Riser top tension can be obtained from (3.9.28) by letting k = N.

3.10. Static Offset of Tanker

The mean wind and current forces acting on the tanker in x-direction are given by the following empirical formulae for VLCCs (67):

Longitudinal wind force (in tf),

$$F_{xw} = C_{xw} \left(\frac{\rho_w}{7600}\right) V_w^2 \cdot A_T \qquad (3.10.1)$$

Current force,

$$F_{xc} = C_{xc} \left(\frac{\rho_c}{7600}\right) V_c^2 \cdot h \cdot L \qquad (3.10.2)$$

where

C_{xw} , C_{xc} = wind and current force coefficients respectively

V_w = mean wind speed at 10m above MWL (kts)

V_c = current velocity at surface (kts)

A_T = projected cross sectional area (m^2)

ρ_w , ρ_c = air and sea water densities (expressed in $kg\,\frac{sec^2}{m^4}$)

h = tanker draft (m)

Mean slow drift force on tanker in surge given by Faltinsen (22) can be written as

$$F_{sd} = \frac{\rho g L}{8} \cdot Q_1^{*2} \cdot H_s^2 \qquad (3.10.3)$$

where

Q_1^* = coefficient given in Appendix C

H_s = significant wave height for irregular seas which can be taken as $\frac{H}{2}$ (half design wave) here.

Mean drag force on buoy due to interaction of waves and current (see Ref. 45) is given by

$$F_{db} = \frac{1}{2}\rho \cdot C_D \cdot D_b \cdot \frac{L_b}{\pi}\left[(2V_{cb}^2 + u_m^2)\,\bar{\phi} + 4 V_{cb} \cdot u_m \cdot \cos(\bar{\phi}) - \frac{1}{2} u_m^2 \sin(2\bar{\phi}) \right] \qquad (3.10.4)$$

where

V_{cb} = current velocity at buoyancy cylinder

$$\bar{\phi} = \sin^{-1}(V_{cb} / u_m) \quad ; \quad V_{cb} < u_m \qquad (3.10.5)$$

$$\bar{\phi} = \pi \quad ; \quad V_{cb} \geq u_m \qquad (3.10.6)$$

$$u_m = \sqrt{\left\{ u_o \cos[k(\tfrac{L}{2} + l_2)] - \omega x_o \right\}^2 + u_o^2 \sin^2[k(\tfrac{L}{2} + l_2)]} \qquad (3.10.7)$$

$$u_o = \frac{\omega H}{2} e^{-k y_b} \qquad (3.10.8)$$

High frequency motions of the system can be calculated at various arbitrary positions falling within the static offset and slowly varying positions of tanker. Therefore only a

rough estimate of the static offset will be carried out here. Static forces acting on the system are shown below. Assuming that resultant wind load acts at the tanker pivot and taking moments about the pivot we have

$$T_o \simeq \frac{F_B \cdot l_2 - M_y \cdot g \cdot X_{CG} - (F_{xc} + F_{sd}) \cdot l_3' - F_{db} \cdot l_5}{(l_1 + l_2)} \qquad (3.10.9)$$

Static offset can now be found by horizontal force equilibrium

$$X_s \simeq \frac{(F_{xw} + F_{xc} + F_{sd} + F_{db}) \cdot N \cdot l}{T_o} \qquad (3.10.10)$$

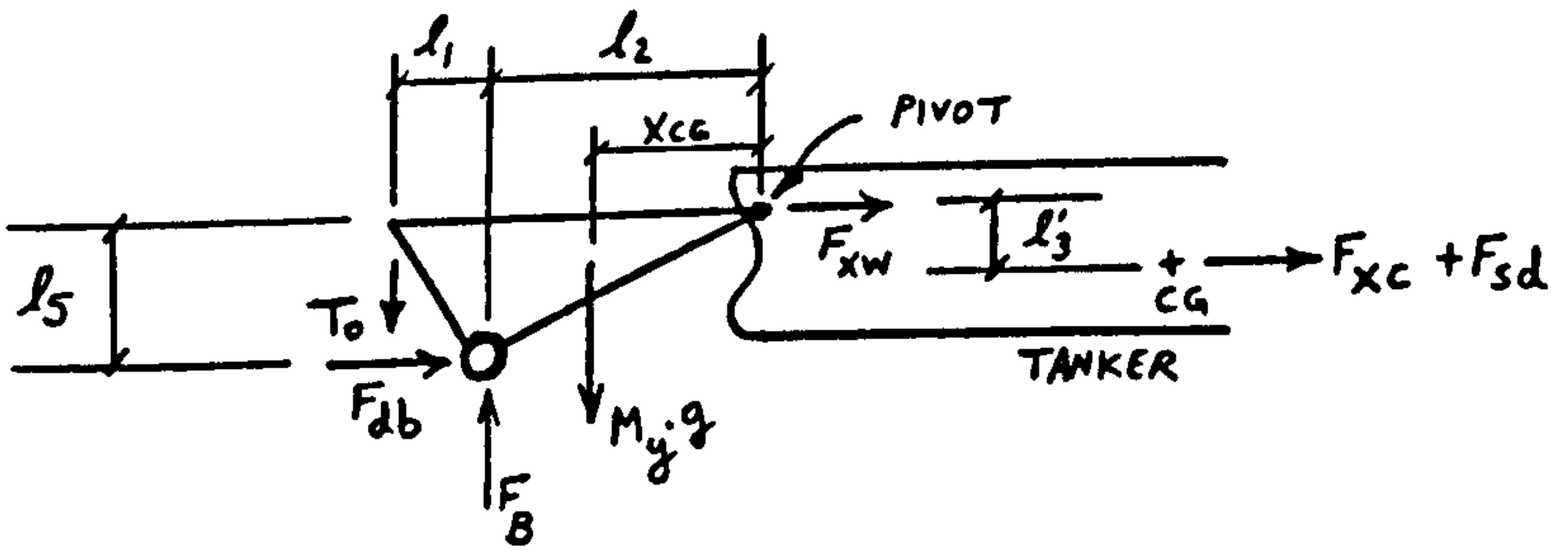

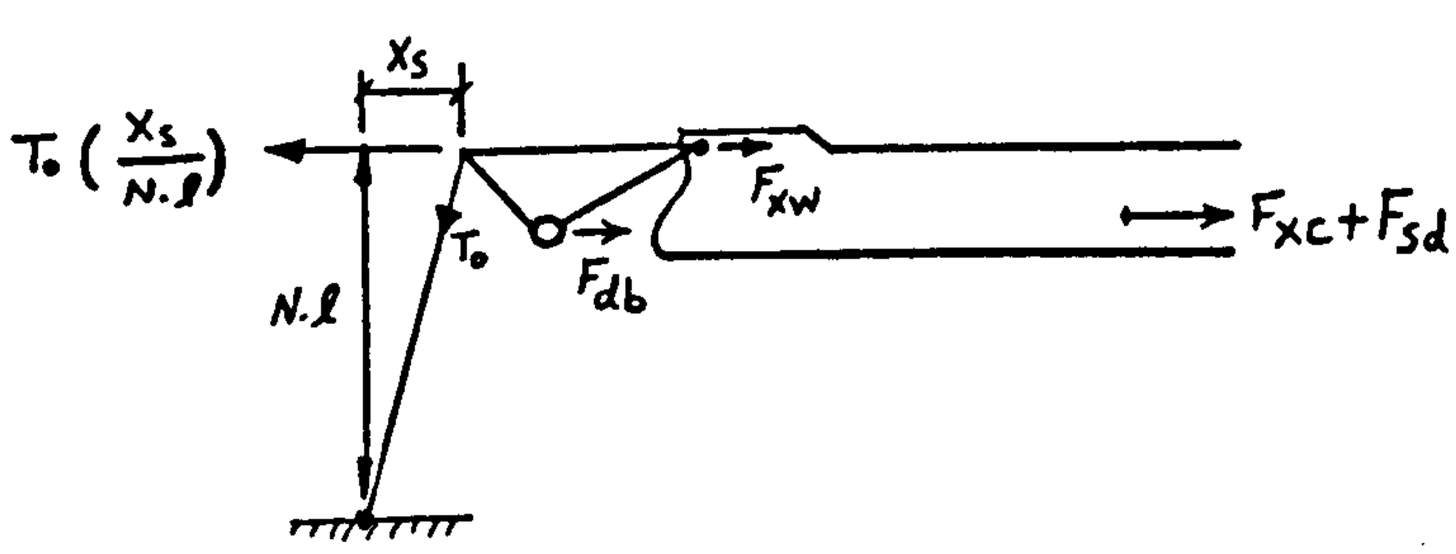

3.11. Numerical Data

Tanker:

	Full Draft	Half Draft
Structural mass (t)	240,000	120,000
Added mass in surge (t)	12,000	6,000
Draft, h (m)	18.9	9.45
$\overline{GM}$ (m)	423	846
ℓ_3' (m)	13.0	21.45
ℓ_3 (m)	3.55	13.0
Length, L (m)	310	
Beam, B (m)	47.0	

Table 3.4 Particulars of Tanker

Yoke:

Cylindrical buoy diameter, D_b = 7.685m;
length, L_b = 40m;
C_m = 2.0;
C_D = 1.5

All bracing members 876.3mm diameter except members (16), (17), (21) in figure 3.5 which are 965.2mm dia.

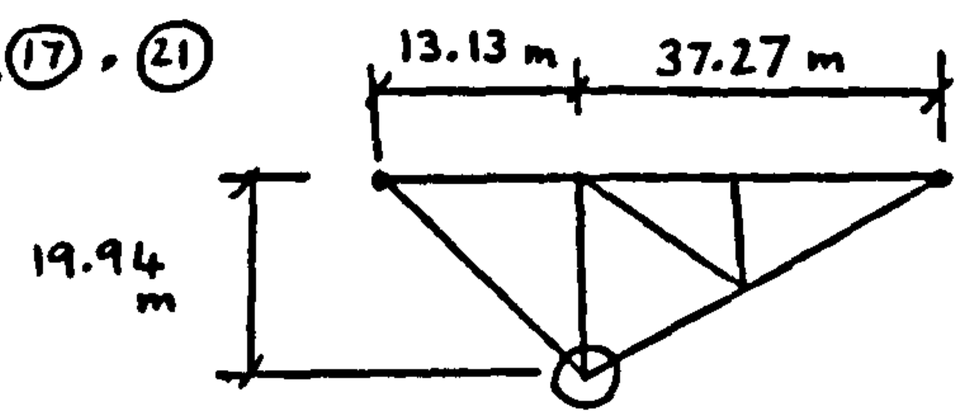

$M_1 = M_2 = M_3 = M_4 = 22.77$ t , $M_5 = M_6 = 21.72$ t , $M_7 = M_8 = M_9 = M_{12} = 26.79$ t ,

$M_{10} = M_{11} = M_{13} = M_{14} = 23.34$ t , $M_{15} = 369.36$ t , $M_{16} = 26.01$ t , $M_{17} = 28.31$ t ,

$M_{18} = 5.14$ t , $M_{19} = 10.91$ t , $M_{20} = 10.29$ t , $M_{21} = 15.99$ t

Riser Links:

No.of links N = 9; Length ℓ = 12.78m;

Diameter D_ℓ = 0.2286m; Mass m = 3975.3kg; C_D = 1.5

Water Depth, d = 115m

Current velocity, V_c = 1.23m/s

From Fig.7 Ref.(67), C_{xc} = 0.07; Fig.2 of Ref.(67) gives C_{xw} = 0.83. Using Figs.2.2,2.3 and Table 2.2 of Ref.(7) together with equations in section 3.10 gives the results summarised in Table 3.5

H (m)	10	15	20	30
T (s)	8.0	9.8	11.3	14.0
V_w (kts)	51	54	57	64
u_m (m/s)	0.98	2.09	2.00	4.71
$\bar{\phi}$ (rad)	π	0.499	0.523	0.214
F_{xw} (MN)	0.43	0.49	0.54	0.68
F_{sd} (MN)	0.32	0.49	0.56	0.71
F_{db} (MN)	0.41	0.66	0.63	1.45
X_s (m)	15.0	20.1	21.1	33.6

Table 3.5. Approximate Mean Loads and Static Offset of Tanker

3.12 Results

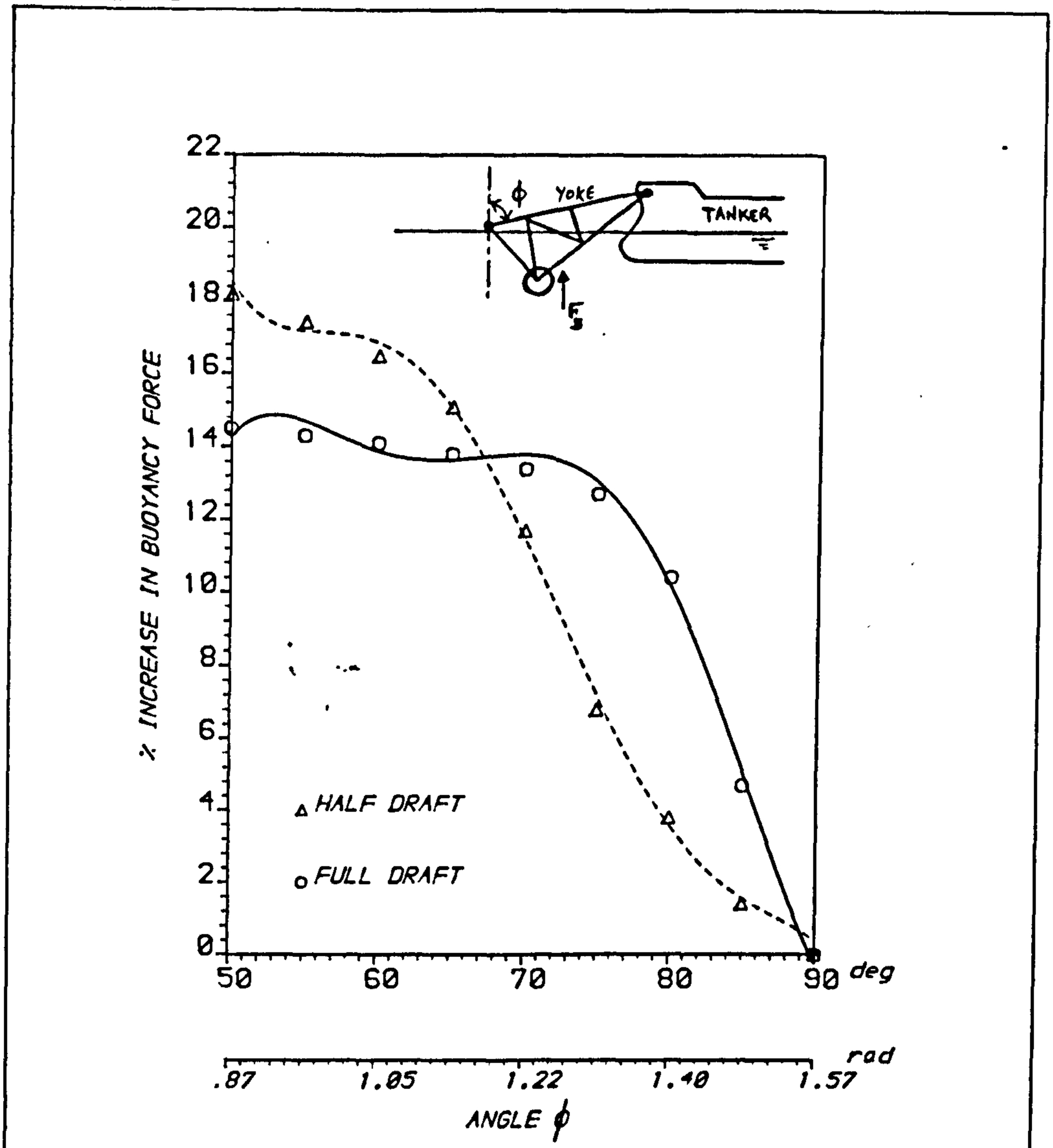

BEST FIT POLYNOMIALS FOR BUOYANCY FORCE:

——— FULL DRAFT

$$F_B = F_{INITIAL}\ (-39.231 + 174.725\,\phi - 298.758\,\phi^2 + 252.169\,\phi^3 - 104.992\,\phi^4 + 17.23\,\phi^5)$$

----- HALF DRAFT

$$F_B = F_{INITIAL}\ (43.384 - 179.099\,\phi + 299.502\,\phi^2 - 246.415\,\phi^3 + 99.674\,\phi^4 - 15.875\,\phi^5)$$

(φ IN RADIANS)

FIG 3.11 VARIATION OF BUOYANCY FORCE WITH YOKE SUBMERSION

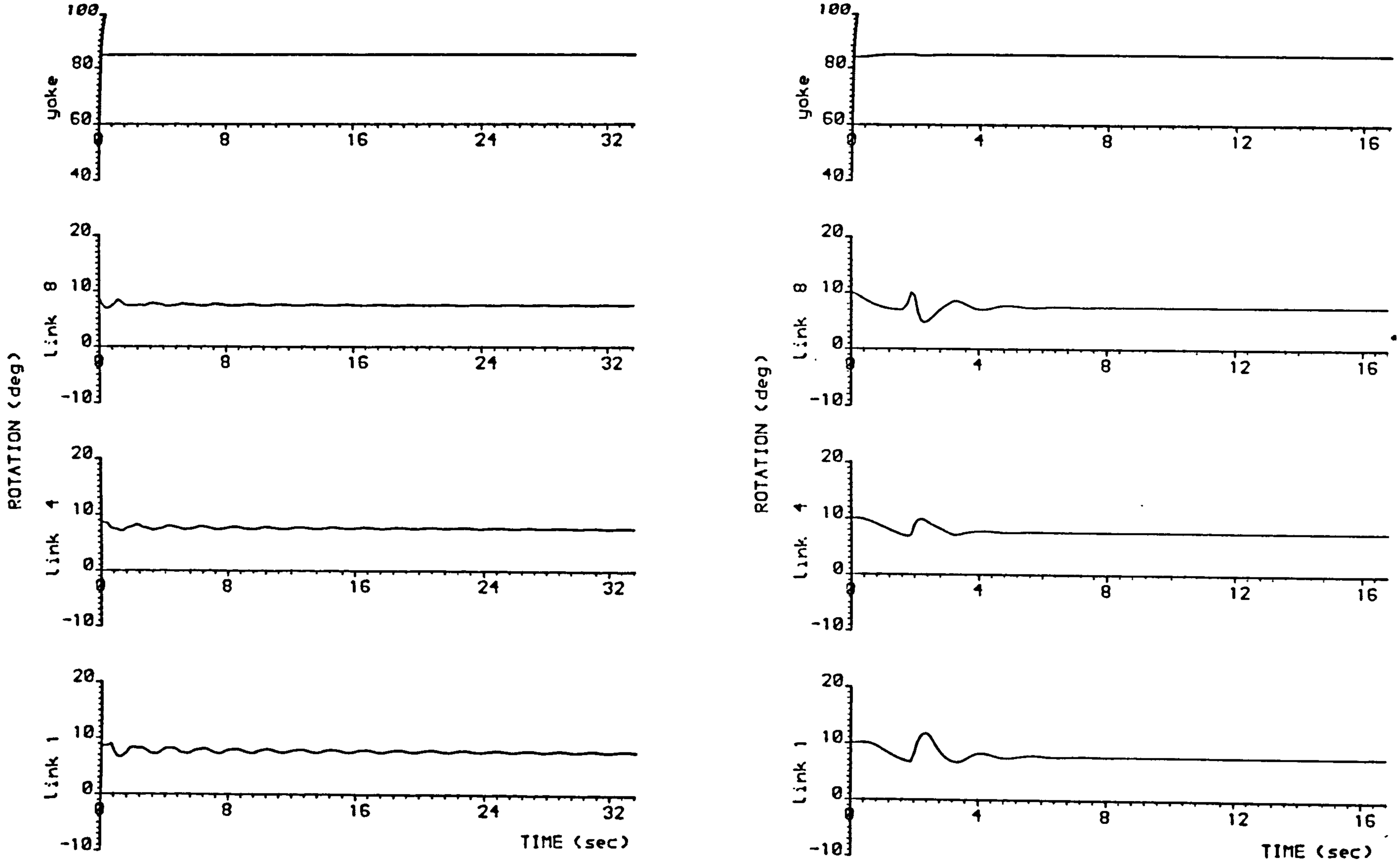

(wave ht.= 0.0 m,wave period= 0.00 sec,water depth= 115.0m,current vel.= 0.0 m/s,tanker offset=15.0 m, portion of buoy volume flooded= 20.0 %)

FIG3.12 RESPONSE OF A DAMAGED SALS SYSTEM

```
**********************************
       DAMAGED SALS SYSTEM
**********************************
 YOKE MASS= 1278.0 t
 PORTION OF BUOY VOLUME FLOODED= 20.0%
 STATIC OFFSET OF TANKER= 15.Cm
  FULL DRAFT

STATIC EQUILIBRIUM POSITION:
----------------------------
 LINK    1= 7.7  deg
         2= 7.7   ,
         3= 7.7   ,
         4= 7.6   ,
         5= 7.6   ,
         6= 7.6   ,
         7= 7.5   ,
         8= 7.5   ,
         9= 7.5   ,
 YOKE ANGLE= 84.8  deg

NATURAL PERIODS AND MODE SHAPES:
--------------------------------
    NATURAL PERIOD (sec)        MODE SHAPE COEFFICIENTS

         1.52

                                 0.53  0.4c  0.34  C.18

                                -0.C1 -0.19 -0.34 -C.4c

         0.75

                                -0.5C -C.2c  0.10  C.41

                                 0.52  0.4C  0.08 -C.2c

         0.49

                                -0.45  0.01  0.45  C.44

                                -0.C1 -0.45 -0.44  C.01

       0.35

                                 0.39 -0.2c -0.47  C.1C

                                 C.5C  C.0E -0.4E -C.24

       0.27

                                 0.32 -C.44 -0.1c  C.49

                                -0.C2 -C.4E  0.18  C.42

       0.22

                                -0.24  0.49 -0.26 -C.23

                                 0.4E -0.2c -0.23  C.4E

       0.18

                                 0.1c -0.41  0.48 -C.32

                                 0.C2  C.2s -0.4c  C.41

            0.1c

                                 0.C5 -0.2:  0.35 -C.44

                                 0.47 -0.45  0.37 -C.25

CRTHOGONALITY OF MODES O.K.
GINO-F MARK 2.c 01/05/80

GINO-F MARK 2.c C1/05/80
```

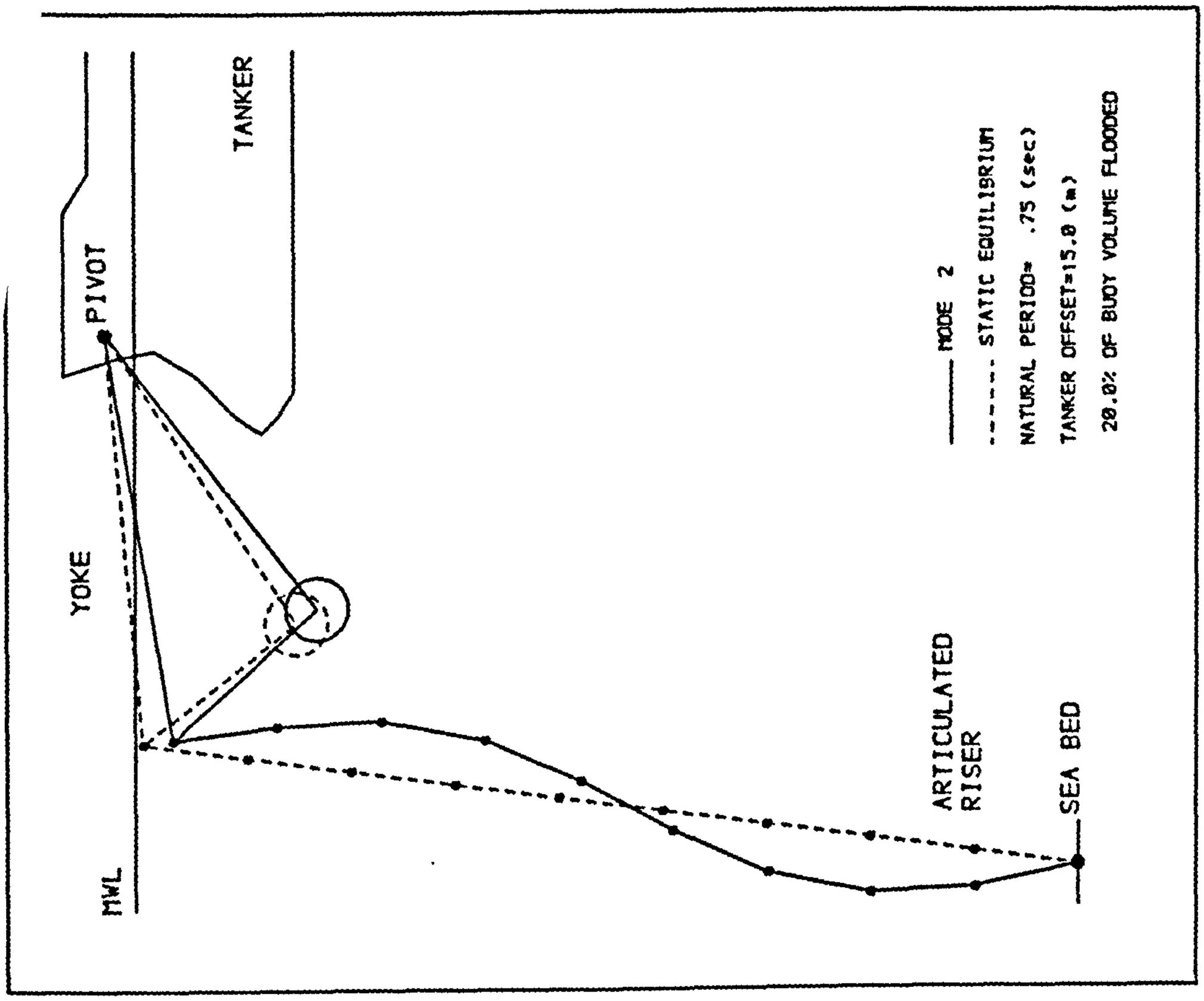

FIG 3.13 DAMAGED SALS SYSTEM. NATURAL PERIODS AND MODE SHAPES (Scale 1:1000)

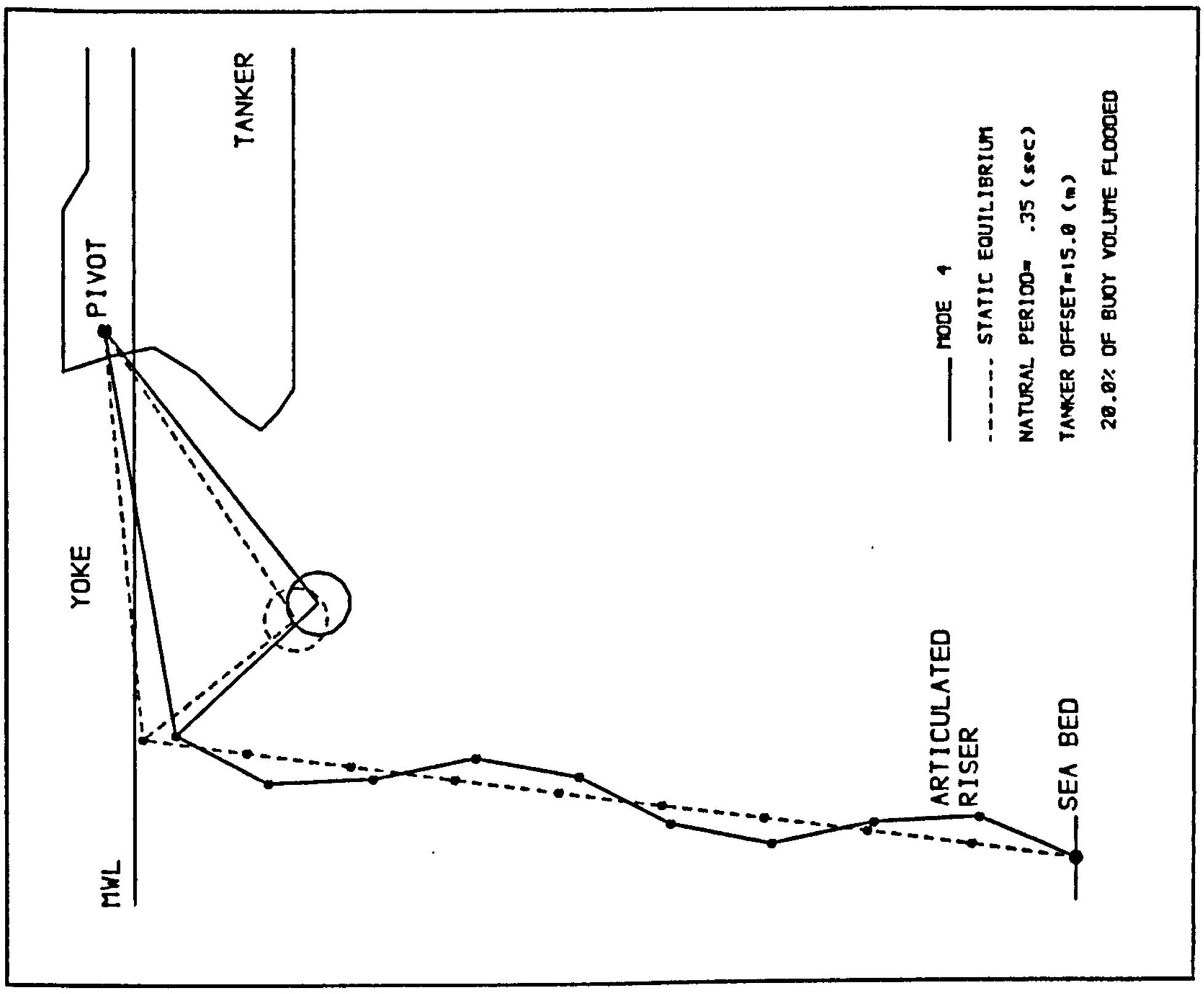

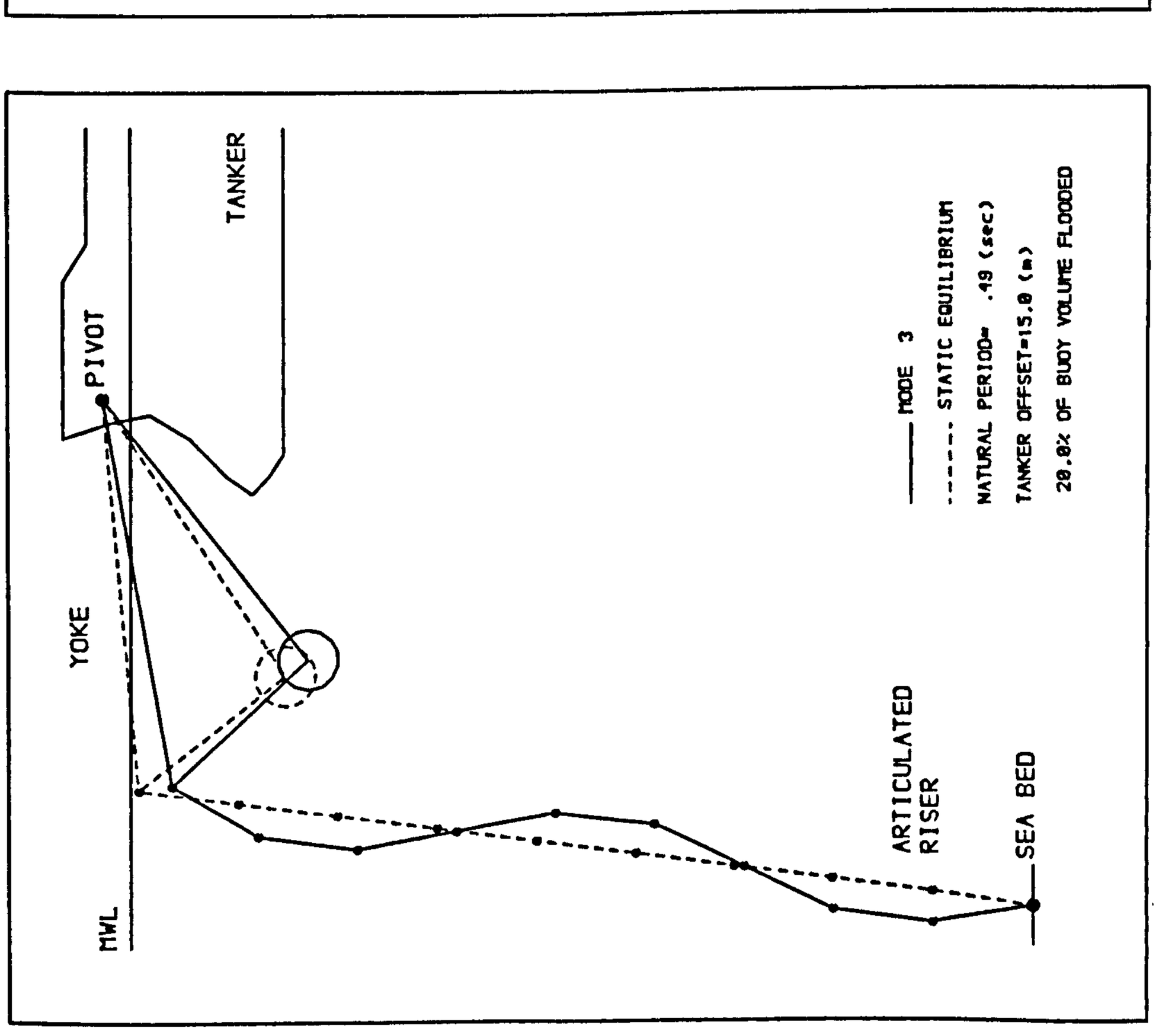

FIG 3.14 DAMAGED SALS SYSTEM. NATURAL PERIODS AND MODE SHAPES (Scale 1:1000)

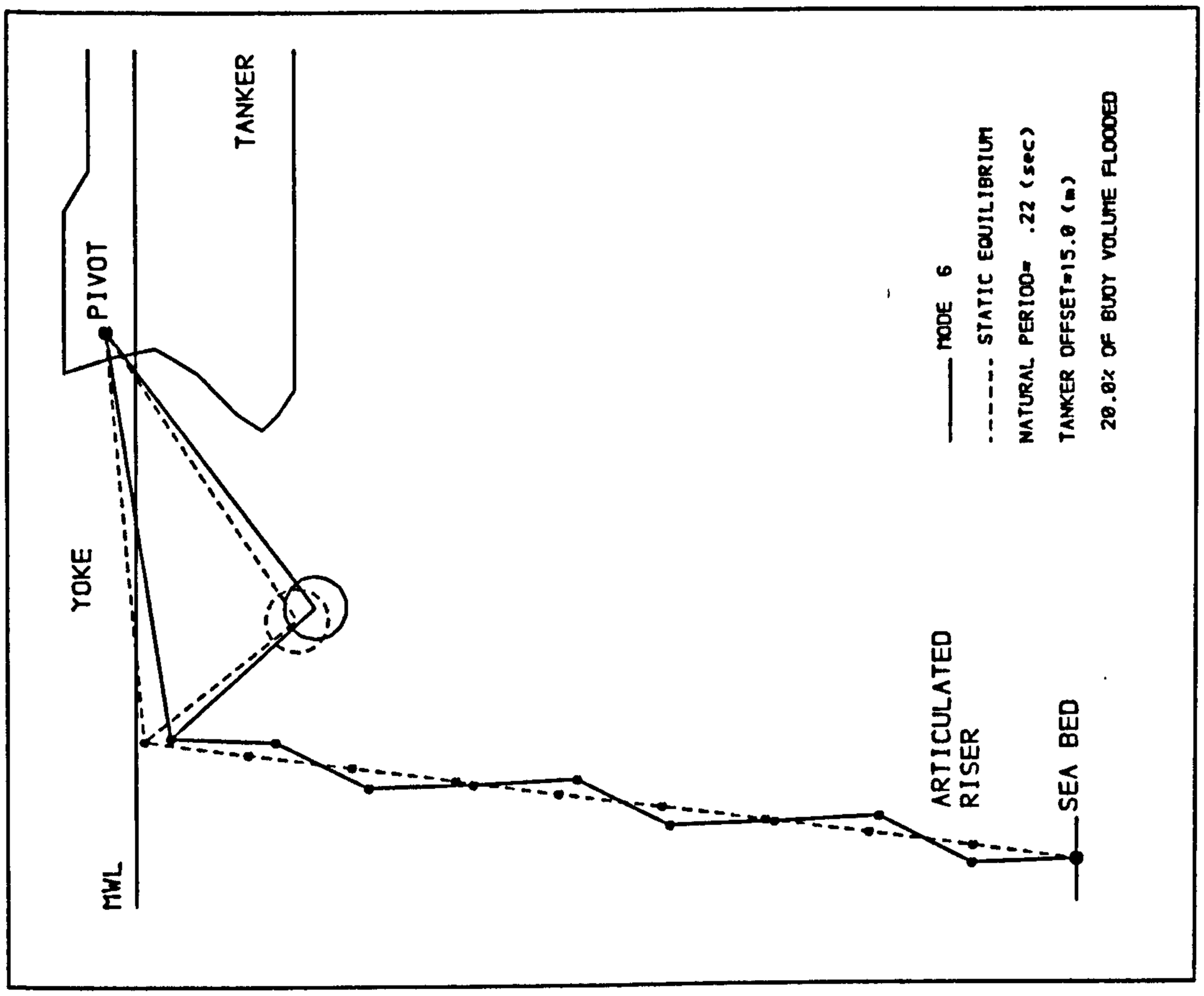

FIG3.15 DAMAGED SALS SYSTEM. NATURAL PERIODS AND MODE SHAPES (Scale 1:1000)

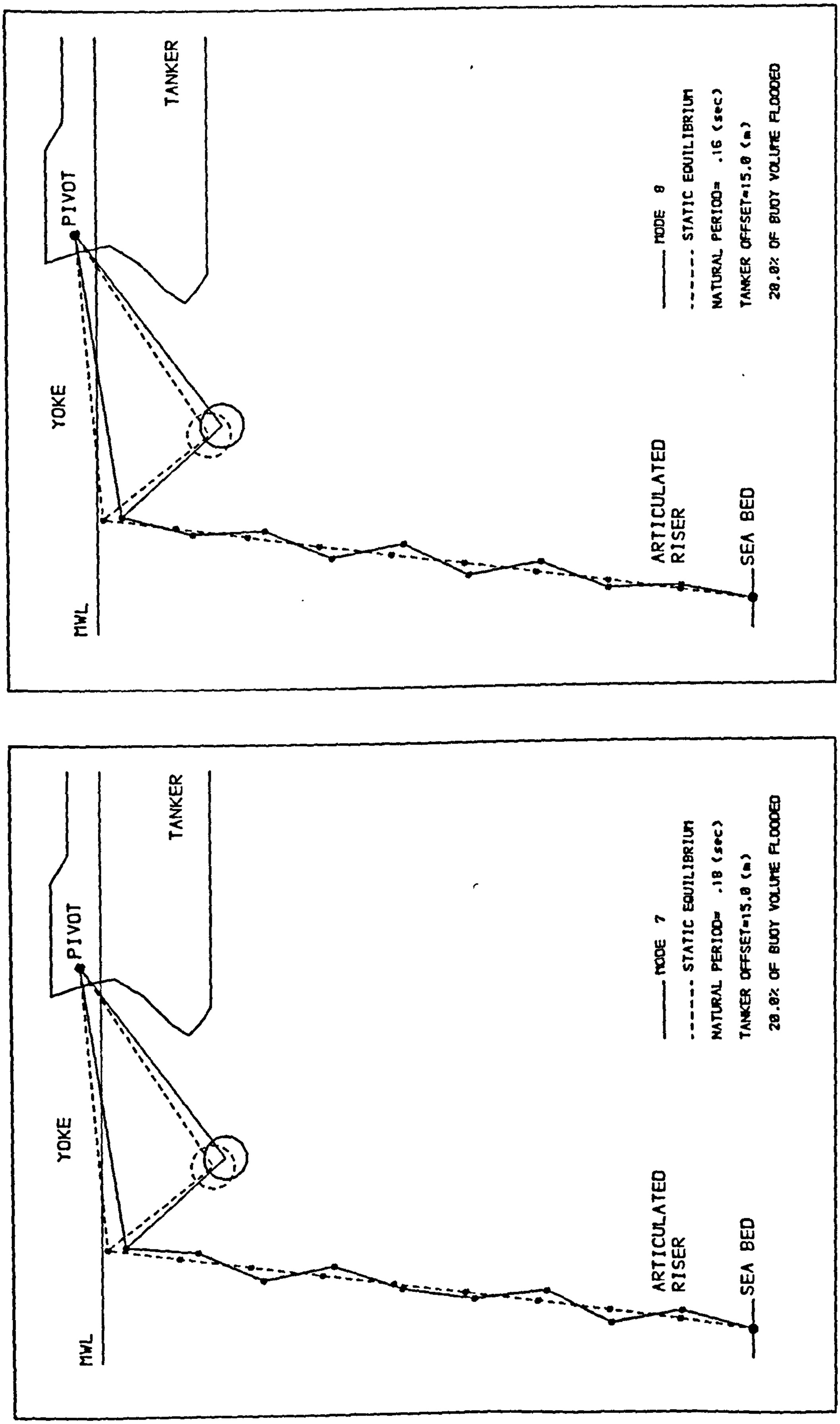

FIG3.16 DAMAGED SALS SYSTEM. NATURAL PERIODS AND MODE SHAPES (Scale 1:1000)

```
**********************************
       DAMAGED SALS SYSTEM
**********************************
 YOKE MASS= 2324.0 t
 PORTION OF BUOY VOLUME FLOODED= 75.0%
 STATIC OFFSET OF TANKER= 15.0m
  FULL DRAFT
STATIC EQUILIBRIUM POSITION:
----------------------------
 LINK    1= 9.5  deg
         2= 8.9   ,
         3= 8.3   ,
         4= 7.9   ,
         5= 7.5   ,
         6= 7.1   ,
         7= 6.7   ,
         8= 6.4   ,
         9= 6.1   ,
 YOKE ANGLE= 84.8  deg
NATURAL PERIODS AND MODE SHAPES:
--------------------------------
    NATURAL PERIOD (sec)        MODE SHAPE COEFFICIENTS

         5.77

                                 0.61  0.47  0.29  0.11

                                -0.06 -0.21 -0.32 -0.40

         2.68

                                 0.55  0.22 -0.18 -0.46

                                -0.49 -0.31 -0.01  0.27

         1.84

                                -0.47  0.12  0.51  0.37

                                -0.10 -0.45 -0.40 -0.03

         1.28

                                 0.43 -0.33 -0.46  0.18

                                 0.48  0.01 -0.44 -0.22

         1.02

                                -0.29  0.51  0.03 -0.50

                                 0.09  0.45 -0.14 -0.41

         0.79

                                -0.26  0.53 -0.36 -0.11

                                 0.45 -0.30 -0.18  0.42

         0.67

                                 0.12 -0.38  0.52 -0.45

                                 0.19  0.18 -0.41  0.30

         0.57

                                -0.06  0.16 -0.20  0.38

                                -0.47  0.51 -0.45  0.28
 ORTHOGONALITY OF MODES O.K.
 GINO-F MARK 2.78 01-JUL-1985 - ISSUE 1

 FORTRAN STOP
 $DEASSIGN/ALL
```

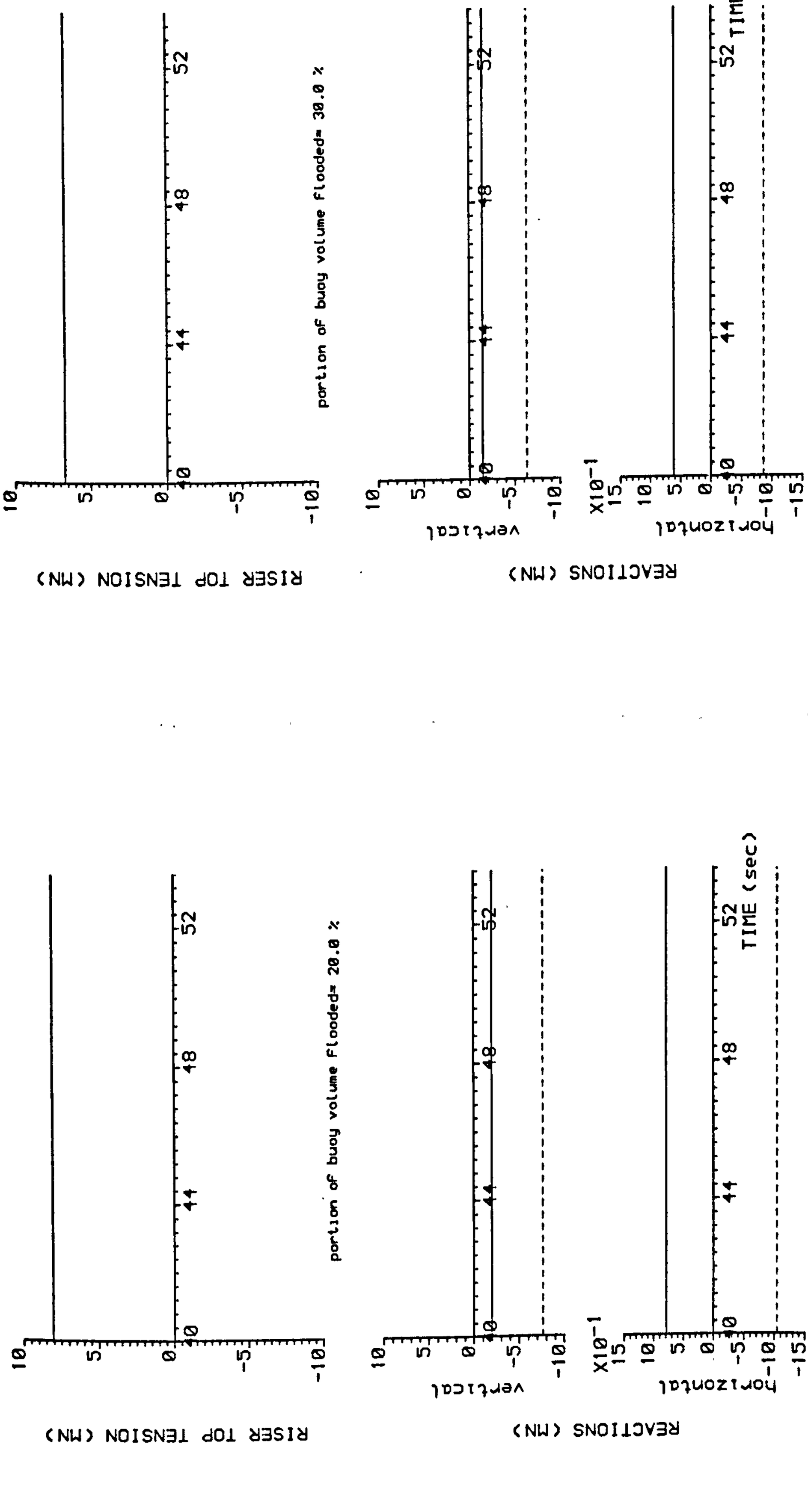

FIG 3.17 DAMAGED SALS SYSTEM: RISER TOP TENSION AND SUPPORT REACTIONS

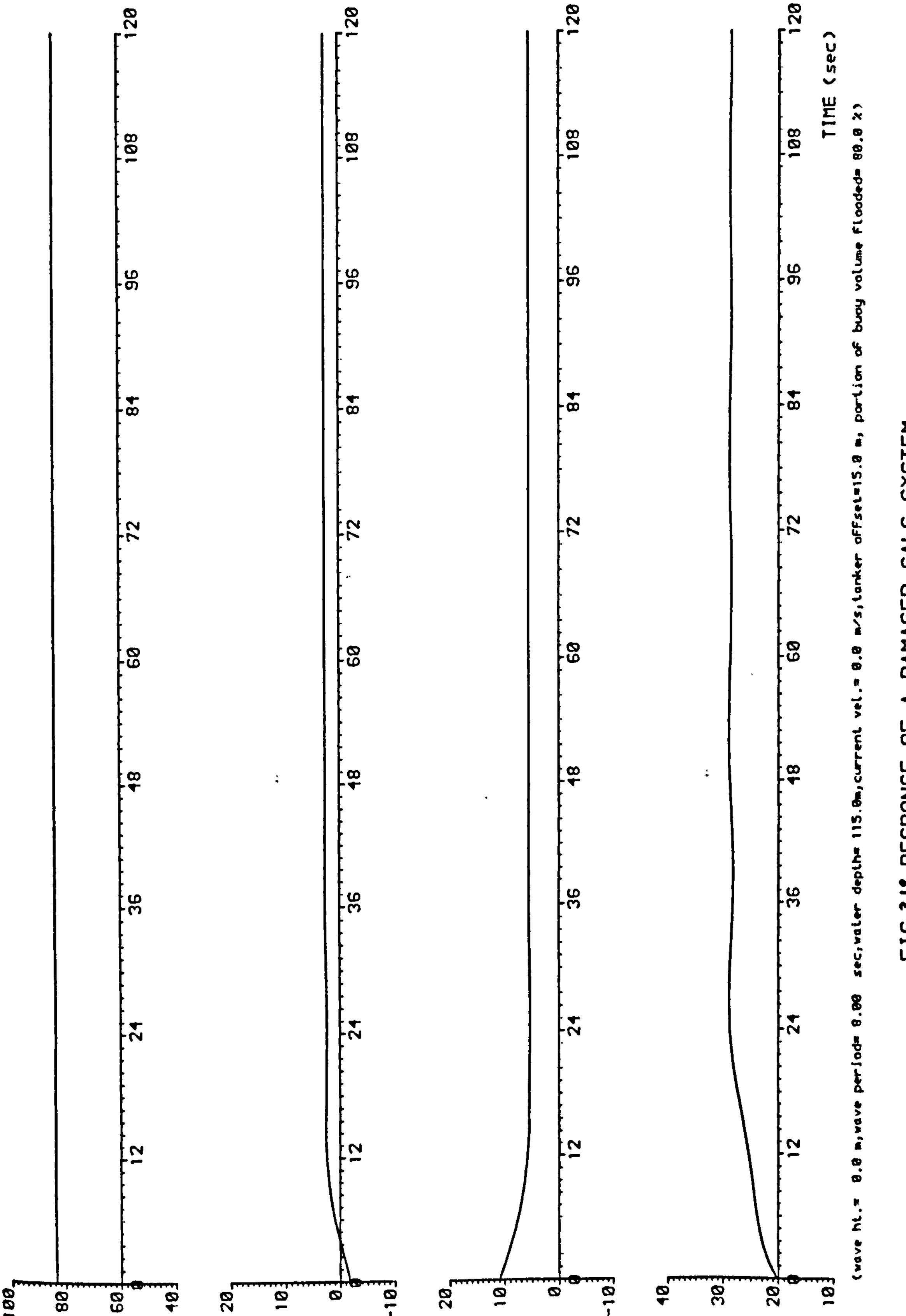

FIG 3.18 RESPONSE OF A DAMAGED SALS SYSTEM

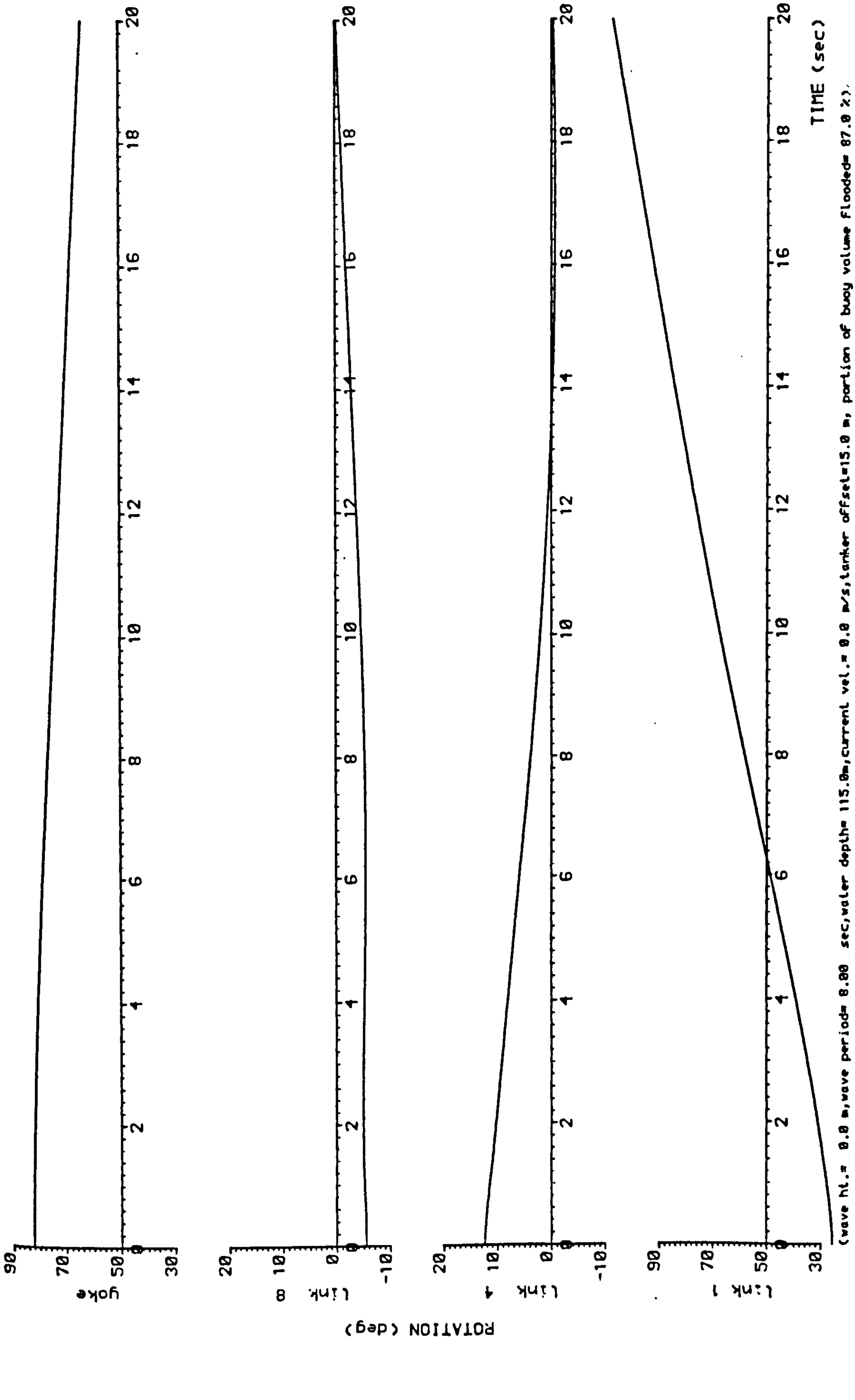

FIG3.11 RESPONSE OF A DAMAGED SALS SYSTEM

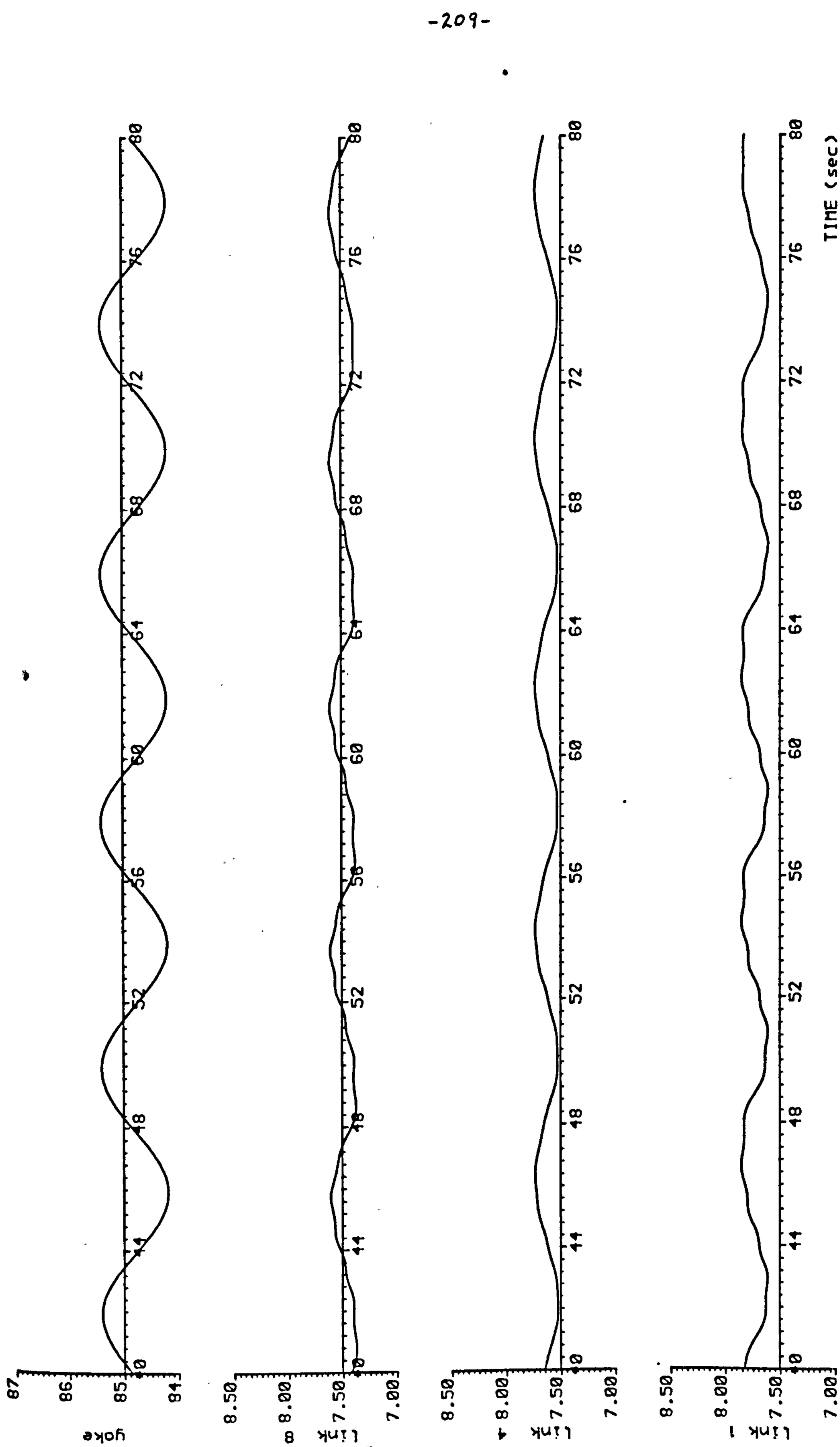

FIG 3.20 RESPONSE OF A DAMAGED SALS SYSTEM

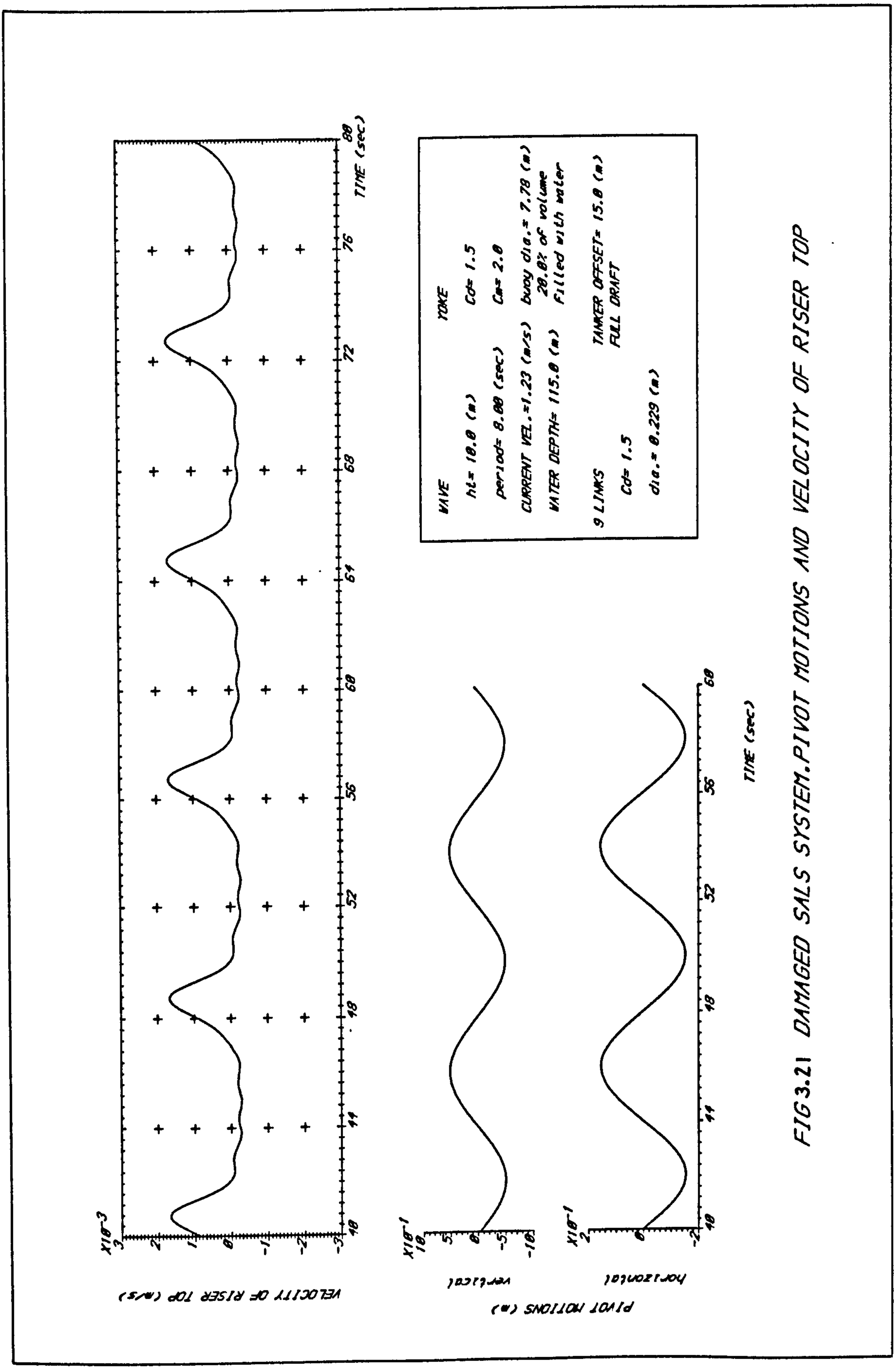

FIG 3.21 DAMAGED SALS SYSTEM. PIVOT MOTIONS AND VELOCITY OF RISER TOP

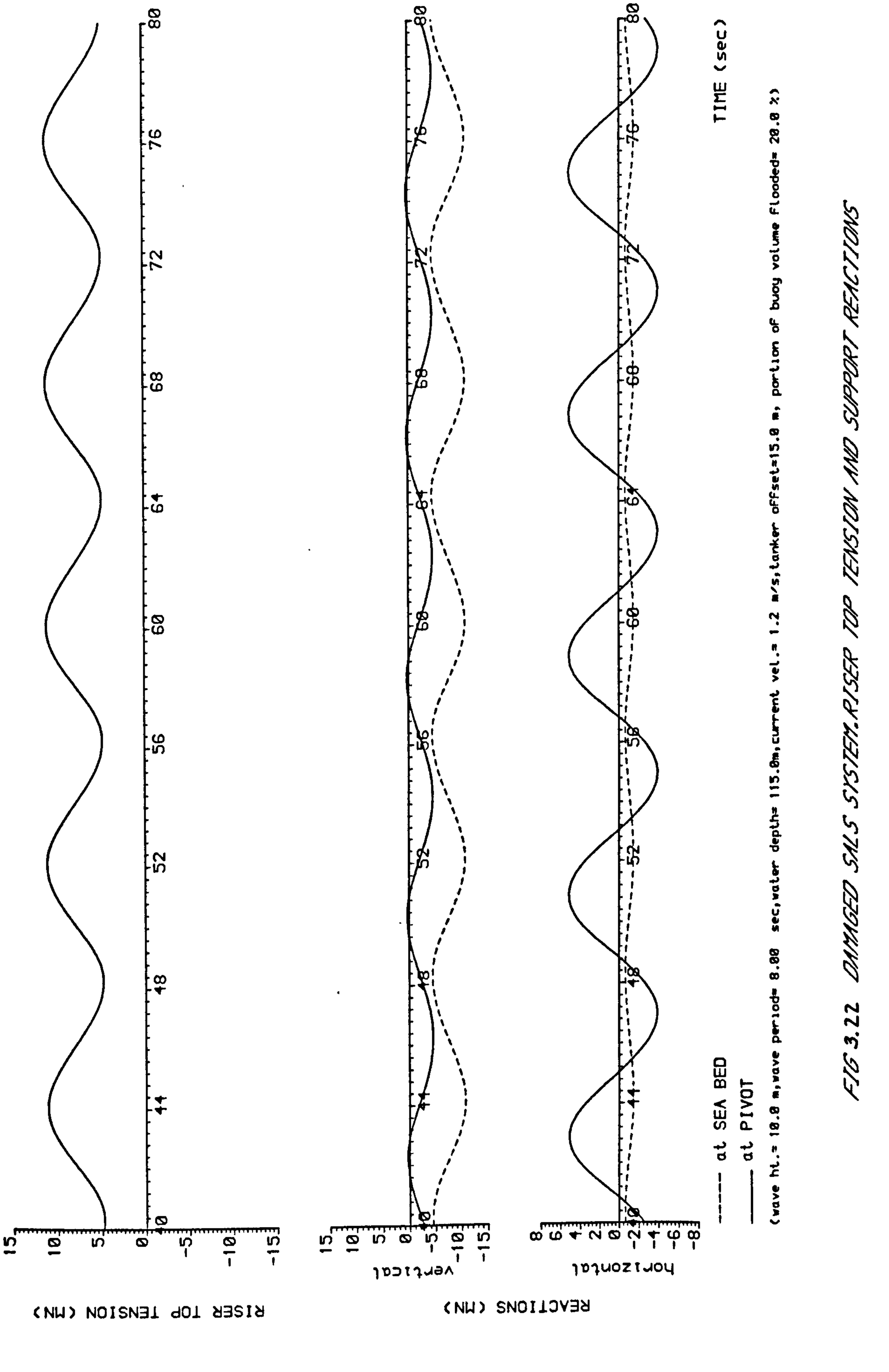

FIG 3.22 DAMAGED SALS SYSTEM.RISER TOP TENSION AND SUPPORT REACTIONS

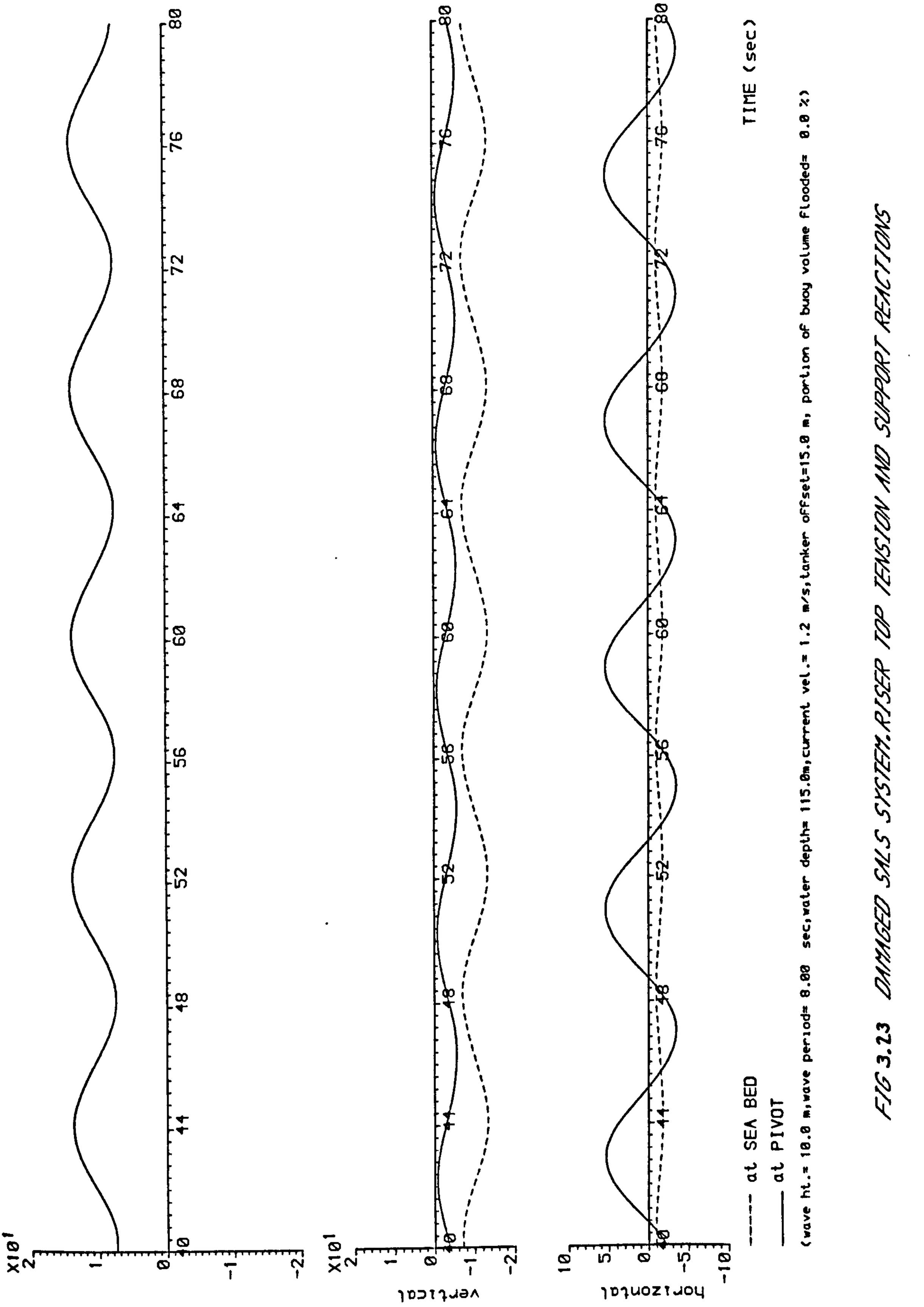

FIG 3.23 DAMAGED SALS SYSTEM. RISER TOP TENSION AND SUPPORT REACTIONS

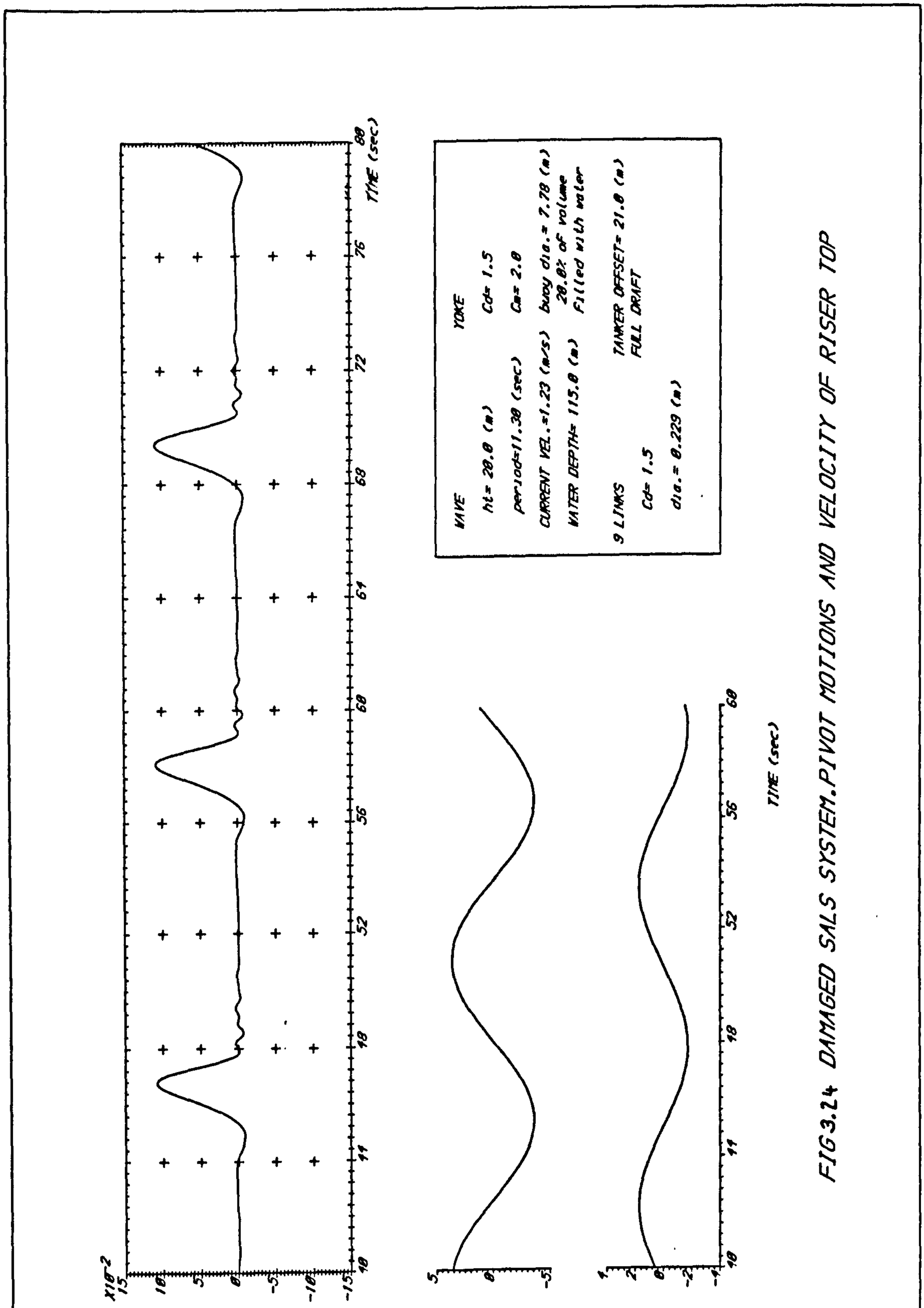

FIG 3.24 DAMAGED SALS SYSTEM. PIVOT MOTIONS AND VELOCITY OF RISER TOP

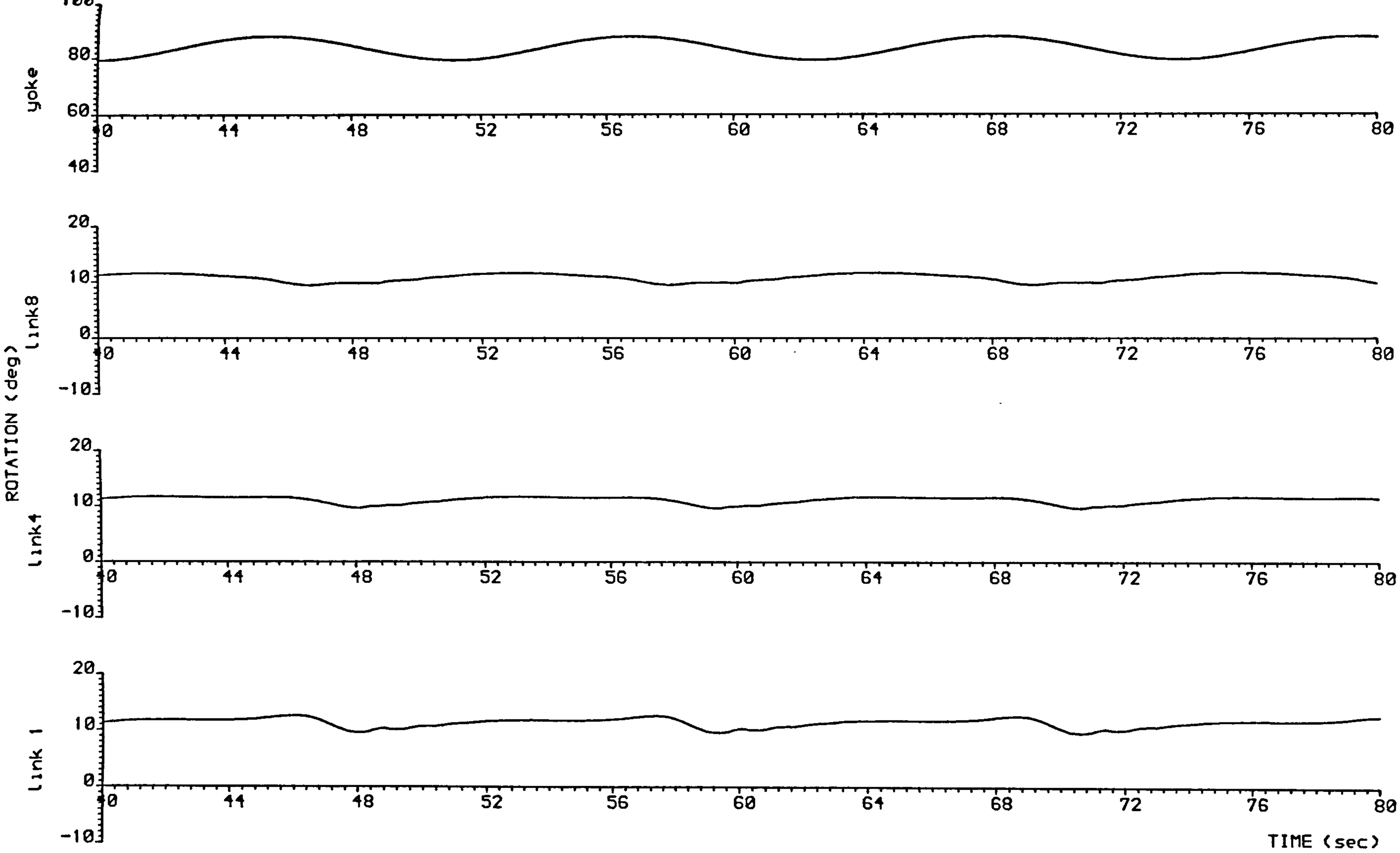

(wave ht.= 20.0 m,wave period=11.30 sec,water depth= 115.0m,current vel.= 1.2 m/s,tanker offset=21.0 m, portion of buoy volume flooded= 20.0 %)

FIG 3.25 RESPONSE OF A DAMAGED SALS SYSTEM

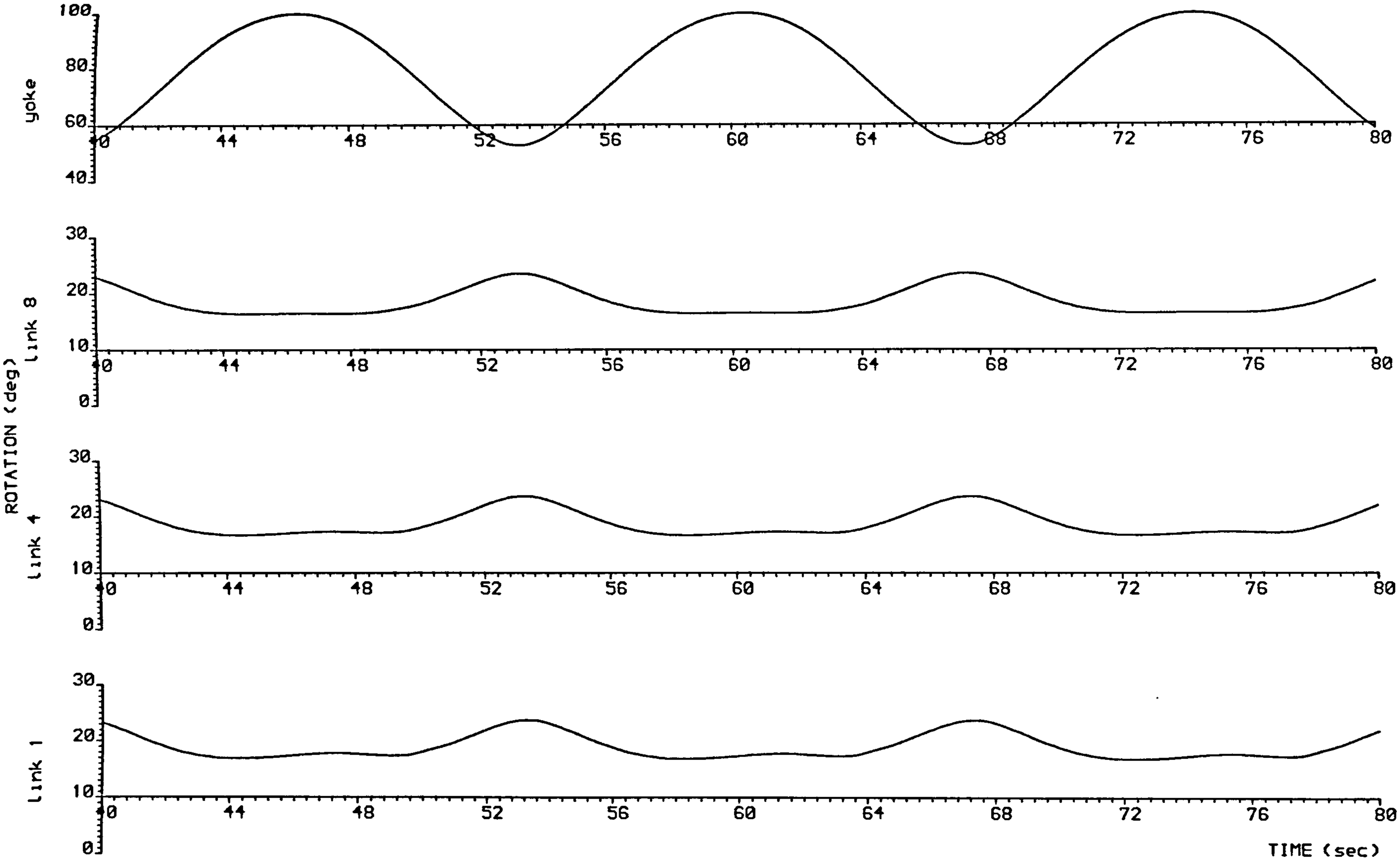

(wave ht.= 30.0 m,wave period=14.00 sec,water depth= 115.0m,current vel.= 1.2 m/s,tanker offset=34.0 m, portion of buoy volume flooded= 0.0 %)

FIG 3.26 RESPONSE OF A DAMAGED SALS SYSTEM

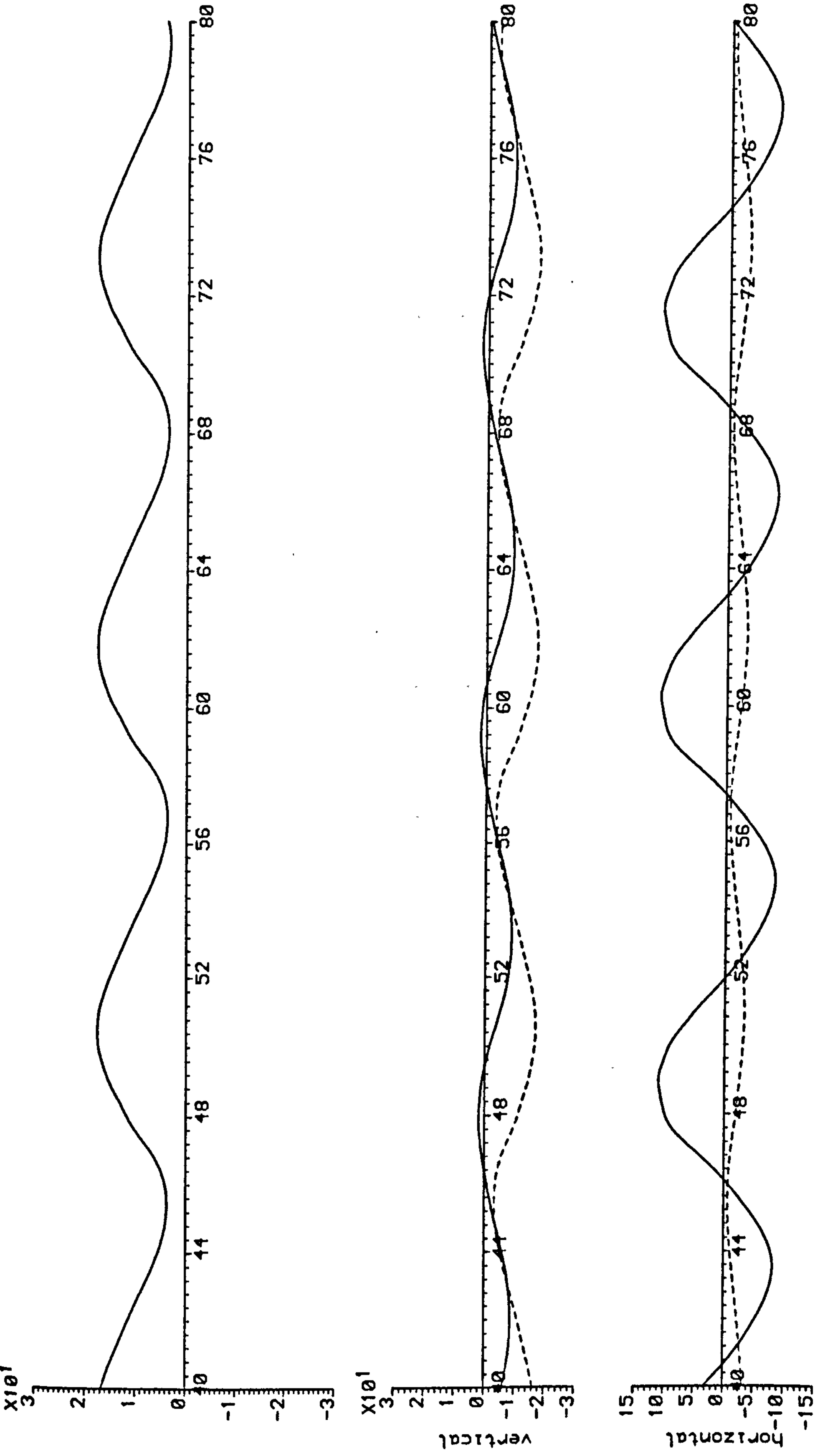

FIG 3.27 DAMAGED SALS SYSTEM. RISER TOP TENSION AND SUPPORT REACTIONS

Wave Height (m)	% Buoy Volume Flooded	Riser Top Tension (MN)		Maximum Reactions (MN)				Max.Velocity of Riser Top (m/s)
				At Tanker Pivot		At Seabed		
		Min.	Max.	Horiz. R1	Vert. R2	Horiz. R3	Vert. R4	
10	0	7.47	13.78	5.37	-5.59	-1.81	-13.36	8.5×10^{-4}
	20	4.8	11.10	5.09	-4.52	-1.45	-10.70	1.7×10^{-3}
	30	3.45	9.76	4.94	-4.04	-1.28	-9.37	3.0×10^{-3}
20	0	3.73	17.54	11.00	-8.77	-3.29	-16.93	2.9×10^{-2}
	20	1.33	14.95	11.06	-7.80	-2.80	-14.39	0.11
30	0	4.09	22.03	24.41	-20.11	-7.98	-20.26	2.4×10^{-2}

Notes
Current velocity = 1.23 m/s
Wave steepness = 1/10
Tanker at full draft

TABLE 3.6. SALS System - Summary of Results for Wave Cases Considered

3.13 Discussion

The equations of motion of the eight degree of freedom, 9-link, yoke/riser system were solved in the time domain by reducing them to 16 first order differential equations and using the Adams variable step - variable order numerical integration algorithm (subroutine D02 CBF (65)) which is suitable for problems in which large numbers of function evaluations are involved and is used in many simulation packages such as ACSL (61). For the system considered this algorithm proved to be almost 30% faster than a Runge-Kutta-Merson algorithm (subroutine DO2BBF(65)). The inverse of the inertia matrix [I] was determined using subroutine F01AAF(65) which employs Crout's method (see Ref.(90)). Since [I] is a 16x16 time varying matrix (see equations 3.6.72 - 3.6.74), its inversion at each time step could prolong the computer run time leading to high costs. It was found that inversion of [I] only at times when variation of angular displacements are larger than 3 degrees would lead to considerable reduction in computing time without affecting the accuracy of results. In order to incorporate variation of buoyancy force F_B in the computer program, use was made of a curve fitting subroutine, E02ACF(65), by finding the best 5th order minimax polynomial fit to the calculated values. Changes in F_B with yoke angle ϕ are shown in Fig.3.11. It can be seen that for large rotations of the yoke assembly changes in F_B can become significant, the large increases being mainly due to submersion of long cylindircal members comprising the yoke upper and lower parts. The polynomial coefficients were found for $50^\circ \leq \phi \leq 90^\circ$ For larger rotations ($\phi < 50^\circ$) the lower part of the yoke structure could come into contact with the tanker hull leading to impact damage. For $90^\circ < \phi < 105^\circ$ changes in F_B were found to be minimal (less than 2%) except for the case of the tanker at half draft where buoyancy cylinder may become only partly submerged. In Fig.3.11 $F_{INITIAL}$ corresponds to the buoyancy force at $\phi = 90^\circ$. In the analysis it was assumed that the centre of buoyancy coincides with the centre of cylindrical chamber at all times, i.e.

the lever arm of the buoyancy force in the equations of motion, which is the horizontal distance from F_B to the riser top articulated joint, is always measured from the cylindrical buoy and not from the actual centre of buoyancy. This assumption, despite significant changes in F_B, was found to be valid for the yoke geometry under consideration. For example, in the case of an 18% increase in F_B, corresponding to $\phi=50^\circ$ with the tanker at half draft, the difference between the two lever arms, one measured from the cylinder the other from centre of buoyancy, was found to be less than 2%.

In deriving an accurate expression for the yoke kinetic energy in section 3.3, its members were considered individually. An approximate method would be to consider the yoke as a concentrated mass acting at its centre of gravity. This led to values of A_m, B_m, D_m (see section 3.3 and equations 3.3.39 - 3.3.41) that were accurate to within 4% of the exact values. Therefore it was found that taking the yoke as a concentrated mass acting at its centre of gravity, an assumption used later in section 3.9 for calculation of riser tension and support reactions and which involves less algebra, could lead to accurate results. It was also assumed that the kinetic energy due to flexural displacements, i.e. bending of links, could be ignored. Simple calculations prove that the natural periods of links in bending are as expected well below the periods of exciting waves. Hence the contribution of link elastic bending to the kinetic energy was found to be very small. For example a wave having H = 30m, T = 14 sec, the angular velocity of links for the rigid body motions are in the order of 0.035 rad/s (see slope of displacements in Fig.3.26) giving a velocity at the top links of the order of $\dot{x}$ = 3-4m/s. Treating the links as simply supported beams subject to uniformly distributed drag load F_D with fluid particle velocity $u \simeq$ 7 m/s (linear wave theory deep water approximation + 1 m/s current) plus the link self weight in fluid gives the maximum deflection $\delta = \frac{5 F_D l^4}{384 EI} \simeq 0.28$ m

and assuming simple harmonic vibrations of amplitude δ and frequency ω gives velocity $\frac{d\delta}{dt} = \omega\delta \simeq 0.13$ m/s. This would roughly make a 7% increase in the kinetic energy which is negligible bearing in mind that the above procedure, although very approximate, is conservative because the inertia relief terms have not been taken into account. In any case flexural kinetic and strain energies do not affect the equations of motion and their effect can be considered separately if a detailed stressing of individual members is required.

The static equilibrium position of the partially flooded yoke/riser system in still water can be found by setting the wave loading to zero. Fig.3.12 shows the response of the system when 20% of the buoy volume is flooded (p=20%) and when there are no waves or current. Note that increase in p with time is assumed to be small and p is taken constant during the simulation. Time histories on the left hand side of Fig.3.12 show that although the initial values of θ_i , ϕ are not far from the final values, i.e. the initial disturbance about the static equilibrium position is not large, transients can take a long time to die out. This is mainly due to small drag damping present. To overcome this problem an artificial linear damping term was used in the program which decreased linearly with time reaching zero after 10 seconds of simulation. The result is shown on the right hand side of Fig.3.12 where despite a higher initial disturbance about the equilibrium position transients died out in less than 10 seconds. Values of angular displacements for this case and the natural periods and mode shapes for small oscillations are given on page 200 . Here, despite a 20% loss of buoyancy the riser remains almost taut. Figs.3.13-3.16 show natural periods and mode shapes of the system for this case. For the higher modes the natural frequencies are shown to be closely spaced which if excited by fluid drag forces can possibly lead to interactions between the modes. The low natural periods are mainly due to the large buoyancy stiffness or tension in the riser. Fig.3.17 shows the static riser top tension (8.03 MN $\simeq$ 800 tf for p = 20%) and the support reactions

when current velocity Vc = 1.23 m/s. Results of the eigenvalue analysis for p = 75% are given on page 205 . The static equilibrium angles show that the riser becomes less taut and the increase in yoke mass, due to flooding, together with the reduction in buoyancy stiffness have increased the natural periods. The first natural period for this case is about 6 seconds indicating the possibility of resonant motions in presence of waves at low sea states (e.g. JONSWAP spectrum, Hs = 4m). For p > 75% (Fig.3.18) the riser becomes very slack resembling the configuration of a catenary mooring chain with the bottom link inclined at 28° to the vertical. If the buoyancy loss is increased further, the stiffness terms in the equations of motion become negative resulting in an unstable system and, as shown in Fig.3.19, the system will continue to sink. Fig.3.20 shows the response of the system to H = 10m, T = 8 sec, V_c = 1.23 m/s, p = 20%. Since D_b = 7.68m and the buoy centre is more than 20 metres below the M.W.L. any potential damping is small and therefore, to reduce the transient oscillations, in addition to the artificial damping mentioned earlier H was linearly increased from zero at t = 0 to 10m at t = 20 sec. The steady state response is shown to consist of oscillations at the exciting wave frequency together with superharmonic components appearing at a 5th of the wave period. The drag force can be expressed in a Fourier series expansion containing harmonics at odd multiples of the exciting frequency (e.g. see Gudmestad and Connor (30)) and therefore the appearance of super-harmonic components in the response can be attributed to quadratic drag resonance due to the fact that the first natural period of the system (T1 = 1.52 sec as shown in Fig.3.13) is very near to 0.2T. Fig.3.21 shows the tanker pivot motions and velocity of the top of the riser for this case. Maximum horizontal and vertical pivot motions are shown to be about ± 0.5m, ± 0.18m respectively. Referring to Fig.B3 in Appendix B the vessel transfer functions are relatively small at high wave frequencies therefore the small amplitude pivot motions are due to the low vessel

response at the wave frequency (0.785 rad/s) under consideration. Time histories of riser tension T_R and support reactions are shown in Fig.3.22. Comparing the maximum value of T_R (11.10 MN) with the static tension T_{RS} in Fig.3.17 (8.03MN) shows that there is an increase in riser top tension of more than 38%. Also comparing the results of Figs.3.22 and 3.23 (no flooding) it is shown that for this case p=20% would reduce the maximum T_R by more than 24%. In Fig.3.22. $T_{R_{MIN}}$ = 4.8 MN = 0.6 T_{RS} (Fig.3.17). Therefore the maximum tension caused solely by dynamic loads is approximately 40% of the static tension. It was also found that the minimum tension in this case was about 45% of the static tension for the undamaged case (T_{RS} = 10.6MN) i.e. the 10m wave together with p = 20% can reduce the riser tension by about 55% during a wave cycle. For H=20m, T=11.3 sec (ω = 0.556 rad/s) the maximum horizontal and vertical pivot motions were found to be ± 1.8 m , ± 2.7 m (Fig.3.24) respectively which appear to be approximately 73 degrees out of phase with each other. Here the vessel transfer functions (see Fig.B3 Appendix B) and fluid loading are higher than the previous case which together lead to larger angular displacements of the yoke as shown in Fig.3.25. Similarly with H=30m, T=14 sec (ω = 0.449 rad/s) the vessel pitch transfer function becomes very large causing vertical pivot motions greater than ± 18 metres leading to large variations in the yoke angle as shown in Fig.3.26. Time histories of T_R and support reactions for the H=20m, with no flooding, are shown in Fig.3.27. and a summary of all results obtained is presented in Table 3.6. All cases considered correspond to a wave steepness of 1/10 with the tanker at full draft. Despite all efforts to minimize the costs, the computer program which was developed to simulate motions of the system proved to be quite expensive to run. For example, to obtain an 80 second simulation record, in some cases, it took 18 hours of CPU time to execute the program on a VAX 11/750 computer. This was generally the case when extreme wave heights and/or high amounts of tension loss in the riser were under consideration

where variations in displacements at both transient and steady states are larger requiring shorter time steps for the numerical integration of equations of motion. In most cases specification of lower accuracy requirements in order to speed up the numerical integration process resulted in unrealistically large values of angular velocities and displacements which subsequently lead to aborted program runs due to numerical overflow in the mathematics library of the computer system.

The sudden application of axial force at the time when the slack riser becomes taut can lead to transient rigid body link oscillations. For the cases considered the slack in the riser was very small and did not lead to high stress levels due to snatch loads. It must be pointed out that when the tanker is at half draft the buoy is nearer to the M.W.L. (70m when $\phi = 90°$) undergoing higher fluid loading which can lead to more severe stresses. In the analysis the effect of elastic riser extension and internal material damping were ignored. A better mathematical model for the study of snatch loads would include the effects of link elasticity. Walton and Polachek (85) studied the dynamics of submerged inextensible cables and later (86) added the effects of cable elasticity to their analysis in which they showed that neglecting cable elasticity would lead to highly conservative (almost double) values of snap loads. An approximate method to find snap loads would be to assume that the kinetic energy at snatch is equal to the strain energy in the links i.e. $\frac{1}{2} M_e \cdot V^2 = \frac{1}{2} K \cdot x^2$ where M_e is an equivalent mass for the yoke, V is the velocity of riser top just prior to snatch, K is the longitudinal stiffness of the links and x = total link extension. This gives a snap load, $F = Kx = V\sqrt{K \cdot M_e}$ where M_e can be taken as a mass concentrated at the riser top and which gives a moment of inertia equal to that of the yoke mass about the tanker bow pivot. For p=20%, M_e = 647.5 tons, K = 74.95×10^6 N/m (Young's modulus x cross sectional area / riser length) and steel

yield stress of 300-600 N/mm², the velocity of riser top to cause yielding of the material at snatch would be in the order of 2-4 m/s. Failure can also occur in the 12 inch diameter pins connecting adjacent links. At each joint the pin acts as a beam supported by two plate connectors at both ends and is subject to snatch load acting at say midspan which can induce excessive bending stresses. Taking the span as 12-13 inches would give riser top velocities, to cause snatch, of the same order as those quoted above for the links. Failure in pure shear for connector plates (6" thick) and the pin were found to be less critical. Although fluid loading and tension are a maximum at the riser top, since the static tension is less at the lower end, segments closer to seabed may experience the slack-taut condition before the upper parts. The extent to which the tension varies along the riser is determined by comparing axial forces in the top and bottom links. For example with H=10m and p=20% (Fig.3.21) bottom tension (in link 1), found from the reactions at the sea bed i.e. by resolving horizontally or vertically, is $T_R = \frac{-R_4}{\cos(\theta_1)} = \frac{-R_3}{\sin(\theta_1)}$ where at time t = 44 sec (when T_R is a maximum) the horizontal and vertical reactions at the sea bed are R_3= -1.45MN and R_4= -10.70MN respectively. From Fig.3.20, θ_1 = 7.7° giving T_R = 10.8 MN which is 3% less than maximum T_R at top however when T_R is a minimum (t = 48 sec) the difference is about 7% and reaches 10% when p=30%. A question arises whether at any particular situation T_R can be completely lost leading to compressive axial loads in the links. Treating each segment of riser as a pin ended column the Euler buckling load $P = \left(\frac{\pi}{\ell_e}\right)^2 EI$, where ℓ_e = effective length of segment = 6.39m, is approximately 6.8MN. Assuming that the riser is hanging freely and is in tension under its own weight only (mass $\simeq$ 31 tons), the downward acceleration of yoke at the top needed to induce a 6.8MN compressive force in the links would have to be higher than 20g which is impossible. A more likely possibility is when the slack riser is subject to high fluid loading

acting in the opposite direction to its sag while the yoke motions cannot compensate for changes in system configuration i.e. the riser acts as an arched beam. In such cases the induced axial compressive force will depend on the riser deflected shape, phase angles between the motions and fluid loads which is not very easy to assess.

The analysis presented in this chapter which made use of Lagrange's constrained equations of motion can also be used for the dynamic analysis of Single Point Mooring (SPM) systems comprising multi-articulated columns and a tanker. Since the algebra involved in determination of Lagrange multipliers can be tedious, a possible alternative analytical method is that presented by Kane (42) which automatically eliminates the computation of these multipliers and which has been used by Wampler et al (87) to generate dynamical equations of motion for constrained systems directly from expressions governing systems without constraints. However Kane's method requires determination of components of body accelerations which can prove to be cumbersome whereas the Lagrangian method, involving kinetic and potential energies, systematically avoids such difficulties. Passerello and Huston (69) combined the advantages of the two methods, that is avoidance of the determination of components of accelerations and automatic elimination of non-working constraint forces i.e. Lagrange multipliers, and Winget and Huston (91) applied the method to cable dynamics. However the method and advantages it can offer here require further investigation. Note that once the riser failure has occurred, say by breaking at the top or the bottom, the system becomes unconstrained and one is interested in the motion of the yoke and freely hanging riser or the yoke alone regarding possible impact with the vessel causing hull damage. Since the mass of the riser is relatively small in comparison with the mass of the yoke, it is expected that the motion of the system would resemble that of the constrained system with the riser in a slack configuration. To ensure safety for the SALS system it is recommended

that parts of the cylindrical buoy susceptible to damage and subsequent flooding be separated in the form of air-tight compartments using bulkheads inside the cylinder such that at the event of any leakage fluid cannot reach the whole length of the cylinder minimizing losses in the riser tension and eliminating possibilities of structural failure due to snatch loads.

CHAPTER FOUR
SIMULATION OF RANDOM SEAS AND ASSOCIATED SECOND ORDER RANDOM PHENOMENA

4.0 INTRODUCTION

As mentioned in the first chapter here we are concerned with two methods of simulating random seas represented by a sum of harmonic wave components and known as wave superposition. The two methods will be used to simulate the low frequency second order response of the tanker in order to estimate the peak slow drift response and its relation to RMS value.

4.1 First Order Random Seas

A general stationary random process $\eta(t)$ having a Gaussian distribution can be represented by a Fourier series expansion (73) as

$$\eta(t) = \sum_{m=1}^{\infty} x_m \cos(\omega_m t) - y_m \sin(\omega_m t) \qquad (4.1.1)$$

where x_m and y_m are independent random variables with a Gaussian distribution having zero mean and ensemble expected values given by

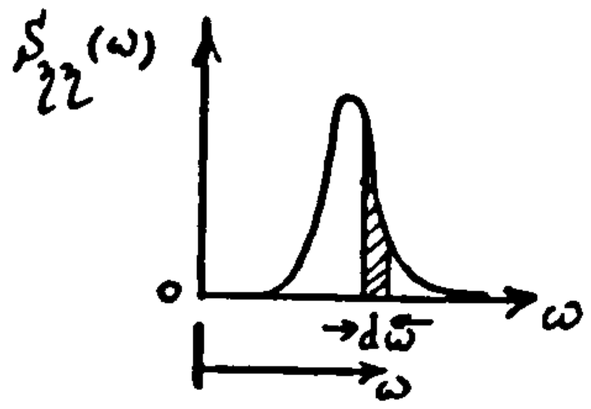

$$E[x_m^2] = E[y_m^2] = S_{\eta\eta}(\omega_m)\, d\omega \qquad (4.1.2)$$

where $S_{\eta\eta}(\omega_m)$ is the one sided power spectral density of the process $\eta(t)$ at frequency ω_m . By changing to polar coordinates and using the expression for joint probability density function of x and y equation (4.1.1) can be written as

$$\left.\begin{aligned} \eta(t) &= \sum_{m=1}^{\infty} a_m \cos(\omega_m t + \psi_m) \\ \psi_m &= \tan^{-1}(y_m / x_m) \end{aligned}\right\} \qquad (4.1.3)$$

where amplitude (or peak value) a_m has a Rayleigh distribution and is commonly taken as

$$a_m = \sqrt{2}\ \sigma_\eta = \sqrt{2 S_{\eta\eta}(\omega_m)\, d\omega} \qquad (4.1.4)$$

(σ_η = RMS OF η)

In the Monte Carlo method ψ_m is a random variable (phase angle) uniformly distributed between 0 and 2π. Equations of the form of (4.1.3) represent a linear random sea surface elevation or wave particle kinematics and can be efficiently simulated using an FFT algorithm. This is achieved by truncating the series of frequency components in (4.1.3) to (LX) terms where (LX) must be sufficiently large. In most FFT subroutines LX = 2^r where r is an integer. Equation (4.1.3) can also be written in complex form

$$\eta(t) = Re\left\{ \sum_{m=1}^{LX} \alpha_m \exp(i\omega_m t) \right\} \qquad (4.1.5)$$

in which

$$\alpha_m = (x_m + i y_m) \qquad (4.1.6)$$

$$x_m = a_m \cos(\psi_m) \qquad (4.1.7)$$

$$y_m = a_m \sin(\psi_m) \qquad (4.1.8)$$

Taking constant frequency and time intervals, $\Delta\omega$ and Δt we have

$$\omega_m = (m-1).\Delta\omega \quad , m = 1, 2, \ldots, LX \qquad (4.1.9)$$

$$t = (q-1).\Delta t \quad , q = 1, 2, \ldots, LX \qquad (4.1.10)$$

For the inverse Fourier transform to be exact we must have

$$\Delta\omega . \Delta t = \frac{2\pi}{LX} \qquad (4.1.11)$$

giving

$$\eta(t) = \eta[(q-1)\Delta t] = R_e \left\{ \sum_{m=1}^{LX} a_m \exp\left[2\pi i (m-1)(q-1)/LX\right] \right\} \qquad (4.1.12)$$

The length of the time history is then $T = (LX-1)\Delta t$.
In using (4.1.9) it is necessary to include frequencies which fall outside the main spectral range as shown in Figure 4.1(a). This results in unnecessary calculations for ω_m and $S_{\eta\eta}(\omega_m)$ and generation of random phase angles of a larger number than is required, which subsequently leads to higher computation costs especially when long time histories are required. A more economic approach is to use only N frequencies within the range of interest, say from ω_{min} to ω_{max} as shown in Figure 4.1(b), and set the remaining values of a_m, ω_m and ψ_m in equation (4.1.12) equal to zero. In

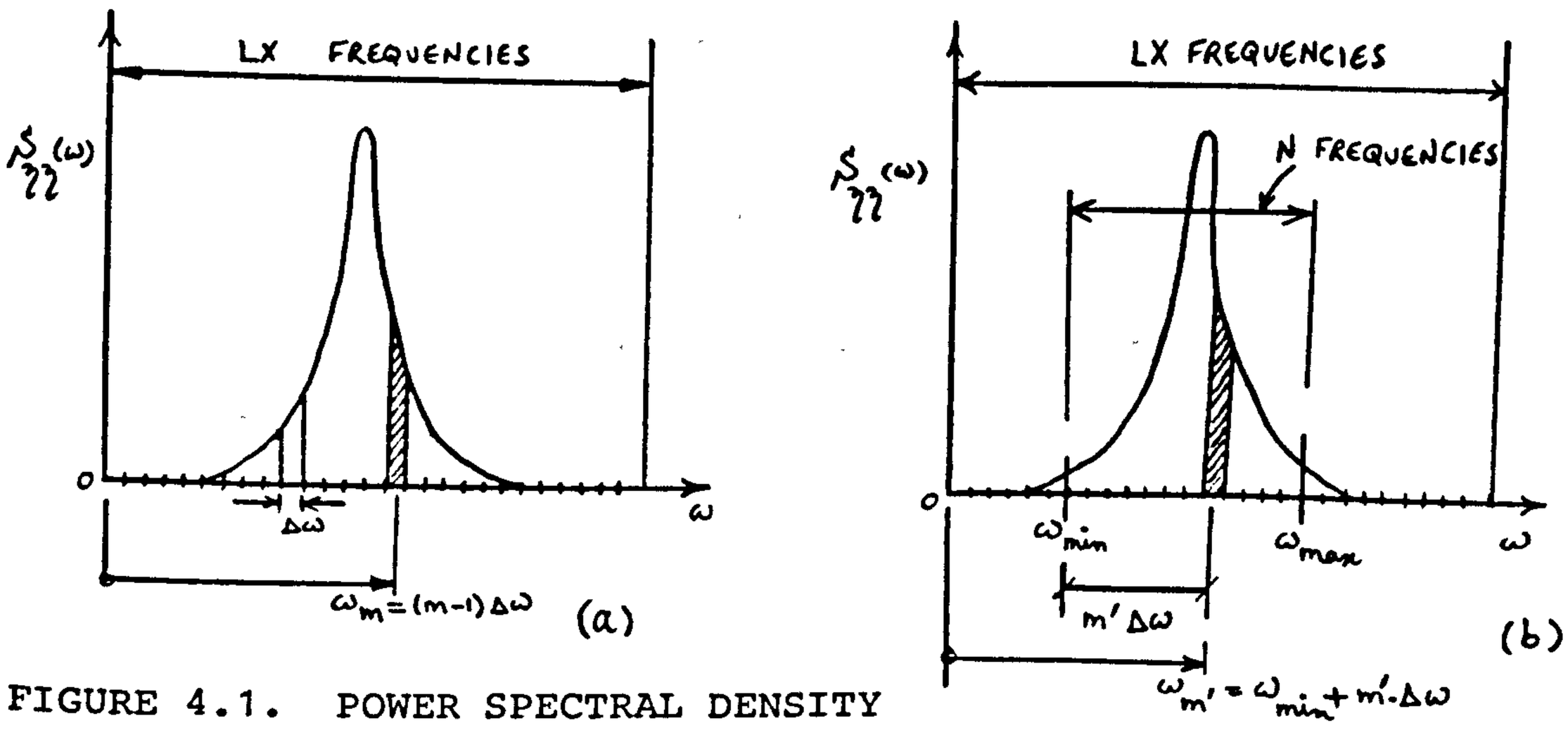

FIGURE 4.1. POWER SPECTRAL DENSITY

this case

$$\omega_{m'} = \omega_{min} + m' \cdot \Delta\omega \qquad ; m' = 1, 2, \ldots, N \tag{4.1.13}$$

In order to cover the spectrum we must have

$$\omega_{min} + N \cdot \Delta\omega \geq \omega_{max}$$

which from (4.1.11) gives

$$N \geq \frac{(\omega_{max} - \omega_{min})\, LX \cdot \Delta t}{2\pi} \tag{4.1.14}$$

also

$$LX \cdot \Delta\omega \geq \omega_{min} + N \cdot \Delta\omega$$

giving

$$N \leq LX\left(1 - \frac{\omega_{min} \cdot \Delta t}{2\pi}\right) \tag{4.1.15}$$

Note: ω_{min} must be chosen as a multiple of $\Delta\omega$.
For example if a sea surface elevation is to be simulated and we have

$$\omega_{min} = 0.196 \text{ rad/s}\ ,\ \omega_{max} = 0.8 \text{ rad/s}\ ,\ \Delta t = 0.5 \text{ s}\ ,\ LX = 2^{11} = 2048$$

then from (4.1.14) and (4.1.15) we have $98 \leq N \leq 2016$. Therefore by using say one hundred frequencies only we can get a time history with 2048 points.

4.2 Second Order Random Seas

Due to the linearization of free surface boundary conditions used in linear wave theory it is not possible to estimate accurately the statistical and spectral properties of wave

kinematics near the free surface and ignoring the nonlinearities can make the random model unrealistic, especially for steeper waves. The second order perturbation solution to the random wave problem (34) is explained in detail in Appendix A where it is proved that the second order components of the random wave field act at frequencies which are determined by the sum and differences of the linear interacting frequency components, i.e. the random model for $\eta(t)$ including the seocnd order terms is

$$\eta(t) = \sum_{m=1}^{LX} x_m \cos(\omega_m t) - y_m \sin(\omega_m t) +$$

$$\sum_{m=1}^{LX}\sum_{n=1}^{LX} F_{mn}\cos(\omega_m+\omega_n)t - G_{mn}\sin(\omega_m+\omega_n)t +$$

$$\sum_{m=1}^{LX}\sum_{n=1}^{LX} H_{mn}\cos(\omega_m-\omega_n)t - P_{mn}\sin(\omega_m-\omega_n)t$$

(4.2.1)

where $F_{mn}, G_{mn}, H_{mn}, P_{mn}$ are functions of the first order components. The double summation terms in (4.2.1) can be reduced to single summations if the frequency interval $\Delta\omega$ is kept constant, i.e. we can write

$$\sum_{m=1}^{LX}\sum_{n=1}^{LX} F_{mn}\cos(\omega_m+\omega_n)t - G_{mn}\sin(\omega_m+\omega_n)t =$$

$$\sum_{k=1}^{(2LX-1)} L_k\cos(\omega_k t) - M_k\sin(\omega_k t)$$

(4.2.2)

and

$$\sum_{m=1}^{LX}\sum_{n=1}^{LX} H_{mn}\cos(\omega_m-\omega_n)t - P_{mn}\sin(\omega_m-\omega_n)t =$$

$$\sum_{i=1}^{LX} Q_i\cos(\omega_i t) - R_i\sin(\omega_i t)$$

(4.2.3)

where

$$\omega_k = (k-1)\,\Delta\omega = \omega_m + \omega_n \qquad (4.2.4)$$

$$\omega_i = (i-1)\,\Delta\omega = \left|\omega_m - \omega_n\right| \qquad (4.2.5)$$

and we note that largest summation frequency is $(\omega_{LX} + \omega_{LX}) = 2(LX-1)\Delta\omega = (k_{max}-1)\Delta\omega$ giving $k_{max} = 2LX-1$ and largest difference frequency is $(\omega_{LX} - \omega_1) = (LX-1)\Delta\omega = (i_{max}-1)\Delta\omega$ resulting in $i_{max} = LX$. Using (4.1.13) we can write

$$\omega_k = (k-1)\,\Delta\omega = (m'+n')\Delta\omega + 2\omega_{min} \qquad (4.2.6)$$

$$\omega_i = (i-1)\,\Delta\omega = \left|m'-n'\right|\Delta\omega \quad ; \; m', n' = 1, 2, \cdots, N \qquad (4.2.7)$$

Dividing (4.2.6) and (4.2.7) throughout by $\Delta\omega$ we get

$$k = m'+n' + \frac{2\omega_{min}}{\Delta\omega} + 1 \qquad (4.2.8)$$

$$i = \left|m'-n'\right| + 1 \qquad (4.2.9)$$

We can then write

$$L_k = \sum_{m'} \sum_{n'} F_{m'n'} \qquad (4.2.10)$$

$$M_k = \sum_{m'} \sum_{n'} G_{m'n'} \qquad (4.2.11)$$

where m' and n' must satisfy equation (4.2.8).

$$Q_i = \sum_{m'} \sum_{n'} H_{m'n'} \qquad (4.2.12)$$

$$R_i = \sum_{m'} \sum_{n'} P_{m'n'} \qquad (4.2.13)$$

where m' and n' must satisfy equation (4.2.9)

Note:

(1) When a difference frequency $(\omega_{m'} - \omega_{n'})$ is negative, i.e. $n' > m'$ the sign of $P_{m'n'}$ in equation (4.2.13) must be adjusted accordingly

(2) The number of single summation terms in (4.2.2) and (4.2.3) can be extended to $LY = 2LX$ instead of $(2LX-1)$ by adding terms $L_{LY} = M_{LY} = o$

Equation (4.2.1) can then be written

$$\eta[(q-1)\Delta t] = R_e \left\{ \sum_{p=1}^{LY} \alpha_p \exp\left[2\pi i (p-1)(q-1)/LY\right] \right\}$$

$$q = 1, 2, \ldots, LY$$
$$p = 1, 2, \ldots, LY \qquad (4.2.14)$$

where

$$LY = 2LX = 2^j \quad ; \quad j = 1, 2, 3, \ldots \qquad (4.2.15)$$

$$\alpha_p = A_p + iB_p \qquad (4.2.16)$$

$$A_p = x_p + L_p + Q_p \qquad (4.2.17)$$

$$B_p = y_p + M_p + R_p \qquad (4.2.18)$$

where L, M, Q, R are given by (4.2.10) to (4.2.13). Thus using (4.2.14) to (4.2.18), $\eta(t)$ can be simulated up to second order.

4.3 A Statistically Realistic Model of Random Seas

As mentioned earlier the amplitudes a_m in equation (4.1.3) are usually calculated deterministically using (4.1.4). This method as noted by Rice (73) can only model a random Gaussian process when infinite number of frequency components are included and truncation of series in (4.1.5) to LX frequencies is not correct unless $LX \rightarrow \infty$. In this method the random nature of $\eta(t)$ arises only from the random phase angles generated with a uniform probability in the range $0 - 2\pi$. Thus different time histories of the process always produce spectra equal to $S_{\eta\eta}(\omega)$ whereas the signal represented by (4.1.5) repeats itself after a time $T = \frac{2\pi}{\Delta\omega}$ and is therefore only a sample of the infinite time history $\eta(t)$, indicating that the spectrum of simulated time history need not be exactly that of the entire signal.

A more accurate way of simulating $\eta(t)$ is to generate x_m and y_m in (4.1.1) randomly from a process with a Gaussian distribution and zero mean, having a variance = $S_{\eta\eta}(\omega_m)\cdot\Delta\omega$ or alternatively generate a_m in (4.1.3) from a Rayleigh distribution with an RMS value of $\sqrt{2\, S_{\eta\eta}(\omega_m)\cdot\Delta\omega}$ Therefore the two approaches are:

1. Deterministic, in which amplitudes are found deterministically and directly from the spectrum of the process

2. Random, in which amplitudes are generated randomly using a Rayleigh distribution.

As mentioned in Chapter One the deterministic approach cannot accurately predict the wave group statistics of a random sea while the wave grouping can have significant influence on the second order excitations and low frequency oscillations of floating structures.

4.4 Slow Drift Force on Tanker (Pinkster's Time Domain Method)

The method presented by Pinkster (71) for calculating second order forces and moments acting on a floating body involves the direct integration of the first and second order fluid pressure over the body surface. The pressure p at any point within the fluid region is given by Bernoulli's equation

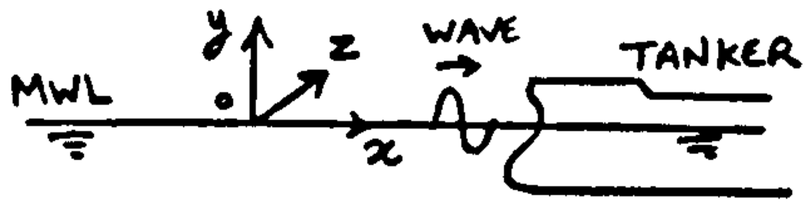

$$\frac{p}{\rho} = -g y - \frac{\partial \phi}{\partial t} - \frac{1}{2}(u^2 + v^2 + w^2) \qquad (4.4.1)$$

where

ϕ = total velocity potential

$-y$ = vertical distance of the point below the mean water level

u, v, w = fluid particle velocities in x,y and z directions where (x,y,z) is the cartesian coordinate system as shown

The total fluid force acting on the body is then determined by integration,i.e.

Force, $$F = -\int_S \int p.\bar{n}.dS \qquad (4.4.2)$$

in which

S = instantaneous wetted surface

$\bar{n}$ = instantaneous outward normal vector to the surface element

If equation (4.4.1) is expanded up to second order terms then, assuming simple harmonic motions in all six degrees of freedom of the floating structure, the second order part

of F in (4.4.2) will be produced by the following:

1. Integration of first order terms over the region of relative surface elevation (between wave elevation and displaced water line)

2. First order velocity squared terms integrated over the mean position of vessel.

3. Integration of pressure gradient over the mean position of submerged surface.

4. Rotation of body which produces second order hydrodynamic force components equal to products of structural inertia forces and first order angular displacements

5. Integration of terms due to second order potential consisting of undisturbed incoming wave potential, diffracted wave potential and body motion potentials over the mean position of vessel.

Detailed derivation of above is given in (71) and for irregular waves the low frequency second order longitudinal force is expressed by

$$F^{(2)} = \sum_n \sum_m a_n a_m \left\{ T_{nm}^c \cos(\alpha^-) + T_{nm}^s \sin(\alpha^-) \right\} \qquad (4.4.3)$$

in which T_{nm}^c and T_{nm}^s are quadratic transfer functions with the property

$$T_{nm}^c = T_{mn}^c$$

$$T_{nm}^s = -T_{mn}^s$$

and

$$\bar{\alpha} = (\omega_n - \omega_m)t + (\psi_n - \psi_m)$$

Assuming that the second order potential contribution is negligible we have

$$T_{nm}^{s} = 0 \qquad (4.4.4)$$

and using values of transfer functions for mean forces in regular waves we can write

$$T_{nm}^{c} = T^{c}(\omega_n, \omega_m) \simeq T^{c}\left(\frac{\omega_m+\omega_n}{2}, \frac{\omega_m+\omega_n}{2}\right) \qquad (4.4.5)$$

Equations (4.4.4) and (4.4.5) together form Newman's approximation (64). Equation (4.4.5) implies that T_{nm}^{c} is replaced by a mean value lying on the diagonal of the matrix of quadratic functions at a mean frequency equal to $\left(\frac{\omega_m+\omega_n}{2}\right)$. Equation (4.4.3) then becomes

$$F^{(2)} \simeq \sum_{n}\sum_{m} a_n a_m T_{nm}^{c} \cos(\bar{\alpha}) \qquad (4.4.6)$$

Then (4.4.6) can be reduced to a single summation term as described in the previous section and simulated using a FFT algorithm. Thus

$$F^{(2)} = \sum_{q=1}^{LX} A_q \cos(\omega_q t) - B_q \sin(\omega_q t) =$$

$$R_e\left\{ \sum_{q=1}^{LX} (A_q + iB_q) \exp(i\omega_q t)\right\} \qquad (4.4.7)$$

where

$$q = |n-m| \tag{4.4.8}$$

$$A_q = \sum_n \sum_m C_{nm} \tag{4.4.9}$$

$$B_q = \sum_n \sum_m D_{nm} \tag{4.4.10}$$

$$C_{nm} = a_n a_m T^c_{nm} \cos(\psi_n - \psi_m) \tag{4.4.11}$$

$$D_{nm} = a_n a_m T^c_{nm} \sin(\psi_n - \psi_m) \tag{4.4.12}$$

The one sided power spectral density of $F^{(2)}$ can then be written as

$$S_F(\omega_q) = \frac{1}{2\Delta\omega} \sum_{m,n} \left[a_n a_m T^c_{nm} \right]^2 \tag{4.4.13}$$

where m,n satisfy equation (4.4.8) and we have

$$\omega_q = |\omega_n - \omega_m| \tag{4.4.14}$$

4.5 Second Order Surge Response of Tanker

Taking the equation of motion of tanker in surge as

$$(M+M_{ax})\ddot{x} + c\dot{x} + kx = F^{(1)} + F^{(2)} \tag{4.5.1}$$

in which

$(M+M_{ax})$ = Tanker structural mass + added mass in surge

c, k = Approximate damping and stiffness coefficients respectively

$F^{(1)}$ = First order force

The second order steady state surge response can then be found by substituting (4.4.7) into (4.5.1) to give

$$x^{(2)} = \sum_{q=1}^{Lx} X_q \cos(\omega_q t) - Y_q \sin(\omega_q t) = Re\left\{ \sum_{q=1}^{Lx} (X_q + i Y_q) \exp(i\omega_q t) \right\} \quad (4.5.2)$$

where

$$X_q = (s_q \cdot A_q + r_q \cdot B_q)/z_q \quad (4.5.3)$$

$$Y_q = (s_q \cdot B_q - r_q \cdot A_q)/z_q \quad (4.5.4)$$

$$s_q = [\, k - (M + M_{ax})\, \omega_q^2 \,] \quad (4.5.5)$$

$$r_q = c \cdot \omega_q \quad (4.5.6)$$

$$z_q = s_q^2 + r_q^2 \quad (4.5.7)$$

Equation (4.5.2) can be simulated using the two previously mentioned methods, one deterministic the other random, in section 4.3. Simulation is carried out for a number of times, each one with different sets of phase angles and in the case of random approach, with different sets of wave amplitudes. The following statistical properties of response are investigated:

(a) Mean response from ith time history,

$$\overline{x}_i = \frac{1}{LX} \sum_{j=1}^{LX} x_j^{(2)} \qquad (4.5.8)$$

(b) Mean squared response from ith time history

$$\overline{x}_i^2 = \frac{1}{LX} \sum_{j=1}^{LX} \left[x_j^{(2)} - \overline{x}_i \right]^2 \qquad (4.5.9)$$

(c) Peak values and number of peaks in each record.

(d) Highest peak value in each record, x_{Pmax} , and ensemble average of highest peaks,

$$\overline{x}_{Pmax} = \frac{1}{(NR)} \sum_{i=1}^{(NR)} (x_{Pmax})_i \qquad (4.5.10)$$

where (NR) = number of records or simulations

(e) Ensemble rms defined as

$$x_{RMS} = \sqrt{\frac{1}{(NR)} \sum_{i=1}^{(NR)} \overline{x}_i^2} \qquad (4.5.11)$$

(f) Peak/rms ratio

$$R = \frac{\frac{1}{(NR)} \sum_{i=1}^{(NR)} \left[(x_{pmax})_i - \overline{x}_i \right]}{x_{RMS}} \qquad (4.5.12)$$

4.6 Numerical Data

Tanker: Mass = 240000t, surge added mass = 12000t,
Beam = 47.2m, Length = 310.0m, Draft = 18.9m

ω_2 \ ω_1	0.354	0.444	0.523	0.600	0.713	0.803	0.887
0.354	2.0	8.7	10.4	24.5	10.0	38.4	37.5
0.444		7.0	20.8	19.4	25.7	12.1	35.2
0.523			12.4	16.4	8.3	14.3	14.2
0.600				14.0	9.5	18.0	14.9
0.713					8.6	4.3	6.7
0.803						9.2	4.7
0.887							8.6

T_{12} in tf/m^2
Frequencies in rad./sec.

TABLE 4.1. Quadratic Transfer Function of Longitudinal Slow Drift Force on a Tanker in Head Seas (71)

4.7 Results.

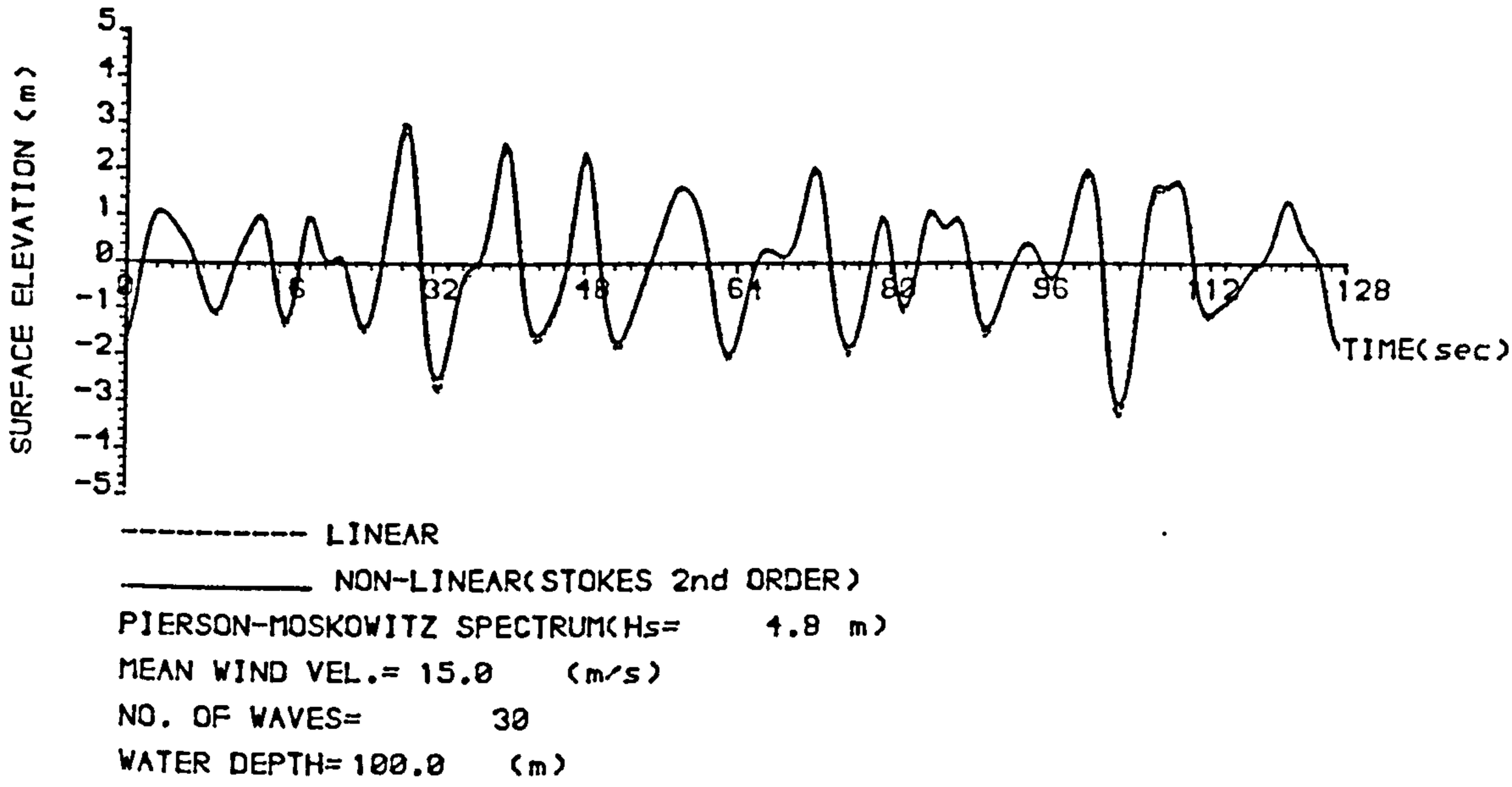

FIG 4.2 RANDOM SEA SURFACE REALIZATIONS

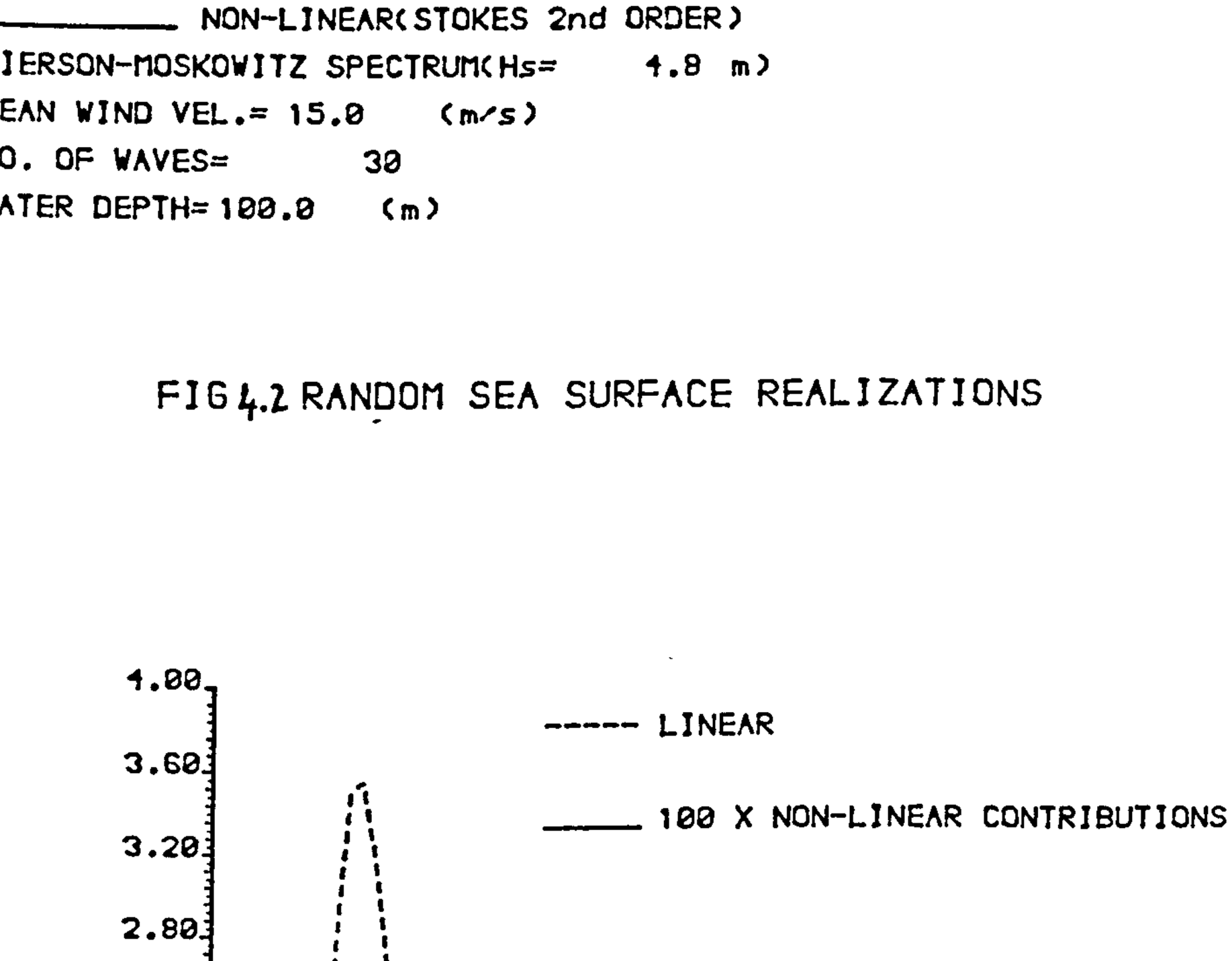

FIG.4.3 POWER SPECTRAL DENSITY OF SIMULATED RANDOM SEA SURFACE

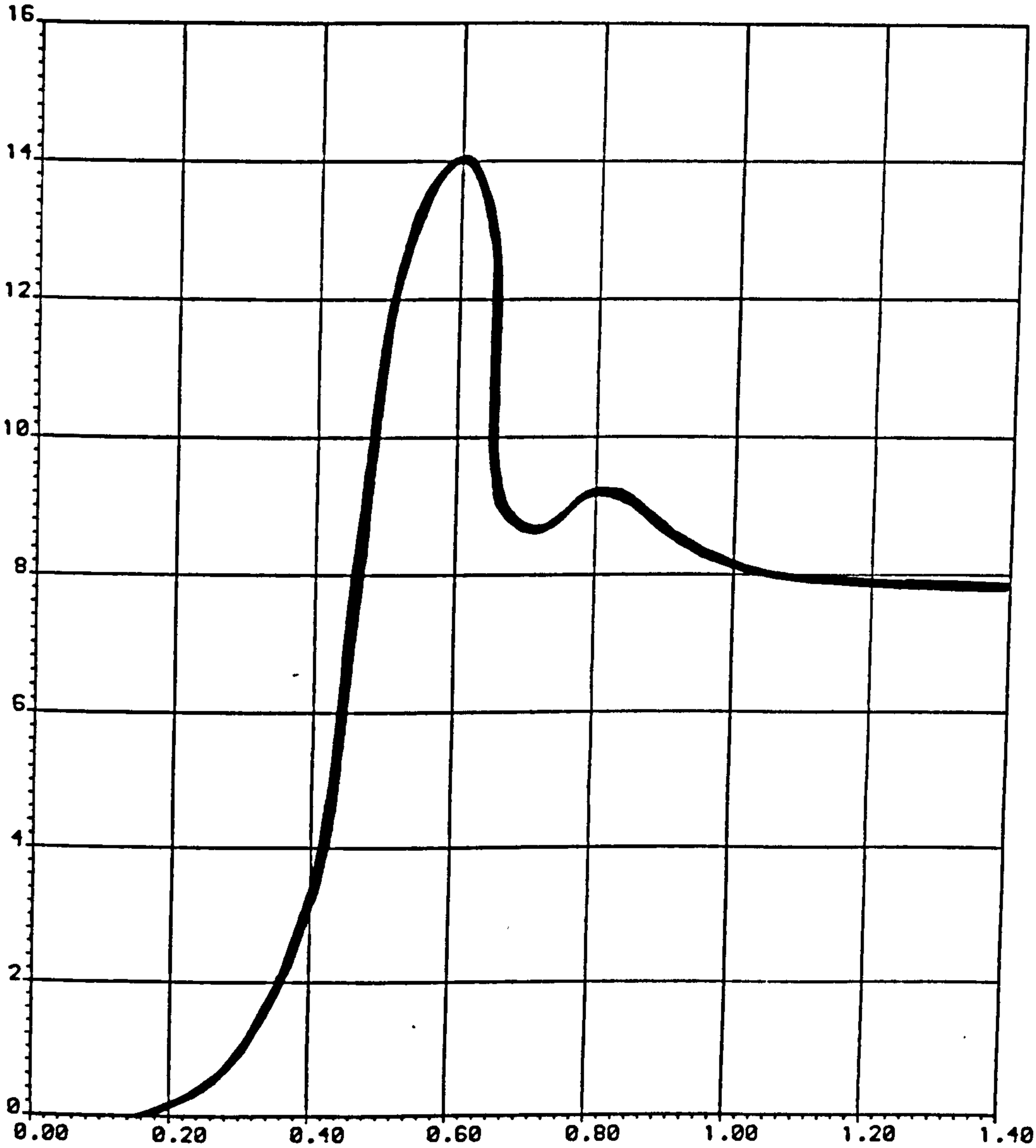

TANKER

Beam 47.17 m
Length 310.0 m
Draft 18.9 m

FIG 4.4 DIAGONAL COSINE TRANSFER FUNCTION OF LONGITUDINAL SLOW DRIFT FORCE ON A TANKER IN HEAD WAVES (Pinkster(71))

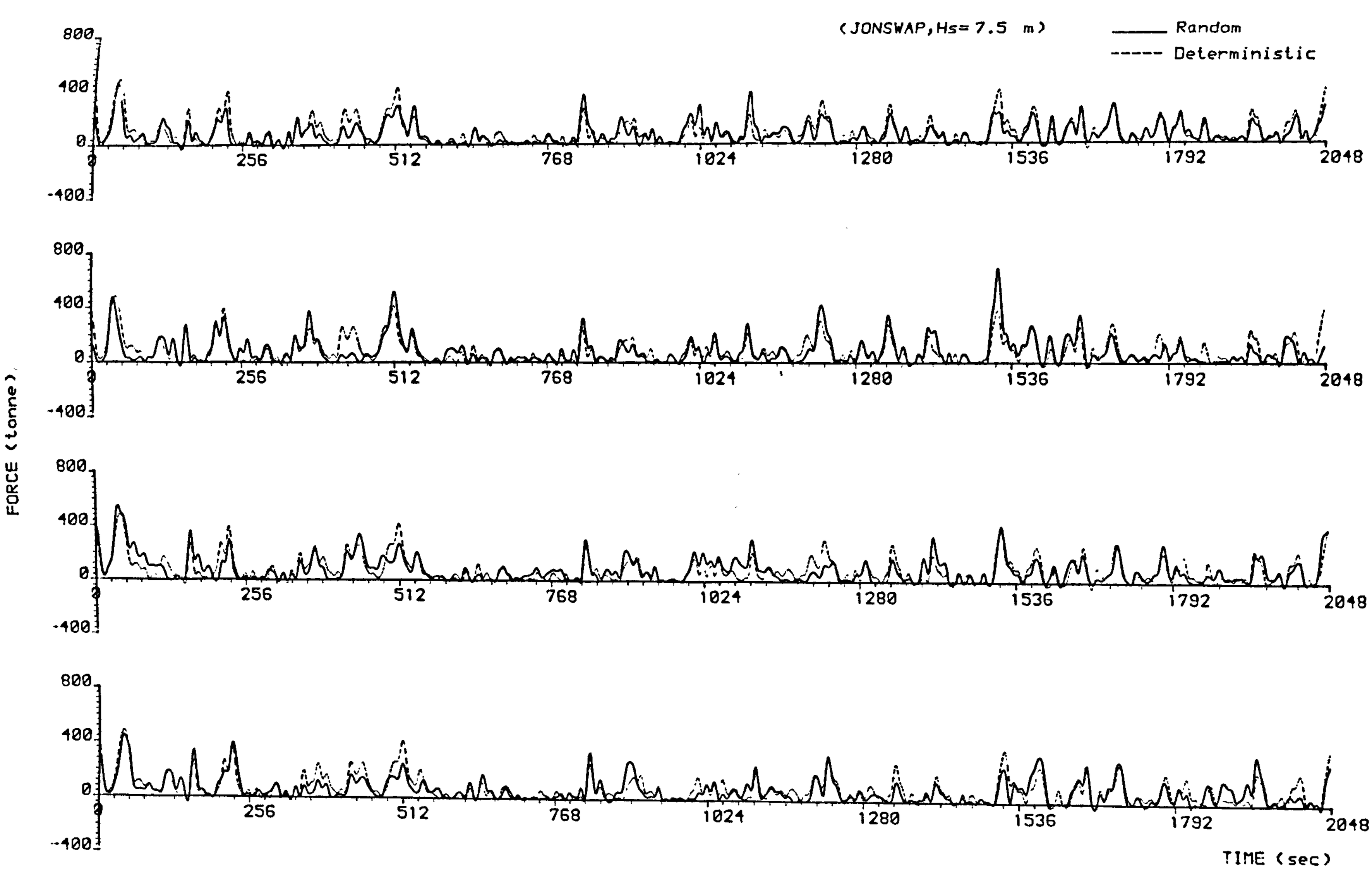

FIG 4.5 TIME HISTORIES OF SLOW DRIFT FORCE ON A TANKER

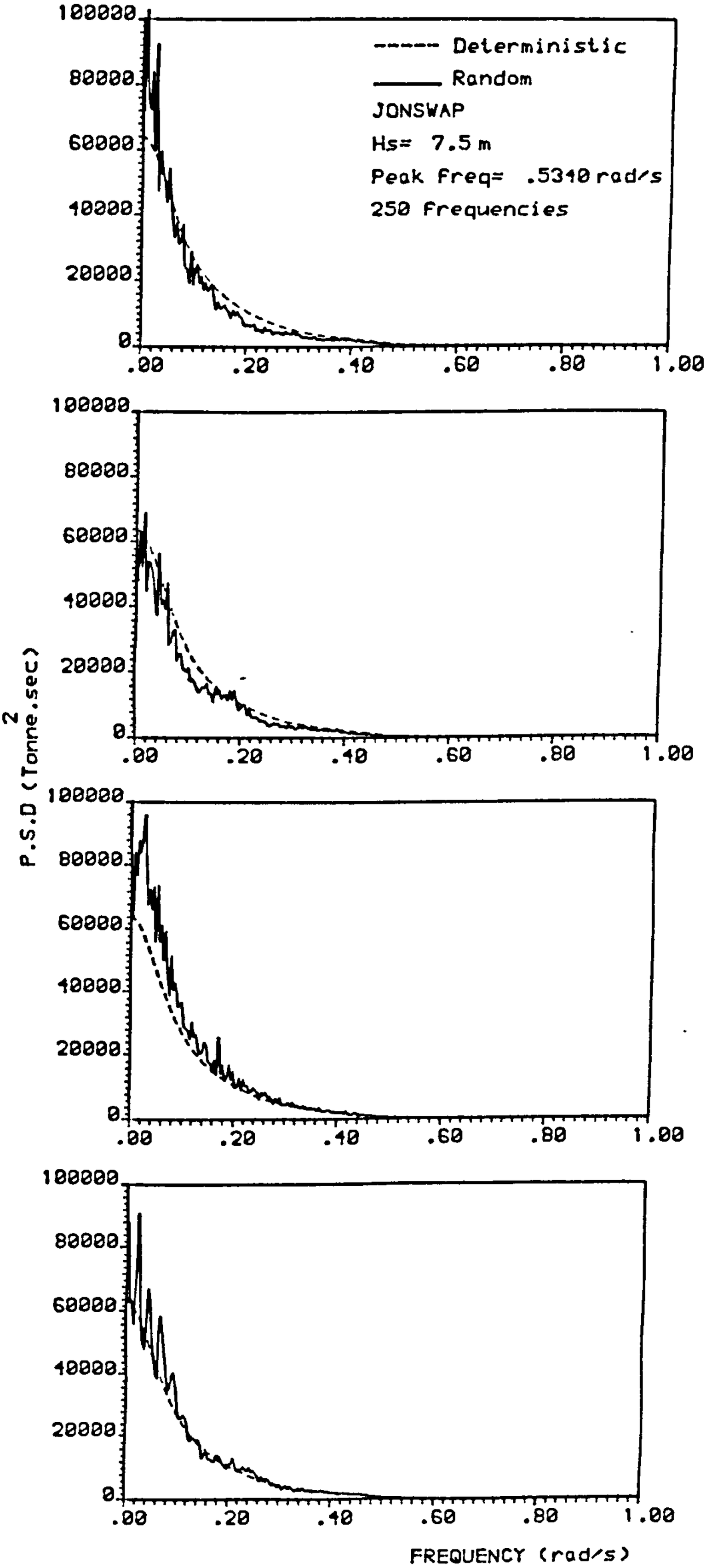

FIG 4.6 POWER SPECTRAL DENSITIES OF SLOW DRIFT FORCE ON A TANKER

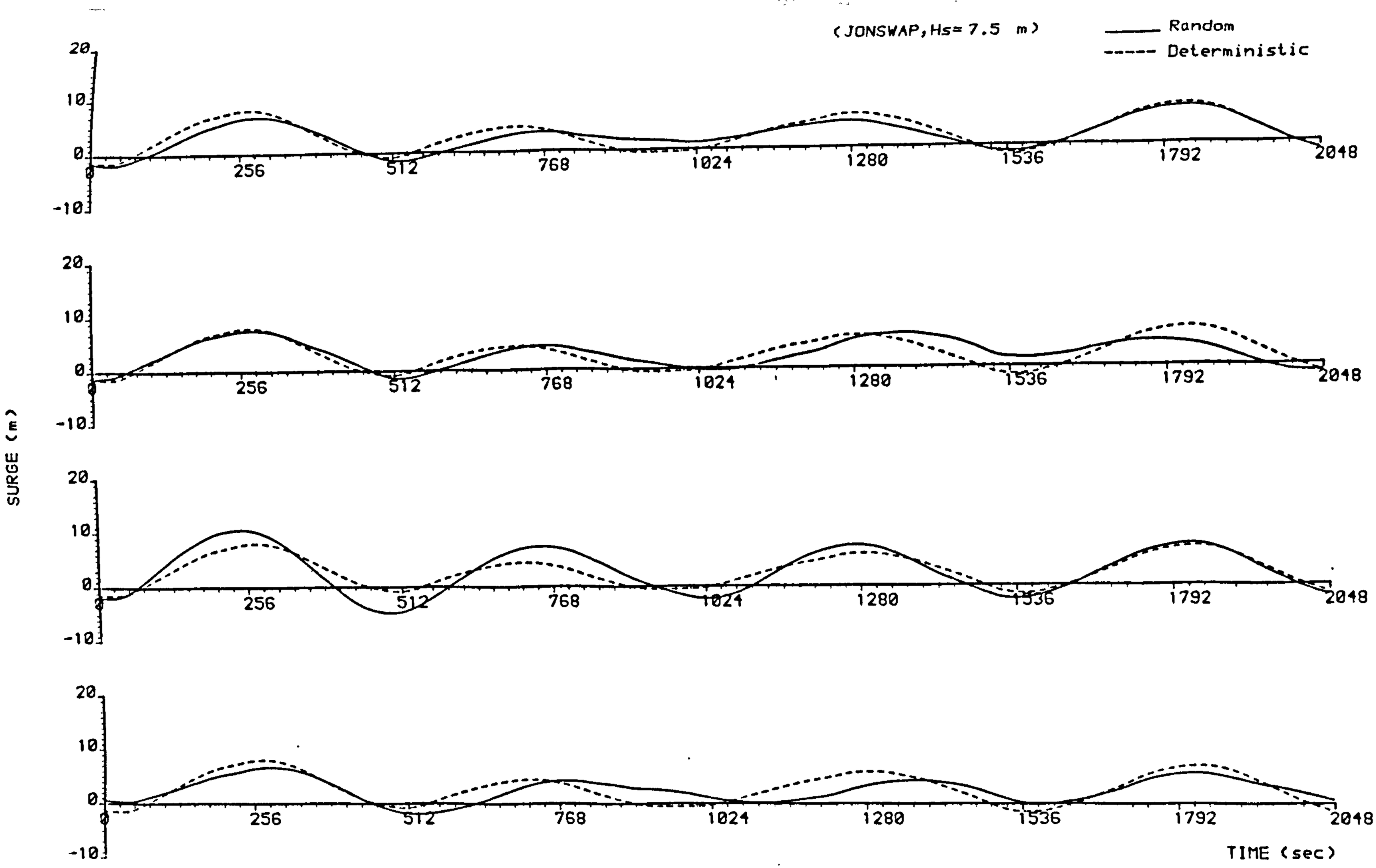

FIG 4.7 TIME HISTORIES OF SLOWLY VARYING SURGE RESPONSE OF A TANKER

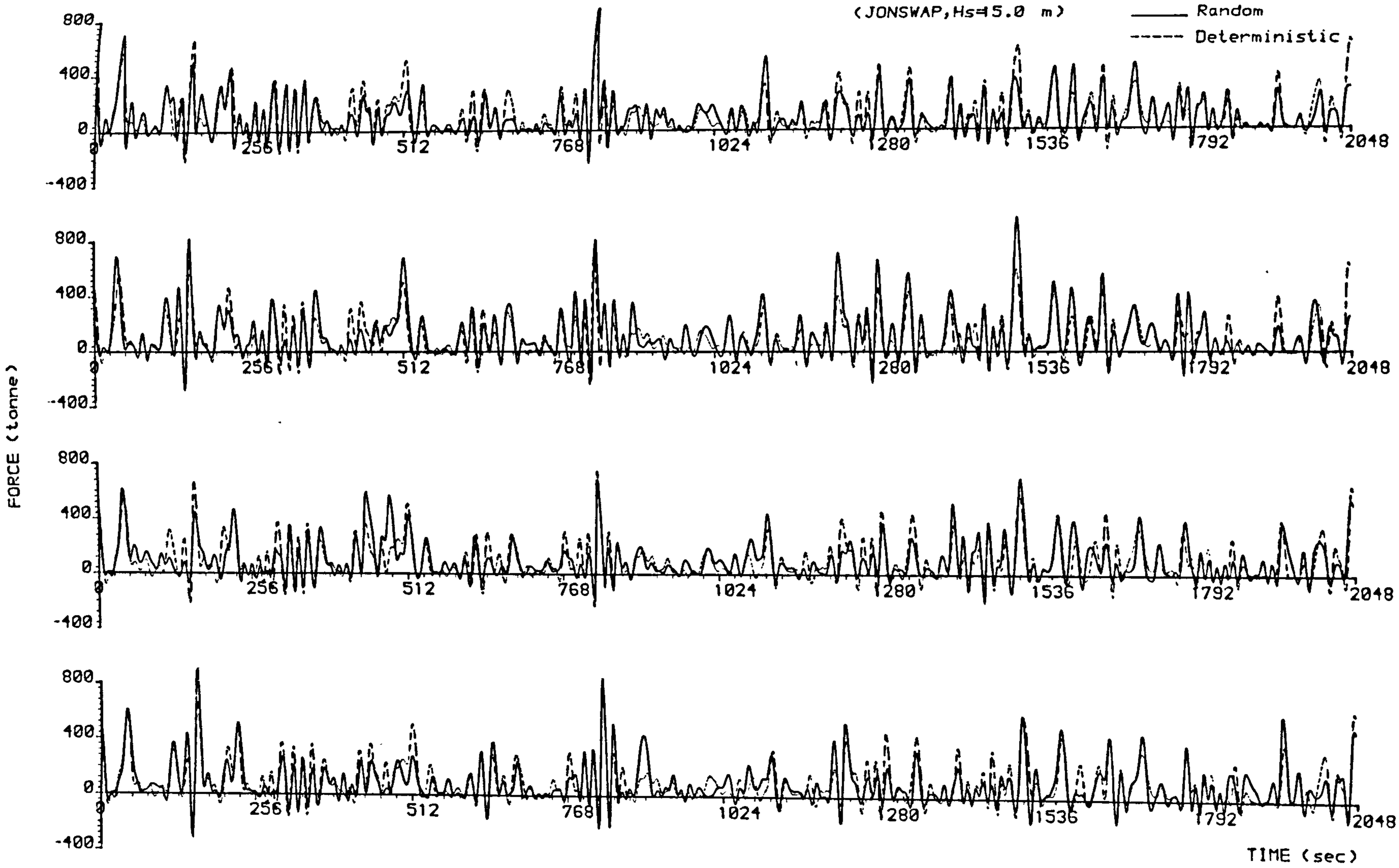

FIG 4.8 TIME HISTORIES OF SLOW DRIFT FORCE ON A TANKER

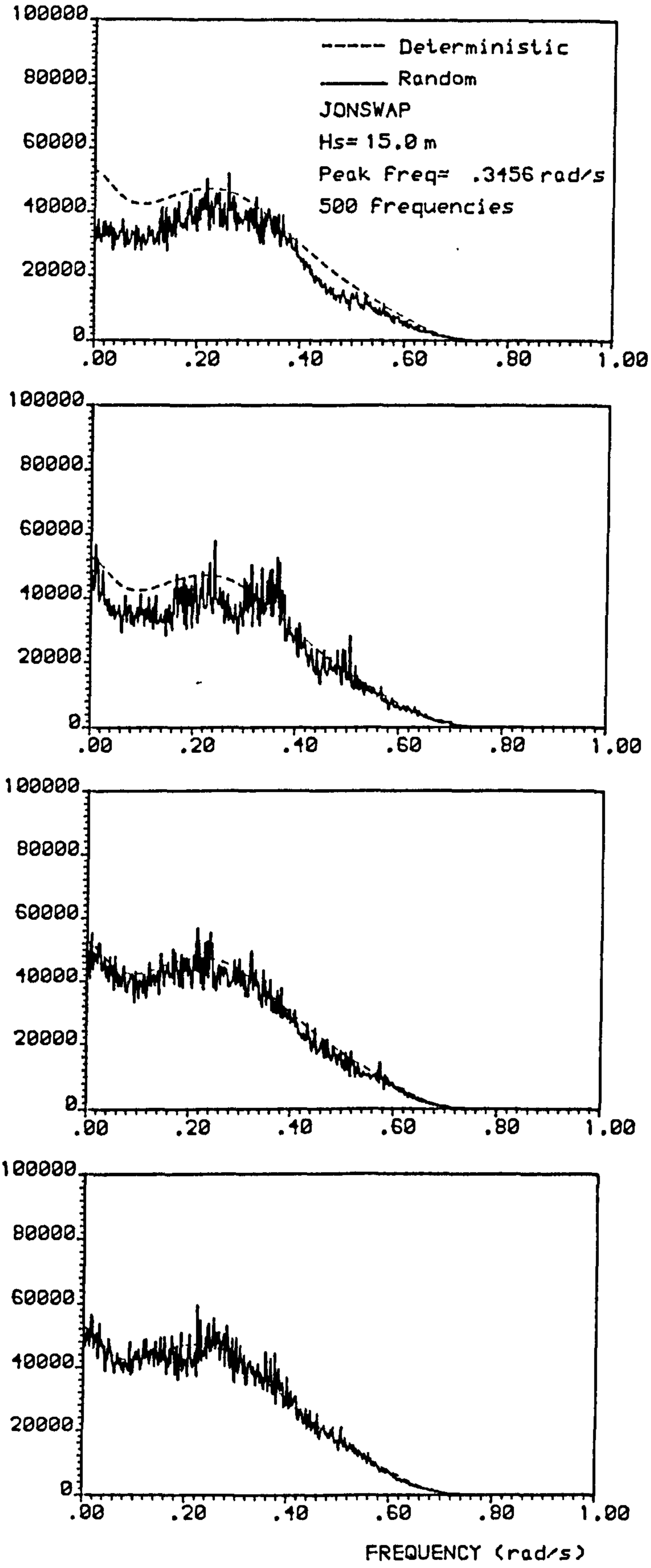

FIG4.1 POWER SPECTRAL DENSITIES OF SLOW DRIFT FORCE ON A TANKER

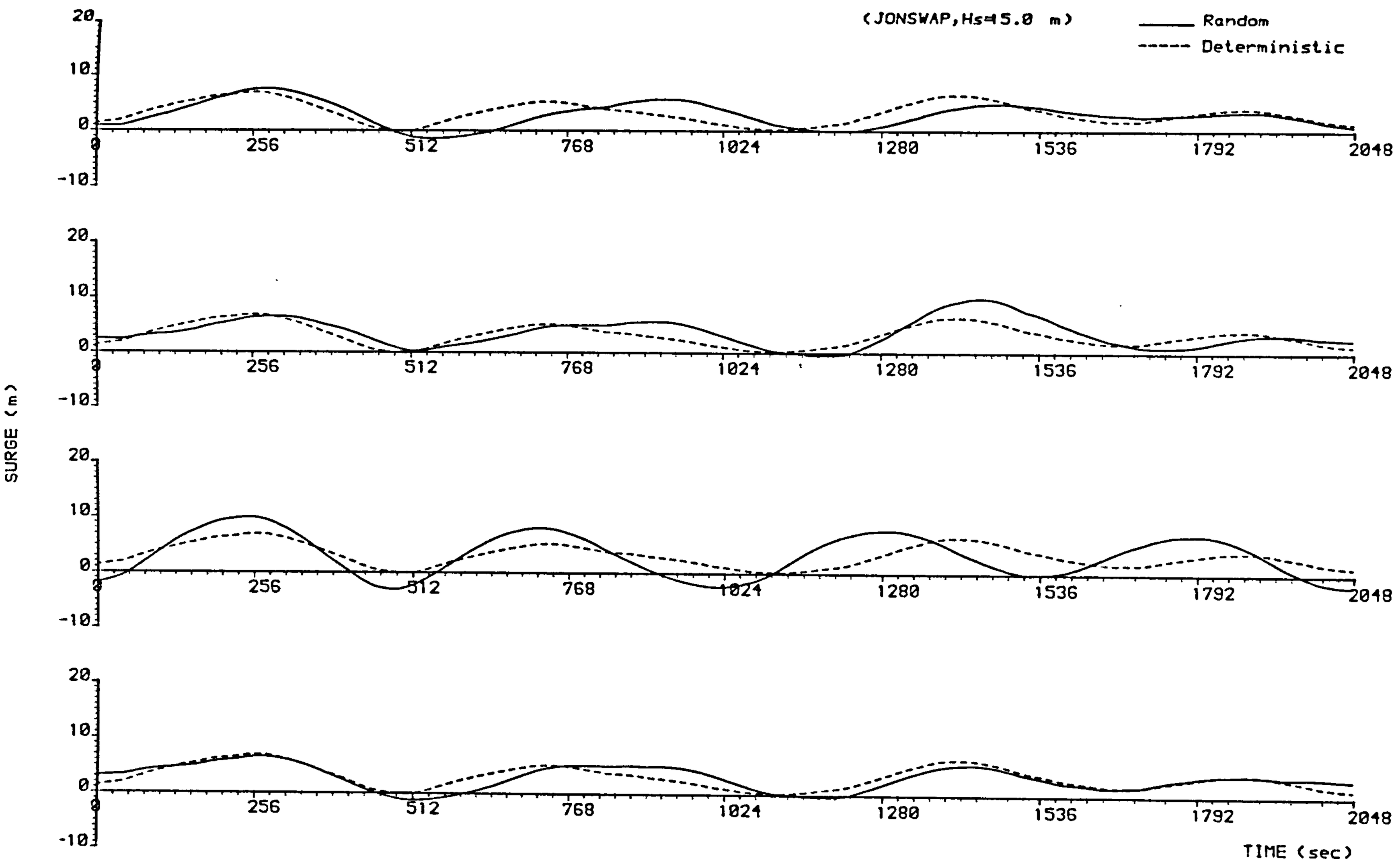

FIG 4.10 TIME HISTORIES OF SLOWLY VARYING SURGE RESPONSE OF A TANKER

```
        SLOW DRIFT RESPONSE OF A TANKER IN SURGE
      **********************************************
 JONSWAP SPECTRUM,HS= 15.00(M),PEAK FREQ.=     0.3456(RAD/SEC)
 SURGE NATURAL PERIOD OF TANKER= 4.00(MIN),DAMPING RATIO= 0.070

    (RANDOM***DETERMINISTIC)

  RECORD NO.       PEAK RESPONSE (M)       NO. OF PEAKS        RMS (M)
==========      ================       ============      ============

     1              1.98***  1.47          34***  33          0.63***  0.54

     2              1.48***  2.32          34***  34          0.56***  0.73

     3              1.75***  1.81          34***  33          0.58***  0.67

     4              1.76***  2.07          34***  35          0.61***  0.61

     5              2.02***  1.82          33***  34          0.75***  0.62
 NO. OF FREQ. COMPONENTS=   750
 DURATION OF EACH RECORD=  2.13 (HRS)
**********************************************************
 ENSEMBLE AVERAGE OF PEAKS= 2.35***  2.47 (M)
 RMS= 0.63***  0.64 (M)
 PEAK/RMS RATIO= 2.85***  2.97
**********************************************************
FORTRAN STOP


        SLOW DRIFT RESPONSE OF A TANKER IN SURGE
      **********************************************
 JONSWAP SPECTRUM,HS= 15.00(M),PEAK FREQ.=     0.3456(RAD/SEC)
 SURGE NATURAL PERIOD OF TANKER= 4.00(MIN),DAMPING RATIO= 0.070

    (RANDOM***DETERMINISTIC)

  RECORD NO.       PEAK RESPONSE (M)       NO. OF PEAKS        RMS (M)
==========      ================       ============      ============

     1              2.10***  1.94          30***  31          0.65***  0.77

     2              1.55***  1.97          36***  33          0.57***  0.65

     3              2.34***  1.53          34***  32          0.67***  0.58

     4              2.60***  2.06          35***  35          0.88***  0.67

     5              2.72***  1.83          33***  33          0.82***  0.76
 NO. OF FREQ. COMPONENTS=   750
 DURATION OF EACH RECORD=  2.13 (HRS)
**********************************************************
 ENSEMBLE AVERAGE OF PEAKS= 2.82***  2.43 (M)
 RMS= 0.73***  0.69 (M)
 PEAK/RMS RATIO= 3.10***  2.71
**********************************************************
FORTRAN STOP


        SLOW DRIFT RESPONSE OF A TANKER IN SURGE
      **********************************************
 JONSWAP SPECTRUM,HS= 15.00(M),PEAK FREQ.=     0.3456(RAD/SEC)
 SURGE NATURAL PERIOD OF TANKER= 4.00(MIN),DAMPING RATIO= 0.070

    (RANDOM***DETERMINISTIC)

  RECORD NO.       PEAK RESPONSE (M)       NO. OF PEAKS        RMS (M)
==========      ================       ============      ============

     1              1.42***  3.49          34***  34          0.54***  0.99

     2              1.63***  1.86          35***  32          0.64***  0.76

     3              2.33***  2.06          34***  34          0.65***  0.61

     4              2.38***  1.62          35***  35          0.86***  0.54

     5              2.92***  2.38          33***  34          0.78***  0.83
 NO. OF FREQ. COMPONENTS=   750
 DURATION OF EACH RECORD=  2.13 (HRS)
**********************************************************
 ENSEMBLE AVERAGE OF PEAKS= 2.72***  2.85 (M)
 RMS= 0.71***  0.76 (M)
 PEAK/RMS RATIO= 3.02***  2.99
**********************************************************
FORTRAN STOP
```

SLOW DRIFT RESPONSE OF A TANKER IN SURGE

****

JONSWAP SPECTRUM,HS= 15.00(M),PEAK FREQ.= 0.3456(RAD/SEC)

SURGE NATURAL PERIOD OF TANKER= 4.00(MIN),DAMPING RATIO= 0.070

(RANDOM***DETERMINISTIC)

RECORD NO.	PEAK RESPONSE (M)	NO. OF PEAKS	RMS (M)
1	2.63*** 1.82	16*** 16	1.00*** 0.65
2	1.85*** 1.88	16*** 17	0.63*** 0.71
3	2.54*** 1.80	16*** 15	0.89*** 0.66
4	1.36*** 1.14	19*** 19	0.65*** 0.48
5	2.38*** 1.61	18*** 17	0.86*** 0.67
6	2.94*** 1.44	16*** 16	0.79*** 0.74
7	2.11*** 1.97	17*** 16	0.71*** 0.78
8	2.11*** 1.83	16*** 16	0.95*** 0.62
9	1.88*** 1.99	16*** 18	0.69*** 0.67
10	1.43*** 2.41	16*** 17	0.63*** 0.74

NO. OF FREQ. COMPONENTS= 375

DURATION OF EACH RECORD= 1.07 (HRS)

****

ENSEMBLE AVERAGE OF PEAKS= 2.72*** 2.36 (M)

RMS= 0.79*** 0.68 (M)

PEAK/RMS RATIO= 2.68*** 2.65

****

FORTRAN STOP

SLOW DRIFT RESPONSE OF A TANKER IN SURGE

JONSWAP SPECTRUM,HS= 15.00(M),PEAK FREQ.= 0.3456(RAD/SEC)
SURGE NATURAL PERIOD OF TANKER= 4.00(MIN),DAMPING RATIO= 0.070

(RANDOM***DETERMINISTIC)

RECORD NO.	PEAK RESPONSE (M)	NO. OF PEAKS	RMS (M)
1	1.51*** 2.17	36*** 32	0.49*** 0.67
2	1.51*** 1.92	33*** 36	0.53*** 0.63
3	2.04*** 2.01	30*** 33	0.69*** 0.69
4	2.06*** 1.57	36*** 32	0.52*** 0.68
5	2.20*** 1.64	34*** 33	0.71*** 0.62
6	1.93*** 1.71	35*** 35	0.65*** 0.58
7	1.98*** 2.16	34*** 34	0.56*** 0.73
8	1.93*** 2.04	33*** 31	0.73*** 0.77
9	2.13*** 1.59	34*** 32	0.67*** 0.68
10	1.75*** 2.18	33*** 36	0.58*** 0.79
11	2.56*** 2.80	33*** 33	0.72*** 0.88
12	2.99*** 2.29	34*** 35	0.80*** 0.77
13	1.80*** 1.81	34*** 35	0.60*** 0.61
14	2.19*** 2.51	34*** 34	0.85*** 0.79
15	1.64*** 2.00	33*** 36	0.63*** 0.56
16	2.10*** 1.53	34*** 33	0.68*** 0.64
17	2.28*** 2.66	34*** 34	0.70*** 0.79
18	2.68*** 1.62	34*** 36	0.77*** 0.57
19	2.29*** 1.93	34*** 33	0.66*** 0.76
20	2.06*** 1.96	32*** 35	0.69*** 0.63

NO. OF FREQ. COMPONENTS= 750
DURATION OF EACH RECORD= 2.13 (HRS)

ENSEMBLE AVERAGE OF PEAKS= 2.64*** 2.52 (M)
RMS= 0.67*** 0.70 (M)
PEAK/RMS RATIO= 3.11*** 2.69

FORTRAN STOP

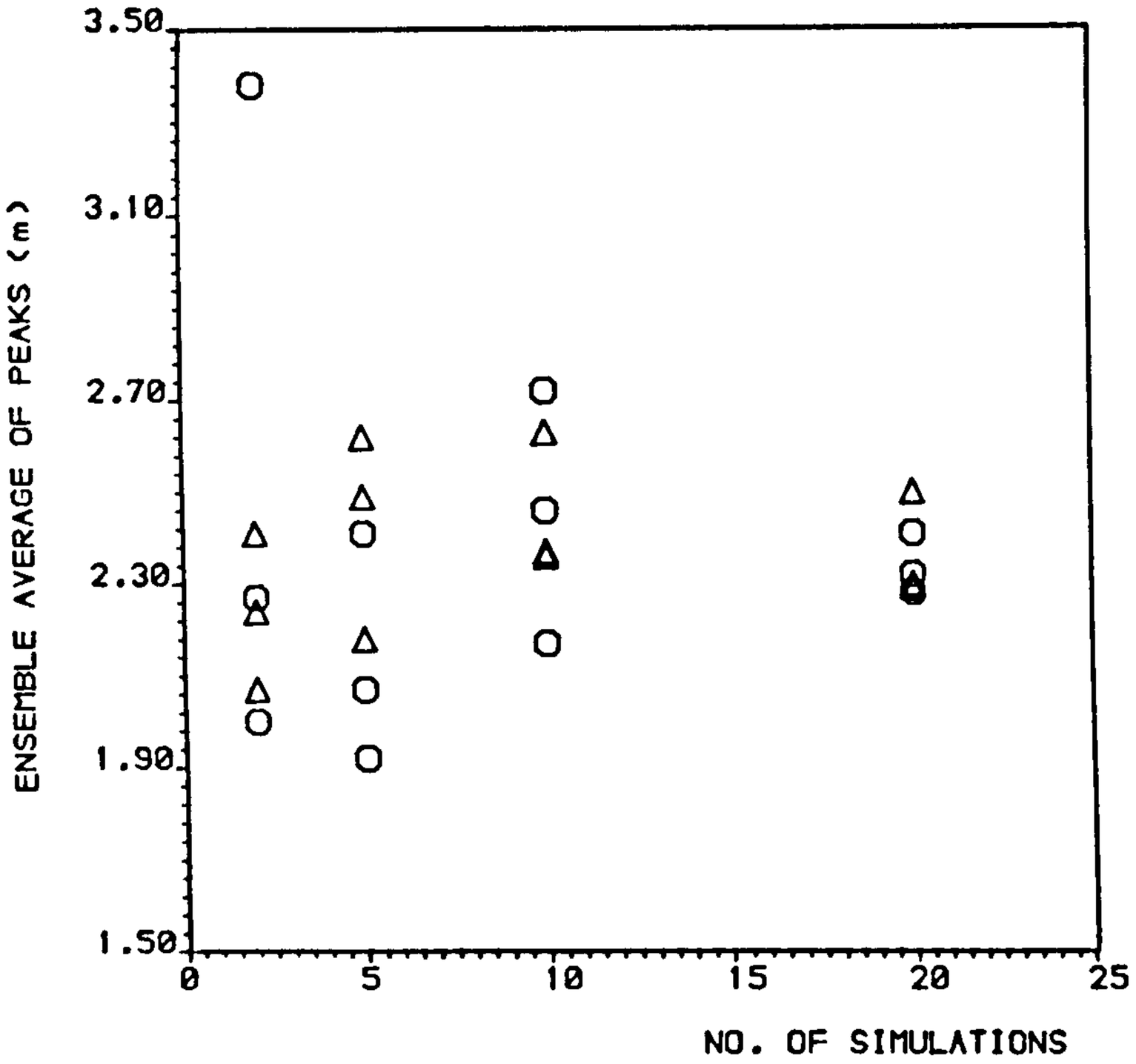

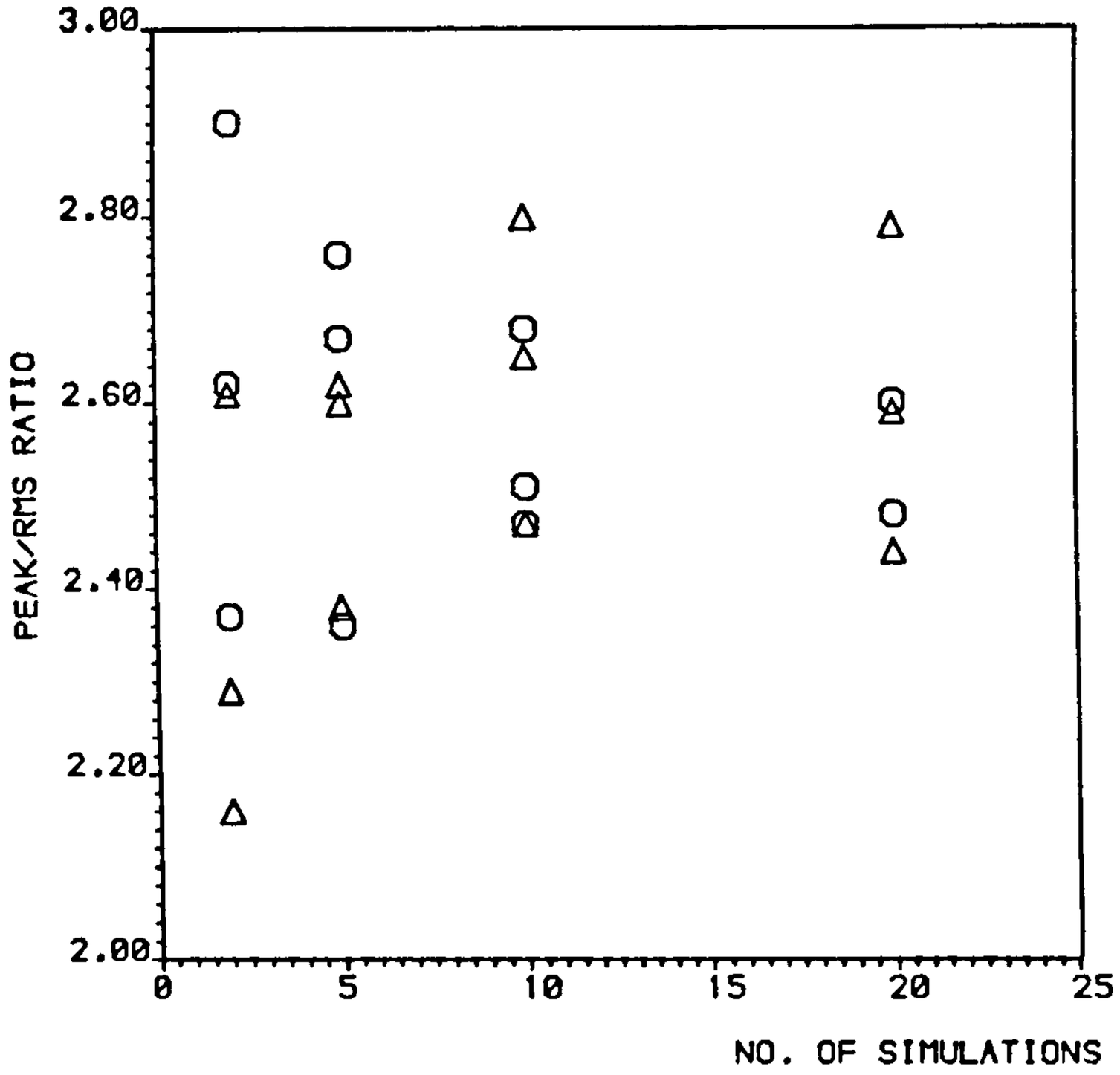

O *RANDOM*

Δ *DETERMINISTIC*

JONSWAP spectrum, Hs=15.0 m, Peak Frequency= 0.3156 rad/s
Surge Natural Period of Tanker=1.00 min., Damping Ratio=0.07
Length of each Record=1.07 hrs.

FIG 4.11 SIMULATION RESULTS FOR LOW FREQUENCY SURGE RESPONSE OF A TANKER IN HEAD SEAS

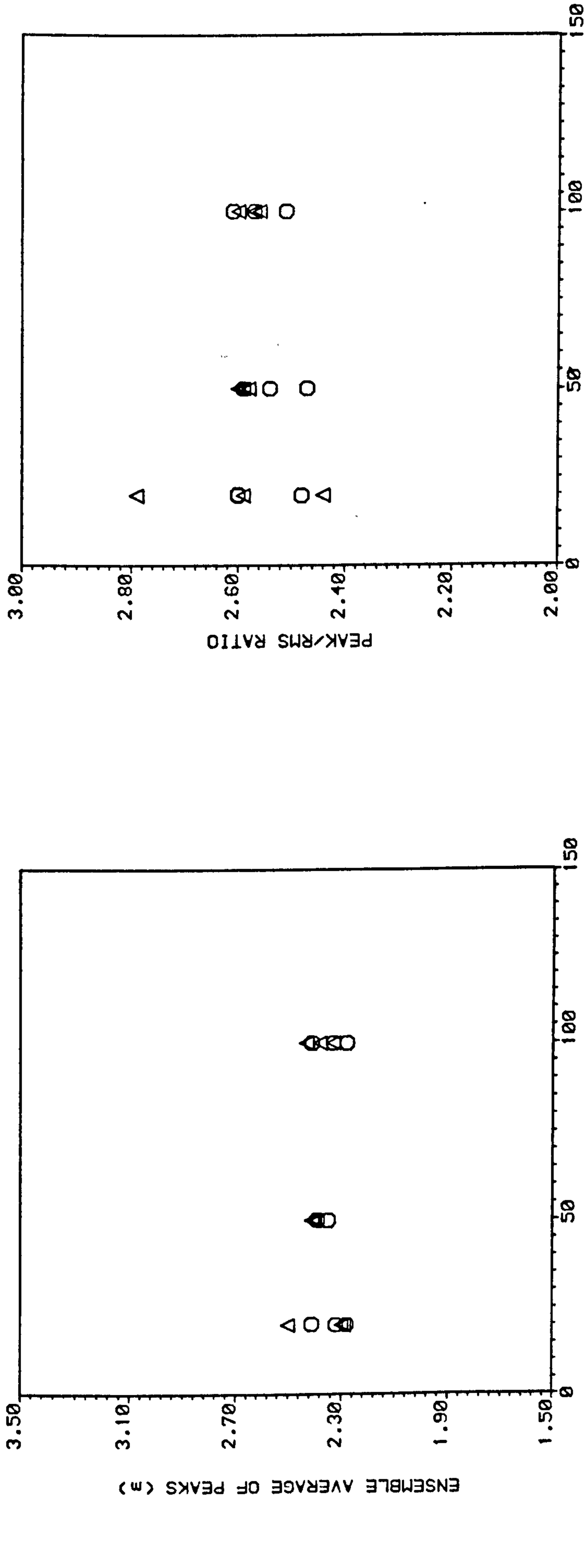

JONSWAP spectrum, Hs=15.0 m, Peak Frequency= 0.3156 rad/s
Surge Natural Period of Tanker=1.00 min.; Damping Ratio=0.07
Length of each Record=1.07 hrs.

○ RANDOM
△ DETERMINISTIC

FIG 4.12 SIMULATION RESULTS FOR LOW FREQUENCY SURGE RESPONSE OF A TANKER IN HEAD SEAS

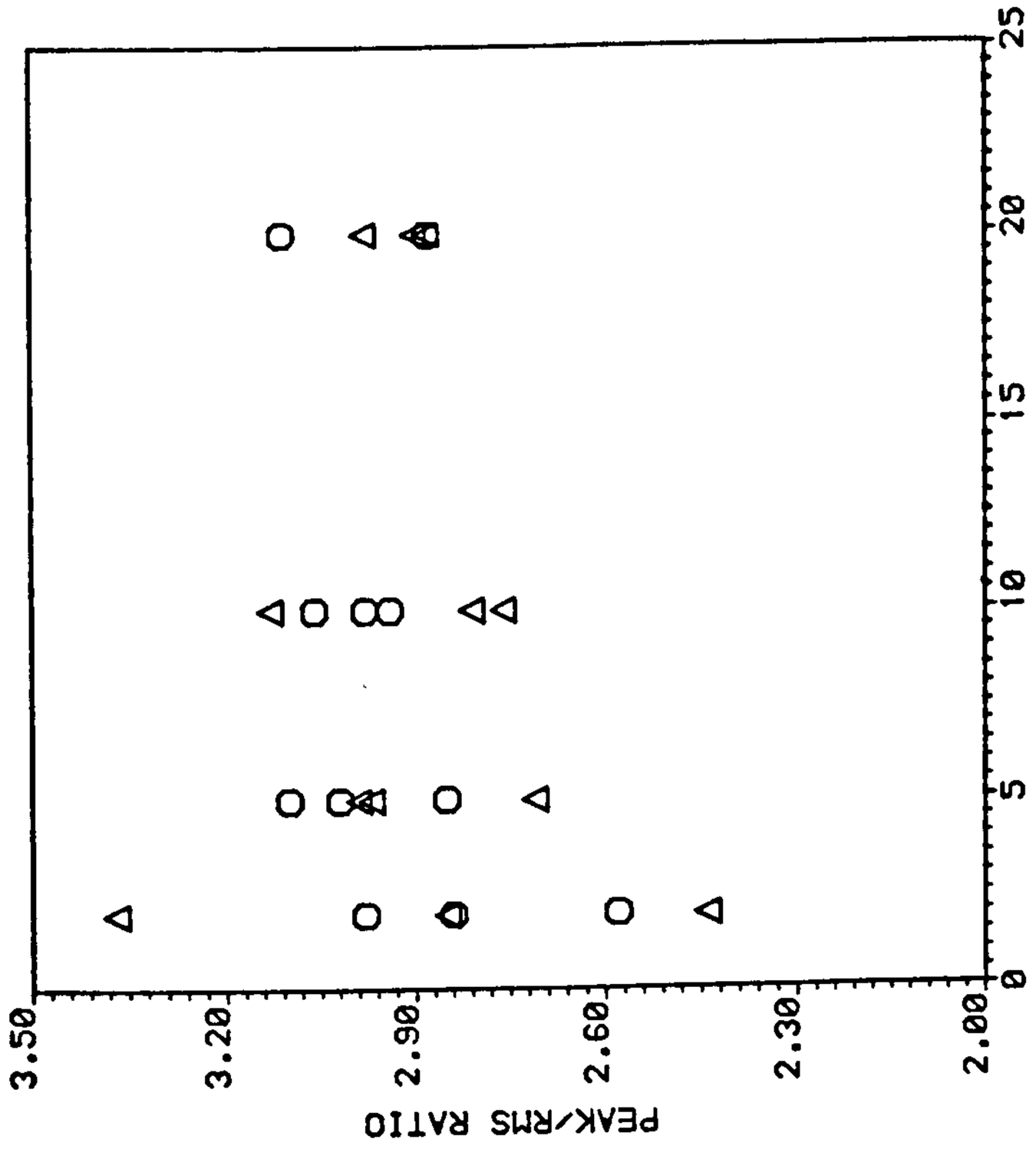

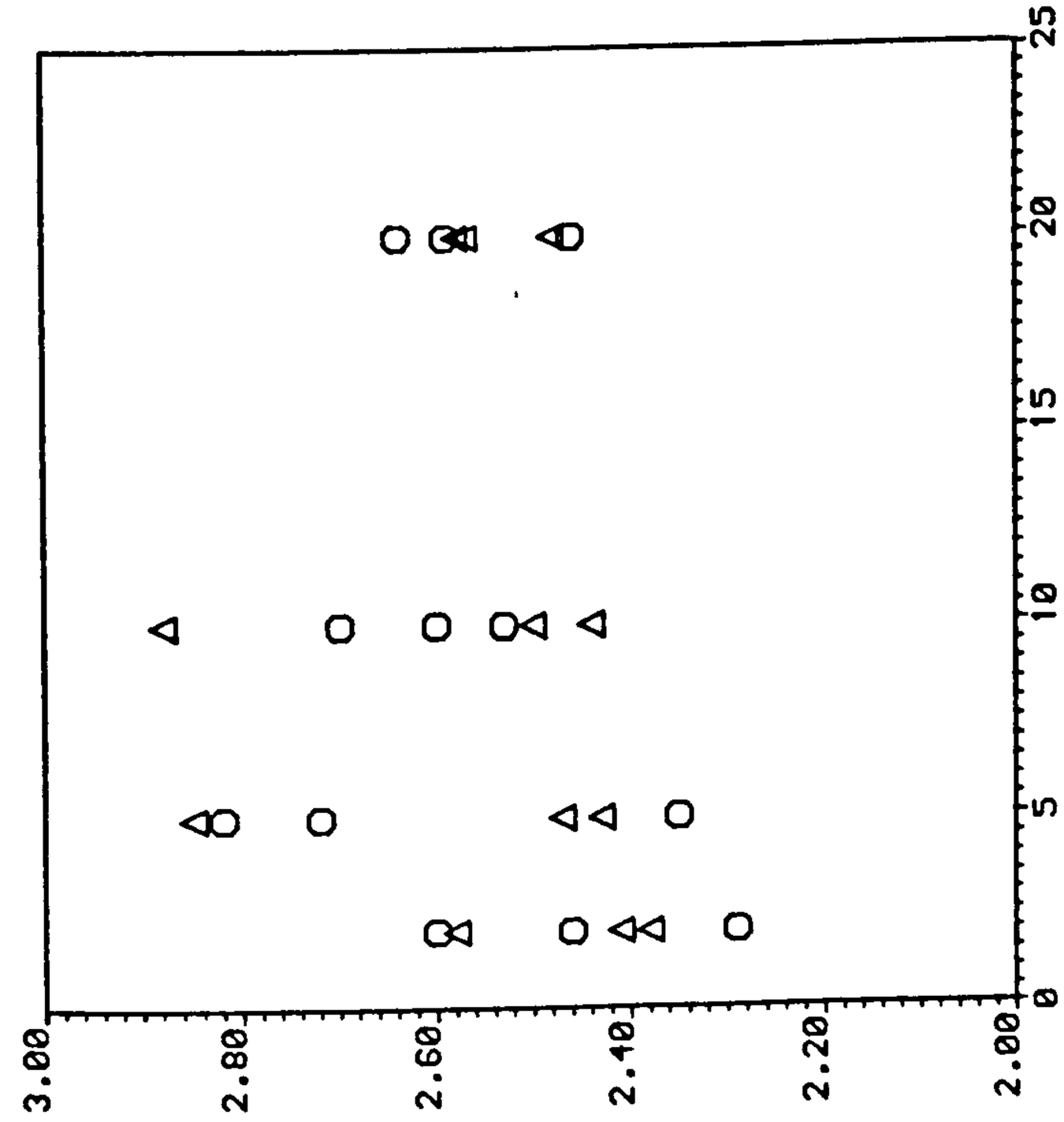

FIG 4.13 SIMULATION RESULTS FOR LOW FREQUENCY SURGE

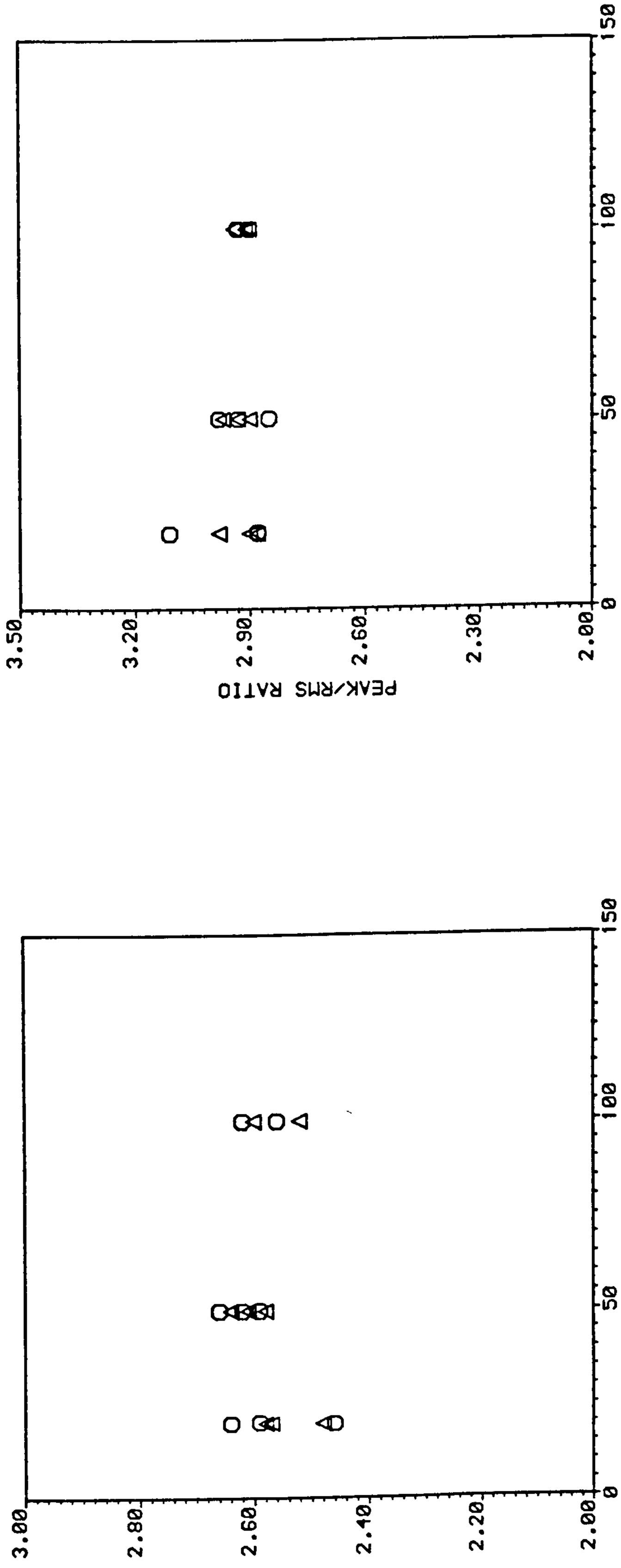

JONSWAP spectrum, Hs=15.0 m, Peak Frequency= 0.3456 rad/s
Surge Natural Period of Tanker=1.00 min., Damping Ratio=0.07
Length of each Record=2.13 hrs.

○ RANDOM
△ DETERMINISTIC

FIG 4.14 SIMULATION RESULTS FOR LOW FREQUENCY SURGE RESPONSE OF A TANKER IN HEAD SEAS

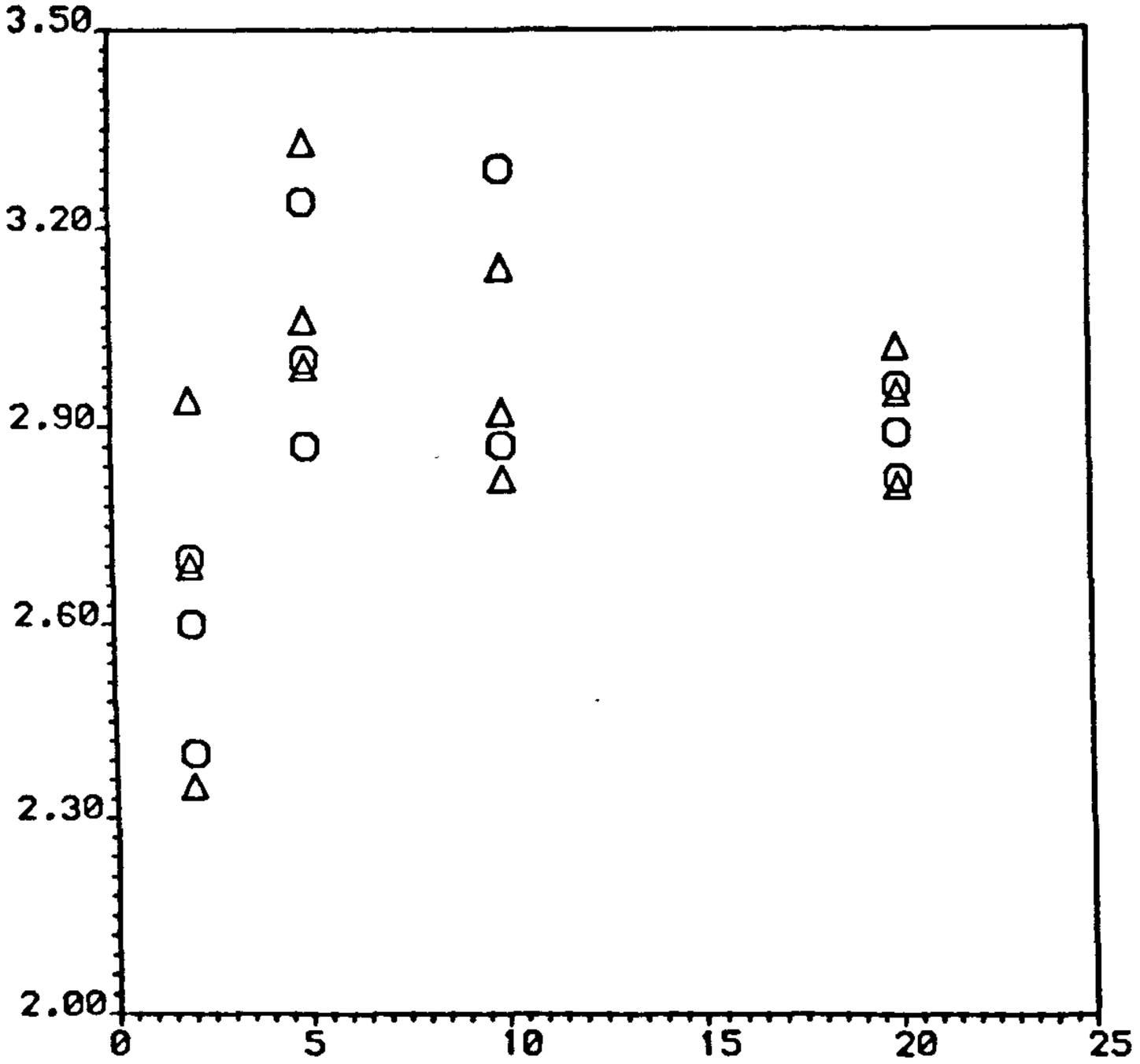

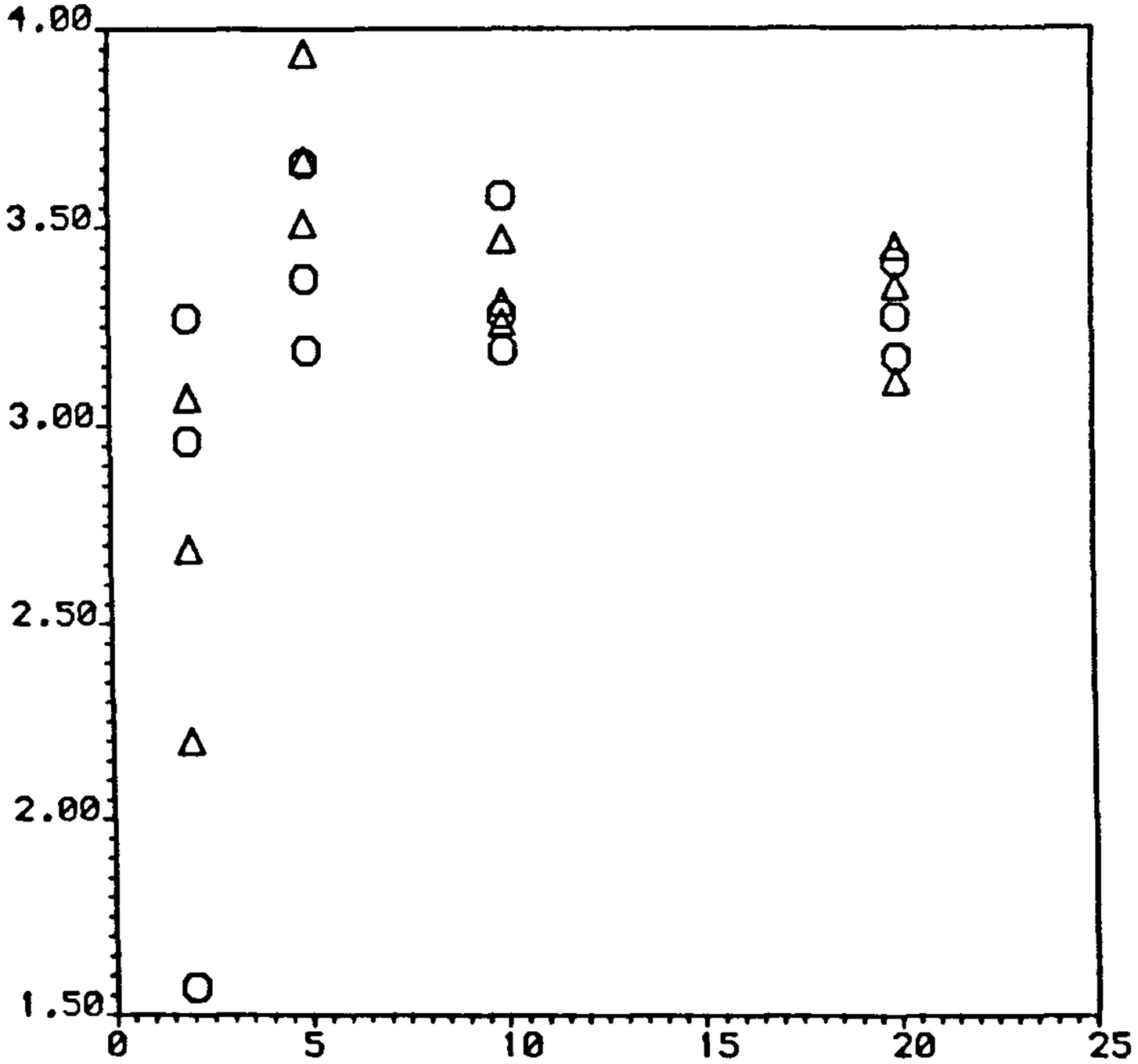

O *RANDOM*

Δ *DETERMINISTIC*

JONSWAP spectrum, Hs=15.0 m, Peak Frequency= 0.3456 rad/s
Surge Natural Period of Tanker=1.00 min., Damping Ratio=0.07
Length of each Record=4.27 hrs.

FIG 4.15 SIMULATION RESULTS FOR LOW FREQUENCY SURGE RESPONSE OF A TANKER IN HEAD SEAS

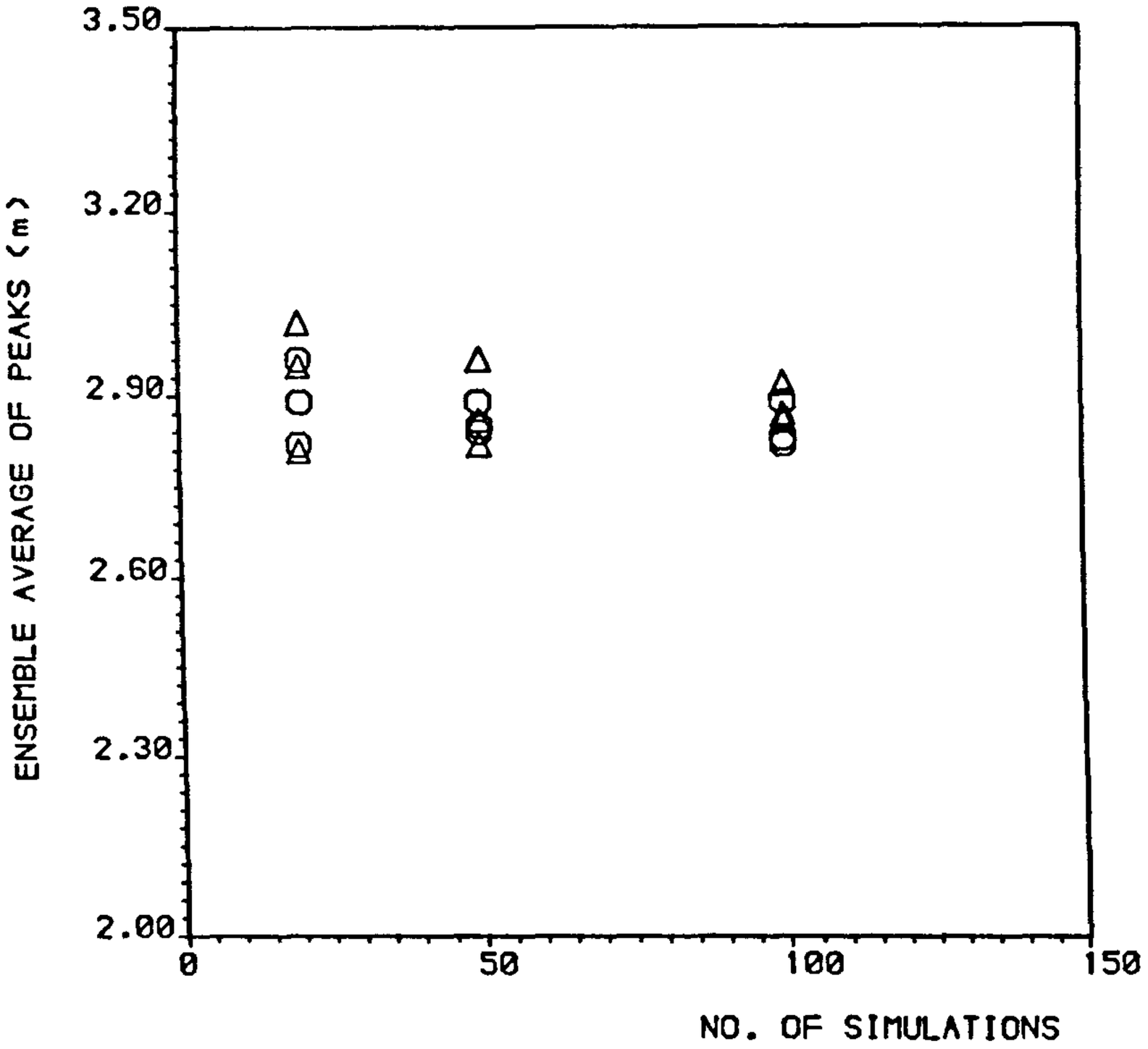

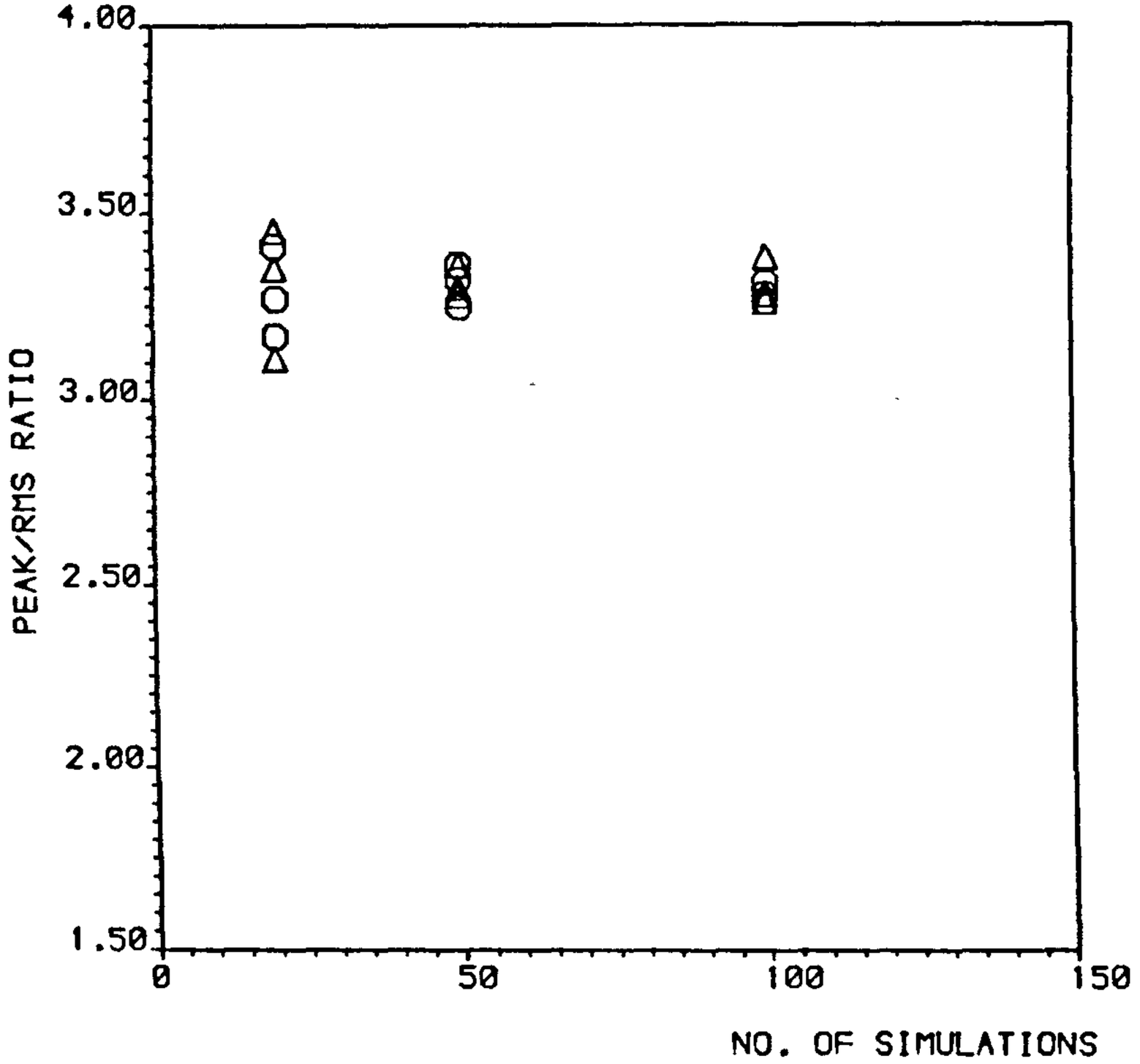

O *RANDOM*

Δ *DETERMINISTIC*

JONSWAP spectrum, Hs=15.0 m, Peak Frequency= 0.3456 rad/s
Surge Natural Period of Tanker=4.00 min., Damping Ratio=0.07
Length of each Record=4.27 hrs.

FIG 4.16 SIMULATION RESULTS FOR LOW FREQUENCY SURGE RESPONSE OF A TANKER IN HEAD SEAS

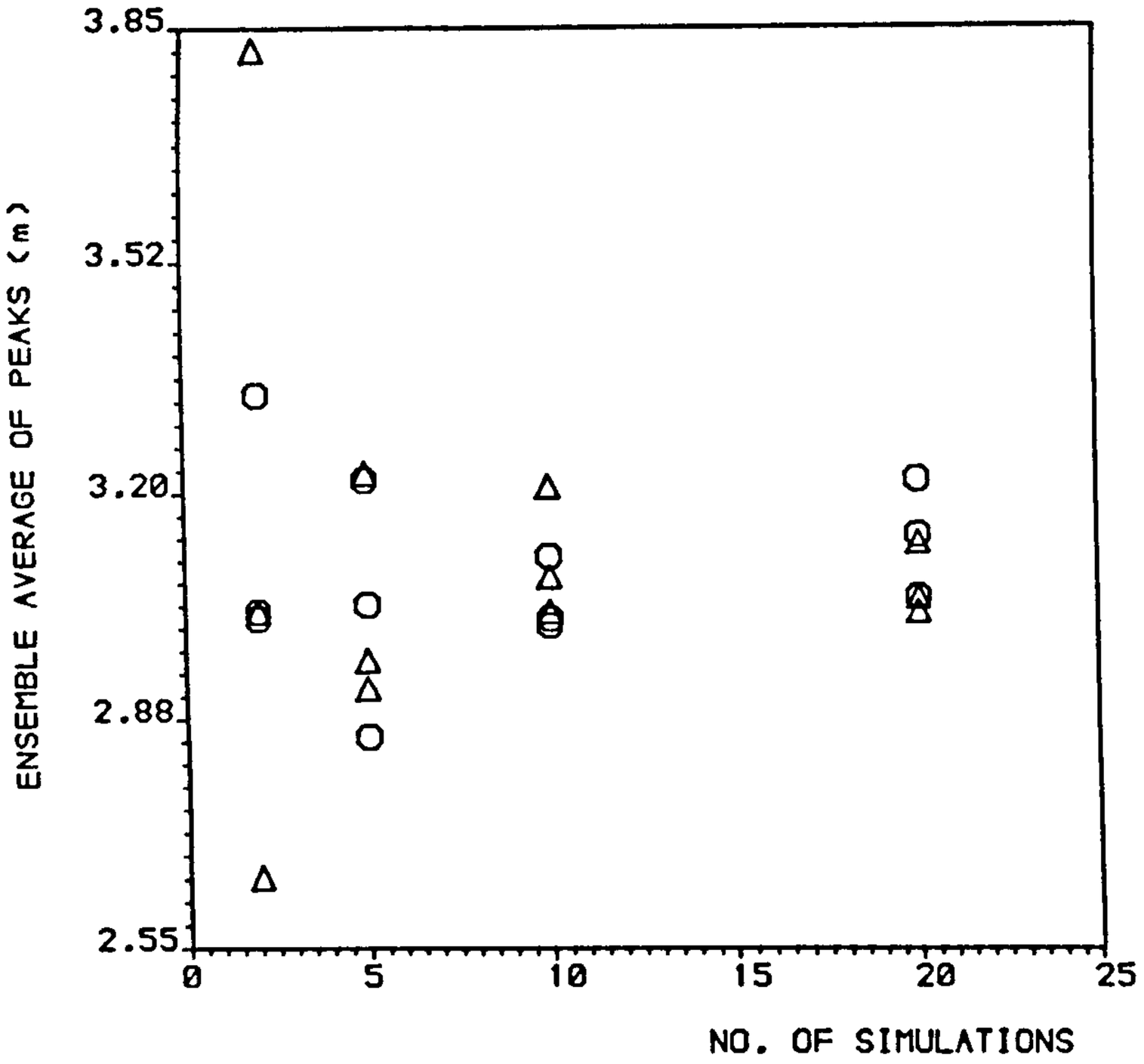

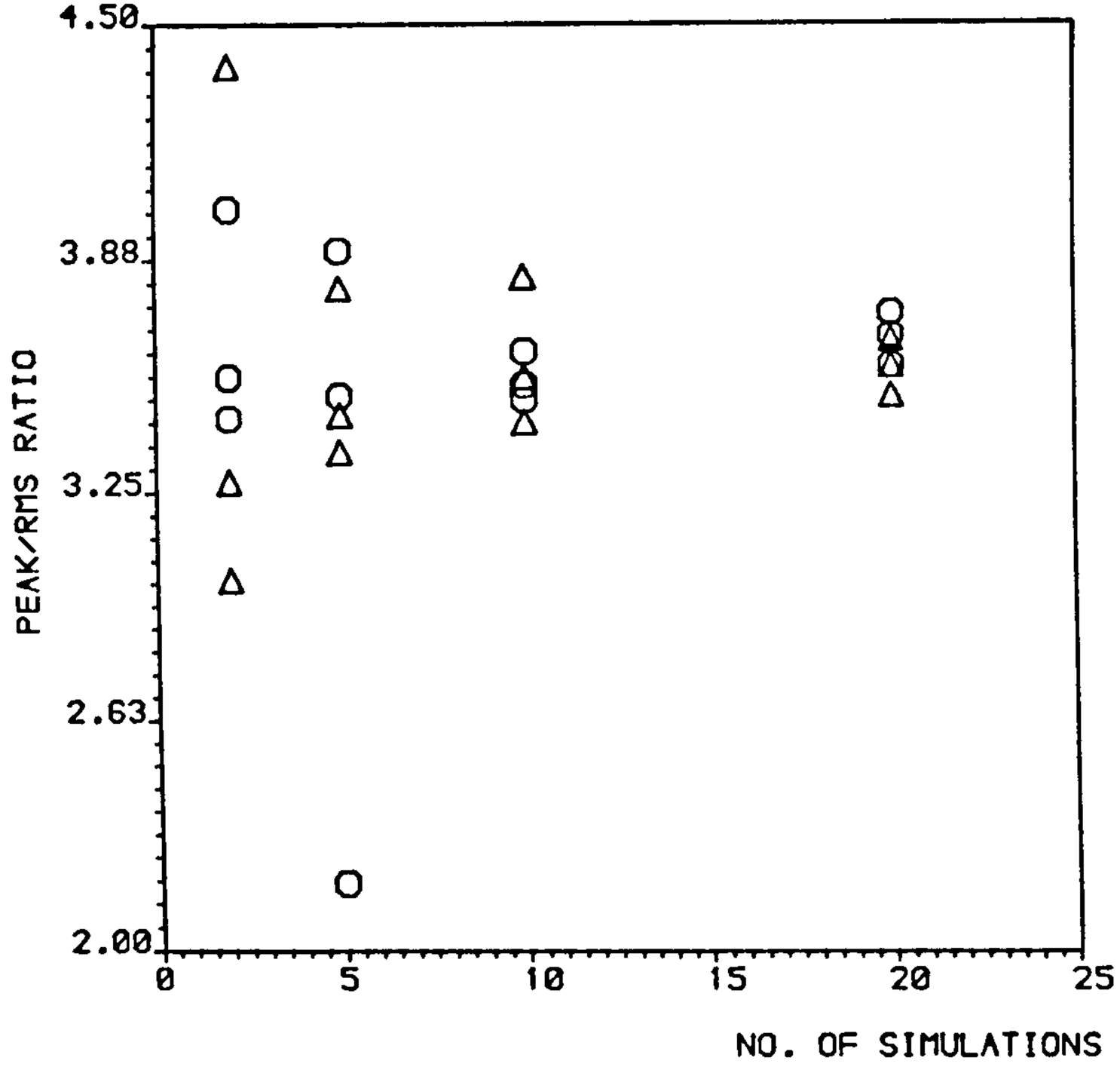

O *RANDOM*

Δ *DETERMINISTIC*

JONSWAP spectrum, Hs=15.0 m, Peak Frequency= 0.3156 rad/s
Surge Natural Period of Tanker=1.00 min., Damping Ratio=0.07
Length of each Record=8.53 hrs.

FIG 4.17 SIMULATION RESULTS FOR LOW FREQUENCY SURGE RESPONSE OF A TANKER IN HEAD SEAS

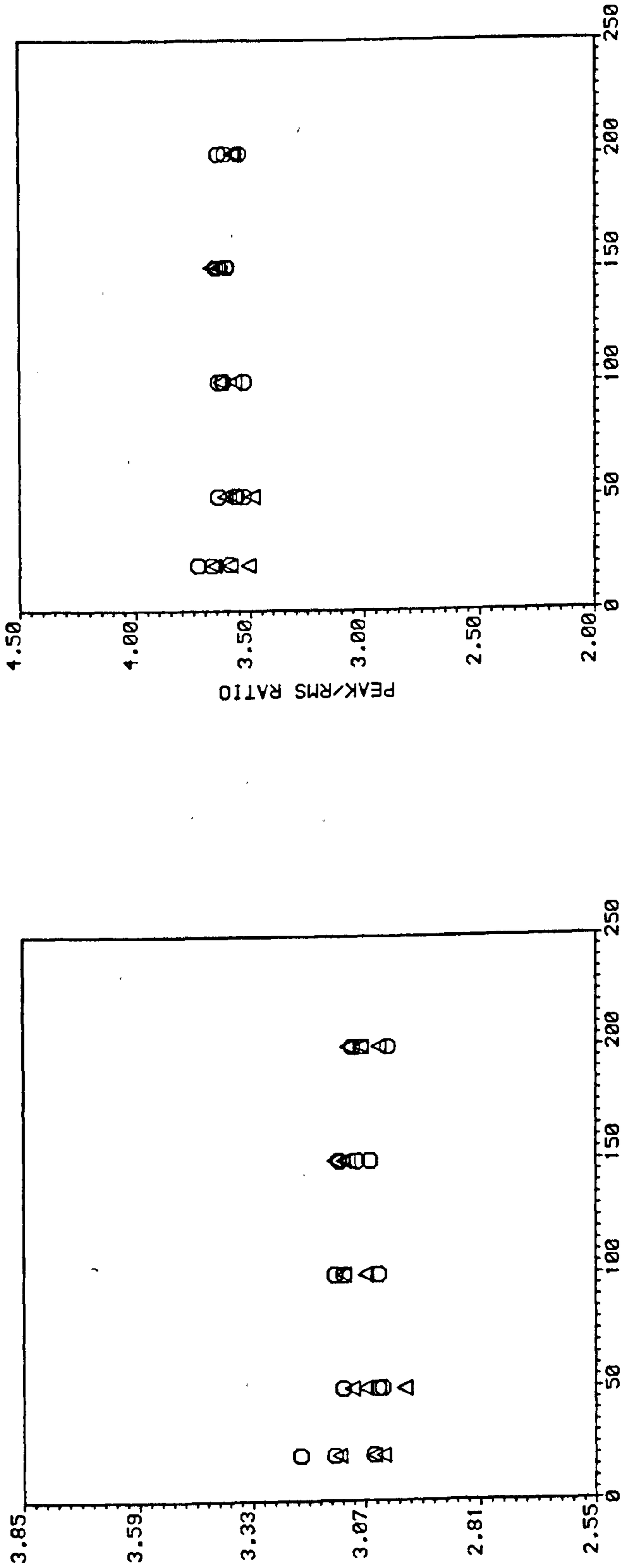

FIG 4.18 SIMULATION RESULTS FOR LOW FREQUENCY SURGE RESPONSE OF A TANKER IN HEAD SEAS

4.8 Discussion

For the simulation of the 1st and 2nd order random processes considered here use was made of the pseudo-random number generator routines G05DAF, G05DPF and G05DDF (65) on a VAX 11/750 computer. All pseudo-random numbers have a finite cycle length after which the sequence repeats itself and it has been recommended (65) never to use more numbers than the square root of the cycle length in any one sequence of numbers so that the statistical properties are not impaired. The cycle length of the routines mentioned above is 2^{57} and initialisation of the sequences was performed by calling the subroutine G05CCF (65) which sets the basic generator routine to a non-repeatable initial state using the setting of the real-time clock. In this way different sequences of random numbers are generated in various runs of the computer program yielding different time histories of the process at each run. Note that the statistical properties are guaranteed within the sequences of random numbers and not between the sequences. Fig.4.2 shows the 1st and 2nd order random sea surface realisations using the deterministic method of simulation mentioned in the previous sections. Use was made of the Pierson-Moskowitz spectrum (70), shown in Fig.4.3, and the simulation was carried out via the FFT algorithm subroutine C06ADF (65). This routine was also used to simulate the slow drift force and the response of a tanker in head seas. Pinkster's results for the diagonal transfer functions of the slow drift force on a tanker were plotted and the graph is presented in Fig. 4.4. In order to incorporate this graph into the computer program the curve was approximated by short linear segments. The curve represents the data on the diagonal of the matrix of transfer functions ($\omega_1 = \omega_2$) given in Section 4.6. which are the amplitudes of the force for zero difference frequencies corresponding to the mean drift force in regular waves. These are analogous to reflection coefficients used in the calculation of the 2nd order low frequency forces on floating bodies and tend to a constant value at high frequencies at which the vessel motions become

negligible and it can be assumed that total reflection of the waves occurs. Note that the Newman approximation is only valid for cases where the contribution of the 2nd order nonlinear potentials (item 5 in Section 4.4) and the difference frequencies are small. Pinkster's comparisons with model tests and computations indicate that the approximation is valid for mean frequencies above 0.4 rad/s. However the objective here is not the accurate estimation of the slow drift force but to find the statistics of the tanker response. It is also pointed out that more computations and model tests are required to verify the accuracy of available results for slow drift force. A sample of simulation results for the slow drift force on a tanker is shown in Fig.4.5. The JONSWAP spectrum with H_S = 7.5m was used with only one simulation using the deterministic approach being shown. Also in this case the random phase angles were the same for both simulation methods. Fig.4.6 shows the power spectral densities of the force when the first order wave spectrum was split into 250 frequency components. It can be seen that the differences between the two approaches can be quite large in each simulation record. Fig.4.7 shows a sample of the results for the slowly varying surge response of a tanker in head seas. Roberts (74) has shown that when damping is very light it can be assumed that the response statistics are independent of the exciting force statistics, however this assumption may not be justified when the actual levels of damping on a floating structure are considered. In Section 4.5 the low frequency damping of the tanker was assumed linear, based on the model test results of Wichers and Sluijs (89) for a LNG carrier and a VLCC. They concluded that due to small velocities of the low frequency surge motion the damping coefficient can be considered linear. Based on results of a 200,000 DWT VLCC a damping ratio of 0.07 was chosen for further time simulations. It was also assumed that the stiffness term in the equation of motion is linear which is applicable to some floating structures such as a SALS system or a TLP, however, when structures such as a Single Buoy Storage (SBS) system or a semi-submersible are considered

the catenary moorings can introduce highly nonlinear stiffness into the equations of motion which can play a dominant role in determining the statistics of vessel response for large displacements.

To simulate tanker response various time histories with different durations were considered. The number of simulations (records) in the computer program varied from NR = 2 to 200 and the duration of each record was between 1 and 8.5 hours. The program was run 3 times for each case. Some of the simulation results are presented on pages 250-252 The two values appearing in each column correspond to the results of (i) the random approach (on the left) and (ii) the deterministic method (on the right). The results for all cases considered and relating to the extreme response of the tanker in head seas are presented in Figs.4.11 - 4.18. With NR $<$ 20 the scatter in the results can become very large but as NR is increased they converge. For example in Figs.4.17 and 4.18 it is shown that for NR $>$ 50 the ensemble average of peaks $\bar{x}_{Pmax}$ = 3.1m and the peak/rms ratio is R = 3.6. However when NR = 2, in one case $\bar{x}_{Pmax}$ was found to be underestimated by about 15% or in another record with NR = 5 the value of R was underestimated by nearly 40%. Therefore in order to arrive at accurate results it is extremely important to obtain a sufficient number of simulation records, say NR $\geq$ 50, in each program run. The length of each record can be adjusted to the estimated duration of the sea state. For all cases considered here the random approach did not offer any advantages over the deterministic method and for accurate results (at high values of NR) the predictions of both methods were identical. Although here the values of R and $\bar{x}_{Pmax}$ are predicted accurately by the deterministic approach points made by Tucker et al (83) concerning wave group statistics and the results of Langley (54) show that this approximate method can underpredict the 4th statistical moments of the force and response. As mentioned earlier when damping tends to zero the response of the system becomes Gaussian and is independent

of the statistics of the exciting force. For a narrow banded Gaussian process Cartwright and Longuet-Higgins (8) derived $R=\sqrt{2\ln N_p}+\frac{0.5772}{\sqrt{2\ln N_p}}$ in which N_p = number of peaks in the simulated record. Regarding the levels of damping present in the equations of motion and the random dynamic analysis of offshore structures, this equation is frequently used for the estimation of the peak values. Here the number of peaks occuring in the 8.5 hour records was found to be in the range 129-142 giving R = 3.3 by the Cartwright-Longuet-Higgins formula which is about 8% less than the simulation results. Such differences would increase with higher levels of damping and therefore the use of the above formula could result in a gross underestimation of the peak values. It must also be added that although exact simulation results are presented here, in order to improve the accuracy of the simulations and to arrive at more realistic predictions the directionality of the sea spectra and the non-stationary nature of the force and the response processes should also be taken into account.

CHAPTER FIVE

CONCLUSIONS

1. For the fixed horizontal and vertical cylinders and the environmental conditions considered the use of a particular wave theory did not affect the choice of C_D and C_m.

2. Predictions of Stokes Vth and stream function wave theories were found to be in good agreement except at high Ursell parameters.

3. For the fixed horizontal cylinders Airy theory invariably overpredicted the load range within a cycle which can lead to large errors in the estimated contribution to fatigue damage of jacket members. For the fixed vertical cylinder, the results of linear wave theory for the maximum shear force were in good agreement with those by the stream function and Stokes Vth theories when integration of forces were carried up to the MWL, however, in some cases the maximum bending moments were underestimated. In most cases the differences between predictions of Airy and nonlinear wave theories were large especially for calculation of forces at locations near the free surface.

4. When integration of forces were extended to the free surface the increase in base shear force, bending moment and stress range were very large, indicating that variable submergence effects cannot be neglected. However more experimental data are required to validate the predictions of wave theories for the particle kinematics near the free surface zone.

5. Convective acceleration terms in the Morison's equation had little effect on the maximum values of the fluid inertia forces. For highly nonlinear waves with large

Ursell parameters and when stress ranges for fatigue calculations are under consideration the differences between the local and total acceleration terms can become important.

6. Although displacements of the articulated towers were small relative to wave length, calculation of forces at the instantaneous position of the tower resulted in large increases in response (about 20%). In some cases this effect considerably influenced the distributed fluid loading causing an increase in the maximum shear force and bending moment. The effect of both variable submergence and calculation of forces at the displaced position of the tower was to increase the loading by 52% and the tower response by 75% in the worst case which require experimental verification.

7. Predictions of the eigenvalue analysis for the dynamic stability of the tower was justified by the simulation results. However it was shown that when drag loads are mobilised, viscous damping can play an important role in limiting the response of the tower and for more reliable results a time domain analysis should be performed.

8. For the SALS system considered it was found that variations of the buoyancy force with yoke submersion can become significant at large rotations of the yoke assembly.

9. The natural periods of the yoke/riser system at moderate levels of buoyancy loss were found to be low indicating that resonant motions are unlikely to occur except in the form of superharmonic excitations caused by drag loading when a natural frequency of the system coincides with an odd multiple of the exciting wave frequency. At high levels of flooding in the buoyancy chamber the increase in the natural periods of the yoke/riser system can lead to resonant motions or

result in total submersion of the yoke structure causing impact damage to the tanker hull.

10. For the cases considered the slack (curvature) in the articulated riser was found to be small and did not lead to high stresses due to snatch loads. Riser links nearer to the sea bed may experience slack-taut condition before the upper segments and it is unlikely that the links can undergo compression leading to buckling failure.

11. Exclusion of riser elastic extension in the analysis can lead to conservative estimates of snatch loads (Ref.85,86) and a better mathematical model for the study of such conditions would include the effects of link elasticity.

12. Time simulation of random second order phenomena, such as the slow drift force on a tanker, represented by a sum of wave harmonics can be efficiently performed via the FFT algorithm by reducing the double summation terms in the time series to a single summation term using a constant frequency interval for the wave harmonics and by considering only the wave amplitudes which correspond to the main frequency components in the wave spectrum.

13. The limited number of simulation records in some cases resulted in gross underestimation of extreme tanker response values and it is extremely important to perform sufficient simulation runs.

14. Comparing the results of the extreme vessel response obtained by the random and deterministic methods of simulation, the random approach did not offer any advantages over the deterministic method and for accurate results with sufficiently large numbers of simulations, the predictions of both methods yield identical values.

15. The simulation records indicate that for practical levels of damping the commonly used method of calculating the peak values based on the Cartwright-Longuet-Higgins formula can underestimate the extreme low frequency response of the vessel by about 8%.

REFERENCES

1. ABRAMOWITZ,M. STEGUN,I.A. — Handbook of Mathematical Functions Dover, N.Y., 1964.

2. ALAGHEBAND-OSKOUI,S. — A Study of Anchoring Methods for Offshore Structures,M.Sc.Thesis, Cranfield Inst.of Tech,1982.

3. BASU,A.K. JAIN,A.K. — Treatment of Variable Submergence Effects for Offshore Towers, Proc.1st Indian Conf.Ocean Engg., Madras, 1981.

4. BISHOP,J.R. — Wave Force Investigation at the Second Christchurch Bay Tower, Summary Report OT-O-82100,NMI Ltd., 1982.

5. BOLOTIN,V.V. — The Dynamic Stability of Elastic Systems, Holden-Day Inc.,1964.

6. BORGMAN,L.E. — Ocean Wave Simulation for Engineering Design, J.Waterways and Harbours Div., ASCE,Vol.95,No.WW4,1969.

7. BRITISH STANDARDS INSTITUTION — BS 6235: Code of Practice for Fixed Offshore Structures, 1982

8. CARTWRIGHT,D.E. LONGUET-HIGGINS,M.S. — The Statistical Distribution of the Maxima of a Random Function, Proc. Royal Soc.London,Series A,1956.

9. CHAKRABARTI,S.K. — Laboratory Generated Waves and Wave Theories, J.Waterways Port Coastal and Ocean Div.,ASCE,Vol.106,No.WW3, 1980.

10. CHAKRABARTI,S.K. COTTER,D.C. — Motion Analysis of Articulated Tower, J.Waterways Port Coastal and Ocean Div.,ASCE,Vol.105,No.WW3,1979.

11. CHAKRABARTI,S.K. COTTER,D.C. — Transverse Motion of Articulated Tower, J.Waterways Port Coastal and Ocean Div., ASCE,Vol.106,No.WW1, 1980.

12. CHAPLIN,J.R. ANASTASIOU,K. — Some Implications of Recent Advances in Wave Theories, Proc.17th Int.Conf. Coastal Engg.,Vol.1,ASCE,1980.

13. CONTE,S.D. DE BOOR,C. — Elementary Numerical Analysis: An Algorithmic Approach, McGraw-Hill, N.Y., 1972.

14. COOLEY,J.W. TUKEY,J.W. — An Algorithm for the Machine Calculation of Complex Fourier Series, Math.of Comp.,Vol.19,No.90,1965.

15. DEAN,R.G. Stream Function Representation of Nonlinear Ocean Waves, J.Geophys. Res.,Vol.70,1965.

16. DEAN,R.G. Evaluation and Development of Water Wave Theories for Engineering Application, Vol.1 & 2, U.S.Army, Coastal Eng.Res.Centre,Special Report No.1, 1974.

17. DEAN,R.G. Relative Validities of Water Wave Theories, J.Waterways Harbours and Coastal Engg.Div.,ASCE,Vol.96, No.WW1, 1970.

18. DELFT HYDRAULICS LABORATORY Wave Kinematics in Irregular Waves, Report M1628/MaTS VM-1-4,Delft,1982.

19. EATOCK-TAYLOR,R. DUNCAN,P.E. Fluid Induced Inertia and Damping in Vibrating Offshore Structures, J.App.Ocean Res.,Vol.2,No.1,1980

20. EATOCK-TAYLOR,R. DRAKE,K.R. DUNCAN,P.E. The Dynamics of a Flexible Articulated Column in Waves, J.Engg.Struct., Vol.5,No.3, 1983.

21. EYKHOUT,F. FOOLEN,J.A. An Integrated Floating Production Storage and Offloading System-SALS - in 380Feet Water Depth, OTC, Paper 3142, Houston, 1978.

22. FALTINSEN,O.M. Sea Loads and Motions of Marine Structures, Norwegian Inst.of Tech, 1979.

23. FENTON,J.D. A High-Order Cnoidal Wave Theory, J.Fluid Mech.,Vol.94,Pt.1,1979.

24. FOX,C. Tower Again for Beryl Loading Replacement, Offshore Engineer December 1985.

25. FROBERG,C.E. Introduction to Numerical Analysis Addison-Wesley, 1965.

26. GARRISON,C.J. Hydrodynamic Loading of Large Offshore Structures: Three Dimensional Source Distribution Methods,Numerical Methods in Offshore Engineering (O.C.Zienkiewicz,R.W.Lewis and K.G.Stagg,eds),Wiley,N.Y.,1978.

27. GRANVILLE,A.J. FISHER,P.M. Articulated Loading Column-Maureen Field, Design in Offshore Structures, Proc.ICE, London, 1983.

28. GREENHILL,A.G. — The Application of Elliptic Functions McMillan, 1892.

29. GRIM,O. — Oscillations of Buoyant Two Dimensional Bodies - Calculation of Hydrodynamic Forces, HS-V Report No.1171,1959.

30. GUDMESTAD,O.T. CONNOR,J.J. — Linearisation Methods and the Influence of Current on the Nonlinear Hydrodynamic Drag Force, J.App. Ocean Res.,Vol.5,No.4, 1983

31. GUDMESTAD,O.T. CONNOR,J.J. — Engineering Approximations to Non-Linear Hydrodynamic Deepwater Waves., J.App.Ocean Res., to be published.

32. HAGEDORN,P. — Nonlinear Oscillations, Oxford Univ. Press, 1982.

33. HALLAM,M.G. HEAF,N.J. WOOTON,L.R. — Dynamics of Marine Structures: Methods of Calculating the Dynamic Response of Fixed Structures Subject to Wave and Current Action, Report UR8, Atkins Research and Development, CIRIA, 1977.

34. HASSELMANN, K. — On the Nonlinear Energy Transfer in a Gravity-Waved Spectrum, Pt.1, General theory,J.Fluid Mech.Vol.12, 1962.

35. HOOFT,J.P. — Advanced Dynamics of Marine Structures, Wiley, N.T., 1982.

36. HOGBEN,N. — Wave Loads on Structures, Int.Conf. BOSS, Vol.1, Trondheim, 1976

37. HUDSPETH R.J. CHEN,M.C. — Digital Simulation of Nonlinear Random Waves, J.Waterways Port Coastal and Ocean Div.,ASCE,Vol.105,No.WW1, 1979.

38. HUDSPETH,R.T. DALRYMPLE,R.A. — Comparison of Wave Forces Computed by Linear and Stream Function Methods, OTC Paper 2037, Houston, 1974.

39. IPPEN,A.T.(ed). — Estuary and Coastline Hydrodynamics McGraw-Hill, N.Y., 1966.

40. ISAACSON,M. — Nonlinear Inertia Forces on Bodies, J.Waterways Port Coastal and Ocean Div.,ASCE,Vol.105, No.WW3, 1979.

41. IWAGAKI,Y. SAKAI,T. — Horizontal Water Particle Velocity of Finite Amplitude Waves, Proc.12th Conf.Coastal Engg.,Washington,1970.

42. KANE,T.R. — Dynamics of Nonholonomic Systems, J.App.Mech.,ASME,Vol.83,1961.

43. KIRK,C.L. JAIN,R.K. — Response of Articulated Towers to Waves and Currents, OTC paper 2798, Houston, 1977.

44. KIRK,C.L. BOSE,P. — Dynamic Response of Articulated Platforms in Random Seas, Int.Conf. Flow Induced Vibrations in Fluid Engg.,Paper C1, Reading, 1982.

45. KIRK,C.L. — Approximate Dynamic Analysis of Single Anchor Leg Storage System, Ocean Eng.,Vol.11,No.5,1984.

46. KOKKINOWRACHOS,K. BUTT,H.G. — Design and Systematic Concept Development of Articulated Offshore Towers, Offshore Brazil, 1978

47. KOKKINOWRACHOS,K. MITZLAFF,A. — Dynamic Analysis of One and Multi-Column Articulated Structures, Int. Symp.Hydrodyn.Ocean Engg.,Norway,1981.

48. KORTWEG,D.J. DE VRIES,G. — On the Change of Form of Long Waves Advancing in a Rectangular Canal and on a New Type of Long Stationary Wave, Phil.Mag.,5th Series,Vol.39, 1985.

49. KOTERAYAMA,W. — Wave Forces Exerted on Submerged Circular Cylinders Fixed in Deep Water,Research Report,Kyushu Univ., Vol.27,No.84,1979.

50. LAITONE,E.V. — The Second Approximation to Cnoidal and Solitary Waves, J.Fluid Mech., Vol.9,1961.

51. LAITONE,E.V. — Limiting Conditions for Cnoidal and Stokes Waves, J.Geophys.Res,Vol.67, No.4, 1962.

52. LAMB,H. — Hydrodynamics, Dover, N.Y., 1945

53. LANGLEY,R.S. KIRK,C.L. — Random Dynamic Analysis of an Offshore Single Anchor Leg Storage System,J.App.Ocean Res.,Vol.4, No.4, 1982.

54. LANGLEY,R.S. — On the Time Domain Simulation of Second Order Wave Forces and Induced Responses, J.App.Ocean Res., to be published.

55. LE MAHAUTE,B. — An Introduction to Hydrodynamics and Water Waves, Springer-Verlag, 1976.

56. LE MEHAUTE,B. DIVOKY,D. LIN,A. — Shallow Water Waves: A Comparison of Theories and Experiments, Proc. 11th Coastal Engg.Conf.,London,1968.

57. LONGUET-HIGGINS,M.S. — On the Statistical Distribution of the Height of Sea Waves, J.Mar. Res.,Vol.11,1952.

58. MAULL,D.J. NORMAN,S.G. — A Horizontal Circular Cylinder Under Waves, Mechanics of Wave Induced Forces on Cylinders (ed. T.L.Shaw), Pitman, 1979.

59. McIVER,D.B. — Parametrically Excited Oscillations in Offshore Structures, Int.Conf. BOSS, Vol.2, 1976.

60. MEI,C.C. — Numerical Methods in Water Wave Diffraction and Radiation, Ann. Rev.Fluid Mech.,Vol.10, 1978.

61. MITCHELL & GAUTHER ASSOC.INC. — Advanced Continuous Simulation Language (ACSL), User Guide/ Reference Manual, Mass.,1981.

62. MORISON,J.R. O'BRIEN,M.P. JOHNSON,J.W. SCHAAF,S.A. — The Force Exerted by Surface Waves on Piles, Petrol Trans.,AIME, Vol.189, 1950.

63. NATH,J.H. KOBUNE,K. — Periodic Theory Velocity Prediction in Random Waves, Proc.16th Coastal Engg.Conf.,Hamburg, 1978.

64. NEWMAN,J.N. — Second Order Slowly Varying Forces on Vessels in Irregular Waves, Proc.Int.Symp.Dynamics of Marine Structures and Vehicles in Waves, Paper 19, 1974.

65. NUMERICAL ALGORITHMS GROUP (NAG) — NAG Library Manuals, Vol.1-6, 1984.

66. OHMART,R.D. GRATZ,R.L. — A Comparison of Measured and Predicted Ocean Wave Kinematics, OTC Paper 3276, Houston, 1978.

67. OIL COMPANIES INTERNATIONAL MARINE FORUM (OCIMF) — Prediction of Wind and Current Loads on VLCCs, London, 1977

68. OLSEN,O.A.
BRAATHEN,A.
LOKEN,A.E.
NYHUS,K.A.
TORSET,O.P.
Slow and High Frequency Motions and Loads of Articulated Single Point Mooring Systems for Large Tankers, Norwegian Maritime Res., No.2, 1978.

69. PASSERELLO,C.E.
HUSTON,R.L.
Another Look at Nonholonomic Systems J.App.Mech.,ASME,Vol.40,No.1,1973.

70. PIERSON,W.J.
MOSKOWITZ,L.
A Proposed Spectral Form for Fully Developed Wind Seas Based on the Similarity Theory of S.A.Kitaigorodskii, J.Geophys Res., Vol.69, 1964.

71. PINKSTER,J.A.
Low Frequency Second Order Wave Exciting Forces on Floating Structures, Publication No.650, Netherlands Ship Model Basin, Wagenigen, 1980.

72. RAMBERG,S.E.
NIEDZWECKI,J.M.
Some Uncertainties and Errors in Wave Force Computations, OTC, Paper 3597, Houston, 1979.

73. RICE,S.O.
Mathematical Analysis of Random Noise, Bell System Tech.J.,Vol.23 and 24, 1944-45; also in selected papers on Noise and Stochastic Processes, N.Wax (Ed), Dover,N.Y., 1954

74. ROBERTS,J.B.
Nonlinear Analysis of Slow Drift Oscillations of Moored Vessels in Random Seas, J.Ship.Res., Vol.25 No.2, 1981.

75. SARPKAYA,T.
ISAACSON,M.
Mechanics of Wave Forces on Offshore Structures, Van Nostrand Reinhold, N.Y., 1981.

76. SARPKAYA,T.
Vortex Shedding and Resistance in Harmonic Flow about Smooth and Rough Circular Cylinders at High Reynold's Number, Report No.NPS-69 SL 76062, Naval Postgraduate School,Monterey,1976.

77. SKJELBREIA,L.
HENDRICKSON,J.A.
Fifth Order Gravity Wave theory, Proc.7th Coastal Engg.Conf.,The Hague, 1960.

78. SPANSBERG,S.
JACOBSON,B.K.
The Effect of Wave Grouping on Slow Drift Oscillations of an Offshore Structure, Int.Symp.Ocean Engg.Ship Handling, Swedish Maritime Res Centre, 1980.

79. STOKES,C.G. — On the Theory of Oscillatory Waves Trans.Camb.Phil.Soc.,Vol.8.1847.

80. TAKAHASHI,K. — An Approach to Investigate the Instability of the Multiple Degree of Freedom Parametric Dynamic Systems, J.Sound and Vibration, 78(4),1981.

81. TIMOSHENKO,S.P. YOUNG,D.H. — Advanced Dynamics, McGraw-Hill, N.Y. 1948.

82. TSUCHIYA, Y. YAMAGUCHI,M. — Some Consideration on Water Particle Velocities of Finite Amplitude Wave Theories,Coastal Engg.in Japan,Vol.15,1972.

83. TUCKER,M.J. CHALLENOR,P.G. CARTER,D.J.T. — Numerical Simulation of a Random Sea: A Common Error and its Effect upon Wave Group Statistics, J.App. Ocean Res.,Vol.6,No.2,1984.

84. TUMA,J.J. — Engineering Mathematics Handbook McGraw-Hill, 1979.

85. WALTON,T.S. POLACHEK,H. — Calculation of Transient Motion of Submerged Cables, J.Math and Comp.,Vol.14,1960

86. WALTON,T.S. POLACHEK,H. — Calculation of Nonlinear Transient Motion of Cables, J.Math and Comp., 1963

87. WAMPLER,C. BUFFINTON,K. SHU-HUI,J. — Formulation of Equations of Motion for Systems Subject to Constraints, J.App.Mech.,ASME,Vol.52,1985.

88. WHEELER,J.D. — Method for Calculating Force Produced by Irregular Waves, OTC Paper 1006, Houston, 1969.

89. WICHERS,J.E.W. SLUIJS,M.F. — The Influence of Waves on the Low Frequency Hydrodynamic Coefficients of Moored Vessels, OTC Paper 1500, Houston, 1979.

90. WILKINSON,J.H. REINSCH,C. — Handbook of Automatic Computation Vol.2, Linear Algebra, Springer-Verlag, 1971.

91. WINGET,J.M. HUSTON,R.L. — Cable Dynamics - A Finite Segment Approach,J.Comp and Struct,Vol.6, 1976.

92. ZIENKIEWICZ,O.C.
BETTES,P.

Dynamic Fluid-Structure Interaction: Numerical Modelling of the Coupled Problem, Numerical methods in Offshore Engineering (O.C.Zienkiewicz, R.W.Lewis,K.G.Staggs,eds), Wiley, N.Y.,1978.

APPENDIX A
NONLINEAR WAVE THEORIES AND SECOND ORDER NONLINEAR RANDOM WAVES

GENERAL

The following give details of some of the nonlinear wave theories suitable for calculating hydrodynamic forces on offshore structures and used in this thesis.

Much of the theoretical development and many points not mentioned in the referenced published work are included. Also many of the equations presented do not appear in the literature and it is hoped that these will provide a better understanding of the nonlinear wave theories and enable the reader more readily to use them on practical problems.

A.1. STOKES SECOND ORDER RANDOM WAVES (34)

The boundary value problem of two dimensional flow with a horizontal sea bed and assuming incompressible, irrotational fluid is formulated bleow, the derivation of which can be found in many text books on wave theory and hydrodynamics (e.g. see (39) or (52)).

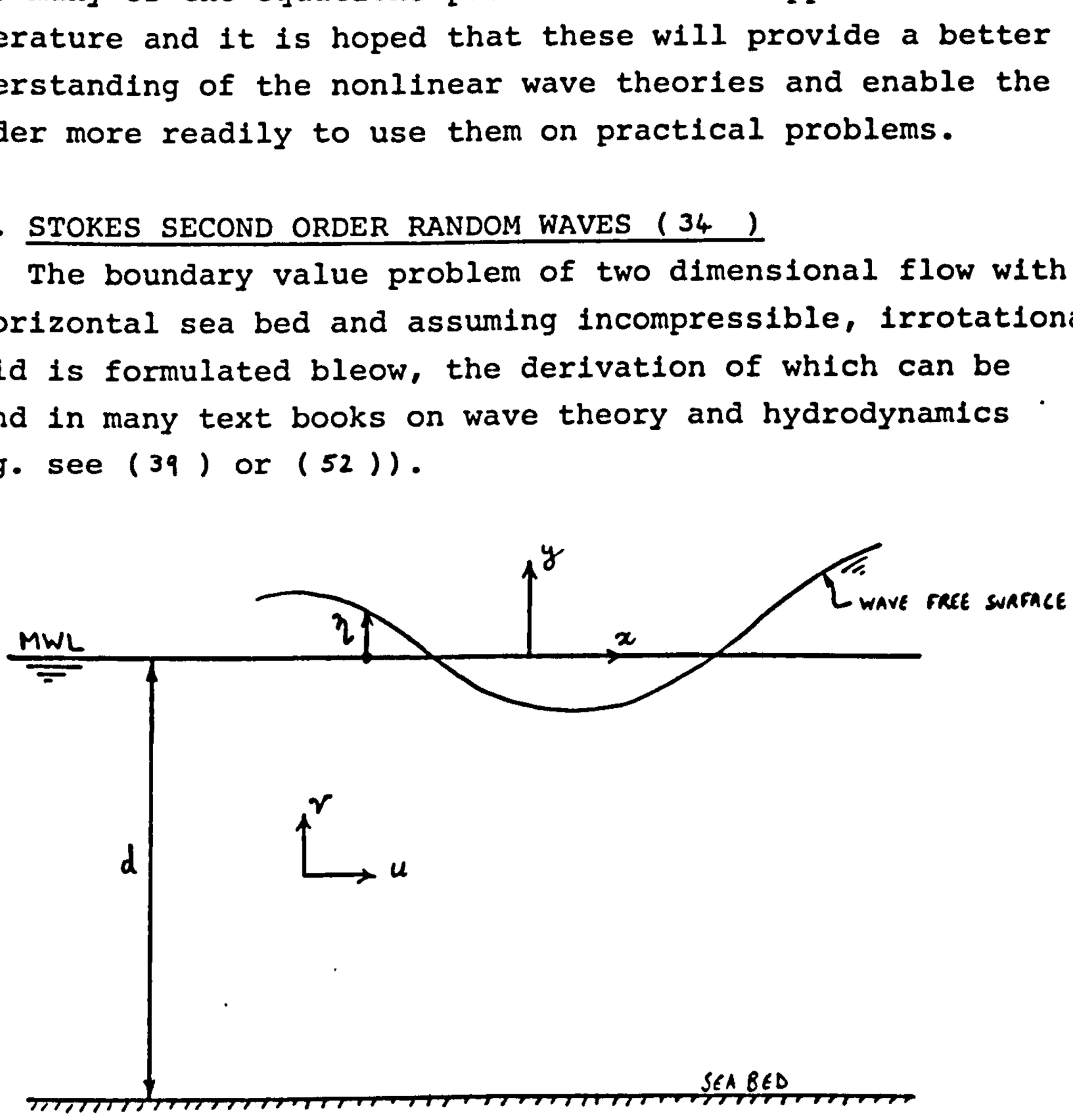

FIGURE A.1. Coordinate System, Definition Sketch.

The x, y coordinate system, fixed at the still water level, is defined as shown and the following terminology will be used.

d = mean water depth

$\eta(x,t)$ = free surface elevation

$\phi(x,y,t)$ = velocity potential of flow field

$u = \frac{\partial \phi}{\partial x}$
= horizontal fluid particle velocity

$v = \frac{\partial \phi}{\partial y}$
= vertical fluid particle velocity

The differential equation to be solved is Laplace's equation of continuity

$$\frac{\partial^2 \phi}{\partial x^2} + \frac{\partial^2 \phi}{\partial y^2} = 0 \qquad \text{(A.1.1)}$$

The boundary condition to be satisfied at the sea bed is that of zero vertical particle velocity

$$v = \frac{\partial \phi}{\partial y}\bigg|_{y=-d} = 0 \qquad \text{(A.1.2)}$$

The kinematic free surface boundary condition (KFSBC) states that a particle on the free surface always remains on the surface, i.e. a particle on the surface at time t_1 with y-coordinate $y_1 = \eta_1$ will have a y-coordinate $y_2 = \eta_2$ at time t_2 and will not move to say y_x below the surface elevation as shown below.

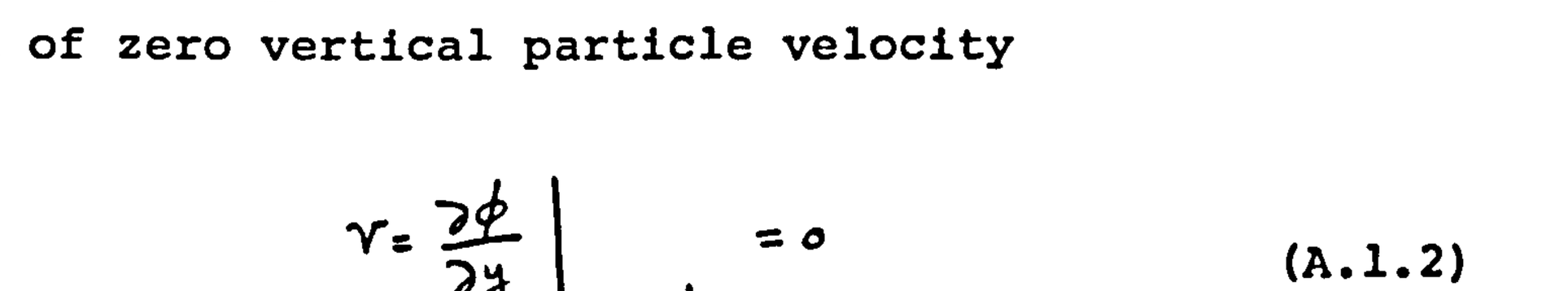

Thus $\frac{d}{dt}(y-\eta)=0$, at $y=\eta$

but

$$\frac{dy}{dt}=v$$

hence

$$\frac{d\eta(x,t)}{dt}=\frac{\partial\eta}{\partial t}+u\frac{\partial\eta}{\partial x}$$

The KFSBC can then be written as

$$\frac{\partial\eta}{\partial t}+\frac{\partial\phi}{\partial x}\cdot\frac{\partial\eta}{\partial x}-\frac{\partial\phi}{\partial y}=0 \quad , \text{ AT } y=\eta \qquad \text{(A.1.3)}$$

The dynamic free surface boundary condition (DFSBC), assuming zero air pressure, is given by Bernoulli's equation as

$$\frac{\partial\phi}{\partial t}+\frac{1}{2}(u^2+v^2)+g\eta = \text{an arbitrary constant usually set to zero} \qquad \text{(A.1.4)}$$

This can be written as

$$\eta=-\frac{1}{g}\left[\frac{\partial\phi}{\partial t}+\frac{1}{2}\left(\frac{\partial\phi}{\partial x}\right)^2+\frac{1}{2}\left(\frac{\partial\phi}{\partial y}\right)^2\right] \quad , \text{ AT } y=\eta \qquad \text{(A.1.5)}$$

Differentiating (A.1.5) with respect to t and x gives

$$\frac{\partial\eta}{\partial t}=-\frac{1}{g}\left[\frac{\partial^2\phi}{\partial t^2}+\frac{1}{2}\frac{\partial}{\partial t}\left(\frac{\partial\phi}{\partial x}\right)^2+\frac{1}{2}\left(\frac{\partial\phi}{\partial y}\right)^2\right] , \text{ AT } y=\eta \qquad \text{(A.1.6)}$$

$$\frac{\partial\eta}{\partial x}=-\frac{1}{g}\left[\frac{\partial^2\phi}{\partial x\partial t}+\frac{1}{2}\frac{\partial}{\partial x}\left(\frac{\partial\phi}{\partial x}\right)^2+\frac{1}{2}\frac{\partial}{\partial x}\left(\frac{\partial\phi}{\partial y}\right)^2\right], \text{ AT } y=\eta \qquad \text{(A.1.7)}$$

Substituting for $\frac{\partial\eta}{\partial t}$ and $\frac{\partial\eta}{\partial x}$ in equation (A.1.3) and multiplying both sides by (-g) gives

$$\frac{\partial^2\phi}{\partial t^2} + g\frac{\partial\phi}{\partial y} + \frac{1}{2}\frac{\partial}{\partial t}\left[\left(\frac{\partial\phi}{\partial x}\right)^2 + \left(\frac{\partial\phi}{\partial y}\right)^2\right] + \frac{1}{2}\frac{\partial\phi}{\partial x}\cdot\frac{\partial}{\partial x}\left[\left(\frac{\partial\phi}{\partial x}\right)^2 + \left(\frac{\partial\phi}{\partial y}\right)^2\right] + \frac{\partial\phi}{\partial x}\cdot\frac{\partial^2\phi}{\partial x\,\partial t} = 0 \quad , \text{AT } y=\eta \tag{A.1.8}$$

now

$$\frac{\partial}{\partial t}\left(\frac{\partial\phi}{\partial x}\right)^2 = \frac{\partial u^2}{\partial t} = 2u\cdot\frac{\partial u}{\partial t} = 2\frac{\partial\phi}{\partial x}\cdot\frac{\partial^2\phi}{\partial x\,\partial t} \tag{A.1.9}$$

similarly

$$\frac{\partial}{\partial t}\left(\frac{\partial\phi}{\partial y}\right)^2 = 2\frac{\partial\phi}{\partial y}\cdot\frac{\partial^2\phi}{\partial y\,\partial t} \tag{A.1.10}$$

Adding (A.1.9) and (A.1.10) gives

$$\frac{\partial}{\partial t}\left[\left(\frac{\partial\phi}{\partial x}\right)^2 + \left(\frac{\partial\phi}{\partial y}\right)^2\right] = 2\left[\frac{\partial\phi}{\partial x}\cdot\frac{\partial^2\phi}{\partial x\,\partial t} + \frac{\partial\phi}{\partial y}\cdot\frac{\partial^2\phi}{\partial y\,\partial t}\right] \tag{A.1.11}$$

As η is a function of x and t only, differentiating (A.1.5) with respect to y gives

$$\frac{\partial\eta}{\partial y} = -\frac{1}{g}\left[\frac{\partial^2\phi}{\partial y\,\partial t} + \frac{1}{2}\frac{\partial}{\partial y}\left(\frac{\partial\phi}{\partial x}\right)^2 + \frac{1}{2}\frac{\partial}{\partial y}\left(\frac{\partial\phi}{\partial y}\right)^2\right] = 0, \text{ AT } y=\eta \tag{A.1.12}$$

$$\frac{\partial^2\phi}{\partial y\,\partial t} = -\frac{1}{2}\frac{\partial}{\partial y}\left[\left(\frac{\partial\phi}{\partial x}\right)^2 + \left(\frac{\partial\phi}{\partial y}\right)^2\right] \quad , \text{AT } y=\eta \tag{A.1.13}$$

Substituting (A.1.13) into (A.1.11) gives

$$\frac{\partial\phi}{\partial x}\cdot\frac{\partial^2\phi}{\partial x\,\partial t} = \frac{1}{2}\frac{\partial}{\partial t}\left[\left(\frac{\partial\phi}{\partial x}\right)^2 + \left(\frac{\partial\phi}{\partial y}\right)^2\right] + \frac{1}{2}\frac{\partial\phi}{\partial y}\cdot\frac{\partial}{\partial y}\left[\left(\frac{\partial\phi}{\partial x}\right)^2 + \left(\frac{\partial\phi}{\partial y}\right)^2\right], \text{ AT } y=\eta \tag{A.1.14}$$

Substituting from (A.1.14) into the last term of (A.1.8) yields

$$\frac{\partial^2\phi}{\partial t^2} + g\frac{\partial\phi}{\partial y} + \left[\frac{\partial}{\partial t} + \frac{1}{2}\frac{\partial\phi}{\partial x}\cdot\frac{\partial}{\partial x} + \frac{1}{2}\frac{\partial\phi}{\partial y}\cdot\frac{\partial}{\partial y}\right] \times$$

$$\left[\left(\frac{\partial\phi}{\partial x}\right)^2 + \left(\frac{\partial\phi}{\partial y}\right)^2\right] = 0 \text{ , AT } y=\eta \qquad \text{(A.1.15)}$$

If $f(y)=0$ at $y=\eta$, using a Taylor series expansion we have

$$f(y) + \eta\frac{\partial f}{\partial y} + \frac{1}{2!}\eta^2\frac{\partial^2 f}{\partial y^2} + \cdots = 0 \text{ , AT } y=0 \qquad \text{(A.1.16)}$$

Assume a perturbation solution for the nonlinear potential ϕ and wave profile η

$$\phi = \varepsilon\phi_1 + \varepsilon^2\phi_2 + \varepsilon^3\phi_3 + \cdots \qquad \text{(A.1.17)}$$

$$\eta = \varepsilon\eta_1 + \varepsilon^2\eta_2 + \varepsilon^3\eta_3 + \cdots \qquad \text{(A.1.18)}$$

where ε is a perturbation parameter.

Applying (A.1.16) to (A.1.15) we have

$$\frac{\partial^2\phi}{\partial t^2} + g\frac{\partial\phi}{\partial y} + \left[\frac{\partial}{\partial t} + \frac{1}{2}\frac{\partial\phi}{\partial x}\cdot\frac{\partial}{\partial x} + \frac{1}{2}\frac{\partial\phi}{\partial y}\cdot\frac{\partial}{\partial y}\right]\left[\left(\frac{\partial\phi}{\partial x}\right)^2 + \left(\frac{\partial\phi}{\partial y}\right)^2\right] +$$

$$\eta\frac{\partial}{\partial y}\left\{\frac{\partial^2\phi}{\partial t^2} + g\frac{\partial\phi}{\partial y} + \left[\frac{\partial}{\partial t} + \frac{1}{2}\frac{\partial\phi}{\partial x}\cdot\frac{\partial}{\partial x} + \frac{1}{2}\frac{\partial\phi}{\partial y}\cdot\frac{\partial}{\partial y}\right]\left[\left(\frac{\partial\phi}{\partial x}\right)^2 + \left(\frac{\partial\phi}{\partial y}\right)^2\right]\right\} + \cdots = 0 \text{ ,}$$

AT $y=0$ (A.1.19)

Substituting for ϕ and η from (A.1.17) and (A.1.18) into (A.1.19) and neglecting third and higher order terms (i.e. including ε and ε^2 terms only) we have

$$\varepsilon\frac{\partial^2\phi_1}{\partial t^2}+\varepsilon^2\frac{\partial^2\phi_2}{\partial t^2}+g\varepsilon\frac{\partial\phi_1}{\partial y}+g\varepsilon^2\frac{\partial\phi_2}{\partial y}+\left[\frac{\partial}{\partial t}+\frac{1}{2}\left(\varepsilon\frac{\partial\phi_1}{\partial x}+\varepsilon^2\frac{\partial\phi_2}{\partial x}\right)\frac{\partial}{\partial x}+\frac{1}{2}\left(\varepsilon\frac{\partial\phi_1}{\partial y}+\varepsilon^2\frac{\partial\phi_2}{\partial y}\right)\frac{\partial}{\partial y}\right]\cdot\left[\varepsilon^2\left(\frac{\partial\phi_1}{\partial x}\right)^2+\varepsilon^2\left(\frac{\partial\phi_1}{\partial y}\right)^2\right]+\left(\varepsilon\eta_1+\varepsilon^2\eta_2\right)\frac{\partial}{\partial y}\left\{\varepsilon\frac{\partial^2\phi_1}{\partial t^2}+\varepsilon^2\frac{\partial^2\phi_2}{\partial t^2}+g\varepsilon\frac{\partial\phi_1}{\partial y}+g\varepsilon^2\frac{\partial\phi_2}{\partial y}+\left[\frac{\partial}{\partial t}+\frac{1}{2}\left(\varepsilon\frac{\partial\phi_1}{\partial x}+\varepsilon^2\frac{\partial\phi_2}{\partial x}\right)\frac{\partial}{\partial x}+\frac{1}{2}\left(\varepsilon\frac{\partial\phi_1}{\partial y}+\varepsilon^2\frac{\partial\phi_2}{\partial y}\right)\frac{\partial}{\partial y}\right]\left[\varepsilon^2\left(\frac{\partial\phi_1}{\partial x}\right)^2+\varepsilon^2\left(\frac{\partial\phi_1}{\partial y}\right)^2\right]\right\}+\cdots\cdots=0,$$

AT $y=0$

(A.1.20)

Multiplying throughout and retaining terms of up to second order only and equating the equal powers of ε we get

ε:

$$\frac{\partial^2\phi_1}{\partial t^2}+g\frac{\partial\phi_1}{\partial y}=0$$

which is the result of linear wave theory, and

ε^2:

$$\frac{\partial^2\phi_2}{\partial t^2}+g\frac{\partial\phi_2}{\partial y}=-\eta_1\frac{\partial}{\partial y}\left[\frac{\partial^2\phi_1}{\partial t^2}+g\frac{\partial\phi_1}{\partial y}\right]-\frac{\partial}{\partial t}\left[\left(\frac{\partial\phi_1}{\partial x}\right)^2+\left(\frac{\partial\phi_1}{\partial y}\right)^2\right] \qquad \text{(A.1.21)}$$

Similarly (A.1.5) gives

$$\eta_2=-\frac{1}{g}\left[\frac{\partial\phi_2}{\partial t}+\eta_1\frac{\partial^2\phi_1}{\partial y\partial t}+\frac{1}{2}\left(\frac{\partial\phi_1}{\partial x}\right)^2+\frac{1}{2}\left(\frac{\partial\phi_1}{\partial y}\right)^2\right] \qquad \text{(A.1.22)}$$

Euqations (A.1.21) and (A.1.22) express ϕ_2 and η_2 directly in terms of ϕ_1 and η_1 which are the results of linear wave theory, also ϕ_1 and η_1 have exact

solutions therefore ε can be set equal to unity.

RANDOM NONLINEAR WAVES

The boundary value problem presented above was originally developed for a single wave. Since the fluid is inviscid, the potential for the superposition of N-coplanar waves representing a random sea is given by the sum of the separate potentials.

$$\phi = \sum_{m=1}^{N} \phi_{(m)}$$

where from linear wave theory

$$\phi_1 = \sum_{m=1}^{N} \phi_{(m)} = \sum_{m=1}^{N} g \frac{a_m \cdot \cosh[k_m(d+y)]}{\omega_m \cdot \cosh(k_m d)} \cdot \sin(k_m \cdot x - \omega_m \cdot t - \psi_m) \qquad \text{(A.1.23)}$$

where

a_m = amplitude of m^{th} wave component

$$= \sqrt{2 S_{\eta\eta}(\omega_m)\, d\omega_m} \quad , m=1,2,\ldots,\infty$$

$S_{\eta\eta}(\omega_m)$ = power spectral density of wave surface elevation

k_m = m^{th} wave number

ω_m = frequency of m^{th} wave component

$d\omega_m$ = width of spectral element

ψ_m = m^{th} random phase angle, uniformly distributed between 0 and 2π

For linear waves $\eta = -\frac{1}{g}\frac{\partial \phi}{\partial t}$ therefore we can write

$$\eta = \sum_{m=1}^{N} \eta_{(m)}$$

where for linear waves

$$\eta_1 = \sum_{m=1}^{N} \eta_{(m)} = \sum_{m=1}^{N} a_m \cos(k_m \cdot x - \omega_m \cdot t - \psi_m) \qquad \text{(A.1.24)}$$

Similarly since fluid particle velocities and accelerations are also linear derivatives of ϕ , they can be superposed.

Substituting for η_1 and ϕ_1 into (A.1.21) and (A.1.22), after some algebraic manipulation gives

$$\phi_2 = \sum_{m=1}^{N}\sum_{n=1}^{N} a_m a_n A_{mn} \frac{\cosh[(k_m+k_n)(d+z)]}{\cosh[(k_m+k_n)d]} \sin(\alpha^+) + \sum_{m=1}^{N}\sum_{n=1}^{N} a_m a_n B_{mn} \frac{\cosh[(k_m-k_n)(d+z)]}{\cosh[(k_m-k_n)d]} \sin(\alpha^-)$$

(A.1.25)

$$\eta_2 = \sum_{m=1}^{N}\sum_{n=1}^{N} a_m a_n C_{mn} \cos(\alpha^+) + \sum_{m=1}^{N}\sum_{n=1}^{N} a_m a_n D_{mn} \cos(\alpha^-)$$

(A.1.26)

$$A_{mn} = \frac{2(\omega_m+\omega_n)(g^2 k_m k_n - \omega_m^2\omega_n^2) + \omega_m(k_n^2 g^2 - \omega_n^4) + \omega_n(k_m^2 g^2 - \omega_m^4)}{4\omega_m\omega_n\{(\omega_m+\omega_n)^2 - g(k_m+k_n)\tanh[(k_m+k_n)d]\}}$$

(A.1.27)

$$B_{mn} = \frac{2(\omega_m - \omega_n)(g^2 k_m k_n + \omega_m^2 \omega_n^2) + \omega_m(\omega_n^4 - k_n^2 g^2) - \omega_n(\omega_m^4 - k_m^2 g^2)}{4\omega_m \omega_n \left\{(\omega_m - \omega_n)^2 - g(k_m - k_n)\tanh[(k_m - k_n)d]\right\}} \qquad \text{(A.1.28)}$$

$$C_{mn} = \left[4\omega_m \omega_n A_{mn}(\omega_m + \omega_n) - g^2 k_m k_n + \omega_m^2 \omega_n^2 + \omega_m \omega_n(\omega_m^2 + \omega_n^2)\right] / 4g\omega_m \omega_n$$

(A.1.29)

$$D_{mn} = \left[4\omega_m \omega_n B_{mn}(\omega_m - \omega_n) - g^2 k_m k_n - \omega_m^2 \omega_n^2 + \omega_m \omega_n(\omega_m^2 + \omega_n^2)\right] / 4g\omega_m \omega_n$$

(A.1.30)

$$\alpha^+ = (k_m + k_n)x - (\omega_m + \omega_n)t - (\psi_m + \psi_n)$$

(A.1.31)

$$\alpha^- = (k_m - k_n)x - (\omega_m - \omega_n)t - (\psi_m - \psi_n)$$

(A.1.32)

Note that in the above expressions some symmetrizations are made for computational convenience, e.g. $\sum_m \sum_n f_m^2 f_n = \sum_m \sum_n \frac{1}{2} f_m f_n (f_m + f_n)$

$$\left.\begin{aligned} A_{mn} &= A_{nm} \\ B_{mn} &= -B_{nm} \\ C_{mn} &= C_{nm} \\ D_{mn} &= D_{nm} \end{aligned}\right\} \qquad \text{(A.1.33)}$$

The particle velocity and acceleration terms up to second order can now be written as

$$u = \sum_{m=1}^{N} g \frac{a_m k_m \cosh[k_m(d+y)]}{\omega_m \cosh(k_m d)} \cos(k_m x - \omega_m t - \psi_m) +$$

$$\sum_{m=1}^{N}\sum_{n=1}^{N} a_m a_n A_{mn}(k_m + k_n) \frac{\cosh[(k_m+k_n)(d+y)]}{\cosh[(k_m+k_n)d]} \cos(\alpha^+) +$$

$$\sum_{m=1}^{N}\sum_{n=1}^{N} a_m a_n B_{mn}(k_m - k_n) \frac{\cosh[(k_m-k_n)(d+y)]}{\cosh[(k_m-k_n)d]} \cos(\alpha^-)$$

(A.1.34)

$$v = \sum_{n=1}^{N} g \frac{a_m k_m \sinh[k_m(d+y)]}{\cosh(k_m d) \cdot \omega_m} \sin(k_m x - \omega_m t - \psi_m) +$$

$$\sum_{m=1}^{N}\sum_{n=1}^{N} a_m a_n (k_m + k_n) \frac{\sinh[(k_m+k_n)(d+y)]}{\cosh[(k_m+k_n)d]} \sin(\alpha^+) +$$

$$\sum_{m=1}^{N}\sum_{n=1}^{N} a_m a_n (k_m - k_n) \frac{\sinh[(k_m-k_n)(d+y)]}{\cosh[(k_m-k_n)d]} \sin(\alpha^-)$$

(A.1.35)

$$\dot{u} = \sum_{m=1}^{N} g a_m k_m \frac{\cosh[k_m(d+y)]}{\cosh(k_m d)} \sin(k_m x - \omega_m t - \psi_m) +$$

$$\sum_{m=1}^{N}\sum_{n=1}^{N} a_m a_n A_{mn} \frac{(k_m+k_n)\cosh[(k_m+k_n)(d+y)]}{\cosh[(k_m+k_n)d](\omega_m+\omega_n)} \sin(\alpha^+) +$$

$$\sum_{m=1}^{N}\sum_{n=1}^{N} a_m a_n B_{mn} \frac{(k_m-k_n)\cosh[(k_m-k_n)(d+y)]}{\cosh[(k_m-k_n)d](\omega_m-\omega_n)} \sin(\alpha^-)$$

(A.1.36)

$$\dot{v} = -\sum_{m=1}^{N} g\, a_m k_m \frac{\sinh[k_m(d+y)]}{\cosh(k_m d)} \cos(k_m x - \omega_m t - \psi_m) -$$

$$\sum_{m=1}^{N}\sum_{n=1}^{N} a_m a_n \frac{(k_m+k_n)\sinh[(k_m+k_n)(d+y)]}{(\omega_m+\omega_n)\cosh[(k_m+k_n)d]} \cos(\alpha^{+}) -$$

$$\sum_{m=1}^{N}\sum_{n=1}^{N} a_m a_n \frac{(k_m-k_n)\sinh(k_m-k_n)(d+y)}{(\omega_m-\omega_n)\cosh[(k_m-k_n)d]} \cos(\alpha^{-}) \qquad \text{(A.1.37)}$$

A.2 STOKES FIFTH ORDER WAVE THEORY (77)

The development of the fifth order wave theory by Skjelbreia and Hendrickson(1960) required a prodigious degree of algebraic manipulation which in the early days inevitably lead to errors. This section represents a summary of a detailed derivation by the author of the fifth order wave theory which is used in this thesis.

A convenient starting point is the simpler second order waves discussed in the previous section. Assuming that the coordinate system x, y in Figure A.1. moves with the wave under its crest, and with velocity $\bar{c}$ (wave celerity $= L/T$), the time dependent terms in the boundary conditions will vanish. Thus the free surface boundary conditions can be written as (c.f. A.1.3 and A.1.4).

$$\frac{\partial \eta}{\partial x} = \frac{v}{u-\bar{c}} \quad , \text{AT } y = \eta \qquad \text{(A.2.1)}$$

$$(u-\bar{c})^2 + v^2 = -2g(Q+\eta) + \bar{c}^2 \quad , \text{AT } y = \eta \qquad \text{(A.2.2)}$$

where Q is a new constant in Bernoulli's equation.

Following a perturbation technique discussed in the previous section, a solution up to the fifth order can be given. Thus for the potential

$$\frac{k\phi}{c} = (\lambda A_{11} + \lambda^3 A_{13} + \lambda^5 A_{15}) \cosh[k(d+y)] \sin\theta +$$

$$(\lambda^2 A_{22} + \lambda^4 A_{24}) \cosh[2k(d+y)] \sin 2\theta +$$

$$(\lambda^3 A_{33} + \lambda^5 A_{35}) \cosh[3k(d+y)] \sin 3\theta +$$

$$\lambda^4 A_{44} \cosh[4k(d+y)] \sin 4\theta +$$

$$\lambda^5 A_{55} \cosh[5k(d+y)] \sin 5\theta$$

(A.2.3)

and for the wave profile

$$k\eta = \lambda \cos\theta + (\lambda^2 B_{22} + \lambda^4 B_{24}) \cos 2\theta +$$

$$(\lambda^3 B_{33} + \lambda^5 B_{35}) \cos 3\theta +$$

$$\lambda^4 B_{44} \cos 4\theta +$$

$$\lambda^5 B_{55} \cos 5\theta$$

(A.2.4)

$$kQ = \lambda^2 . C_3 + \lambda^4 . C_4 \qquad \text{(A.2.5)}$$

$$k\bar{c}^2 = C_0^2 \left(1 + \lambda^2 . C_1 + \lambda^4 . C_2\right) \qquad \text{(A.2.6)}$$

where

θ = phase angle = $2\pi . \frac{x}{L}$

k = wave number = $\frac{2\pi}{L}$

L = wave length

λ = parameter to be determined

Coefficients A_{ij} , B_{ij} and C_i are obtained as follows:

1. Find $\frac{u-\bar{c}}{\bar{c}}$ and $\frac{v}{\bar{c}}$ from (A.2.3) and $k\frac{\partial \eta}{\partial x}$ from (A.2.4)

2. Substitute these into (A.2.1) and (A.2.2) including terms up to fifth order (i.e. up to λ^5).

3. Expand (A.2.1) and (A.2.2) about $y = o$ using a Taylor series up to fifth order terms.

4. Group the resulting equations in powers of λ and subgroup them according to powers of $\sin\theta$ or $\cos\theta$ on the left hand side of the equation.

5. The equations must hold for any value of θ , thus terms in each subgroup are set to zero and coefficients are obtained by solving the resulting equations.

Taking $s = \sinh(kd)$ and $c = \cosh(kd)$ we get

$$C_o^2 = g \tanh(kd) \qquad \text{(A.2.7)}$$

$$A_{11} = \frac{1}{s} \qquad \text{(A.2.8)}$$

$$A_{13} = \frac{-c^2(5c^2+1)}{8s^5} \qquad \text{(A.2.9)}$$

$$A_{15} = \frac{-(1184c^{10} - 1440c^8 - 1992c^6 + 2641c^4 - 249c^2 + 18)}{1536\, s^{11}} \qquad \text{(A.2.10)}$$

$$A_{22} = \frac{3}{8s^4} \qquad \text{(A.2.11)}$$

$$A_{24} = \frac{(192c^8 - 424c^6 - 312c^4 + 480c^2 - 17)}{768\, s^{10}} \qquad \text{(A.2.12)}$$

$$A_{33} = \frac{(13 - 4c^2)}{64 s^7} \qquad \text{(A.2.13)}$$

$$A_{35} = \frac{(512c^{12} + 4224c^{10} - 6800c^8 - 12808c^6 + 16704c^4 - 3154c^2 + 107)}{4096\, s^{13}\,(6c^2 - 1)} \qquad \text{(A.2.14)}$$

$$A_{44} = \frac{(80c^6 - 816c^4 + 1338c^2 - 197)}{1536\, s^{10}\,(6c^2 - 1)} \qquad \text{(A.2.15)}$$

$$A_{55} = -\left\{ 2880\,c^{10} - 72480\,c^{8} + 324000\,c^{6} - 432000\,c^{4} + 163470\,c^{2} - 16245 \right\} / \left[61440\,s^{11}(6c^{2}-1)(8c^{4}-11c^{2}+3) \right]$$

(A.2.16)

$$B_{22} = \frac{(2c^{2}+1)\,c}{4s^{3}}$$

(A.2.17)

$$B_{24} = \frac{c(272\,c^{8} - 504\,c^{6} - 192\,c^{4} + 322\,c^{2} + 21)}{384\,s^{9}}$$

(A.2.18)

$$B_{33} = \frac{3(8c^{6}+1)}{64\,s^{6}}$$

(A.2.19)

$$B_{35} = \left\{ 88128\,c^{14} - 208224\,c^{12} + 70848\,c^{10} + 54000\,c^{8} - 21816\,c^{6} + 6264\,c^{4} - 54\,c^{2} - 81 \right\} / \left[12288\,s^{12}(6c^{2}-1) \right]$$

(A.2.20)

$$B_{44} = \frac{c(768\,c^{10} - 448\,c^{8} - 48\,c^{6} + 48\,c^{4} + 106\,c^{2} - 21)}{384\,s^{9}(6c^{2}-1)}$$

(A.2.21)

$$B_{55} = \left\{ 192000\,c^{16} - 262720\,c^{14} + 83680\,c^{12} + 20160\,c^{10} - 7260\,c^{8} + 7160\,c^{6} - 1800\,c^{4} - 1050\,c^{2} + 225 \right\} / \left[12288\,s^{10}(6c^{2}-1)(8c^{4}-11c^{2}+3) \right]$$

(A.2.22)

$$C_{1} = \frac{8c^{4} - 8c^{2} + 9}{8\,s^{4}}$$

(A.2.23)

$$C_{2} = \left\{ 3840\,c^{12} - 4096\,c^{10} + 2592\,c^{8} - 1008\,c^{6} + 5944\,c^{4} - 1830\,c^{2} + 147 \right\} / \left[512\,s^{10}(6c^{2}-1) \right]$$

(A.2.24)

$$C_{3} = -\frac{1}{4\,s\,c}$$

(A.2.25)

$$C_4 = \frac{(12\,c^8 + 36\,c^6 - 162\,c^4 + 141\,c^2 - 27)}{192\,c.s^9} \qquad (A.2.26)$$

Now to find λ and (kd) we can write wave height,

$$H = \zeta\big|_{\theta=0} - \zeta\big|_{\theta=\pi}$$

and using (A.2.4) gives

$$F_1 = -\tfrac{1}{2}\left(\frac{H}{d}\right) + \frac{1}{(kd)}\left\{\lambda + \lambda^3 . B_{33} + \lambda^5 (B_{35} + B_{55})\right\} = 0 \qquad (A.2.27)$$

Multiplying both sides of (A.2.26) by $\left(\frac{kd}{g}\right)$ and substituting for C_0^2 from (A.2.7) gives

$$F_2 = -\left(\frac{\omega^2 d}{g}\right) + (kd)\tanh(kd)\left\{1 + \lambda^2 . C_1 + \lambda^4 . C_2\right\} = 0 \qquad (A.2.27)$$

λ and (kd) can now be determined by solving (A.2.27) and (A.2.28) numerically. Using Newton's iterative method (see (13)) we have

$$\lambda_{i+1} = \lambda_i - \left[\frac{F_1 \cdot \frac{\partial F_2}{\partial (kd)} - F_2 \cdot \frac{\partial F_1}{\partial (kd)}}{J(F_1, F_2)}\right]_i \qquad (A.2.29)$$

$$(kd)_{i+1} = (kd)_i - \left[\frac{F_2 \cdot \frac{\partial F_1}{\partial \lambda} - F_1 \cdot \frac{\partial F_2}{\partial \lambda}}{J(F_1, F_2)}\right]_i \qquad (A.2.30)$$

where

$$J(F_1,F_2) = \left[\frac{\partial F_1}{\partial \lambda}\cdot\frac{\partial F_2}{\partial (kd)} - \frac{\partial F_2}{\partial \lambda}\cdot\frac{\partial F_1}{\partial (kd)}\right] \qquad \text{(A.2.31)}$$

and

$$\frac{\partial F_1}{\partial \lambda} = \frac{1}{(kd)}\left\{1 + 3\lambda^2 . B_{33} + 5\lambda^4 (B_{35} + B_{55})\right\} \qquad \text{(A.2.32)}$$

$$\frac{\partial F_2}{\partial \lambda} = (kd)\tanh(kd)\left\{2\lambda . C_1 + 4\lambda^3 . C_2\right\} \qquad \text{(A.2.33)}$$

$$\frac{\partial F_1}{\partial (kd)} = \frac{1}{(kd)}\left\{\lambda^3 B'_{33} + \lambda^5 (B'_{35} + B'_{55})\right\} - \frac{1}{(kd)^2}\left\{\lambda + \lambda^3 . B_{33} + \lambda^5 (B_{35} + B_{55})\right\} \qquad \text{(A.2.34)}$$

$$\frac{\partial F_2}{\partial (kd)} = \left[\tanh(kd) + (kd)\operatorname{sech}^2(kd)\right]\left\{1 + \lambda^2 . C_1 + \lambda^4 . C_2\right\} + (kd)\tanh(kd)\left\{\lambda^2 . C'_1 + \lambda^4 . C'_2\right\} \qquad \text{(A.2.35)}$$

where a dash indicates partial differentiation with respect to (kd)

Taking

$$C_n = \cosh(nkd), \quad n = 2, 3, \ldots \qquad \text{(A.2.36)}$$

$$S_n = \sinh(nkd), \quad n = 2, 3, \ldots \qquad \text{(A.2.37)}$$

We have

$$C_1' = (-4c^5 - c^3 + 5c)/2s^7 \qquad \text{(A.2.38)}$$

$$C_2' = \Big\{ \big[22.5\, s_{12} + 145\, s_{10} + 512\, s_8 + 1098\, s_6 + 4356.5\, s_4 + 5047\, s_2 \big]\, Y_1 \cdot Y_2 - \big[1.875\, c_{12} + 14.5\, c_{10} + 64\, c_8 + 183\, c_6 + 1089.125\, c_4 + 2523.5\, c_2 + 1713 \big] \times \big[(10\, s_{10} - 80\, s_8 + 270\, s_6 - 480\, s_4 + 420\, s_2)\, Y_1 + 6\, s_2 \cdot Y_2 \big] \Big\} / (Y_1 \cdot Y_2)^2$$

(A.2.39)

where

$$Y_1 = 3c_2 + 2 \qquad \text{(A.2.40)}$$

$$Y_2 = c_{10} - 10\, c_8 + 48\, c_6 - 120\, c_4 + 210\, c_2 - 126 \qquad \text{(A.2.41)}$$

$$B_{33}' = \Big\{ 64\, s^6 (4.5\, s_6 + 18\, s_4 + 22.5\, s_2) - (0.75\, c_6 + 4.5\, c_4 + 11.25\, c_2 + 10.5) \times (12\, s_6 - 48\, s_4 + 60\, s_2) \Big\} / 4096\, s^{12} \qquad \text{(A.2.42)}$$

$$B_{35}' = \Big\{ 12288\, s^{12}(6c^2-1) \Big[\frac{7639}{64} s_{14} + \frac{2341}{4} s_{12} - \frac{65745}{64} s_{10} - 7911\, s_8 - \frac{1029781}{64} s_6 - \frac{58887}{4} s_4 - \frac{339957}{64} s_2 \Big] - \Big[\frac{1377}{128} c_{14} + \frac{783}{16} c_{12} - \frac{13149}{128} c_{10} - \frac{7911}{8} c_8 - \frac{342927}{128} c_6 - \frac{58887}{16} c_4 - \frac{339957}{128} c_2 - \frac{7101}{8} \Big] \cdot \big[126\, s_{14} - 1152\, s_{12} + 4590\, s_{10} - 10368\, s_8 + 14454\, s_6 - 12672\, s_4 + 6534\, s_2 \big] \Big\} / \big[12288\, s^{12} (6c^2-1) \big]^2 \qquad \text{(A.2.43)}$$

$$B'_{55} = \Bigg\{ 12288\, s^{10} (6c^2-1)(8c^4-11c^2+3)\Big[\frac{375}{4}s_{16} + \frac{55265}{64}s_{14} + 3540\, s_{12} + \frac{571225}{64}s_{10} + \frac{32385}{2}s_8 + \frac{1544085}{64}s_6 + 28770\, s_4 + \frac{1292765}{64}s_2\Big] -$$

$$\Big[288\, s_{16} - 2562\, s_{14} + 10080\, s_{12} - 23250\, s_{10} + 35520\, s_8 - 39114\, s_6 + 32736\, s_4 - 18810\, s_2\Big]\Big[\frac{375}{64}c_{16} + \frac{7895}{128}c_{14} + 295\, c_{12} + \frac{114245}{128}c_{10} + \frac{32385}{16}c_8 + \frac{514695}{128}c_6 + \frac{14385}{2}c_4 + \frac{1292765}{128}c_2 + \frac{370085}{64}\Big] \Bigg\} /$$

$$\Big[12288\, s^{10}(6c^2-1)(8c^4-11c^2+3)\Big]^2$$

(A.2.44)

Note that in derivation above the following have been used:

$$c^2 = \frac{1}{2}(c_2+1) \qquad \text{(A.2.45)}$$

$$c^4 = \frac{1}{8}c_4 + \frac{1}{2}c_2 + \frac{3}{8} \qquad \text{(A.2.46)}$$

$$c^6 = \frac{1}{32}(c_6 + 6c_4 + 15c_2 + 10) \qquad \text{(A.2.47)}$$

$$c^8 = \frac{1}{128}(c_8 + 8c_6 + 28c_4 + 56c_2 + 35) \qquad \text{(A.2.48)}$$

$$c^{10} = \frac{1}{512}(c_{10} + 10c_8 + 45c_6 + 120c_4 + 210c_2 + 126) \qquad \text{(A.2.49)}$$

$$c^{12} = \frac{1}{2048}\left(C_{12} + 12\,C_{10} + 66\,C_8 + 220\,C_6 + 495\,C_4 + 792\,C_2 + 462 \right)$$

(A.2.50)

$$c^{14} = \frac{1}{8192}\left(C_{14} + 14\,C_{12} + 91\,C_{10} + 364\,C_8 + 1001\,C_6 + 2002\,C_4 + 3003\,C_2 + 1716 \right)$$

(A.2.51)

$$c^{16} = \frac{1}{32768}\left(C_{16} + 16\,C_4 + 120\,C_{12} + 560\,C_{10} + 1820\,C_8 + 4368\,C_6 + 8008\,C_4 + 11440\,C_2 + 6435 \right)$$

(A.2.52)

which have been derived using the following formulae (84)

$$s_n = n.s.c^{n-1} + \binom{n}{3} s^3 . c^{n-3} + \binom{n}{5} s^5 . c^{n-5} + \ldots\ldots$$

$$c_n = c^n + \binom{n}{2} s^2 . c^{n-2} + \binom{n}{4} s^4 . c^{n-4} + \ldots\ldots$$

where

$$\binom{n}{k} = \frac{n!}{(n-k)!\;k!}$$

Therefore by specifying values of $\left(\frac{\omega^2 d}{g}\right)$ and $\left(\frac{H}{d}\right)$ in (A.2.27) and (A.2.28) we can now find (kd) and λ using (A.2.29) to (A.2.44). The starting values for (A.2.29) and (A.2.30) can be the linear deep water approximations, i.e. $(kd)_1 \simeq \frac{\omega^2 d}{g}$ and from (A.2.4), $\lambda_1 = \frac{1}{2} k H \simeq \frac{1}{2}\left(\frac{\omega^2 d}{g}\right)\left(\frac{H}{d}\right)$
Returning to the fixed coordinate system x,y for a wave travelling from left to right we have

$$\eta = d \sum_{n=1}^{5} a_n C_n \left[n(kx - \omega t) \right]$$

(A.2.53)

where

$$a_1 = \lambda / (kd)$$

(A.2.54)

$$a_2 = (\lambda^2 . B_{22} + \lambda^4 . B_{24}) / (kd) \qquad \text{(A.2.55)}$$

$$a_3 = (\lambda^3 . B_{33} + \lambda^5 . B_{35}) / (kd) \qquad \text{(A.2.56)}$$

$$a_4 = \lambda^4 . B_{44} / (kd) \qquad \text{(A.2.57)}$$

$$a_5 = \lambda^5 . B_{55} / (kd) \qquad \text{(A.2.58)}$$

From (A.2.6) and (A.2.7)

$$C^* = \left(\frac{\bar{C}}{\sqrt{gd}}\right)\left[\tanh(kd)(1+\lambda^2 . C_1 + \lambda^4 . C_2)/(kd)\right]^{\frac{1}{2}} \qquad \text{(A.2.59)}$$

Using this and differentiating (A.2.3) with respect to x we arrive at expression for horizontal particle velocity:

$$u = \sqrt{gd} \sum_{n=1}^{5} b_n \cosh[nk(d+y)] . \cos[n(kx-\omega t)] \qquad \text{(A.2.60)}$$

where

$$b_1 = C^* (\lambda . A_{11} + \lambda^3 . A_{13} + \lambda^5 . A_{15}) \qquad \text{(A.2.61)}$$

$$b_2 = 2 C^* (\lambda^2 . A_{22} + \lambda^4 . A_{24}) \qquad \text{(A.2.62)}$$

$$b_3 = 3C^*(\lambda^3 . A_{33} + \lambda^5 . A_{35}) \qquad \text{(A.2.63)}$$

$$b_4 = 4C^* . \lambda^4 . A_{44} \qquad \text{(A.2.64)}$$

$$b_5 = 5C^* . \lambda^5 . A_{55} \qquad \text{(A.2.65)}$$

Similarly the vertical particle velocity is given by

$$v = \sqrt{gd} \sum_{n=1}^{5} b_n \sinh[nk(d+y)] \sin[n(kx-\omega t)] \qquad \text{(A.2.66)}$$

Horizontal particle acceleration,

$$\frac{\partial u}{\partial t} = g \sum_{n=1}^{5} d_n \cosh[nk(d+y)] . \sin[n(kx-\omega t)] \qquad \text{(A.2.67)}$$

vertically,

$$\frac{\partial v}{\partial t} = -g \sum_{n=1}^{5} d_n \sinh[nk(d+y)] . \cos[n(kx-\omega t)] \qquad \text{(A.2.68)}$$

where

$$d_n = n\sqrt{\frac{\omega^2 d}{g}} . b_n \qquad \text{(A.2.69)}$$

Global acceleration terms can be written as

$$\frac{Du}{Dt} = \frac{\partial u}{\partial t} + u\frac{\partial u}{\partial x} + v\frac{\partial u}{\partial y}$$

$$\frac{Dv}{Dt} = \frac{\partial v}{\partial t} + u\frac{\partial v}{\partial x} + v\frac{\partial v}{\partial y}$$

$$\frac{\partial u}{\partial x} = -k\sqrt{gd} \sum_{n=1}^{5} n b_n \cosh[nk(d+y)] \sin[n(kx-\omega t)]$$

(A.2.70)

$$\frac{\partial u}{\partial y} = k\sqrt{gd} \sum_{n=1}^{5} n b_n \sinh[nk(d+y)] \cos[n(kx-\omega t)]$$

(A.2.71)

$$\frac{\partial v}{\partial x} = \frac{\partial u}{\partial y} \qquad \text{(A.2.72)}$$

$$\frac{\partial v}{\partial y} = -\frac{\partial u}{\partial x} \qquad \text{(A.2.73)}$$

For deep water or large values of (nkd) , coefficients and b_n , d_n become too small and we can write

$$u = \sqrt{gd} \sum_{n=1}^{5} B_n e^{nky} \cdot \cos[n(kx-\omega t)] \qquad \text{(A.2.74)}$$

$$v = \sqrt{gd} \sum_{n=1}^{5} B_n e^{nky} \cdot \sin[n(kx-\omega t)] \qquad \text{(A.2.75)}$$

where

$$B_n = b_n \cosh(nkd) \qquad \text{(A.2.76)}$$

$$\frac{\partial u}{\partial t} = g \sum_{n=1}^{5} D_n e^{nky} \cdot \sin[n(kx-\omega t)] \qquad \text{(A.2.77)}$$

$$\frac{\partial v}{\partial t} = g \sum_{n=1}^{5} D_n e^{nky} \cdot \cos[n(kx-\omega t)] \qquad \text{(A.2.78)}$$

$$D_n = n\sqrt{\frac{\omega^2 d}{g}} \cdot B_n \qquad \text{(A.2.79)}$$

$$\frac{\partial u}{\partial x} = -k\sqrt{gd} \sum_{n=1}^{5} n B_n e^{nky} \cdot \sin[n(kx-\omega t)] \qquad \text{(A.2.80)}$$

$$\frac{\partial u}{\partial y} = k\sqrt{gd} \sum_{n=1}^{5} n B_n e^{nky} \cdot \cos[n(kx-\omega t)] \qquad \text{(A.2.81)}$$

Equations of this section were implemented in a computer program and coefficients were computed for a range of (H/d) and $(\omega^2 d/g)$ values. Results are presented graphically in Figures A.2 to A.35. Values of (kd) are given in Tables A.1 to A.3. Coefficients b_n for n = 3, 4 and 5 can be found in terms of B_n using (A.2.76). Values of d_n can be found in terms of b_n using (A.2.69). Similarly D_n can be found in terms of B_n using (A.2.79). Coefficients B_4 and B_5 for small values of (H/d) become negligible and are not given.

w2d/g=	1.50	2.00	2.50
H/d			
****			
0.03	1.6209	2.0635	2.5283
0.04	1.6202	2.0620	2.5256
0.05	1.6193	2.0602	2.5221
0.06	1.6182	2.0579	2.5179
0.07	1.6168	2.0552	2.5130
0.08	1.6153	2.0522	2.5074
0.09	1.6136	2.0488	2.5011
0.10	1.6117	2.0450	2.4941
0.11	1.6096	2.0408	2.4866
0.12	1.6074	2.0363	2.4784
0.13	1.6049	2.0315	2.4698
0.14	1.6023	2.0263	2.4606
0.15	1.5994	2.0209	2.4509
0.16	1.5964	2.0151	2.4408
0.17	1.5933	2.0091	2.4303
0.18	1.5900	2.0028	2.4194
0.19	1.5865	1.9962	2.4082
0.20	1.5829	1.9894	2.3967
0.21	1.5791	1.9824	2.3850
0.22	1.5752	1.9752	2.3730
0.23	1.5712	1.9678	2.3609
0.24	1.5670	1.9603	2.3486
0.25	1.5627	1.9526	2.3362
0.26	1.5583	1.9448	2.3237
0.27	1.5538	1.9369	2.3111
0.28	1.5492	1.9288	2.2985
0.29	1.5445	1.9207	2.2858
0.30	1.5397	1.9125	2.2732
0.31	1.5348	1.9042	2.2606
0.32	1.5298	1.8959	2.2480
0.33	1.5248	1.8875	2.2355
0.34	1.5197	1.8791	2.2230
0.35	1.5146	1.8707	2.2107
0.36	1.5094	1.8623	2.1984
0.37	1.5042	1.8539	2.1862
0.38	1.4989	1.8455	2.1741
0.39	1.4936	1.8371	2.1622
0.40	1.4882	1.8288	2.1503
0.41	1.4829	1.8205	2.1386
0.42	1.4775	1.8122	*******
0.43	1.4721	1.8040	*******
0.44	1.4667	1.7958	*******

TABLE A1 .VALUES OF kd.
Stckes 5th Order waves.

H/d	w2d/g= 3.00	3.50	4.00
0.03	3.0085	3.4968	3.9884
0.04	3.0038	3.4894	3.9775
0.05	2.9979	3.4801	3.9637
0.06	2.9908	3.4689	3.9472
0.07	2.9824	3.4559	3.9281
0.08	2.9730	3.4412	3.9067
0.09	2.9624	3.4249	3.8832
0.10	2.9509	3.4072	3.8578
0.11	2.9384	3.3882	3.8308
0.12	2.9251	3.3681	3.8025
0.13	2.9109	3.3470	3.7729
0.14	2.8961	3.3250	3.7425
0.15	2.8806	3.3023	3.7114
0.16	2.8646	3.2790	3.6798
0.17	2.8481	3.2552	3.6478
0.18	2.8311	3.2311	3.6157
0.19	2.8139	3.2067	3.5836
0.20	2.7964	3.1822	3.5515
0.21	2.7786	3.1576	3.5197
0.22	2.7607	3.1331	3.4881
0.23	2.7428	3.1086	3.4569
0.24	2.7247	3.0843	3.4261
0.25	2.7067	3.0601	3.3957
0.26	2.6886	3.0362	3.3659
0.27	2.6707	3.0126	*******
0.28	2.6528	2.9893	*******
0.29	2.6351	2.9662	*******
0.30	2.6175	*******	*******
0.31	2.6001	*******	*******
0.32	2.5828	*******	*******
0.33	2.5658	*******	*******
0.34	2.5490	*******	*******
0.35	*******	*******	*******

TABLE A2 .VALUES OF kd.
Stokes 5th Order Waves.

H/d	w2d/g= 4.50	5.00	5.50
0.03	4.4809	4.9727	5.4634
0.04	4.4654	4.9517	5.4356
0.05	4.4460	4.9253	5.4010
0.06	4.4228	4.8941	5.3602
0.07	4.3962	4.8585	5.3141
0.08	4.3666	4.8191	5.2635
0.09	4.3343	4.7766	5.2093
0.10	4.2997	4.7315	5.1524
0.11	4.2633	4.6844	5.0935
0.12	4.2254	4.6358	5.0334
0.13	4.1863	4.5862	4.9726
0.14	4.1464	4.5361	4.9117
0.15	4.1060	4.4858	4.8511
0.16	4.0653	4.4356	4.7912
0.17	4.0246	4.3857	4.7321
0.18	3.9840	4.3365	4.6742
0.19	3.9438	4.2880	4.6176
0.20	3.9039	4.2404	*******
0.21	3.8647	*******	*******
0.22	3.8260	*******	*******
0.23	3.7881	*******	*******
0.24	*******	*******	*******

TABLE A3 .VALUES OF kd.
Stokes 5th Order Waves.

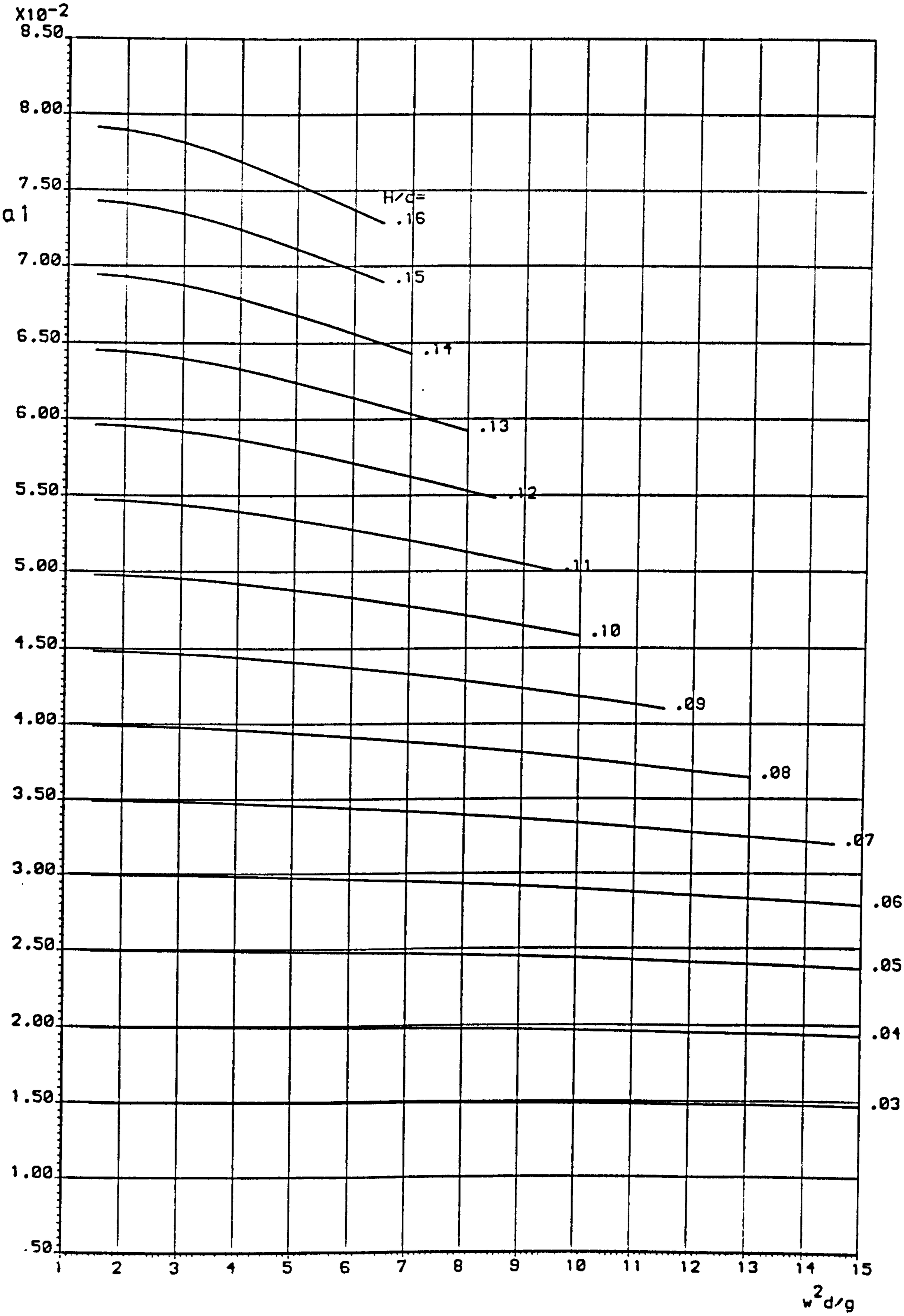

FIG A2 STOKES FIFTH ORDER WAVE COEFFICIENTS

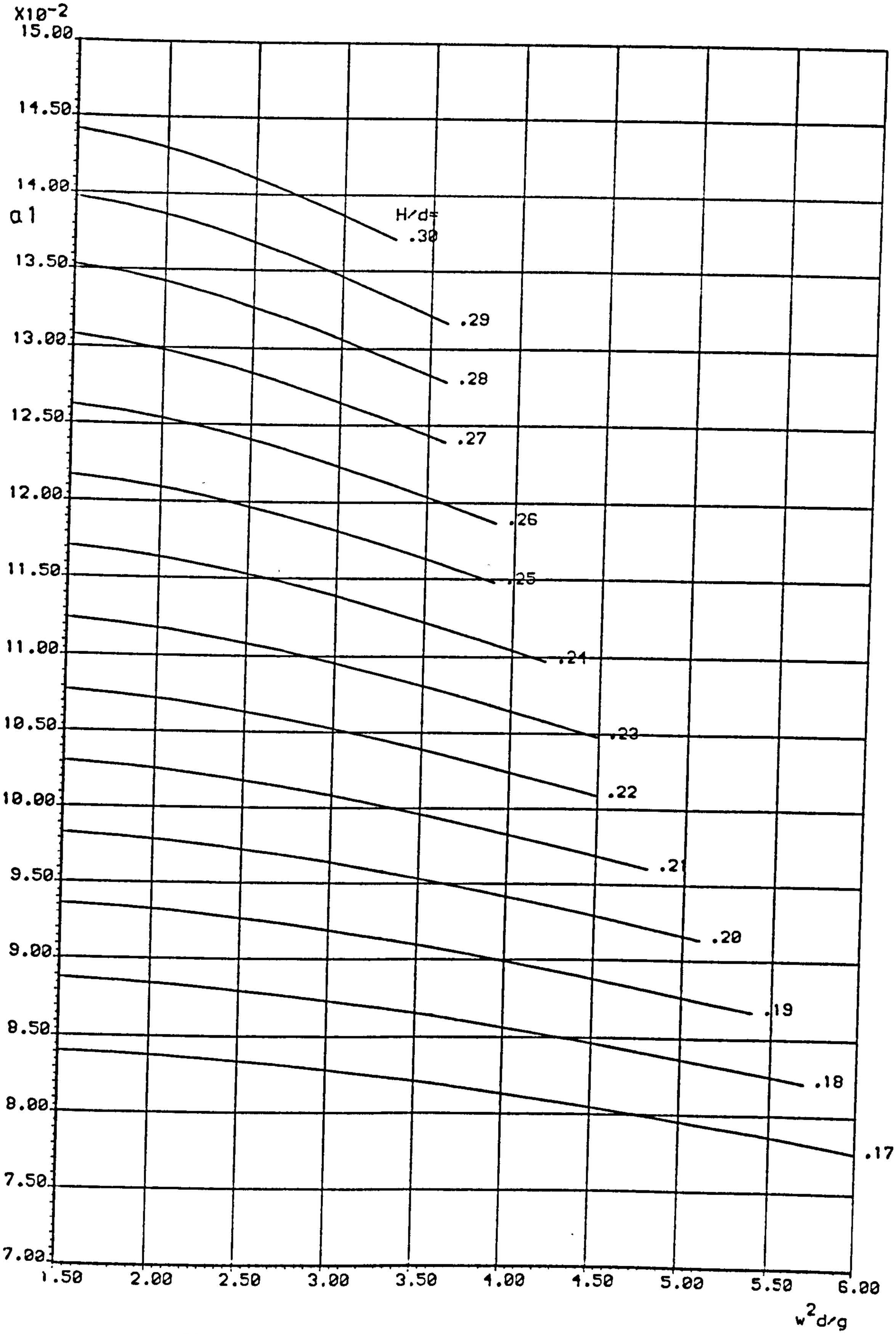

FIG A3 STOKES FIFTH ORDER WAVE COEFFICIENTS

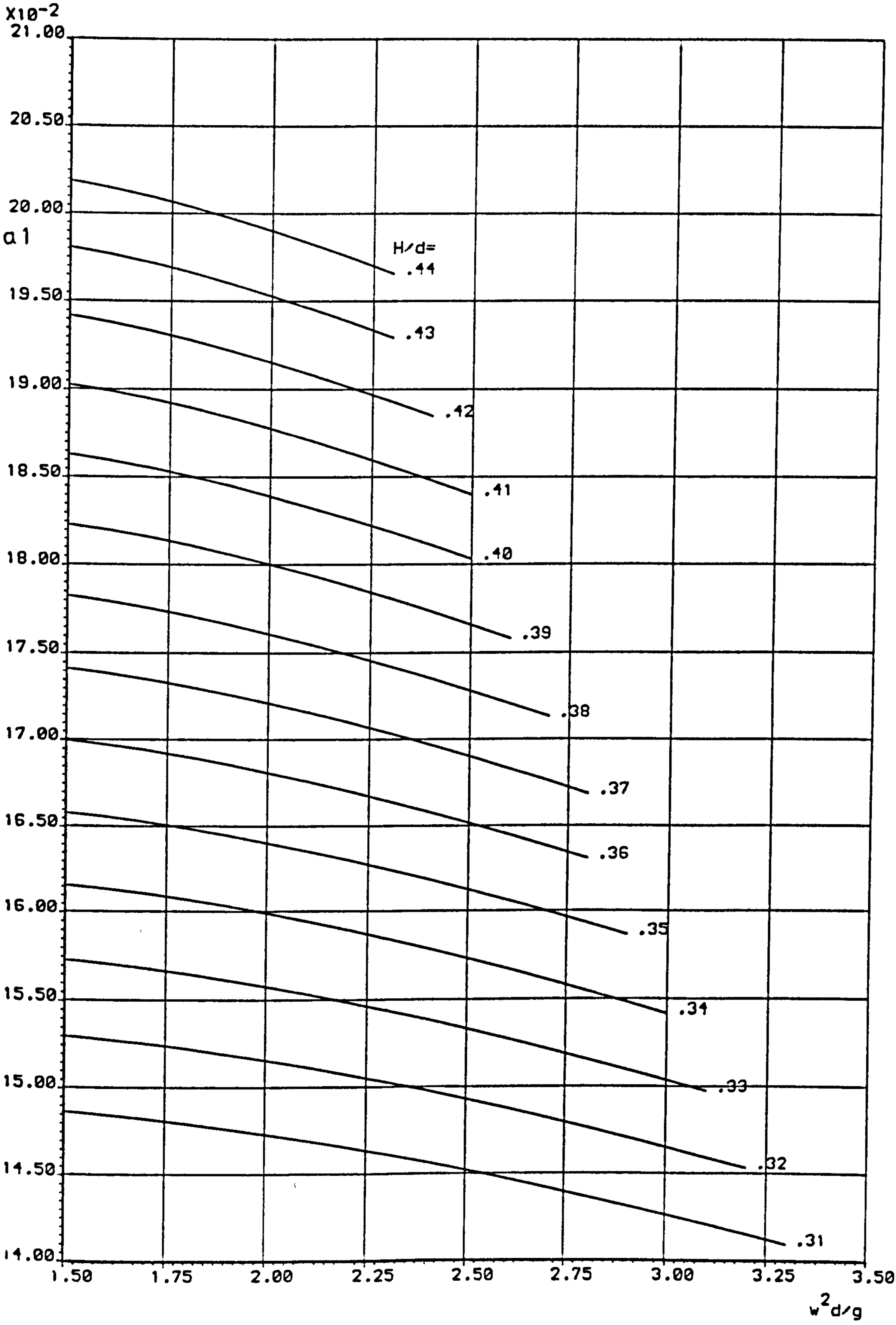

FIG A4 STOKES FIFTH ORDER WAVE COEFFICIENTS

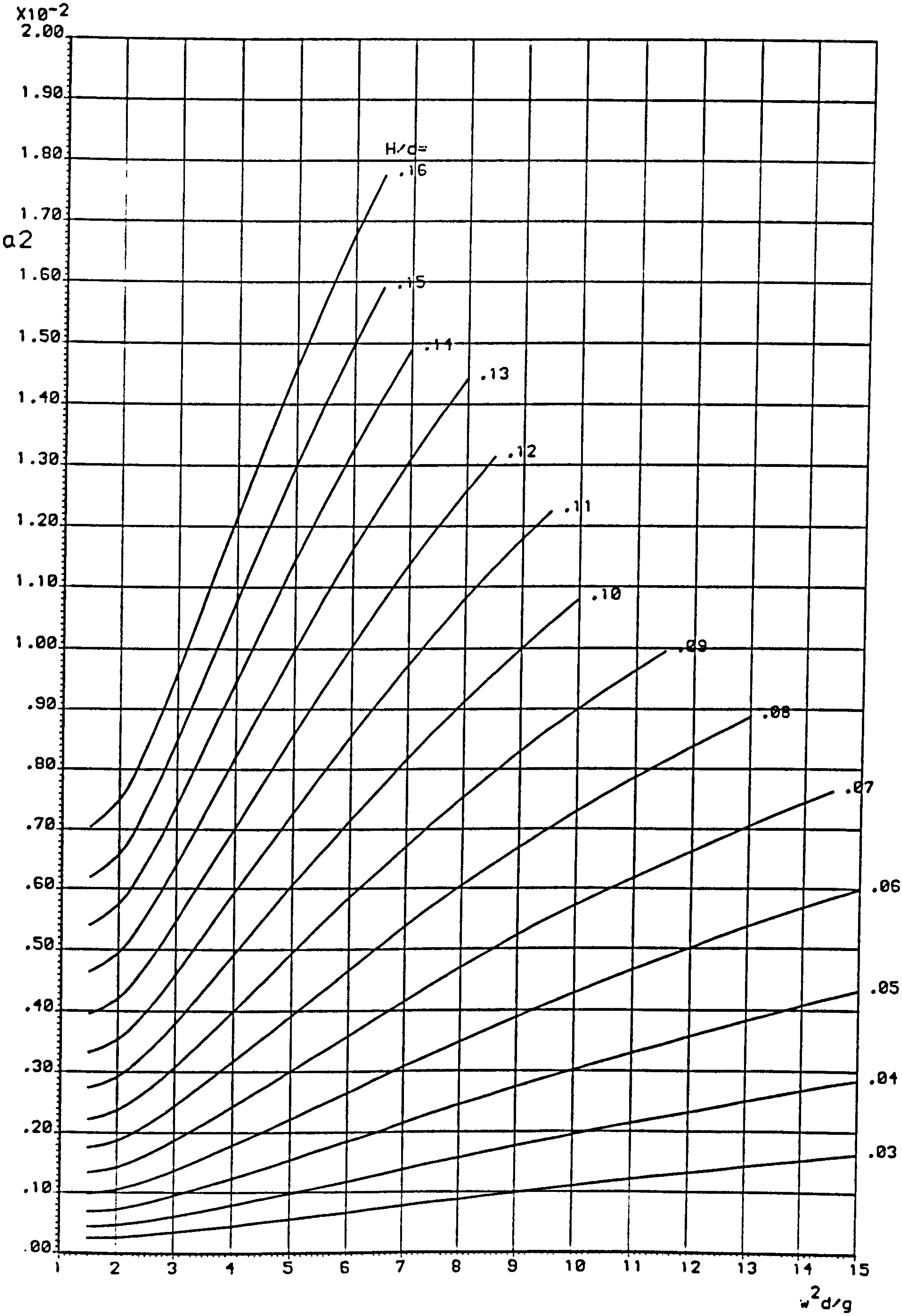

FIG A5 STOKES FIFTH ORDER WAVE COEFFICIENTS

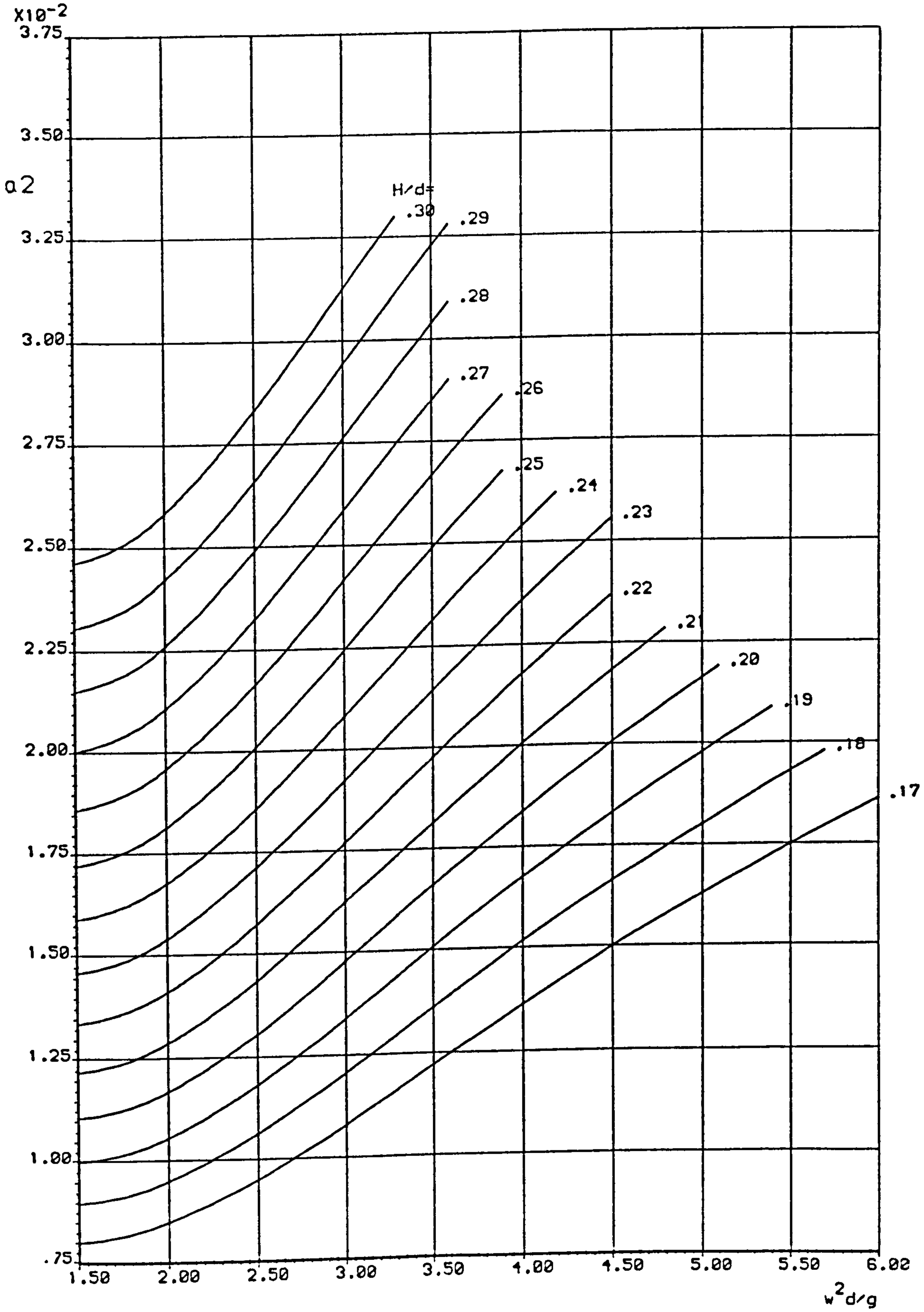

FIG A6 STOKES FIFTH ORDER WAVE COEFFICIENTS

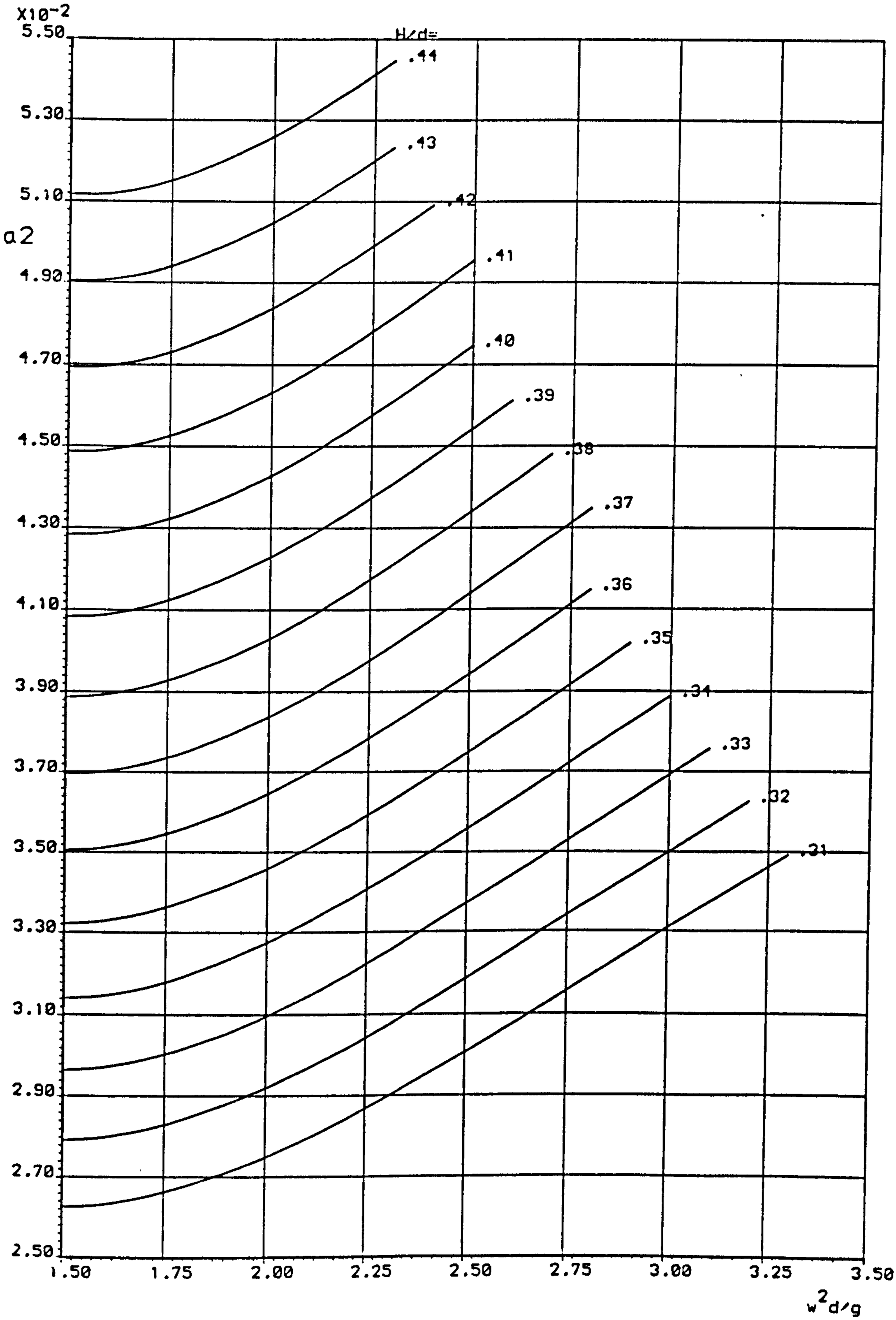

FIG A7 STOKES FIFTH ORDER WAVE COEFFICIENTS

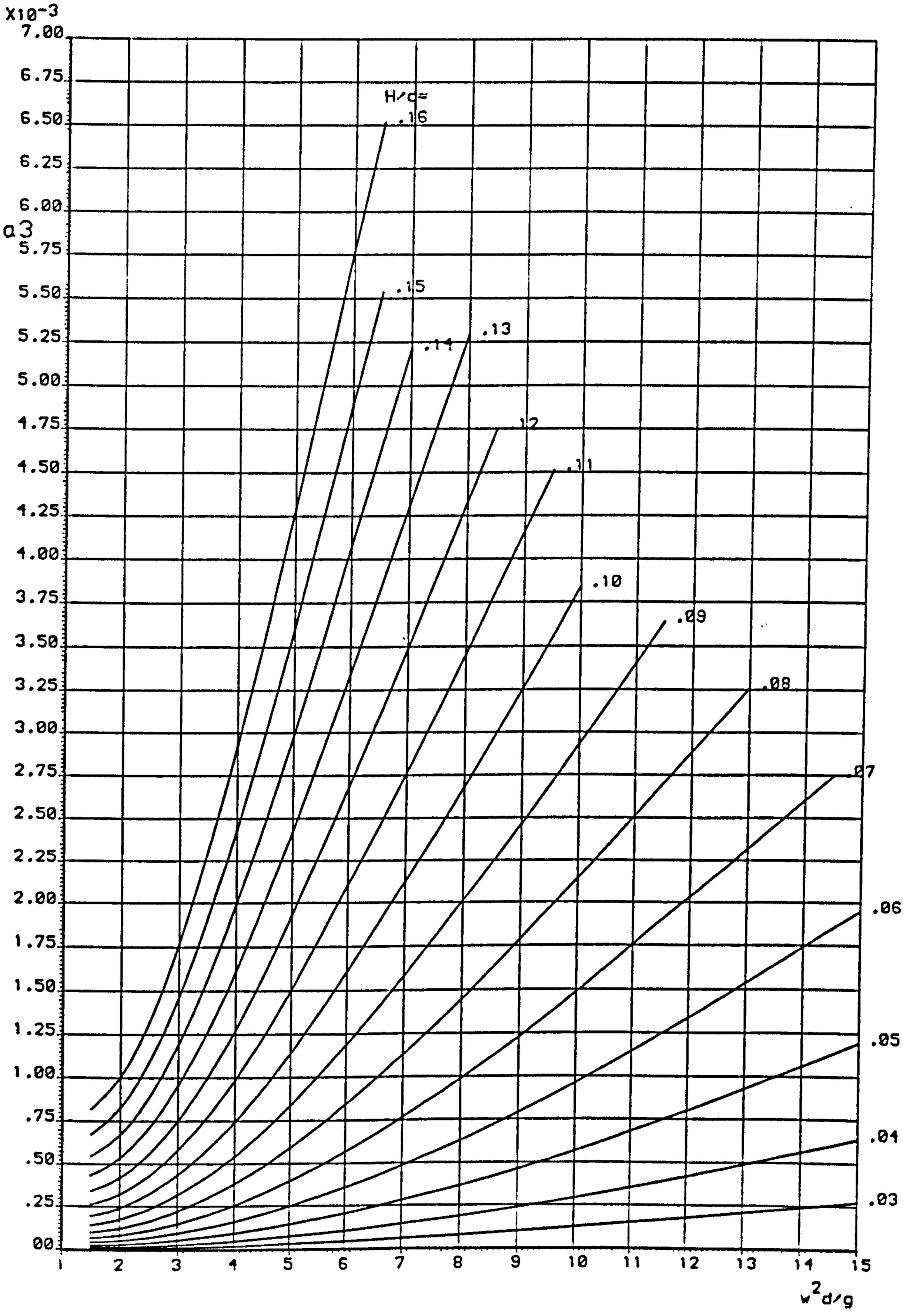

FIG A8 STOKES FIFTH ORDER WAVE COEFFICIENTS

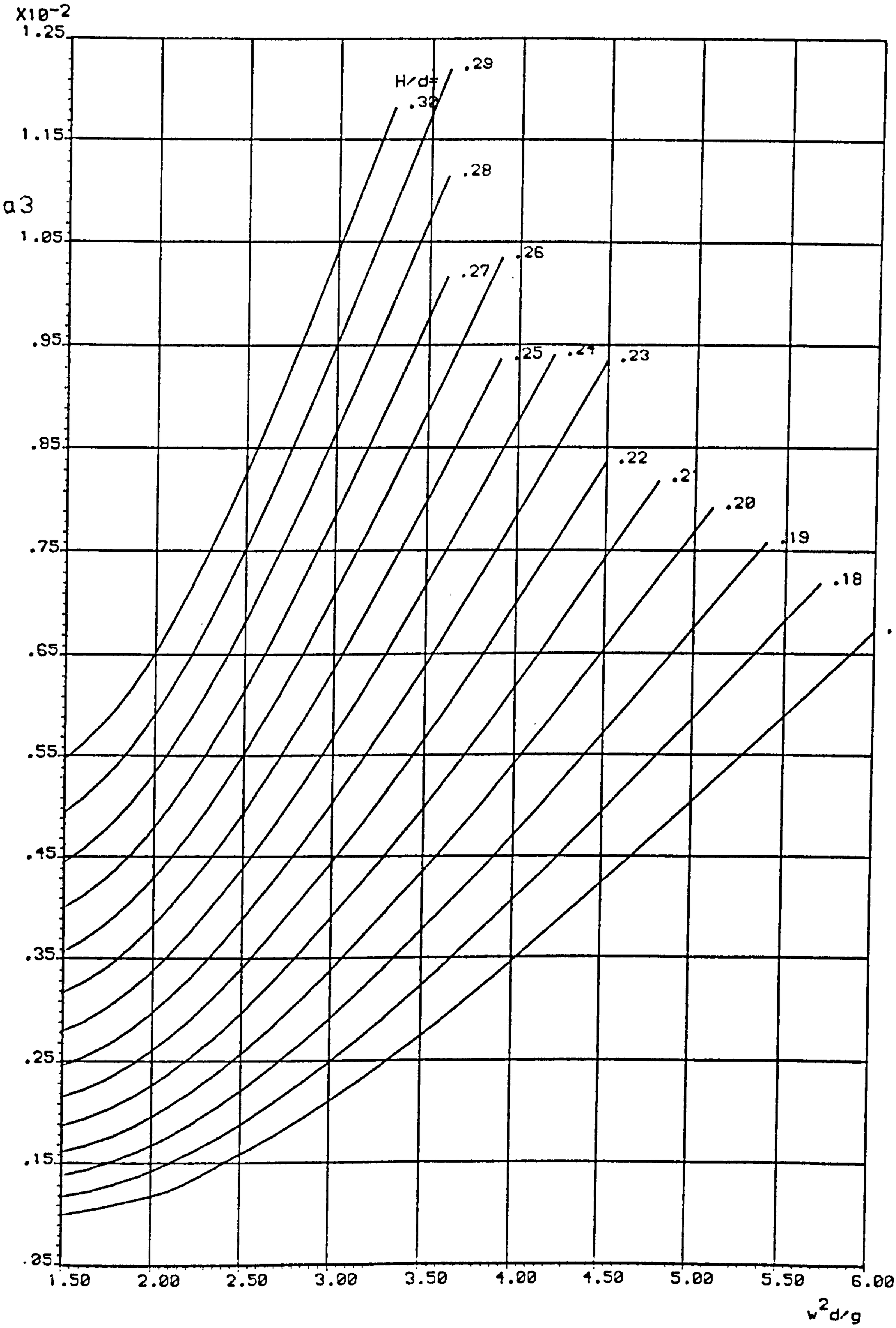

FIG A9 STOKES FIFTH ORDER WAVE COEFFICIENTS

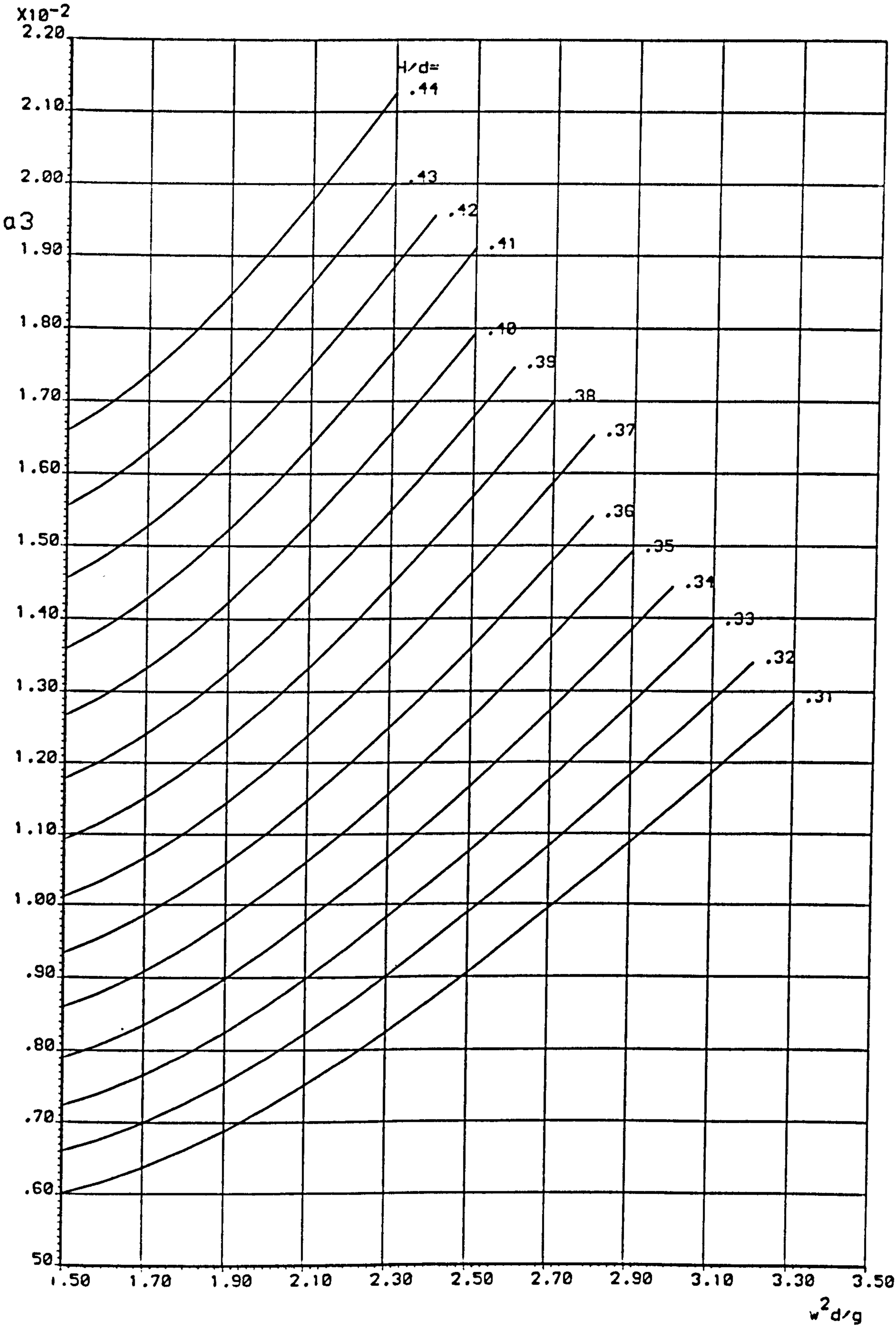

FIG A10 STOKES FIFTH ORDER WAVE COEFFICIENTS

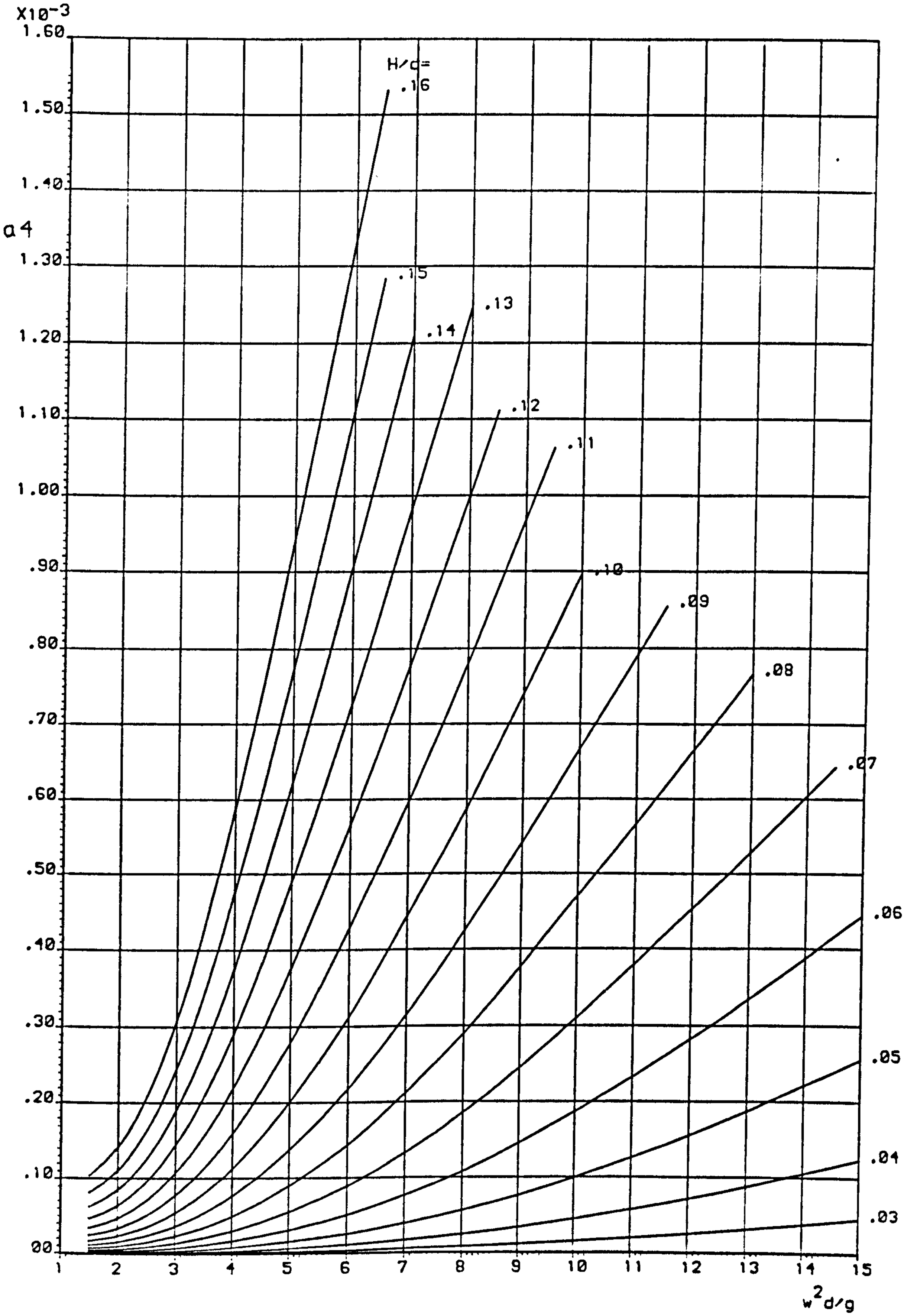

FIG AII STOKES FIFTH ORDER WAVE COEFFICIENTS

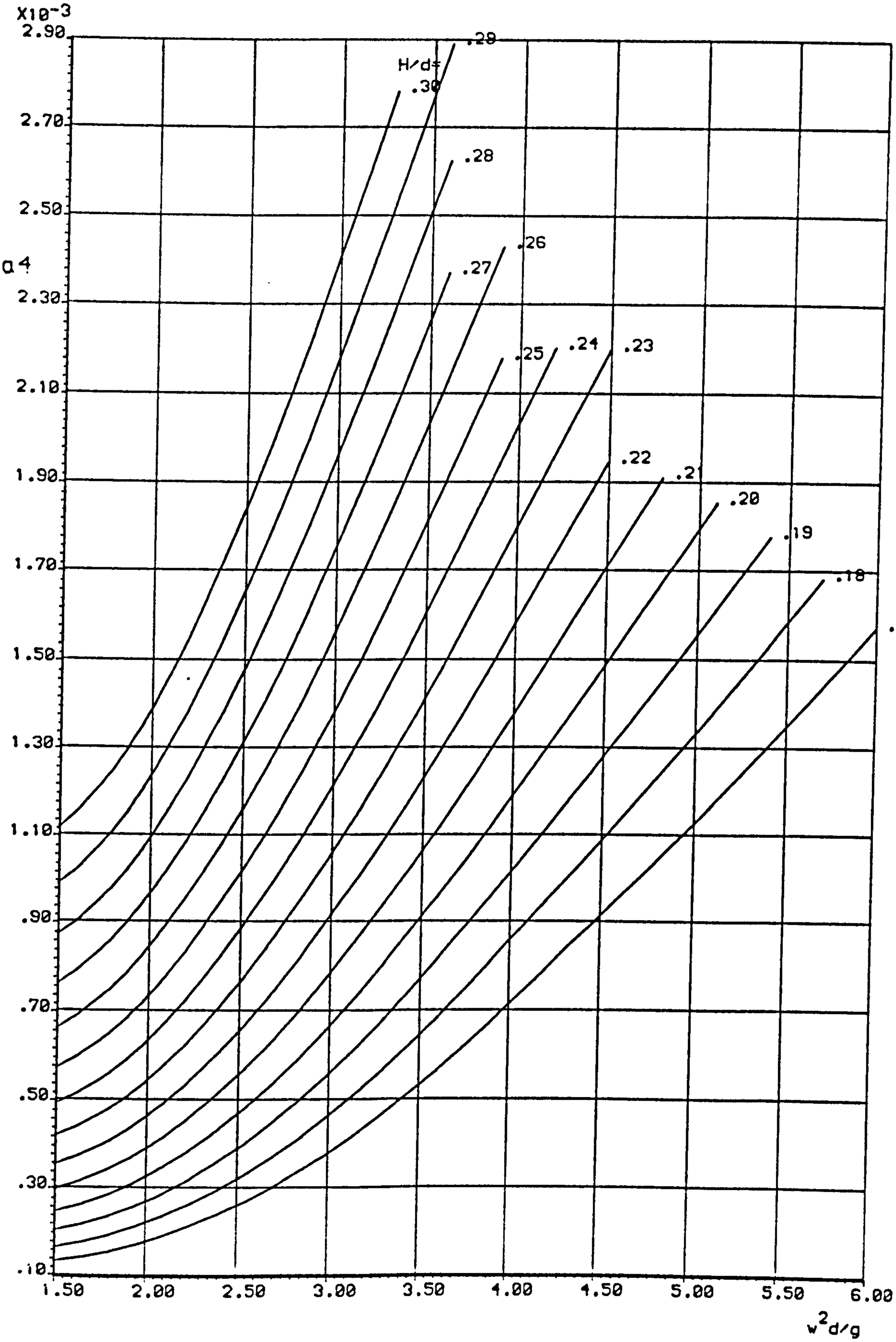

FIG A12 STOKES FIFTH ORDER WAVE COEFFICIENTS

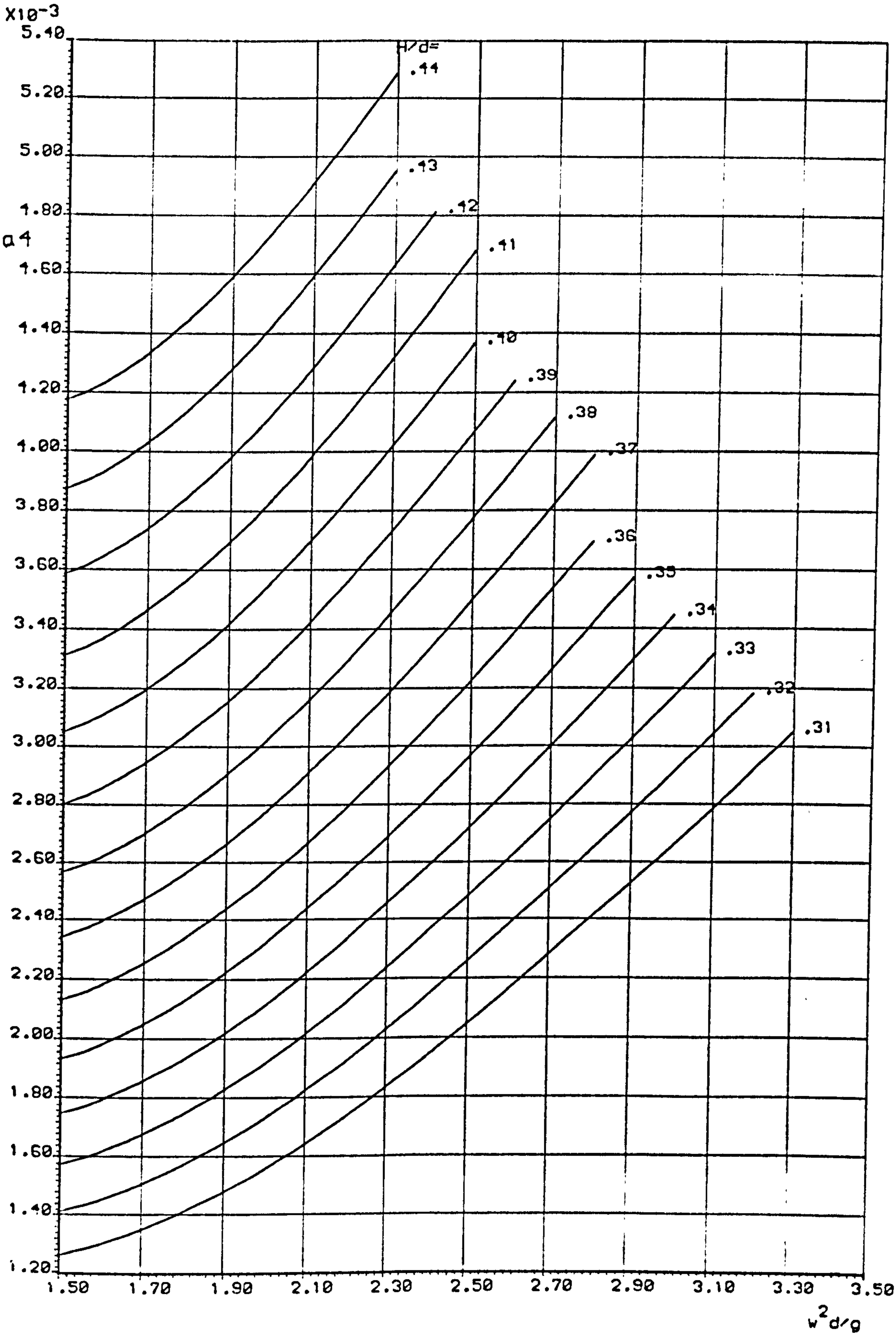

FIG A13 STOKES FIFTH ORDER WAVE COEFFICIENTS

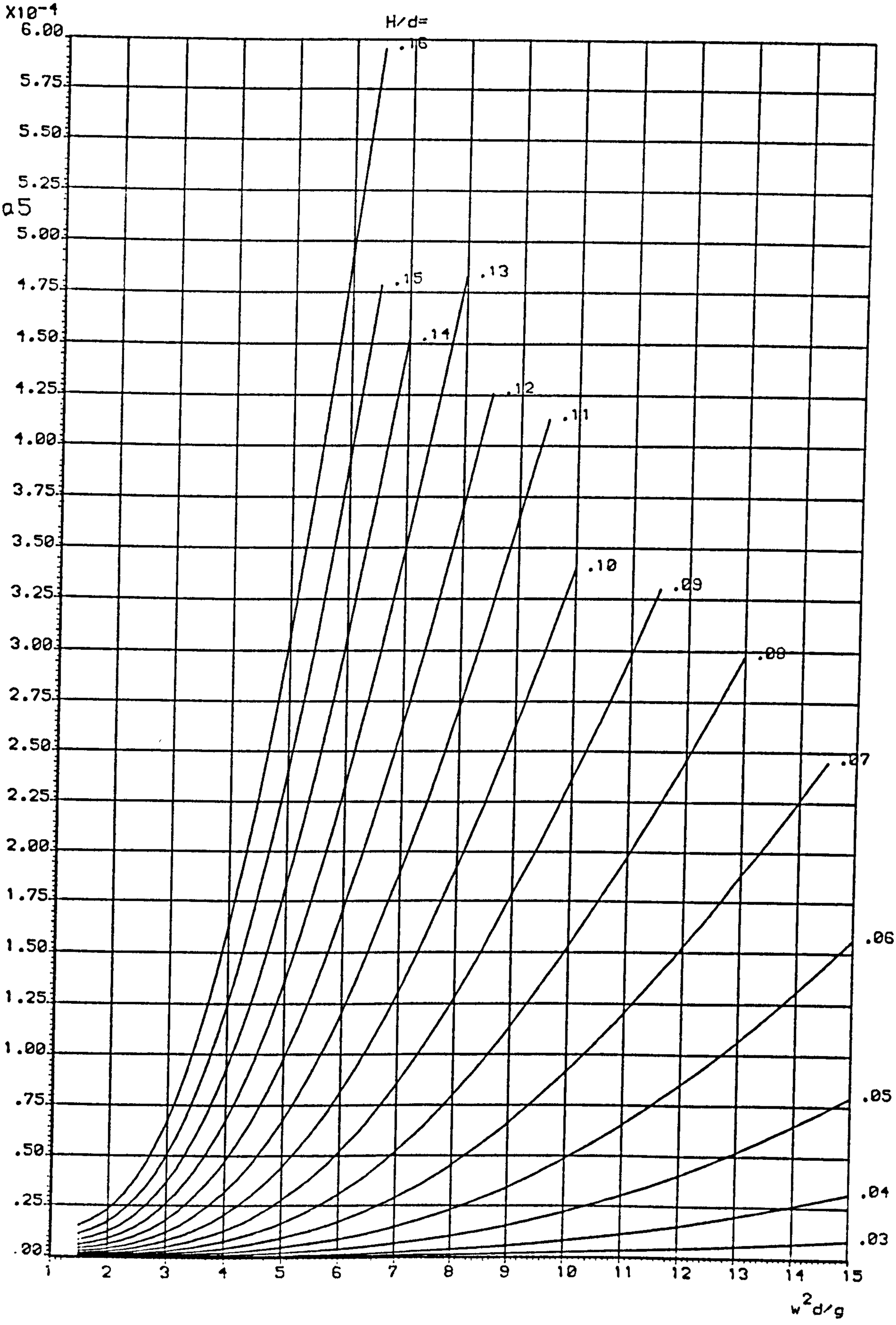

FIG A14 STOKES FIFTH ORDER WAVE COEFFICIENTS

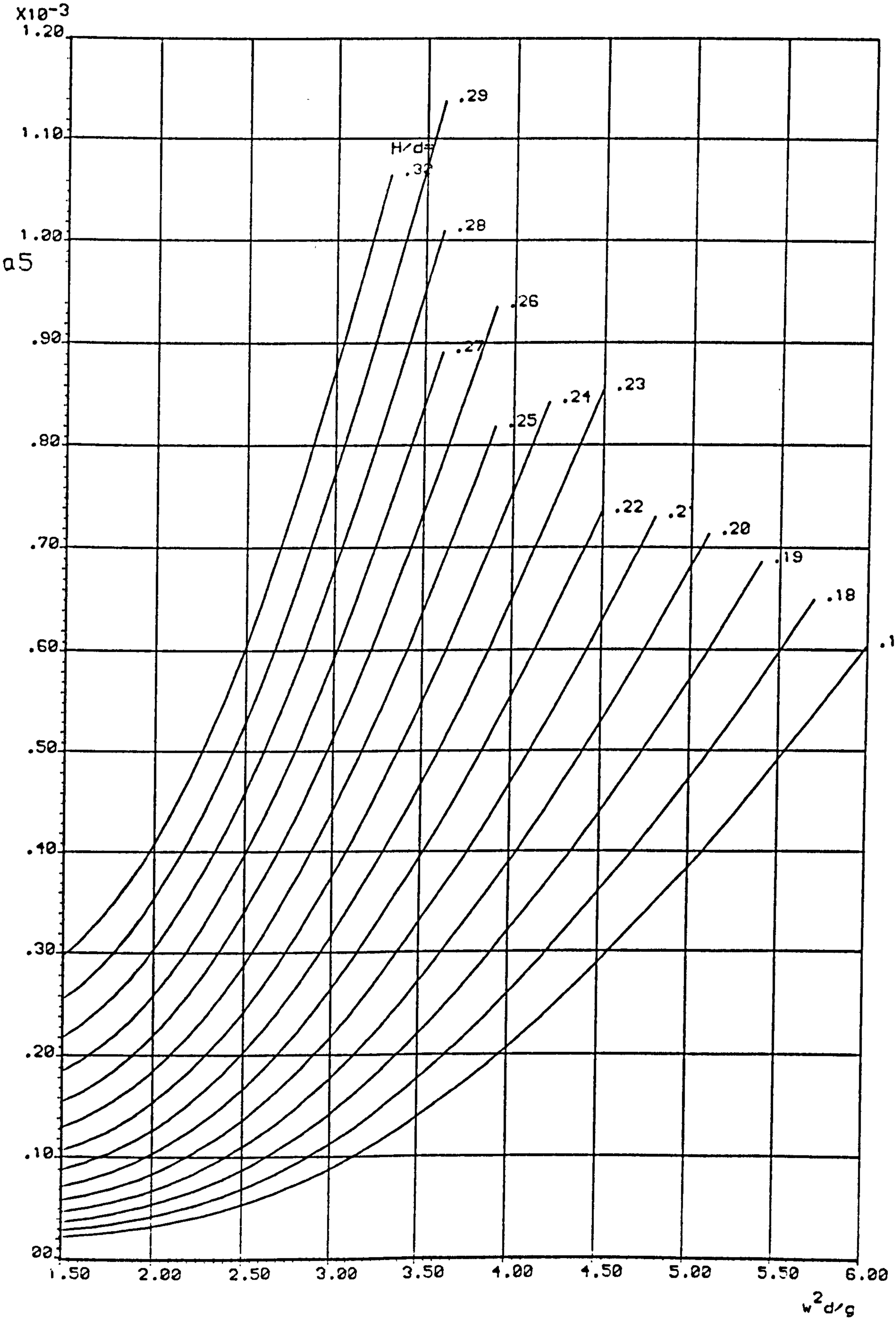

FIG A15 STOKES FIFTH ORDER WAVE COEFFICIENTS

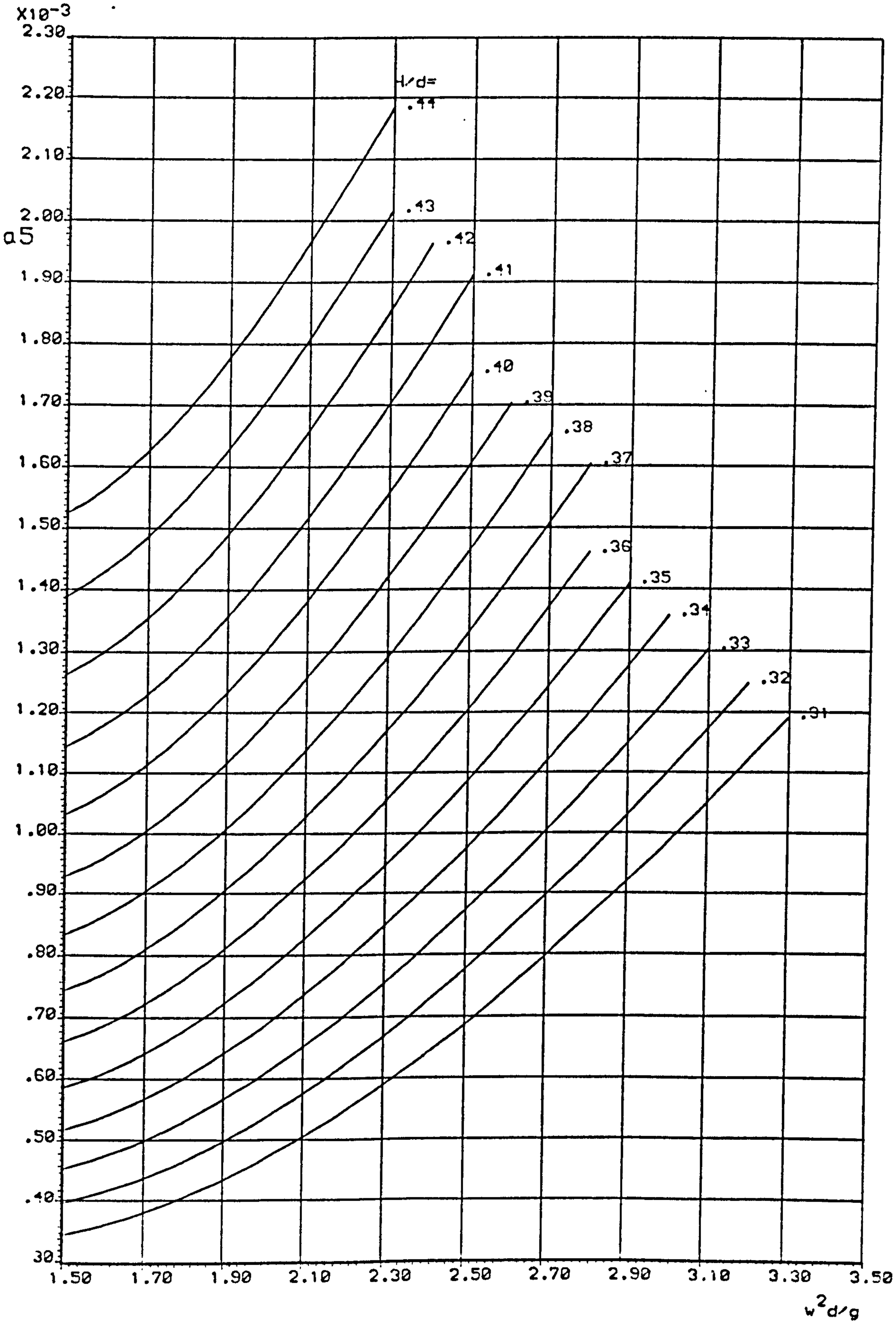

FIG A16 STOKES FIFTH ORDER WAVE COEFFICIENTS

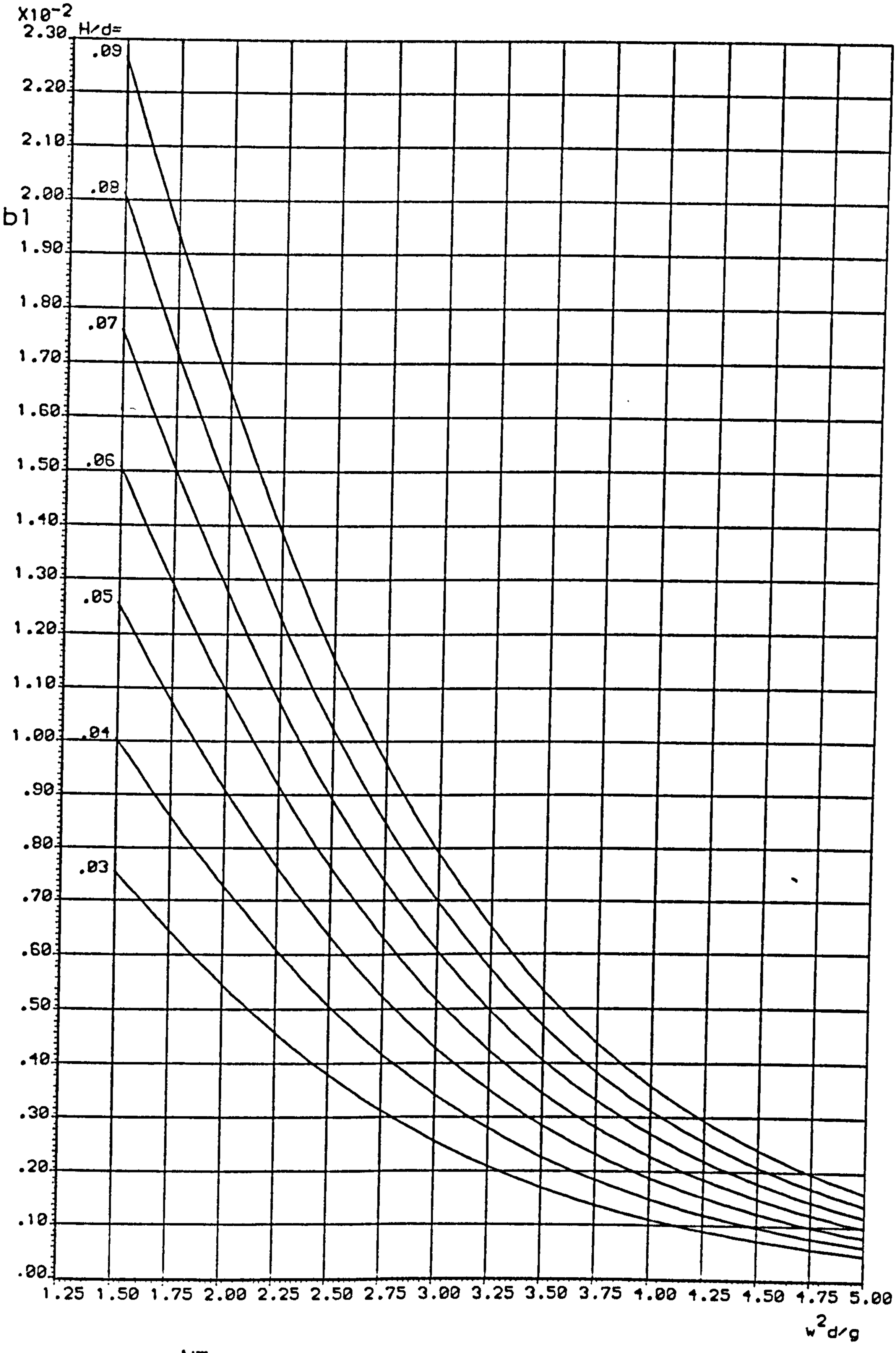

FIG A17 STOKES FIFTH ORDER WAVE COEFFICIENTS

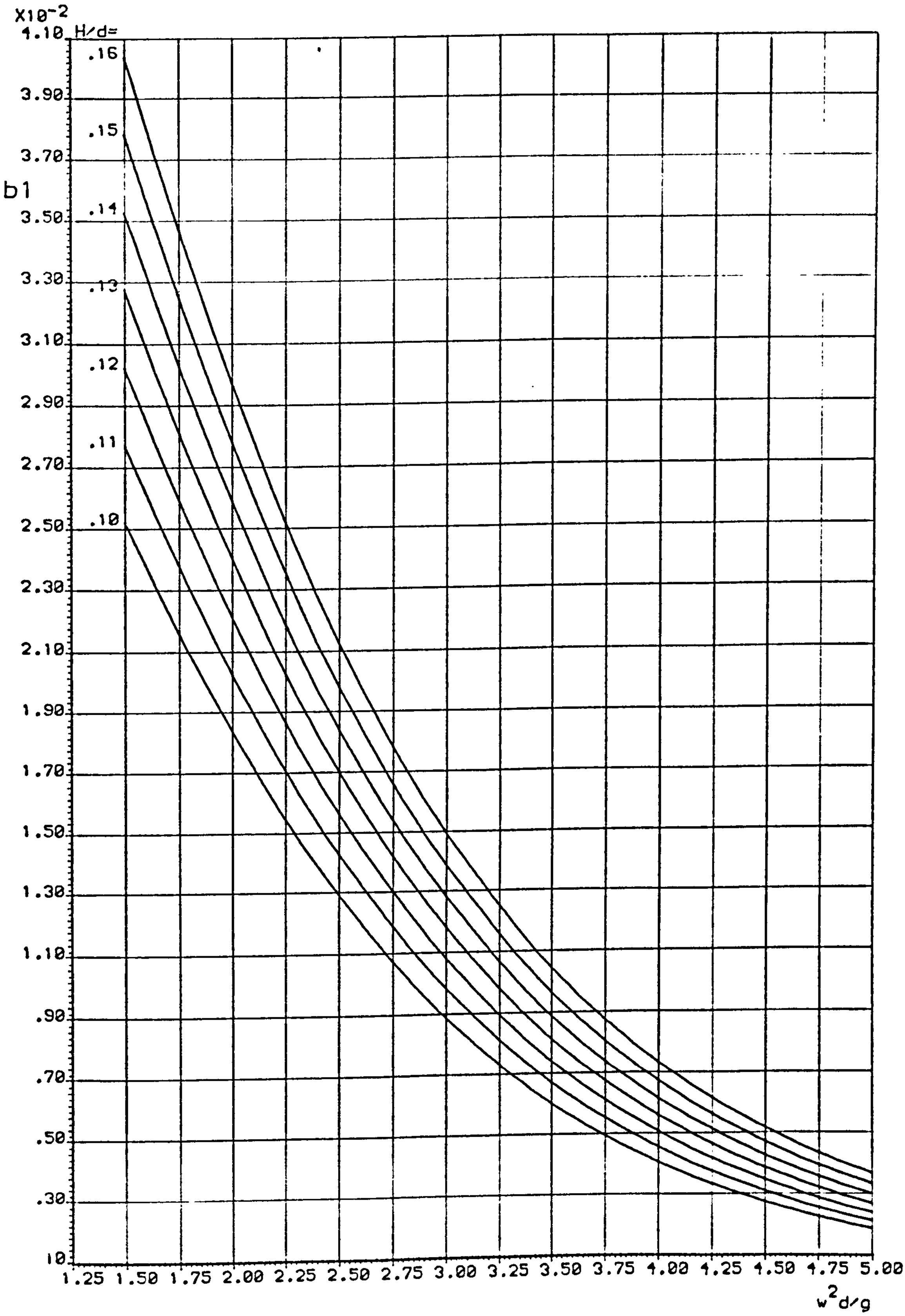

FIG A18 STOKES FIFTH ORDER WAVE COEFFICIENTS

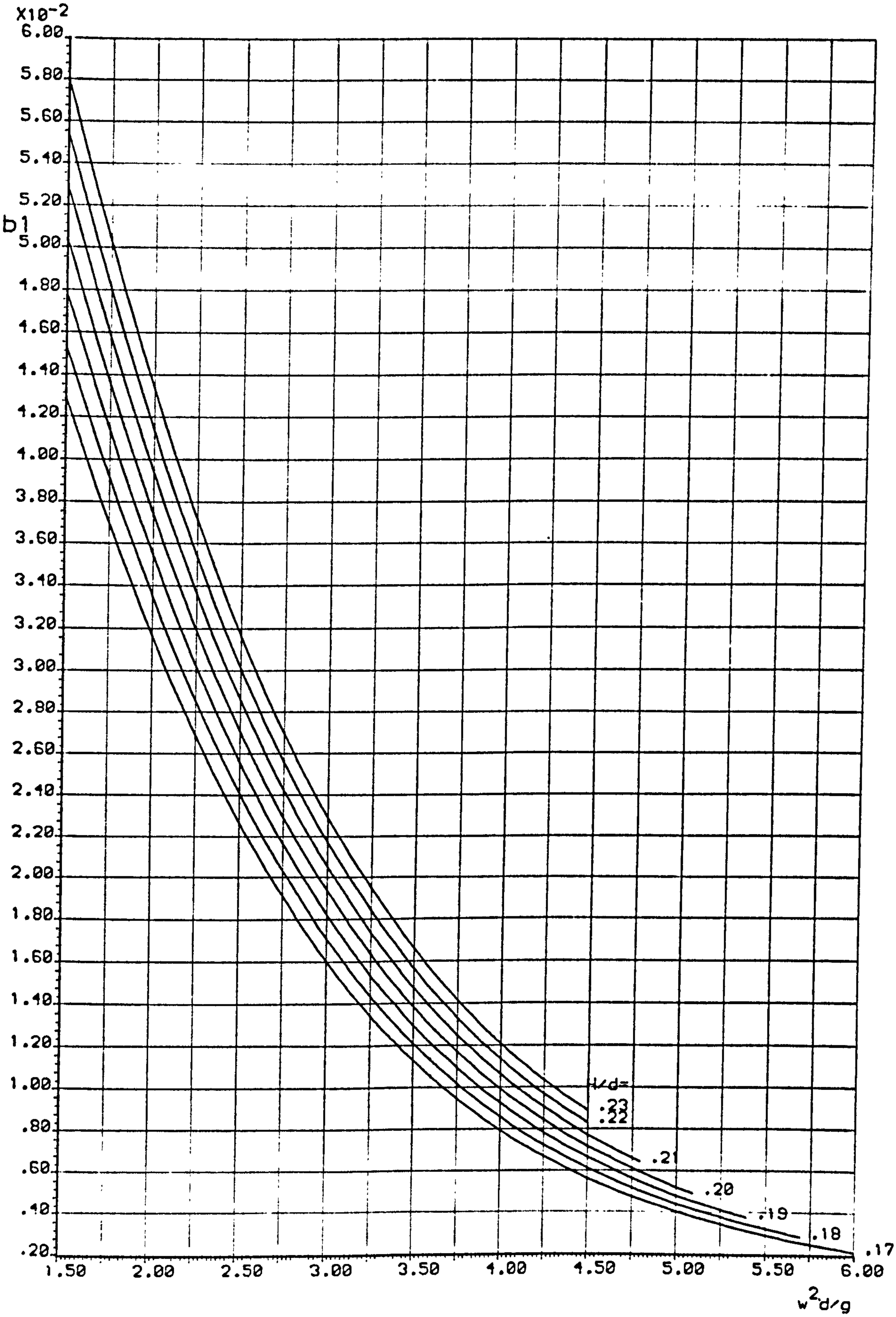

FIG A19 STOKES FIFTH ORDER WAVE COEFFICIENTS

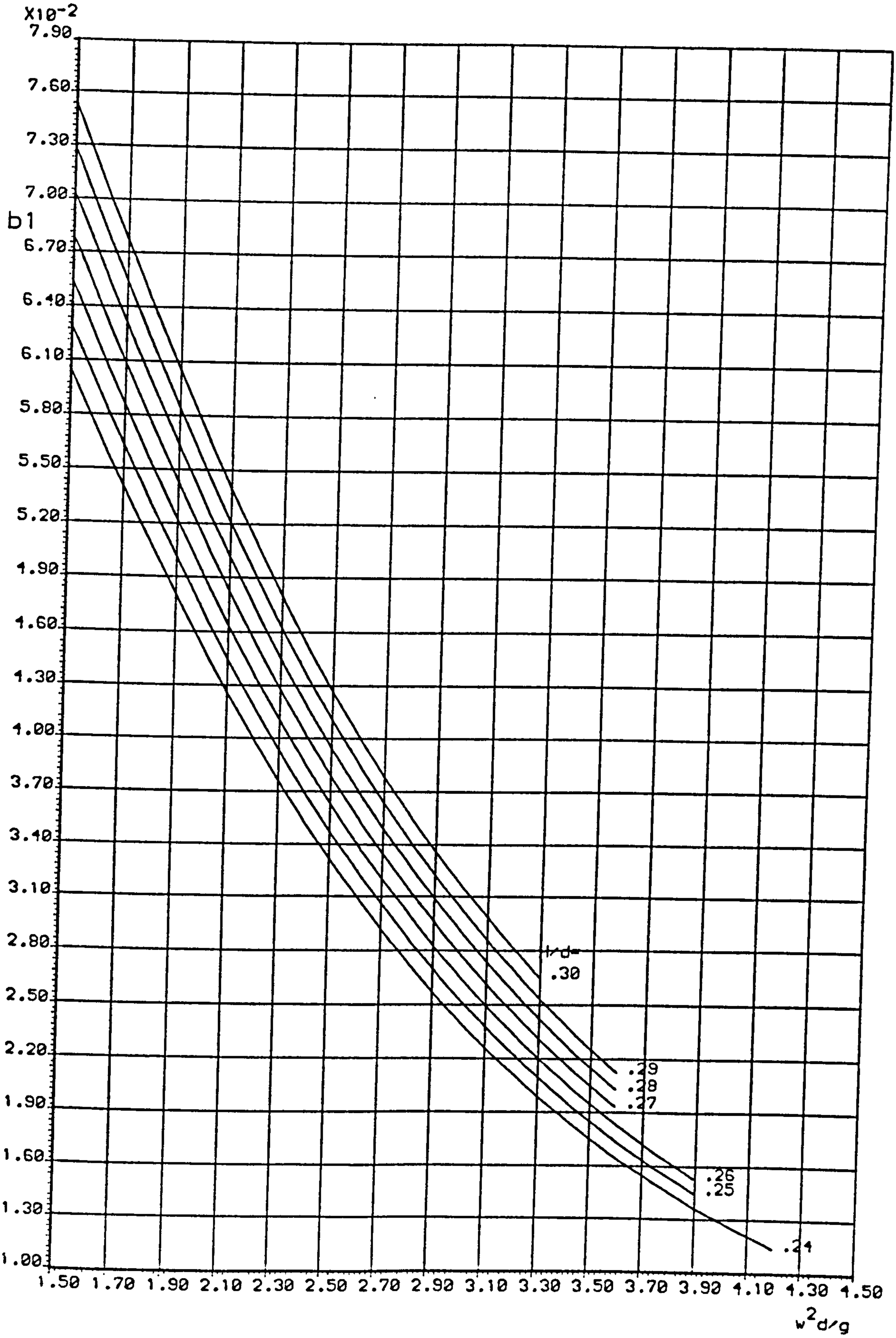

FIG A20 STOKES FIFTH ORDER WAVE COEFFICIENTS

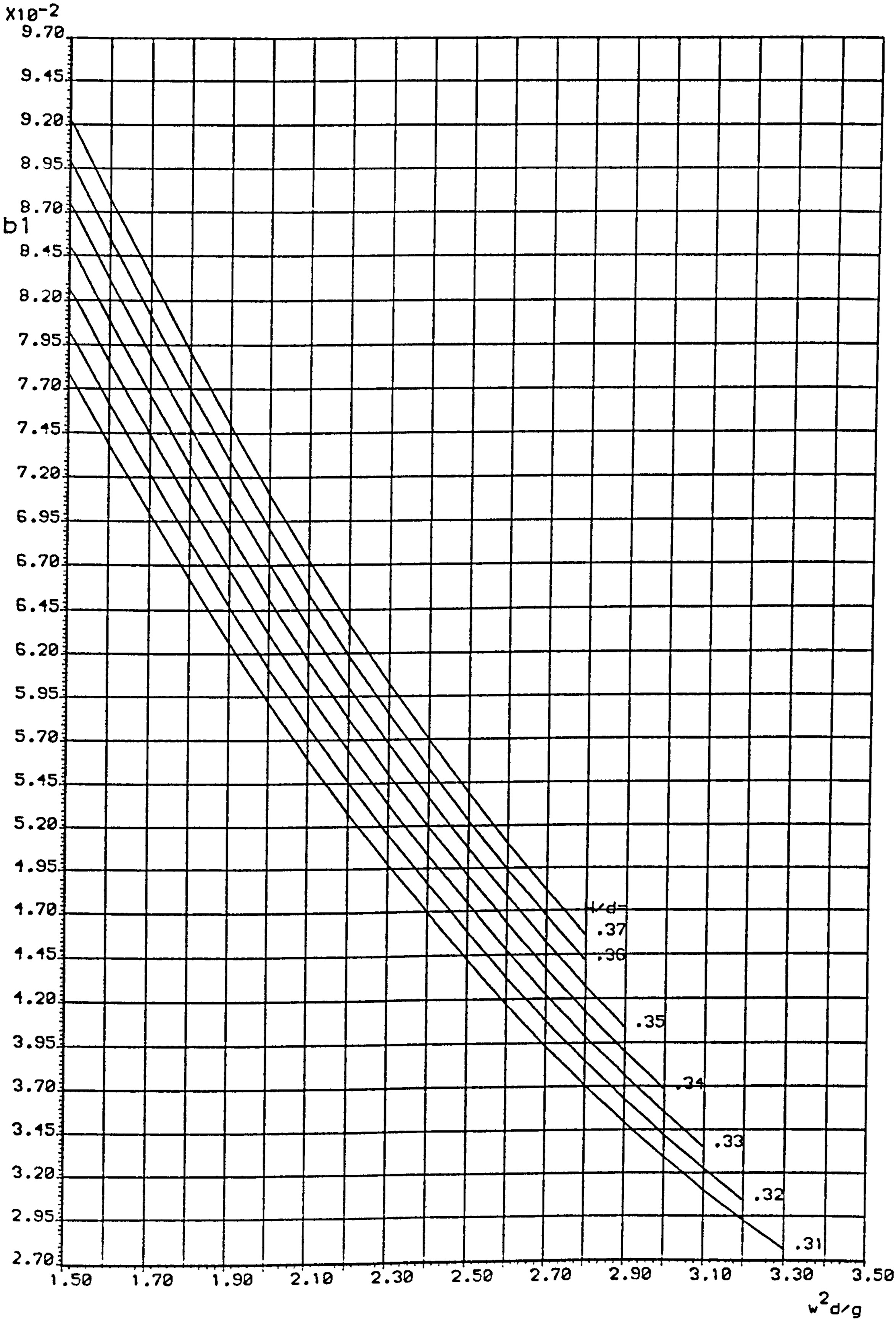

FIG A21 STOKES FIFTH ORDER WAVE COEFFICIENTS

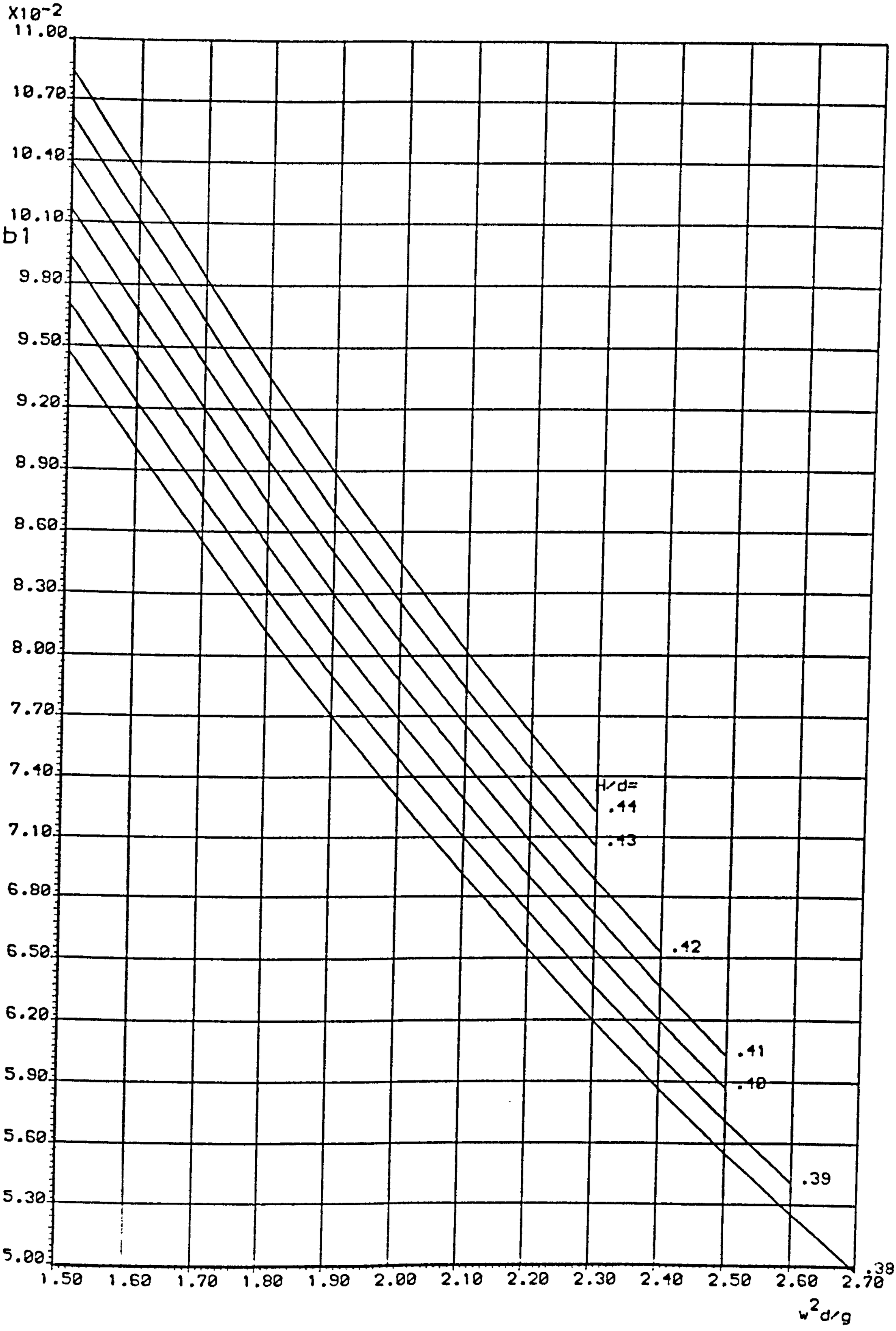

FIG A22 STOKES FIFTH ORDER WAVE COEFFICIENTS

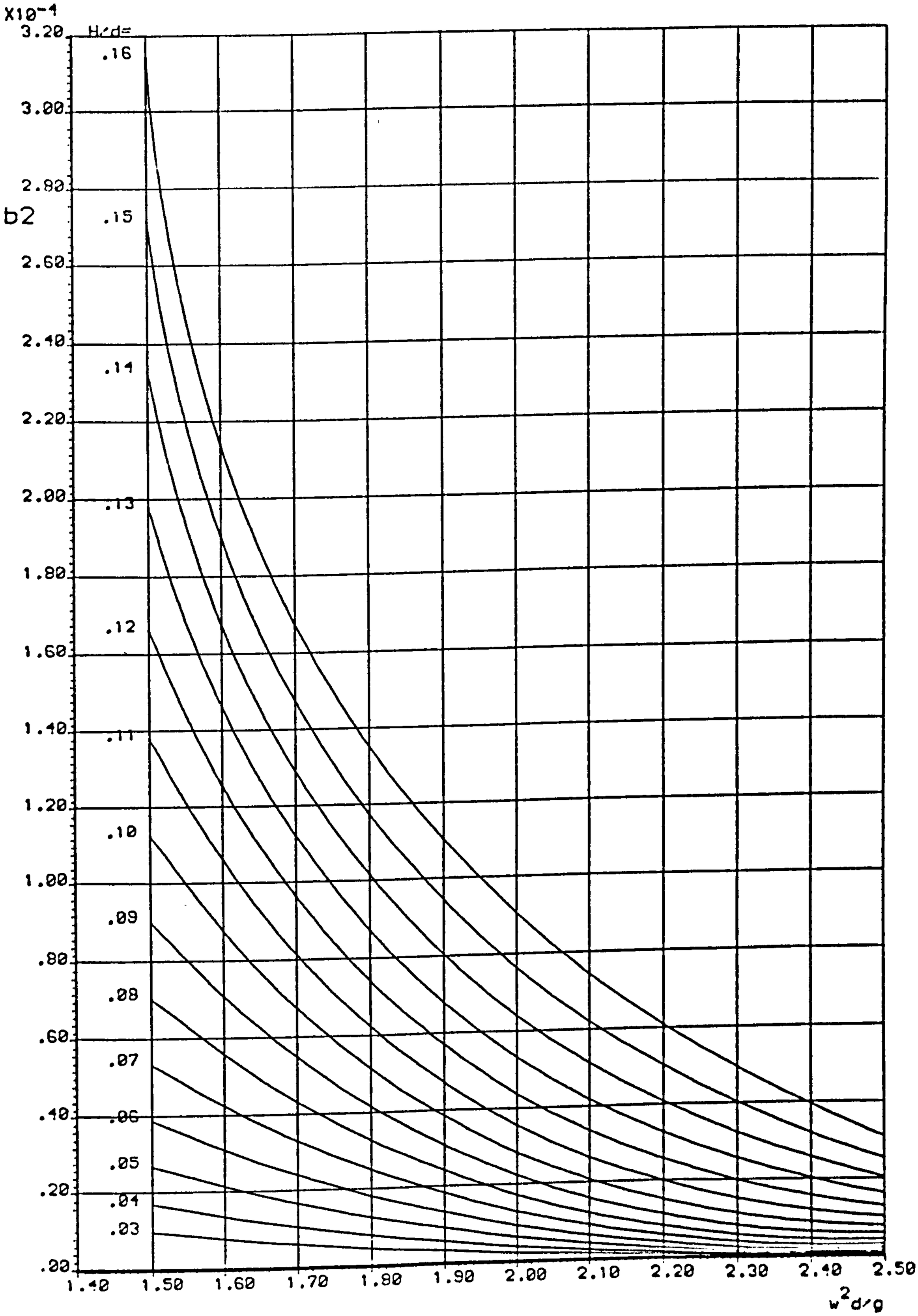

FIG A23 STOKES FIFTH ORDER WAVE COEFFICIENTS

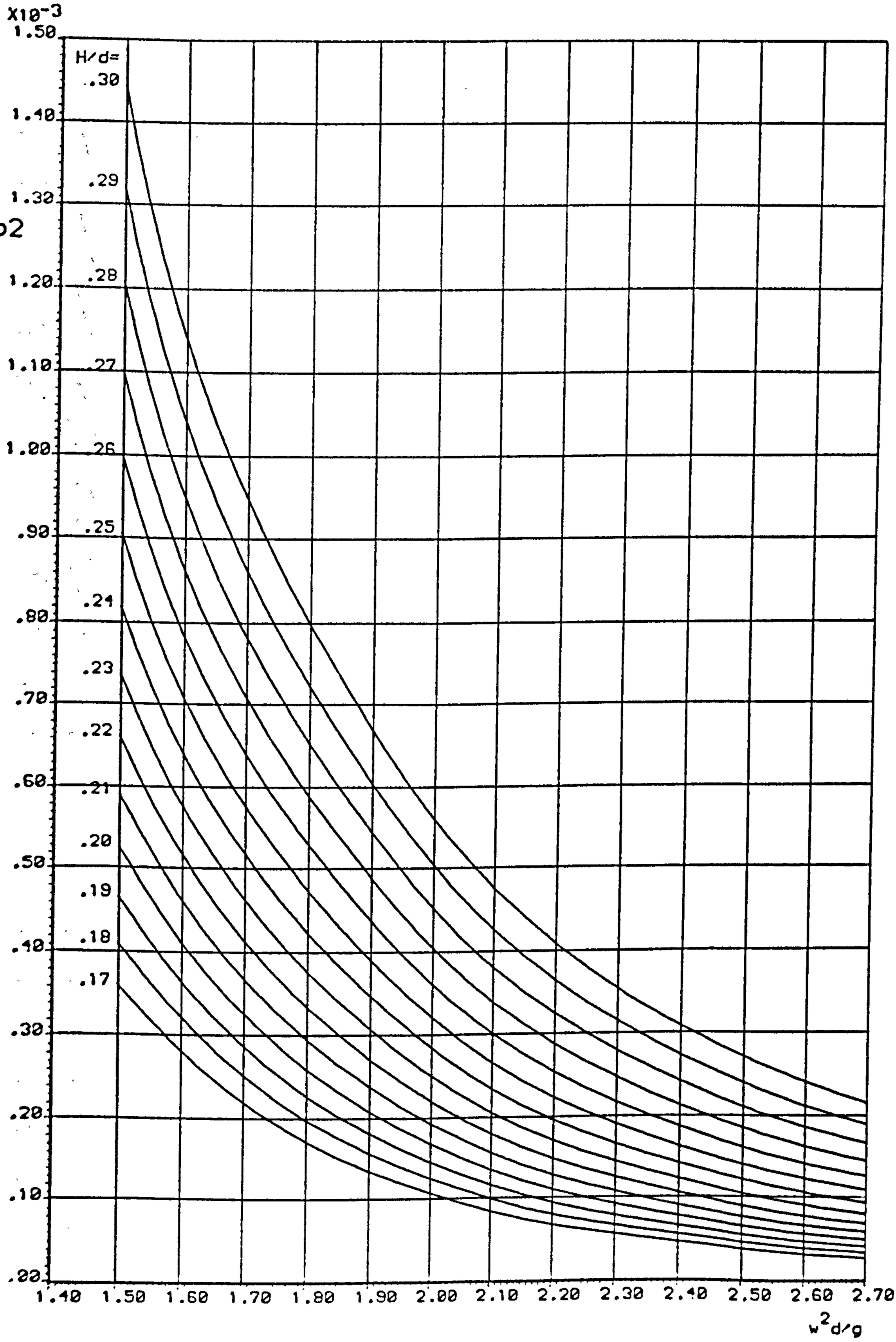

FIG A24 STOKES FIFTH ORDER WAVE COEFFICIENTS

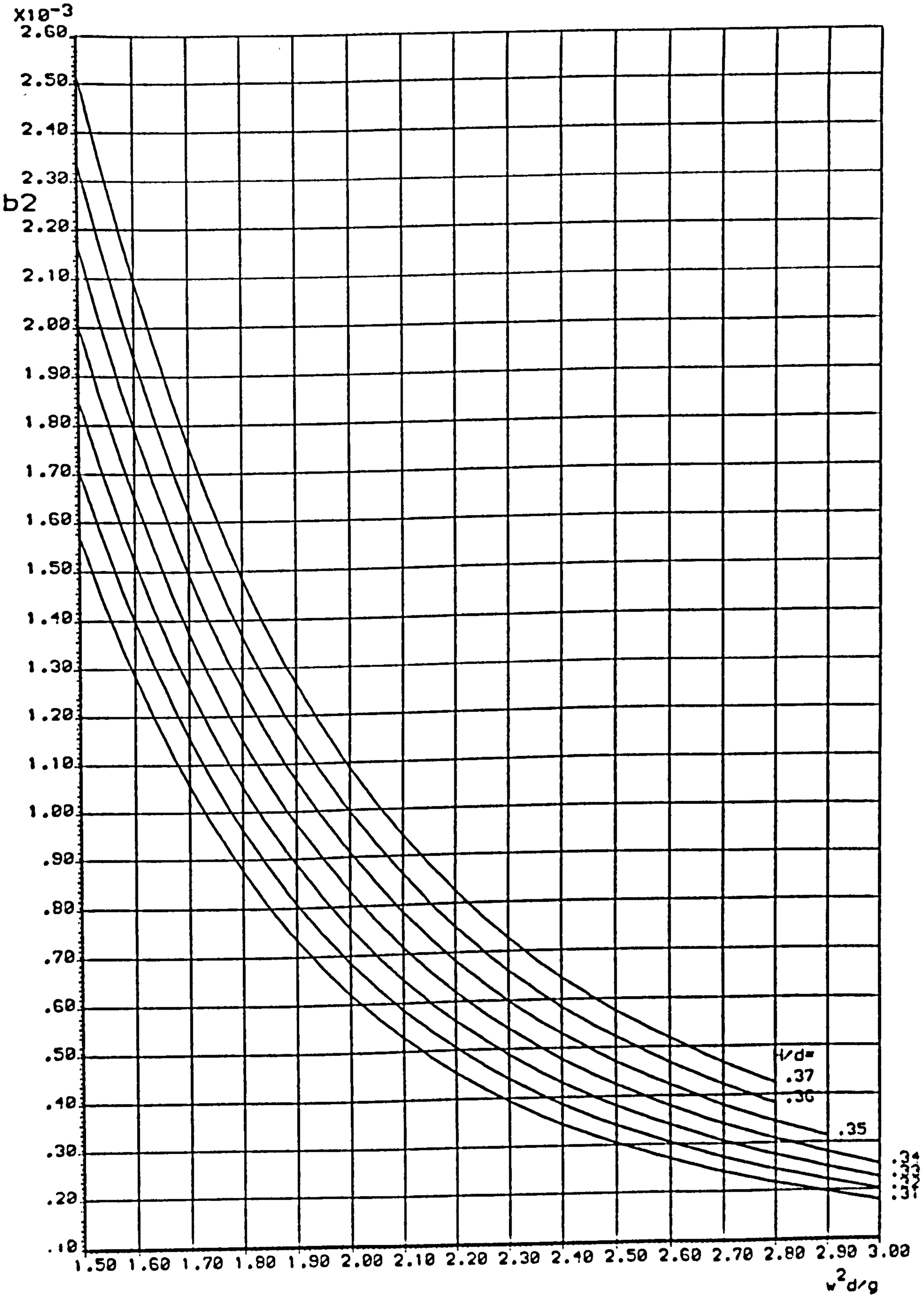

FIG A25 STOKES FIFTH ORDER WAVE COEFFICIENTS

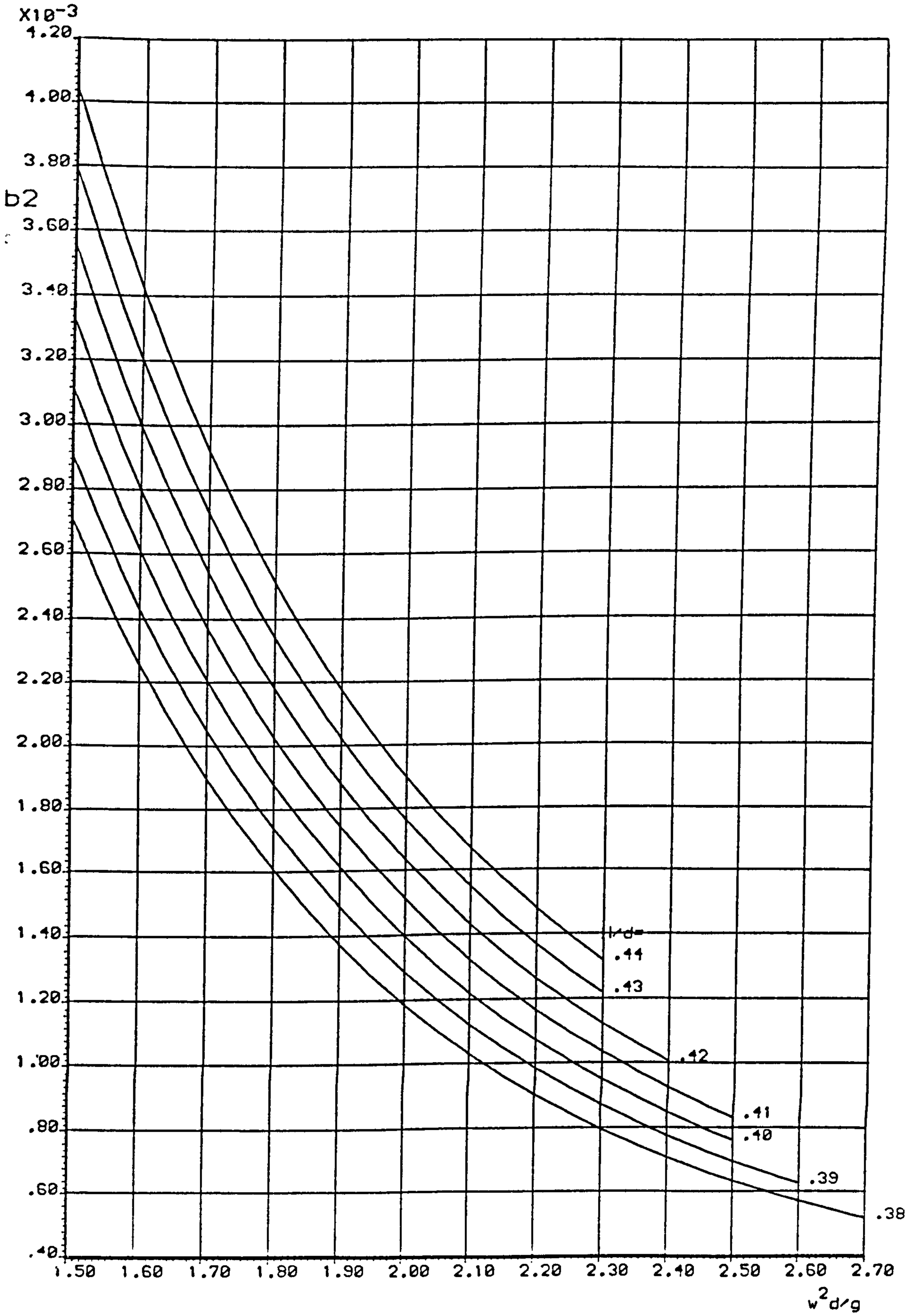

FIG A26 STOKES FIFTH ORDER WAVE COEFFICIENTS

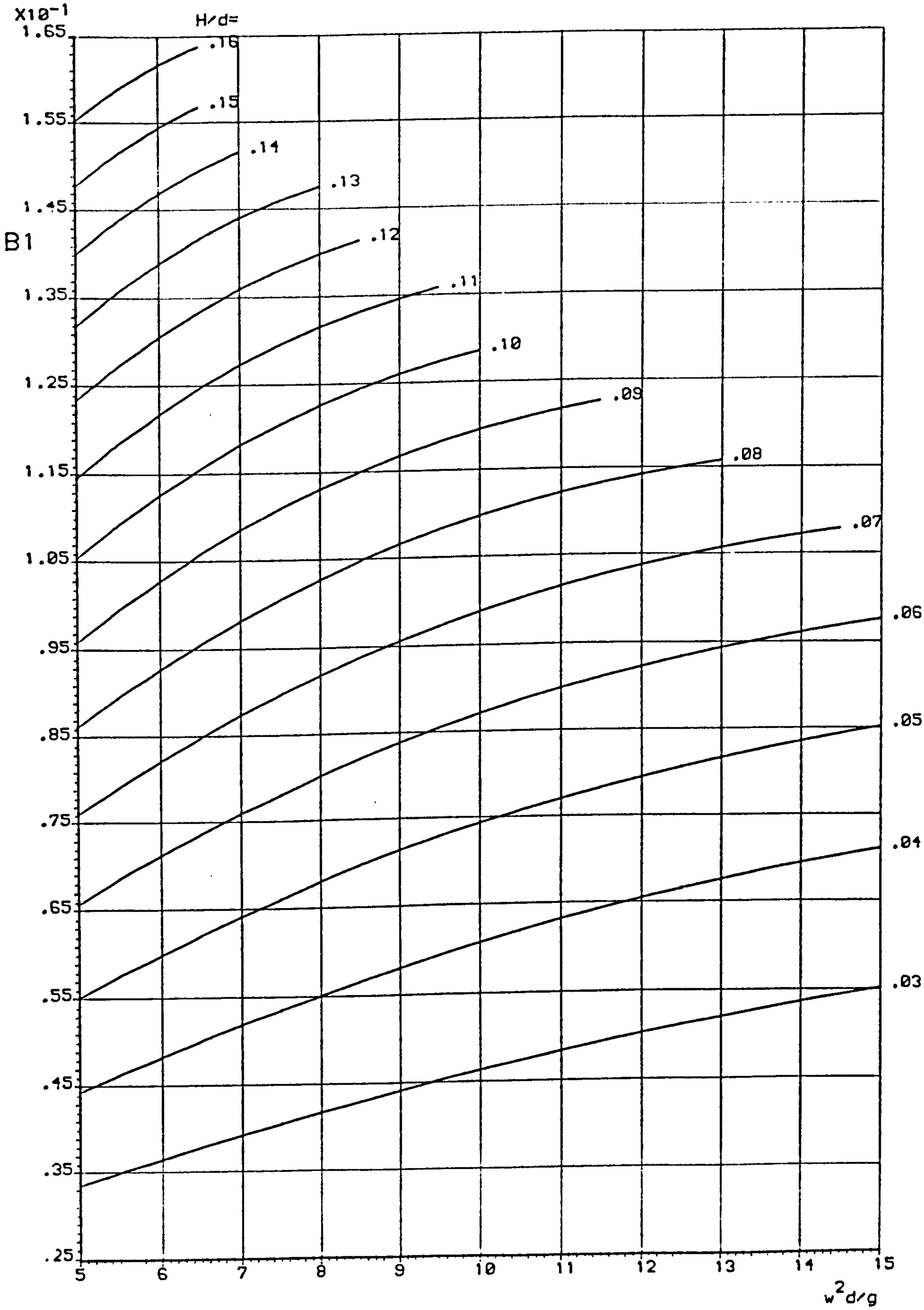

FIG A27 STOKES FIFTH ORDER WAVE COEFFICIENTS

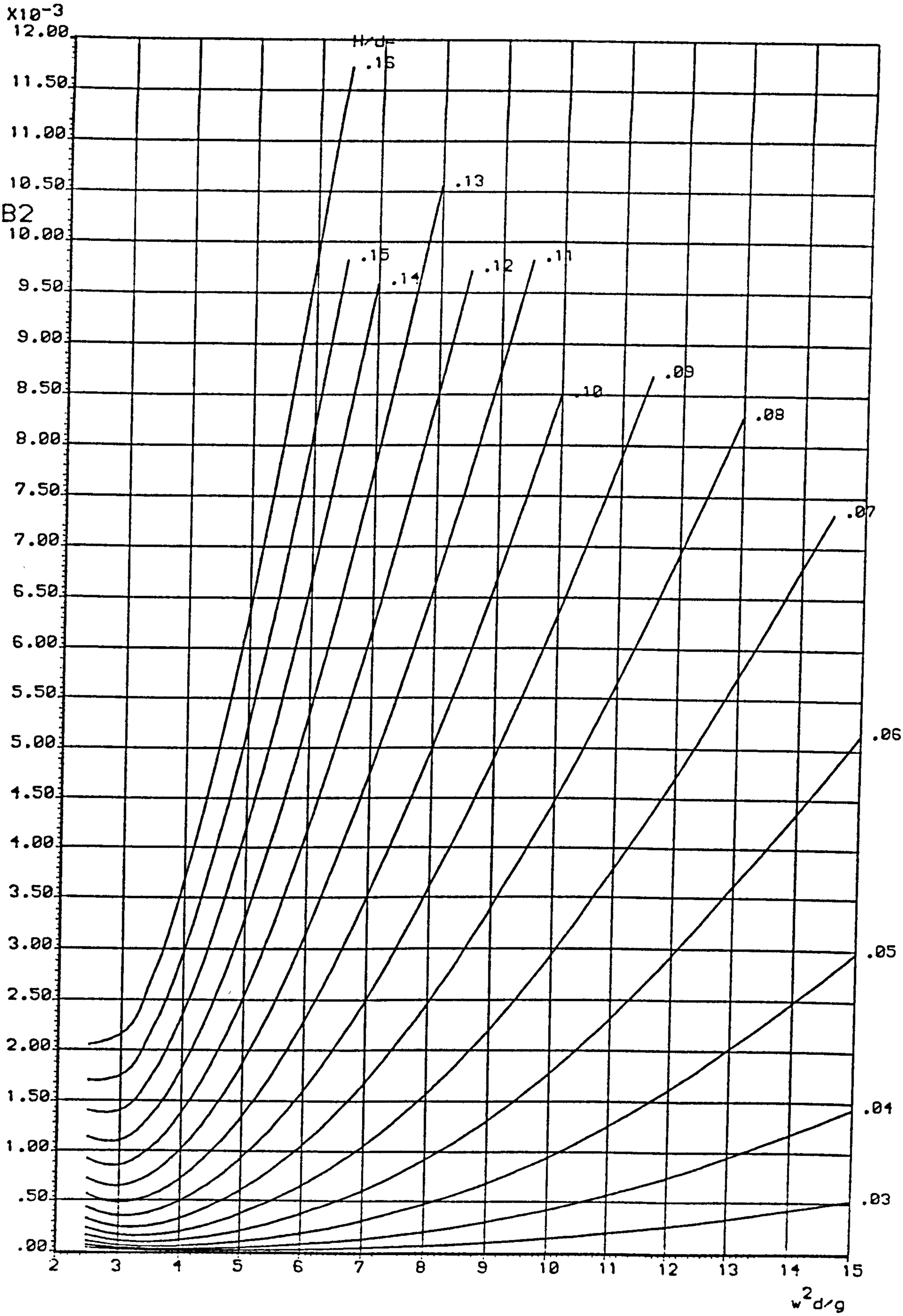

FIG A28 STOKES FIFTH ORDER WAVE COEFFICIENTS

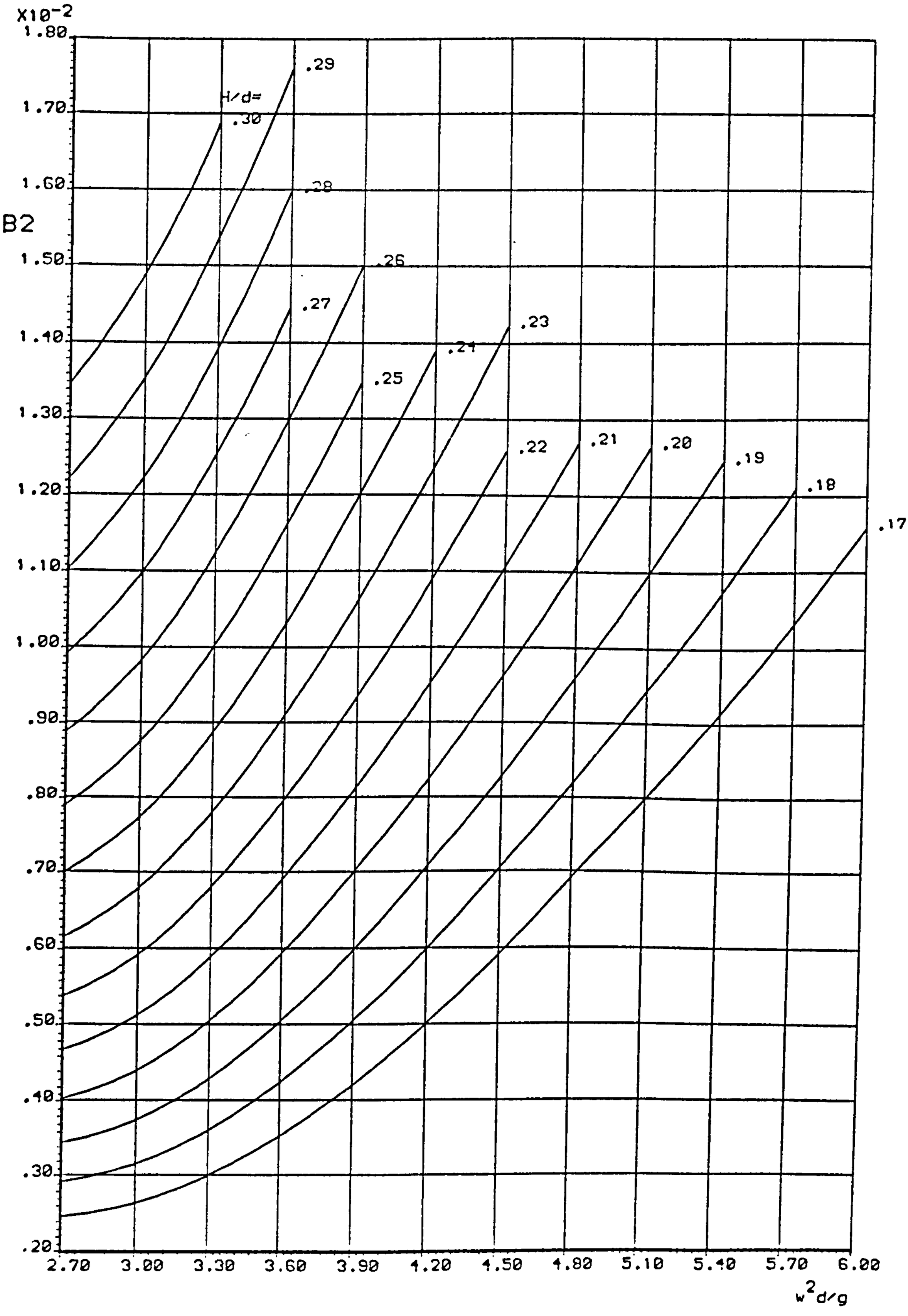

FIG A29 STOKES FIFTH ORDER WAVE COEFFICIENTS

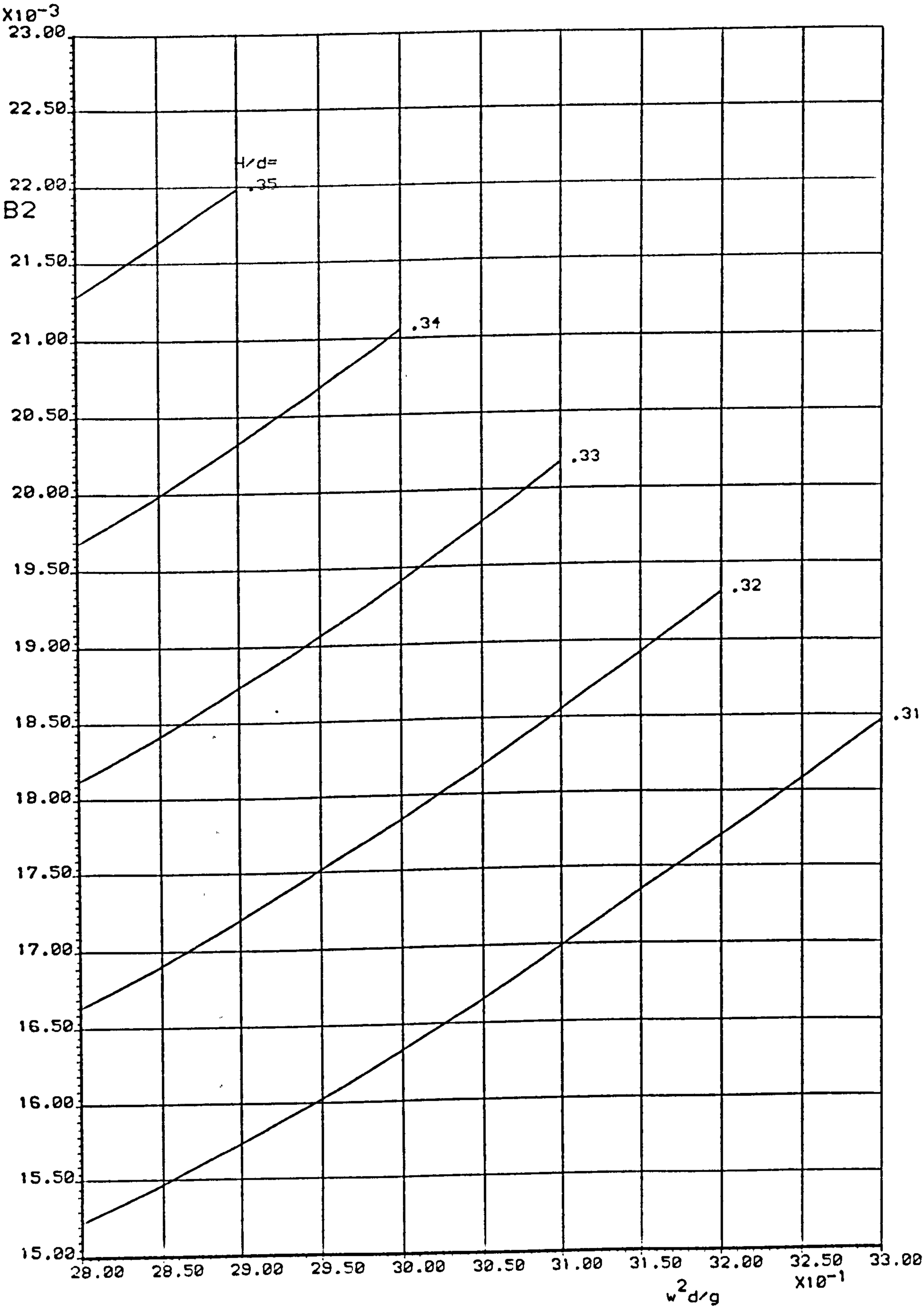

FIG A30 STOKES FIFTH ORDER WAVE COEFFICIENTS

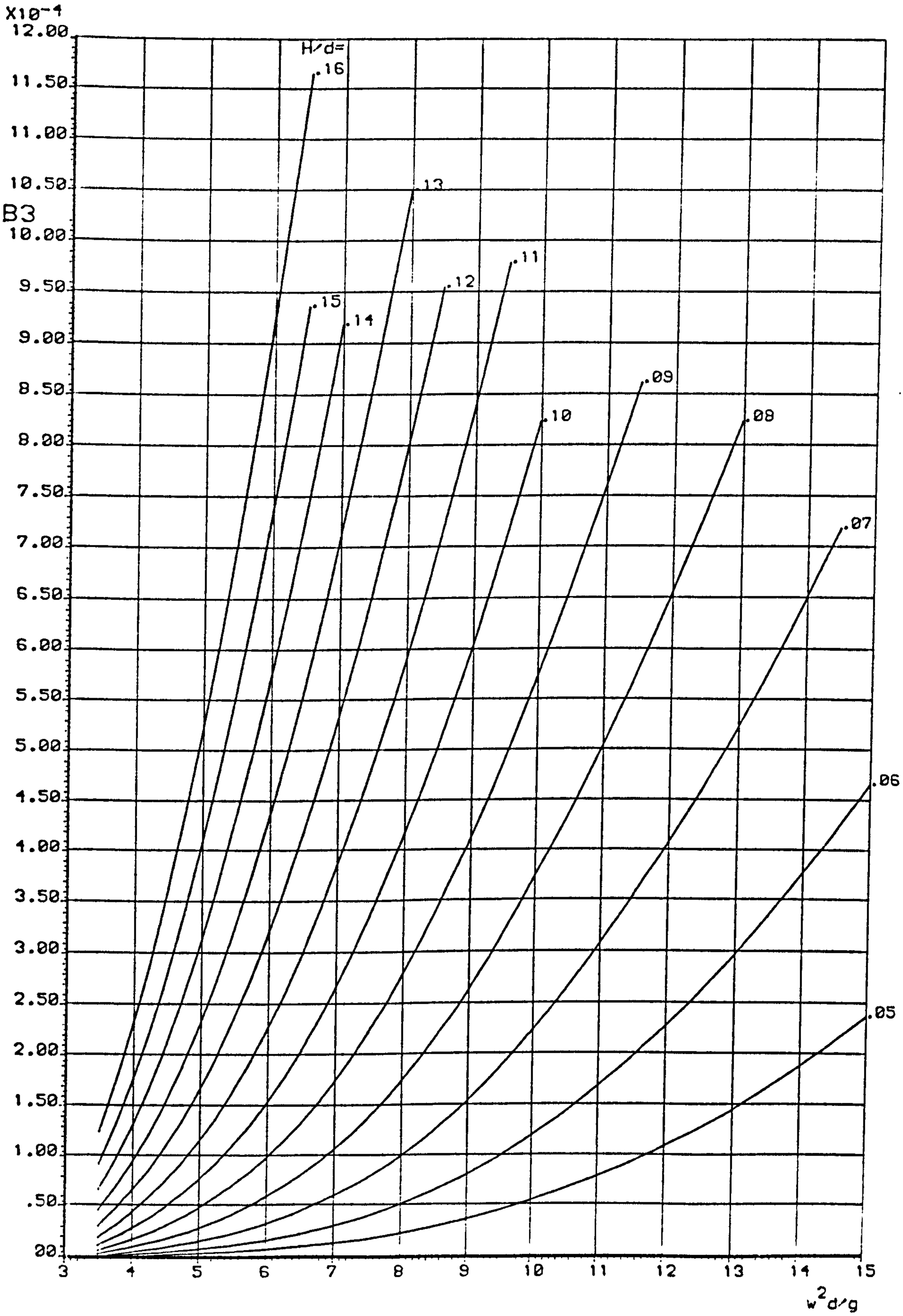

FIG A31 STOKES FIFTH ORDER WAVE COEFFICIENTS

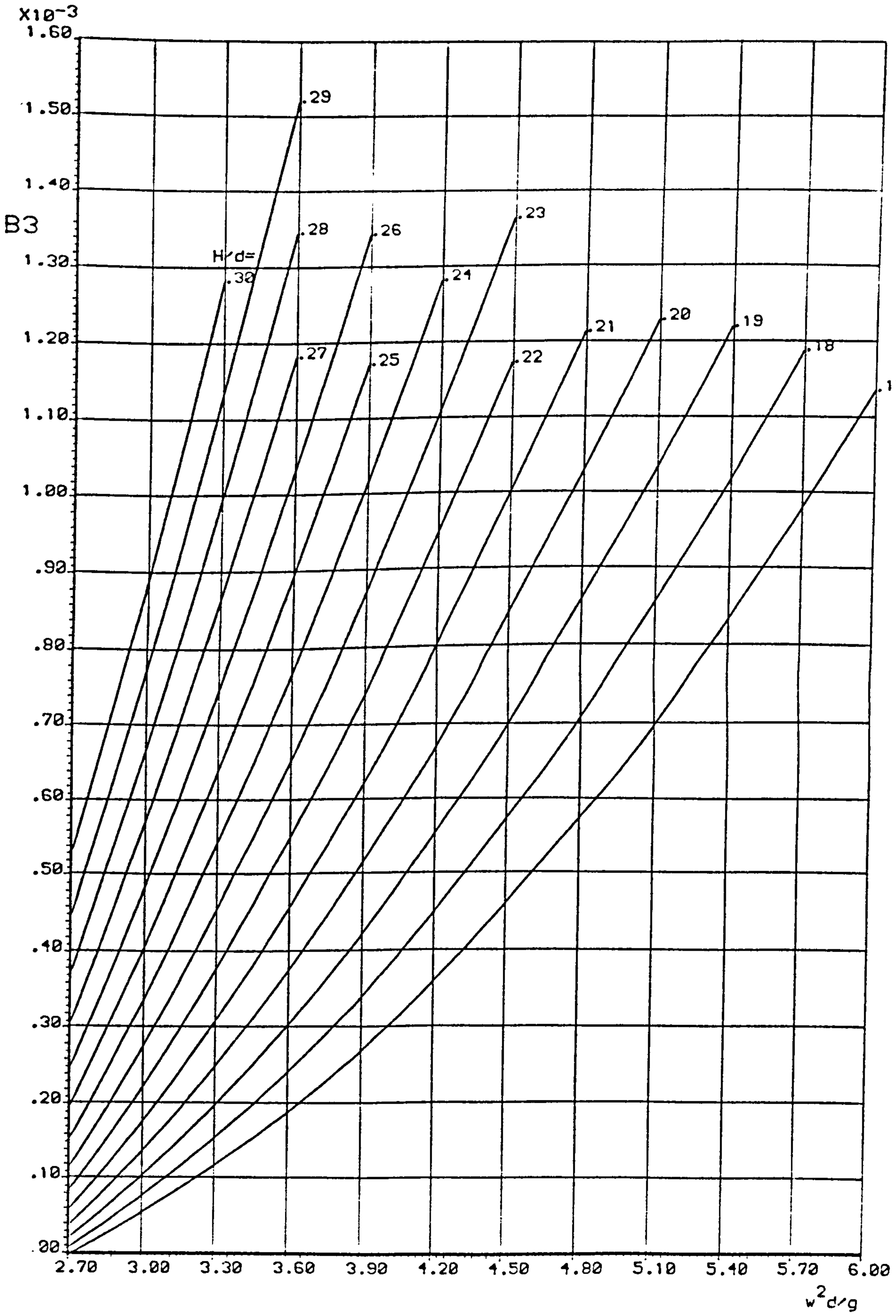

FIG A32 STOKES FIFTH ORDER WAVE COEFFICIENTS

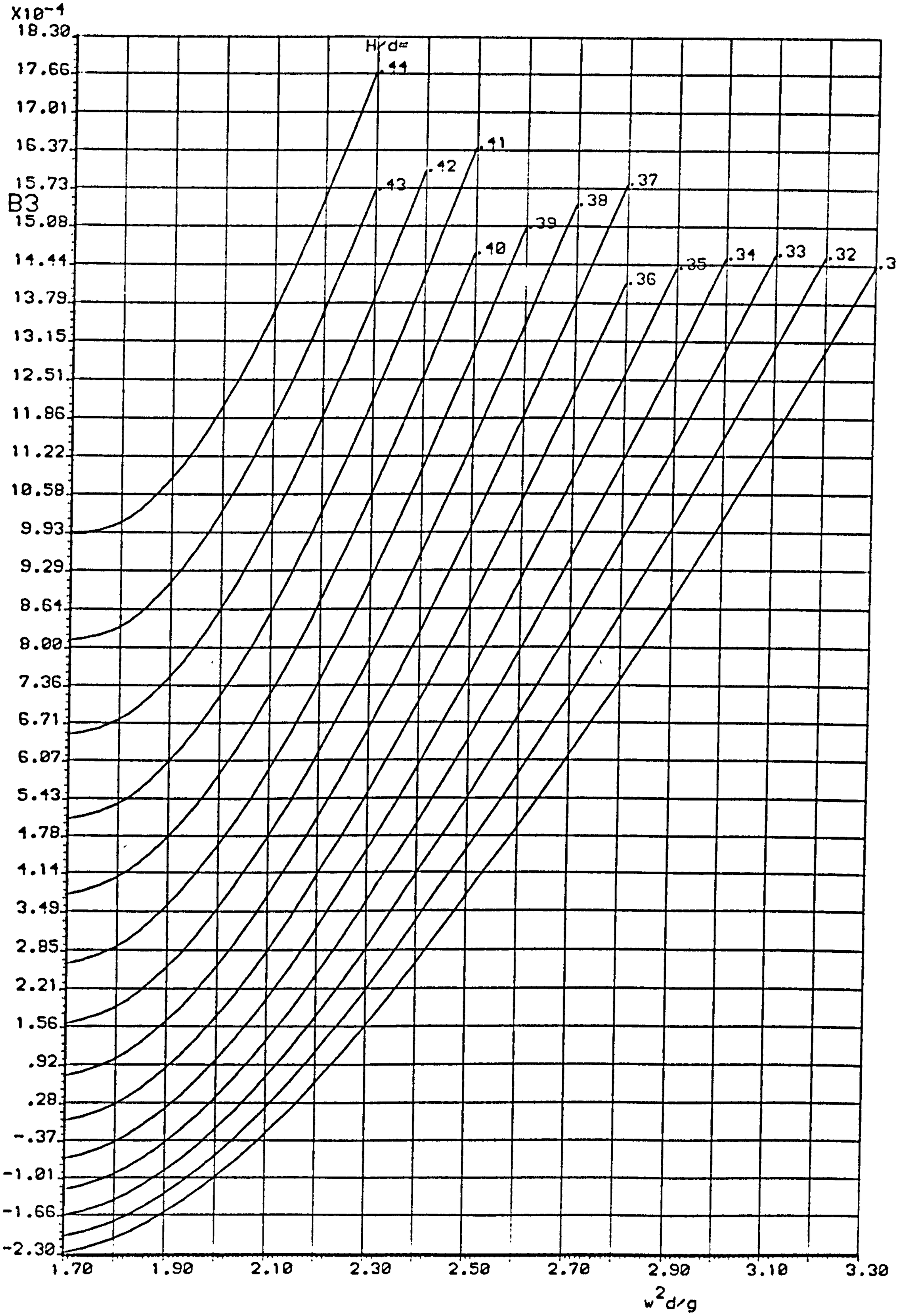

FIG A33 STOKES FIFTH ORDER WAVE COEFFICIENTS

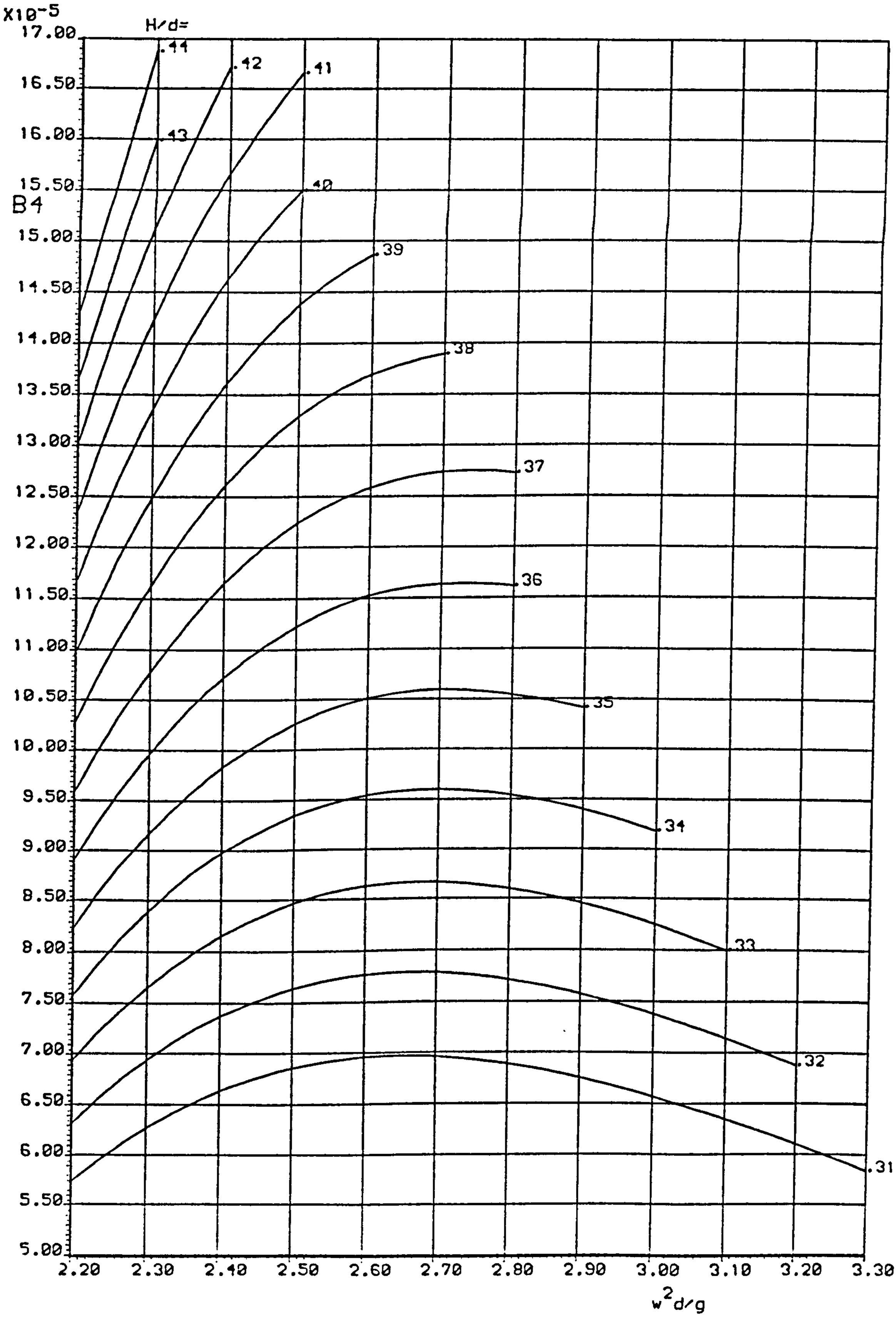

FIG A34 STOKES FIFTH ORDER WAVE COEFFICIENTS

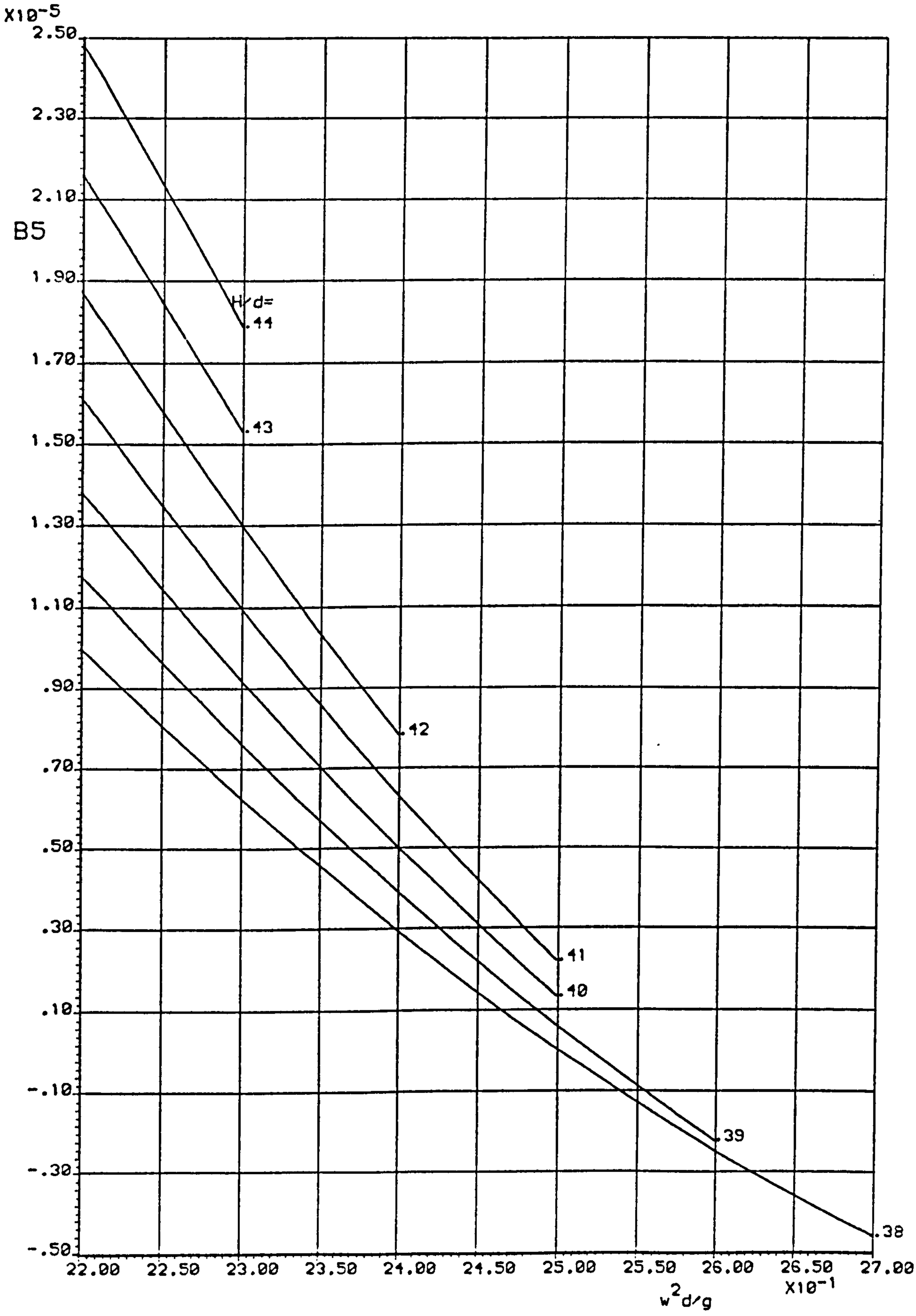

FIG A35 STOKES FIFTH ORDER WAVE COEFFICIENTS

A.3. STREAM FUNCTION THEORY (16)

Considering the coordinate system in Figure A.1 and assuming that it moves with the wave at velocity $\bar{c} = L/T$ a stream function $\psi(x,y)$ must satisfy the Laplace equation

$$\frac{\partial^2 \psi}{\partial x^2} + \frac{\partial^2 \psi}{\partial y^2} = 0 \qquad \text{(A.3.1)}$$

where velocity components u and v are defined as

$$u - \bar{c} = -\frac{\partial \psi}{\partial y} = \frac{\partial \phi}{\partial x} \qquad \text{(A.3.2)}$$

$$v = \frac{\partial \psi}{\partial x} = \frac{\partial \phi}{\partial y} \qquad \text{(A.3.3)}$$

The bottom boundary condition, (A.1.2), and the free surface kinematic and dynamic boundary conditions, (A.2.1) and (A.2.2), still hold. The solution can be written as a Fourier series of linear wave components

$$\psi(x,y) = \bar{c}\cdot y + \sum_{n=1}^{N} X(n) \sinh[nk(d+y)] \cos(nkx) \qquad \text{(A.3.4)}$$

where N represents the order of stream function and $X(n)$ are coefficients to be determined.

Substituting $y = \eta$ in (A.3.4) we get the surface elevation as

$$\eta = \frac{1}{\bar{c}}\psi_\eta - \frac{1}{\bar{c}} \sum_{n=1}^{N} X(n) \sinh[nk(d+\eta)] \cos(nkx) \qquad \text{(A.3.5)}$$

$\psi(x,y)$ satisfies all boundary conditions exactly except for the dynamic free surface boundary condition.

(A.3.5) can be written as

$$\psi_\eta = \bar{c} \cdot \eta(x) + \sum_{n=1}^{N} f_n(\eta(x), x) \qquad \text{(A.3.6)}$$

giving

$$\frac{\partial \psi_\eta}{\partial x} = \bar{c} \cdot \frac{\partial \eta}{\partial x} + \sum_{n=1}^{N} \frac{\partial f_n}{\partial \eta} \cdot \frac{\partial \eta}{\partial x} + \frac{\partial f_n}{\partial x} \qquad \text{(A.3.7)}$$

where

$$\frac{\partial f_n}{\partial \eta} = X(n) \cdot n \cdot k \cdot \cosh[nk(d+\eta)] \cdot \cos(nkx) \qquad \text{(A.3.8)}$$

$$\frac{\partial f_n}{\partial x} = -X(n) \cdot nk \cdot \sinh[nk(d+\eta)] \cdot \sin(nkx) \qquad \text{(A.3.9)}$$

Substituting these into (A.3.7) gives

$$\frac{\partial \psi_\eta}{\partial x} = \bar{c} \cdot \frac{\partial \eta}{\partial x} + \sum_{n=1}^{N} X(n) \cdot nk \cdot \cosh[nk(d+\eta)] \cos(nkx) \cdot \frac{\partial \eta}{\partial x} - X(n) \cdot nk \cdot \sinh[nk(d+\eta)] \sin(nkx) \qquad \text{(A.3.10)}$$

From (A.3.2) and (A.3.3)

$$u = -\sum_{n=1}^{N} X(n) \cdot nk \cdot \cosh[nk(d+\eta)] \cdot \cos(nkx), \text{ AT } y = \eta$$

$$v = -\sum_{n=1}^{N} X(n) \cdot nk \cdot \sinh[nk(d+\eta)] \cdot \sin(nkx), \text{ AT } y = \eta$$

Thus (A.3.7) becomes

$$\frac{\partial \psi_\eta}{\partial x} = \frac{\partial \eta}{\partial x}(\bar{c}-u) + v \qquad \text{(A.3.11)}$$

The kinematic free surface boundary condition, equation (A.2.1), suggests that (A.3.11) is equal to zero, i.e. $v = \frac{\partial \psi_\eta}{\partial x} = 0$. Therefore ψ_η is constant for all x. Taking $L_o = \frac{g T^2}{2\pi}$ where L_o is the deepwater wave length predicted by linear wave theory, equation (A.3.5) can be nondimensionalised as

$$\eta^* = k^* \psi_\eta^* - k^* \sum_{n=1}^{N} X^*_{(n)} \sinh[n k^* H^* (d^* + \eta^*)] \cdot \cos(n \frac{x}{L_o} k^*) \qquad \text{(A.3.12)}$$

Also the nondimensional velocity components are

$$u^* = - \sum_{n=1}^{N} n k^* X^*_{(n)} \cosh[n k^* H^* (d^* + \eta^*)] \cos(n \frac{x}{L_o} k^*) \qquad \text{(A.3.13)}$$

$$v^* = - \sum_{n=1}^{N} n k^* X^*_{(n)} \sinh[n k^* H^* (d^* + \eta^*)] \sin(n \frac{x}{L_o} k^*) \qquad \text{(A.3.14)}$$

and nondimensional celerity

$$c^* = \frac{\bar{c} \cdot T}{L_o} = \frac{2\pi}{k^*} \qquad \text{(A.3.15)}$$

The nondimensional dynamic free surface boundary condition is then given by equation (A.2.2) as

$$\eta^* + \pi H^* (u^{*2} + v^{*2}) - u^* c^* = Q^* \qquad \text{(A.3.16)}$$

where

$$\zeta^* = \zeta / H \qquad \text{(A.3.17)}$$

$$k^* = k.L_o \qquad \text{(A.3.18)}$$

$$\psi_\zeta^* = \psi_\zeta / gHT \qquad \text{(A.3.19)}$$

$$X^*(n) = X(n) / gHT \qquad \text{(A.3.20)}$$

$$H^* = H / L_o \qquad \text{(A.3.21)}$$

$$d^* = d / H \qquad \text{(A.3.22)}$$

$$Q^* = -Q / H \qquad \text{(A.3.23)}$$

The unknowns to be determined are $X^*(n)$, k^* and ψ_ζ^* which are found by minimizing the mean squared error in the equation (A.3.16)

$$E = \frac{1}{J} \sum_{j=1}^{J} (Q_j^* - \overline{Q^*})^2 \qquad \text{(A.3.24)}$$

where $\bar{Q}^* = \bar{Q}/H$ is the nondimensionalised constant in Bernoulli's equation and $\bar{Q}$ can be taken as (P/ρ) where P = atmospheric pressure. The index j is in the range $1 < j < J$ as x takes successive values spanning one complete wave length. Note that $Q^* = Q(x^*(n), k^*)$, thus a nonlinear least square method is used to determine the changes in the unknowns, $\Delta x^*(n)$ and Δk^*, such that error is minimized, i.e.

$$\frac{\partial E}{\partial \Delta k^*} = \frac{\partial E}{\partial \Delta x^*(n)} = 0 \qquad \text{(A.3.25)}$$

Therefore the value of Q^* for j^{th} x-coordinate and at $(i+1)^{th}$ iteration can be found from

$$Q_j^{*(i+1)} = Q_j^{*(i)} + \sum_{n=1}^{N} \left\{ \left(\frac{\partial Q_j^*}{\partial x^*(n)} \right)^{(i)} \cdot \Delta x^*(n) \right\} + \left(\frac{\partial Q_j^*}{\partial k^*} \right)^{(i)} \cdot \Delta k^* \qquad \text{(A.3.26)}$$

and

$$x^{*(i+1)}(n) = x^{*(i)}(n) + \Delta x^*(n) \qquad \text{(A.3.27)}$$

$$k^{*(i+1)} = k^{*(i)} + \Delta k^* \qquad \text{(A.3.28)}$$

Substituting (A.3.26) into (A.3.24) gives the error at $(i+1)^{th}$ iteration as

$$E^{(i+1)} = \frac{1}{J} \sum_{j=1}^{J} \left\{ Q_j^{*(i)} - \bar{Q}^* + \sum_{n=1}^{N} \left(\frac{\partial Q_j^*}{\partial x^*(n)} \right)^{(i)} \cdot \Delta x^*(n) + \left(\frac{\partial Q_j^*}{\partial k^*} \right)^{(i)} \cdot \Delta k^* \right\}^2 \qquad \text{(A.3.29)}$$

Using (A.3.29) and (A.3.25) we have N+1 equations in the unknwons $\Delta X^*(n)$ and Δk^* :

$$\frac{\partial E}{\partial \Delta k^*} = \frac{2}{J}\left\{ \sum_{j=1}^{J} (Q_j^{*(i)} - \bar{Q}^*)\left(\frac{\partial Q_j^*}{\partial k^*}\right)^{(i)} + \sum_{j=1}^{J} \left(\frac{\partial Q_j^*}{\partial k^*}\right)^2 .\Delta k^* + \sum_{j=1}^{J}\sum_{n=1}^{N} \left(\frac{\partial Q_j^*}{\partial k^*}\right)^{(i)} \cdot \left(\frac{\partial Q_j^*}{\partial X^*(n)}\right)^{(i)} .\Delta X^*(n) \right\} = 0$$

(A.3.30)

$$\frac{\partial E}{\partial \Delta X^*(n)} = \frac{2}{J}\left\{ \sum_{j=1}^{J} (Q_j^{*(i)} - \bar{Q}^*)\left(\frac{\partial Q_j^*}{\partial X^*(n)}\right)^{(i)} + \sum_{j=1}^{J} \left(\frac{\partial Q_j^*}{\partial k^*}\right)^{(i)} \cdot \left(\frac{\partial Q_j^*}{\partial X^*(n)}\right)^{(i)} \Delta k^* + \sum_{j=1}^{J}\sum_{m=1}^{N} \left(\frac{\partial Q_j^*}{\partial X^*(m)}\right)^{(i)} \left(\frac{\partial Q_j^*}{\partial X^*(m)}\right)^{(i)} \cdot \Delta X^*(m) \right\} = 0$$

(A.3.31)

Equations (A.3.30) and (A.3.31) can be written in matrix form

$$\{\gamma\} = [A]^{-1}\{B\} \qquad \text{(A.3.32)}$$

where $\{\gamma\}$ and $\{B\}$ are vectors of size $(N+1)$ and $[A]$ is $(N+1)\times(N+1)$ in which

$$g_l = \Delta X^*(l) \qquad , l=1,2,\ldots,N \tag{A.3.33}$$

$$g_{N+1} = \Delta k^* \tag{A.3.34}$$

$$A_{lp} = \sum_{j=1}^{J} \left(\frac{\partial Q_j^*}{\partial x^*(l)}\right)^{(i)} \left(\frac{\partial Q_j^*}{\partial x^*(p)}\right)^{(i)} \quad , \begin{matrix} l=1,2,\ldots,N \\ p=1,2,\ldots,N \end{matrix} \tag{A.3.35}$$

$$A_{lp} = \sum_{j=1}^{J} \left(\frac{\partial Q_j^*}{\partial x^*(l)}\right)^{(i)} \left(\frac{\partial Q_j^*}{\partial k^*}\right)^{(i)} \quad , \begin{matrix} l=1,2,\ldots,N \\ p=N+1 \end{matrix} \tag{A.3.36}$$

$$A_{lp} = \sum_{j=1}^{J} \left(\frac{\partial Q_j^*}{\partial k^*}\right)^2 \qquad , l=p=N+1 \tag{A.3.37}$$

$$B_l = \sum_{j=1}^{J} \left(-Q_j^{*(i)} + \bar{Q}^*\right)\left(\frac{\partial Q_j^*}{\partial x^*(l)}\right)^{(i)} , \quad l=1,2,\ldots,N \tag{A.3.38}$$

$$B_{N+1} = \sum_{j=1}^{J} \left(-Q_j^{*(i)} + \bar{Q}^*\right)\left(\frac{\partial Q_j^*}{\partial k^*}\right)^{(i)} \tag{A.3.39}$$

and derivatives of Q_j^* are found as follows and will be substituted into equations (A.3.32) to (A.3.39)

$$\frac{\partial Q_j^*}{\partial x^*(l)} = \frac{\partial Q_j^*}{\partial \eta_j^*}\cdot\frac{\partial \eta_j^*}{\partial x^*(l)} + \frac{\partial Q_j^*}{\partial u_j^*}\cdot\frac{\partial u_j^*}{\partial x^*(l)} + \frac{\partial Q_j^*}{\partial v_j^*}\cdot\frac{\partial v_j^*}{\partial x^*(l)} \qquad , l=1,2,\ldots,N \tag{A.3.40}$$

$$\frac{\partial Q_j^*}{\partial k^*} = \frac{\partial Q_j^*}{\partial \eta_j^*}\cdot\frac{\partial \eta_j^*}{\partial k^*} + \frac{\partial Q_j^*}{\partial u_j^*}\cdot\frac{\partial u_j^*}{\partial k^*} + \frac{\partial Q_j^*}{\partial v_j^*}\cdot\frac{\partial v_j^*}{\partial k^*} + \frac{\partial Q_j^*}{\partial c^*}\cdot\frac{\partial c^*}{\partial k^*} \tag{A.3.41}$$

taking

$$\theta_j = \frac{k^*}{L_*} x_j = 2\pi\left(\frac{j-1}{J-1}\right) \qquad \text{(A.3.42)}$$

where x_j is the j^{th} x-coordinate along the wave length.
Equation (A.3.12) can be written as

$$\eta_j^* = f_j\left(\eta^*, x^*(n)\right) \qquad , n=1,2,\ldots,N$$

then

$$\frac{\partial \eta_j^*}{\partial x^*(l)} = \frac{\partial f_j}{\partial \eta^*} \cdot \frac{\partial \eta^*}{\partial x^*(l)} + \frac{\partial f_j}{\partial x^*(l)}$$

giving

$$\frac{\partial \eta_j^*}{\partial x^*(l)} = \left(\frac{\partial f_j}{\partial x^*(l)}\right) \Big/ \left(1 - \frac{\partial f_j}{\partial \eta_j^*}\right)$$

thus

$$\frac{\partial \eta_j^*}{\partial x^*(l)} = -k^* \sinh\left[k^* H^* l (d^* + \eta^*)\right] \cos(l\theta_j) \Big/ \left\{1 + \sum_{n=1}^{N} x^*(n) k^{*2} H^* . n \cosh\left[n k^* H^* (d^* + \eta^*)\right] \cos(n\theta_j)\right\}$$

(A.3.43)

From (A.3.16)

$$\frac{\partial Q_j^*}{\partial \eta_j^*} = \frac{\partial Q_j^*}{\partial u_j^*} \cdot \frac{\partial u_j^*}{\partial \eta_j^*} + \frac{\partial Q_j^*}{\partial v_j^*} \cdot \frac{\partial v_j^*}{\partial \eta_j^*} + 1$$

also

$$\frac{\partial u_j^*}{\partial x^*(l)} = \frac{\partial u_j^*}{\partial \eta_j^*} \cdot \frac{\partial \eta_j^*}{\partial x^*(l)} - k^* l \cosh\left[k^* H^* l (d^* + \eta^*)\right] \cos(l\theta_j) \qquad \text{(A.3.44)}$$

$$\frac{\partial v_j^*}{\partial x^*(l)} = \frac{\partial v_j^*}{\partial \eta_j^*} \cdot \frac{\partial \eta_j^*}{\partial x^*(l)} - k^* l \sinh\left[k^* H^* l (d^* + \eta^*)\right] \sin(l\theta_j) \qquad \text{(A.3.45)}$$

Substituting these into (A.3.40) we get

$$\frac{\partial Q_j^*}{\partial x^*(l)} = 2\left[\frac{\partial Q_j^*}{\partial u_j^*} \cdot \frac{\partial u_j^*}{\partial \eta_j^*} + \frac{\partial Q_j^*}{\partial v_j^*} \cdot \frac{\partial v_j^*}{\partial \eta_j^*} + \frac{1}{2}\right]\left(\frac{\partial \eta_j^*}{\partial x^*(l)}\right) -$$
$$k^* l \cosh\left[k^* H^* l (d^* + \eta^*)\right] \cos(l\theta_j)\left(\frac{\partial Q_j^*}{\partial u_j^*}\right) -$$
$$k^* l \sinh\left[k^* H^* l (d^* + \eta^*)\right] \sin(l\theta_j)\left(\frac{\partial Q_j^*}{\partial v_j^*}\right) \qquad \text{(A.3.46)}$$

where from (A.3.16)

$$\frac{\partial Q_j^*}{\partial u_j^*} = 2u^* \pi H^* - \frac{2\pi}{k^*} =$$
$$-2\pi H^* \sum_{n=1}^{N} n X^*(n) k^* \cosh\left[n k^* H^* (d^* + \eta_j^*)\right] \cdot \cos(n\theta_j) - \frac{2\pi}{k^*} \qquad \text{(A.3.47)}$$

$$\frac{\partial Q_j^*}{\partial v_j^*} = 2v^* \pi H^* =$$
$$-2\pi H^* \sum_{n=1}^{N} n X^*(n) k^* \sinh\left[n k^* H^* (d^* + \eta_j^*)\right] \sin(n\theta_j) \qquad \text{(A.3.48)}$$

$$\frac{\partial u_j^*}{\partial \eta_j^*} = - \sum_{n=1}^{N} n^2 X^*(n) k^{*2} H^* \sinh\left[n k^* H^* (d^* + \eta_j^*)\right] \cos(n\theta_j)$$

(A.3.49)

$$\frac{\partial \nu_j^*}{\partial \eta_j^*} = -\sum_{n=1}^{N} n^2 X^*(n) k^{*2} H^* \cosh\left[n k^* H^* (d^* + \eta_j^*)\right] \sin(n\theta_j) \qquad \text{(A.3.50)}$$

Similarly (A.3.41) is written as

$$\frac{\partial Q_j^*}{\partial k^*} = 2\left[\frac{\partial Q_j^*}{\partial u_j^*} \cdot \frac{\partial u_j^*}{\partial \eta_j^*} + \frac{\partial Q_j^*}{\partial \nu_j^*} \cdot \frac{\partial \nu_j^*}{\partial \eta_j^*} + \frac{1}{2}\right]\left(\frac{\partial \eta_j^*}{\partial k^*}\right) -$$

$$\left(\frac{\partial Q_j^*}{\partial u_j^*}\right) \sum_{n=1}^{N} \left\{ \cosh\left[n k^* H^* (d^* + \eta_j^*)\right] + \right.$$

$$\left. n k^* H^* (d^* + \eta_j^*) \sinh\left[n k^* H^* (d^* + \eta_j^*)\right] \right\} n X^*(n) \cos(n\theta_j) -$$

$$\left(\frac{\partial Q_j^*}{\partial \nu_j^*}\right) \sum_{n=1}^{N} \left\{ \sinh\left[n k^* H^* (d^* + \eta_j^*)\right] + \right.$$

$$\left. n k^* H^* (d^* + \eta_j^*) \cosh\left[n k^* H^* (d^* + \eta_j^*)\right] \right\} n X^*(n) \sin(n\theta_j) -$$

$$\left(\frac{2\pi}{k^*}\right) \sum_{n=1}^{N} n X^*(n) \cosh\left[n k^* H^* (d^* + \eta_j^*)\right] \cos(n\theta_j)$$

(A.3.51)

where from (A.3.12) we get

$$\frac{\partial \eta_j^*}{\partial k^*} = \psi_\eta^* - \sum_{n=1}^{N} \left\{ \sinh\left[n k^* H^* (d^* + \eta_j^*)\right] + \right.$$

$$\left. n k^* H^* (d^* + \eta_j^*) \cosh\left[n k^* H^* (d^* + \eta_j^*)\right] \right\} X^*(n) \cos(n\theta_j)$$

(A.3.52)

Values of $\frac{\partial Q^*}{\partial x^*}$ and $\frac{\partial Q^*}{\partial k^*}$ can now be found using equations (A.3.40) to (A.3.52) and equation (A.3.32) can be solved for $\Delta X^{*(n)}$ and Δk^*. Subsequently values of Q_j^*, $X^{*(n)}$ and k^* at $(i+1)^{th}$ iteration are determined from (A.3.26) to (A.3.28) and mean squared error E is found from (A.3.29). Values of η_j^* at $(i+1)^{th}$ iteration can be recalculated from (A.3.12) as

$$\eta_j^{*(i+1)} = k^{*(i+1)} \cdot \psi_\eta^{*(i)} - k^{*(i+1)} \sum_{n=1}^{N} X^{*(i+1)}_{(n)} \sinh\left[n k^{*(i+1)} \cdot H^* (d^* + \eta_j^{*(i)})\right] \cdot \cos(n\theta_j), \quad j = 1, 2, \ldots, J \tag{A.3.53}$$

Also ψ_η^* is redetermined such that the mean water level remains constant, i.e.

$$\int_0^L \eta \, dx = 2 \int_0^{(L/2)} \eta^* \, dx = 2 \int_0^{[\partial T^2 / 2k^{*(i+1)}]} \eta^* \, dx = 0$$

Using (A.3.12) this gives

$$\psi_\eta^{*(i+1)} = \frac{2}{\partial T^2} \int_0^{[\partial T^2 / 2k^{*(i+1)}]} \left\{ k^{*(i+1)} \sum_{n=1}^{N} X^{*(i+1)}_{(n)} \sinh\left[n k^{*(i+1)} H^* (d^* + \eta^{*(i+1)})\right] \cdot \cos\left(\frac{n k^{*(i+1)}}{L_o} \cdot x\right) \right\} dx. \tag{A.3.54}$$

which can be integrated numerically using say Simpson's rule. Summary of the steps to be taken to find $X^{*(n)}$ and k^* is then:

1. Assume an initial value of $k^* = 2\pi T$ (linear wave theory for deep water)

2. Using (A.3.43) to (A.3.50) find $\frac{\partial Q_j^*}{\partial X^*(\ell)}$ and using (A.3.47) to (A.3.52) find $\frac{\partial Q_j^*}{\partial k^*}$ for $j = 1, 2, \cdots, J$ and $\ell = 1, 2, \cdots, N$

3. Using (A.3.33) to (A.3.39) form $[A]$ and $\{B\}$ to solve equation (A.3.32) and find $\Delta X^*(n)$; and Δk^*

4. Find $Q_j^{*(i+1)}$, $X^{*(n)}{}^{(i+1)}$ and $k^{*(i+1)}$ from (A.3.26) to (A.3.28)

5. Find error at $(i+1)^{th}$ iteration from (A.3.29)

6. Find $\eta_j^{*(i+1)}$ for $j = 1, 2, \cdots, J$ and $\psi_\eta^{*(i+1)}$ from (A.3.53) and (A.3.54)

7. Repeat steps 2 to 6 until successive reductions in the error ε are sufficiently small and the crest to trough distance is within an acceptable limit of the original wave height (say 1%)

8. Values of $X(n)$, k and ψ_η can be found using (A.3.18) to (A.3.20).

Note that for a fixed frame of reference x,y we have

$$\psi = \sum_{n=1}^{N} X(n) \sinh[nk(d+y)] \cos[n(kx-\omega t)] \qquad \text{(A.3.55)}$$

$$u = -k \sum_{n=1}^{N} n X(n) \cosh[nk(d+y)] \cos[n(kx-\omega t)] \qquad \text{(A.3.56)}$$

$$v = -k \sum_{n=1}^{N} n X(n) \sinh[nk(d+y)] \sin[n(kx-\omega t)] \qquad \text{(A.3.57)}$$

$$\frac{\partial u}{\partial t} = -k\omega \sum_{n=1}^{N} n^2 X(n) \cosh[nk(d+y)] \sin[n(kx-\omega t)] \quad \text{(A.3.58)}$$

$$\frac{\partial v}{\partial t} = k\omega \sum_{n=1}^{N} n^2 X(n) \sinh[nk(d+y)] \cos[n(kx-\omega t)] \quad \text{(A.3.59)}$$

$$\frac{\partial u}{\partial x} = k^2 \sum_{n=1}^{N} n^2 X(n) \cosh[nk(d+y)] \sin[n(kx-\omega t)] \quad \text{(A.3.60)}$$

$$\frac{\partial v}{\partial x} = -k^2 \sum_{n=1}^{N} n^2 X(n) \sinh[nk(d+y)] \cos[n(kx-\omega t)] \quad \text{(A.3.61)}$$

Values of coefficients for a wide range of conditions are given by Dean (16).

A.4. FIFTH ORDER CNOIDAL WAVE THEORY (23)

Considering the coordinate system X,Y on the sea bed and moving beneath the wave crest in phase with the wave, the boundary value problem, as already mentioned in the previous sections, can be written in terms of a stream function ψ as

$$u = \frac{\partial \psi}{\partial y} \qquad \text{(A.4.1)}$$

$$v = -\frac{\partial \psi}{\partial x} \qquad \text{(A.4.2.)}$$

$$\frac{\partial^2 \psi}{\partial x^2} + \frac{\partial^2 \psi}{\partial y^2} = 0 \qquad \text{(A.4.3.)}$$

$$\psi = 0 \quad , \text{ON } Y=0 \qquad \text{(A.4.4.)}$$

$$\psi = -\psi_\eta = \text{CONSTANT} \quad , \text{AT } Y = \eta(x) \qquad \text{(A.4.5.)}$$

$$\frac{1}{2}\left[\left(\frac{\partial \psi}{\partial x}\right)^2 + \left(\frac{\partial \psi}{\partial y}\right)^2\right]_{y=\eta} + g\eta = R \qquad \text{(A.4.6.)}$$

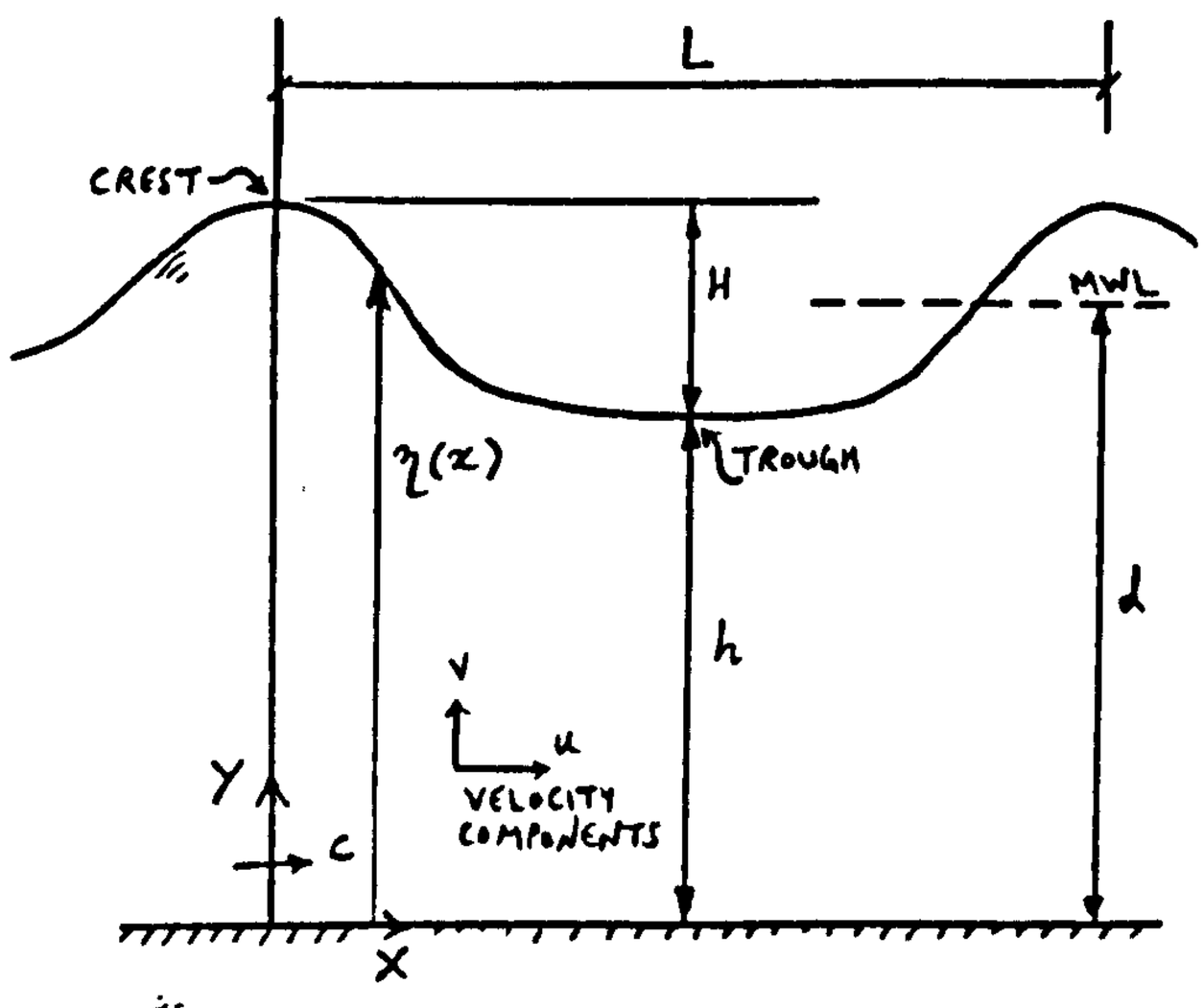

FIG.A36. CNOIDAL WAVES - COORDINATE SYSTEM

A general power series solution to ψ which satisfies Laplace equation (A.4.3.) as well as the bottom boundary condition (A.4.4.) can be given by

$$\psi = -\sin\left[\gamma \mathcal{D} f(x)\right] \qquad \text{(A.4.7.)}$$

where $\mathcal{D}$ is the differential operator and $f(x)$ is a function to be determined by free surface boundary conditions Equation (A.4.7.) can be expanded as

$$\psi = -\gamma \frac{df(x)}{dx} + \frac{\gamma^3}{3!}\cdot\frac{d^3 f(x)}{dx^3} - \frac{\gamma^5}{5!}\cdot\frac{d^5 f(x)}{dx^5} + \cdots \qquad \text{(A.4.8.)}$$

and $f'(x) = \dfrac{df(x)}{dx}$ is the horizontal fluid velocity at Y = O. From (A.4.8.) we have

$$\frac{d\psi}{dY} = -\frac{df(x)}{dx} + \frac{\gamma^2}{2!}\cdot\frac{d^3 f(x)}{dx^3} - \frac{\gamma^4}{4!}\cdot\frac{d^5 f(x)}{dx^5} + \cdots \qquad \text{(A.4.9.)}$$

$$\frac{d\psi}{dx} = -\gamma\frac{d^2 f(x)}{dx^2} + \frac{\gamma^3}{3!}\cdot\frac{d^4 f(x)}{dx^4} - \frac{\gamma^5}{5!}\cdot\frac{d^6 f(x)}{dx^6} + \cdots \qquad \text{(A.4.10)}$$

(A.4.5.) and (A.4.6.) can be written as

$$\psi_\zeta = \zeta\frac{df(x)}{dx} - \frac{\zeta^3}{3!}\cdot\frac{d^3 f(x)}{dx^3} + \frac{\zeta^5}{5!}\cdot\frac{d^5 f(x)}{dx^5} - \cdots \qquad \text{(A.4.11)}$$

$$\frac{1}{2}\left[\left(-\zeta\frac{d^2 f(x)}{dx^2} + \frac{\zeta^3}{3!}\cdot\frac{d^4 f(x)}{dx^4} - \frac{\zeta^5}{5!}\cdot\frac{d^6 f(x)}{dx^6} + \cdots\right)^2 + \left(-\frac{df(x)}{dx} + \frac{\zeta^2}{2!}\cdot\frac{d^3 f(x)}{dx^3} - \frac{\zeta^4}{4!}\cdot\frac{d^5 f(x)}{dx^5} + \cdots\right)^2\right] + \partial\zeta = R \qquad \text{(A.4.12)}$$

To non-dimensionalise these let

$$X_* = x/h \qquad \text{(A.4.13)}$$

$$\eta_* = \eta/h \qquad \text{(A.4.14)}$$

$$f_* = f(x)/\psi_\eta \qquad \text{(A.4.15)}$$

$$g_* = g h^3/\psi_\eta^2 \qquad \text{(A.4.16)}$$

$$r_* = R h^2/\psi_\eta^2 \qquad \text{(A.4.17)}$$

Note that η = distance from sea bed to surface elevation and h = distance from sea bed to wave trough.

Therefore (A.4.11) and (A.4.12) become

$$\eta_* \frac{df_*}{dX_*} - \frac{\eta_*^3}{3!}\frac{d^3 f_*}{dX_*^3} + \frac{\eta_*^5}{5!}\frac{d^5 f_*}{dX_*^5} - \cdots = 1 \qquad \text{(A.4.18)}$$

$$\frac{1}{2}\left[\left(-\eta_* \frac{d^2 f_*}{dX_*^2} + \frac{\eta_*^3}{3!}\frac{d^4 f_*}{dX_*^4} - \frac{\eta_*^5}{5!}\frac{d^6 f_*}{dX_*^6} + \cdots\right)^2 + \left(-\frac{df_*}{dX_*} + \frac{\eta_*^2}{2!}\frac{d^3 f_*}{dX_*^3} - \frac{\eta_*^4}{4!}\frac{d^5 f_*}{dX_*^5} + \cdots\right)^2\right] + g_* \eta_* = r_* \qquad \text{(A.4.19)}$$

Differentiating (A.4.18) with respect to X_* and noting that

$$\frac{d}{dX_*}\left(\frac{\eta_*^3}{3!}\right) = \frac{d}{dX_*}\left[\left(\frac{\eta}{x}\right)^3 \cdot \frac{X_*^3}{3!}\right] = \left(\frac{\eta}{x}\right)^3 \cdot \frac{X_*^2}{2!} =$$

$$\left(\frac{\eta}{x}\right)^2 \cdot \frac{X_*^2}{2!}\left(\frac{\eta}{x}\right) = \frac{\eta_*^2}{2!} \cdot \frac{d\eta_*}{dX_*}$$

or generally

$$\frac{d}{dx_*}\left(\frac{\zeta_*^{2n+1}}{2n+1}\right) = \frac{d\zeta_*}{dx_*}\left(\frac{\zeta_*^{2n}}{2n!}\right) \qquad , n = 1, 2, \ldots.$$

we get

$$\frac{d\zeta_*}{dx_*}\left[\frac{df_*}{dx_*} - \frac{\zeta_*^2}{2!}\cdot\frac{d^3f_*}{dx_*^3} + \frac{\zeta_*^4}{4!}\frac{d^5f_*}{dx_*^5} - \ldots.\right] = \left(-\zeta_*\frac{d^2f_*}{dx_*^2} + \frac{\zeta_*^3}{3!}\cdot\frac{d^4f_*}{dx_*^4} - \ldots.\right)$$

Using this in (A.4.19) we have

$$\frac{1}{2}\left[1+\left(\frac{d\zeta_*}{dx_*}\right)^2\right]\left[1-\frac{\zeta_*^2}{2!}\cdot\frac{d^3f_*}{dx_*^3} + \frac{\zeta_*^4}{4!}\cdot\frac{d^5f_*}{dx_*^5} - \ldots.\right]^2 +$$

$$g_*\zeta_* - r_* = 0 \qquad \text{(A.4.20)}$$

Equations (A.4.18) and (A.4.20) can be written in terms of $f'_* = \frac{df_*}{dx_*}$ as

$$\zeta_* f'_* - \frac{\zeta_*^3}{3!}\cdot\frac{d^2(f'_*)}{dx_*^2} + \frac{\zeta_*^5}{5!}\cdot\frac{d^4(f'_*)}{dx_*^4} + \ldots. - 1 = 0 \qquad \text{(A.4.21)}$$

$$\frac{1}{2}\left[1+\left(\frac{d\zeta_*}{dx_*}\right)^2\right]\left[1-\frac{\zeta_*^2}{2!}\cdot\frac{d^2(f'_*)}{dx_*^2} + \frac{\zeta_*^4}{4!}\cdot\frac{d^4(f'_*)}{dx_*^4} - \ldots.\right]^2 + g_*\zeta_* - r_* = 0$$

(A.4.22)

Equations (A.4.21) and (A.4.22) have the trivial solution of $\zeta_* = f'_* = g_* = 1$ and $r_* = \frac{3}{2}$ and all quantities will be expanded about this state. Assuming variations with

X_* to be as αX_* where α is a parameter to be determined and because even derivatives of f'_* occur in (A.4.21) and (A.4.22) terms like $\frac{d^{2n}}{d(X_*)^{2n}}\left[\frac{df_*(\alpha X_*)}{d(\alpha X_*)}\right]$ will occur. Noting that

$$\frac{d^{2n}}{dX_*^{2n}}\left[\frac{df_*(\alpha X_*)}{d(\alpha X_*)}\right] = (\alpha^2)^n \frac{d^{(2n+1)}}{d(\alpha X_*)^{2n+1}}\left[f_*(\alpha X_*)\right]$$

e.g. If n = 1 and $f_*(\alpha X_*) = a + (\alpha X_*) + (\alpha X_*)^2 + (\alpha X_*)^3 + \cdots$

$$f'_* = 1 + 2(\alpha X_*) + 3(\alpha X_*)^2 + 4(\alpha X_*)^3 + \cdots$$

$$\frac{d^2 f'_*}{dX_*^2} = 6\alpha^2 + 24\alpha^3 X_*$$

$$\frac{d^3 f_*}{d(\alpha X_*)^3} = 6 + 24(\alpha X_*)$$

giving

$$\frac{d^2 f'_*}{dX_*^2} = \alpha^2 \frac{d^3 f_*}{d(\alpha X_*)^3}$$

It can be seen that powers of α^2 occur in the expansions. Hence we can expand in terms of α^2 i.e. we can write

$$\eta_* = 1 + \sum_{i=1}^{\infty} (\alpha^2)^i \; Y_i(\alpha X_*) \qquad \text{(A.4.23)}$$

$$f'_* = 1 + \sum_{i=1}^{\infty} (\alpha^2)^i \; F_i \; (\alpha X_*) \qquad \text{(A.4.24)}$$

$$g_* = 1 + \sum_{i=1}^{\infty} (\alpha^2)^i \; g_i \qquad \text{(A.4.25)}$$

$$r_* = \frac{3}{2} + \sum_{i=1}^{\infty} (\alpha^2)^i \; r_i \qquad \text{(A.4.26)}$$

Substitution of these into (A.4.21) and using derivatives of (A.4.24) gives

$$[1 + \alpha^2 Y_1 + \alpha^4 Y_2 + \alpha^6 Y_3 + \cdots][1 + \alpha^2 F_1 + \alpha^4 F_2 + \alpha^6 F_3 + \cdots] -$$

$$\frac{1}{3!}[1 + \alpha^2 Y_1 + \alpha^4 Y_2 + \alpha^6 Y_3 + \cdots]^3 [\alpha^4 F_1'' + \alpha^6 F_2'' + \alpha^8 F_3''] + \cdots - 1 = 0 \qquad \text{(A.4.27)}$$

Where a dash indicates differentiation with respect to X_*
Equating coefficients of each α^{2i} to zero we have

α^2:

$$F_1 + Y_1 = 0 \qquad \text{(A.4.28)}$$

$$F_1 + Y_1 + g_1 - r_1 = 0 \qquad \text{(A.4.29)}$$

α^4:

$$F_2 + Y_2 + F_1 Y_1 - \frac{1}{6} F_1'' = 0 \qquad \text{(A.4.30)}$$

$$F_2 + Y_2 + g_2 - r_2 - \frac{1}{2} F_1'' + \frac{1}{2} F_1^2 - g_1 Y_1 = 0 \qquad \text{(A.4.31)}$$

Subtracting (A.4.30) from (A.4.31) gives

$$F_1'' = 3\left[(\partial_2 - r_2) - \partial_1 F_1 + \frac{3}{2} F_1^2 \right] \qquad \text{(A.4.32)}$$

Multiplying this by F_1' and integrating with respect to (αX_*) we get

$$(F_1')^2 = 3\left[(\partial_2 - r_2) F_1 - 3\partial_1 F_1 + 3F_1^3 \right]$$

Implying that F_1' can be written as

$$F_1' = \sqrt{(F_1-\beta)(F_1-\gamma)(F_1-\Omega)} \quad , \Omega > \beta > \gamma$$

Note that η_* and γ_1 are always positive (see A.4.23) and using (A.4.28) it can be seen that F_1 is negative. Writing the standard Jacobian elliptic integral of the first kind as

$$(\alpha X_*) = \int_{\gamma}^{F_1} \frac{dF_1}{\sqrt{(F_1-\beta)(F_1-\gamma)(F_1-\Omega)}} = C_n^{-1}\left(\sqrt{\frac{\beta - F_1}{\beta-\gamma}} \backslash m \right)$$

where C_n is the Jacobian elliptic function with modulus $m = \frac{\beta-\gamma}{\Omega-\gamma}$, $1 \geq m \geq 0$ (see (28)) and noting that $\beta = 0$ here, we get a solution of the form

$$F_1 = \gamma C_n^2 (\alpha X_* \backslash m)$$

and

$$m = \frac{-\gamma}{\Omega - \gamma}$$

This gives

$$F_1' = -2\gamma \left[Cn \cdot Sn \cdot dn \right]$$

$$F_1'' = -2\gamma \left\{ -m\, Sn^2\, Cn^2 - dn^2\, Sn^2 + dn^2\, Cn^2 \right\}$$

Substituting these into (A.4.32) and using $Sn^2 = 1 - Cn^2$ and $dn^2 = 1 + m(Cn^2 - 1)$ we get

$$(g_2 - r_2) + \frac{2\gamma}{3}(-4m + 2)\, Cn^2 + 2\gamma m\, Cn^4 +$$

$$\frac{2\gamma(m-1)}{3} + \frac{3}{2}\gamma^2 Cn^4 - g_1 \gamma\, Cn^2 = 0 \qquad \text{(A.4.33)}$$

Now each power of Cn must satisfy (A.4.33), giving

$$\gamma = -\frac{4}{3} m \qquad \text{(A.4.34)}$$

$$g_1 = \frac{4}{3}(1 - 2m) \qquad \text{(A.4.35)}$$

$$r_2 - g_2 = \frac{8}{9} m(1 - m) \qquad \text{(A.4.36)}$$

and

$$F_1 = -\frac{4}{3} m\, Cn^2 \left(\alpha X_* \backslash m \right) \qquad \text{(A.4.37)}$$

Functions of Cn and Cn^2 have real periods of $4K(m)$ and $2K(m)$ respectively, where K is the complete elliptic integral of the first kind given by (see (1))

$$K(m) = \frac{\pi}{2}\left[1 + \left(\frac{1}{2}\right)^2 m + \left(\frac{1\cdot 3}{2\cdot 4}\right)^2 m^2 + \left(\frac{1\cdot 3\cdot 5}{2\cdot 4\cdot 6}\right)^2 m^3 + \ldots\right]$$

(A.4.38)

Using (A.4.37) and (A.4.28) equation (A.4.23) gives

$$\eta_* = 1 + \frac{4}{3} m \alpha^2 Cn^2(\alpha X_* \backslash m) + O(\alpha^4)$$

Using the boundary condition that $\eta_* = 1 + H/h$ at crest we get

$$\alpha = \left(\frac{3}{4m}\cdot\frac{H}{h}\right)^{\frac{1}{2}} + O\left((H/h)^{\frac{3}{2}}\right)$$

and

$$\eta_* = 1 + (H/h)\, Cn^2(\alpha X_* \backslash m) + O\left((H/h)^2\right)$$

Similarly by considering higher order terms of α^2 and assuming that $F_n = \sum_{k=0}^{n}\sum_{l=0}^{n} F_{nkl}\,(Cn^2)^k\, m^l$, where F_{nkl} are coefficients found by requiring that each power of Cn^2 satisfies the appropriate differential equation (as in A.4.33), higher order solutions can be obtained. Note that parameter α is found in terms of (H/h) and m using $\eta_*(0) = 1 + H/h = 1 + \alpha^2 \gamma_1(0) + \alpha^4 \gamma_2(0) + \cdots$. To convert the expansion parameter α to the more commonly used dimensionless wave height parameter, $\varepsilon = H/h$, the series in α^2 can be reverted using a computer to give α^2 as a series in ε

Taking

$$\bar{\varepsilon} = H/d \qquad \text{(A.4.39)}$$

$$\varepsilon = H/h = \bar{\varepsilon}/(h/d) \qquad \text{(A.4.40)}$$

$$(\varepsilon/m) = a \qquad \text{(A.4.41)}$$

$$(\bar{\varepsilon}/m) = \bar{a} \qquad \text{(A.4.42)}$$

α up to the fifth order can be expressed as

$$\alpha = \left(\frac{3}{4}a\right)^{\frac{1}{2}} \left\{ 1 + a(0.25 - 0.875\,m) + a^2(0.03125 - 0.34375\,m + 0.86719\,m^2) + \right.$$

$$a^3(-0.37743 + 0.51146\,m + 0.13743\,m^2 - 0.833\,m^3) +$$

$$\left. a^4(0.20322 + 0.44278\,m - 1.38145\,m^2 + 0.54282\,m^3 + 0.76773\,m^4) \right\}$$

(A.4.43)

and the wave profile is given by

$$\eta_* = (\eta/h) = 1 + a\,m\,G_n^2 + a^2\left[0.75\,m^2(-G_n^2 + G_n^4)\right] +$$

$$a^3\left[0.7625\,m^2(-G_n^2 + G_n^4) + m^3(1.3875\,G_n^2 - 2.65\,G_n^4 + 1.2625\,G_n^6)\right] +$$

$$a^4 \left[0.80533\, m^2 \left(-C_n^2 + C_n^4\right) + m^3 \left(2.48904\, C_n^2 - 4.33146\, C_n^4 + 1.84242\, C_n^6\right) + \right.$$

$$\left. m^4 \left(-3.05188\, C_n^2 + 7.40646\, C_n^4 - 6.52546\, C_n^6 + 2.17088\, C_n^8\right) \right] +$$

$$a^5 \left[0.43643\, m^2 \left(C_n^2 - C_n^4\right) + m^3 \left(1.9228\, C_n^2 - 4.66167\, C_n^4 + 2.73888 C_n^6\right) + \right.$$

$$m^4 \left(-7.04588\, C_n^2 + 17.45561\, C_n^4 - 15.316977\, C_n^6 + 4.90723\, C_n^8\right) +$$

$$m^5 \left(6.54722\, C_n^2 - 19.80887\, C_n^4 + 25.34187\, C_n^6 - \right.$$

$$16.32709\, C_n^8 +$$

$$\left. 4.24687\, C_n^{10}\right) \Bigg]$$

(A.4.44)

Defining the wave celerity as $c = \frac{1}{L}\int_0^L u.dx$ and taking

$$b = E(m) \,/\, K(m) \qquad \text{(A.4.45)}$$

where E(m) is the complete elliptic integral of second kind given by

$$E(m) = \frac{\pi}{2}\left[1 - \left(\frac{1}{2}\right)^2 \frac{m}{1} - \left(\frac{1\cdot 3}{2\cdot 4}\right)^2 \frac{m^2}{3} - \left(\frac{1\cdot 3\cdot 5}{2\cdot 4\cdot 6}\right)^2 \frac{m^3}{5} - \ldots\right]$$

(A.4.46)

Results of this theory are as follows:

DIMENSIONLESS WAVE PERIOD

$$T_* = T(g/d)^{\frac{1}{2}} = \frac{4K(m)}{(3\bar{a})^{\frac{1}{2}}}\left\{1+\bar{a}(0.25-0.125m)+\bar{a}^2[0.01458-1.08333b+b^2+m(-0.01458+0.54167b)-0.07656m^2]+\bar{a}^3[0.36121+2.50417b-4.5b^2+2b^3+m(-0.54182-2.50417b+2.25b^2)+m^2(0.41216+0.33229b)-0.11578m^3]+\bar{a}^4[-1.86885-4.22859b+15.19111b^2-13.66667b^3+4b^4+m(3.73770+6.34288b-15.19111b^2+6.83333b^3)+m^2(-2.73031-1.88433b+2.69111b^2)+m^3(0.86147-0.11498b)-0.07582m^4]\right\}$$

(A.4.47)

$$\frac{h}{\bar{\eta}} = 1+\bar{a}\{1-b-m\}+\bar{a}^2\{-0.5+0.5b+m[0.5-0.25b]\}+\bar{a}^3\{0.665-1.165b+0.5b^2+m[-0.99750+1.165b-0.25b^2]+m^2[0.33250-0.04b]\}+\bar{a}^4\{-1.62667+3.20667b-2.08b^2+0.5b^3+m[3.25333-4.81b+2.08b^2-0.25b^3]+m^2[-2.454+2.17633b-0.14250b^2]+m^3[0.82733-0.28650b]\}+\bar{a}^5\{4.86659-10.74409b+8.62250b^2-3.245b^3+0.5b^4+m[-12.16647+21.48818b-12.93375b^2+3.245b^3-0.25b^4]+m^2[11.79929-16.00776b+6.09025b^2-0.30750b^3]+m^3[-5.53247+5.26318b-0.88950b^2]+m^4[1.03306-0.20555b]\}$$

(A.4.48)

DIMENSIONLESS WAVE CELERITY

$$C_* = \frac{c}{(gh)^{\frac{1}{2}}} = 1+a\{0.5-b\}+a^2\{-0.10833+0.33333b+m[-0.01667+0.08333b]-0.025m^2\}+a^3\{-0.17190+0.09333b+m[0.33911-0.34333b]+m^2[-0.16006+0.21833b]+0.04643m^3\}+a^4\{0.02097+0.37690b+m[0.17293-0.68202b]+m^2[-0.56238+1.04889b]+m^3[0.39861-0.56668b]-0.08531m^4\}+a^5\{0.11046-0.94038b+m[-0.31285+1.22117b]+m^2[-0.11262+0.35314b]+m^3[0.91605-1.75325b]+m^4[-0.73881+1.00619b]+0.15763m^5\}$$

(A.4.49)

$$\frac{u(x_*,y_*,t)}{(gh)^{\frac{1}{2}}} = C_* - 1 - \left\{a\{-0.5+m[1-C_n^2(\gamma)]\}+a^2\{0.225+m[-0.6+0.75y_h^2+C_n^2(\gamma)(1-1.5y_h^2)]+m^2[0.225-0.75y_h^2+C_n^2(\gamma)(-1.25+3.0y_h^2)+C_n^4(\gamma)(1.0-2.25y_h^2)]\}+a^3\{-0.07857+\right.$$

$$m\left[0.14911-0.375\,y_h^2+0.18750\,y_h^4+Cn^2(z)\left(-0.4+0.75\,y_h^2-0.375\,y_h^4\right)\right]+m^2\left[0.16161-0.56250\,y_h^4+Cn^2(z)\left(1.35-5.25\,y_h^2+3.18750\,y_h^4\right)+Cn^4(z)\left(-1.7+7.125\,y_h^2-2.8125\,y_h^4\right)\right]+m^3\left[-0.17857+0.375\,y_h^2+0.375\,y_h^4+Cn^2(z)\left(-0.475+3.0\,y_h^2-3.18750\,y_h^4\right)+Cn^4(z)\left(1.9-10.875\,y_h^2+5.625\,y_h^4\right)+Cn^6(z)\left(-1.2+7.5\,y_h^2-2.81250\,y_h^4\right)\right]\Big\}+a^4\Big\{0.39788+m\left[-0.74576+0.01875\,y_h^2+0.01875\,y_h^6+Cn^2(z)\left(0.09643-0.0375\,y_h^2-0.0375\,y_h^6\right)\right]+m^2\left[0.73477-0.09375\,y_h^2+0.14063\,y_h^4-0.17813\,y_h^6+Cn^2(z)\left(-0.46431+5.625\,y_h^2-4.78125\,y_h^4+1.23750\,y_h^6\right)+Cn^4(z)\left(0.81967-7.25625\,y_h^2+6.0\,y_h^4-1.18125\,y_h^6\right)\right]+m^3\left[-0.67908+0.66562\,y_h^2+0.14063\,y_h^4+0.31875\,y_h^6+Cn^2(z)\left(0.55694-7.55625\,y_h^2+9.70312\,y_h^4-3.48750\,y_h^6\right)+Cn^4(z)\left(-3.04667+29.025\,y_h^2-33.42187\,y_h^4+7.0875\,y_h^6\right)+Cn^6(z)\left(2.90133-25.2\,y_h^2+24.375\,y_h^4-3.93750\,y_h^6\right)\right]+m^4\left[0.23701-0.59063\,y_h^2-0.28125\,y_h^4-0.15938\,y_h^6+Cn^2(z)\left(0.17018+3.0375\,y_h^2-4.07812\,y_h^4+2.325\,y_h^6\right)+Cn^4(z)\left(1.03417-17.07188\,y_h^2+27.09375\,y_h^4-7.08750\,y_h^6\right)+Cn^6(z)\left(-3.10267+33.525\,y_h^2-42.42187\,y_h^4+7.875\,y_h^6\right)+Cn^8(z)\left(1.576-18.9\,y_h^2+19.68750\,y_h^4-2.95313\,y_h^6\right)\right]\Big\}+a^5\Big\{-0.82992+m\left[1.76991-0.57050\,y_h^2-0.01875\,y_h^4+0.00937\,y_h^6+0.001\,y_h^8+Cn^2(z)\left(-0.78281+1.141\,y_h^2+0.03750\,y_h^4-0.01875\,y_h^6-0.00201\,y_h^8\right)\right]+m^2\left[-0.99629+1.44569\,y_h^2-0.45\,y_h^4+0.11719\,y_h^6-0.03415\,y_h^8+Cn^2(z)\left(0.89794-4.45837\,y_h^2+3.84375\,y_h^4-1.59375\,y_h^6+0.26016\,y_h^8\right)+Cn^4(z)\left(0.49893+2.27950\,y_h^2-3.91875\,y_h^4+1.80938\,y_h^6-0.25614\,y_h^8\right)\right]+m^3\left[-0.41272-1.29006\,y_h^2+0.96797\,y_h^4-0.25313\,y_h^6+0.12656\,y_h^8+Cn^2(z)\left(-0.66324+5.86650\,y_h^2-16.09219\,y_h^4+9.84375\,y_h^6-1.64833\,y_h^8\right)+Cn^4(z)\left(1.20740-31.13156\,y_h^2+63.225\,y_h^4-31.55625\,y_h^6+3.70647\,y_h^8\right)+Cn^6(z)\left(-2.26014+31.778\,y_h^2-53.23125\,y_h^4+22.96875\,y_h^6-2.21484\,y_h^8\right)\right]+m^4\left[0.83138-0.38012\,y_h^2-1.6016\,y_h^4+0.05156\,y_h^6-0.15569\,y_h^8+Cn^2(z)\left(0.70429-2.12075\,y_h^2+16.30547\,y_h^4-13.23750\,y_h^6+2.77634\,y_h^8\right)+Cn^4(z)\left(-2.71917+42.62962\,y_h^2-110.93203\,y_h^4+73.18125\,y_h^6-9.58259\,y_h^8\right)+Cn^6(z)\left(7.12267-110.618\,y_h^2+225.63750\,y_h^4-115.5\,y_h^6+11.70703\,y_h^8\right)+Cn^8(z)\left(-4.96993+74.07\,y_h^2-131.90625\,y_h^4+55.61719\,y_h^6-4.74609\,y_h^8\right)\right]+m^5\left[-0.34250+0.795\,y_h^2+0.66094\,y_h^4+0.075\,y_h^6+0.06228\,y_h^8+Cn^2(z)\left(-0.26144-2.23875\,y_h^2-5.39297\,y_h^4+4.875\,y_h^6-1.38817\,y_h^8\right)+Cn^4(z)\left(0.43733-11.405\,y_h^2+47.56406\,y_h^4-41.7\,y_h^6+6.38839\,y_h^8\right)+Cn^6(z)\left(-2.69367+61.73675\,y_h^2-162.53203\,y_h^4+103.68750\,y_h^6-11.70703\,y_h^8\right)+Cn^8(z)\left(5.21186-91.44\,y_h^2+204.75\,y_h^4-102.375\,y_h^6+9.49219\,y_h^8\right)+Cn^{10}(z)\left(-2.19396+42.552\,y_h^2-85.05\,y_h^4+35.43750\,y_h^6-2.84766\,y_h^8\right)\right]\Big\}\Big\}\Big\} \tag{A.4.50}$$

NOTE THAT $y_h = (Y/h)$

$$\frac{v}{(gh)^{\frac{1}{2}}} = -2\alpha\, Cn(z)\, sn(z)\, dn(z)\Big\{\Big\{a\left\{-m\,y_h\right\}+a^2\left\{m\left[y_h-0.5\,y_h^3\right]+m^2\left[-1.25\,y_h+y_h^3+Cn^2(z)\left(2\,y_h-1.5\,y_h^3\right)\right]\right\}+$$

$$a^3\left\{m[-0.4y_h+0.25y_h^3-0.075y_h^5]+m^2[1.35y_h-1.75y_h^3+0.6375y_h^5+Cn^2(3)(-3.4y_h+4.75y_h^3-1.125y_h^5)]+m^3[-0.475y_h+y_h^3-0.6375y_h^5+Cn^2(3)(3.8y_h-7.25y_h^3+2.25y_h^5)+Cn^4(3)(-3.6y_h+7.5y_h^3-1.6875y_h^5)]\right\}+a^4\left\{m[0.09643y_h-0.0125y_h^3-0.00536y_h^7]+m^2[-0.46431y_h+1.875y_h^3-0.95625y_h^5+0.176786y_h^7+Cn^2(3)(1.63934y_h-4.8375y_h^3+2.4y_h^5-0.3375y_h^7)]+m^3[0.55694y_h-2.51875y_h^3+1.940624y_h^5-0.498214y_h^7+Cn^2(3)(-6.09334y_h+19.35y_h^3-13.368748y_h^5+2.025y_h^7)+Cn^4(3)(8.70399y_h-25.2y_h^3+14.625y_h^5-1.6875y_h^7)]+m^4[0.17018y_h+1.0125y_h^3-0.815624y_h^5+0.332143y_h^7+Cn^2(3)(2.06834y_h-11.381253y_h^3+10.8375y_h^5-2.025y_h^7)+Cn^4(3)(-9.30801y_h+33.525y_h^3-25.453122y_h^5+3.375y_h^7)+Cn^6(3)(6.304y_h-25.2y_h^3+15.75y_h^5-1.687503y_h^7)]\right\}+a^5\left\{m[-0.78281y_h+0.380333y_h^3+0.0075y_h^5-0.002678y_h^7-0.000223y_h^9]+m^2[0.89794y_h-1.486123y_h^3+0.76875y_h^5-0.227678y_h^7+0.028907y_h^9+Cn^2(3)(0.99786y_h+1.519667y_h^3-1.5675y_h^5+0.516966y_h^7-0.05692y_h^9)]+m^3[-0.66324y_h+1.9555y_h^3-3.218438y_h^5+1.40625y_h^7-0.183148y_h^9+Cn^2(3)(2.4148y_h-20.754373y_h^3+25.29y_h^5-9.016071y_h^7+0.82366y_h^9)+Cn^4(3)(-6.78042y_h+31.778y_h^3-31.93875y_h^5+9.84375y_h^7-0.73828y_h^9)]+m^4[0.70429y_h-0.706917y_h^3+3.261094y_h^5-1.891071y_h^7+0.308482y_h^9+Cn^2(3)(-5.43834y_h+28.419746y_h^3-44.372812y_h^5+20.908928y_h^7-2.129464y_h^9)+Cn^4(3)(21.36801y_h-110.618y_h^3+135.3825y_h^5-49.5y_h^7+3.902343y_h^9)+Cn^6(3)(-19.87972y_h+98.76y_h^3-105.525y_h^5+31.781251y_h^7-2.109373y_h^9)]+m^5[-0.26144y_h-0.74625y_h^3-1.078594y_h^5+0.696428y_h^7-0.154241y_h^9+Cn^2(3)(0.87466y_h-7.60333y_h^3+19.025624y_h^5-11.914285y_h^7+1.419642y_h^9)+Cn^4(3)(-8.08101y_h+61.73675y_h^3-97.519218y_h^5+44.4375y_h^7-3.902343y_h^9)+Cn^6(3)(20.84744y_h-121.92y_h^3+163.8y_h^5-58.5y_h^7+4.218751y_h^9)+Cn^8(3)(-10.9698y_h+70.92y_h^3-85.05y_h^5+25.3125y_h^7-1.582033y_h^9)]\right\}\right\} \qquad (A.4.51)$$

$$\frac{1}{g}\frac{\partial u}{\partial t}=-C_*\left(\frac{h}{g}\right)^{\frac{1}{2}}\frac{\partial u}{\partial x} \quad \text{AND} \quad \frac{1}{g}\frac{\partial v}{\partial t}=-C_*\left(\frac{h}{g}\right)^{\frac{1}{2}}\frac{\partial v}{\partial x}$$

WHERE (A.4.52)

$$\left(\frac{h}{g}\right)^{\frac{1}{2}}\frac{\partial u}{\partial x}=-\left(\frac{h}{g}\right)^{\frac{1}{2}}\frac{\partial v}{\partial y}=2\alpha\, Cn(3).sn(3).dn(3)\left\{\right.$$

$$a\{-m\}+a^2\left\{m[1.0-1.5y_h^2]+m^2[-1.25+3.0y_h^2+2Cn^2(3)(1.0-2.25y_h^2)]\right\}+a^2\left\{m[-0.4+0.75y_h^2-0.375y_h^4]+m^2[1.35-5.25y_h^2+3.1875y_h^4+2Cn^2(3)(-1.7+7.125y_h^2-2.8125y_h^4)]\right\}+a^4\left\{m[0.09643-0.03750y_h^2-0.03750y_h^6]+m^2[-0.46431+5.625y_h^2-4.78125y_h^4+1.23750y_h^6+2Cn^2(3)(0.81967-$$

$$7.25625\,y_h^2+6.0\,y_h^4-1.18125\,y_h^6)]+m^3[0.55694-7.55625\,y_h^2+9.70312\,y_h^4-3.48750\,y_h^6+2\,Cm^2(3)(-3.04667+29.025\,y_h^2-33.42187\,y_h^4+7.08750\,y_h^6)+3\,Cm^4(3)(2.90133-25.2\,y_h^2+24.375\,y_h^4-3.93750\,y_h^6)]+m^4[0.17018+3.03750\,y_h^2-4.07812\,y_h^4+2.325\,y_h^6+2\,Cm^2(3)(1.03417-17.07188\,y_h^2+27.09375\,y_h^4-7.0875\,y_h^6)+3\,Cm^4(3)(-3.10267+33.525\,y_h^2-42.42187\,y_h^4+7.875\,y_h^6)+4\,Cm^6(3)(1.576-18.9\,y_h^2+19.68750\,y_h^4-2.95313\,y_h^6)]\}+$$

$$a^5\{m[-0.78281+1.141\,y_h^2+0.0375\,y_h^4-0.01875\,y_h^6-0.00201\,y_h^8]+m^2[0.89794-4.45837\,y_h^2+3.84375\,y_h^4-1.59375\,y_h^6+0.26016\,y_h^8+2\,Cm^2(3)(0.49893+2.2795\,y_h^2-3.91875\,y_h^4+1.80938\,y_h^6-0.25614\,y_h^8)]+m^3[-0.66324+5.8665\,y_h^2-16.09219\,y_h^4+9.84375\,y_h^6-1.64833\,y_h^8+2\,Cm^2(3)(1.2074-31.13156\,y_h^2+63.225\,y_h^4-31.55625\,y_h^6+3.70647\,y_h^8)+4\,Cm^4(3)(-2.26014+31.778\,y_h^2-53.23125\,y_h^4+22.96875\,y_h^6-2.21484\,y_h^8)]+m^4[0.70429-2.12075\,y_h^2+16.30547\,y_h^4-13.23750\,y_h^6+2.77634\,y_h^8+2\,Cm^2(3)(-2.71917+42.62962\,y_h^2-110.93203\,y_h^4+73.18125\,y_h^6-9.58259\,y_h^8)+3\,Cm^4(3)(7.12267-110.618\,y_h^2+225.6375\,y_h^4-115.5\,y_h^6+11.70703\,y_h^8)+4\,Cm^6(3)(-4.96993+74.07\,y_h^2-131.90625\,y_h^4+55.61719\,y_h^6-4.74609\,y_h^8)]+m^5[-0.26144-2.23875\,y_h^2-5.39297\,y_h^4+4.875\,y_h^6-1.38817\,y_h^8+2\,Cm^2(3)(0.43733-11.405\,y_h^2+47.56406\,y_h^4-41.7\,y_h^6+6.38839\,y_h^8)+3\,Cm^4(3)(-2.69367+61.73675\,y_h^2-162.53203\,y_h^4+103.6875\,y_h^6-11.70703\,y_h^8)+4\,Cm^6(3)(5.21186-91.44\,y_h^2+204.75\,y_h^4-102.375\,y_h^6+9.49219\,y_h^8)+5\,Cm^8(3)(-2.19396+42.552\,y_h^2-85.05\,y_h^4+35.4375\,y_h^6-2.84766\,y_h^8)]\}\Big\}$$

(A.4.53)

$$\left(\frac{h}{g}\right)^{\frac{1}{2}}\frac{\partial u}{\partial y}=\left(\frac{h}{g}\right)^{\frac{1}{2}}\frac{\partial v}{\partial x}=-2\Big\{a^2\{m[0.75\,y_h+Cm^2(3)(-1.5\,y_h)]+m^2[-0.75\,y_h+Cm^2(3)(3.0\,y_h)+Cm^4(3)(-2.25\,y_h)]\}+a^3\{m[-0.375\,y_h+0.375\,y_h^3+Cm^2(3)(0.75\,y_h-0.75\,y_h^3)]+m^2[-1.125\,y_h^3+Cm^2(3)(-5.25\,y_h+6.375\,y_h^3)+Cm^4(3)(7.125\,y_h-5.625\,y_h^3]+m^3[0.375\,y_h+0.75\,y_h^3+Cm^2(3)(3.0\,y_h-6.375\,y_h^3)+Cm^4(3)(-10.875\,y_h+11.25\,y_h^3)+Cm^6(3)(7.5\,y_h-5.625\,y_h^3)]\}+a^4\{m[0.01875\,y_h+0.05625\,y_h^5+Cm^2(3)(-0.0375\,y_h-0.1125\,y_h^5)]+m^2[-0.09375\,y_h+0.28126\,y_h^3-0.53439\,y_h^5+Cm^2(3)(5.625\,y_h-7.5625\,y_h^3+3.7125\,y_h^5)+Cm^4(3)(-7.25625\,y_h+12.0\,y_h^3-3.54375\,y_h^5)]+m^3[0.66562\,y_h+0.28126\,y_h^3+0.95625\,y_h^5+Cm^2(3)(-7.55625\,y_h+19.40624\,y_h^3-10.4625\,y_h^5)+Cm^4(3)(29.025\,y_h-66.84374\,y_h^3+21.2625\,y_h^5)+Cm^6(3)(-25.2\,y_h+48.75\,y_h^3-11.8125\,y_h^5)]+m^4[-0.59063\,y_h-0.5625\,y_h^3-0.47814\,y_h^5+Cm^2(3)(3.0375\,y_h-8.15624\,y_h^3+6.975\,y_h^5)+Cm^4(3)(-17.07188\,y_h+54.1875\,y_h^3-21.2625\,y_h^5)+Cm^6(3)(33.525\,y_h-84.84374\,y_h^3+23.625\,y_h^5)+Cm^8(3)(-18.9\,y_h+39.375\,y_h^3-8.85939\,y_h^5)]\}+a^5\{m[-0.5705\,y_h-0.03775\,y_h^3+$$

$$0.02811\,y_h^5 + 0.004\,y_h^7 + C_m^2(3)\left(1.141\,y_h + 0.075\,y_h^3 - 0.05625\,y_h^5 - 0.00804\,y_h^7\right)] +$$
$$m^2\left[1.44569\,y_h - 0.9\,y_h^3 + 0.35157\,y_h^5 - 0.1366\,y_h^7 + C_m^2(3)\left(-4.45837\,y_h + 7.6875\,y_h^3 - \right.\right.$$
$$\left.4.78125\,y_h^5 + 1.04064\,y_h^7\right) + C_m^4(3)\left(2.2795\,y_h - 7.8375\,y_h^3 + 5.42814\,y_h^5 - 1.07456\,y_h^7\right)] +$$
$$m^3\left[-1.29006\,y_h + 1.93594\,y_h^3 - 0.75939\,y_h^5 + 0.50624\,y_h^7 + C_m^2(3)\left(5.8665\,y_h - \right.\right.$$
$$32.18438\,y_h^3 + 29.53125\,y_h^5 - 6.59332\,y_h^7\Big) + C_m^4(3)\left(-31.13156\,y_h + 126.45\,y_h^3 - 94.66875\,y_h^5 + \right.$$
$$\left.14.82588\,y_h^7\right) + C_m^6(3)\left(31.778\,y_h - 106.4625\,y_h^3 + 68.90625\,y_h^5 - 8.85936\,y_h^7\right)] +$$
$$m^4\left[-0.38012\,y_h - 2.32032\,y_h^3 + 0.15468\,y_h^5 - 0.62276\,y_h^7 + C_m^2(3)\left(-2.12075\,y_h + \right.\right.$$
$$32.61094\,y_h^3 - 39.7125\,y_h^5 + 11.10536\,y_h^7\Big) + C_m^4(3)\left(42.62962\,y_h - 221.86406\,y_h^3 + \right.$$
$$219.54375\,y_h^5 - 38.33036\,y_h^7\Big) + C_m^6(3)\left(-110.618\,y_h + 451.275\,y_h^3 - 346.5\,y_h^5 + \right.$$
$$\left.46.82812\,y_h^7\right) + C_m^8(3)\left(74.07\,y_h - 263.8125\,y_h^3 + 166.85157\,y_h^5 - 18.98436\,y_h^7\right)] +$$
$$m^5\left[0.795\,y_h + 1.32188\,y_h^3 + 0.225\,y_h^5 + 0.24912\,y_h^7 + C_m^2(3)\left(-2.23875\,y_h - \right.\right.$$
$$10.78594\,y_h^3 + 14.625\,y_h^5 - 5.55268\,y_h^7\Big) + C_m^4(3)\left(-11.405\,y_h + 95.12812\,y_h^3 - \right.$$
$$125.1\,y_h^5 + 25.55356\,y_h^7\Big) + C_m^6(3)\left(61.73675\,y_h - 325.06406\,y_h^3 + \right.$$
$$311.0625\,y_h^5 - 46.82812\,y_h^7\Big) + C_m^8(3)\left(-91.44\,y_h + 409.5\,y_h^3 - 307.125\,y_h^5 + \right.$$
$$\left.\left.37.96876\,y_h^7\right) + C_m^{10}(3)\left(42.552\,y_h - 170.1\,y_h^3 + 106.3125\,y_h^5 - 11.39064\,y_h^7\right)]\right\}\Big\}$$

(A.4.54)

Changing the coordinates to a stationary frame x,y on the sea bed we have

$$x = X + ct$$

$$x_* = \frac{x}{h} = X_* + x_c^*(t) \qquad \text{(A.4.55)}$$

where

$$x_c^*(t) = \frac{ct}{h} \qquad \text{(A.4.56)}$$

and

$$c = c_* \sqrt{gh}$$

also

$$u(x,y,t) = u(X,Y) + c$$
$$v(x,y,t) = v(X,Y)$$

and arguments of all elliptic functions used will be $\eta = \alpha(x_* - x_c^*(t))$ instead of αX_*

Note that for calculation of elliptic functions the following can be used (1)

$$sn(z\backslash m) = \frac{2\pi}{\sqrt{m}\ K(m)} \sum_{n=0}^{\infty} \frac{q^{n+\frac{1}{2}}}{1-q^{2n+1}} \sin[(2n+1)w] \qquad \text{(A.4.57)}$$

$$cn(z\backslash m) = \frac{2\pi}{\sqrt{m}\ K(m)} \sum_{n=0}^{\infty} \frac{q^{n+\frac{1}{2}}}{1+q^{2n+1}} \cos[(2n+1)w] \qquad \text{(A.4.58)}$$

$$dn(z\backslash m) = \frac{\pi}{2K(m)} + \frac{2\pi}{K(m)} \sum_{n=1}^{\infty} \frac{q^n}{1+q^{2n}} \cos(2nw) \qquad \text{(A.4.59)}$$

where

$$q = e^{-\pi K'(m_1)/K(m)} \qquad \text{(A.4.60)}$$

$$W = \pi z / 2K(m) \qquad \text{(A.4.61)}$$

$$m_1 = 1 - m \qquad \text{(A.4.62)}$$

$$K'(m_1) = \frac{\pi}{2}\left[1 + \left(\frac{1}{2}\right)^2 m_1 + \left(\frac{1\cdot 3}{2\cdot 4}\right)^2 m_1^2 + \left(\frac{1\cdot 3\cdot 5}{2\cdot 4\cdot 6}\right)^2 m_1^3 + \cdots\right] \qquad \text{(A.4.63)}$$

Also note that C_n^2 has a period of 2K(m). Therefore if θ is phase angle in degrees, then

$$z = \frac{\theta \cdot K(m)}{180} \qquad \text{(A.4.64)}$$

$$W = \frac{\pi \cdot \theta}{360} \qquad \text{(A.4.65)}$$

Given wave height, period and water depth, equations (A.4.50 -A.4.54) can be evaluated taking the following steps:

1. Find m from (A.4.47) by iteration using say the method of bisection (the starting value can be taken as 0.5).

2. Find h from (A.4.48)

3. Determine α from (A.4.43)

4. C_* can be found using (A.4.49)

5. Elliptic functions can be evaluated using (A.4.57 - A.4.65).

APPENDIX B

SALS SYSTEM RESPONSE TRANSFER FUNCTIONS (45)

B.1. SURGE MOTION

The high frequency motion is inertia force dominated therefore neglecting damping the steady state surge is

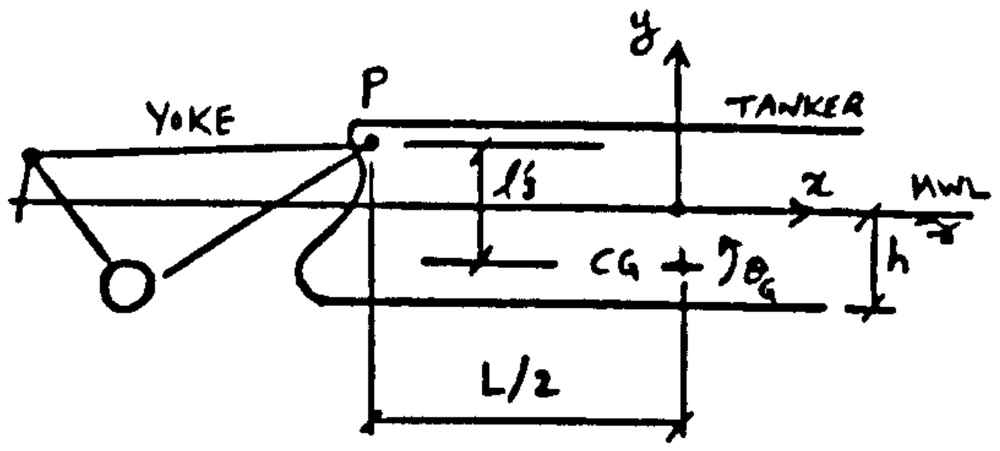

FIG.B.1.SCHEMATIC OF SALS

$$x_G = x_0 \sin(\omega t) \qquad \text{(B.1.1)}$$

where

$$\frac{x_0}{H} = \frac{G_x}{(M + M_{ax})\omega^2} \qquad \text{(B.1.2)}$$

$$G_x = \rho \beta B \omega^2 (1 + C_{xx}) \left[1 - \frac{\sinh k(d-h)}{\sinh kd}\right] \sin\left(\tfrac{1}{2} kL\right)/k^2 \qquad \text{(B.1.3)}$$

ω = wave frequency

H = wave height

B = tanker width

L = tanker length

β = hull shape factor

ρ = fluid density

C_{xx} = added mass coefficient in surge

M_{ax} = added mass in surge (taken as 5% of structural mass)

h = tanker draft

d = water depth

k = wave number

From equation (B.1.1)

$$\dot{x}_G = \omega x_o \cos(\omega t) \qquad \text{(B.1.4)}$$

$$\ddot{x}_G = -\omega^2 x_G \qquad \text{(B.1.5)}$$

B.2. HEAVE MOTION

Assuming heave and pitch motions are uncoupled, averaging the vertical acceleration over the volume of fluid and taking the mean of wave elevation over the water plane area, equation of heave motion is

$$\ddot{y}_G + 2\beta_y \cdot \omega_y \cdot \dot{y}_G + \omega_y^2 \cdot y_G = H\left(G_{y_1} \cdot \cos\omega t - G_{y_2} \sin\omega t\right) \qquad \text{(B.2.1)}$$

where

$$G_{y_1} = \frac{\rho g B}{(M+M_{ay})}\left[1-\beta(1+C_{yy})\left\{1-\frac{\cosh k(d-h)}{\cosh kd}\right\}\right]\frac{\sin(\frac{1}{2}kL)}{k} \qquad \text{(B.2.2)}$$

$$G_{y_2} = \frac{\rho g}{(M+M_{ay})}\left[1-\frac{\cosh k(d-h)}{\cosh kd}\right]\left[\frac{g^2\bar{A}^2}{h\omega^4}\right]\frac{\sin(\frac{1}{2}kL)}{k} \qquad \text{(B.2.3)}$$

Undamped natural frequency

$$\omega_y = \left[L B \rho g / (M+M_{ay})\right]^{\frac{1}{2}} \qquad \text{(B.2.4)}$$

damping ratio

$$\beta_y = B_y / 2(M+M_{ay})\omega_y \qquad \text{(B.2.5)}$$

$$B_y = \rho g^2 \bar{A}^2 L / \omega^3 \qquad \text{(B.2.6)}$$

M_{ay} = added mass in heave

$\bar{A}$ = generated wave amplitude/heave amplitude given by (29)

C_{yy} = heave added mass coefficient (29)

Steady state solution is

$$y_G = y_0 \cos(\omega t + \psi) \qquad \text{(B.2.7)}$$

where

$$\frac{y_0}{H} = \left[\frac{G_{y_1}^2 + G_{y_2}^2}{(\omega_y^2 - \omega^2)^2 + (2\beta_y \cdot \omega \cdot \omega_y)^2} \right]^{\frac{1}{2}} \qquad \text{(B.2.8)}$$

$$\tan\psi = \left[\frac{G_{y_2}(\omega_y^2 - \omega^2) - 2 G_{y_1} \cdot \beta_y \cdot \omega \cdot \omega_y}{G_{y_1}(\omega_y^2 - \omega^2) + 2 G_{y_2} \cdot \beta_y \cdot \omega \cdot \omega_y} \right] \qquad \text{(B.2.9)}$$

Also

$$\dot{y}_G = -y_0 \omega \sin(\omega t + \psi) \qquad \text{(B.2.10)}$$

$$\ddot{y}_G = -\omega^2 y_G \qquad \text{(B.2.11)}$$

B.3. PITCH MOTION

Neglecting pitch moments due to horizontal fluid forces, the equation of pitch motion is

$$\ddot{\theta}_G + 2\beta_\theta \cdot \omega_\theta \cdot \dot{\theta}_G + \omega_\theta^2 \cdot \theta_G = H(G_{\theta 1} \sin\omega t + G_{\theta 2} \cos\omega t) \qquad (B.3.1)$$

where

$$G_{\theta 1} = \frac{\rho g B}{(I+I_\theta)} \left[1-\beta(1+C_{yy})\left\{1-\frac{\cosh k(d-h)}{\cosh kd}\right\}\right] \frac{\sin(\frac{1}{2}kL)-\frac{1}{2}kL\cos(\frac{1}{2}kL)}{k^2}$$

(B.3.2)

$$G_{\theta 2} = \frac{\rho g}{(I+I_\theta)} \left[\frac{g^2\bar{A}^2}{h\omega^4}\right] \left\{1-\frac{\cosh k(d-h)}{\cosh kd}\right\} \frac{\sin(\frac{1}{2}kL)-\frac{1}{2}kL\cos(\frac{1}{2}kL)}{k^2}$$

(B.3.3)

Natural frequency

$$\omega_\theta = \left[\, g.M.\,\overline{GM} \,/\, (I+I_\theta)\,\right]^{\frac{1}{2}} \qquad (B.3.4)$$

where $\overline{GM}$ is the pitch metacentre height.

Damping ratio

$$\beta_\theta = B_\theta \,/\, 2(I+I_\theta)\omega_\theta \qquad (B.3.5)$$

$$B_\theta = \rho g^2 \bar{A}^2 L^3 \,/\, 12\omega^3 \qquad (B.3.6)$$

Total moment of inertia

$$(I+I_\theta) = (M+M_{ay})L^2/12 \qquad \text{(B.3.7)}$$

Steady state solution to (B.3.1) is

$$\theta_G = \theta_0 \cos(\omega t + \mathcal{T}) \qquad \text{(B.3.8)}$$

where

$$\frac{\theta_0}{H} = \left[\frac{G_{\theta 1}^2 + G_{\theta 2}^2}{(\omega_\theta^2 - \omega^2)^2 + (2\beta_\theta . \omega . \omega_\theta)^2}\right]^{\frac{1}{2}} \qquad \text{(B.3.9)}$$

$$\tan \mathcal{T} = -\left[\frac{G_{\theta 1}(\omega_\theta^2 - \omega^2) + 2 G_{\theta 2} . \beta_\theta . \omega . \omega_\theta}{G_{\theta 2}(\omega_\theta^2 - \omega^2) - 2 G_{\theta 1} . \beta_\theta . \omega . \omega_\theta}\right] \qquad \text{(B.3.10)}$$

also

$$\dot{\theta}_G = -\theta_0 \omega \sin(\omega t + \mathcal{T}) \qquad \text{(B.3.11)}$$

$$\ddot{\theta}_G = -\omega^2 \theta_G \qquad \text{(B.3.12)}$$

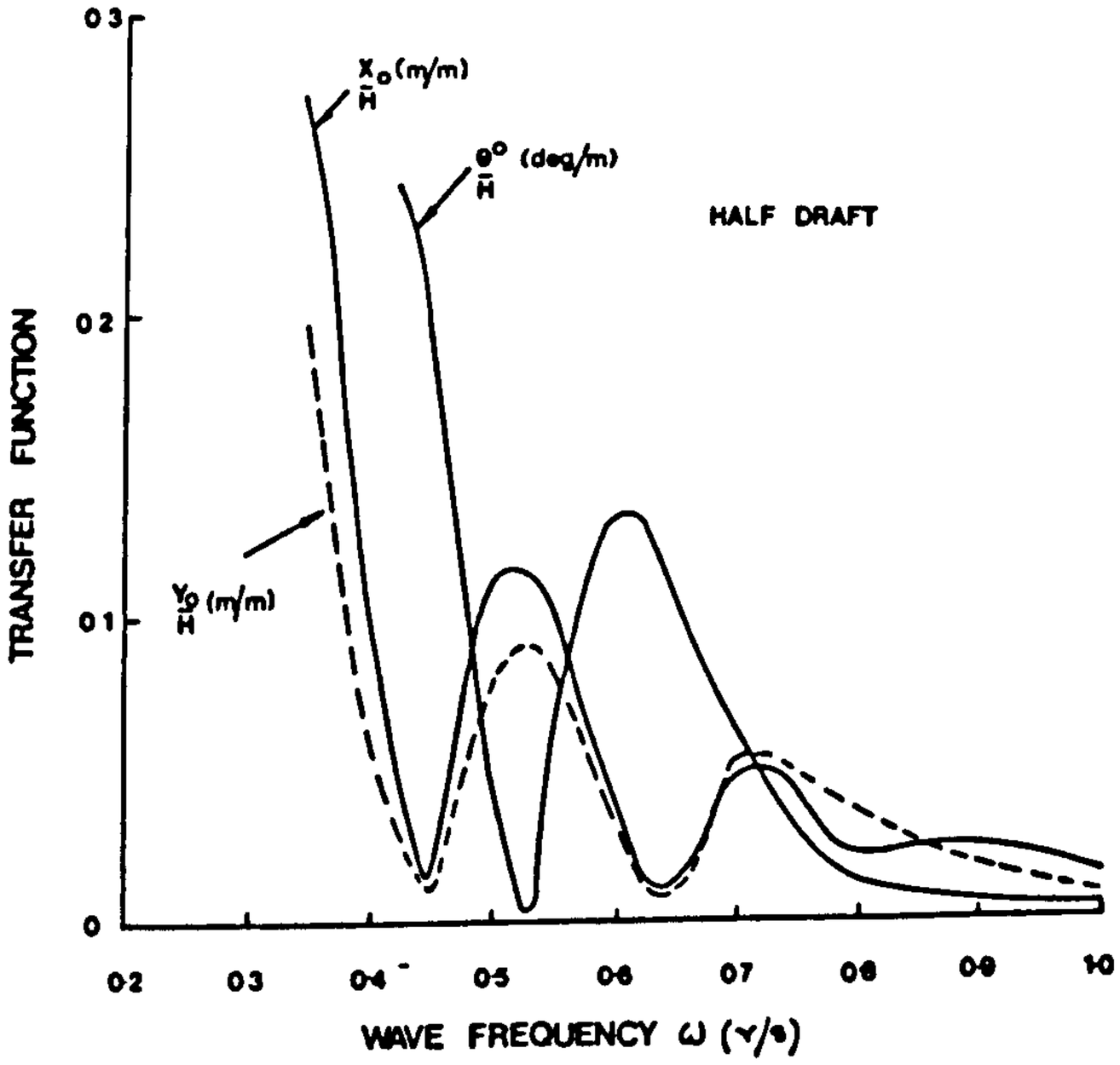

FIGURE B.2. Vessel transfer functions for surge, heave and pitch - half draft

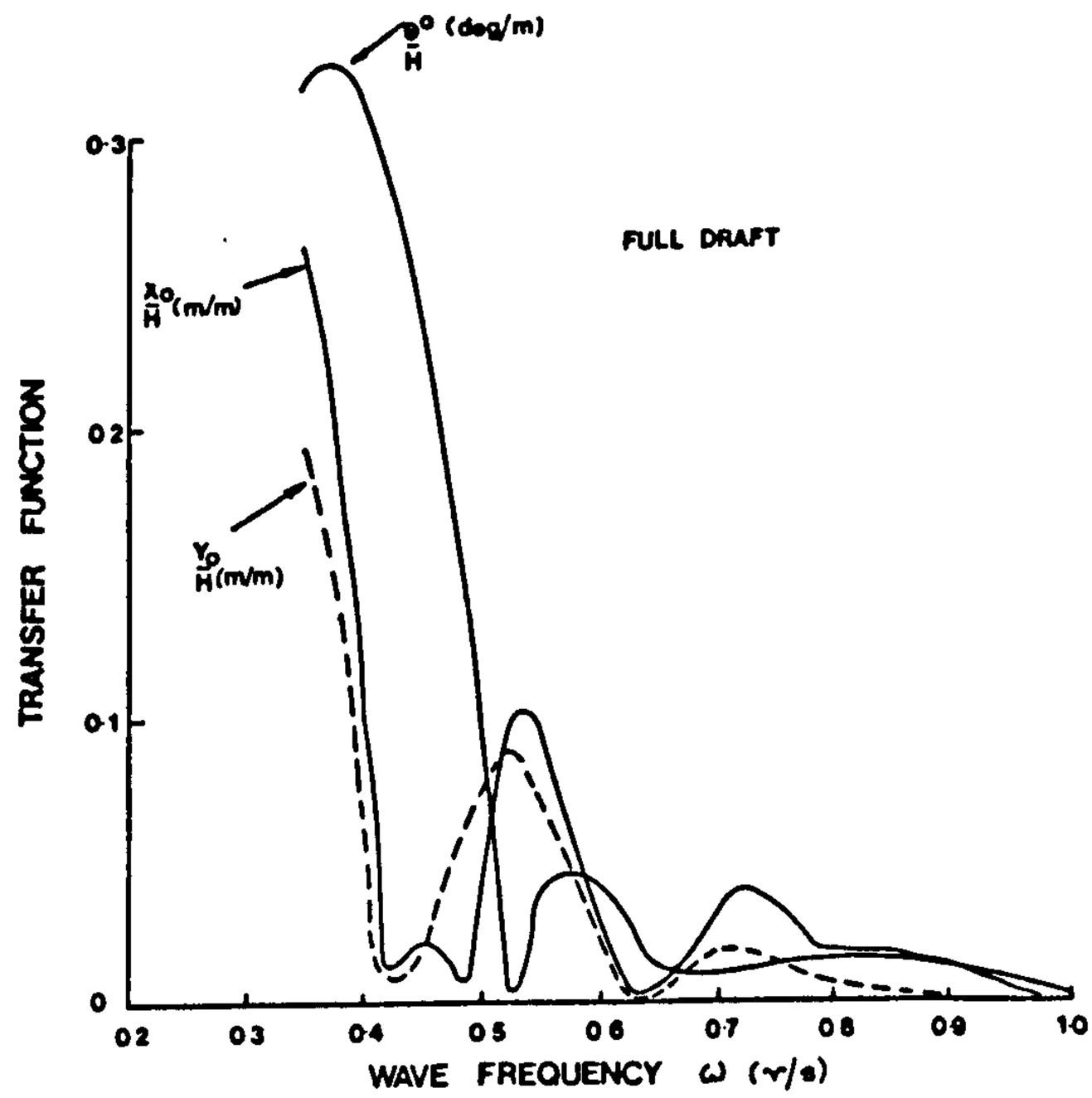

FIGURE B.3. Vessel transfer functions for surge, heave and pitch - full draft

APPENDIX C

FORCE COEFFICIENTS

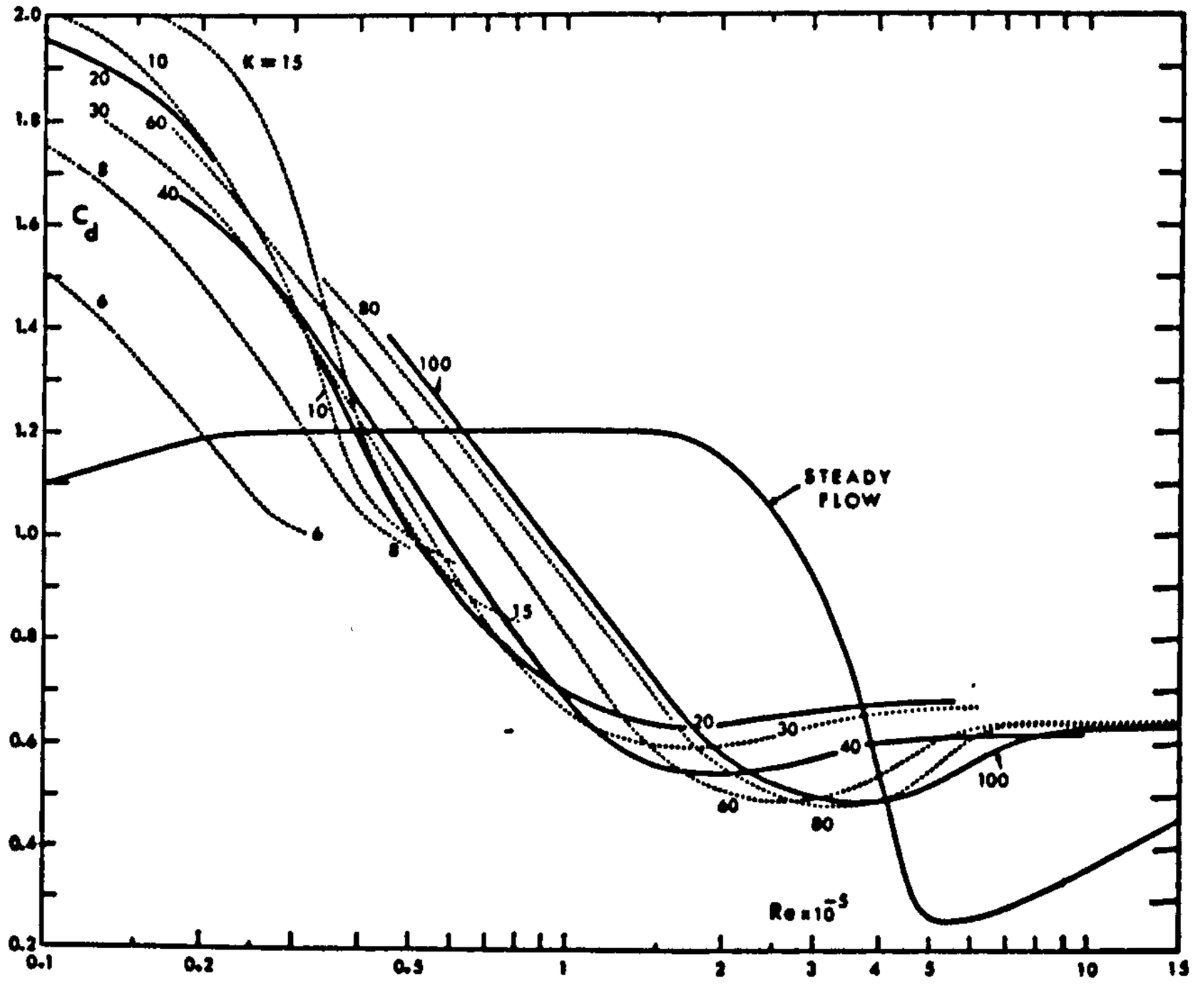

FIGURE C.1. Drag coefficient versus Reynold's number (75)

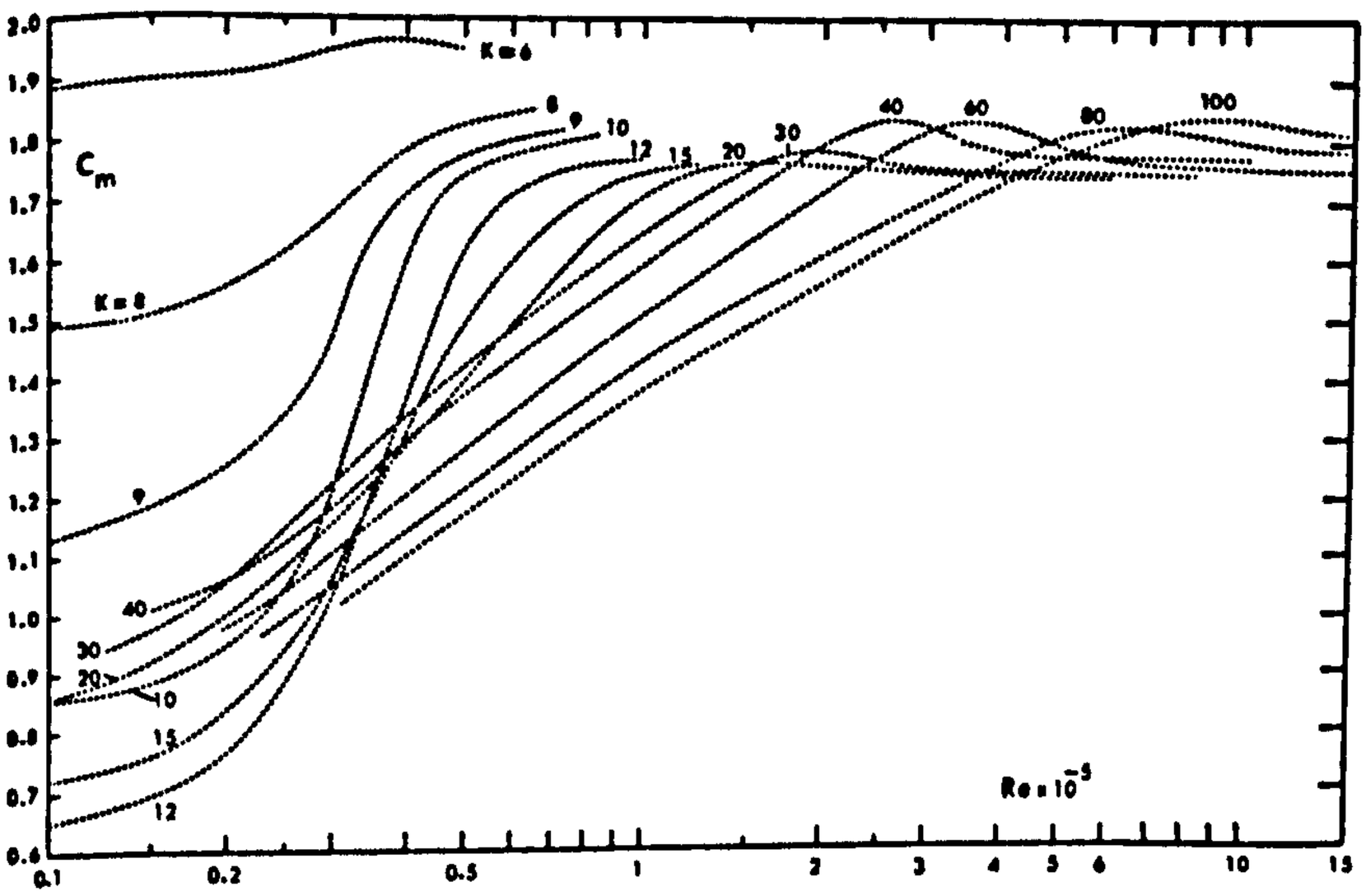

FIGURE C.2. Inertia Coefficient versus Reynold's number (75)

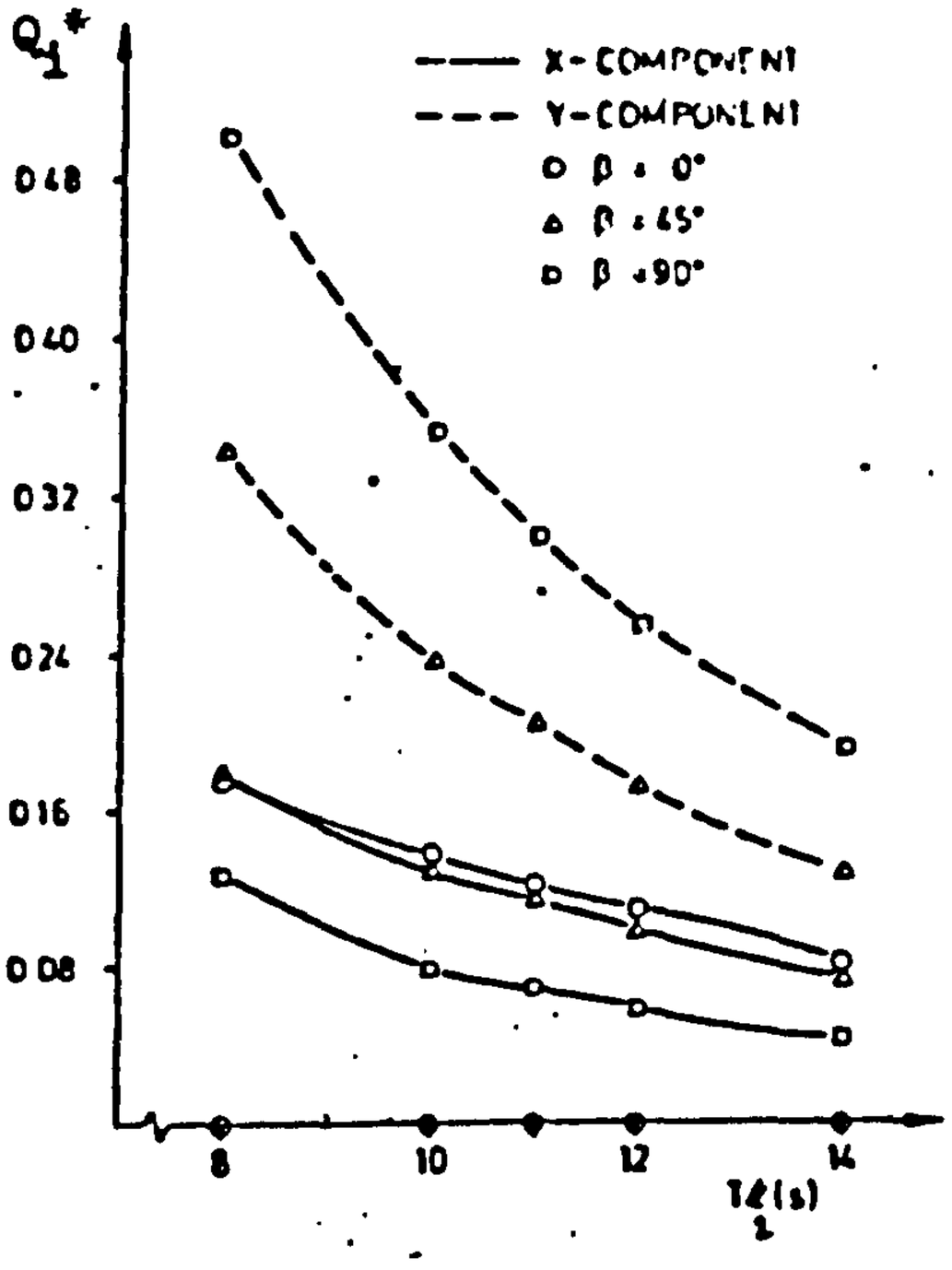

FIGURE C.3. Slow drift force coefficient on VLCC (22)

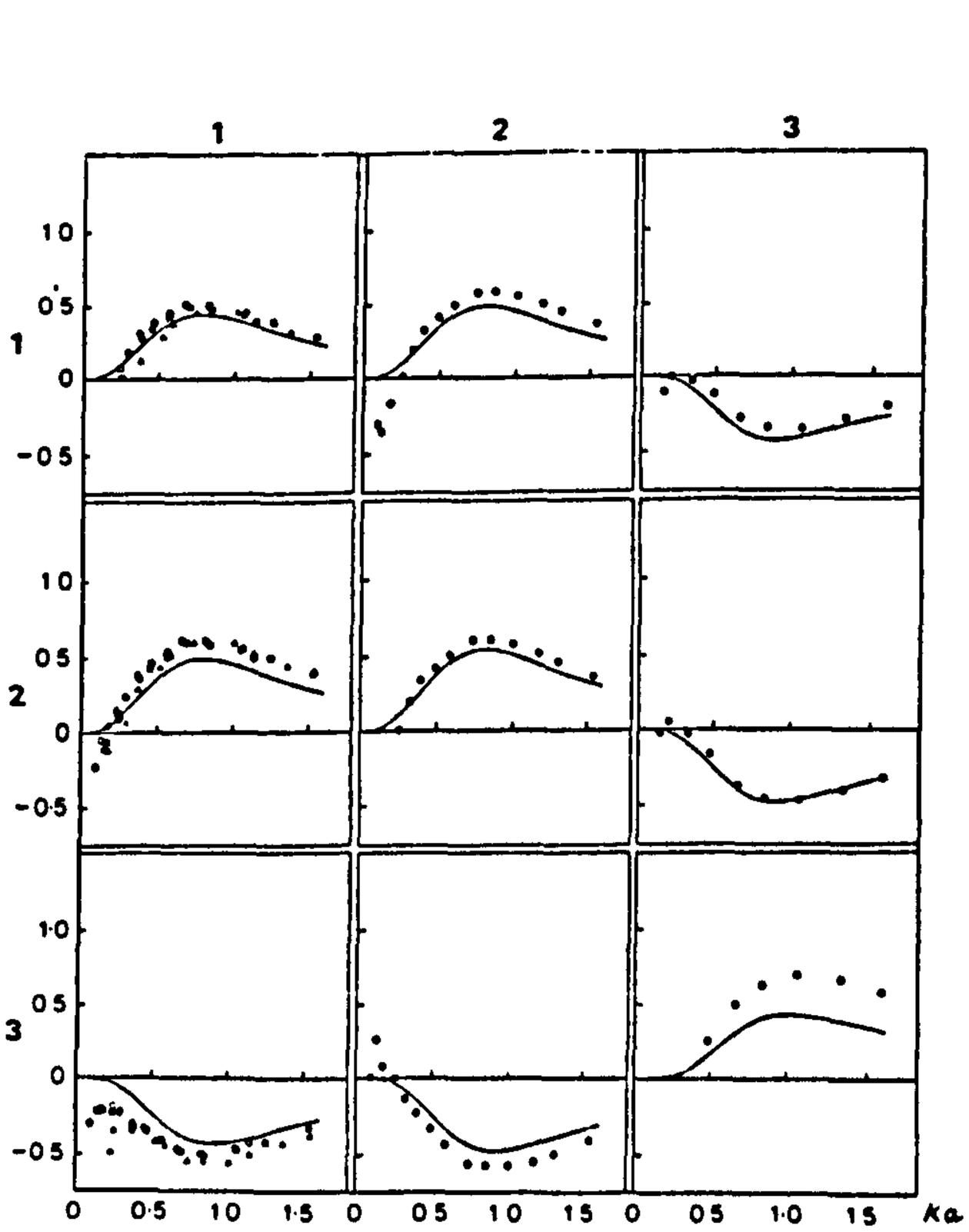

FIGURE C4. NONDIMENSIONAL DAMPING MATRIX FOR AN OSCILLATING COLUMN (19)

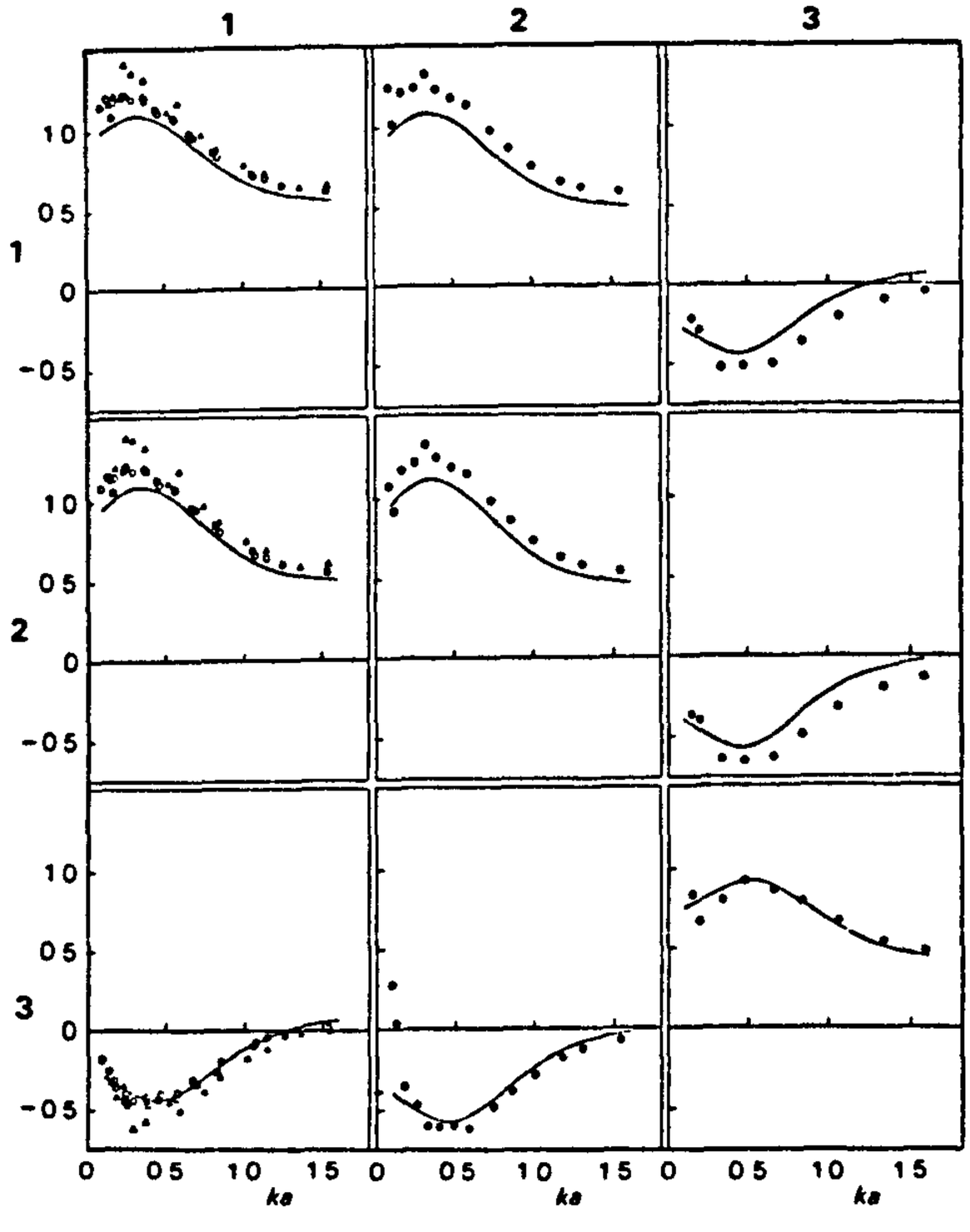

FIGURE C5. NONDIMENSIONAL ADDED INERTIA MATRIX FOR AN OSCILLATING COLUMN (19)

FOR ALC :

$$(I + I_a)\ddot{\theta} + c\dot{\theta} + K\theta = F(t)$$

$$\alpha_{11} = \frac{I_a}{\bar{M}^*} \quad , \beta_{11} = \frac{c}{\omega \bar{M}^*}$$

$$\bar{M}^* = \int_{-l_t}^{0} \rho \frac{\pi D^2}{4} y^2 \, dy$$